(1)

The Electrochemical Society, Inc.

181st Meeting Program

Including:

State-of-the-Art Program on Compound Semiconductors XVI
Fullerenes: Chemistry, Physics, and New Directions
Quantum Confinement
Micromachining and Microstructures
Electronics/Dielectric Science & Technology Joint Recent News Papers

Adam's Mark Hotel
St. Louis, Missouri
May 17-22, 1992

ST. LOUIS, MO, MEETING ORGANIZATION

Host Chairman

V. H. Branneky

The Electrochemical Society, Inc., Headquarters Staff

Roque J. Calvo, Executive Secretary
Brian E. Rounsavill, Meetings and Programs Manager
Sarah A. Kilfoyle, Publications Manager
Ellen Tiano, Information Systems Manager
Carolyn Pylypiak, Financial Manager
Barbara J. Baggott, Secretary to Roque J. Calvo
Stephen M. Shier, Administrative Assistant

The Electrochemical Society, Inc.
10 South Main Street
Pennington, NJ 08534-2896
(609) 737-1902

Printed in the United States of America

SECURITY CLASSIFICATION OF THIS PAGE

REPORT DOCUMENTATION PAGE

Form Approved
OMB No. 0704-0188

1a. REPORT SECURITY CLASSIFICATION: (U)	1b. RESTRICTIVE MARKINGS: NA
2a. SECURITY CLASSIFICATION AUTHORITY: NA	3. DISTRIBUTION / AVAILABILITY OF REPORT: Distribution Unlimited
2b. DECLASSIFICATION / DOWNGRADING SCHEDULE: NA	
4. PERFORMING ORGANIZATION REPORT NUMBER(S): The Electrochemical Society, Inc.	5. MONITORING ORGANIZATION REPORT NUMBER(S): NA
6a. NAME OF PERFORMING ORGANIZATION: The Electrochemical Society, Inc. / 6b. OFFICE SYMBOL (If applicable): NA	7a. NAME OF MONITORING ORGANIZATION: Office of Naval Research
6c. ADDRESS (City, State, and ZIP Code): Pennington, New Jersey 08534-2896	7b. ADDRESS (City, State, and ZIP Code): 33 Third Avenue, New York, NY 10003-9998
8a. NAME OF FUNDING / SPONSORING ORGANIZATION: Office of Naval Research / 8b. OFFICE SYMBOL (If applicable): ONR	9. PROCUREMENT INSTRUMENT IDENTIFICATION NUMBER: N00014-92-J-1413
8c. ADDRESS (City, State, and ZIP Code): 33 Third Avenue, New York, NY 10003-9998	10. SOURCE OF FUNDING NUMBERS: PROGRAM ELEMENT NO. / PROJECT NO. / TASK NO. / WORK UNIT ACCESSION NO.

11. TITLE (Include Security Classification): Fullerenes: Chemistry, Physics and New Directions

12. PERSONAL AUTHOR(S): K. M. Kadish and R. S. Ruoff

13a. TYPE OF REPORT	13b. TIME COVERED	14. DATE OF REPORT (Year, Month, Day)	15. PAGE COUNT
Annual	FROM 4/92 TO 9/92	91/4/28	

16. SUPPLEMENTARY NOTATION

17. COSATI CODES			18. SUBJECT TERMS (Continue on reverse if necessary and identify by block number)
FIELD	GROUP	SUB-GROUP	Fullerenes

19. ABSTRACT (Continue on reverse if necessary and identify by block number)

The Fullerene Symposium is organized with the intention of providing a forum for the presentation of latest developments on these fascinating new allotropes of carbon. Papers on recent advances or on the state of the field are solicited in the following areas; Fundamental understanding of the Physical Properties and Structures, Synthesis and separation, Chemical reactions and new derivative, Charge transfer reactions and electrochemistry, Conductivity and super conductivity, Possible applications and New directions.

20. DISTRIBUTION / AVAILABILITY OF ABSTRACT	21. ABSTRACT SECURITY CLASSIFICATION
☐ UNCLASSIFIED/UNLIMITED ☐ SAME AS RPT ☐ DTIC USERS	
22a. NAME OF RESPONSIBLE INDIVIDUAL	22b. TELEPHONE (Include Area Code) / 22c. OFFICE SYMBOL

DD Form 1473, JUN 86 — Previous editions are obsolete — SECURITY CLASSIFICATION OF THIS PAGE

S/N 0102-LF-014-6603

St. Louis — The Gateway City

St. Louis Skyline

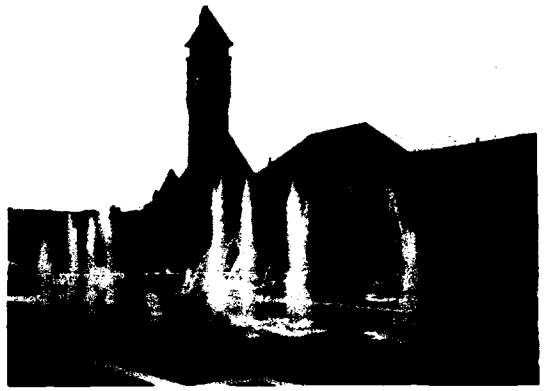

Union Station

When the French fur trader Pierre Laclede came upon the swirling confluence of the Missouri and Mississippi Rivers in 1764, he instantly recognized its potential as a trading center. Landing at the first available prime spot south of the joining of the two rivers, he founded the village of St. Louis. In the 1800s St. Louis grew, and heavy river traffic between New Orleans and St. Paul made the city a major port. The city became known as the "Gateway West." It was from here that the explorers Lewis and Clark started out on their westward expedition.

The Gateway Arch, the 630 foot high stainless steel monument that dominates the downtown skyline, commemorates the role of St. Louis in the nation's surge westward. Beneath the Gateway Arch is the Museum of Westward Expansion which chronicles 19th century St. Louis history with displays of covered wagons, Texas longhorns, Indian ponies, and teepees. Nearby is the restored Old Courthouse, site of the famous Dred Scott decision.

St. Louis today is a bustling city of 2.5 million people, ranking in the top 15 in population among U.S. metro areas. It is the nation's second largest inland port, with barge connections to 29 American centers and, via the Mississippi and the Gulf of Mexico, to the rest of the world. It is also the nation's third largest rail center.

While not geographically located at the precise center of the U.S., St. Louis claims to be the population center of the nation. The city is accessible by air from almost anywhere in the 48 contiguous United States in three hours or less. Nearly 35 percent of the country's population lives within a 500 mile radius of St. Louis.

St. Louis has a rich musical tradition with something for everyone. For those who like classical music, there is the St. Louis Symphony, the nation's second oldest symphony orchestra. For those who like ragtime, a visit to the restored Scott Joplin house is a must. In addition to the second floor where the "King of Ragtime" lived between 1900 and 1903, there are exhibition galleries and a musical performance room. Blues and jazz buffs can hear their favorite music in the bohemian Soulard neighborhood or at Laclede's Landing.

Forest Park, a 1300 acre park (bigger than New York's Central Park) in the city proper, contains many attractions for the visitor. On its wooded grounds is the St. Louis Art Museum which was the Fine Arts Palace during the 1904 World's Fair. Also in Forest Park are the Muny Opera (an outdoor musical theater) and the Missouri Historical Society. One of the city's major attractions, the St. Louis Zoo, which is famous for displaying animals in their natural habitat, is also located in the park. The park is also home to the Missouri Botanical Garden, a 79 acre historical landmark founded by Henry Shaw in 1859. The Botanical Garden offers the Climatron, the world's first geodesic domed greenhouse which houses a tropical rain forest, the country's largest authentic Japanese garden, and an English woodland garden.

The city offers many other spots of interest. There is The Cathedral of St. Louis which is famous for its dazzling mosaic-covered domes, arches, wall panels, and ceilings. Also not to be missed is Laclede's Landing, the site of the original fur-trading settlement. Cobblestone streets and cast iron street lamps surround dozens of century-old buildings housing offices, small shops and boutiques, unusual restaurants, and a collection of nightspots that make this one of the city's premiere entertainment districts. It is situated on the last remaining example of the street pattern laid out when St. Louis was founded as a French trading village in 1764.

Union Station, now a Historical Landmark, was built in 1894 when the railroad was king. In recent years the terminal fell into disrepair and was nearly torn down. The old station has been renovated from top to bottom, and the station building is now a hotel. The hotel has a breathtaking Grand Hall (the former station lobby) which features a 65 foot vaulted ceiling, gold leaf, stained glass windows, and sculptures. The Romanesque limestone facade resembles a medieval castle. The station's old train shed now contains myriad shops and restaurants.

St. Louis has always been a big sports city. Busch Stadium, home to baseball's St. Louis Cardinals, contains the Sports Hall of Fame with displays on baseball, football, basketball, golf, soccer, tennis, and hockey. For those who prefer to watch ice hockey, there are the St. Louis Blues. The St. Louis Storm provides entertainment for indoor soccer fans. For those who would rather engage in sports than watch them, there are numerous parks in and around the city offering opportunities for boating, fishing, hiking, swimming, and horseback riding.

As the Gateway to the West in the 19th century, St. Louis offered travelers from the East their last opportunity for a fine meal as they prepared for the trek toward the Rocky Mountains. That tradition of great food continues today. In the many restaurants throughout the city, one will find a diversity of cuisine representing the rich and diverse cultural heritage of the area.

Your visit to St. Louis is one you are not likely to soon forget. It is a unique blend of old and new, a city rich in history and diversified entertainment. Come and enjoy all that the "Gateway City" has to offer you.

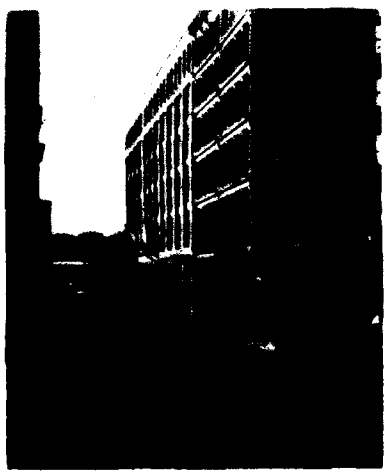

Laclede's Landing

Fox Theatre

Representative George E. Brown, Jr., to Deliver The Electrochemical Society Lecture

The Honorable George E. Brown, Jr., Democrat of the 36th District (Riverside, San Bernadino, and Coltin), California, has been selected to deliver The Electrochemical Society Lecture at the Plenary Session of the 181st Meeting of the Society in St. Louis, Missouri. His lecture entitled "Government Initiatives in Materials Science," will be presented at 9:00 a.m. on Monday, May 18, 1992 in Promenade Ballroom C and D, 2nd level of The Adam's Mark Hotel.

Representative Brown has been an aggressive proponent of the notions of open and free communication within the national and international science community, and a leader in our nation's efforts to broaden science and engineering career opportunities for women and minorities and to improve science literacy. In addition, his strong support for institutionalizing long-range planning and investment in science and technology distinguishes Rep. Brown as a consistently creative and supportive leader in advancing science.

First elected to the U.S. House of Representatives in 1962, he has worked to strengthen America's scientific and technological base. His participation in hearings and legislation led to the formation of the

charter for the National Science Foundation in 1965. He also led the efforts to create the Office of Technology Assessment and the Office of Science and Technology Policy.

Long before it became an issue, Rep. Brown recognized that the United States needed to aggressively pursue alternative energy systems and nonpolluting technologies. He played an important role in developing a National Energy Policy in the wake of the oil embargo of 1973 and has chaired numerous hearings on solar, wind-powered, geothermal, and other forms of alternative energy systems. Most recently, legislation authored by Rep. Brown to develop new hydrogen research and development programs at the Department of Energy was signed into law by President Bush.

Representative Brown has introduced dozens of pieces of legislation to protect valuable natural ecosystems, remove cancer causing pesticides from our food supplies, and increase funding for federal environmental protection programs. He was instrumental in achieving passage of the nation's first Clean Air Act and helped to establish the Environmental Protection Agency in 1970.

A self-avowed space enthusiast, Rep. Brown has spent a considerable part of his congressional career promoting the civilian space program and working to prevent the militarization of space. Previously a member of the Science, Space and Technology Committee, Rep. Brown will serve as Chairman of this House Committee for the 102nd Congress.

Ernest B. Yeager to Receive the Vittorio de Nora Award

Ernest B. Yeager has been selected to receive the Vittorio de Nora Award for electrochemical engineering and technology. According to the citation: "The nomination of Professor Ernest B. Yeager is made in consideration of his leadership role in advancing the field of electrochemical technology as demonstrated through the foundation and growth of the Case Center for Electrochemical Sciences. In particular, his role in the development of fuel cell and battery technology through work in oxygen electrochemistry, electrocatalysis, and carbon electrochemistry is cited." He will be presented with the Award at the Vittorio de Nora Award Banquet on Tuesday, May 19, 1992 at 7:45 P.M. in the Rose Garden, 4th level of The Adam's Mark Hotel.

Dr. Yeager's award address entitled "Opportunities for O_2 Cathodes in Batteries, Fuel Cells, and Industrial Electrolytic Processes" will be delivered immediately following the presentation of awards at the Awards and Recognition Session to be held on Tuesday, May 19 at 4:30 P.M. in Promenade Ballroom C and D, 2nd level.

Ernest Yeager is a native of Orange, New Jersey. He received his B.A. (summa cum laude) from Montclair State College (New Jersey) in 1945 and his M. S. and Ph.D. in physical chemistry at Western Reserve University in 1946 and 1948, respectively. He then joined the faculty and advanced to the rank of Professor of Chemistry at what is now Case Western Reserve University.

From 1969 to 1972, he served as Chairman of the Chemistry Department and in 1972-1973 as Chairman of the University Faculty Senate. In 1976 he became the Director of the newly established Case Center for Electrochemical Sciences. In 1983 he was appointed to the Frank Hovorka Chair in Chemistry and in 1991 was given emeritus status.

Professor Yeager is a past President and Honorary Member of The Electrochemical Society which he joined in 1950. He is also a past President and Honorary Member of the International Society of Electrochemistry, a past Vice-President and Fellow of the Acoustical Society of America and a Fellow of the American Association for the Advancement of Science. His awards include the Technical Award (1954) and the Distinguished Service Award (1982) of the Cleveland Technical Societies Council, the Biennial Award of the Acoustical Society of America in 1956, the Navy Certificate of Commendation in 1972, the Acheson Medal of The Electrochemical Society in 1980, the Morley Medal of the Cleveland Section of the American Chemical Society in 1981, the Distinguished Achievement Medal of Western Reserve College in 1983, and an honorary doctorate from Montclair State College in 1983.

Professor Yeager's research publications involve many areas of electrochemistry including electrochemical kinetics, electrocatalysis, the electrochemistry of oxides, spectroscopic studies of electrochemical interfaces, lithium electrochemistry, the passivation of metals, underpotential deposition, the electrochemistry of single-crystal noble metals, and the relaxational properties of electrolytes and colloidal systems. In recent years, his research group has given particular attention to oxygen electrochemistry and to various electrocatalytic reactions including the oxidation of small organics. He is the editor or co-editor of sixteen books on electrochemistry and has published 258 papers.

His nonscientific interests include music, particularly the piano.

Ken Nobe to Receive the Henry B. Linford Award for Distinguished Teaching

Ken Nobe, Professor of Chemical Engineering at the University of California, Berkeley, has been selected to be the sixth recipient of the Henry B. Linford Award for Distinguished Teaching of The Electrochemical Society. The Award of a silver medal and a bronze replica and $1000 will be presented at the Awards and Recognition Session at the 181st Meeting of the Society in St. Louis, Missouri, Tuesday, May 19. The Linford Award is presented biennially to recognize excellence in teaching in subject area of interest to the Society. Funding is derived from an endowment by Samuel Rubin honoring the late Henry B. Linford, former Professor of Chemical Engineering at Columbia University.

Ken Nobe was born in Berkeley, California. After serving as an infantryman in Europe during World War II, he studied chemistry and chemical engineering at the University of California, Berkeley, receiving a B.S. in 1951. From 1951-1952 he was a chemical engineer at Air Reduction Research Laboratories in Murray Hill, New Jersey, working on the fabrication of copper-catalyzed polyacetylene for testing of its physical properties.

At the University of California, Los Angeles, where he received his Ph.D. in December 1956, he taught thermodynamics as an assistant in engineering (1955-1956), and in January 1957 became an Assistant Professor. During 1958-1959 he took an industrial leave of absence at the Ramo-Wooldridge Corp. (now TRW) in El Segundo, California. He was Chairman of the Chemical, Nuclear and Thermal Engineering Department

(1978-1983), and Founding Chairman of the Chemical Engineering Department (1983-1984); he was also Chairman of the Faculty of the School of Engineering and Applied Science (1987-1988).

A member of the Society since 1962, he has served the Society as Chairman of the Southern California-Nevada Section (1965-1966); Chairman of the Corrosion Division (1978-1980); Chairman of the Corrosion Monograph Series (1980-1986) and a Corrosion Division Editor of the *Journal* (1967-1991). He was also Division Editor of *Electrochimica Acta* (1977-1985).

For the past thirty years the interests of his research group have been directed to kinetic studies of uninhibited and inhibited metal and alloy electrodissolution and, more recently, electrodeposition. He collaborated in paired synthesis research with Manuel Baizer after the latter's retirement from Monsanto (1978) until his death in 1988. Their last collaboration was on bioelectrochemical-enzyme reactions, which was funded just before Dr. Baizer's death, and is still ongoing. In recent years, Dr. Nobe and his collaborators have focused on studies of nonlinear electrode kinetic instabilities during high rate electrodissolution of metals and alloys.

Since the mid-1950s to the early 1980s, he and his co-workers had also been active in studies of the catalytic combustion of hydrocarbons and carbon monoxide, and catalytic reduction of nitrogen oxides for pollution control of automotive and stationary source emissions. In this area, seminal contributions of his group included demonstrating the efficacy of rhodium catalysts for application in automotive catalytic converters and the development of the V_2O_5-Al_2O_3 and V_2O_5/TiO_2 catalysts for the selective catalytic reduction of nitrogen oxides from stationary sources.

He has gained great satisfaction from his collaboration in applied catalysis and electrochemistry with more than 110 graduate students and postgraduate scholars. Although he had developed and taught undergraduate and graduate courses in catalysis, corrosion, and electrochemistry, he still derives his greatest satisfaction in teaching thermodynamics. Perhaps this can be traced back to that charismatic teacher of thermodynamics and renaissance man, C. W. Tobias.

Stanley I. Raider to Receive the Thomas D. Callinan Award of the Dielectric Science and Technology Division

Stanley I. Raider has been selected as the recipient of the 1992 Thomas D. Callinan Award of the Dielectric Science and Technology Division of The Electrochemical Society. The award will be presented at the Awards and Recognition Session on Tuesday, May 19, 1992, at 4:30 P.M. in the Promenade Ballroom C and D, 2nd level of the Adam's Mark Hotel. His award address, "Carbon Impurities at a Si-SiO_2 Interface," will be given on Wednesday, May 20 at 8:15 a.m. in the Promenade Ballroom F, 2nd level.

Dr. Raider received a B.S. degree in chemistry from Brooklyn College in 1955 and a B.Ch.E. degree from Brooklyn Polytechnic Institute in 1957. During employment by the U.S. Naval Powder Plant in 1956 and by Hooker Chemical Company which he joined in 1958, he was involved in applied polymer research on coatings and rigid foams. In 1967, he earned his Ph.D. in chemistry at the State University of New York at Stony Brook. His doctoral research involved the synthesis and spectroscopic analysis of new silyl-aluminum hydride and germyl hydride compounds.

In 1967, Dr. Raider joined the IBM Components Division at East Fishkill, New York. He transferred to the IBM T.J. Watson Research Center in 1975 where he is a Research Staff Member. He is presently on temporary assignment in IBM at Thornwood, New York.

Dr. Raider's research at IBM has primarily focused on how device properties and processing relate to the chemistry that occurs at interfaces between thin insulator films and semiconducting or superconducting substrates. He was among the first to use x-ray photoelectron spectroscopy as a tool to characterize interfaces and has applied this technique to study the Si-SiO_2 interface, the oxidation of silicon nitride, and the Nb/Nb oxide interface formed during Josephson tunnel barrier processing. From studies of Si-SiO_2 interfacial reactions involving N_2 or carbon impurities, processes were identified which affect Si oxidation kinetics, initiate interfacial reactions at local sites, and produce electrically active intermediates at the interface. He has found that MOS capacitor breakdowns are enhanced by field assisted transport of sodium ions into SiO_2 when Si is negatively biased and has shown that the times to breakdown are proportional to the applied field as described by Peek's law. Based on interface studies with superconducting films, he has developed processes for preparing high quality, reproducible Nb/Nb oxide/Pb alloy Josephson tunnel junctions, for trimming tunnel junction currents by ion implantation, and for fabricating new three-terminal, nonequilibrium superconducting devices. He has studied conduction in granular NbN superconducting films using scanning tunneling microscopy at liquid helium temperatures and is currently evaluating the uniformity of deposited high T_c superconducting film properties using magneto-optic glasses.

Dr. Raider has received two IBM Outstanding Contribution Awards for his work on time-dependent breakdown of metal oxide semiconductor capacitors and for developing the process that IBM used in their Josephson program to produce stable, reproducible Josephson tunnel junctions. He is

the recipient of four IBM Invention Awards, the author of more than 50 technical papers, and holds five issued patents. He is an editor of two Electrochemical Society proceeding volumes on low-temperature electronics and high-temperature superconductivity.

In The Electrochemical Society, he has served in the Dielectric Science and Technology Division as Nominating Committee Chairman and as a member-at-large, and as a member of the New Technology Subcommittee. He has organized and participated in symposia on new research topics for the Society, has organized and moderated a panel discussion on low temperature electronics and superconductivity in 1987, and has chaired sessions in symposia on Si oxidation and dielectric breakdown. He is a member of the Materials Research Society, has served on the Applied Superconductivity Planning Committee (1987), and has chaired symposia at Applied Superconductivity Conferences.

Gottlieb S. Oehrlein to Receive the Electronics Division Award

Gottlieb S. Oehrlein, a physicist at the IBM T.J. Watson Research Center, has been selected to receive the 1992 Electronics Division Award of The Electrochemical Society at the Awards and Recognition Session to be held at 4:30 p.m. on Tuesday, May 19, 1992 in Promenade Ballroom C and D, 2nd level of the Adam's Mark Hotel.

Dr. Oehrlein will present his award address, "Surface Studies of Reactive Ion Etching Processes in Silicon Technology: From Surface Damage to High Resolution Depth Profiling" at 2:00 p.m. on Monday, May 18, 1992, in the Promenade Ballroom C, 2nd level of the Adam's Mark Hotel.

Dr. Oehrlein is a Research Staff Member in the Silicon Technology Department at the IBM T.J. Watson Research Center. He received a Vordiplom degree in physics from Wuerzburg University in West Germany in 1976 and his M.S. and Ph.D. degrees in physics from the State University of New York at Albany in 1978 and 1981, respectively. He subsequently joined IBM at the T.J. Watson Research Center, where he has worked on exploratory materials and plasma-based processes.

His early research interests have included nucleation of oxygen precipitates and oxygen-related thermal donors during heat-treatment of Czochralski-grown silicon, rapid thermal processing of ion implanted silicon, and enhanced diffusion mechanisms of dopants. He also has worked on the deposition and characterization of Ta_2O_5 for applications as the storage capacitor dielectric in DRAMs.

More recently, Dr. Oehrlein has been interested in understanding fundamental aspects of reactive ion etching (RIE), in particular the plasma-surface interactions responsible for the achievement of etch selectivity and etch directionality but which may also result in dry etch damage. He and his coworkers characterized and elucidated the mechanistic details of silicon near-surface defects and surface contamination in selective oxide RIE and other plasma processes. A new approach to spatially resolve *in situ* analysis of semiconductor microstructures (using blanket surface analysis techniques) was demonstrated which exploited the topographic and insulating characteristics of the structures. This approach enabled the study of the surface chemistry of contact hole etching processes using actual structures and also made possible the first *in situ* studies of the chemistry of sidewall passivation layers formed in Si trench etching using fluorine-, chlorine-, and bromine-based plasmas. Additionally, using real-time ellipsometry during RIE of Si, SiO_2, SiGe, etc., the kinetic aspects of etch selectivity could be studied. The combination of RIE and ellipsometry also has enabled high-resolution compositional depth profiling of ultra-thin films, *e.g.*, oxide-nitride-oxide dielectric stacks, or determining the Ge profile in epitaxial SiGe alloy/Si superlattices.

Oehrlein has been a Fellow of the Institute of International Education (New York) and received the SUNY at Albany Chancellor's "Honors Convocation Award for Academic Excellence and a Distinguished Dissertation" in 1982. Dr. Oehrlein was awarded the 1986 Solid-State Science and Technology Young Authors Award of The Electrochemical Society. He received several IBM internal awards, including an IBM Outstanding Technical Achievement Award for his work in the area of reactive ion etching. He is a member of the American Vacuum Society, The Electrochemical Society, and the American Physical Society, and served on the program committee of the 1983 Electronic Materials Conference and the 1990 Gordon Research Conference on Plasma Chemistry. He was a Visiting Scientist at the Forsvarets Forskningsanstalt, Linkoping, Sweden, and the Centre National d'Etudes des Telecommunications, Grenoble, France, during the summers of 1981 and 1989, respectively. In 1988 he was appointed the first visiting professor of the SUNY Albany/RPI Joint Laboratories of Advanced Materials.

Dr. Oehrlein's research has resulted in over 100 publications, numerous invited lectures at conferences and universities, and several patents. Currently, he is working on the characterization of high-density plasma surface interactions and integration of plasma-based processes in vacuum cluster tools.

Robert A. Osteryoung to Receive the Max Bredig Award in Molten Salt Chemistry of the Physical Electrochemistry Division

The Max Bredig Award will be presented to Robert A. Osteryoung at the Awards and Recognition Session to be held on Tuesday, May 19, 1992, at 4:30 p.m. in Promenade Ballroom C and D, 2nd level of the Adam's Mark Hotel. "Through the Years and Temperatures: Adventures in Molten Salt Land" is the title of his award address which he will deliver after dinner (approximately 8 p.m.) Wednesday, May 20, in the St. Louis Ballroom H, 4th level of the Adam's Mark Hotel.

Robert Osteryoung was born in Cleveland, Ohio, in 1927. He served in the U.S. Navy and then obtained the degree of B.S. in Chemistry in 1949 from Ohio University. In 1951 he received his M.S. from the University of Illinois and obtained his Ph.D. in 1954 from the same institution. From 1951 to 1952 he worked for the Harshaw Chemical Company. From 1954 through 1959 he was Assistant, then Associate, Professor of Chemistry at Rensselaer Polytechnic Institute, Troy, New York. In 1959 he joined the staff of Atomics International Division of what is now Rockwell International, Los Angeles. He moved to Rockwell's Science Center Laboratory as Group Leader of Physical Chemistry in 1966 and in 1968 was named Associate Director. He also served, from 1966 to 1968, as Director of the Materials and Process Laboratory of Rockwell's Autonetics Division. He was also a Visiting Associate in Chemistry at the California Institute of Technology from 1962 to 1968.

In 1968 he was named Professor and Chairman, Department of Chemistry, Colorado State University, Ft. Collins, Colorado, where he served as Chairman through June

1978. From July 1977p through June 1978 he was on leave as a Program Manager at the Air Force Office of Scientific Research in Washington, DC. He joined the faculty of the State University of New York at Buffalo in 1979. He will move to North Carolina State University in Raleigh, North Carolina, as Research Professor in July 1992.

His research interests are in molten salt chemistry and electrochemistry, in electroanalytical chemistry, with emphasis on fast pulse voltammetric methods, and in the online use of computers in electrochemistry. He has published over 200 research papers in these areas. A past Chairman of the Gordon Research Conference on Electrochemistry, he has been an invited speaker at Gordon Research Conferences in electrochemistry, analytical chemistry, and molten salt chemistry. He has also been an invited speaker at numerous other scientific meetings in the United States and abroad.

Having joined The Electrochemical Society in 1969, he has served as Secretary-Treasurer, Vice-Chairman, and Chairman of the Physical Electrochemistry Division, and member of the Board of Directors, and currently serves on the Finance Committee. He was twice nominated as Vice-President of the Society. From 1979-1986 he served as a Divisional Editor of the *Journal of the Electrochemical Society*.

He is a past member of the Advisory Board of *Analytical Chemistry*, a past Chairman of the Division of Analytical Chemistry of the American Chemical Society, and is currently an Alternate Councilor of that Division to the ACS Council. As Chairman of the Division of Analytical Chemistry's Professional Status Committee, he operated the Division's Summer Intern Program for thirteen years. He was Program Chairman of the Division's 1984 Summer Symposium. He currently serves as an Associate Editor of *Analytical Chemistry* for electroanalytical chemistry.

He was the 1978 recipient of the Distinguished Service Award of the Colorado Section of the American Chemical Society, the 1987 recipient of the Charles N. Reilley Award in Electroanalytical Chemistry of the Society for Electroanalytical Chemistry, was the winner of the 1990 Schoellkopf Medal of the Western New York section of the American Chemical Society, and, in 1991, received the American Chemical Society's Division of Analytical Chemistry Award in Electrochemistry. He was selected as a Fellow of the Electrochemical Society in 1990.

His other professional affiliations include: founding member and past member of the Board of Directors of the Society of Electroanalytical Chemistry, the International Society of Electrochemistry, Phi Beta Kappa, Sigma Xi, and fellow of the American Association for the Advancement of Science.

THE ADAM'S MARK HOTEL

2nd Level

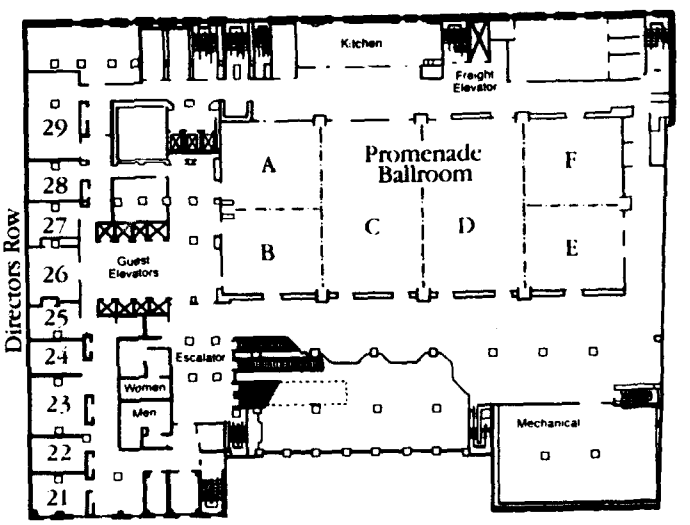

4th Level

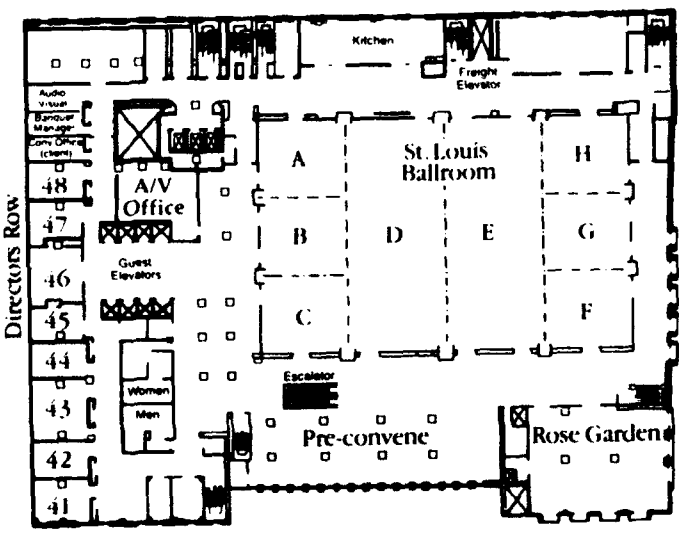

181st Meeting of The Electrochemical Society, Inc.
Adam's Mark Hotel, May 17-22, 1992

		Monday May 18	Tuesday May 19	Wednesday May 20	Thursday May 21	Friday May 22
Room 26 2nd Level	A.M.	**Physical Electrochemistry—** General Session Abs. 447-455	**Physical Electrochemistry—** General Session Abs. 456-464	**Physical Electrochemistry—** Electrochemistry of High Temperature Superconductors Abs. 434-441	**Physical Electrochemistry—** Electrochemistry of High Temperature Superconductors Abs. 442-446	
	P.M.					
Room 29 2nd Level	A.M.		**Corrosion/IE&EE—** Cathodic Protection Systems Abs. 54-61	**New Technology Subcommittee/Sensor/ Electronics/DS&T—** Micromachining and Microstructures	**New Technology Subcommittee/ Sensor/Electronics/DS&T—** Micromachining and Microstructures	
	P.M.		**New Technology Subcommittee/Sensor/ Electronics/DS&T—** Micromachining and Microstructures			
Promenade Ballroom A 2nd Level	A.M.	**HTM/DS&T—** Synthesis and Processing for High-Temperature Materials in the Year 2000 Abs. 341-347	**HTM/DS&T—** Synthesis and Processing for High-Temperature Materials in the Year 2000 Abs. 348-354	**Electronics/DS&T—** Joint General Session Abs. 269-293	**Electronics/DS&T—** Joint Recent News Paper Session	
Promenade Ballroom B 2nd Level	A.M.		**IE&EE—** Industrial Electro-Organic Process Abs. 408-413	**Organic and Biological Electrochemistry—** Electro-Organic Synthesis with Homogeneous and Heterogeneous Catalysts Abs. 414-423	**Organic and Biological Electrochemistry—** Electro-Organic Synthesis with Homogeneous and Heterogeneous Catalysts Abs. 424-433	
	P.M.	**IE&EE—** Industrial Electro-Organic Processes Abs. 401-407				
Promenade Ballroom C 2nd Level	A.M.	**DS&T/Electronics—** 9th Symposium on Plasma Processing Abs. 62-76	**DS&T/Electronics—** 9th Symposium on Plasma Processing Abs. 77-88	**DS&T/Electronics—** 9th Symposium on Plasma Processing Abs. 89-105	**DS&T/Electronics—** 9th Symposium on Plasma Processing Abs. 106-123	**DS&T/Electronics—** 9th Symposium on Plasma Processing Abs. 124-132
	P.M.					
	Evening			**DS&T/Electronics—** 9th Symposium on Plasma Processing Informal Discussion		
Promenade Ballroom E 2nd Level	A.M.	**Electronics/DS&T—** 5th International Symposium on Silicon-on-Insulator Technology and Devices Abs. 153-161	**Electronics/DS&T—** 5th International Symposium on Silicon-on-Insulator Technology and Devices Abs. 162-173	**Electronics/DS&T—** 5th International Symposium on Silicon-on-Insulator Technology and Devices Abs. 174-184	**Electronics/DS&T—** 5th International Symposium on Silicon-on-Insulator Technology and Devices Abs. 185-195	
Promenade Ballroom F 2nd Level	A.M.	**Electronics/DS&T—** 2nd Symposium on the Physics and Chemistry of SiO_2 and the Si-SiO_2 Interface Abs. 210-222	**Electronics/DS&T—** 2nd Symposium on the Physics and Chemistry of SiO_2 and the Si-SiO_2 Interface Abs. 223-235	**Electronics/DS&T—** 2nd Symposium on the Physics and Chemistry of SiO_2 and the Si-SiO_2 Interface Abs. 236-252	**Electronics/DS&T—** 2nd Symposium on the Physics and Chemistry of SiO_2 and the Si-SiO_2 Interface Abs. 253-268	
Room 43 4th Level	A.M.	**Electronics/DS&T—** Materials and Processing Issues for Large Scale Integrated Electronic and Photonic Arrays Abs. 196-204	**Electronics/DS&T—** Materials and Processing Issues for Large Scale Integrated Electronic and Photonic Arrays Abs. 205-209	**Electronics/DS&T—** State-of-the-Art Program on Compound Semiconductors (SOTAPOCS XVI)	**Electronics/DS&T—** State-of-the-Art Program on Compound Semiconductors (SOTAPOCS XVI)	
	P.M.		**Electronics/DS&T—** State-of-the-Art Program on Compound Semiconductors (SOTAPOCS XVI)			

Room 46 **4th Level**	**A.M.** **P.M.**	**Energy Technology/Physical Electrochemistry/Corrosion—** Fractals in Electrochemistry Abs. 308-320	**Energy Technology/Physical Electrochemistry/Corrosion—** Fractals in Electrochemistry Abs. 321-326	**Energy Technology/Physical Electrochemistry/Electronics/ DS&T—** Electrochemical Characterization of Thin Solid Films Abs. 327-334 **HTM—** Stability of Refractory Materials Abs. 335-340	**Corrosion—** General Session Abs. 41-53	
St. Louis Ballroom A **4th Level**	**A.M.** **P.M.**	**IE&EE—** Electrochemistry in Mineral and Metal Processing III Abs. 366-374	**IE&EE—** Electrochemistry in Mineral and Metal Processing III Abs. 375-383	**IE&EE—** Electrochemistry in Mineral and Metal Processing III Abs. 384-394	**IE&EE—** Electrochemistry in Mineral and Metal Processing III Abs. 395-400	
St. Louis Ballroom B **4th Level**	**A.M.** **P.M.**	**Physical Electrochemistry/High Temperature Materials—** 8th International Symposium on Molten Salts Abs. 482-496	**Physical Electrochemistry/High Temperature Materials—** 8th International Symposium on Molten Salts Abs. 497-510	**Physical Electrochemistry/High Temperature Materials—** 8th International Symposium on Molten Salts Abs. 511-528	**Physical Electrochemistry/High Temperature Materials—** 8th International Symposium on Molten Salts Abs. 530-543	
St. Louis Ballroom C **4th Level**	**A.M.** **P.M.**	***Physical Electrochemistry/ DS&T/Electronics—*** Fullerenes: Chemistry, Physics and New Directions	***Physical Electrochemistry/ DS&T/Electronics—*** Fullerenes: Chemistry, Physics and New Directions	***Physical Electrochemistry/ DS&T/Electronics—*** Fullerenes: Chemistry, Physics and New Directions	**Physical Electrochemistry/ DS&T/Electronics—** Fullerenes: Chemistry, Physics and New Directions	**Physical Electrochemistry/ DS&T/Electronics—** Fullerenes: Chemistry, Physics and New Directions
	Evening			**Physical Electrochemistry/ DS&T/Electronics—** Fullerenes: Chemistry, Physics and New Directions Poster Session	**Physical Electrochemistry/ DS&T/Electronics—** Fullerenes: Chemistry, Physics and New Directions Open Discussion/Late News	
St. Louis Ballroom D **4th Level**	**A.M.** **P.M.**	**Battery/Energy Technology—** Joint General Session Abs. 1-13	**Battery/Energy Technology—** Joint General Session Abs. 14-18	**Energy Technology—** Surface Processing in Energy Technologies Abs. 294-307		
St. Louis Ballroom E **4th Level**	**A.M.** **P.M.**	**Sensor—** Electrochemical Sensors in Medical Science Abs. 544-556	***Sensor—*** Electrochemical Sensors in Medical Science Abs. 557-564	**HTM/Sensor/Battery—** High Temperature Sensors Abs. 355-365		
St. Louis Ballroom F **4th Level**	**A.M.** **P.M.**	**Physical Electrochemistry/ Electrodeposition—** Micromorphology in Electrocrystallization Abs. 465-474	**Physical Electrochemistry/ Electrodeposition—** Micromorphology in Electrocrystallization Abs. 475-481 **New Technology Subcommittee/ Electronics/DS&T** Quantum Confinement	**New Technology Subcommittee/ Electronics/DS&T—** Quantum Confinement		
St. Louis Ballroom G **4th Level**	**A.M.** **P.M.**	**DS&T/Electronics—** 2nd International Symposium on Reduced-Thermal-Budget Processing for the Fabrication of Microelectronic Devices Abs. 133-144	**DS&T/Electronics—** 2nd International Symposium on Reduced-Thermal-Budget Processing for the Fabrication of Microelectronic Devices Abs. 145-152			
St. Louis Ballroom H **4th Level**	**A.M.** **P.M.**	**Battery/Energy Technology/ Physical Electrochemistry—** Direct Electrochemical Oxidation of Methanol and Small Organic Molecules Abs. 19-28	**Battery/Energy Technology/ Physical Electrochemistry—** Direct Electrochemical Oxidation of Methanol and Small Organic Molecules Abs. 29-40			
	Evening			**Max Bredig Award Address** Abs. 529		

SCHEDULE OF SYMPOSIA/SESSIONS BY DIVISIONS AND GROUPS

Thursday, May 21, 1992

Friday, May 22, 1992

ELECTRODEPOSITION

Monday, May 18, 1992

Tuesday, May 19, 1992

ELECTRONICS

Monday, May 18, 1992

Tuesday, May 19, 1992

Wednesday, May 20, 1992

Thursday, May 21, 1992

PHYSICAL ELECTROCHEMISTRY

Monday, May 18, 1992

Tuesday, May 19, 1992

Wednesday, May 20, 1992

Thursday, May 21, 1992

Friday, May 22, 1992

SENSOR

Monday, May 18, 1992

Tuesday, May 19, 1992

Wednesday, May 20, 1992

NEW TECHNOLOGY SUBCOMMITTEE

Tuesday, May 19, 1992

Wednesday, May 20, 1992

ST. LOUIS, MISSOURI MEETING

Symposium and General Session Organizing Chairmen

Battery/Energy Technology Joint General Session

E. Gagnon
A. Landgrebe

Direct Electrochemical Oxidation of Methanol and Small Organic Molecules

J. Fenton
V. Jalan
W. O'Grady
P. Ross, Jr.

Corrosion General Session

H. Isaacs

Cathodic Protection Systems

K. Nisancioglu
R. White

Ninth Symposium on Plasma Processing

D. Hess
G. Mathad

Second International Symposium on Reduced-Thermal-Budget Processing for the Fabrication of Microelectronic Devices

J. Osenbach
G. Schwartz

Fifth International Symposium on Silicon-on-Insulator Technology and Devices

W. Bailey
S. Cristoloveanu
G. Cullen
P. Hemment
K. Izumi

Materials and Processing Issues for Large Scale Integrated Electronic and Photonic Arrays

D. Buckley
R. Enstrom
R. Levy

Second Symposium on the Physics and Chemistry of SiO_2 and the Si-SiO_2 Interface

B. Deal
C. Helms

State-of-the-Art Program on Compound Semiconductors XVI

D. Buckley
B. Etienne
T. Kamijoh
A. Katz
V. Swaminathan
G. Valco

Electronics/Dielectric Science & Technology Joint General Session

A. Harrus
R. Jaccodine

Electronics/Dielectric Science & Technology Joint Recent News Paper Session

L. White

Surface Processing in Energy Technologies

A. Czanderna
A. Landgrebe

Fractals in Electrochemistry

J. Kaufman
J. Talbot
M. Tomkiewicz

Electrochemical Characterization of Thin Solid Films

M. Orazem
P. Sides

Stability of Refractory Materials

D. Jacobson
K. Shin

Synthesis and Processing for High-Temperature Materials for the Year 2000

M. Allendorf
J. Dismukes
J. Wagner, Jr.

High Temperature Sensors

A. Khandkar
M. Liu
W. Worrell

Electrochemistry in Mineral and Metal Processing III

P. Richardson
R. Woods

Industrial Electro-Organic Processes

C. King
P. Pintauro
N. Weinberg

Electro-Organic Synthesis with Homogeneous and Heterogeneous Catalysts

D. Peters
J. Toomey

Electrochemistry of High Temperature Superconductors

J. McDevitt

Physical Electrochemistry General Session

B. Conway

Micromorphology in Electrocrystallization

T. Hepel
G. Whitney

Fullerenes: Chemistry, Physics and New Directions

K. Kadish
R. Ruoff

Eighth International Symposium on Molten Salts

G. Blomgren
R. Gale
H. Kojima

Electrochemical Sensors in Medical Science

D. Harrison
R. Wightman

Quantum Confinement

E. Nicollian
R. Tsu

Micromachining and Microstructures

P. Barth
H. Gray
J. Zemel

PROGRAM

ST. LOUIS, MISSOURI

The Electrochemical Society, Inc.

May 17 - 22, 1992
Sunday through Friday

HOTEL INFORMATION

The 1992 Spring Meeting will be held at the Adam's Mark Hotel, Fourth and Chestnut, St. Louis, MO 63102. The telephone number for the hotel is 314-241-7400. The standard convention rates are $108 for single rooms and $118 for double rooms.

Hotel reservation cards have been sent to all members, authors of papers and Technical Session Chairmen and Vice-Chairmen. It is suggested that you use the special reservation envelope. If you call for a reservation you MUST mention that you are attending The Electrochemical Society Meeting to obtain these special convention rates. DEADLINE FOR HOTEL RESERVATIONS IS APRIL 10, 1992.

TRAVEL INFORMATION

In order to reduce expenses for attendees, TWA has been named the official carrier for this Spring Meeting. Arrangements have been made for attendees to obtain a special reduced airfare. This special airfare, which is not available elsewhere, will be guaranteed to all registrants who wish to use the special Fugazy International Travel meeting service telephone number listed below.

To make a reservation at the special reduced airfare, which can be as low as a 45% discount, you can call Fugazy International Travel directly. The phone numbers are: 800-828-4488 (anywhere in the Continental US) or 908-828-4488 in the state of New Jersey.

Call between the hours of 8:30 AM and 5:30 PM Eastern Time, Monday through Friday or 10:00 AM to 2:00 PM on Saturday. Please mention that you are attending The Electrochemical Society Meeting in St. Louis, Missouri.

REGISTRATION

The registration area will be located on the Fourth Level in the Coat Room Foyer of The Adam's Mark Hotel.

Advance Registration

Advance registration is suggested if you plan to attend the Spring Meeting. Forms are available from The Electrochemical Society, Inc., 10 South Main Street, Pennington, New Jersey 08534-2896, phone number 609-737-1902, or FAX: 609-737-2743. DEADLINE FOR RECEIPT OF ADVANCE REGISTRATION, INCLUDING PAYMENT, IS MAY 1, 1992. Written requests for refunds will be honored only if received at Society Headquarters in Pennington before May 8, 1992.

Note: Meeting registration fees and all tickets are discounted if purchased with Advance Registration.

Registration at the Meeting

The registration hours are:

Sunday, May 17	2:00 P.M. to 7:00 P.M.
Monday, May 18	7:30 A.M. to 3:30 P.M.
Tuesday, May 19	7:30 A.M. to 3:30 P.M.
Wednesday, May 20	7:30 A.M. to 3:30 P.M.
Thursday, May 21	7:30 A.M. to 1:30 P.M.
Friday, May 22	8:00 A.M. to 10:00 A.M.

REGISTRATION FEES

All participants and attendees are required to pay a registration fee. Payment can be made by cash, check, or travelers checks in U.S. funds. Credit cards, only Mastercard or Visa, are accepted. The schedule of fees is as follows:

Technical Session Registration Fees

	ADVANCE	AT MEETING
Members	$170.00	$190.00
Nonmembers	$255.00*	$275.00*
Student Members	$10.00	$10.00
Nonmember Students	$20.00*	$20.00*
Nontechnical Registrants Fee	$30.00	$40.00
Emeritus and Honorary Members	Complimentary	
Last Day Registration (Friday only)		
Members		$40.00
Nonmembers		$55.00

**If a nonmember submits an Application for Admission within four months of the Meeting and is subsequently elected to membership in the Society, the difference between the nonmember and member registration fee will be applied to the 1992 dues, which are $85.00.*

MEETING INFORMATION

Meeting Registration	Coat Room Foyer, 4th Level
Information/Message Center	Coat Room Foyer, 4th Level
Nontechnical Registrants Headquarters	Rose Garden, 4th Level
Society Headquarters Office	Room 27, 2nd Level

GENERAL FUNCTIONS

Sunday, May 17

Sunday Evening Get-Together

An informal Sunday Evening Get-Together will be held in the St. Louis Ballroom D, Fourth Level from 7:30 to 9:30 P.M. All meeting registrants are invited to attend.

Monday, May 18

Monday--Plenary Session

At 9:00 A.M. the Plenary Session will be held in the Promenade Ballroom C & D, Second Level. The Honorable George E. Brown, Jr., California State Representative, will deliver The Electrochemical Society Lecture entitled, "Government Initiatives in Materials Science."

Monday Evening Mixer

An informal gathering will be held in the Pre-Convene, Second Level from 6:00 to 7:15 P.M. Beer, soft drinks, and snacks will be served on a complimentary basis. In addition, there will be a cash bar for those who prefer mixed drinks or wine. All meeting registrants are invited to attend.

Tuesday, May 19

Awards and Recognition Session

The Awards and Recognition Session will begin at 4:30 P.M. in the Promenade Ballroom C & D, Second Level.

At this session, the Thomas D. Callinan Award of the Dielectric Science and Technology Division will be presented to Stanley I. Raider. The Electronics Division Award will be presented to Gottlieb S. Oehrlein. The Henry B. Linford Award for Distinguished Teaching will be presented to Ken Nobe.

Vittorio de Nora Award Address

Immediately following the Awards and Recognition Session, Ernest B. Yeager will deliver the Vittorio de Nora Award Address entitled, "Opportunities for O_2 Cathodes in Batteries, Fuel Cells and Industrial Electrolytic Processes."

Vittorio de Nora Award Reception and Banquet

Beginning at 7:00 PM, a reception and banquet will be held in the Rose Garden Room, Fourth Level, to honor Ernest B. Yeager. After dinner, he will be presented with the Vittorio de Nora Medal and Prize. Tickets for this event will be $40.00 in advance and $45.00 at the meeting.

Wednesday, May 20

Max Bredig Award in Molten Salt Chemistry Dinner and Address

Begining at 6:00 P.M., a dinner will be held in the St. Louis Ballroom H, 4th Level of the Adam's Mark Hotel, to honor Robert A. Osteryoung. After dinner he will deliver the Max Bredig Award Address entitled, "Through the Years and Temperatures: Adventures in Molten Salt Land." Tickets for this event will be $22.00 in advance and $27.00 at the meeting.

Cruisin' Down the Mighty Mississippi

Enjoy a moonlight cruise down the Mississippi River aboard the Huck Finn Riverboat which has been reserved exclusively for Society Meeting attendees. The Huck Finn Riverboat is a replica of a 19th century stern-wheeler with all the modern conveniences. Cash bars are located on the first and second floors, with an open-air deck, perfect for star gazing.

A Dixieland band greets you on your arrival, and continues to entertain you throughout the evening. After the boat has crusied for a while, you will be served a buffet-style dinner of baked ham, chicken a la orange, vegetables, pastas, salads, rolls and deserts.

Your cruise down the Mighty Mississippi River will be a memorable part of your stay in St. Louis. Buses depart from the 4th Street Exit of the Adam's Mark Hotel at 6:30 PM. If you would prefer to walk, the equivalent of four city blocks, simply cross Memorial Drive, pass the Gateway Arch, and walk down the stairs to the dock where you can board the riverboat at approximately 7:00 PM.

Buses will return to the Adam's Mark Hotel at approximately 10:30 P.M. PRICE: $43.50 per person in advance, $45.00 after April 17, 1992. Tickets are available at the *Images and Ideas* hospitality desk located in the Meeting Registration Area.

COMMITTEE MEETINGS

Committee Meeting Rooms 21 through 29 are located on the Second Level to the left of the entrance to the Promenade Ballrooms. Committee Meeting Rooms 41 through 48 are located on the Fourth Level to the left of the entrance to the St. Louis Ballrooms.

Sunday, May 17

2:00 P.M.	Electronics Division Subcommittee on Silicon Dioxide/Silicon Interface	Room 26
3:00 P.M.	Electronics Division Subcommittee on ULSI Science and Technology	Room 24
3:00 P.M.	Electronics Division Subcommittee on Compound Semiconductors	Room 25
4:00 P.M.	Dielectric Science and Technology Division Executive Committee	Room 23
4:00 P.M.	Ad Hoc Long Range Planning Committee	Room 21
5:00 P.M.	External Awards Subcommittee	Room 22
5:30 P.M.	Electronics Division Technical Program Planning Subcommittee	Room 26
7:00 P.M.	Fellow Selection Committee	Room 25
7:00 P.M.	Physical Electrochemistry Division-David C. Grahame Award Committee	Room 24
7:00 P.M.	Sensor Group Executive Committee	Room 22
7:00 P.M.	Council of Local Sections	Room 29
8:00 P.M.	Physical Electrochemistry Division Symposium Planning Committee	Room 23
8:00 P.M.	Editorial Board	Room 21
8:00 P.M.	Electronics Division Executive Committee	Promenade Ballroom B

Monday, May 18

7:30 A.M.	High Temperature Materials Division Executive Committee	Room 25
7:30 A.M.	Industrial Electrolysis and Electrochemical Engineering Division Executive Committee	Room 28
7:30 A.M.	Physical Electrochemistry Division Executive Committee	Room 22
7:30 A.M.	Dielectric Science and Technology Division Long Range Symposium Planning Committee	Room 23
10:00 A.M.	Solid State Science & Technology Award Subcommittee	Room 22
10:30 A.M.	Education Committee	Room 21
1:30 P.M.	Society Meeting Committee	Room 21
2:00 P.M.	New Technology Subcommittee	Room 24
4:00 P.M.	Honors and Awards Committee	Room 21
4:30 P.M.	Division/Group/Local Section Representatives to Individual Membership Committee	Room 28
7:00 P.M.	Dielectric Science and Technology Division Governing Body/Symposium Planning Committee	Room 23
7:00 P.M.	Energy Technology Division Executive Committee	Room 25

Tuesday, May 19

7:30 A.M.	Symposium Subcommittee	Room 23
9:00 A.M.	Publication Committee	Room 21
10:30 A.M.	Executive Session of the Individual Membership Committee	Room 25
1:30 P.M.	Technical Affairs Committee	Room 21
6:00 P.M.	Organic and Biological Electrochemistry Division Executive Committee	Room 25

Wednesday, May 20

7:30 A.M.	Finance Committee	Room 21
7:30 A.M.	Council of Past Presidents' Breakfast	Room 23
7:30 A.M.	Solid State Monograph Committee	Room 25
10:00 A.M.	Ways and Means Committee	Room 21
1:30 P.M.	Financial Policy Advisory Committee	Room 21
2:30 P.M.	Contributing Membership Committee	Room 25
5:30 P.M.	Organic and Biological Electrochemistry Division Mixer	Room 41
6:00 P.M.	Max Bredig Award in Molten Salt Chemistry Dinner	St. Louis Ballroom H

Thursday, May 21

7:30 A.M.	Solid State Division/Group Chairmen's Breakfast	Room 25
9:00 A.M.	Board of Directors' Meeting	Promenade Ballroom D
5:00 P.M.	Ninth International Symposium on Molten Salts Planning Meeting	Room 24

LUNCHEONS AND BUSINESS MEETINGS

(Luncheon tickets are $13.00 in Advance and $17.00 at the Meeting)

Monday, May 18

12:15 P.M.	Physical Electrochemistry Division	St. Louis Ballroom D (Northern Section)
12:15 P.M.	Electronics Division	Rose Garden
12:15 P.M.	Industrial Electrolysis and Electrochemical Engineering Division	St.Louis Ballroom E (Northern Section)

Tuesday, May 19

12:15 P.M.	Annual Society	Rose Garden

Wednesday, May 20

12:15 P.M.	Dielectric Science and Technology Division	Rose Garden
12:15 P.M.	Energy Technology Division	Promenade Ballroom D
12:15 P.M.	Organic and Biological Electrochemistry Division	St. Louis Ballroom H

TECHNICAL SESSION CHAIRMEN ORIENTATION

All Session Chairmen and Vice-Chairmen are urged to attend an orientation meeting on the day of their participation. The meeting is scheduled from 7:30 to 8:00 A.M., each day, in Room 24, Second Level of the Adam's Mark Hotel. All Session Chairmen and Vice-Chairmen have been sent the necessary information and materials needed to conduct their Technical Sessions. Should you have any questions or specific problems that you would like to discuss, a member of the Society Headquarters Staff will be available in Room 24 from 7:30 to 8:00 AM on the day of your participation.

NONTECHNICAL REGISTRANTS PROGRAM

For details of the evening social events, please refer to the category GENERAL FUNCTIONS.

The headquarters for the Nontechnical Registrants will be located in the Rose Garden Room, Fourth Level of the Adam's Mark Hotel, Monday, May 18 through Thursday, May 21. Those individuals registered as Nontechnical Registrants are cordially invited to a continental breakfast each morning from 8:30 AM to 10:00 A.M., Monday through Thursday.

During this period plans can be made with old and new acquaintances to enjoy one of the many sightseeing tours available through *Images and Ideas*, the exclusive tour operator for the Society's 181st Meeting. The Tour Registration Desk will be located in the Meeting Registration area on the fourth level adjacent to the escalators. The registration hours are: Sunday - 2:00 P.M. to 7:00 P.M., Monday through Wednesday - 8:00 A.M. - 10:30. Buses for all tours depart from the 4th Street Exit of the Adam's Mark Hotel.

Monday, May 18

IMAGES AND IDEAS ORIENTATION - 9:30 AM - 10:00 AM

The *Images and Ideas* Hostess will provide an orientation in the Rose Garden Room of all tours being offered during the week.

DISCOVER ST. LOUIS - 10:30 A.M. - 3:30 P.M.

Begin with a drive through Laclede's Landing where cobblestone streets and cast-iron streetlamps surround century old buildings that house small shops, boutiques and unusual restaurants. Continue your tour along the historic riverfront passing boats and stern-wheelers on one side and the magnificent stainless steel Gateway Arch on the other. View St. Louis' oldest church, the Old Cathedral, recognized as the Oldest Church west of the Mississippi and the Old Courthouse, once the tallest building in St. Louis and the scene of the Dred Scott trial.

From the riverfront, your tour will proceed to St. Louis' Historic South Side where Anheuser-Busch, the largest brewery in the United States, is located. Also in this area is the DeMenil ante-bellum Mansion, built in the 1800's and the Lemp Mansion, which Life Magazine named as one of the ten most haunted houses in the United States.

Your first stop will be Union Station. Built in 1894, this former train station is a National Historic Landmark. Enjoy lunch on your own and still have time to browse through some shops before reboarding your motorcoach to continue your tour to the Cathedral of St. Louis. A visit to this magnificent Church is definitely one of the highlights of any tour. Built in 1907, it contains one of the largest collections of mosaic art in the world.

The final stop will be the Missouri Botanical Gardens. May is the most spectacular month for viewing the gardens. This 79-acre National Historic Landmark is ablaze with color featuring the country's largest Japanese garden and a rose garden displaying 200 varieties of roses.

Discover some of the more popular sights of St. Louis on this incredible tour of the city. PRICE: $22.00 per person in advance, $24.00 after April 17, 1992.

Tuesday, May 19

FOX THEATRE AND SCIENCE CENTER - 10:00 A.M. - 3:00 P.M.

This tour begins with a short drive to "Fox Theatre" where arrangements have been made to tour the incredible theatre, built in 1929 by William Fox of 20th Century Fox fame, as crown jewel of his empire. It has earned the name "The Fabulous Fox" due to the lavish interior decorations; a mixture of cultures that make it "beautifully bizarre". Once a movie palace, it is now used for entertainment featuring Broadway shows and Super Star variety shows ranging form rock to classical. This theatre must be seen to be believed.

After lunch on your own in the Central West End, we continue the tour to St. Louis' newest jewel - the St. Louis Science Center. Opened in November of 1991, it is ranked among the top ten in the world. The four galleries represent Ecology and the Environment, Human Adventure, Technology and Space Science. Experience an earthquake or tornado, create your own rainbow, take a journey into the basic building block of life through a three-dimensional cell model, or launch a hot air balloon.

The Fox Theatre and St. Louis Science Center are spectacular sites that should not be missed by anyone visiting this wonderful city. PRICE: $24.00 per person in advance, $26.00 after April 17, 1992.

Wednesday, May 20

1904 WORLD'S FAIR REVISITED - 10:00 A.M. - 3:00 P.M.

This tour offers you the opportunity to spend the day in Forest Park, St. Louis' cultural center where our city's science center, history museum, zoo, art museum and the famous "Muny Opera" theatre are located. It was also the site of the 1904 World's Fair, one of the most famous World Fairs ever held.

The first stop will be the History Museum where the history of Missouri and St. Louis comes alive as you stroll through this museum which houses collections on the 1904 World's Fair, Charles Lindbergh, riverboats, antique guns, and period costumes.

You will also have the opportunity to visit the St. Louis Zoo and/or the Art Museum. The Zoo contains over 2800 animals in their natural setting and is considered one of the top zoos in the United States. See Big Cat Country, The Jungle of the Apes, and the newest addition to the zoo, "The Living World".

If you prefer the world of art, a visit to the Art Museum may be more to your liking. This impressive building sits atop Art Hill and is guarded by a 47-foot statue of St. Louis the Crusader. The museum was the Fine Arts Palace of the 1904 World's Fair, and is today considered among the top ten art museums in the country. Enjoy lunch on your own at either the Painted Giraffe at the Zoo or in the Art Museum Cafe. PRICE: $20.00 per person in advance, $22.00 after April 17, 1992.

Thursday, May 21

HISTORIC ST. CHARLES - 10:00 A.M. - 2:00 P.M.

This tour's destination is historic St. Charles, located on the wide Missouri River. Founded in 1769, it is the oldest city on the Missouri River and was Missouri's first state capitol as well as the site of the beginning of the Lewis & Clark expedition.

Enjoy lunch on your own in one of the quaint restaurants located in this unique, historic area. You will still have time to stroll through the many craft and antique shops that line the cobblestone streets or relax in the garden of one of the small wineries. Tours can also be taken through Missouri's First State Capitol.

This tour has been designed to let you enjoy the ambiance of this historic area at your leisure. PRICE: $19.00 per person in advance, $20.00 after April 17, 1992.

DISCUSSION

No recording will be made of the oral discussions. Those contributing to the discussion of a paper and desiring their remarks to be published should send the discussion to the Publications Manager, JOURNAL OF THE ELECTROCHEMICAL SOCIETY, 10 South Main Street, Pennington, New Jersey 08534-2896. The discussion will then be referred to the author for a reply. Publication of the discussion and the comments of the author(s) depends on the publication of the paper in the JOURNAL.

Written discussion of a published paper should be submitted within two months following the publication of the article.

EMPLOYMENT SERVICES

There will be a special bulletin board in the Registration Area for employment posters. Companies desiring to recruit employees are requested to place their announcements on this special board. Please note that these announcements should be no larger than 8 1/2" x 11".

NOTE

Photographing of slides, charts, etc., will be permitted unless specifically prohibited by the speaker. PHOTO FLASH AND PHOTO FLOODS ARE PROHIBITED. TAPE RECORDINGS, EXCEPT ON BEHALF OF THE SOCIETY, ARE PROHIBITED.

TECHNICAL SESSIONS

MONDAY, MAY 18, 1992

9:00 A.M.	Society Plenary Session, Promenade Ballroom C and D, 2nd Level. The Honorable George E. Brown, Jr., California State Representative, will deliver The Electrochemical Society Lecture, " Government Initiatives in Materials Science."
12:15 P.M.	Physical Electrochemistry Division Luncheon and Business Meeting, St. Louis Ballroom D (Northern Section), 4th Level.
12:15 P.M.	Electronics Division Luncheon and Business Meeting, Rose Garden, 4th Level.
12:15 P.M.	Industrial Electrolysis and Electrochemical Engineering Division Luncheon and Business Meeting, St. Louis Ballroom E (Northern Section), 4th Level.

JOINT GENERAL SESSION
Battery/Energy Technology

E. G. Gagnon, Chairman; A. R. Landgrebe, Vice-Chairman
St. Louis Ballroom D, 4th Level

10:00	Experimental Determination of the Transport Number of Water in Nafion 117® Membrane - T. F. Fuller and J. Newman	1
10:20	High Utilization Gas Diffusion Electrodes for Proton Exchange Membrane Fuel Cells - E. B. Anderson, E. J. Taylor, K. Donohue, and N. R. K. Vilambi	2
10:40	Temperature and Pressure Dependence of the Electrode Kinetics of Oxygen Reduction at the Platinum Microelectrode/Nafion Interface - A. Parthasarathy, S. Srinivasan, A. J. Appleby, and C. R. Martin	3
11:00	Spontaneous Hydrous Oxide Formation on Platinum and Its Relevance in Oxygen Gas Reduction - L. D. Burke, J. K. Casey, and A. J. Morrissey	4
11:20	Effect of Platinum Loading on Proton Exchange Membrane Fuel Cell Performance - A. C. Ferreira, S. Srinivasan, and A. J. Appleby	5
11:40	The Hydrogen Diffusion Porous Electrode Catalyzed by Tungsten Carbide - Z.-E. Lu, A.-P. Huang, T.-G. Zhong, and G.-N. Fang	6

A. R. Landgrebe, Chairman; E. G. Gagnon, Vice-Chairman

2:00	Optimization of Electrode Structure to Further Minimize the Platinum Loading in Proton Exchange Membrane Fuel Cells - A. C. Ferreira, S. Srinivasan, and A. J. Appleby	7
2:20	A Thin Film Solid Oxide Fuel Cell Prepared Using Reactive DC Magnetron Sputtering - L.-S. Wang and S. A. Barnett	8
2:40	Effects of a Sputtered Film of Pt on Performance of Proton Exchange Membrane Fuel Cells: Electrode Kinetic and Morphological Characteristics - S. Mukerjee, S. Srinivasan, and A. J. Appleby	9
3:00	Mechanism of Mixed Fuel/Oxidant Solid-State Thin Film Fuel Cells - B. M. Coffey, T. O. Poehler and P. C. Searson	10
3:20	Ten-minute intermission	
3:30	New Aspects in the Development of Proton Exchange Membrane Electrolyzers - K. Ledjeff, F. Mahlendorf, and A. Heinzel	11
3:50	Calorimetric Concentration and Mass Flow Monitor for Gas Phase Ozone - P. C. Foller	12
4:10	SPEFC Development at the Centre for Electrochemical and Energy Research, SPIC Science Foundation - S. Parthasarathy	13

DIRECT ELECTROCHEMICAL OXIDATION OF METHANOL AND SMALL ORGANIC MOLECULES
Battery/Energy Technology/Physical Electrochemistry

W. E. O'Grady, Chairman; J. M. Fenton, Vice-Chairman
St. Louis Ballroom H, 4th Level

10:10	Direct Electro-Oxidation of Methanol in Acid Medium at Modified Electrodes with Low Precious Metal Loadings - J.-M. Leger, G. Meli, and C. Lamy	19
10:35	The Influence of Surface Acid-Base Properties of Pt/C Catalysts on the Electrochemical Oxidation of Methanol - A. S. Arico, V. Antonucci, P. A. Simonov, P. L. Antonucci, and N. Giordano	20
11:00	Carbon Supported Platinum Alloy Catalysts for Methanol Oxidation - M. Gauthier, A. Gelb, E. B. Anderson, and E. J. Taylor	21
11:25	Methanol Oxidation on NiTi - R. Manoharan and J. B. Goodenough	22

J. M. Fenton, Chairman; E. J. Taylor, Vice-Chairman

2:00	The Effect of Specific Adsorption of Anions and Cations on the Kinetics of Methanol Electro-Oxidation on Pt Single Crystal Surfaces - P. N. Ross and N. Markovic	23
2:25	Oxidation of Methanol on Single Crystal Platinum Electrodes in Sodium Hydroxide and Sodium Carbonate Solutions - R. Adzic, N. Marinkovic, A. Tripkovic, and N. Markovic	24
2:50	Partial Oxidation of Methane on $YBa_2Cu_3O_x$ Electrodes in a High Temperature Solid-State Electrochemical Cell - T. M. Gur, H. Wise, and R. A. Huggins	25
3:15	Fifteen-minute intermission	
3:30	Methanol Oxidation on Platinum-Tin Catalysts Dispersed on Poly(3-methyl)thiophene Conducting Polymer - S. Swathirajan and Y. M. Mikhail	26
3:55	Methanol Oxidation on Novel Conductive Polymeric Porphyrins - D. MacArthur, E. Kubaszewski, J. Fish, and T. Malinski	27
4:20	Nafion Supported Catalysts for the Electrochemical Oxidation of Methanol in Acid Media - A. Kowalak, W. O'Grady, and D. Rolison	28

NINTH SYMPOSIUM ON PLASMA PROCESSING
Dielectric Science and Technology/Electronics

T. O. Mantei, Chairman; S. Butler, Vice-Chairman
Promenade Ballroom C, 2nd Level

Modeling and Mechanisms

10:00	Feature Scale Simulation of Oxide Plasma Etching - J. P. McVittie, J. C. Rey, and M. M. IslamRaja	62
10:20	Use of Overhang Test Structure to Understand RIE Lag in Oxide Etching - S-I. Dohmae and J. P. McVittie	63
10:40	Modeling of Plasma Etching Reactors Including Wafer Heating Effects - D. J. Economou and E. Aydil	64
11:00	Optimally Uniform ECR Plasma Generation for Precise Patterning - S. Samukawa, T. Nakamura, and A. Ishitani	65
11:20	Variation of Ion Energy and Ion Flux in Various Gas Plasmas with 13.56 MHz Cathode Coupled Parallel-Plate Plasma Equipment - S. Hasaka, I. Natori, T. Yamashita, and T. Ohmi	66
11:40	Dependencies of Negative Ions from Pulsed Radio-Frequency Discharges - L. J. Overzet, L. Luo, and Y. Lin	67

D. Economou, Chairman; S. V Nguyen, Vice-Chairman

Modeling and Mechanisms (cont'd)

2:00	ELECTRONICS DIVISION AWARD ADDRESS: Surface Studies of Reactive Ion Etching Processes in Silicon Technology: From Surface Damage to High-Resolution Depth Profiling - G. S. Oehrlein	68

MONDAY CONTINUED

Diagnostics and Measurements

SECOND INTERNATIONAL SYMPOSIUM ON REDUCED-THERMAL-BUDGET PROCESSING FOR THE FABRICATION OF MICROELECTRONIC DEVICES

Dielectric Science and Technology/Electronics

J. W. Osenbach, Chairman; G. C. Schwartz, Vice-Chairman
St. Louis Ballroom G, 4th Level

G. C. Schwartz, Chairman; J. W. Osenbach, Vice-Chairman

FIFTH INTERNATIONAL SYMPOSIUM ON SILICON-ON-INSULATOR TECHNOLOGY AND DEVICES

Electronics/Dielectric Science and Technology

W. Bailey, Chairman; G. W. Cullen, Vice-Chairman
Promenade Ballroom E, 2nd Level

Applications for SIMOX

J. Gautier, Chairman; S. Cristoloveanu, Vice-Chairman

Novel Device Concepts

MATERIALS AND PROCESSING ISSUES FOR LARGE SCALE INTEGRATED ELECTRONIC AND PHOTONIC ARRAYS

Electronics/Dielectric Science and Technology

D. N. Buckley, Chairman; R. A. Levy, Vice-Chairman
Room 43, 4th Level

N. Bouadma, Chairman; R. E. Enstrom, Vice-Chairman

MONDAY CONTINUED

4:55 Be^+ Ion Implantation in Ga(Al)Sb Layers: Radiation Damage - M. Perotin, A. Perez, H. Luquet, L. Gouskov, and A. Sabir 204

SECOND SYMPOSIUM ON THE PHYSICS AND CHEMISTRY OF SiO_2 AND THE Si-SiO_2 INTERFACE

Electronics/Dielectric Science and Technology

E. A. Irene, Chairman; M. Hirose, Vice-Chairman
Promenade Ballroom F, 2nd Level

Thermal Oxidation Mechanisms and Modeling

10:00 Silicon Oxides and Silicon Oxidation - A. M. Stoneham 210
10:30 Use of ^{18}O Labeling to Study Growth Mechanisms in Dry Oxidation of Silicon - I. Trimaille, J.-J. Ganem, S. Rigo, S. I. Raider, and N. A. Penebre 211
10:50 Strain Dependent Diffusion during Dry Thermal Oxidation of Crystalline Si - C. H. Bjorkman and G. Lucovsky 212
11:10 Oxidation of Silicon in Oxygen: Measurement of Film Thickness and Kinetics - S.-C. Kao and R. H. Doremus 213
11:30 Modeling Process-Dependent Thermal Silicon Dioxide (SiO_2) Films on Silicon - H. Wei, A. K. Henning, J. Slinkman, and J. Rogers 214

S. Rigo, Chairman; B. E. Deal, Vice-Chairman

Novel Oxidation Methods and Characterization

1:45 New Approach to Chemically Enhanced Oxidation - A Review - R. J. Jaccodine 215
2:15 Kinetics of Oxidation of Silicon by Electron Cyclotron Resonance Plasma - J. Joseph 216
2:35 Mechanisms of Oxidation Rate Enhancement in Negative-Point Oxygen Corona Discharge Processing of SiO_2 Films on Si - L. M. Landsberger 217
2:55 High Pressure, Low Temperature Oxidation of $Si_{1-x}Ge_x$: *Promise for MOS-Quality Passivation* - C. Caragianis, Y. Shigesato, and D. C. Paine 218
3:15 Ten-minute intermission
3:25 A New Ellipsometry Technique for Interface Analysis: Application to Si-SiO_2 - E. A. Irene and V. A. Yakovlav 219
3:55 Infrared-Dichroism on a Thin Silicon Oxide Layer - S. Fujimura, K. Ishikawa, and T. Ogawa 220
4:15 Deconvolution of Thickness-Averaged Structural and Optical Properties of Thermally Grown and RPECVD SiO_2 Films - C. E. Shearon, Jr., C. H. Bjorkman, and G. Lucovsky 221
4:35 TEM Investigations of the Oxidation Kinetics of Amorphous Silicon Films - M. Reiche 222

FRACTALS IN ELECTROCHEMISTRY

Energy Technology/Physical
Electrochemistry/Corrosion

J. H. Kaufman, Chairman; M. Tomkiewicz, Vice-Chairman
Room 46, 4th Level

10:10 Introductory remarks by M. Tomkiewicz
10:15 Effects of Anisotropy on Pattern Formation in Electrochemical Deposition - F. Family and K. C. B. Chan 308
10:35 Interfacial Dynamics and Induced Convective Transport in Electrodeposition - D. P. Barkey 309
10:55 Diffusion to Patterned Electrodes - Y. Dassas and P. Duby 310
11:15 Electro-Convection Around Two-Dimensional Ramified Copper Aggregates - V. Fleury, J. N. Chazalviel and M. Rosso 311
11:35 Electrochemical Aspects of Fractal Zinc Electrodeposition - F. Sagues, J. Claret, L. Lopez-Tomas, J. Mach, F. Mas, and P. P. Trigueros 312

B. Sapoval, Chairman; T. Pajkossy, Vice-Chairman

2:00 Morphology Transitions in Rapid Electrodeposition - L. M. Sander 313
2:20 Columnar Growth and Kinetic Roughening in Electrochemical Deposition - P-z. Wong, G. L. M. K. S. Kahanda, X-q. Zou, and R. Farrell 314
2:40 Evidence for a Kosterlitz-Thouless Transition in the Threshold Screening Model: Critical Region of Fractal Growth - J. H. Kaufman and O. R. Melroy 315
3:00 Probing Electrocrystallization Mechanisms of Molecular Solids - A. C. Hillier and M. D. Ward 316
3:20 Fifteen-minute intermission
3:35 Multifractal Fluctuations in Diffusion in Disordered Systems - S. Havlin 317
4:00 Fractals in Electrochemical Photovoltaics - A. J. McEvoy and M. Gratzel 318
4:20 Morphology and Kinetics of Fractal Growths - D. B. Hibbert and S. N. Atchison 319
4:40 Photocatalysis on Porous Substrates - M. Tomkiewicz and H. Wang 320

SYNTHESIS AND PROCESSING FOR HIGH-TEMPERATURE MATERIALS IN THE YEAR 2000

High Temperature Materials/Dielectric Science and Technology

J. B. Wagner, Jr., Chairman; M. D. Allendorf, Vice Chairman
Promenade Ballroom A, 2nd Level

10:30 Introductory remarks
10:40 Materials Research in the U.S.: The Development of a National Agenda - L. H. Schwartz 341
11:20 Expanding Horizons for Chemical Vapor Deposition Synthesis - K. E. Spear 342

J. Dismukes, Chairman; S. C. Singhal, Vice-Chairman

2:00 Chemical Vapor Deposition Process Aspects for the Year 2000 - J.-O. Carlsson 343
2:40 Computational Analysis of Fluid Flow and Chemical Kinetics in Chemical Vapor Deposition - R. J. Kee, G. H. Evans, and M. E. Coltrin 344
3:20 Ten-minute intermission
3:30 Processing and Fabrication of Ceramic Composites in the 21st Century - R. W. Rice 345
4:10 Chemical Vapor Infiltration - T. M. Besmann, D. P. Stinton, and R. A. Lowden 346
4:50 High-Tech Fibers - G. G. Tibbetts 347

ELECTROCHEMISTRY IN MINERAL AND METAL PROCESSING III

Industrial Electrolysis and Electrochemical Engineering

R. Woods, Chairman; I. Iwasaki, Vice-Chairman
St. Louis Ballroom A, 4th Level

10:00 Requirements for Industrial Collectorless Flotation - N. Arbiter and J. E. Gebhardt 366
10:30 Surface Electron Structures of Galena and Pyrite Related to Collectorless Flotation - S. Sun, D. Wang, and B. Li 367
11:00 Electrochemical Aspects of Cast Iron Grinding Media Wear and Its Effect on Flotation - I. Iwasaki and V. Rajagopal 368
11:30 An Electrochemical Study of Sulfide Mineral-Grinding Medium Contact and Its Relevance to Flotation - X. Li and I. Iwasaki 369

G. H. Kelsall, Chairman; D. R. Nagaraj, Vice-Chairman

2:00 Mechanism of Thionocarbamate Interaction in Flotation Systems - R. H. Yoon and C. I. Basilio 370
2:30 The Role of Pulp Redox Potentials and Modifiers in Complex Sulfide Flotation with Dithiophosphinates - A. Gorken, D. R. Nagaraj, and P. J. Riccio 371
3:00 The Mechanism of Sulfide Depression with Functionalized Synthetic Polymers - D. R. Nagaraj, C. S. Basilio, and R. H. Yoon 372
3:30 Fifteen-minute intermission
3:45 Interaction of Ethyl Xanthate with Silver and Silver/Gold Alloys - R. Woods, C. I. Basilio, D. S. Kim, and R. H. Yoon 373
4:15 Interpretation of Electrode Responses with the Help of a Multivariate Technique - B. I. Palsson and E. Oberg 374

MONDAY CONTINUED

INDUSTRIAL ELECTRO-ORGANIC PROCESSES
Industrial Electrolysis and Electrochemical Engineering

P. N. Pintauro, Chairman; C. King, Vice-Chairman
Promenade Ballroom B, 2nd Level

2:00 Organic Electrosynthesis at Extended Area Nickel Electrodes - C. J. Brown and D. Pletcher 401
2:25 Oxidation of Methanol on a Metallized Polymer Electrolyte Membrane - R. Liu and P. Fedkiw 402
2:50 The Electrocatalytic Hydrogenation of Soybean Oil - G. Yusem and P. N. Pintauro 403
3:15 Ten-minute intermission
3:25 Direct and Indirect Electrochemical Epoxidation of Olefins in a Sieve Plate Reactor - C. F. Oduoza and K. Scott 404
3:50 A Comparison of Some Insoluble Oxide Catalysts in the Electro-Oxidation of Thioethers in Aqueous Surfactant Suspensions - T. C. Franklin, R. Nnodimele, and R. C. Duty 405
4:15 Electrochemical Oxidation of Organic Pollutants for Waste Water Treatment - Ch. Comninellis 406
4:40 Proton-Exchange Membrane Reactor for Removal of Organic and Bacterial Contaminants from Reclaimed Water - L. M. Kaba, S. Srinivasan, A. J. Appleby, G. D. Hitchens and O. J. Murphy 407

GENERAL SESSION
Physical Electrochemistry

B. E. Conway, Chairman; R. P. Buck, Vice-Chairman
Room 26, 2nd Level

10:00 The Effect of Solvent on the Simultaneous Adsorption of Anions and Cations - M. Anbu Kulandainathan and S. Venkatakrishna Iyer 447
10:30 Manipulation of Double Layer in Metal Insulator Electrolyte - K. Ghowsi 448
11:00 Molecular Recognition at Interfaces: Specific Binding of an Electroactive Tetrathiafulvalene (TTF) Derivative to Organosulfur Monolayers by Hydrogen Bonding - L. M. Frostman and M. D. Ward 449
11:30 Kinetics of Electron Hopping in Langmuir Monolayers at the Air/Water Interface - M. Majda, D. H. Charych, and J. T. Orr 450

R. P. Buck, Chairman; B. E. Conway, Vice-Chairman

2:00 Effects of Monosubstituted Phenol Additives on the Conductivity of Electrochemically Synthesized Polypyrrole - M. Fukuyama, N. Nanai, T. Kojima, Y. Kudoh, and S. Yoshimura 451
2:30 Impedance and Voltammetric Characterization of Electrochemically Deposited (Poly)aniline Conducting Films - P. Vanysek and G. Sandi 452
3:00 A Cathodically Polymerized Binuclear Cobalt Complex and Its Electrocatalytic Reduction of Carbon Dioxide - X. Ren, S. K. Mandal, and P. Pickup 453
3:30 *Fifteen-minute intermission*
3:45 The Electrochemical Reduction of CO_2 on Ag and Au Electrodes: The Effect of Trace Impurities - R. Kostecki, P. Kedzierzawski, and J. Augustynski 454
4:15 Redox Potential of N-Hexadecyl-N'-Methyl Viologen $(^{2+/+})$ Solubilized in Cetyltrimethylammonium Chloride Micelle - C.-W. Lee and M.-K. Oh 455

MICROMORPHOLOGY IN ELECTROCRYSTALLIZATION
Physical Electrochemistry/Electrodeposition

T. Hepel, Chairman; G. Whitney, Vice-Chairman
St. Louis Ballroom F, 4th Level

10:00 Introductory remarks by T. Hepel
10:10 Study of Unidirectional Crystallization of 1-D Quantum Conductors - A. R. Hillman, D. C. Loveday, and M. Hepel 465
10:35 Electrodeposition of Epitaxial Films of $Ag(Ag_2O_4)_2NO_3$ - B. E. Breyfogle and J. A. Switzer 466
11:00 Ten-minute intermission
11:10 *In Situ* Characterization of p-Type Copper Thiocyanate Films by Raman Spectroelectrochemistry - Y. Son, N. R. de Tacconi, and K. Rajeshwar 467
11:35 Electrochemical Architecture of Nanomodulated Tl-Pb-O Superlattices - J. A. Switzer, R. J. Phillips, and R. P. Raffaelle 468

A. R. Hillman, Chairman; G. Whitney, Vice-Chairman

2:00 Introductory remarks by A. R. Hillman
2:05 Electrosynthesis, Characterization, and Modeling of Highly Efficient Polyrryrrole/Pt Nanocomposite Catalysts - C. S. C. Bose, C. C. Chen, and K. Rajeshwar 469
2:30 Electrodeposition of Metals on Polypyrrole Coated Au/Quartz Piezoelectrodes - M. Hepel, S. Perkins, and T. Hepel 470
2:55 Localized I/V and I/Z Measurements on Conducting Poly-n-methyl Pyrrole Thin Films Performed with a Scanning Tunneling Microscope - S. Creager 471
3:20 Fifteen-minute intermission
3:35 Factors Affecting Electrochemical Metallization of Insulating Substrates Precoated by Conducting Polymer Films - F. A. Uribe, A. J. Rudge, and S. Gottesfeld 472
4:00 When Anodic Polymerization of Dibenzo-18-Crown-6 Leads to a New Artifical Membrane: Changes of Micromorphology upon Different Modes of Doping - J. Simonet, J. Rault-Berthelot, V. Questaigne, and L. Angely 473
4:25 Formation and Removal of p-SnS Patterns and Characters on Transparent, Conductive Oxide Glass by Mask-Defined Photoelectrodeposition and Dissolution - R. D. Engelken, C. Brinkley, L. N. Chang, and L. Yu 474

FULLERENES: CHEMISTRY, PHYSICS AND NEW DIRECTIONS
Physical Electrochemistry/Dielectric Science and Technology/Electronics

R. S. Ruoff, Chairman; P. Eklund, Vice-Chairman
St. Louis Ballroom C, 4th Level

10:00 The program and abstracts will be published in the April issue of the *Journal* and included in the program booklet distributed at the Meeting.

K. Kadish, Chairman; R. Malhotra, Vice-Chairman

2:00 The program and abstracts will be published in the April issue of the *Journal* and included in the program booklet distributed at the Meeting.

EIGHTH INTERNATIONAL SYMPOSIUM ON MOLTEN SALTS
Physical Electrochemistry/High Temperature Materials

G. Mamantov, Chairman; D. Newman, Vice-Chairman
St. Louis Ballroom B, 4th Level

10:00 On Charging Palladium in an Al/LiCl-KCl Eutectic, Excess LiH(D)/Pd Cell - B. Y. Liaw, P.-I. Tao, and B. E. Liebert 482
10:30 Structure of Molten Iron Chloride - D. L. Price, M.-L. Saboungi, S. C. Moss, and S. Hashimoto 483
10:50 Electronic Conduction in Molten KBr-K Solutions - G. M. Haarberg and J. J. Egan 484
11:10 Electronic Polarizabilities of LiCl-CsCl, LiI-KI and LiI-CsI Binary Melts - M. Endo, Z. Hongmin, Y. Sato, and T. Yamamura 485
11:30 Computer Assisted Data Acquisition and Analyses of Brillouin Spectra of $ZnCl_2$ Single and $ZnCl_2$-NaCl Binary Melts - Z. Hongmin, Y. Sato, T. Yamamura, and K. Sugimoto 486
11:50 Preparation, Vapor Pressure, and Thermochemistry of Tin(II) Bromide - T. R. Brumleve, S. R. Walston, S. A. Mucklejohn, and N. W. O'Brien 487

D. Newman, Chairman; G. Mamantov, Vice-Chairman

2:00 Development of Raman Spectroscopic Sensors for the Determination of Magnesium in a Molten Salt System - G. Mamantov, S. Dai, G. M. Begun, J. P. Young, and J. E. Coffield 488

MONDAY CONTINUED

2:20 Structural Properties of Zinc Halide Melts - E. A. Pavlatou and G. N. Papatheodorou 489
2:40 Structural Investigation of Molten Lithium Bromide - S. Itoh 490
3:00 Use of Raman Spectroscopy for Determining the Corrosion of Ceramics in Molten Fluorides - C. G. Kontoyannis and N. S. Tziafos 491
3:20 Raman and Infrared Spectroscopic Studies of the Platinum Electrode-Molten Nitrates Interface - M. M. Gaphurov, and V. D. Prisyaznhyi 492
3:40 Ten-minute intermission
3:50 Selective Precipitation of Oxide Superconductors from Molten Hydroxide and Molten Nitrate - A. M. Stacy, S. L. Stoll, L. N. Marquez, and S. W. Keller 493
4:10 A New Series of Complex Metal Oxides: Crystallization of AB_3MO_8 (A = Na, Li; B = Ba, Sr; M = Bi, Sb) from Hydroxide Melts - V. A. Carlson and A. M. Stacy 494
4:30 Investigation of a Molten Salt Extraction/Electrolysis Process for Converting Ilmenite to Iron and a High Grade TiO_2 Feedstock - K. J. Leary 495
4:50 New Principles for the Processing of Carnallitites in the Domain of Molten Salt Hydrates - H.-H. Emons and T. Fanghanel 496

ELECTROCHEMICAL SENSORS IN MEDICAL SCIENCE
Sensor

D. Belanger, Chairman; D. J. Harrison, Vice-Chairman
St. Louis Ballroom E, 4th Level

10:10 Introductory remarks by D. J. Harrison
10:15 Development of an Implantable Glucose Sensor - G. S. Wilson, Y. Zhang, D. Moatti-Sirat, V. Poitout, G. Reach, and D. R. Thevenot 544
10:40 Permeability of Glucose and Other Neutral Molecules in Nafion Films Cured at 25° and 120°C - J. D. Harrison and Z. Fan 545
11:00 Amperometric Glucose Sensors Based on Glucose Oxidase Immobilized in Nafion® - T. A. Zawodzinski, Jr., S. Gottesfeld, and J. Rishpon 546
11:20 Development of a Transdermal Electrochemical Sensor for the Continuous Monitoring/Recording of Alcohol Vapor - L. Swette, N. Kackley, A. B. LaConti, and R. M. Swift 547
11:40 Progress in the Development of Amperometric Sensors for Measuring the Partial Pressure of Oxygen in Blood - J. S. Foos 548

D. J. Harrison, Chairman; K. Seiler, Vice-Chairman

2:00 Moving Sensors from the Journal to the Clinical Lab: Some Real World Consideration - R. W. Mason 549
2:20 Improved Adhesion of Hydrophilic Membranes on Planar Silicon Based Oxygen Sensors - E. Aw, J. Lee, C.-Y. Aw, and J. C. Patton 550
2:40 A Thin Platinum Island Film Glucose Sensor - B. Kasapbasioglu, P. J. Hesketh, W. C. Hanly, and J. Maclay 551
3:00 Evaluation of Sensing Surfaces for Use in LAPS-Based Biosensor Devices - L. Bousse, B. van der Schoot, and N. F. de Rooij 552
3:20 Ten-minute intermission
3:30 Design, Fabrication and Testing of Flexible Ion Microsensors for Cardiovascular Applications - R. P. Buck, E. Lindner, V. V. Cosofret, R. P. Kusy, T. A. Johnson, and M. P. Neuman 553
4:00 Measurement of Guinea Pigs Heart Intracellular Potassium Ion Concentration with Potassium Microelectrodes - Y. M. Liu, Z. Q. Huang, J. S. Xiao, and S. Z. Yan 554
4:20 Carrier Based Optodes - K. Seiler and W. Simon 555
4:40 Towards Reversible Sensors Based on Photochemical-Electrochemical Switching - M. J. Preigh and S. G. Weber 556

TUESDAY, MAY 19, 1992

12:15 P.M. Annual Society Luncheon and Business Meeting, Rose Garden, 4th Level.
4:30 P.M. Awards and Recognition Session, Promenade Ballroom C and D, 2nd Level. Ernest B. Yeager will deliver the Vittorio de Nora Award Address, "Opportunities for O_2 Cathodes in Batteries, Fuel Cells, and Industrial Electrolytic Processes.

JOINT GENERAL SESSION
Battery/Energy Technology

E. G. Gagnon, Chairman; A. R. Landgrebe, Vice-Chairman
St. Louis Ballroom D, 4th Level

9:00 A Model for the Deliverable Capacity of the TiS_2 Electrode in a Li/TiS_2 Cell - Z. Mao and R. E. White 14
9:20 The Rechargeable Li_xTiS_2/$LiAlCl_4$/$Li_{1-x}CoO_2$ Solid-State Cell - W. K. Behl, E. J. Plichta, D. Vujic, H. S. W. Wang, and D. M. Schleich 15
9:40 Electrochemical Properties of Polyaniline and Substituted Derivatives - P. V. Madsen, T. O. Poehler, J. Gopal, D. O. Cowan, and P. C. Searson 16
10:00 Ten-minute intermission
10:10 Investigations on a Novel Zn/KOH/DDH Primary Cell System - R. Udhayan, D. P. Bhatt, and P. B. Mathur 17
10:30 Low Temperature Removal of Hydrogen Sulfide from Sour Gas and Its Utilization for Hydrogen and Sulfur Production - K. M. Petrov, S. Srinivasan, and A. J. Appleby 18

DIRECT ELECTROCHEMICAL OXIDATION OF METHANOL AND SMALL ORGANIC MOLECULES
Battery/Energy Technology/Physical Electrochemistry

P. Ross, Jr, Chairman; W. E. O'Grady, Vice-Chairman
St. Louis Ballroom H, 4th Level

8:30 *In Situ* FTIR Characterization of Electrocatalysts for the Oxidation of Methanol - W. Vielstich, T. Iwasita, F. C. Nart, and B. Lopez 29
8:55 Adsorption and Electro-Oxidative Pathways for Small Organic Molecules on Gold and Transition-Metal-Coated Gold Electrodes as Probed by Real-Time Surface-Enhanced Raman Spectroscopy - Y. Zhang and M. J. Weaver 30
9:20 Variable Angle *In Situ* FTIR Reflectance Spectroscopy of High Surface Area Electrodes: A New Method for Studying Electrocatalytic Systems - P. W. Faguy 31
9:45 *In Situ* Infrared and Electrochemical Studies of the Oxidation of Ethylene on Single Crystal and Polycrystalline Platinum Electrodes - Q. Zhao and E. B. Yeager 32
10:10 Applications of Real-Time Infrared Spectroscopy to Electrocatalysis at Bimetallic Surfaces: Electro-Oxidation of Ethylene Glycol on *Bismuth-Modified* Pt (111) - X. Jiang and M. J. Weaver 33
10:35 Ten-minute intermission
10:45 Potential Step and NMR Investigation of the Oxidation and Adsorption of Methanol on Platinum Surfaces - A. Wieckowski, K. Franaszczuk, P. Slezak, C. K. Rhee, and P. Zelenay 34
11:10 XAS Studies of UPD Metal/Pt Electrocatalysts - J. McBreen 35
11:35 Premonolayer Formation of Active Oxides and the Role of the Latter in the Oxidation of Small Organic Molecules - L. D. Burke, D. T. Buckley, and J. K. Casey 36

TUESDAY CONTINUED

V. Jalan, Chairman; W. E. O'Grady, Vice-Chairman

2:00 Direct Methanol Fuel Cells with Aqueous Carbonate Electrolytes - E. J. Cairns, F. R. McLarnon, and B. R. Rauhe 37
2:25 A Methanol-Aqueous Carbonate Fuel Cell - J. A. Kosek, S. Sarangapani, and J. Giner 38
2:50 Ten-minute intermission
3:00 Direct Electrochemical Oxidation of Methanol Vapor on Au-PEM Electrode - A. S. Lin and W. E. O'Grady 39
3:25 Methanol Electro-Oxidation: Problems, Progress, and Prospects - S. Mukerjee, S. Srinivasan, and A. J. Appleby 40

CATHODIC PROTECTION SYSTEMS
Corrosion/Industrial Electrolysis and Electrochemical Engineering

K. Nisancioglu, Chairman; R. E. White, Vice-Chairman
Room 29, 2nd Level

9:00 Influence of Al_3Fe Intermetallic Inclusions on Depassivation of Al-6061 Alloys - C.-H. Paik and R. C. Alkire 54
9:20 Oxygen Reduction on Steel in Basic Aqueous Solution with Relevance to Disbonding of Coatings from Cathodically Protected Steel - D. Gervasio and J. H. Payer 55
9:40 Formation of Calcareous Deposits on Cathodically Protected Steel in Seawater - R. E. White, J.-F. Yan, T. V. Nguyen, and R. B. Griffin 56
10:00 *Some Results of Cathodic Polarization Experiments* - M. de Lourdes, M. Magalhaes, and L. Sathler 57
10:20 Ten-minute intermission
10:30 Graded-Mesh and Adaptive-Mesh Finite Element Methods in Electrochemical Systems - S. Crockett and W. H. Smyrl 58
10:50 Cathodic Protection Design with Time-Dependent Boundary Conditions - K. Nisancioglu and P. O. Gartland 59
11:10 Boundary Elements Applied to Dynamic Simulation of Cathodic Protection Systems - J. A. F. Santiago, J. C. F. Telles, W. J. Mansur, and L. Sathler 60
11:30 Numerical Simulation of a Wet Christmas Tree Cathodic Protection System - J. C. F. Telles, W. J. Mansur, J. A. F. Santiago, S. L. Delarue, and W. Baptista 61
11:50 Closing remarks

MICROMACHINING AND MICROSTRUCTURES
New Technology Subcommittee/
Sensor/Electronics/Dielectric Science and Technology

H. F. Gray, Chairman; J. N. Zemel, Vice-Chairman
Room 29, 2nd Level

2:00 The program and abstracts will be published in the April issue of the *Journal* and included in the program booklet *distributed at the Meeting.*

NINTH SYMPOSIUM ON PLASMA PROCESSING
Dielectric Science and Technology/Electronics

G. S. Oehrlein, Chairman; S. J. Fonash, Vice-Chairman
Promenade Ballroom C, 2nd Level

Diagnostics and Measurements (cont'd)

9:00 Electrical Measurement of Etching Parameters in an Oxide RIE System - S.-I. Dohmae and J. P. McVittie 77

Device Damage

9:20 Gate Oxide Breakdown Phenomena in Magnetron Plasma - M. Sekine, K. Horioka, H. Okano, Y. Matsunaga, T. Matsushita, K. Hishioka, and Y. Yoshida 78
10:00 Gate Edge Effects on Oxide Damage during Polycide Etching - C. Gabriel 79
10:20 Spectroscopic Ellipsometry and Schottky Barrier Characterization of RIE Exposures of Thin Si-SiO_2 Structures Exposed to Poly-Si Overetch - T. Gu, R. A. Ditizio, R. W. Collins, S. J. Fonash, J. F. Rembetski, and X.-C. Mu 80
10:40 A Model for Thin Oxide Damage in Nonuniform Discharges - S. Fang and J. P. McVittie 81
11:00 Ion Bombardment Effects on Silicon Surface Properties in Plasma Etching - G. S. Oehrlein, D. Vender, and Y. Zhang 82
11:20 Reactive Ion Etch Induced Device Characteristics Changes in Thin Film Transistor - Y. Kuo 83
11:40 Assessment of the Effects of Magnetic Field Strength and of Post-Etching Ozone Cleaning on Substrate Damage and Contamination in MERIE Contact Etching - R. A. Ditizio, T. Gu, R. W. Collins, J. R. Ruzyllo, S. J. Fonash, and H. J. Leary 84

D. W. Hess, Chairman; J. I. McOmber, Vice-Chairman

Plasma Particles

2:00 A Model of Particulates in Glow Discharge Plasmas - D. B. Graves, M. G. Kilgore, J. E. Daugherty, and R. K. Porteous 85
2:40 Detection and Control of Particle Contamination in Production Plasma Equipment - G. S. Selwyn, E. F. Patterson, and K. L. Haller 86
3:20 Trapped Contamination Particulates in an RF Processing Plasma - R. N. Carlile and S. G. Geha 87
3:40 Particle Contamination on Silicon Wafers Etched in RF Plasmas - M. M. Smadi, G. Y. Kong, R. N. Carlile, and S. E. Beck 88

SECOND INTERNATIONAL SYMPOSIUM ON REDUCED-THERMAL-BUDGET PROCESSING FOR THE FABRICATION OF MICROELECTRONIC DEVICES
Dielectric Science and Technology/Electronics

J. W. Osenbach, Chairman; G. C. Schwartz, Vice-Chairman
St. Louis Ballroom G, 4th Level

9:00 A Highly Reliable Rapid Thermal Sintering Process for Aluminum Alloy Metallization - A. Husain 145
9:20 Thermal Stability of Thin Submicrometer Lines of $CoSi_2$ - O. Wang, C. M. Osburn, P. L. Smith, C. A. Canovai, and G. E. McGuire 146
9:40 *Effects of Dopants in Polysilicon on Titanium Silicide* Degradation - T. Koch 147
10:00 Fifteen-minute intermission
10:15 Low Temperature Sub-Atmospheric CVD USG/PSG for Gap Filling and Planarization of Advanced Submicron Memory Devices - D. Cote, H. Nobel, C. Basa, K. Kwok, E. Yieh, B. C. Nguyen, and Bg. Neureither 148
10:35 Water Trapping and Detrapping in Thin Film Dielectrics: Temperature Dependence and Water-Trap Dynamics - J. N. Cox, J. Z. Ren, J. M. Van Horn, and K. W. Kwok 149
10:55 Characterization of Remote Plasma-Enhanced CVD ONO Structures Using Electron Holography and Energy Loss Microscopy - G. L. Waytena, P. Rez, J. K. Weiss, W. J. DeRuijter, S. V. Hattangady, and G. G. Fountain 150
11:15 BPSGs Viscosity Determination for Rapid Flow Annealing Optimization - A. Tissier, J.-F. Teissier, A. Poncet, and D. Sanchez 151
11:35 Autodoping of Boron from BSG Glass - K. D. Beyer, G. Fitzgibbon, and P. A. Ronsheim 152

FIFTH INTERNATIONAL SYMPOSIUM ON SILICON-ON-INSULATOR TECHNOLOGY AND DEVICES
Electronics/Dielectric Science and Technology

S. Cristoloveanu, Chairman; J. Gautier, Vice-Chairman
Promenade Ballroom E, 2nd Level

Floating Body Effects

8:50 Introductory remarks

TUESDAY CONTINUED

9:00 Improved Physical Modeling of Bipolar Effects in SOI Transistors - G. A. Armstrong and W. D. French 162
9:20 A Simple Subthreshold Model for Floating Body SOI MOSFETs - G. Liu, P. Liu, Y. H. Chang, G. P. Li, and J. White 163
9:40 Voltage Limitations of Submicron CMOS on Thin SOI - J. Seliskar, F. Brady, L. K. Wang, and N. Haddad 164
10:00 Study of the Kink-Related Excess Low-Frequency Noise in SOI NMOSFETs at Room Temperature and 77 K - C. Claeys and E. Simoen 165
10:20 Ten-minute intermission

M. Matloubian, Chairman; G. Campisi, Vice-Chairman

Reliability Issues

10:30 Advantages and Limitations of Thin Film SIMOX MOSFETs: Reliability Aspects - J. Gautier and G. Reimbold 166
11:10 Hot-Carrier-Induced Degradation in Partially and Fully Depleted SIMOX MOSFETs - S. M. Gulwadi, S. Cristoloveanu, D. E. Ioannou, G. Campisi, and H. L. Hughes 167
11:30 Back-Channel Hot-Electron Effect on the Drain Breakdown Voltage in Thin-Film SOI MOSFETs - B. Zhang and T. P. Ma 168
11:50 Numerical Analysis of Short-Channel and Drain Engineering Effects for Fully Depleted SOI MOSFETs in a Radiation Environment - J. H. Smith, R. Lawrence, and G. Campisi 169

G. Campisi, Chairman; M. Matloubian, Vice-Chairman

Device-Based Characterization

2:00 Device-Based Electrical Characterization for SOI Technology Development - D. E. Ioannou 170
2:40 Evaluation of ZMR SOI Films for BICMOS Application by Low Frequency Noise Investigations - B. Tillack, R. Banisch, F. Januschewski, A. Chovet, K. Hoeppner, and H. H. Richter 171
3:00 Measurements and Analysis of Random Telegraph Signals in Small Area SOI MOSFETs - O. Roux dit Buisson, G. Ghibaudo, J. Brini, and T. Ouisse 172
3:20 A New Transient Drain Current Technique for Interface Characterization in SOI MOSFETs - S. Cristoloveanu, H. Haddara, and M. T. Elewa 173

MATERIALS AND PROCESSING ISSUES FOR LARGE SCALE INTEGRATED ELECTRONIC AND PHOTONIC ARRAYS

Electronics/Dielectric Science and Technology

S. Yamkoshi, Chairman; D. N. Buckley, Vice-Chairman
Room 43, 4th Level

9:00 Integrated Optoelectronic Device Technology - S. R. Forrest 205
9:40 Devices and Processes for Integrated Photoreceivers on InP - A. Scavennec, L. Giraudet, P. Blanconnier, G. Post, J. P. Praseuth, and A. Temmar 206
10:20 Fifteen-minute intermission
10:35 GaAs-on-InP, Receiver-Transmitter Optoelectronic Integrated Circuit - P. J. O'Sullivan and D. A. Allan 207
11:15 Computer Simulation and Characterization of MBE Growth of AlGaAs/GaAs Heterostructures - P. B. Kosel and T. R. Krishna 208
11:35 Formation of Epitaxial $CoSi_2$ Films on (001) Silicon Using Ti-Co Alloy and Bimetal Source Materials - S. L. Hsia, T. Y. Tan, P. L. Smith, and G. E. McGuire 209

STATE-OF-THE-ART PROGRAM ON COMPOUND SEMICONDUCTORS XVI

Electronics/Dielectric Science and Technology

V. Swaminathan, Chairman; J. P. Vilcot, Vice-Chairman
Room 43, 4th Level

2:00 **The program and abstracts will be published in the April issue of the *Journal* and included in the program booklet distributed at the Meeting.**

SECOND SYMPOSIUM ON THE PHYSICS AND CHEMISTRY OF SiO_2 AND THE Si-SiO_2 INTERFACE

Electronics/Dielectric Science and Technology

D. Griscom, Chairman; S. I. Raider, Vice-Chairman
Promenade Ballroom F, 2nd Level

Deposition and Properties of SiO_2

8:30 Thermal and X-Ray Production of Point Defects in Vitreous SiO_2 - F. L. Galeener 223
9:10 Nonstoichiometry and Defects in Bulk a-SiO_2 - H. Kawazoe and K. Awazu 224
9:50 The Paramagnetic Defects in Crystalline SiO_2 - J. A. Weil, R. J. McEachern, and M. M. Mombourquette 225
10:20 Ten-minute intermission
10:30 *Formation of Si/SiO_2 Heterostructures* by Low-Temperature, Plasma-Assisted Oxidation and Deposition Processes - G. Lucovsky, Y. Ma, T. Yasuda, and S. Habermehl 226
11:00 Growth and Characterization of SiO_2 Thin Films Deposited by DECR-PECVD at Low Temperature - B. Agius, M. C. Hugon, N. Jiang, M. Puech, G. Ravel, and F. Plais 227
11:20 Low Temperature Synthesis and Characterization of Silicon Dioxide Films - G. S. Chakravarthy, R. A. Levy, and J. M. Grow 228
11:40 *Fundamental Spectroscopic Studies of SiO_2 Deposition* from TEOS - J. E. Crowell, H.-C. Cho, and L. L. Tedder 229

T. Ohmi, Chairman; G. Lucovsky, Vice-Chairman

Chemical Properties of Si Surfaces Related to Oxidation and Oxide Deposition

1:30 Native Oxide Growth and Hydrogen Bonding Features on Chemically Cleaned Silicon Surfaces - M. Hirose, M. Takakura, T. Yasaka, and S. Miyazaki 230
2:00 *Understanding the Surface Chemical and Structural* Implications of HF Solution Cleaning of Silicon - G. S. Higashi 231
2:30 Pre-Gate Oxide Si Surface Control - M. Morita and T. Ohmi 232
3:00 Chemical Structures of Native Oxides Formed during Wet Chemical Treatments on Atomically Flat Si(111) Surface - H. Ogawa and T. Hattori 233
3:20 Silicon Surface Analysis and Very Thin Silicon Oxide Characterization after HF/Ethanol Preoxidation Silicon Cleaning - J. R. Morante, B. Garrido, J. Samitier, F. Gessin, J. L. Prom, and G. Sarrabayrouse 234
3:40 Effects of Metallic Impurities upon Thin Gate Oxide Integrity and Related Bulk Electrical Properties in CZ Si - K.-C. Cho, J.-G. Park, Y.-S. Kwak, D.-J. Lee, C.-S. Lim, C.-K. Shin, and S. Hahn 235

FRACTALS IN ELECTROCHEMISTRY

Energy Technology/Physical
Electrochemistry/Corrosion

S. Havlin, Chairman; C. Thompson, Vice-Chairman
Room 46, 4th Level

9:00 Equivalent Circuit Study of Fractal Electrodes - B. Sapoval 321
9:20 The Double Layer Impedance: Effects of Electrode Roughness - T. C. Halsey 322
9:40 Theory of Interfacial Constant Phase Element in Electrode-Electrolyte Systems - S. H. Liu 323
10:00 Fifteen-minute intermission
10:15 Noise Analysis Applied to Electrochemical Systems - U. Bertocci 324
10:35 Surface Morphology Characterization with X-Ray Scattering - C. Thompson 325
11:05 Electrochemical Fractal Dimension Measurement on Rough Surfaces - T. Pajkossy, A. Imre, and L. Nyikos 326

TUESDAY CONTINUED

SYNTHESIS AND PROCESSING FOR HIGH-TEMPERATURE MATERIALS IN THE YEAR 2000

High Temperature Materials/Dielectric Science and Technology

S. C. Singhal, Chairman; J. Dismukes, Vice Chairman
Promenade Ballroom A, 2nd Level

M. D. Allendorf, Chairman; J. B. Wagner, Jr., Vice-Chairman

ELECTROCHEMISTRY IN MINERAL AND METAL PROCESSING III

Industrial Electrolysis and Electrochemical Engineering

R.-H. Yoon, Chairman; S. Chander, Vice-Chairman
St. Louis Ballroom A, 4th Level

J. Ralston, Chairman; K. Osseo-Asare, Vice-Chairman

INDUSTRIAL ELECTRO-ORGANIC PROCESSES

Industrial Electrolysis and Electrochemical Engineering

C. King, Chairman; J. W. Van Zee, Vice-Chairman
Promenade Ballroom B, 2nd Level

GENERAL SESSION

Physical Electrochemistry

A. Lasia, Chairman; P. Vanysek, Vice-Chairman
Room 26, 2nd Level

P. Vanysek, Chairman; A. Lasia, Vice-Chairman

MICROMORPHOLOGY IN ELECTROCRYSTALLIZATION

Physical Electrochemistry/Electrodeposition

R. C. Alkire, Chairman; T. Hepel, Vice-Chairman
St. Louis Ballroom F, 4th Level

TUESDAY CONTINUED

QUANTUM CONFINEMENT
New Technology Subcommittee/Electronics/Dielectric Science and Technology

E. Nicollian, Chairman; R. Tsu, Vice-Chairman
St. Louis Ballroom F, 4th Level

2:00 The program and abstracts will be published in the April issue of the *Journal* and included in the program booklet distributed at the Meeting.

FULLERENES: CHEMISTRY, PHYSICS AND NEW DIRECTIONS
Physical Electrochemistry/Dielectric Science and Technology/Electronics

J. Bernholc, Chairman; B. Dunlap, Vice-Chairman
St. Louis Ballroom C, 4th Level

9:00 The program and abstracts will be published in the April issue of the *Journal* and included in the program booklet distributed at the Meeting.

D. M. Cox, Chairman; D. Tomanek, Vice-Chairman

2:00 The program and abstracts will be published in the April issue of the *Journal* and included in the program booklet distributed at the Meeting.

EIGHTH INTERNATIONAL SYMPOSIUM ON MOLTEN SALTS
Physical Electrochemistry/High Temperature Materials

E. J. Cairns, Chairman; D. G. Lovering, Vice-Chairman
St. Louis Ballroom B, 4th Level

9:00 Molten Carbonate Fuel Cell Reaction Mechanisms - K. Hemmes, R. C. Makkus, R. Weewer, and J. H. W. de Wit 497
9:20 IMHEX® Molten Carbonate Fuel Cell Program Status - G. L. Reznikov and R. Donelson 498
9:40 A Comparative Study of Electrochemical Systems of Oxygen in Molten Alkaline Carbonates at 500°-750°C - J. Devynck, G. Moutiers, M. Cassir, and B. Tremillon 499
10:00 High Temperature Corrosion of Nickel Coated with Molten Alkali Carbonates - K.-i. Ota, B.-u. Kim, H. Yoshitake, and N. Kamiya 500
10:20 Ten-minute intermission
10:30 Galvanic Corrosion of Coupled Pt-Ni System in Molten Na_2CO_3 at 1173 K - Y. Shinata, M. Hara, and S. Hashimoto 501
10:50 Development of Cathodes for an Aluminum-Chlorine Fuel Cell in High Temperature Chloride Melts - T. Ishikawa, T. Sasaki, and S. Konda 502
11:10 Application of Molten Salts in Pyrochemical Processing of Reactive Metals - B. Mishra, D. L. Olson, and W. A Averill 503
11:30 Investigations at Los Alamos National Laboratory of Calcium Chloride Based Molten Salts Systems - S. D. Owens, K. M. Axler, G. L. DePoorter, and G. D. Bird 504
11:50 Voltammetric Study of a Planar Electrode with Supermeniscus Film in Molten Carbonate - G. L. Lee and J. R. Selman 505

D. G. Lovering, Chairman; E. J. Cairns, Vice-Chairman

2:20 Material-Deposition Processes in the Separator of Li-Alloy/Fe/S_2 Thermal Cells - M. C. Hash, J. A. Smaga, R. A. Guidotti, and F. W. Reinhardt 506
2:40 Performance of a Sodium/Selenium (IV) Molten Chloroaluminate Cell for an Electric Vehicle - M. Matsunaga, M. Morimitsu, G. Mori, S. Obata, T. Kitazaki, and K. Hosokawa 507
3:00 The Modification of Flemion Membranes for Use in Energy Generating Devices - D. S. Newman, S. Li, and T. Howard 508
3:20 Molten Salt Regular Mixture Theory Applied to Ion Exchange Membranes - K. S. Forland, T. Okada, and S. K. Ratkje 509
3:40 Theory of Thermocells: Transported Entropies and Heat of Transfer in Ag_2SO_4-Li_2SO_4 - A. Grimstvedt and S. K. Ratjke 510

ELECTROCHEMICAL SENSORS IN MEDICAL SCIENCE
Sensor

G. Wilson, Chairman; L. Bousse, Vice-Chairman
St. Louis Ballroom E, 4th Level

9:00 Electrochemical Methods for Quantitation of Peroxidase and Alkaline Phosphatase - H. Song and D. G. Hafeman 557
9:20 Bienzyme Amperometric Sensors Using a Polymeric Electron Transfer Mediator - A. C. Michael and M. G. Garguilo 558
9:40 Glutamate Electrodes: Construction, Function, and Applications - J. R. Woodward, R. B. Spokane, S. Parker, T. D. Gibson, J. N. Hulbert, and L. C. Clark, Jr. 559
10:00 Glutamate Dehydrogenase-Modified Carbon Fiber Microelectrodes with Millisecond Response Times - W. G. Kuhr and P. Pantano 560
10:20 Ten-minute intermission
10:30 Application of ω-Thiocarboxylic Acid Monolayers for the Detection of Dopamine in the Presence of High Concentration of Ascorbic Acid - D. Mandler and F. Malem 561
10:50 Controlled Binding and Electrorelease of Metal Ions, Drugs, and Neurotransmitters from Cation Gate Composite Polymer Films Studied by Piezoelectric Sensor Technique - M. Hepel and L. Dentrone 562
11:10 The Effect of Overoxidation on the Electrochemical Behavior of Polypyrrole Films Doped with Various Anionic Species - D. Belanger and F. Provencher 563
11:30 Polypyrrole-Enzyme Film Electrode Mediated by Electropolymerized Catalytic Polymer Film - H. Tachikawa, Z. Sun, and H. Ge 564

WEDNESDAY, MAY 20, 1992

12:15 P.M. Dielectric Science and Technology Division Luncheon and Business Meeting, Rose Garden, 4th Level.
12:15 P.M. Energy Technology Division Luncheon and Business Meeting, Promenade Ballroom D, 2nd Level.
12:15 P.M. Organic and Biological Electrochemistry Division Luncheon and Business Meeting, St. Louis Ballroom H, 4th Level.

NINTH SYMPOSIUM ON PLASMA PROCESSING
Dielectric Science and Technology/Electronics

R. N. Carlile, Chairman; D. W. Hess, Vice-Chairman
Promenade Ballroom C, 2nd Level

Plasma Cleaning

9:00 Plasma and Surface Diagnostics of ECR Hydrogen Cleaning of Native Silicon Oxide - W. Tsai, M. Delfino, B. C. Chung, T. Sheng, and S. Salimian 89
9:20 Process and Module for Low Temperature Hydrogen Cleaning for Silicon Wafers - F.-P. Steiner, E. Beck, and J. Ramm 90
9:40 *In Situ* Chamber Dry Cleaning for HBr RIE - K. Iizuka and M. Nakamura 91

Low Temperature Etching

10:00 Ion Beam-Assisted Etching of Si (111) with Fluorine at 77K - J. W. Coburn and C. B. Mullins 92

WEDNESDAY CONTINUED

10:40 A New Method of Sidewall Protection for Anisotropic Etching Using Sulfur Deposition - T. Tatsumi, T. Nagayama, and S. Kadomura 93

11:00 Cooling Wafer Stage for Low Temperature Dry Etching - M. Kanetomo, T. Kure, K. Tsujimoto, and S. Tachi 94

Silicon Etching

11:20 Problems of Low Pressure Single Crystal Silicon Etching - M. Engelhardt 95

11:40 Highly Selective Low Pressure Polysilicon Etching in High Density, Low Energy RF Plasmas - M. Engelhardt 96

G. S. Mathad, Chairman; S. Salimian, Vice-Chairman

Silicon Etching (cont'd)

2:00 Selective High-Rate Etching of Polysilicon in Microwave ECR Discharges: A Comparision of ECR Configurations - T. O. Mantei, D. Dane, and P. Gadgil 97

2:20 Quarter-Micron Deep Trench Etch for ULSI - Y. T. Lii and T. V. Rajeevakumar 98

2:40 MRIE 0.1 μm Polysilicon Lines by Using HBr - Y. T. Lii, C. M. Reeves, D. A. Danner, P. J. Coane, and L.-K. Wang 99

3:00 Fundamental Processing Limit of Gate Oxide Thickness for Polysilicon Gate Definition - A. S. Yapsir 100

Aluminum/Alloy Etching

3:20 200 mm Aluminum Etch in MERIE System - S. Mak, S. Arias, and C. S. Rhoades 101

3:40 Dry Etching of Al Alloy Films Using HBr Mixed Gases - K. Fujino and T. Oku 102

4:00 One-Step Electron Cyclotron Resonance Etching of Submicron Al-Si-Cu - D. X. Ma and C.-H. Chen 103

4:20 Low Energy Ion Etching of Aluminum Oxide Films and Native Aluminum Oxide - M. E. Day, S. Salimian, and M. Delfino 104

4:40 Analysis of Post-Metal Etch Processes Causing Submicron Technology Corrosion Defects - K. E. Mautz 105

G. S. Selwyn, Chairman; D. B. Graves, Vice-Chairman

Plasma Generated Particles

7:00 Informal discussion

FIFTH INTERNATIONAL SYMPOSIUM ON SILICON-ON-INSULATOR TECHNOLOGY AND DEVICES

Electronics/Dielectric Science and Technology

P. L. F. Hemment, Chairman; J. Margail, Vice-Chairman
Promenade Ballroom E, 2nd Level

Characterization of Materials I

9:00 Introductory remarks

9:10 Defects in SIMOX Structures: Characterization and Some Formation Mechanisms - J. Margail, J. M. Lamure, J. Stoemenos, and A. M. Papon 174

9:50 Effect of Thermal Ramping Conditions on Defect Formation in Oxygen Implanted Silicon-on-Insulator Material - S. Krause, J. D. Lee, J. C. Park, P. Roitman, and M. El-Ghor 175

10:10 Screen Oxide Effects on the SIMOX Material Quality Observed by Raman Microprobe Measurements - A. Perez-Rodriguez, J. R. Morante, E. Martin, J. Jimenez, J. Margail, and A. M. Papon 176

10:30 Fifteen-minute intermission

10:45 Kinetics of Oxygen Precipitation in Low Fluence SIMOX - L. Meda, C. Spaggiari, G. F. Cerofolini, S. Bertoni, and R. Canteri 177

11:15 Novel Approach to Defect Etching in Thin Film SOI - H. Gassel, J. Peter-Weidemann, and H. Vogt 178

J. Margail, Chairman; P. L. F. Hemment, Vice-Chairman

Characterization of Materials II

2:00 Correlation Between X-Ray Moire' Pattern and Dislocation Density in SIMOX - M. K. El-Ghor, K. A. Joyner, and G. A. Rozgonyi 179

2:20 Raman Scattering and FTIR Spectroscopy as Characterization Techniques of SIMOX Structures - J. Samitier, A. Perez-Rodriguez, J. R. Morante, E. Martin, J. Jimenez, and P. L. F. Hemment 180

2:40 Electro-Optical Characterization of SIMOX Structures by Photoconductive Based Techniques - J. Macia, A. Perez-Rodriguez, J. R. Morante, M. A. Lourenco, P. L. F. Hemment, and K. P. Homewood 181

3:00 Ten-minute intermission

3:10 The Effects on Carrier Lifetime of SIMOX Anneal Process Parameters: A Designed Experiment - K. A. Joyner 182

3:30 Nondestructive SOI Process Evaluation Using Recombination Lifetime Measurements - A. Buczkowski, F. Shimura, B. Cordts, and G. A. Rozgonyi 183

3:50 Investigation of Local Isolation Structures on SIMOX Substrates with Micro-Raman Spectroscopy and Correlation with XTEM - I. De Wolf, A. Romano-Rodriguez, I. Vanhellemont, H. Norstrom, and H. E. Maes 184

SECOND SYMPOSIUM ON THE PHYSICS AND CHEMISTRY OF SiO_2 AND THE Si-SiO_2 INTERFACE

Electronics/Dielectric Science and Technology

T. Hattori, Chairman; C. R. Helms, Vice-Chairman
Promenade Ballroom F, 2nd Level

Chemical, Structural, and Microroughness Effects at the Si-SiO_2 Interface

8:15 T. D. CALLINAN AWARD ADDRESS: Carbon Impurities at Si-SiO_2 Interfaces - S. I. Raider 236

8:50 Microscopic Structure of the Si/SiO_2 Interface - F. J. Himpsel 237

9:20 High Resolution Transmission Electron Microscope Image of the SiO_2/(001)Si Interface - H. Akatsu, Y. Sumi, and I. Ohdomari 238

9:50 Dependence of Surface Microroughness on Types of Silicon Substrates - T. Ohmi, T. Tsuga, and J. Takano 239

10:20 Ten-minute intermission

10:30 The Effect of Surface Roughness on Gate Oxide Leakage Currents - M. Chonko and V. Kaushik 240

10:50 A Double Sacrificial Oxide Process for Smoother 150 Å SiO_2 Gate Oxide Interfaces - H.-H. Tseng and P. J. Tobin 241

11:10 Effect of Solidification Induced Defects in CZ-Silicon upon Thin Gate Oxide Integrity - H. Suga, H. Abe, H. Koya, T. Yoshimi, I. Suzuki, H. Yoshioka, and N. Kagawa 242

11:30 Effects of D-Defects in CZ Silicon upon Thin Gate Oxide Integrity - J.-G. Park, S.-P. Choi, G.-S. Lee, Y.-J. Jeong, Y.-S. Kwak, C.-K. Shin, S. Hahn, and P. Mascher 243

11:50 Oxidation-Induced Changes in the Si Surface Microroughness - V. Nayar, A. J. Pidduck, and C. Pickering 244

A. Goodman, Chairman; W. T. Lynch, Vice-Chairman

Novel Structures, Processes, and Phenomena

1:45 Properties of SIMOX and Related Systems - S. Cristoloveanu 245

2:15 Reoxidized Nitrided Oxide Gate Dielectrics for Advanced CMOS - G. J. Dunn 246

2:45 Interface Properties and Device Reliability of High Quality PECVD Oxide for MOS Applications - L. K. Wang, C. C-H. Hsu, and W. Chang 247

3:05 Charge Trapping in an ONO Gate Dielectric - R. B. Klein and N. S. Saks 248

3:25 Interface Trap Density Reduction and Oxide Profiling for Fluorinated MOS Capacitors - D. Kouvatsos, R. J. Jaccodine, and F. A. Stevie 249

3:45 Ten-minute intermission

3:55 Physics of Extreme Quantum Confinement Examplified by Si/SiO_2 Systems - R. Tsu 250

4:25 Integrity of Very Thin Silicon Films Deposited on SiO_2 - M. Chonko, D. Vandenberg, and D. Keitz 251

4:45 Researches of SiO_2 on InP and GaAs MOS Structures - Y. K. Su and C. J. Hwang 252

WEDNESDAY CONTINUED

STATE-OF-THE-ART PROGRAM ON COMPOUND SEMICONDUCTORS XVI

Electronics/Dielectric Science and Technology

J. P. Vilcot, Chairman; V. Swaminathan, Vice-Chairman
Room 43, 4th Level

9:00 The program and abstracts will be published in the April issue of the *Journal* and included in the program booklet distributed at the Meeting.

D. N. Buckley, Chairman; T. Kamijoh, Vice-Chairman

2:00 The program and abstracts will be published in the April issue of the *Journal* and included in the program booklet distributed at the Meeting.

JOINT GENERAL SESSION

Electronics/Dielectric Science and Technology

R. J. Jaccodine, Chairman; A. Harrus, Vice-Chairman
Promenade Ballroom A, 2nd Level

9:00 *Suppression of WSi_x Peeling in 0.8 μ BiCMOS Technology* - B. L. Mantha and C. S. Wang 269

9:15 Characterization of WSi_x Films Deposited by Dichlorosilane Reduction Process for MOS VLSI - A. Ookawa, S. Moribe, S. Morita, and A. Koike 270

9:30 Effect of Underlying TiW Thickness on the Electromigration of Vias - D. Pramanik and V. Jain 271

9:45 Microstructure Control and Thermal Stability of Titanium Silicide - R. W. Mann and C. Racine 272

10:00 The Direct Observation of Atom Column Defects in $MoSi_2$ and W/Si_2 - K. M. Pollack, D. S. Schwartz, T. C. Bryant, and P. Fraundorf 273

10:15 Poly-Void Formation in Poly Buffer LOCOS Process - H. S. Yang, C. S. Han, W. G. Lee, K. M. Lee, H. S. Park, and K. H. Oh 274

10:30 Fifteen-minute intermission

10:45 Influence of Field Isolation Stress on Gate Oxide Reliability - K. Shiozaki, K. Shimanoe, K. Kato, and J. Nakano 275

11:00 A Comparison of Interstitial Oxygen Calculated by Different Techniques - J. W. Medernach and J. O. Stevenson 276

11:15 The Warpage of As-Received and Oxygen Precipitated CZ Silicon Wafers - J. Jeong and H.-D. Chiou 277

11:30 Modeling of Phosphorus Precipitation - S. Dunham 278

11:45 Accurate and Computationally Efficient Modeling of BF_2 Implants into Single-Crystal Silicon - S. J. Morris, V. Do, P. Gupa, S.-H. Yang, C. Park, K. M. Klein, A. F. Tasch, R. B. Simonton, and G. E. Lux 279

A. Harrus, Chairman; R. J. Jaccodine, Vice-Chairman

2:00 Investigation of Ion-Surface Interaction in Ar Plasma Etching of Si and PECVD of SiO_2 Film by High-Frequency C-V Method - C. Pavelescu, J. P. McVittie, C. Chang, K. C. Saraswat, and J. Y. Leong 280

2:15 Trace Moisture Analysis in Monosilane-Hydrogen Mixtures at Atmospheric Pressure and Ion-Molecule Reactions - T. Irie, S. Iijima, and Y. Mitsui 281

2:30 Chemical Foundations in Understanding the Step Coverage Problem in CVD Using the Silane Chemistry - C. Pavelescu and K. C. Saraswat 282

2:45 *Characterization of Band-Pattern Polishing Marks* Induced during Waxless/Wax Polishing Process Using Magic Mirror Method - K. H. Cho, H. Y. Cho, S. Hahn, D. Feindel, F. Mason, P. R. Blaustein, and K. W. Kim 283

3:00 Highly Reliable Electrostatic Chucks Employing Plasma-Sprayed Aluminum-Oxide Coating for Advanced Semiconductor Processing - H. Uetake, K. Morizuka, and T. Ohmi 284

3:15 Investigation of Single-Layer p-SnS:M and Double Layer p-SnS:M/n-MS:Sn. (M=Zn or Cd)-Based Photoconductive Cells Produced by a Combined Chemical Bath Deposition/Ion Exchange Process - R. Engelken, C. Brinkley, L. N. Chang, and L. Yu 285

3:30 *Fifteen-minute intermission*

3:45 Mix-Cation Oxide Powders via Resin Intermediates *Derived from Water Soluble Polymers* - L.-W. Tai and H. U. Anderson 286

4:00 A Novel Evaluation Technique of Carrier Concentration by Noncontact Eddy Current Measurement - S. Washizuka, Y. Yoneda, A. Watanabe, and T. Ohta 287

4:15 ZrO_2-CeO_2 Spherical Powders Prepared by Sol-Gel Process: Synthesis, Sintering, and Characterization - F. Croce, M. Carewska, and A. Deptula 288

4:30 A Characterization of the Effect of Deposition Temperature on Polysilicon Properties: Morphology, Dopability, Etchability, and Polycide Properties - E. Ibok and S. Garg 289

4:45 Effect of Back-Surface Polycrystalline Silicon Layer on Oxygen Precipitation in CZ Silicon Wafer - M. Kadoi, H. Furuya, T. Shingyouji, and Y. Shimanuki 290

5:00 $HfN/Hf_xO_yN_z$ Thin Films by LPCVD - C. Orfescu, A. J. Fortini, R. La Feria, A. J. Sherman, and E. H. Liu 291

5:15 Damage and Its Rapid Thermal Annealing Kinetics in Ar^+ Ion Implanted CZ Silicon - Y.-K. Kwon, K.-I. Kim, Y.-H. Bae, W.-J. Chung, E. K. McIntyre, Jr., T. Hara, H. Hagiwara, H. Suzuki, W. L. Smith, S. Hahn, L. Larson, C. B. Yarling, and R. Meinecke 292

5:30 Low Resistance Molybdenum Silicide - Molybdenum Thin Films - S. Vasile and D. Nicolaescu 293

SURFACE PROCESSING IN ENERGY TECHNOLOGIES

Energy Technology

A. W. Czanderna, Chairman; A. R. Landgrebe, Vice-Chairman
St. Louis Ballroom D, 4th Level

8:30 Introductory remarks by A. W. Czanderna

8:50 Photoelectrochemical and Electrochemical Polishing of Epi β-SiC and CVD - R. D. Rauh, T. H. Nguyen, M. M. Carrabba, and T. D. Plante 294

9:10 Characterization of Electrocatalytically Active Ni-Co Amorphous and Crystalline Alloys - K. Lian, D. W. Kirk, and S. J. Thorpe 295

9:30 Influence of Pretreatment on the Unusual Redox Behavior of Noble Metal Electrodes - L. D. Burke and J. K. Casey 296

9:50 Ten-minute intermission

10:00 Catalyst Layer and Interface Properties of Directly Catalyzed Polymer Electrolyte Membranes - M. S. Wilson, T. A. Zawodzinski, Jr., T. E. Springer, J. Valerio, and S. Gottesfeld 297

10:20 Chemical Bath Deposition of Cadmium Sulfide Thin Films, *In Situ* Growth and Structural Studies by Combined Quartz Crystal Microbalance and Impedance Techniques - D. Lincot and R. Ortega 298

10:40 *Study of the Bandedge Shifts of n- and p-type $CuInSe_2$* Semiconducting Electrodes in Various Aqueous Electrolytes - W. Siripala, J. Vedel, D. Lincot, and D. Cahen 299

11:00 Highly Oriented *vs.* Microcrystalline Thick Cadmium Films Deposited on Polycrystalline Nickel from a Molten Salts Electrolyte - R. R. Agarwal 300

11:20 Surface Modification of Sintered Plates Negative *Electrodes of Nickel Cadmium Battery* - S. Tamil Selvan, R. Sabapathi, and N. Venkatakrishnan 301

A. R. Landgrebe, Chairman; A. W. Czanderna, Vice-Chairman

2:00 Introductory remarks by A. R. Landgrebe

2:20 Properties and Modification of Perfluorosulfonic Acid Membrane Surfaces - T. A. Zawodzinski, Jr., M. Shoichet, N. Hamel, G. Gard, T. J. McCarthy, and S. Gottesfeld 302

2:40 *In Situ* Study of the Chemical Bath Deposition Mechanism of Cadmium Sulfide Thin Films on Gold and Copper Indium Diselenide Substrates - D. Lincot, R. Ortega, and J. Vedel 303

3:00 Electrochemical Vapor Deposition of CeO_2 Thin Film Electrolytes for Solid Oxide Fuel Cells - J.-F. Jue and A. V. Virkar 304

3:20 Ten-minute intermission

WEDNESDAY CONTINUED

3:30 Evaluation of Doped Ceria With and Without Zirconia Coating for Application in Low-Temperature Solid Oxide Fuel Cells - K. Mehta and A. V. Virkar 305

3:50 Kinetics of the Cadmium Electrode in Alkaline Solution - S. Tamil Selvan, R. Sabapathi, and N. Venkatakrishnan 306

4:10 Evaluation of Electrodeposited Electrocatalytic Composite Metal Film Coatings for Cathodic H_2 Evolution in Water Electrolyzers - B. E. Conway, R. Simpraga, and R. Brousseau 307

ELECTROCHEMICAL CHARACTERIZATION OF THIN SOLID FILMS

Energy Technology/Physical Electrochemistry/Electronics/Dielectric Science and Technology

P. J. Sides, Chairman; M. E. Orazem, Vice-Chairman
Room 46, 4th Level

9:00 *In Situ Infrared Spectroscopy of Corrosion Processes* at Lacquer Coated Metals - S. N. Port, A. Bewick, and J. Casper 327

9:20 Coulometric Reduction of Thin Tarnish Films Formed on Copper - B. I. Rickett and J. H. Payer 328

9:40 Impedance Characterization of Polypyrroles - P. G. Pickup, G. L. Duffitt, and X. Ren 329

10:00 Electrochemical Observation of Intermediates during the Formation of Conducting Polypyrrole - D. J. Harrison and D. E. Raymond 330

10:20 Ten-minute intermission

10:30 Electrochemical Quartz Crystal Microbalance Studies of Electroactive Polymer Bilayers - A. R. Hillman and A. Glidle 331

10:50 Modeling of the $GaInP_2$/Aqueous Electrolyte Interface Utilizing Electrochemical Impedance Spectroscopy - S. S. Kocha and B. E. Liebert 332

11:10 The Effect of Preparation Conditions on the Ion Diffusion and Electrochromic Properties of Li_xWO_3 - J.-G. Zhang, C. E. Tracy, and D. K. Benson 333

11:30 Electrode Surface Modification with ZnO and ZnO-CdS Semiconductor Colloidal Particles - P. V. Kamat and S. Hotchandani 334

STABILITY OF REFRACTORY MATERIALS

High Temperature Materials

D. L. Jacobson, Chairman; A. Luo, Vice-Chairman
Room 46, 4th Level

2:00 The Performance of W Single Crystal Faceted Coating Surface Having (110) Preference Orientation of TEC Cylindrical Electrodes - R. V. Savvov, A. V. Vizgalov, V. I. Yarygin, and Z. B. Skrebova 335

2:20 Ionic Conductivity and Phase Transformation in Gd_2O_3 - Stabilized Bi_2O_3 - P. Su and A. V. Virkar 336

2:40 Platinum-Tungsten and Rhodium-Tungsten Alloys for AMTECH Electrodes - M. A. Ryan, R. M. Williams, B. Jeffries-Nakamura, M. L. Underwood, and D. O'Connor 337

3:00 The High Temperature Work Function of Sintered Dilute Solution Tungsten, Iridium Alloys - L. A. D'Cruz, D. R. Bosch, and D. L. Jacobson 338

3:20 Dispersion Particle Strengthening in Tungsten at High Temperatures - A. Luo and D. L. Jacobson 339

3:40 High Temperature Electron Emission and Vaporization of Tungsten- Iridium Alloys - R. N. Wall, D. L. Jacobson, and D. R. Bosch 340

HIGH TEMPERATURE SENSORS

High Temperature Materials/Sensor/Battery

C. B. Alcock, Chairman; P. Moseley, Vice-Chairman
St. Louis Ballroom E, 4th Level

9:00 Sensor Applications of Oxygen Pumping with ZrO_2 Electrochemical Cells - E. M. Logothetis, J. H. Visser, R. E. Soltis, and L. Rimai 355

9:30 Kinetics of the Electrode Reaction at the H_2-H_2O, Porous Pt/Stabilized Zirconica Interface - J. Mizusaki, H. Tagawa, M. Tajika, K. Isobe, I. Koshiro, H. Maruyama, and K. Hirano 356

10:00 Mixed Potential Gas Sensors - P. T. Moseley and R. Peat 357

10:20 Ten-minute intermission

10:30 New Ideas, How to Use Mixed Ionic Electronic Conductors, Instead of Solid Electrolytes, in Potentiometric Sensors - I. Riess 358

10:50 A Study on Properties of Electrode Materials for Oxygen Sensors - H. Arai, K. Eguchi, and T. Inoue 359

11:10 Novel Solid Electrolyte CO_2 Sensor Using Sodium Ion Conductor and Lithium-Based Carbonate Electrode - N. Yamazoe, S. Yao, Y. Shimizu, and N. Miura 360

11:30 Development of Solid-State Electrochemical Sensors for Measurement of Elements in Molten Metals - R. V. Kumar and D. J. Fray 361

C. C. Liu, Chairman; N. Yamazoe, Vice-Chairman

2:00 Miniaturization of High Temperature Oxygen Sensor Employing Film Electrolyte and Electrodes - E. B. Makovos, F. W. Montague, M. A. Stuczynski, and C.-C. Liu 362

2:20 Humidity Sensor for High Temperature Using a Limiting Current Type Plane Oxygen Sensor - H. Yagi 363

2:40 The Relationship Between Microstructure and Properties of Native Insulators Used in High Temperature-Thin Film Sensor Applications - A. S. Lawing, O. J. Gregory, and S. Mina 364

3:00 A Novel Polymer Blend for Solid-State Ammonia Sensor - R. D. A. Paulmer, R. S. Srinivasa, and A. R. Kulkarni 365

ELECTROCHEMISTRY IN MINERAL AND METAL PROCESSING III

Industrial Electrolysis and Electrochemical Engineering

M. Wadsworth, Chairman; E. Suoninen, Vice-Chairman
St. Louis Ballroom A, 4th Level

9:00 Photoelectrochemical Behavior of Chalcopyrite ($CuFeS_2$) in Alkaline Solutions - G. H. Kelsall and F. W. H. Dean 384

9:30 Electrochemical Oxidation of Chalcopyrite ($CuFeS_2$) in Alkaline Solutions - G. H. Kelsall, K. E. R. England, D. J. Vaughan, and Q. Yin 385

10:00 The Photoelectrochemistry of *In Situ* Fractured Pyrite Electrodes - P. E. Richardson, Y. Li, and R.-H. Yoon 386

10:30 Fifteen-minute intermission

10:45 Interfacial Electrochemistry of Semiconductor Pyrite - K. K. Mishra and K. Osseo-Asare 387

11:15 Electrochemical Studies of Iron Sulfides in Relation to Their Atmospheric Oxidation and Prevention of Acid Drainage: Part II - S. M. Ahmed and E. Giziewicz 388

J. B. Hiskey, Chairman; A. Buckley, Vice-Chairman

2:00 Transpassive Oxidation of Pyrite - X. Zhu, J. Li, D. M. Bodily, and M. E. Wadsworth 389

2:30 Comparative Studies of Surface Properties of Pyrite from Coal and Ore Sources - X.-H. Wang, C. L. Jiang, A. M. Raichur, J. W. Leonard, and B. K. Parekh 390

3:00 Electrochemical Kinetics of Silver Dissolution in Cyanide Solutions - J. Li and M. E. Wadsworth 391

3:30 *Fifteen-minute intermission*

3:45 Thermodynamic Equilibrium Calculations on Au/Ag-Lixiviant Systems Relevant to Gold Extraction from Complex Ores - X.-H. Wang 392

4:15 Gold Leaching and Recovery: The Bromide Process - A. Dadgar and J. Howarth 393

4:45 Complex Technology of Electrochemical Water Treatment with Regeneration of Valuable Components in Electroplating Production - V. A. Kolesnikov, E. A. Shalyt, and P. K. Aarinola 394

WEDNESDAY CONTINUED

ELECTRO-ORGANIC SYNTHESIS WITH HOMOGENEOUS AND HETEROGENEOUS CATALYSTS

Organic and Biological Electrochemistry

D. G. Peters, Chairman; J. E. Toomey, Jr., Vice-Chairman
Promenade Ballroom B, 2nd Level

9:00 Introductory remarks by D. G. Peters
9:05 Mediated Reductive Dechlorination of PCBs in Surfactant Dispersions and Microemulsions - I. U. Haque, E. C. Couture, S. Zhang, and J. F. Rusling 414
9:35 Electrocatalytic Hydrogenation at Palladium Black Electrodes - S. J. C. Cleghorn and D. Pletcher 415
10:05 The Electrochemical Reduction of Nitroaromatic Compounds to Amines in Basic Solutions at Porous Metallic Electrodes - J. Lessard, M.-J. Lessard, Y. Couture, A. Martel, and C. Roy 416
10:35 Fifteen-minute intermission
10:50 Role of Sulfide Ion as Mediator in the Electroreduction of Nitroaromatics - A. Tandon, P. S. Verma, S. K. Mukerji, and K. N. Tandon 417
11:20 Indirect Reduction of Sulfonium Salts by Means of p-Acceptor Radical Anions (in Liquid Phase) and N-Doped Electroactive Polymers (in Solid Phase): Application to Functionnalization Reactions - J. Simonet, P. Martigny, H. Le Deit, and J. Rault-Berthelot 418

J. E. Toomey, Jr., Chairman; D. G. Peters, Vice-Chairman

2:00 On the *ipso*-Substitution in Aromatic Compounds by Electrogenerated Radicals - H. Lund, K. Pang, and Q. Chen 419
2:30 Production of Pyrene Quinone by Indirect Electro-Oxidation of Suspended Pyrene - T. Nonaka, A. Yoshiyama, M. Wakamatsu, S. Tsuji, and I. Okubo 420
3:00 Fifteen-minute intermission
3:15 Electro-Oxidation of Propene in Aqueous Zeolite Suspensions - J. Z. Stemple and D. R. Rolison 421
3:45 Mediated Reduction of Aryl Bromides at Tin Cathodes - E. G. Gunderson, E. Kariv-Miller, and V. Svetlicic 422
4:15 Fluoride Ion Promoted Anodic Substitution. Regioselective Anodic Alkoxylation of Sulfides - T. Fuchigami, H. Yano, A. Konno, and T. Nonaka 423

ELECTROCHEMISTRY OF HIGH TEMPERATURE SUPERCONDUCTORS

Physical Electrochemistry

C. Lieber, Chairman; J. T. McDevitt, Vice-Chairman
Room 26, 2nd Level

9:00 Introductory remarks
9:15 Progress in Observing Electrochemical Processes at Superconducting Electrode/Molecular Solvent Interfaces - S. R. Peck, L. S. Curtin, L. M. F. Tender, J. N. Richardson, and R. W. Murray 434
9:55 Low Temperature Electrochemistry on High T_c Superconductors - W. J. Lorenz, G. Saemann-Ischenko, and M. W. Breiter 435
10:35 Fifteen-minute intermission
10:50 Corrosion Reactivities of Various Copper Oxide and Fullerene High Temperature Superconductor Phases - J. T. McDevitt, D. R. Riley, J.-P. Zhou, A. Manthiram, and D. Jurbergs 436
11:30 Electrochemical Rate Data of Superconductor Materials and Their Lithium Insertion Compounds as Electrodes - N. A. Fleischer and J. Manassen 437

J. T. McDevitt, Chairman; C. Lieber, Vice-Chairman

2:00 The Surface Structure and Electronic States of High-Tc Superconductors by STM - C. M. Lieber and Z. Zhang 438
2:40 Physical and Chemical Characterization of Electrodeposited Superconducting Bismuthates - M. L. Norton and H.-Y. Tang 439
3:20 Fifteen-minute intermission
3:35 Synthesis of Superconducting Films via an Electrochemical Pathway - A. Weston, N. Ali, and S. B. Lalvani 440
3:55 Superconductor Oxide Films via an Electrodeposition Process - R. N. Bhattacharya, P. A. Parilla, and R. D. Blaugher 441

FULLERENES: CHEMISTRY, PHYSICS AND NEW DIRECTIONS

Physical Electrochemistry/Dielectric Science and Technology/Electronics

W. Goddard, III, Chairman; C. Reed, Vice-Chairman
St. Louis Ballroom C, 4th Level

9:00 The program and abstracts will be published in the April issue of the *Journal* and included in the program booklet distributed at the Meeting.

M. Parinello, Chairman; F. Wudl, Vice-Chairman

2:00 The program and abstracts will be published in the April issue of the *Journal* and included in the program booklet distributed at the Meeting.

B. Bell, Chairman; J. Cioslowski, Vice-Chairman
Poster Session

7:00 The program and abstracts will be published in the April issue of the *Journal* and included in the program booklet distributed at the Meeting.

EIGHTH INTERNATIONAL SYMPOSIUM ON MOLTEN SALTS

Physical Electrochemistry/High Temperature Materials

G. Blomgren, Chairman; R. Carlin, Vice-Chairman
St. Louis Ballroom B, 4th Level

9:00 The Nature of Proton in Ambient-Temperature Chloroaluminate Molten Salts - R. A. Osteryoung and P. C. Trulove 511
9:30 The Chemistry of Proton in Ambient-Temperature Chloroaluminate Molten Salts - P. C. Trulove and R. A. Osteryoung 512
9:50 Ionic Equilibria in Ambient Temperature Molten Salts - J. L. E. Campbell and K. E. Johnson 513
10:10 Dual Spin Probe NMR Relaxation Studies of Microdynamics in Chloroaluminate Melts - W. R. Carper, C. E. Keller, P. A. Shaw, M. Parrish, and J. S. Wilkes 514
10:30 Ten-minute intermission
10:40 NMR Measurements in Solutions of Dialylimidazolium Haloaluminates - S. Takahashi, J. Rathke, and M.-L. Saboungi 515
11:00 The Electrochemistry of Aluminum and Protons in Room Temperature Chloroaluminate Molten Salts Buffered with Sodium Chloride - T. L. Riechel and J. S. Wilkes 516
11:20 Reduction Potentials for Lithium and Sodium in Ambient-Temperature Chloroaluminate Molten Salts - R. T. Carlin and C. Scordilis-Kelley 517
11:40 Physico-Chemical Behavior and Liquid Crystalline Properties of Molten Alkali Metal Alkanoates - T. A. Mirnaya and S. V. Volkov 518

R. Carlin, Chairman; G. Blomgren, Vice-Chairman

2:00 Low Temperature Molten Salt Electrolytes Based on Quaternary Alkylphosphonium Salts - G. E. Blomgren and S. D. Jones 519
2:20 New, Stable, Ambient-Temperature Molten Salts - E. I. Cooper and E. J. M. O'Sullivan 520
2:40 Mixed Chloroborate and Chloroaluminate Room Temperature Melts - R. J. Gale and J. Liu 521
3:00 Electrochemistry of 9,10-Anthraquinone in the Presence of Proton and Tetrachloroaluminate in Ambient Temperature Molten Salts - M. T. Carter and R. A. Osteryoung 522
3:20 Electrochemical Reduction of Aromatic Ketones in a Room Temperature Molten Salt - G. T. Cheek 523
3:40 Ten-minute intermission

WEDNESDAY CONTINUED

3:50 Studies on Characteristics of Room Temperature Molten Salts $AlCl_3$-1-butylpyridinium Chloride - N. Koura, K. Ueda, and K. Takeishi 524

4:10 Electrodeposition of Metals from Room-Temperature Chloroaluminate Molten Salts - I. Xu and C. L. Hussey 525

4:30 Electrodeposition of Palladium onto Electrodes from Acidic, Neutral, Neutral-Buffered, and Basic MEIC-$AlCl_3$ Molten Salts - H. C. Delong and J. S. Wilkes 526

4:50 Nucleation and Morphology Studies of Aluminum Deposited from an Ambient-Temperature Chloroaluminate Molten Salt - R. T. Carlin, W. Crawford, T.-L. Liu, and M. Bersch 527

5:10 Ionic Conductivity, Thermodynamics and IR-Spectroscopy of Tetra-n-Pentylammonium Thiocyanate-Benzoic Acid System - A. M. Elias and M. E. Elias 528

R. J. Gale, Chairman; C. Hussey, Vice-Chairman
St. Louis Ballroom H, 4th Level

8:00 **MAX BREDIG AWARD ADDRESS:** Through the Years and Temperatures: Adventures in Molten Salt Land - R. A. Osteryoung 529

QUANTUM CONFINEMENT
New Technology Subcommittee/Electronics/Dielectric Science and Technology

R. Tsu, Chairman; E. Nicollian, Vice-Chairman
St. Louis Ballroom F, 4th Level

9:00 The program and abstracts will be published in the April issue of the *Journal* and included in the program booklet distributed at the Meeting.

E. Nicollian, Chairman; R. Tsu, Vice-Chairman

2:00 The program and abstracts will be published in the April issue of the *Journal* and included in the program booklet distributed at the Meeting.

MICROMACHINING AND MICROSTRUCTURES
New Technology Subcommittee/
Sensor/Electronics/Dielectric Science and Technology

J. N. Zemel, Chairman; P. W. Barth, Vice-Chairman
Room 29, 2nd Level

9:00 The program and abstracts will be published in the April issue of the *Journal* and included in the program booklet distributed at the Meeting.

P. W. Barth, Chairman; H. F. Gray, Vice-Chairman

2:00 The program and abstracts will be published in the April issue of the *Journal* and included in the program booklet distributed at the Meeting.

THURSDAY, MAY 21, 1992

GENERAL SESSION
Corrosion

B. R. MacDougall, Chairman; R. G. Kelly, Vice-Chairman
Room 46, 4th Level

9:00 Laser Initiated Corrosion Pits on Aluminum - D. Buzza and R. C. Alkire 41

9:25 The Characterization of Crevice Solution Chemistry during the Initiation Stage of Crevice Corrosion - B. K. Nash and R. G. Kelly 42

9:50 Stress Corrosion Behavior of TIG Welded 304 Stainless Steel - S.-H. Chen, T.-P. Cheng, and I.-J. Yang 43

10:15 Ten-minute intermission

10:25 Laser Raman Spectroelectrochemical Studies of Fe, Ni, Cr, and Their Glassy Metal Alloys with Phosphorus - M. Pankuch, C. A. Melendres, J. C. Kang, S. Lalvani, and Y. S. Li 44

10:50 Surface Analysis and Corrosion Studies of Iron-Based Metals in Para-Toluene Sulfonic Acids - M.-Y. Teng and I.-J. Yang 45

11:15 Film Thickness Effects on Flash-Rusting Measured by Spectrophotometry and Atomic Absorption - M. R. Van De Mark, E. Sianawati and N. Mason 46

11:40 The Analysis of Atmospheric Corrosion on Fe Particle Magnetic Tape - J. F. Dante and R. G. Kelly 47

J. A. Bardwell, Chairman; P. Kovacs, Vice-Chairman

2:00 Corrosion of Alloys in a Marine Environment under AC Conditions - M. A. Pagano, W.-W. Qiu, and S. B. Lalvani 48

2:25 A Model for the Evaluation of Electrochemical Impedance Spectra - P. Kovacs 49

2:50 Anodization of Copper in Ethylene Glycol-Water Mixture - A Study Using Microelectrode - J. Osteryoung and K. Wikiel 50

3:15 Fifteen-minute intermission

3:30 Polarization Characteristics of Ni and Inconel 600 in Aggressive and Inhibitive Acidic Media - A. A. Abd El-Fattah, E. M. Mabrouk, H. E. Megahid, and M. Abd-Allah 51

3:55 Corrosion of Mg and Its Alloy in Aqueous $Mg(ClO_4)_2$ Battery Electrolyte. A RDE Study - R. Udhayan and D. P. Bhatt 52

4:20 Ellipsometric Study on Inhibition Effect of Molybdate for Cooling Water - S. F. Xie, Y. R. Yang, and Z. Q. Huang 53

NINTH SYMPOSIUM ON PLASMA PROCESSING
Dielectric Science and Technology/Electronics

M. Engelhardt, Chairman; M. Sekine, Vice-Chairman
Promenade Ballroom C, 2nd Level

Aluminum/Alloy Etching (cont'd)

9:00 Pattern Density Effects on Corrosion of Aluminum Alloy/Refractory Metal Interconnects - C. Gabriel and R. Wallach 106

9:20 Dry Corrosion Control in Aluminum Etch Using O_2/NH_3 in Microwave Downstream Plasma - S. Mak and J. Hwang 107

9:40 Microcontamination Reduction and Corrosion Prevention for Aluminum Etch Through Loadlock Improvements - E. DeLaurentis and J. Hwang 108

10:00 RIE-Related Sidewall Voiding in Al-Cu Alloy Metallization for ICs - T. H. Daubenspeck and H. K. Lee 109

Tungsten Etching

10:20 Wafer Clamping Effects on Etchback of CVD Tungsten Films - L. Shen, L. Wilson, and Y. Chu 110

10:40 Mechanism of Residue Formation in Low Temperature Tungsten Interconnect Etch - U. C. Sridharan, D. Hartman, R. Wright, and M. Kent 111

11:00 A Kinetic Study of Reactive Ion Etching of Tungsten in SF_6/O_2 RF Plasmas - M.-C. Peignon, C. Cardinaud, and G. Turban 112

11:20 Optical Emission Studies of Etching Tungsten Silicide and Polysilicon Films - X. Y. Qian, D. J. Hemker, and G. W. Hills 113

THURSDAY CONTINUED

Dielectric Etching

11:40 Effect of Wafer-Average and Within-Die Polysilicon Pattern Density on Transistor Gate-Length Definition for Cell-Based ASIC CMOS Designs - D. Dimitrelis, M. Carneiro, and V. Dunton 114

D. E. Ibbotson, Chairman; J. D. Chapple-Sokol, Vice-Chairman

Dielectric Etching (cont'd)

2:00 Reactor Characterization for a Process to Etch Si_3N_4 Formed on Thin SiO_2 - P. E. Riley, J. C. Sum, and D. Figueredo 115

2:20 A Sub-Half Micron Deep UV Integrated Arc Process - T. Ta, K. Reinhardt, P. Westerfield, S. Sethi, E. Capsuto, J. Kochan, R. Fuller, and A. White 116

2:40 Photoresist Swelling in Hydrogen-Containing Freon Plasmas - Y. Kuo 117

3:00 Comparison of Nonline of Sight Resist Ashing Using Microwave or Radio Frequency Plasma Generation - J. I. McOmber, J. T. Davies, J. Howden, M. Wright, and K. Saul 118

3:20 Analytical Study on the Mechanism of High Dose Ion Implanted Photoresist Ashing in a True Downstream Plasma - X. C. Mu 119

3:40 Selective Etching of Bilayer Photoresist Using Multipolar Electron Cyclotron Resonance Source - S. W. Pang, K. T. Sung, and K. K. Ko 120

PECVD

4:00 Plasma CVD of a-SiC:H for X-Ray Mask Membranes Using a Helical Resonator Discharge - A. D. Johnson, D. E. Ibbotson, and J. A. Mucha 121

4:40 Composition and Stability of Plasma-Deposited Fluorinated Silicon Nitride Thin Films - R. Costantino, C. Marinensi, G. Tigani, and A. Zanobi 122

5:00 Modeling and Simulation of Plasma Enhanced Chemical Vapor Deposition of Silicon Nitride - M. Mazhar IslamRaja, A J. Bariya, J. P. McVittie, M. A. Cappelli, K. C. Saraswat, L. Moberly, and R. Lahri 123

FIFTH INTERNATIONAL SYMPOSIUM ON SILICON-ON-INSULATOR TECHNOLOGY AND DEVICES

Electronics/Dielectric Science and Technology

K. Izumi, Chairman; S. Cristoloveanu, Vice-Chairman
Promenade Ballroom E, 2nd Level

Materials Quality

8:50 Introductory remarks

9:00 Dislocation-Free SIMOX Substrates - A. Yoshino 185

9:40 Effects of High Temperature Anneal Variables on SIMOX Films - K. A. Joyner, M. K. El-Ghor, H. H. Hosack, and A. K. Rai 186

10:00 The Effects of HCl in SIMOX Annealing: A Time Series Experiment - K. A. Joyner and G. A. Brown 187

10:20 Fifteen-minute intermission

10:35 Post-Oxygen-Implant Anneal Effects on SOI Transistor Electrical Characteristics - G. V. Rouse, R. D. Cherne, and W. A. Krull 188

10:55 A High-Quality SIMOX Wafer and Its Application to Ultrathin-Film MOSFETs - S. Nakashima, Y. Omura, and K. Izumi 189

11:15 The Effects of Dose and Target Temperature on the Low Energy (70 keV) SIMOX Layers - Y. Li, J. A. Kilner, R. J. Chater, P. L. F. Hemment, A. Nejim, A. K. Robinson, K. J. Reeson, C. D. Marsh, and G. R. Booker 190

11:35 Etch-Stop Layer in Silicon Produced by Implantation of Electrically Inactive Impurities - Q.-Y. Tong, G. Cha, H.-M. You, U. Gosele, and D. Feijoo 191

S. Cristoloveanu, Chairman; K. Izumi, Vice-Chairman

Materials

2:00 SIMOX: An Efficient Etch-Stop to Fabricate Silicon Membranes with Well-Defined Thickness - H. Gassel, H. G. Dura, W. Mokwa, and H. Vogt 192

2:20 Reactive Ion Etching of SOI (ZMR and SIMOX) Silicon in $CF_4 + O_2$ and $SF_6 + O_2$ Plasmas - O. W. Purbo, C. R. Selvakumar, and D. Misra 193

2:40 Gettering of Bonded SOI Layers - H.-D. Chiou, F. Secco d'Aragona, and E. Strickland 194

3:00 50 nm Thick SOI Fabrication by Advanced ELO: Tunnel Epitaxy - A. Ogura, A. Furuya, and R. Koh 195

SECOND SYMPOSIUM ON THE PHYSICS AND CHEMISTRY OF SiO_2 AND THE Si-SiO_2 INTERFACE

Electronics/Dielectric Science and Technology

E. H. Poindexter, Chairman; N. S Saks, Vice-Chairman
Promenade Ballroom F, 2nd Level

Defects and Hot Carrier Induced Damage in Si-SiO_2 Systems I

8:45 Generation of Telegraph Noise via Single Interfacial Defects - M. J. Uren and D. H. Cobden 253

9:15 Single Electron Transfer from the Channel in Sub-μm MOSFETs to an Individual Interface Trap - M. Schulz and A. Pappas 254

9:45 ^{17}O Hyperfine Study of the P_b Center - J. H. Stathis, S. Rigo, and I. Trimaille 255

10:15 The Influence of Crystal Orientation and Processing Conditions on the Energy Distribution of Traps at the Si-SiO_2 Films Interface - C. H. Bjorkman, Y. Ma, T. Yasuda, and G. Lucovsky 256

10:35 Ten-minute intermission

M. Schulz, Chairman; M. A. Stroscio, Vice-Chairman

Defects and Hot Carrier Induced Damage in Si-SiO_2 Systems II

10:45 Charge Trapping and Degradation of Thin Dielectric Layers - M. M. Heyns, A. v. Schwerin, S. Verhaverbeke, and A. Kelleher 257

11:15 Charging and Discharging Properties of Electron Traps Created by Hot-Carrier-Injections in Gate Oxide of n-MOSFET - D. Vuillaume 258

11:35 Optically Induced Nitrogen Dangling Bonds in Amorphous Silicon Nitride Thin Films - W. L. Warren, J. Kanicki, P. J. McWhorter, and E. H. Poindexter 259

M. Heyns, Chairman; D. J. DiMaria, Vice-Chairman

Radiation and Hydrogen Induced Effects in Si-SiO_2 Systems

1:30 Impact Ionization and Positive Charges in SiO_2 - D. J. DiMaria, D. Arnold, and E. Cartier 260

2:00 Hot-Electron Dynamics in SiO_2 Studied by Photon-Induced Electron Transmission Through Thin Films - E. Cartier, E. A. Eklund, D. Arnold, D. J. DiMaria, and F. R. McFeely 261

2:20 Constant Current Stress Breakdown in Ultra Thin SiO_2 Films - T. Kubota, D. Apte, and K. Saraswat 262

2:40 Ten-minute intermission

2:50 Radiation-Induced Interface Traps in MOS Devices - N. S. Saks and D. B. Brown 263

3:20 Hydrogen Related E' Centers and Positive Charge in Irradiated Oxide Films - M. E. Zvanut, R. E. Stahlbush, W. E. Carlos, and H. L. Hughes 264

3:40 Molecular Orbital Studies of Oxygen-Related Hole Traps and of Their Interactions with Hydrogen Atoms and Molecules - A. H. Edwards 265

4:00 Removal of Traps in Process-Damaged MOS Structures by Room-Temperature Hydrogenation - S. Kar 266

4:20 Hot-Electron Induced Hydrogen Redistribution in SiO_2 - D. A. Buchanan, A. Marwick, L. Dori, and D. J. DiMaria 267

4:40 H_2 Cracking in Irradiated MOSFETs and H^+ Formation - R. E. Stahlbush and A. H. Edwards 268

THURSDAY CONTINUED

STATE-OF-THE-ART PROGRAM ON COMPOUND SEMICONDUCTORS XVI

Electronics/Dielectric Science and Technology

T. Kamijoh, Chairman; D. N. Buckley, Vice-Chairman

Room 43, 4th Level

9:00 The program and abstracts will be published in the April issue of the *Journal* and included in the program booklet distributed at the Meeting.

A. Katz, Chairman; G. Valco, Vice-Chairman

2:00 The program and abstracts will be published in the April issue of the *Journal* and included in the program booklet distributed at the Meeting.

JOINT RECENT NEWS PAPER SESSION

Electronics/Dielectric Science and Technology

L. K White, Chairman; D. Bailey, Vice-Chairman
Promenade Ballroom A, 2nd Level

9:00 The Joint Recent News Paper Program will be sent to all members of the Electronics and Dielectric Science and Technology Divisions in April. Copies of the Recent News Paper abstracts will be available at the Session.

D. Bailey, Chairman; L. K. White, Vice-Chairman

2:00 The Joint Recent News Paper Program will be sent to all members of the Electronics and Dielectric Science and Technology Divisions in April. Copies of the Recent News Paper abstracts will be available at the Session.

ELECTROCHEMISTRY IN MINERAL AND METAL PROCESSING III

Industrial Electrolysis and Electrochemical Engineering

P. E. Richardson, Chairman; T. J. O'Keefe, Vice-Chairman
St. Louis Ballroom A, 4th Level

8:45 A Comparative EIS Study on Cermet and Platinum Anodes for the Electrolyic Production of Aluminum - C. F. Windisch, Jr. 395

9:15 Solid Metal Reductive Stripping of Cerium from Tri-n-Butyl Phosphate - T. J. O'Keefe and J. D. Dillon III 396

9:45 The Electrochemical Behavior of Group V Elements during Copper Deposition - J. B. Hiskey and Y. Maeda 397

10:15 *Fifteen-minute intermission*

10:30 Mass Transport in High-Current-Density Zinc Electrowinning - K. J. Cathro 398

11:00 Full-Scale Hydrogen Diffusion Anodes for Immersed Tank Electrowinning and Electroplating - P. C. Foller, R. J. Allen, and R. Vora 399

11:30 Cathodic Reduction of Hg(II)-Cl(I) Complex on Ag-Hg Electrode - Q. Yin 400

ELECTRO-ORGANIC SYNTHESIS WITH HOMOGENEOUS AND HETEROGENEOUS CATALYSTS

Organic and Biological Electrochemistry

D. G. Peters, Chairman; J. E. Toomey, Jr., Vice-Chairman
Promenade Ballroom B, 2nd Level

9:00 Use of [2,2'-Ethylenebis(nitrilomethylidyne) diphenolato]nickelate(I) as a Homogeneous and Polymer-Based Catalyst for Reduction of Organic Halides - D. G. Peters, C. E. Dahm, and M. S. Mubarak 424

9:30 Long Life Anion Radicals from ArX or RX Type Compounds: Mediators, or Ar and R Providing Species? Case of Otho-Bis(alkylsulphonyl) Benzenes - J. Simonet 425

10:00 Conversion of - isoSafrole to Piperonal Using Electrolytically Recycled Higher Oxides of Manganese - J. Grimshaw and C. Hua 426

10:30 Fifteen-minute intermission

10:45 Mechanism of Electron Transfer Activation of Organic Substrates in the Presence of Organometallic Catalysts. Application to Homogeneous Catalysis under Reductive Conditions - A. Jutand, C. Amatore, and M. Nielsen 427

11:15 Electrochemistry of 9,9'-Spirobifluorene Derivatives: 2,2'-Diacetyl 9,9'-Spirobifluorene - L. Mattiello and L. Rampazzo 428

F. M. Hawkridge, Chairman; D. G. Peters, Vice-Chairman

2:00 A Study of Substituted Catechols as Electron Transfer Mediators in Electrocatalytic Enzyme Reactions - T. J. Moore and L. A. Coury 429

2:30 Electroreductive Cleavage of the C-Cl Bond of 9-Chlorofluorenes - F. Maran and E. Vianello 430

3:00 Fifteen-minute intermission

3:15 Electrochemical Behavior of Cytochrome c_3 Hildenborough on a Gold Electrode - B. A. Gorecka and G. S. Wilson 431

3:45 The Anodic Oxidation of Hydrazones - M. R. Van De Mark, E.-C. Lin, and W. Elderi 432

4:15 Pin Loosening in External Skeletal Fixation: *In Vivo* Electrochemical Impedance Study of the Pin Bone Interface - O. A. Velev, B. H. Palmer, S. Srinivasan, D. A. Hulse, H. W. Sampson, and W. H. Hyman 433

ELECTROCHEMISTRY OF HIGH TEMPERATURE SUPERCONDUCTORS

Physical Electrochemistry

M. Norton, Chairman; J. T. McDevitt, Vice-Chairman
Room 26, 2nd Level

9:00 Reactivity of Compound Superconductors: Cuprates, Bismuthates, Fullerides - B. Miller and J. M. Rosamilia 442

9:40 Controlled Room Temperature Formation of Weak Link or Josephson Junction in Thin Film $YBa_2Cu_3O_{7-x}$ - D. Cahen and Y. Scolnik 443

10:20 Fifteen-minute intermission

10:35 High Temperature Electrochemical Behavior of $YBa_2Co_3O_x$ Electrodes on Stabilized Zirconia Solid Electrolyte - T. M. Gur and R. A. Huggins 444

10:55 Electrochemical Response of $YBa_2Cu_3O_x$ as a Function of Oxygen Content - D. R. Riley and J. T. McDevitt 445

11:15 Application of High Temperature Electrochemical Techniques to $YBa_2Cu_3O_{7-\delta}$ - R. V. Kumar, D. J. Fray, J. E. Evetts, H. W. Williams, and A. Misson 446

FULLERENES: CHEMISTRY, PHYSICS AND NEW DIRECTIONS

Physical Electrochemistry/Dielectric Science and Technology/Electronics

L. Chiang, Chairman; D. Bethune, Vice-Chairman
St. Louis Ballroom C, 4th Level

9:00 The program and abstracts will be published in the April issue of the *Journal* and included in the program booklet distributed at the Meeting.

S. Iijima, Chairman; C. Lieber, Vice-Chairman

2:00 The program and abstracts will be published in the April issue of the *Journal* and included in the program booklet distributed at the Meeting.

K. M. Kadish, Chairman; R. S. Ruoff, Vice-Chairman

7:00 Open Discussion/Late News

Abstracts

JOINT GENERAL SESSION

Battery/Energy Technology

1 Experimental Determination of the Transport Number of Water in Nafion 117® Membrane: *T. F. Fuller* and *J. Newman*, Lawrence Berkeley Laboratory, and Dept. of Chemical Engineering, University of California, Berkeley, California 94720

The transport number of water in Nafion® 117 membrane over a wide range of water contents is determined experimentally using a concentration cell. The transport number of water, the ratio t_o^m/z_m, is about 1.4 for a membrane equilibrated with saturated water vapor at 25°C, decreases slowly as the membrane is dehydrated, and falls sharply toward zero as the concentration of water approaches zero. The relationship between the transference number, the transport number, and the electroosmotic drag coefficient is presented, and their relevance to water-management in solid-polymer-electrolyte fuel cells is discussed. Results are compared with other data available in the literature and with the theoretical maximum.

2 High Utilization Gas Diffusion Electrodes for Proton Exchange Membrane Fuel Cells: *E. B. Anderson, E. J. Taylor, K. Donohue*, and *N. R. K. Vilambi*, PSI Technology Co., 20 New England Business Center, Andover, MA 01810

We are developing an electrochemical catalyzation (ECC) technique to prepare high utilization carbon supported platinum electrocatalysts for proton exchange membrane fuel cells (PEMFCs). We prepared anodes and cathodes containing ≤0.05 mg Pt/cm² and evaluated their performance in a single cell PEMFC. For the anodes, we observe equivalent performance as with unsupported platinum electrocatalyst and both anodes and cathodes exhibit improved mass and specific activities due to improved platinum utilization.

3 Temperature and Pressure Dependence of the Electrode Kinetics of Oxygen Reduction at the Platinum Microelectrode/Nafion Interface: *A. Parthasarathy*, Dept. of Chemistry, Colorado State University, Fort Collins, CO 80523, *S. Srinivasan* and *A. J. Appleby*, Center for Electrochemical Systems and Hydrogen Research, Texas A&M University, College Station, TX 77843-3402, *C. R. Martin*, Dept. of Chemistry, Colorado State University, Fort Collins, CO 80523

Electrode kinetics of oxygen reduction at the platinum/Nafion interface is important in solid polymer electrolyte fuel cell research. Investigations of the oxygen reduction reaction at a platinum microelectrode/Nafion interface were previously carried out at ambient conditions. Electrode kinetic parameters for oxygen reduction at fuel cell operating conditions are now necessary. From the temperature dependence study, activation energies for the oxygen reduction reaction were obtained. From the pressure dependence of electrode kinetics, the reaction order of oxygen was determined.

4 Spontaneous Hydrous Oxide Formation on Platinum and Its Relevance in Oxygen Gas Reduction: *L. D. Burke, J. K. Casey*, and *A. J. Morrissey*, Chemistry Dept., University College Cork, Cork, Ireland

It has been established from studies of the interaction of gaseous oxygen with platinum clusters that the finely divided metal oxidizes more readily than continuous platinum. A similar effect was reported recently for platinum in aqueous media. Oxygen gas reduction in acid solution at finely divided platinum surfaces, prepared by electrodeposition or wet chemical reduction (Pt on C) techniques, exhibits significant inhibition until the spontaneously formed incipient hydrous oxide species are reduced.

5 Effect of Platinum Loading on Proton Exchange Membrane Fuel Cell Performance: *A. C. Ferreira, S. Srinivasan*, and *A. J. Appleby*, Center for Electrochemical Systems and Hydrogen Research, Texas A&M University, College Station, TX 77843-3402

The objectives of this work are to attain high energy efficiencies and long lifetimes in PEMFC. Performances of proton exchange membrane fuel cell with porous gas diffusion electrodes containing Pt loadings 0.4-10 mg/cm² were investigated. Electrodes with 5 and 10 mg/cm² (unsupported) of Pt showed practically identical performance. The performance of the cell with 2.5 mg/cm² (unsupported Pt) of Pt is somewhat lower. Single cells with carbon supported platinum electrocatalysts (0.4 mg/cm², 20%) exhibited cell potentials 50-100 mV lower than in cells with unsupported Pt electrocatalysts at the same current densities.

6 The Hydrogen Diffusion Porous Electrode Catalyzed by Tungsten Carbide: *Z.-E. Lu,* A.-P. Huang, T.-G. Zhong*, and *G.-N. Fang*, Dept. of Chemistry, East China Institute of Chemical Technology, Shanghai (200237), China

In the weakly polarized region of the hydrogen diffusion electrode catalyzed by WC in HCl solution, the current varies linearly with the potential. The slopes in both the anodic and cathodic regions are equal. In the moderately polarized anodic region there are two Tafel lines with the latter slope doubling the former. The polarization curves of both regions are corelated by the factor r/i_oS^*, predicted by the plate-like model of thin layers, and verified in this experiment.

7 Optimization of Electrode Structure to Further Minimize the Platinum Loading in Proton Exchange Membrane Fuel Cells: *A. C. Ferreira, S. Srinivasan*, and *A. J. Appleby*, Center for Electrochemical Systems and Hydrogen Research, Texas A&M University, College Station, TX 77843-3402

One of the promising approaches to develop and commercialize proton exchange membrane fuel cell power sources for electric vehicles is to minimize the platinum loading. Previous work on this topic showed that the electrode structure is of vital importance to increase the platinum utilization. Improvements in the structure of porous gas diffusion electrodes are being made by optimizing the composition of the electrodes (supported electrocatalyst, Teflon and pore formers) and using the rolling method for the fabrication of fuel cell electrodes. Platinum loadings have been reduced from 0.4 mg/cm² (state-of-the-art) to 0.09 mg/cm² in this work. The fuel cell performances with this reduction demonstrate that the platinum requirements can be reduced from 2.0 to 0.6 g/kW. The cell has been operated at current densities, as high as in cells with high Pt loading electrodes, without mass transport problems.

8 A Thin Film Solid Oxide Fuel Cell Prepared Using Reactive DC Magnetron Sputtering: *Li.-S. Wang* and *S. A. Barnett*, Dept. of Materials Science and Engineering, Northwestern University, Evanston, IL 60208

The structure and properties of a thin film solid oxide fuel cell deposited using reactive magnetron sputtering has been studied. The thin film fuel cell is composed of a 20 μm thick yttria-stabilized zirconia (YSZ) thin film electrolyte, with 1 μm thick porous Ag-YSZ cermet cathode and Ni-YSZ anode. The open-circuit voltage on the H_2, H_2O (3%), Ni-YSZ|$(Y_2O_3)_{0.1}(ZrO_2)_{0.9}$|Ag-YSZ, air fuel cell was 0.84 V at 600°-800°C; the maximum output current density and power density were 140 mA/cm² and 30 mW/cm² at 750°C.

9 Effects of a Sputtered Film of Pt on Performance of Proton Exchange Membrane Fuel Cells: Electrode Kinetic and Morphological Characteristics: *S. Mukerjee, S. Srinivasan*, and *A. J. Appleby*, Center for Electrochemical Systems and Hydrogen Research, Texas A&M University, College Station, TX 77843-3402

Localization of Pt electrocatalyst as a sputtered thin film (50 Å) on supported electrocatalyst (20% Pt/C, 0.4 mg/cm² loading) have been known to exhibit higher performances as compared to supported electrodes with approximately the same Pt loading. This study compares the pressure and temperature effects on the electrode kinetics with and without the sputtered films. The results indicate lower pressure and temperature effects on performance of electrodes with sputtered films as compared to those without. The morphological changes of the electrodes with sputter deposition have also been examined by SEM/EDAX.

10 Mechanism of Mixed Fuel/Oxidant Solid-State Thin Film Fuel Cells: *B. M. Coffey, T. O. Poehler*, and *P. C. Searson*, Dept. of Materials Science, Johns Hopkins University, Baltimore, MD 21218

The fabrication and characterization of thin solid-state fuel cells has been investigated. These devices are of planar construction with a substrate mounted inner Pt electrode, separated from a porous outer Pt electrode by a solid electrolyte. Total cell thickness is less than 1 μm. A gaseous fuel/oxidant mixture is fed to the porous outer electrode. Potentials of up to 700 mV and low current densities have been obtained in operation with H_2/O_2. Reference electrodes have been incorporated into experimental cells to study potential changes at the inner/outer electrodes, as a function of gas partial pressures, with the objective of elucidating the mechanism by which they operate.

11 New Aspects in the Development of Proton Exchange Membrane Electrolyzers: *K. Ledjeff, F. Mahlendorf*, and *A. Heinzel*, Fraunhofer-Institute for Solar Energy Systems, Oltmannsstrasse 22, W-7800 Freiburg, Germany

For solar energy systems, long term energy storage with a high efficiency is required. Hydrogen is a suitable energy carrier and its generation by water electrolysis is a well-established technique. Electrolyzers based on proton exchange membranes are known for their high energy density, good efficiency, and long term performance. We present results of a 500 W pressure electrolyzer (max. 15 bar). In lab-scale electrolysis cells maximum currents of 15 A/cm² have been realized. These advanced electrodes increase the flexibility substantially. Low installed power can cope with peak currents as supplied by solar cells or wind turbines, due to its excellent overload capabilities.

12 Calorimetric Concentration and Mass Flow Monitor for Gas Phase Ozone: *P. C. Foller*, 2000 Commonwealth Ave., Unit 1110, Boston, MA 02135

An inexpensive calorimetric ozone mass flow and concentration sensor has been developed using catalyzed platinum resistance thermometer elements. A heated element is compared with an unheated reference to yield flow rate, and a catalyzed element is compared to a reference to yield concentration. Stored calibrations are indexed based on flow rate, and then concentration is de-

---

***An asterisk by a name indicates which author will present the paper.**

THURSDAY CONTINUED

EIGHTH INTERNATIONAL SYMPOSIUM ON MOLTEN SALTS
Physical Electrochemistry/High Temperature Materials

H. Kojima, Chairman; J. R. Selman, Vice-Chairman
St. Louis Ballroom B, 4th Level

9:00 Synthesis of Molybdenum-Doped Alkaline Metal *Vanadium Bronzes* by Molten Salts Electrolysis - Y. Kaneko, H. Ishikawa, and H. Kojima 530
9:20 Electrodeposition of Molybdenum and Molybdenum Carbide Coatings from Oxide-Based Molten Salts - J. R. Selman, B. Aladjov, and D. Topor 531
9:40 A Novel Pulsating Current Technique Used in the Study of Platinum and Molybdenum Electrodes in Molten Silicates, Borates, and Phosphates - J. K. Higgins 532
10:00 Anodic Reaction on Nickel in a Molten CsF-NH_4F-HF System - A. Tasaka, K. Mizuno, K. Miki, A. Kamata, H. Teruta, W. Sato, and K. Yanagawa 533
10:20 Ten-minute intermission
10:30 Electrochemical Formation of Thin Carbon Film from Molten Chloride System - Y. Ito, T. Shimada, and H. Kawamura 534
10:50 Melting Behavior for Powder/Hydrated Melt($CaCl_2$.nH_2O n:6.00, 7.35) Coexisting Systems - S. Deki, M. Mizuhata, A. Kajinami, and Y. Kanaji 535
11:10 Transference Numbers in Molten Fluorides by an Operationally Defined EMF-Method - T. Forland, S. K. Ratkje, and H. Rajabu 536
11:30 Thermodynamics of Li_2O-LiF-CaF_2 Melts - S. T. G. Sampath Kumar, A. Narayan, and R. G. Reddy 537

J. R. Selman, Chairman; H. Kojima, Vice-Chairman

2:00 Predominance Area Diagram of Niobium Species in Molten LiCl+KCl Eutectic - G. S. Picard and P. Bocage 538
2:20 Thermogravimetric Study of the 800°C Reaction of Zirconia Stabilizing Oxides with SO_3-$NaVO_3$ - R. L. Jones 539
2:40 Electroanalytical Study of the Reduction of K_2WCl_6 in Molten LiCl-KC1 Eutectic - C. A. C. Sequeira 540
3:00 Electrochemical Behavior of Tantalum in Halide Melts - E. Polyakov and L. Polyakova 541
3:20 Ten-minute intermission
3:30 Models of Alumina Dissolution in Cryolite - R. G. Haverkamp, B. J. Welch, and J. B. Metson 542
3:50 The Effects of pH and Temperature on the Structure and Properties of Molten Sn(2+) Dicarboxylates - T. A. Ibidapo 543

MICROMACHINING AND MICROSTRUCTURES
New Technology Subcommittee/
Sensor/Electronics/Dielectric Science and Technology

H. F. Gray, Chairman; J. N. Zemel, Vice-Chairman
Room 29, 2nd Level

9:00 The program and abstracts will be published in the April issue of the *Journal* and included in the program booklet distributed at the Meeting.

J. N. Zemel, Chairman; P. W. Barth, Vice-Chairman

2:00 The program and abstracts will be published in the April issue of the *Journal* and included in the program booklet distributed at the Meeting.

FRIDAY, MAY 22, 1992

NINTH SYMPOSIUM ON PLASMA PROCESSING
Dielectric Science and Technology/Electronics

J. P. McVittie, Chairman; G. S. Mathad, Vice-Chairman
Promenade Ballroom C, 2nd Level

PECVD (cont'd)

9:00 Characterization of PECVD Nitride Films Used in VLSI Applications - A. K. Stamper, S. L. Pennington, and G. Bazan 124
9:20 Deposition of Silicon Nitride Films by ECR-Enhanced CVD - J. D. Chapple-Sokol and D. E. Kotecki 125
9:40 *Plasma Deposition and Characterization of Fluorinated* Silicon Nitride - S. V. Nguyen, D. Dobuzinsky, R. Gleason, and M. Gibson 126
10:00 Modeling of PECVD TEOS Oxide Step Coverage Using an Overhang Structure - C. Chang, J. P. McVittie, and K. C. Saraswat 127
10:20 Low Temperature Deposition of SiO_2 by DECR-PECVD - B. Agius 128
10:40 Effects of RF Frequencies and Deposition Rates on the Moisture Resistance of PECVD TEOS-Based Oxide Films - S. A. Robles, M. Galiano, and B. C. Nguyen 129
11:00 Formation of High Quality Tantalum Thin Films on SiO_2 by Dual-Frequency-Excitation Plasma Process - H. Wakamatsu, S. Aoyama, J. Watanabe, N. Konishi, and T. Ohmi 130
11:20 Control of Stress, Stability, and Mechanical Properties of PECVD Dielectric Films for GaAs and Si Applications - T. H. Wu, L. A. Schneggenburger, B. van Schravendijk, B. Sparks, A. S. Harrus, and D. G. Hemmes 131
11:40 Formation and Characterization of Zirconia Films by Plasma-Enhanced Chemical Vapor Deposition - C. C. Chen, M. M. Nasrallah, H. U. Anderson, and W. J. James 132

FULLERENES: CHEMISTRY, PHYSICS AND NEW DIRECTIONS
Physical Electrochemistry/Dielectric Science and Technology/Electronics

S. Saito, Chairman; D. Lorents, Vice-Chairman
St. Louis Ballroom C, 4th Level

9:00 The program and abstracts will be published in the April issue of the *Journal* and included in the program booklet distributed at the Meeting.

M. Schluter, Chairman; H. N. Shinohara, Vice-Chairman

2:00 The program and abstracts will be published in the April issue of the *Journal* and included in the program booklet distributed at the Meeting.

termined via the resistance of the catalyzed PRT. Use is forecast in multiple remote sensing reporting to a central display, a task not readily accomplished with conventional ultraviolet spectrophotometric technology.

13 SPEFC Development at the Centre for Electrochemical and Energy Research, SPIC Science Foundation: *S. Parthasarathy,* Contribution from the Centre for Electrochemical & Energy Research, SPIC Science Foundation, Madras 600032, India

SPEFC development has been initiated at SPIC Science Foundation, as SPEFC is an ideal candidate for transportation for a number of reasons. This paper describes the work in progress since 1989 in collaboration with CESHR, Texas A&M University. Considerable progress has been made in reducing platinum loading and optimizing the process for fabrication of electrodes. The results of characterization of electrodes using cyclic voltammetry and assessment of platinum utilization are correlated with electrode performance. Hydrogen Storage Laboratory setup at the Centre, is briefly described.

14 A Model for the Deliverable Capacity of the TiS_2 Electrode in a Li/TiS_2 Cell: *Z. Mao* and *R. E. White,* Center for Electrochemical Engineering, Dept. of Chemical Engineering, Texas A&M University, College Station, Texas 77843-3122

The mathematical model for porous TiS_2 electrodes developed by West *et al.* has been reformulated for galvanostatic discharge mode and has been extended to include the effect of the electrolyte in the separator. It has been shown that use of a thinner separator would result in a considerable increase in the deliverable capacity of the electrode. In order to predict realistically the performance of the electrode as a function of design parameters, it is shown that the effect of the electrolyte in the separator should be included in the mathematical analysis.

15 The Rechargeable Li_xTiS_2/$LiAlCl_4$/$Li_{1-x}CoO_2$ Solid-State Cell: *W. K. Behl* and *E. J. Plichta,* U.S. Army Electronics Technology and Devices Laboratory, Fort Monmouth, NJ 07703-5601, *D. Vujic, H. S. W. Wang,* and *D. M. Schleich,* Polytechnic University, Brooklyn, NY 11201

An all solid-state cell employing lithium tetrachloroaluminate ($LiAlCl_4$) as the lithium ion conducting solid electrolyte and using lithium intercalating compounds, titanium disulfide (TiS_2) and lithium cobalt (III) oxide ($LiCoO_2$), as the electroactive materials in the "rocking chair" configuration is described. The cell was operated at 100°C and exhibited an open circuit potential of 2.1 V in the charged state. The cell showed excellent discharge characteristics at current densities up to 0.1 mA/cm² and also showed no significant loss of capacity over one hundred charge-discharge cycles.

16 Electrochemical Properties of Polyaniline and Substituted Derivatives: *P. V. Madsen, T. O. Poehler, J. Gopal, D. O. Cowan,* and *P. C. Searson,* Dept. of Materials Science and Engineering, Johns Hopkins University, Baltimore, MD 21218

Polymerization and characterization of polyaniline and substituted derivates are described. The thickness of the polymer is studied in relation to the polymerization conditions. The charge capacity from the current-potential curves of each polymer is found in different solutions and shows linear relationship to the thickness of the polymer over a wide range of thicknesses. The chemical structure of these polymers has been determined from XPS-data.

17 Investigations on a Novel Zn/KOH/DDH Primary Cell System: *R. Udhayan, D. P. Bhatt,* and *P. B. Mathur,* Central Electrochemical Research Institute, Karaikudi-623 006, India

The work described in this paper relates to the studies on a novel alkaline primary cell involving N,N'-dichlorodimethyl-hydantoin (DDH) as a cathodic depolarizer and the commercial zinc as an anodic material. The novelty of the system lies in the fact that the organic cathode material employed in this investigation possesses nontoxic property and the zinc cell system, reported here, in conjunction with DDH shows high energy density of 212 Wh(kg of DDH)$^{-1}$ at the higher operating voltage of ~2.0 V. Workable current density of this system is reported up to the figure of 13 mA cm^{-2}.

18 Low Temperature Removal of Hydrogen Sulfide from Sour Gas and Its Utilization for Hydrogen and Sulfur Production: *K. M. Petrov, S. Srinivasan,* and *A. J. Appleby,* Center for Electrochemical Systems and Hydrogen Research, Texas A&M University, College Station, TX 77843-3402

The anodic oxidation of sulfide ions, formed by scrubbing H_2S with sodium hydroxide and adjusting the pH of anolyte with more NaOH to a pH of nearly 14 produced polysulfide ions. In this cell the catholyte was pure NaOH, and the cathodic product was hydrogen. The sodium polysulfide was transferred to a separate chamber through which H_2S, with or without CO_2, was passed. Crystalline sulfure is produced. The filtrate is mixed with the solution obtained by hydrogen sulfide scrubbing and returned to the electrolytic cell. Hydrogen and sulfur with high purity are produced at low cell voltage (E_{cell} = 1 V) and at a high current density (i = 300 mA/cm²). This investigation demonstrates that the process can be made continuous.

DIRECT ELECTROCHEMICAL OXIDATION OF METHANOL AND SMALL ORGANIC MOLECULES

Battery/Energy Technology/Physical Electrochemistry

19 Direct Electro-Oxidation of Methanol in Acid Medium at Modified Electrodes with Low Precious Metal Loadings: *J.-M. Léger, G. Méli,* and *C. Lamy,* Laboratoire de Chimie 1, Electrochimie et Interactions, URA CNRS No. 350, Université de Poitiers, 86022 Poitiers, France

The direct electro-oxidation of methanol in acid medium is an attractive way to develop fuel cells. For practical applications, the metal loading must be decreased and the electrocatalytic activity increased. Modified electrodes, using ionomer membranes with low platinum loadings, display much less poisoning than bulk electrode. By adding a second metal (ruthenium or tin), the potential of methanol oxidation shifts negatively. The performances are hugely enhanced by feeding methanol from the gaseous phase.

20 The Influence of Surface Acid-base Properties of Pt/C Catalysts on the Electrochemical Oxidation of Methanol: *A. S. Arico, V. Antonucci,* and *N. Giordano,* Institute CNR-TAE, 98126 S. Lucia Messina, Italy, *P. A. Simonov,* Institute of Catalysis, Novosibirsk 630090, U.S.S.R., *P. L. Antonucci,* University of Reggio Calabria, Faculty of Engineering, 89100 Reggio Calabria, Italy

Pt supported carbon black catalysts have been investigated by surface adsorption measurements and cyclic voltammetry in sulfuric acid and methanol. The peak potential of Pt oxide reduction showed a volcano-shaped correlation as a function of the pH_{zpc} with a maximum at about pH_{zpc} = 6. The methanol oxidation process showed higher overpotentials for catalysts having extreme pH_{zpc} values. This behavior may be interpreted in terms of different metal-support interactions.

21 Carbon Supported Platinum Alloy Catalysts for Methanol Oxidation: *M. Gauthier, A. Gelb, E. B. Anderson,* and *E. J. Taylor,* PSI Technology Co., 20 New England Business Ctr., Andover, MA 01810

We are investigating carbon supported platinum alloy electrocatalysts for methanol oxidation. The alloy electrocatalysts were selected from the binary systems Pt-Au and Pt-Ru and from the ternary system Pt-Au-Ru. We are preparing the electrocatalysts using both chemical and electrochemical techniques and are characterizing the alloys using TEM and XRD. We report the electrochemical activity for methanol oxidation as a function of alloy composition and chemical *vs.* electrochemical preparation.

22 Methanol Oxidation on NiTi: *R. Manoharan* and *J. B. Goodenough,* Center for Materials Science and Engineering, University of Texas, Austin, TX 78712-1084

The 50-50 NiTi ordered alloy, which is stable in acid, was chosen as an initial candidate in a search for platinum-free alloy electrodes for the methanol-oxidation reaction (MOR). We report observation of the MOR on this alloy; it appears to proceed at surface O^{2-}-ions of a passivating Ni-Ti oxyhydroxide film. Electron transfer from the film surface to the electrode is argued to occur via a Ni^{3+2+} redox band in the passivating layer.

23 The Effect of Specific Adsorption of Anions and Cations on the Kinetics of Methanol Electro-Oxidation on Pt Single Crystal Surfaces: *N. Ross* and *N. Markovic,* Materials Sciences Div., Lawrence Berkeley Laboratory, University of California, Berkeley, CA 94720

The kinetics of the electrochemical oxidation of methanol on Pt(111) and Pt(100) single crystal electrodes were studied in acid and alkaline electrolytes containing small quantities of various ions, both cations and anions, which interact to varying extent with the Pt surface. The Pt surfaces were prepared in open hydrogen-air flame and in UHV, and characterized by LEED and AES before transfer to the electrochemical cell via a differentially pumped manifold. Specifically adsorbing anions like bisulfate and chloride and cation like cesium have a strongly negative effect on the kinetics. The maximum in reaction rate in acid electrolytes (NHE) is shown to be due to the formation of a critical coverage of adsorbed anions, and not due to the formation of "Pt oxide" as previously supposed. The maximum in reaction rate in the alkaline electrolyte containing cesium is observed in the region where Cs is incorporated in the "Pt OH" layer which, surprisingly has an inhibiting rather than a catalitic effect on methanol oxidation.

24 Oxidation of Methanol on Single Crystal Platinum Electrodes in Sodium Hydroxide and Sodium Carbonate Solutions: *R. Adžić, N. Marinković, A. Tripković,* and *N. Marković,* Institute of Electrochemistry, University of Belgrade, Njegoševa 12, Belgrade, Yugoslavia

Oxidation of methanol on platinum in sodium hydroxide and sodium carbonate solutions has a pronounced dependence on the crystallographic orientation of the electrode surface, contrary to some reports in the literature. The rates of reaction are considerably higher than in acid solutions. The (111) oriented surface, due to the least poisoning, shows the highest current peak, but the onset of the reaction is at least negative potentials for the (110) surface. Different Tafel slopes, obtained from slow sweeps, were found for Pt(111) (120 mV/dec) and Pt(100) (60 mV/dec). Stepped surfaces, vicinal to Pt(111) cause a shift of the onset of the oxida-

tion of methanol to more negative potentials, but decrease of the current peak. Vicinals of Pt(100) cause increase of the current peak, without effect on the onset of the reaction.

25 Partial Oxidation of Methane on $YBa_2Cu_3O_x$ Electrodes in a High Temperature Solid-State Electrochemical Cell: *T. M. Gür*, Center for Materials Research, Stanford, CA 94305-4045, *H. Wise* and *R. A. Huggins*, Depart. of Materials Science and Engineering, Stanford University, Stanford, CA 94305-2205

Because of the wide oxygen nonstoichiometry and fast diffusion rate of oxide ions exhibited by the mixed-conducting $YBa_2Cu_3O_x$, its potential as an oxidation catalyst for methane was examined. For this purpose, a solid-state electrochemical reactor was employed, in which a $YBa_2Cu_3O_x$ electrode was deposited on a yttria-stabilized zirconia (YSZ) solid electrolyte. A porous platinum electrode was used as the counterelectrode in contact with air. Oxygen needed for the oxidation of methane was electrochemically pumped through the YSZ solid electrolyte from the air side onto the $YBa_2Cu_3O_x$ electrode in contact with methane. Under electrochemically controlled conditions, the partial oxidation of methane to carbon monoxide and methanol was achieved.

26 Methanol Oxidation on Platinum-Tin Catalysts Dispersed on Poly(3-methyl)thiophene Conducting Polymer: *S. Swathirajan* and Y. M. Mikhail*, Physical Chemistry Dept., RCEL, General Motors Research Laboratories, Warren, MI 48090-9055

Platinum-tin catalysts were electrodeposited on poly(3-methyl)thiophene, to investigate the effect of Pt loading and the catalyst deposition conditions on the electrochemical oxidation of methanol. The Pt-Sn catalyst deposited in the hydrogen adsorption potential region showed a higher surface area. Rutherford backscattering spectrometric studies enabled an estimation of the thickness and the distribution of the catalyst layer in the conducting polymer support. Methanol oxidation currents were negligible at catalyst loadings less than 60 $\mu g/cm^2$.

27 Methanol Oxidation on Novel Conductive Polymeric Porphyrins: *D. MacArthur, E. Kubaszewski, J. Fish*, and *T. Malinski*, Dept. of Chemistry, Oakland University, Rochester, MI 48309-4401

The characterization and catalytic oxidation of methanol on several novel polymeric conductive porphyrins with uridine, pyridinium, paracyclophane, and 3-methoxy-4-hydroxy substituents are described. Free base and zinc, cobalt, nickel, iron, manganese, and ruthenium metalated porphyrins were investigated. Oxidation of methanol in acidic and basic media was studied. A significant shift of potential and a high steady current density was observed for methanol oxidation for several of these polymeric porphyrins.

28 Nafion Supported Catalysts for the Electrochemical Oxidation of Methanol in Acid Media: *A. Kowalak*, Dept. of Chemistry, University of Mass-Lowell, Lowell, MA 01854, *W. O'Grady*, and *D. Rolison*, Code 6170, Naval Research Laboratory, Washington, DC 20375

We have studied the electrochemical oxidation of methanol in sulfuric acid and trifluoromethanesulfonic acid (TFMSA). The electrode catalysts used were mixtures of Pt-carbon particles (Prototech Co.) in Nafion supported on a glassy carbon disk. Data were taken at room temperature and 60°C with 1*M* CH_3OH in H_2SO_4 or TFMSA of various concentrations. The Prototech in H_2SO_4 shows lower activity as the concentration of sulfuric acid is increased. TFMSA results show greater activity than sulfuric acid.

29 *In Situ* FTIR Characterization of Electrocatalysts for the Oxidation of Methanol: *W. Vielstich, T. Iwasita, F. C. Nart*, and *B. Lopez*, Institute for Physical Chemistry, University of Bonn, D-5300 Bonn 1, Germany

In-Situ FTIR spectra have been taken from smooth noble metal catalysts, suitable for methanol oxidation in acid solutions. Starting with 1*M* methanol solution and using a procedure to obtain absolute bands, besides linear-, bridge- and multi-bonded CO, for the first time a band due to adsorbed COH is observed. An 81:15 Pt-Ru alloy shows a much weaker signal of the CO poison than platinum. CO_2-formation starts already below 300 mV RHE. At the same CO coverage the IR absorption frequency is shifted to higher wave numbers for active catalysts. In this sense, ternary Pt-metal combinations showed the best performance. Current-potential plots for finely divided metal on carbon are given. At 70°C, 150 mA/cm^2 are obtained already below +400 mV.

30 Adsorption and Electro-Oxidative Pathways for Small Organic Molecules on Gold and Transition-Metal-Coated Gold Electrodes as Probed by Real-Time Surface-Enhanced Raman Spectroscopy: *Y. Zhang* and *M. J. Weaver*, Dept. of Chemistry, Purdue University, West Lafayette, IN 47907

The adsorption and electro-oxidation of methanol, formic acid as well as carbon monoxide have been studied on gold, platinum-, rhodium-, and ruthenium- coated gold electrodes by means of real-time surface-enhanced Raman scattering (SERS). The charge coupled device (CCD) detector used now makes it feasible to characterize and study adsorbed reactive intermediates produced during a voltammetric potential excursion. New insights have been gained regarding the interfacial reaction pathways followed by the archetypically important electrocatalytic processes.

31 Variable Angle *In Situ* FTIR Reflectance Spectroscopy of High Surface Area Electrodes: A New Method for Studying Electrocatalytic Systems: *P. W. Faguy*, Dept. of Chemistry, University of Louisville, Louisville, KY 40292

A new method for the infrared investigation of electrocatalytic reactions on high-surface area electrodes is described. Variable angle reflectance spectroscopy provides a tool for separating the various attenuation and scattering components associated with the reflection of infrared light from a high-surface area electrode under potential control. The potential dependent distribution of the products of the direct oxidation of methanol on Pt-carbon electrodes is measured, *in situ*, using this technique.

32 *In Situ* Infrared and Electrochemical Studies of the Oxidation of Ethylene on Single Crystal and Polycrystalline Platinum Electrodes: *Q. Zhao* and *E. B. Yeager*, Case Center for Electrochemical Sciences and Dept. of Chemistry, Case Western Reserve University, Cleveland, OH 44106

The adsorption and electro-oxidation of ethylene at different temperatures have been investigated on polycrystalline platinum with *in situ* FTIR and linear sweep voltammetry. Linearly adsorbed carbon monoxide was detected as the main adsorbed species. A small amount of bridged carbon monoxide was also detected at more negative potentials. Raising the temperature enhanced the oxidation kinetics and C—C bond rupture of ethylene adsorbed on the electrode surface. The oxidation kinetics have also been examined on the low-index surfaces of single crystal platinum and found to be surface structure dependent.

33 Applications of Real-Time Infrared Spectroscopy to Electrocatalysis at Bimetallic Surfaces: Electro-Oxidation of Ethylene Glycol on Bismuth-Modified Pt(111): *X. Jiang* and *M. J. Weaver*, Dept. of Chemistry, Purdue University, West Lafayette, IN 47907

The influence of predosed bismuth upon the electro-oxidation of ethylene glycol on Pt(111) in 0.1*M* perchloric acid is examined by means of voltammetry combined with real-time infrared spectroscopy. It was found that two major oxidation products, oxalic acid and carbon dioxide, are formed via distinct reaction pathways. The predosed bismuth adatoms significantly alter the selectivity of the model electrocatalyst in that the production of carbon dioxide increases monotonically with the bismuth coverage at the expense of the oxalic acid yield.

34 Potential Step and NMR Investigation of the Oxidation and Adsorption of Methanol on Platinum Surfaces: *A. Wieckowski, K. Franaszczuk, P. Slezak, C. K. Rhee*, and *P. Zelenay*, Dept. of Chemistry, University of Illinois, Urbana, IL 61801

The rate of methanol oxidation on smooth, polycrystalline Pt and on oriented surfaces was investigated. A complex pulse sequence for the pretreatment of the platinum surface was applied to seek an initially clean substrate. The effect of isotopic substitution was examined. It was found that the electrochemical step alone is not rate determining in methanol oxidation process. The initial adsorption step should be taken into consideration. Multiple methanol-derived CO bonding to a polycrystalline platinum electrode was detected in *in situ* NMR experiments with external control of the electrode potential.

35 XAS Studies of UPD Metal/Pt Electrocatalysts: *J. McBreen*, Dept. of Applied Science, Brookhaven National Laboratory, Upton, NY 11973

X-ray absorption spectroscopy (XAS) results were obtained for both the UPD Cu and UPD Sn on carbon supported Pt in 0.5*M* H_2SO_4. Spectra were recorded at the respective K edges of the UPD species and at the L_3 edge of the Pt. In the case of UPD Cu the adsorbed species is in the Cu^{+1} state and there is a partial charge transfer to the Pt. UPD Sn is associated with labile oxygen, which varies reversibly with potential. The UPD Sn displaces adsorbed sulfate species and has no effect on the electronic structure of the Pt.

36 Premonolayer Formation of Active Oxides and the Role of the Latter in the Oxidation of Small Organic Molecules: *L. D. Burke, D. T. Buckley*, and *J. K. Casey*, Chemistry Dept., University College Cork, Cork, Ireland

The oxidation of methanol at low potentials on platinum in aqueous media is inhibited due to formation of deactivating species, *e.g.*, CO_{ads}. The improved performance of certain alloys, *e.g.*, Pt/Ru, is due to the provision of active oxide species (by the second component in the mixture) that promote conversion of CO_{ads} to CO_2. Evidence for the formation of active oxides on platinum at unusually low potentials, and their role in electrocatalytic oxidations, are presented.

37 Direct Methanol Fuel Cells with Aqueous Carbonate Electrolytes: *E. J. Cairns, F. R. McLarnon*, and *B. R. Rauhe*, Lawrence Berkeley Laboratory, Berkeley, CA 94720

In a study of the effects of electrode macrostructure on the performance of the direct methanol fuel cell anode, the authors found that concentrated Cs_2CO_3 worked well as an intermediate-temperature (100°-140°C) electrolyte. A Pt/Ru on graphitized carbon catalyst exhibited much higher catalytic activity in this electrolyte than platinum alone; overpotential was reduced approximately 300 mV at 10 mA/cm^2 in 72 w/o Cs_2CO_3. Results indicate incomplete utilization of catalyst sites due to poor wetting. Present efforts are focused on modifying Teflon content and pore characteristics to increase accessibility of the catalyst.

38 A Methanol-Aqueous Carbonate Fuel Cell: *J. A. Kosek, S. Sarangapani,* and *J. Giner,* Giner, Inc., Waltham, MA 02154

Methanol adsorption on Pt, measured by H_2 displacement in 1*M* K_2CO_3, over a bulk methanol concentration range of 0.01-1.0*M*, yielded a bell-shaped potential dependence. Tafel plots show that methanol oxidation in carbonate has better kinetics than in an acid electrolyte. Complete methanol-oxygen aqueous carbonate fuel cell testing yielded iR-corrected performance of up to 570 mV at 150 mA/cm^2. The absence of any long-term poisoning effects was demonstrated.

39 Direct Electrochemical Oxidation of Methanol Vapor on Au-PEM Electrode: *A. S. Lin* and *W. E. O'Grady,* Naval Research Laboratory, Washington, DC 20375

The study of gold as a catalyst on proton exchange membrane has demonstrated the enhancement for direct electrochemical oxidation of methanol. A vapor deposited gold thin film on Nafion was used as electrode to study the methanol vapor reaction. An Astris QUICKCELL® unit was used in the gas fed configuration. Oxidation current occurs near the potential of Au oxide growth region. The result suggests that the active sites on gold surface are not deactivated by the strongly adsorbed intermediates.

40 Methanol Electro-Oxidation: Problems, Progress, and Prospects: *S. Mukerjee, S. Srinivasan,* and *A. J. Appleby,* Center for Electrochemical Systems and Hydrogen Research, Texas A&M University, College Station, TX 77843-3402

The development of high performance direct methanol air fuel cells is of vital importance for defense and civilian applications. In order to achieve the performance levels of indirect methanol reformer fuel cells (power densities >200 mW/cm^2), the challenging problems are to find electrocatalysts which have high electrocatalytic activities and which are not poisoned by the intermediates. Recently, significant advances have been made with bifunctional electrocatalysts utilizing platinum or platinum-ruthenium along with refractory metal oxides (Zr, Ta, Mo). The metal or the alloy (Pt or Pt/Ru) functions as the electrocatalyst, while the latter serve as promoters for methanol oxidation. Furthermore, amorphous metallic alloys (Pt with Pd, Zr or Mo) have been found to be more stable than crystalline counterparts and exhibit higher catalytic activities. Here too the catalysts are bifunctional, by, providing active O or OH sites for oxidation of intermediates during methanol oxidation. Prospects for applications of these electrocatalysts at the electrode/solid polymer electrolyte interfaces are encouraging because in perfluorosulfonic acids an increased activity for methanol oxidation has been demonstrated. An alternative approach is to use the fluorinated aids as additives to phosphoric acid and operate the cells at about 200°C.

GENERAL SESSION

Corrosion

41 Laser Initiated Corrosion Pits on Aluminum: *D. Buzza* and *R. Alkire,* Dept. of Chemical Engineering, University of Illinois, Urbana, IL 61801

A focused laser beam was used to initiate corrosion pits on 99.999% pure aluminum immersed in 1M NaCl, pH 11 solution and held under potentiostatic control. The shape of the pits as measured by a post-electrolysis 3-D SEM method was compared with the measured net anodic current. In order to investigate the shape evolution of a group of pits, the laser initiation technique was adapted to initiate ordered arrays of pits.

42 The Characterization of Crevice Solution Chemistry during the Initiation Stage of Crevice Corrosion: *B. K. Nash* and *R. G. Kelly,* Center for Electrochemical Science and Engineering, Dept. of Materials Science, University of Virginia, Charlottesville, VA 22903

This work is concerned with identifying the mechanism of crevice corrosion initiation in 304 stainless steel. It has been suggested that acidification of the crevice solution by chromium hydrolysis is not the mechanism responsible for initiation, but that exceeding a critical chloride and thiosulfate concentration is the condition leading to depassivation. Through the use of ion chromatography, this study will quantitatively determine the crevice concentrations of sulfur species and transition metals present in actual 304 SS crevice solutions during the initiation period. The results will allow an assessment of the critical crevice solution which develops prior to initiation of crevice corrosion in 304 stainless steel.

43 Stress Corrosion Behavior of TIG Welded 304 Stainless Steel: *S.-H. Chen,* T. P. Cheng,* and *I.-J. Yang,* Materials Research Laboratories, Chutung, Hsinchu, Taiwan, China

The sulfide stress corrosion cracking (SSCC) of TIG welded 304 stainless steel was studied by slow strain rate test (SSRT) in NACE solutions. The microhardness test of welded specimen showed that a lower hardness region was obtained in the heat affected zone (HAZ) in comparison with those in fusion zone and base metal. The failure time of the welded specimen decreased with the increase of H_2S concentration. Failure was found at the border, which had a maximum hardness value of 190 Hv, of the heat affected zone and the fusion zone for all specimens studied.

44 Laser Raman Spectroelectrochemical Studies of Fe, Ni, Cr, and Their Glassy Metal Alloys with Phosphorus: *M. Pankuch* and *C. A. Melendres,* Argonne National Laboratory, Materials Science and Chemical Technology Div., Argonne, IL 60439-4837, *J. C. Kang* and *S. Lalvani,* Dept. of Mechanical Engineering and Energy Processes, Southern Illinois University Carbondale, IL 62901, *Y. S. Li,* Dept. of Chemistry, Memphis State University, Memphis, TN 38152

The spectroelectrochemical behavior of Fe, Ni, and Cr was studied in 0.15*M* NACl solution and compared with their glassy metal alloys with phosphorus. While a significant alteration in the corrosion and anodic dissolution behavior of the metals is observed on alloying, the composition of the surface films formed appears to be essentially the same. $Fe(OH)_2$, Fe_3O_4, and FeOOH were found on the Fe surface and Cr_2O_3 on the Cr. No evidence of phosphate incorporation into the films was observed.

45 Surface Analysis and Corrosion Studies of Iron-Based Metals in Para-Toluene Sulfonic Acids: *M.-Y. Teng** and *I.-J. Yang,* Materials Research Laboratories, Chutung, Hsinchu, Taiwan, China

Potentiodynamic and surface analysis techniques were performed to evaluate the corrosion properties of metals in para-toluene sulfonic acids. A typical polarization curve showed the active, passive, and transpassive regions were observed, with the exception of the electrochemical behavior of pure iron. The passive current densities were substantially reduced when Fe alloyed with Cr or/and Ni due to the enrichment of Cr content in the passive films. Surprisingly, the critical current densities of pure Fe decreased with increasing of PTSA and a pseudo-passive range was observed.

46 Film Thickness Effects on Flash-Rusting Measured by Spectrophotometry and Atomic Absorption: *M. R. Van De Mark,* E. Sianawati,* and *N. Mason,* Dept. of Chemistry University of Missouri-Rolla, Rolla, MO 65401

The use of latex paint on ferrous substrates usually results in the formation of corrosion products denoted as flash rusting. This paper entails further evaluation of spectral reflectance measurements as a new method of qualification of flash rusting. The spectral method is compared to atomic absorption analysis and used to study latex paint thickness effects on corrosion. Correlations are also made with respect to the coatings adhesion. Both uninhibited and post added inhibited coatings were used.

47 The Analysis of Atmospheric Corrosion on Fe Particle Mag netic Tape: *J. F. Dante* and *R. G. Kelly,* Center for Electrochemical Sciences and Engineering, Dept. of Materials Science and Engineering, University of Virginia, Charlottesville, VA 22903

The degradation of metal particle magnetic recording tape during atmospheric exposure has been studied. Corrosion rates were measured using a quartz crystal microbalance (QCM). The composition of the adsorbed electrolyte layer has been analyzed using ion chromatography. The effects of relative humidity, temperature, pollutant gas type (SO_2, NO_2, and Cl_2) and concentrations were investigated. The individual contributions of the degradation of the various components of the tape on the degradation of performance are presented and discussed.

48 Corrosion of Alloys in a Marine Environment under AC Conditions: *M. A. Pagano, W.-W. Qiu,* and *S. B. Lalvani,* College of Engineering and Technology, Southern Illinois University, Carbondale, IL 62901

Sinusoidal alternating voltage (AV) was used to study the effects of periodic fields on the corrosion of 1018 carbon steel and 90/10 Cu/Ni in simulated seawater. Experimental data show that under the influence of AV, the corrosion rate of carbon steel increases with applied peak voltage then decreases in the range 100-600 mV. Increasing the voltage above 600 mV results in an exponential increase in corrosion rate. For 90/10 Cu/Ni, the corrosion rate increases monotonically with applied voltage (0-1500 mV). To help understand this phenomena, other types of experimental analysis were performed: (*i*) potentiodynamic polarization, (*ii*) characterization of corroded specimens with SEM and EDS, and (*iii*) computer modeling of the corrosion system based on dc polarization results. Additional effects of frequency and rectification of signals are also determined and discussed.

49 A Model for the Evaluation of Electrochemical Impedance Spectra: *P. Kovacs,* Orthopaedic Research Dept., Smith & Nephew Richards, Inc., Memphis, TN 38116

As the evaluation of electrochemical impedance spectra is model-dependent, there is a need for general models that can be applied to a variety of systems and have the necessary physical meaning, too. Employing only circuit elements that can be related directly to single physical processes, a model is proposed in this paper, and its general applicability is demonstrated by a number of examples. The model, which takes into account the presence of diffusion zones with and without electrochemical reactions, seems to be very useful for the evaluation of the electrochemical impedance spectra of both active and passive metals and alloys. The interpretation of the results on extremely corrosion resistant materials like surgical implant alloys may also become less difficult, despite the more complex nature of the spectra.

50 Anodization of Copper in Ethylene Glycol-Water Mixture. A Study Using Microelectrode: *J. Osteryoung,* and *K. Wikiel,* Dept. of Chemistry, SUNY at Buffalo, Buffalo NY 14214

Anodization of copper ultramicroelectrode in 50% ethylene glycol-water mixture in the presence of chloride ions was studied by means of normal and reverse pulse voltammetry, and constant potential step methods. Anodic behavior of copper in the presence of chloride ions in ethylene glycol-water solution does not basically differ from the behavior in pure chloride ion-water system. The product of anodic dissolution of copper, in solutions containing more than 0.05*M* chloride ion, is the soluble dichlorocomplex of monovalent Cu, provided that the oxidation overpotential is not very high and the potential is not applied to the electrode for a long time (milliseconds time scale). The analysis of the plot of potential shift *vs.* log chloride concentration gives the coordination number of copper chlorocomplex as 2 and the stability constant of $CuCl_2^-$ complex, in ethylene glycol-water mixture, as $\log \beta_2 = 5.6$.

51 Polarization Characteristics of Ni and Inconel 600 in Aggressive and Inhibitive Acidic Media: *A. A. Abd El-Fattah, E. M. Mabrouk, H. E. Megahid,* and *M. Ahd-Allah,* Chemistry Dept., Faculty of Science, Zagazig University, Benha, Egypt

The pitting corrosion potential of nickel and Inconel 600 varies with the concentration of Cl^- ions according to a segmoidal S. shaped curves. These curves were explained on the basis of formation of passivatable, active, and continuously propagated pits depending on the range of Cl^- ion concentration. Addition of the sodium salts of chromate, tungstate, molybdate, phosphate dibasic, and carbonate shifts the pitting potential of the electrode samples to noble direction denoting increased resistance of pitting attack.

52 Corrosion of Mg and Its alloy in Aqueous $Mg(ClO_4)_2$ Battery Electrolyte-A RDE Study: *R. Udhavan* and *D. P. Bhatt,* Central Electrochemical Research Institute, Karaikudi-623 006, India

This paper reports the first results pertaining to the corrosion aspects of magnesium and its AZ 31 alloy in aqueous $Mg(ClO_4)_2$ battery electrolyte employing a versatile RDE technique. From the current-potential profiles, the pitting potential regions, kinetic currents, etc., have been determined, and the results have been discussed in terms of the film formation and the convective diffusion controlled mechanisms. Interestingly, the mechanism of the dissolution process has been found uniform at all the chosen potentials which is considered as an important criteria from the viewpoint of battery application.

53 Ellipsometric Study on Inhibition Effect of Molybdate for Cooling Water: *S. F. Xie, Y. R. Yang,* and *Z. Q. Huang,* Dept. of Applied Chemistry, Chongqing University Chongqing, 630044, China

In consideration that it is difficult to obtain information about processes through the electrochemical method, this paper describes the investigation of the inhibition effect of cooling water through the ellipsometric technique. The optical constant, thickness of film, and coverage are calculated from Δ, Ψ measured. The inhibition mechanism is also discussed in detail.

CATHODIC PROTECTION SYSTEMS

Corrosion/Industrial Electrolysis and Electrochemical Engineering

54 Influence of Al_3Fe Intermetallic Inclusions on Depassivation of Al-6061 Alloys: *C.-H. Paik* and *R. C. Alkire,* Dept. of Chemical Engineering and Materials Research Laboratory, University of Illinois, Urbana, IL 61801

Pitting of aluminum alloy (Al-6061-T6) in 0.1*M* NaCl begins at the edges of Al_3Fe inclusions, where, due to the facility of oxygen reduction on the inclusions, the local pH can reach high values and cause depassivation of the adjacent Al phase. To simulate the localized corrosion, sectioned electrodes have been fabricated consisting of Al_3Fe (diameter 10 ~100 μm) embedded in the center of and insulated from an Al disk. The pH distribution around an artificial Al_3Fe inclusion was monitored by using a tungsten pH microsensor (tip diameter < 1 μm). The pH sensed 0.25 mm above an Al_3Fe electrode, was found to increase to 12.

55 Oxygen Reduction on Steel in Basic Aqueous Sol[illegible] with Relevance to Disbonding of Coatings from Ca[illegible]lically Protected Steel: *D. Gervasio* and *J. H. Payer,* Dept. of Material Science and Engineering, Case Western Reserve University, Cleveland, Ohio 44106-7204

The mechanism of oxygen reduction on cathodically protected steel is being examined as an important part of a project to develop an improved model for the cathodic disbonding of protective coatings. Buried steel pipelines are protected from corrosion by a combination of an insulating coating and cathodic polarization. The electrochemical and chemical processes accompanying cathodic protection can lead to a loss of adhesion between the steel and the protective coating, *i.e.*, cathodic disbonding. Oxygen reduction was examined using a rotating ring disk electrode (RRDE). At 400 rpm, oxygen reduction occurred between -0.2 and -1.2 V *vs.* SCE on an ASTM A516 steel disk in aqueous borate buffer (pH = 9.8) with 1 atm oxygen over solution. The peroxide oxidation current on the Au ring was greatest when the disk potential was at -0.5 V and was on the order of several percent of the oxygen reduction current. Peroxide is chemically reactive and may adversely affect protective coatings on cathodically protected surfaces. The peroxide generation must be addressed in any mechanism for cathodic disbonding.

56 Formation of Calcareous Deposits on Cathodically Protected Steel in Seawater: *R. E. White, J.-F. Yan,* and *T. V. Nguyen,* Dept. of Chemical Engineering, Texas A&M University, College Station, TX 77843-3122 and *R. B. Griffin,* Dept. of Mechanical Engineering, Texas A&M University, College Station, TX 77843

Cathodic protection has been recognized as an effective method for protecting offshore structures from corroding. One feature associated with the marine cathodic protection is the formation of calcareous deposits on cathodically protected surfaces. These porous deposits, mostly $CaCO_3$ and $Mg(OH)_2$, reduce cathodic current requirements by decreasing the active surface area involved in cathodic reactions such as oxygen reduction and hydrogen evolution. A rotating disk electrode technique was used to grow calcareous deposits on low carbon steel in artificial seawater in the laboratory. Scanning electron microscopy was used to analyze the composition and morphology of the deposits. A mathematical model was also developed. The effects of rotation speed, electrode potential and seawater chemistry, such as pH and dissolved oxygen, are included in the model. The drop in current density with time predicted by the model agrees well with the experimental results.

57 Some Results of Cathodic Polarization Experiments: *M. de Lourdes, M. Magalhaes,* and *L. Sathler,* Lab. de Corrosao "Prof. Manoel de Castro" UFRJ, Rio de Janeiro, Brazil

Cathodic protection has been proving to be an effective method to reduce the corrosion of structures in marine environment. One consequence of protecting a metal structure in seawater by this method is the formation of calcareous deposits that usually modify the conditions for this protection. This paper is a contribution to the study of kinetics development in the surface of polarized steel in natural seawater.

58 Graded-Mesh and Adaptive-Mesh Finite Element Methods in Electrochemical Systems: *S. Crockett* and *W. H. Smyrl,* Corrosion Research Center, Dept. of Chemical Engineering and Materials Science, University of Minnesota, Minneapolis, MN 55455

Two approaches to generating meshes for use in finite element method solutions of the model equations for a corrosion system are presented. The first, a graded mesh, incorporates *a priori* knowledge of the behavior of the system into a fixed, nonuniform mesh which concentrates computing power in regions of high gradient. The second an adaptive mesh approach, simultaneously finds the solution of the model equations and modifies the mesh for a more accurate solution.

59 Cathodic Protection Design with Time-Dependent Boundary Conditions: *K. Nisancioglu,* Dept. of Chemistry, Laboratories of Industrial Electrochemistry, Norwegian Institute of Technology, N-7034 Trondheim, Norway, *P. O. Gartland,* SINTEF Corrosion Center, N-7034 Trondheim, Norway

A boundary element model is described for calculating current and potential distribution on a cathodically protected steel structure in seawater with time-dependent and nonlinear boundary conditions. The model takes into account the effect of steel surface morphology, the flow rate of seawater, and the deposition/dissolution of calcareous scale. The model is validated by predicting the potential-time behavior of an experimental offshore rig protected by sacrificial anodes. It is shown further that certain unusual current-time histories observed on cathodically protected structures can be rationalized.

60 Boundary Elements Applied to Dynamic Simulation of Cathodic Protection Systems: *J. A. F. Santiago, J. C. F. Telles, W. J. Mansur,* and *L. Sathler,* COPPE/Federal University of Rio de Janeiro, CEP 21945 Rio de Janeiro, Brazil

The present paper is concerned with the boundary element modeling of potential and current density distribution in cathodic protection systems. This phenomenon is governed by Laplace equation, subjected to nonlinear time-varying boundary conditions, relating potential and current density, described by dynamic polarization curves determined from potentiostatic experiments. Two solution methods are studied in order to simulate the dynamic polarization curves as time advances, namely, fictitious time and fictitious potential.

61 Numerical Simulation of a Wet Christmas Tree Cathodic Protection Sys[illegible] *J. C. F. Telles, W. J. Mansur, J. A. F. Santiago,* and *S. L. De[illegible]rue,* COPPE/Federal University of Rio de Janeiro, CEP 21945, Rio de Janeiro, Brazil, *W. Baptista,* CENPES/PETROBRAS, Ilha do Fundao, 21910 Rio de Janeiro, Brazil

Wet christmas trees are used to direct and block oil production. This equipment is safeguarded against corrosion by means of galvanic cathodic protection, used in association with organic coatings. The current needed to provide this cathodic protection, and consequently the number of anodes required, are at present calculated based on a coated submerged region and on a noncoated buried region. The parameters used, such as coating efficiency

and current flow to the buried region, are those found in the literature. With the purpose of ascertaining current distribution and electrochemical potential in the two regions, cathodic protection systems for wet x-trees were numerically analyzed through the PROCAT computer program, which is based on the boundary elements method.

NINTH SYMPOSIUM ON PLASMA PROCESSING

Dielectric Science and Technology/Electronics

62 Feature Scale Simulation of Oxide Plasma Etching: *J. P. McVittie, J. C. Rey,* and *M. M. IslamRaja,* Center for Integrated Circuits, Stanford University, Stanford, CA 94305-4070

This paper discusses the use of a profile simulator to help understand the mechanisms leading to experimentally observed profiles and the use of special experimental test structures to extract needed parameters for anisotropic oxide etching processes. The focus is on developing correct models for the mechanisms which control wall slopes and RIE lag effects in CHF_3 based oxide etching.

63 Use of Overhang Test Structure to Understand RIE Lag in Oxide Etching: *S.-I. Dohmae* and *J. P. McVittie,* Center for Integrated Systems, Stanford University, Stanford, CA 94305-4070

Overhang test structures which eliminate sidewall effects were used to study the mechanisms responsible for the RIE lag effect in CHF_3/O_2 oxide etching. RIE lag was observed in these structures and is not restricted to sidewall mechanisms. Bottom etch widths and the linear dependence of the etch rate on aspect ratio suggest that neutral transport controls the lag in these test structures.

64 Modeling of Plasma Etching Reactors Including Wafer Heating Effects: *D. J. Economou,* Dept. of Chemical Engineering, University of Houston, Houston, TX 77204-4792, *E. Aydil,* AT&T Bell Laboratories, Murray Hill, NJ 07974

A comprehensive model for chlorine etching of polysilicon has been developed including wafer heating effects. Spatiotemporal variations of atom density, etch rate, and wafer temperature were predicted. Wafer heating caused the etch rate to increase with time despite the fact that the etchant concentration decreased with time. Etch rate and uniformity were measured in real time using a multichannel laser interferometry technique. Measured etch rate transients were compared to model predictions. Results were found to be sensitive to wafer back-side cooling and the surface kinetics.

65 Optimally Uniform ECR Plasma Generation for Precise Patterning: *S. Samukawa,* VLSI Development Div., NEC Corp., 1120 Shimokuzawa Sagamihara, Kanagawa 229, Japan, *T. Nakamura,* Mechatronics Laboratory, NEC Corp., 4-1-1 Miyazaki Miyamae-ku, Kawasaki 213, Japan, *A. Ishitani,* VLSI Development Div., NEC Corp., 1120 Shimokuzawa Sagamihara, Kanagawa 229, Japan

The nonuniform magnetic field gradient around the ECR position and the parabolic 875 G magnetic field profiles cause the inclination of plasma generation. The ion flight directions are disturbed by the instability in the nonuniform plasma. Conversely, the uniform magnetic field gradient and flat magnetic field distribution result in optimally uniform ECR plasma generation. The uniform ECR plasma prevents microloading effects in subhalf-micron pattern fabrication.

66 Variation of Ion Energy and Ion Flux in Various Gas Plasmas with 13.56 MHz Cathode Coupled Parallel-Plate Plasma Equipment: *S. Hasaka, I. Natori, T. Yamashita,* and *T. Ohmi,* Dept. of Electronics, Faculty of Engineering, Tohoku University, Aza-Aoba, Aramaki, Aoba-ku, Sendai 980, Japan

In various gas plasmas, variation of important plasma parameters such as ion energy, ion flux, and plasma potential has been evaluated by measurement of the RF waveform applied to the RF electrode, which is the substrate surface, without any contamination and disturbance to the process. We have demonstrated that high performance plasma process of low ion energy and high ion flux can be achieved by low bond energy gases excited plasma.

67 Dependencies of Negative Ions from Pulsed Radio-Frequency Discharges: *L. J. Overzet, L. Luo,* and *Y. Lin,* University of Texas at Dallas, Richardson, TX 75083-0688

The negative ion spectra from pulsed RF discharges through etching gases have been measured by direct ion mass spectrometry and multiple negative ions were found in each gas mixture studied. The heavy mass negative ions in some discharges appear related to clustering with etching products. The signal intensity of small mass ions did not vary by a significant amount over long times; but, some large mass negative ions exhibited an "onset" time dependence of approximately 5 min. (This work was supported in part by the National Science Foundation ECS—9009662 and Texas Instruments Inc.)

68 Surface Studies of Reactive Ion Etching Processes in Silicon Technology: From Surface Damage to High-Resolution Depth Profiling: *G. S. Oehrlein,* IBM Res. Div., T.J. Watson Research Center, Yorktown Heights, NY 10598

In situ real-time ellipsometry coupled with comprehensive post-plasma surface analysis has been used to clarify selectivity and directionality mechanisms of dry etching processes of silicon-related materials. Examples of the insights which have been obtained are described. Combining reactive ion etching and ellipsometry also enables high-resolution depth profiling. The profiling of SiGe superlattice structures and ultrathin oxide-nitride-oxide (ONO) films are described.

69 Modeling and Investigation of RF Electrical Signals from Nitride Etch: *S. Watts Butler* and *K. Branker,* Texas Instruments Inc., Dallas, TX 75265

RF current, voltage, and phase data were collected on a nitride etcher. Analysis of the data proved that delivered power was not only a function of power supply setpoint, but also a function of pressure. Using data from the fundamental alone, a satisfactory model of the etch rate was formed. Based on comparison of the data with documented machine maintenance, it is apparent that phase and/or impedance at the harmonics can be used as a diagnostic tool.

70 *In Situ* Ellipsometry during Plasma Processing: *G. M. W. Kroesen,* Dept. of Physics, Eindhoven University of Technology, 5600 MB Eindhoven, The Netherlands, *G. S. Oehrlein,* IBM Research Div., Yorktown Heights, NY 10598, *W. Fukarek,* Dept. of Physics, EMA University, 0-2200 Greifswald, Germany, *J. W. H. G. den Boer,* Dept. of Physics, Eindhoven University of Technology, 5600 MB Eindhoven, The Netherlands

In situ monochromatic and spectroscopic ellipsometry is a very accurate and nonintrusive technique to study the modifications of a surface that is subject to plasma treatment. The paper focuses on three major applications: (*i*) measurement of surface temperatures by HeNe ellipsometry; (*ii*) depth profiling of optical parameters by RIE and HeNe ellipsometry; and (*iii*) study of surface modifications by IR spectroscopic ellipsometry.

71 Optical Emission Comparison of Oxygen and Oxygen/Nitrous Oxide Plasma Generated by Microwave and Radio Frequency Sources Between 80 and 800 nm: *J. I. McOmber, J. T. Davies, J. Howden,* and *E. M. Liston,* GaSonics/IPC, San Jose, CA 95134-1909

Emission spectra from 80 to 800 nm wavelength were used to identify species observed in a non-line of sight downstream asher as a function of the excitation plasma source, 13.56 MHz or 2.45 GHz. The emission spectra are used to explain the atomic, ionic, and molecular reactions and interactions in the plasma and downstream regions of interest to organic ashing. The excitation source has a major effect on the species generated, and thus the downstream ashing characteristics.

72 Plasma Diagnostics for the Etching of Silicon Nitride Thin Films Using Emission Spectroscopy and Multivariate Calibration: *G. Barna,* Texas Instruments, Inc., Dallas, TX 75265, *B. Wangmaneerat* and *T. M. Niemczyk,* Dept. of Chemistry, University of New Mexico, Albuquerque, NM 87131, *D. M. Haaland,* Sandia National Laboratory, Albuquerque, NM 87185

Emission spectroscopy combined with a multivariate calibration technique has been used for the diagnosis of a plasma during the etching of a silicon nitride thin film. A partial least squares algorithm was applied to the emission spectra data obtained in a 2s measurement made during each of the 31 etch experiments. The standard error of prediction from the cross-validated calibrations, used to determine the predictive capability of the calibration model, was about 10% of the mid-range of the five control parameters and the etch rate.

73 Reactive Ion Etch Process Parameter and Etch Rate Estimation Using Principal Component Analysis of Optical Emission Spectroscopy and Mass Spectrometry: *D. Angell,* IBM ASTC, EM1, East Fishkill, NY 12533, *R. Shadmehr,* Dept. of Brain and Cognitive Science, Massachusetts Institute of Technology, Cambridge, MA 02139, *P. B. Chou* and *G. S. Oehrlein,* IBM Research Div., T.J. Watson Research Center, Yorktown Heights, NY 10598

We report on a simple technique that enables estimation of process parameters and etch characteristics from optical emission or mass spectrum measurements. Through principal component analysis, we observe that 99% of the variance in the more than 1100 optical and mass spectra channels are accounted for by very few principal components of each sensor. These principal components, along with the measured dependent variables, are used to build empirical models for real-time monitoring or control of reactive ion etching. To date, both regression analysis and artificial neural networks have been employed. Examples that estimate chamber status, chamber contamination, etch rate, and leak detection are given.

74 Studies of the Reaction of NF_3/Ar and C_2F_6/O_2 Plasmas with Anodized Aluminum Surfaces Using X-Ray Photoelectron Spectroscopy: *J. G. Langan* and *B. S. Felker,* Air Products and Chemicals, Inc., Allentown, PA 18195

We have exposed a series of hard anodized aluminum coupons to NF_3/Ar and C_2F_6/O_2 plasmas under a variety of conditions. The samples were transferred *in vacuo* for XPS analysis. After plasma exposure, the surface shows a decrease in the amount of aluminum

oxide type bonding with a corresponding increase in aluminum fluoride or oxy-fluoride bonding for both source gases. The surfaces of the NF_3/Ar and C_2F_6/O_2 plasma exposed coupons show the same chemical species present; the major difference is increased fluorination of the NF_3 plasma exposed coupons.

75 Diffraction Laser Endpoint for Trench Etch Applications: *M. Birang* and *P. Ebbing*, Applied Materials, Santa Clara, CA 95054

Trench endpoint signal was achieved from small feature sizes on the wafer, 0.85 μm square in cross section and 8 μm deep. This paper talks about the interferometry and diffraction techniques, light dispersion and collection techniques, and signal processing techniques used to build the instrument. The analysis of the signals is shown and the theoretical and actual signals are compared. Then the experimental signals from the above features are shown, and the apparatus used to collect that signal is presented.

76 Diagnostics of an ECR Plasma Using the Langmuir Probes: *Y. Nakagawa, K. Ikeda*, and *T. Tsukada*, Anelva Corp., 5-8-1, Yotsuya, Fuchu-shi, Tokyo, 183 Japan

The plasma characteristics of an ECR plasma etching apparatus were measured by the Langmuir probe techniques for different discharge conditions. A new plasma parameter, plasma power, was defined as the ion transportation capability of a plasma. The properties of the ECR plasma were explained clearly employing this parameter. The plasma power at its maximum has obtained always near the ECR layer. The result of poly-Si etching was also discussed using this parameter.

77 Electrical Measurement of Etching Parameters in an Oxide RIE System: *S. I. Dohmae* and *J. P. McVittie*, Center for Integrated Systems, Stanford University, Stanford, CA 94305-4070

Etching parameters were measured electrically by simple diagnostic techniques in a SiO_2 RIE system and correlated with etching characteristics. The etch yield was found to be a linear function of the square root of the ion energy even in the conventional RIE chamber. This result indicates that more accurate control of etching could be done in commercially available etching systems by making more use of electrical discharge measurements.

78 Gate Oxide Break-down Phenomena in Magnetron Plasma: *M. Sekine, K. Horioka, H. Okano, Y. Matsunaga, T. Matsushita, K. Hishioka*, and *Y. Yoshida*, ULSI Research Center (2PG), Toshiba Corp., 1 Toshiba-cho, Saiwai-ku, Kawasaki 210, Japan

Gate oxide breakdown phenomena in a magnetron plasma were investigated from the view point of magnetic field distribution effect on the damage. It was found that having strong parallel and normal magnetic field regions simultaneously on a wafer induced surface potential difference along the wafer, and could cause oxide breakdown. An optimized magnetic field, consisting of flux lines parallel to the wafer, was verified to cause no degradation in the gate oxide.

79 Gate Edge Effects on Oxide Damage during Polycide Etching: *C. Gabriel*, VLSI Technology, Inc., San Jose, CA 95131

Gate oxide damage from plasma etching of MOS gate electrodes was studied. Three commercial etchers were compared, including a microwave ECR, an RF triode, and an RF diode. Oxide breakdown was measured on large capacitors with various configurations of gate area, gate edge, and isolation edge. From Poisson defect density calculations, most of the oxide damage correlates with the gate edge for gate lengths below about five microns. The defects will affect device reliability more than yield.

80 Spectroscopic Ellipsometry and Schottky Barrier Characterization of RIE Exposures of Thin Si-SiO_2 Structures Exposed to Poly-Si Overetch: *T. Gu, R. A. Ditizio, R. W. Collins*, and *S. J. Fonash*, Center for Electronic Materials and Processing, Pennsylvania State University, University Park, PA 16802, *J. F. Rembetski, M. A. Carlson*, and *P. Westerfield*, SEMATECH, Austin, TX 78741, *X.-C. Mu*, Intel Corp., Santa Clara, CA 95052

Schottky barrier current-voltage measurements have revealed the presence of substrate damage after exposures of thin oxide layers to reactive ion etches designed for poly-Si etching. The amount of damage, and the uniformity of this damage, increases as a function of the overetch exposure time. In this report, we correlate the observed changes in Schottky barrier current-voltage measurements with observations made by spectroscopic ellipsometry. Both techniques reveal the presence of the damage and the saturation of this substrate damage after long exposure times.

81 A Model for Thin Oxide Damage in Nonuniform Discharges: *S. Fang* and *J. P. McVittie*, Center for Integrated System, Stanford University, Stanford, CA 94305-4070

MOS gate oxides can be severely degraded by charge buildup during plasma processing, however, the mechanisms of this charge buildup and subsequent damage are not well understood. In this paper, we present a new model tc explain the role of discharge nonuniformity in this damage, and apply this model via SPICE circuit simulations, and probe and breakdown measurements to both uniform and nonuniform discharges. The model also explains the importance of device structures and the negligible dc bias on this damage.

82 Ion Bombardment Effects on Silicon Surface Properties in Plasma Etching: *G. S. Oehrlein, D. Vender*, and *Y. Zhang*, IBM Research Div., T.J. Watson Research Center, Yorktown Heights, NY 10598

The fluorinated, disordered silicon surface layer formed on the silicon substrate surface in RF diode and/or electron cyclotron resonance (ECR) plasmas fed with fluorine-based etching gases, *e.g.*, CF_4 or SF_6, has been studied using real-time ellipsometry and x-ray induced photoemission spectroscopy after sample transfer in vacuum for various processing conditions. A thin (≈0.5 nm) fluorinated layer is formed for conditions which minimize the ion bombardment of the Si substrate, *e.g.*, ECR processing without additional sample bias. The thickness of the fluorinated layer increases strongly with the sheath voltage at the substrate, but is relatively insensitive to variations of other processing parameters, *e.g.*, pressure. The implications of these findings for our understanding of ion induced etching reactions of silicon are discussed.

83 Reactive Ion Etch Induced Device Characteristics Changes in Thin Film Transistor: *Y. Kuo*, IBM Research Div., T.J. Watson Research Center, Yorktown Heights, NY 10598

We have detected some plasma damage on the inverted, trilayer TFT in a n^+ RIE process. The damage includes a positive V_{th} shift, a high off current, and the divergence of the I_D *vs.* V_G curves. The V_{th} shift increased with the gate dielectric SiN_x thickness and was lowered when half of the SiN_x layer was replaced by TaO_x. These damages were caused mostly by the plasma radiation and slightly by the cathode charge effect. Interfacial traps between a-Si:H and SiN_x were responsible for the anomalous TFT characteristics. This damage appeared to be physical and was easily repaired with a thermal annealing process.

84 Assessment of the Effects of Magnetic Field Strength and of Post-Etching Ozone Cleaning on Substrate Damage and Contamination in MERIE Contact Etching: *R. A. Ditizio, T. Gu, R. W. Collins, J. R. Ruzyllo*, and *S. J. Fonash*, Center for Electronic Materials and Processing, Pennsylvania State University, University Park, PA 16802, *H. J. Leary*, IBM East Fishkill, Hopewell Junction, NY 12533

Spectroscopic ellipsometry and Schottky barrier I-V measurements have been used to assess the lattice damage and residue layer formation produced by MERIE SiO_2 contract etching. In this study, blanket oxides (1000 Å) were exposed to a CHF_3/O_2 contact etching chemistry in an MERIE system under various magnetic field conditions. Samples were then assessed for damage/contamination effects both before and after UV ozone cleans. Our results show the dependence of the resulting residue layer thickness and damage layer thickness on magnetic field strength and on this surface treatment.

85 A Model of Particulates in Glow Discharge Plasmas: *D. B. Graves, M. G. Kilgore, J. E. Daugherty*, and *R. K. Porteous*, Dept. of Chemical Engineering, University of California, Berkeley, CA 94720

Particulates that form in glow discharge plasmas are charged negatively and are often suspended in the plasma by electrostatic forces. It has been observed that dust tends to segregate to certain locations in the discharge. In order to minimize particulate contamination during processing, it is important to understand the nature of the forces particles experience in plasmas. We have constructed a model of particles in plasmas to understand particle segregation in glow discharges.

86 Detection and Control of Particle Contamination in Production Plasma Equipment: *G. S. Selwyn*, IBM T.J. Watson Research Center, Yorktown Heights, NY 10598, *E. F. Patterson*, IBM East Fishkill, Hopewall Junction, NY 12533, *K. L. Haller*, IBM General Technology Div., Essex Junction, VT 05452

Particle contamination is a serious concern in all microelectronics fabrication lines. Tools and processes contribute the greatest share of contamination, especially plasma process tools. This work demonstrates the nature of particle contamination in plasma tools with emphasis on production plasma equipment during normal process conditions. Particle behavior and trapping effects are demonstrated in sputter and PECVD tools, as well as enhanced plasma tools such as magnetron RIE and ECR. The use of grooved electrode design for contamination control is also discussed.

87 Trapped Contamination Particulates in an RF Processing Plasma: *R. N. Carlile* and *S. G. Geha*, Univ. of Arizona, Tucson, AZ 85721

The levitated regions containing high density contamination particulates in RF processing plasmas are investigated in this paper. Using a tuned Langmuir probe in an RF sputter plasma, the plasma potential, electron density, and electron temperature of these regions (or traps) are measured, accompanied by a real-time video record of the dynamics of the particulates. A scenario of trap formation is presented in which we postulate that a trap is system generated and that particulates subsequently flow into a trap and distort its boundaries in such a way that the particulates eventually leak into a pump port.

88 Particle Contamination on Silicon Wafers Etched in RF Plasmas: *M. M. Smadi*, IBM East Fishkill Facility, Hopewall Junction, NY 12533, *G. Y. Kong*, Motorola Inc., Austin, TX 78728, *R. N. Carlile* and *S. E. Beck*, ECE Dept., University of Arizona, Tucson, AZ 85721

Particle contamination and etch depth on silicon wafers etched in SF_6/Ar and CF_4/O_2/Ar plasmas are examined as a function of 13.56 MHz RF power, 100 kHz power, pressure, flow rate, and etch time. Particle deposition and etch depth have a linear dependence on 13.56 MHz RF power, 100 kHz power, and etch time. Also, the particle deposition and etch depth have quadratic dependence on process gas flow rate. In the pressure range explored, particle deposition on the wafers is independent of pressure.

89 Plasma and Surface Diagnostics of ECR Hydrogen Cleaning of Native Silicon Oxide: *W. Tsai,* M. Delfino, B. C. Chung, T. Sheng,* and *S. Salimian,* Edward L. Ginzton Research Center, Varian Associates, Palo Alto, CA 94304-1025

In situ optical emission spectroscopy was used to monitor active species during ECR hydrogen plasma cleaning of native silicon oxide to understand the mechanism of the plasma process. Relative concentration of hydrogen and hydroxyl radicals were measured downstream as a function of operating pressure. Gas phase concentrations were well correlated with the etch rate of native silicon oxide measured using *in situ* x-ray photoelectron spectroscopy. Plasma potential, ion density, and electron temperature of the ECR hydrogen plasma were also measured with a Langmuir probe.

90 Process and Module for Low Temperature Hydrogen Cleaning for Silicon Wafers: *F.-P. Steiner, E. Beck,* and *J. Ramm,* Balzers AG, FL-9496 Balzers, Liechtenstein

An ultra high vacuum compatible process module for silicon wafer cleaning is presented. The cleaning procedure utilizes an argon/hydrogen plasma which is characterized by low discharge voltages (about 25 V) and high discharge currents (up to 100 A). If the wafer is immersed in this plasma, the native oxide as well as hydrocarbons are removed from the surface. Mainly electrons stimulate the surface chemistry and damages by sputtering are avoided. Typical etch rates for thermally grown SiO_2 range from 0.01 to 0.05 nm/s. It was found that 5 min cleaning prepares the silicon wafers for low temperature epitaxial growth of silicon.

91 *In Situ* Chamber Dry Cleaning for HBr RIE: *K. Iizuka* and *M. Nakamura,* Process Development Div., Fujitsu Limited, 1015, Kamikodanaka, Nakahara-ku, Kawasaki 211, Japan

Anisotropy is achieved through the side-wall protection by reaction products in HBr RIE. On the other hand, the reaction products deposit on a wall of reaction chamber to form particles. XPS analysis revealed that the deposition on the wall was the mixture of Si, O, C and Br, but mainly consisted of SiO_2. *In situ* plasma cleaning with O_2 rich mixtures of oxygen and fluorinated gases were found to be effective in removing SiO_2 or the deposition on the chamber wall. The conditions suitable for the dry cleaning are completely different from the usual etching conditions.

92 Ion Beam-Assisted Etching of Si(III) with Fluorine at 77K: *J. W. Coburn,* IBM Research Div., San Jose, CA 95120-6099, *C. B. Mullins,* Dept. of Chemical Engineering, University of Texas, Austin, TX 78712-1062

Recent interest in low temperature RIE has prompted some basic beam studies of Si etching with fluorine at 77K. Etch rates are measured *in situ* using quartz crystal microbalance methods, and the neutral etch products are monitored with modulated beam mass spectrometry. Only a brief transient of spontaneous etching is observed and the ion-assisted etch rates are somewhat larger at 77K than at room temperature. The sputter yields of condensed SiF_4 and $SiCl_4$ were measured to provide an estimate of the etch rates expected if sputtering is needed to remove the etch products.

93 A New Method of Sidewall Protection for Anisotropic Etching Using Sulfur Deposition: *T. Tatsumi, T. Nagayama,* and *S. Kadomura,* ULSI R&D Group, Sony Corp., 4-14-1 Asahi-cho, Atsugi, Kanagawa 243, Japan

The objective of this work is to demonstrate a new dry etch processing technique for ULSI devices. The dry etch method presented in this paper used "sulfur" for sidewall protection. Sulfur can be sublimated by heating the substrate after etch, so protection films did not remain on the etched surface. This concept was applied to poly-Si, W-polycide and Al-alloy films. The deposition and the sublimation of sulfur were confirmed using EDX and TDS.

94 Cooling Wafer Stage for Low Temperature Dry Etching: *M. Kanetomo, T. Kure, K. Tsujimoto,* and *S. Tachi,* Central Research Laboratory, Hitachi, Ltd., Kokubunji, Tokyo 185, Japan

Cooling wafer stage has been developed for low temperature dry etching. Cooling stage temperature during etching is calculated by the finite element method and is compared with experimentally obtained values. Heat transfer convection value between the wafer back side and the cooling stage surface was found to be 0.0002 W/mm²K for 10 sccm of He gas flow to cool the back of the wafer. Suppressing any increase in wafer temperature and wafer temperature control at a constant value are required in the low temperature region below -100°C by the time modulation method.

95 Problems of Low Pressure Single Crystal Silicon Etching: *M. Engelhardt,* Siemens AG, Corporate Research and Development, 8000 Munich 83, Germany

Hardware erosion leading to a deposition of sputtered material onto the wafer was found to be a major drawback of plasma etching at low gas pressures in high density, low energy RF plasmas. The results were obtained with single crystal silicon etching in a magnetically confined reactor using pure chlorine as a process gas. They seem, however, to be generally true for other etch systems operating at similar process conditions such as ECR etch systems.

96 Highly Selective Low Pressure Polysilicon Etching in High Density, Low Energy RF Plasmas: *M. Engelhardt,* Siemens AG, Corporate Research and Development, 8000 Munich 83, Germany

Pure chlorine and pure bromine and mixtures of both were used as process gases in a magnetically confined reactor to achieve highly selective polysilicon etching for multi-Mbit DRAMs at low gas pressures. Extremely high selectivities to gate oxide are achieved when gate oxide erosion is balanced by an oxide deposition resulting from the presence of quartz inserts in the reactor which were installed to prevent metal contamination of the wafer in process.

97 Selective High-Rate Etching of Polysilicon in Microwave ECR Discharges: A Comparison of ECR Configurations: *T. D. Manter, D. Dane,* and *P. Gadgil,* Dept. of Electrical and Computer Engineering, University of Cincinnati, Cincinnati, OH 45221

High polysilicon etch rates have been obtained in combination with high etch selectivities with respect to SiO_2 and photoresist in a microwave electron cyclotron resonance (ECR) etch reactor. Using Cl_2-O_2 at 3 to 4 milliTorr and 700 W input microwave power at 2.45 GHz, undoped polysilicon etch rates in excess of 400 nm/min are obtained in a close-coupled ECR configuration with the etch substrate located close to the resonance zone. The corresponding poly-oxide selectivities are greater than 150, and the poly-resist selectivities are 13-15. This performance is compared with the etch results obtained on the same etch tool in a multipolar-confined flared B-field ECR reactor with remote wafer position.

98 Quarter-Micron Deep Trench Etch for ULSI: *Y. T. Lii* and *T. V. Rajeevakumar,* IBM Research Div., T.J. Watson Research Center, Yorktown Heights, NY 10598

This work demonstrates deep trench etching with openings down to 0.25 x 0.25 μm and aspect ratios as high as 40 with round smooth bottoms and tight critical dimension control. This paper presents results of a recent study of quarter-micron silicon deep trench etching with mixtures of HBr and fluorine-containing gases in a magnetically enhanced RIE reactor. The effects of RIE lag on the trenches down to quarter micron opening were quantified and trench etch rate was found to depend solely on trench aspect ratio.

99 MRIE 0.1 μm Polysilicon Lines by Using HBr: *Y. T. Lii, C. M. Reeves, D. A. Danner, P. J. Cocne,* and *L.-K. Wang,* IBM Research Div., T.J. Watson Research Center, Yorktown Heights, NY 10598

We have demonstrated MRIE (magnetically enhanced reactive ion etching) of polysilicon gates with linewidths down to 0.1 μm with HBr gas chemistry. Either 30 nm nitride or 0.3 μm E-beam resist can be used as the etch mask. High polysilicon etch rate, high selectivity of polysilicon to oxide, and tight linewidth control have been demonstrated. Wafer temperature is a key process parameter for controlling sidewall profile and linewidth. This work also demonstrates the advantage of clustering tools for process integration.

100 Fundamental Processing Limit of Gate Oxide Thickness for Polysilicon Gate Definition: *A. S. Yapsir,* IBM Semiconductor Research and Development Center, Hopewell Junction, NY 12533

A quantitative study of the fundamental processing limit of gate oxide thickness for polysilicon gate RIE definition is presented. To perform the study, an *in situ* scheme for monitoring gate oxide removal during etching, is developed. A criterion for a maximum overetch is defined as the time interval between the initial occurrence of oxide etching and silicon substrate etching. Using this definition, the maximum overetch allowed for a specified gate oxide thickness is measured.

101 200 nm Aluminum Etch in MERIE System: *S. Mak, S. Arias,* and *C. S. Rhoades,* Applied Materials, Santa Clara, CA 95054

A screening experiment was performed to study the 200 mm aluminum etch in a MERIE system, using $BCl_3/Cl_2/N_2/CF_4$ chemistry. Main effects of controllable parameters including gas flows, RF power, magnetic-field, and cathode temperature were investigated over a pressure range of 50-200 mT. Of particular interest were the microloading effect on residue and profile. Better etch performance in terms of aluminum etch rate, selectivity to photoresist, residue, and profile control were achievable by optimizing the process at 200 mT pressure regime.

102 Dry Etching of Al Alloy Films Using HBr Mixed Gases: *K. Fujino,* Semiconductor Process Laboratory, 2-13-29 Kohnan Minato-ku, Tokyo 108 Japan, *T. Oku,* Canon Sales Co., Inc., 2-13-29 Kohnan Minato-ku, Tokyo 108 Japan

Al alloy films were reactive-ion-etched using HBr/BCl_3 or $HBr/BCl_3/Cl_2$ gases. Etching rates of the Al films, self dc bias and

selectivities of photoresist and thermal oxide were studied as functions of RF power, gas pressure, total gas flow rate. An Al etch rate of 2.3 μm/min, a photoresist selectivity of 7.7 and a thermal oxide selectivity of 45.5 were obtained with completely anisotropic Al profile. This is because of chemical properties of HBr.

103 One-Step Electron Cyclotron Resonance Etching of Submicron Al-Si-Cu: *D. X. Ma* and *C.-W. Chen*, Lam Research Corp., Fremont, CA 94538

Al-Si-Cu etching was investigated in a high density, low pressure ECR etch system. An anisotropic one-step BCl_3-Cl_2 process was developed without carbon containing additives. The process achieved high aluminum etch rate (>1000 nm/min), excellent aluminum etch uniformity (<±3.5%), and good selectivities of aluminum to resist (>2.7:1) and to oxide (>12:1). The effects of process parameters on etch performance was studied using an $L_9(3^4)$ orthogonal matrix. A large process latitude was also demonstrated.

104 Low Energy Ion Etching of Aluminum Oxide Films and Native Aluminum Oxide: *M. E. Day, S. Salimian*, and *M. Delfino*, E.L. Ginzton Research Center, Varian Associates, Palo Alto, CA 94304-1025

We report high etch rates of aluminum oxide films and native aluminum oxide at low bias voltages using a microwave ECR-source argon plasma. Aluminum oxide films were prepared by reactively sputtering an aluminum target in an argon/oxygen ambient. X-ray photoelectron spectroscopy (XPS) was used to quantify the oxygen/aluminum ratios of these films and to compare these values with those found in native aluminum oxide films. By using XPS we were able to determine how effective the ECR clean was in removing native aluminum oxide.

105 Analysis of Post-Metal Etch Processes Causing Submicron Technology Corrosion Defects: *K. E. Mautz*, Motorola, Inc., Semiconductor Products Sector, Austin, TX 78762

Post-metal etch corrosion defects on submicron devices using Al/Si/Cu alloy metal films were investigated. Analysis of the process and equipmental factors affecting the corrosion defect types was done and the mechanisms were determined. Significant differences were found in the metal etch corrosion prevention processes, ash equipment technology, and DI water rinse processes. Factors that were not significant were the solvent clean and metal etch chemistry. The defects occur due to localized surface chlorine concentrations.

106 Pattern Density Effects on Corrosion of Aluminum Alloy/Refractory Metal Interconnects: *C. G. Gabriel*, VLSI Technology, Inc., San Jose, CA 95131, *R. Wallach*, Lam Research Corp., Fremont, CA 94538

Corrosion of aluminum after plasma etching of interconnects was found to depend on pattern density, with isolated lines corroding more readily than dense lines. The pattern density effect originates during etch and continues during post-etch passivation. Unlike isolated lines, dense lines do not corrode until a threshold level of residual chlorine is reached. To identify the likely mechanism, corrosion was observed and residual chlorine was measured on etched wafers with various spacings of metal lines.

107 Dry Corrosion Control in Aluminum Etch Using O_2/NH_3 in Microwave Downstream Plasma: *S. Mak* and *J. Hwang*, Applied Materials, Inc., Santa Clara, CA 95054

A post-etch corrosion prevention process using a microwave downstream O_2/NH_3 plasma to strip the photoresist mask and to remove the chlorides from the wafer surface after aluminum etch has been developed. Response surface methodology was applied to study the parameter effects. Over 24 h, corrosion-free results had been demonstrated and repeatability been tested on the Al-1% Si-0.5% Cu/TiN film structure.

108 Microcontamination Reduction and Corrosion Prevention for Aluminum Etch Through Loadlock Improvements: *E. DeLaurentis* and *J. Hwang*, Applied Materials, Santa Clara, CA 95054

A continuous dry nitrogen purge is integrated into the loadlock of a single wafer, multichamber aluminum etch system. The purge allows better control in cross contamination between the etch chamber and the loadlock chamber, and minimizes moisture introduction during atmospheric wafer transfers. The loadlock particle density is reduced by a factor of 5 to 10. Also, problems with inconsistent corrosion performance after the aluminum etch are resolved and corrosion-free results become reproducible.

109 RIE-Related Sidewall Voiding in Al-Cu Alloy Metallization for ICs: *T. H. Daubenspeck* and *H. K. Lee*, IBM General Technology Div., Essex Junction, VT, 05452

Sidewall void formation in submicron Al/Cu alloy wires has been found to occur as a result of the manner in which reactive ion etch (RIE) processing is performed and controlled. These defects are a risk for both reliability and yield. Voids form in response to inappropriate etch process conditions, tool contamination, or by a thermally initiated reaction during resist strip. Void formation data are presented and discussed for both batch and single-wafer RIE reactors.

110 Wafer Clamping Effects on Etchback of CVD Tungsten Films: *L. Shen, L. Wilson*, and *Y. Chu*, Advanced Micro Devices, Sub-Micron Development Center, Sunnyvale, CA 94088-3453

Two blanket tungsten etchback processes were developed for use in contact and via fill applications, the first utilizing a 2.25 mm clamp and the second a 6.0 mm wafer clamp. Designed experiments for both processes produced good agreement between catalyst and RS1. The 2.25 mm process requires multiple steps for uniform plug recession; exposed oxide loading effects are seen. A SEM plug recess study of the 6.0 mm process showed uniform recession with no loading effects; however the factor of helium back-side cooling was shown to produce excessive recession. Plug recess and keyhole size were studied as a function of temperature.

111 Mechanism of Residue Formation in Low Temperature Tungsten Interconnect Etch: *U. C. Sridharan*, Hewlett-Packard, Palo Alto, CA 94303, *D. Hartman* and *R. Wright*, SEMATECH, Austin, TX 78741, *M. Kent*, Drytek/General Signal, Wilmington, MA 01887

A low temperature tungsten etch process was studied in the temperature range from -50° to -10°C using pure SF_6 chemistry. Highly anisotropic tungsten profiles were observed. However two types of residues, namely, "drift" and "spike" were observed under these conditions. Such residue formation was studied in detail. The analyses of the residue indicated the presence of predominantly titanium and fluorine in the drift residue. A mechanism was proposed to account for such residue formation.

112 A Kinetic Study of Reactive Ion Etching of Tungsten in SF_6/O_2 RF Plasmas: *M. C. Peignon, C. Cardinaud*, and *G. Turban*, LPCM, University de Nantes, 44072 Nantes Cedex 03, France

The reactive ion etching of chemical vapor deposited (CVD) tungsten in SF_6/O_2 RF plasma has been investigated by means of optical emission spectroscopy, mass spectrometry, and *in situ* x-ray photoelectron spectroscopy (XPS). This study is particularly focused on the etching of a WO_3/W layer, a native oxide 35-45 Å thick (WO_3) always appearing on the CVD tungsten surface. Actinometry measurements show an excess of the atomic fluorine and oxygen relative concentrations during the etching of the WO_3 layer as compared to that of tungsten. Two etch products of tungsten are detected by mass spectrometry: WF_6 and WOF_4. In pure SF_6 plasma, the main etch product of WO_3 and W is WF_6. In SF_6/O_2 (40/60) plasma, WF_6 is the dominant product of the etching of the WO_3 layer, and WOF_4 that of W. *In situ* XPS analyses show the presence of fluorine, oxygen, and sulfur on the etched tungsten surface. The role of these elements in the formation of the two etch products of tungsten is discussed.

113 Optical Emission Studies of Etching Tungsten Silicide and Polysilicon Films: *X. Y. Qian, D. J. Hemker*, and *G. W. Hills*, Applied Materials, Santa Clara, CA 95054

A diode array spectrometer has been used to study optical emission during the etching of tungsten silicide and polysilicon stack films in $SF_6/HBr/Cl_2/He/O_2$ containing discharges in a MERIE reactor. Experiments are reported on the use of emission from the 440 nm region as a suitable endpoint for these stacked films. Temporal and spatial scans of the optical emission give insight into the plasma and surface chemistries, the influence of the magnetic field and the impact of hardware design on the plasma chemistry.

114 Effect of Wafer-Average and Within-Die Polysilicon Pattern Density on Transistor Gate-Length Definition for Cell-Based ASIC CMOS Designs: *D. Dimitrelis, M. Carneiro*, and *V. Dunton*, VLSI Technology, Inc., San Jose, CA 95131

Cell-based ASIC designs exhibit large transistor-density variation depending upon the logic or memory function they implement. Therefore, the polysilicon etch process for an ASIC manufacturing line must be pattern-density independent. Using a newly designed test chip we characterize the effect of process parameters on uniform gate-length definition as a function of wafer-average and within-die polysilicon pattern density. Results are presented for polysilicon etch of 1.0 μm and smaller geometries using an SF_6/Cl_2 plasma.

115 Reactor Characterization for a Process to Etch Si_3N_4 Formed on Thin SiO_2: *P. E. Riley, J. C. Sum*, and *D. Figueredo*, Hewlett-Packard Circuit Technology R&D, Palo Alto, CA 94303

A process to etch LPCVD Si_3N_4 which has been deposited over thin thermal SiO_2 has been developed with an Applied Materials 8110 hexode system. To insure uniform and repeatable processing with sufficient etch selectivity between Si_3N_4 and thin SiO_2, the system has been characterized as a function of (*i*) reactor pressure, (*ii*) O_2 in a CHF_3/O_2 mixture, and (*iii*) dc bias voltage.

116 A Sub-Half Micron Deep UV Integrated ARC Process: *T. Ta, K. Reinhardt, P. Westerfield, S. Sethi, E. Capsuto, J. Kochan, R. Fuller*, and *A. White*, SEMATECH, Austin, TX 78741

A sub-half micron deep UV process has been implemented using a highly absorbing organic antireflective coating (ARC). The ARC requires plasma etching for pattern delineation. The interaction of the etch gases with the ARC has been studied. To obtain a robust, production-worthy process, the correct choice of etch gases is essential. Various etch compositions and pretreatments of the underlying film surface have been investigated. The final process exhibits stable and repeatable CD control, is devoid of micromasking residues and the ARC is easily stripped after etch.

117 Photoresist Swelling in Hydrogen-Containing Freon Plasmas: *Y. Kuo*, IBM Research Division, T.J. Watson Research Center, Yorktown Heights, NY 10598

A polymer swelling phenomenon has been observed when a positive photoresist pattern was exposed to the hydrogen-containing plasma in a reactive ion etching chamber. The swollen polymer has a mushroom profile and is very resistant to certain plasma attack. The swelling rate decreased with time. FTIR data showed that during the swelling process, (*i*) new bonds were formed, (*ii*) fragments were lost, and (*iii*) hydrogen atoms were added. LAMMA profile showed that fragments with the weight range of 60-360 were lost from the surface. Therefore, this polymer swelling phenomena probably involved several reactions: chain scission, cross-linking, and hydrogenation. The mechanism of the process is delineated. Possible applications of this new structure are also discussed.

118 Comparison of Nonline of Sight Resist Ashing Using Microwave or Radio Frequency Plasma Generation: *J. I. McOmber, J. T. Davies, J. Howden,* and *M. Wright*, GaSonics/IPC, San Jose, CA 95134, *K. Saul*, Hewlett Packard, Northwest I.C. Div., Corvallis, OR 97330

We examined resist ashing in a nonline of sight downstream resist asher powdered with either radio frequency or microwave for reactive species generation. The ashing process is discussed as a function of the plasma excitation source. The process is found to be independent of the plasma excitation source at temperatures of 150°C or less. The microwave powered plasma demonstrates a faster ash rate at the temperatures normally used for production single wafer ashers.

119 Analytical Study on the Mechanism of High Dose Ion Implanted Photoresist Ashing in a True Downstream Plasma: *X. C. Mu*, Intel Corp., Components Research, Santa Clara, CA 95051

In this study, we present our understanding of the basic mechanism of high dose ion-implanted photoresist ashing process in a true downstream plasma reactor. Analytical techniques, such as organic SIMS, thermal desorption mass spectroscopic analysis, and FTIR were employed. It was found that not just the solvent, but mainly the basic resist resin in the photoresist is also capable of desorption, which is the dominant factor for the resist explosion during downstream plasma resist ashing. Some alternative process options were tried to alleviate the problem.

120 Selective Etching of Bilayer Photoresist Using Multipolar Electron Cyclotron Resonance Source: *S. W. Pang, K. T. Sung,* and *K. K. Ko*, Dept. of Electrical Engineering and Computer Science, University of Michigan, Ann Arbor, MI 48109-2122

A bilayer resist typically consists of a thin imaging layer (20 nm) and a thick bottom layer (1 μm). The etching of the bottom layer resist requires high selectivity against the imaging layer, vertical etch profile, and low damage to the underlying substrate. A high density, low pressure electron cyclotron resonance (ECR) source together with a RF-powered electrode can provide more flexibility to meet these requirements than conventional reactive ion etching systems. Effects of microwave power, RF power, ECR source to sample distance, and pressure on resist etch rate in an O_2 plasma are shown. Etch rate was found to increase with microwave and RF power, but decrease with source to sample distance. Photoresist was etched with smooth morphology and fast etch rate up to 1.6 μm/min. The optimal conditions for bilayer resist etching are discussed.

121 Plasma CVD of a-SiC:H for X-Ray Mask Membranes Using a Helical Resonator Discharge: *A. D. Johnson, D. E. Ibbotson,* and *J. A. Mucha*, AT&T Bell Laboratories, Murray Hill, NJ 07974

Smooth, optically transparent, a-SiC:H thin films have been deposited on Si substrates from silacyclobutane, SiC_3H_8 (SCB), in a low pressure, cold wall, helical resonator (HR) plasma CVD reactor. The HR source geometry allows flexibility in the placement of the plasma zone relative to the gas feed and substrate. SCB deposits stoichiometric a-SiC:H (C:Si = 1) over the temperature range 370-685°C, independent of flow rate. Decomposing SCB in a plasma allows stress control over the range 10^{10} dyn/cm^2 compressive to 10^{10} dyn/cm^2 tensile, at constant temperature. ERD has been used to measure the hydrogen content of a-SiC:H for various processing conditions.

122 Composition and Stability of Plasma-Deposited Fluorinated Silicon Nitride Thin Films: *R. Costantino, C. Marinensi, G. Tigani,* and *A. Zanobi*, Eniricerche S.p.A., I-00016 Monterotondo, Rome, Italy

Fluorinated silicon nitride films have been deposited by plasma-enhanced chemical vapor deposition (PE-CVD) using SiH_4-NF_3-N_2 gas mixtures at 13.56 MHz. We studied fluorinated films by varying the relative $[NF_3]/[SiH_4]$ flow ratio in the range 0.1-1.6 and the RF power in the range 50-100 W. The addition of NF_3 to deposition gas mixtures significantly reduces the concentration of H bonded to Si, because strong Si—F bonds replace weak Si—H bonds, and the hydrogen remaining in film is present as stable N—H bonds. Films with larger $[SiH_4]/[NF_3]$ flow ratio hydrolize rapidly to silicon dioxide, while films with lower $[SiH_4]/[NF_3]$ flow ratios remain unchanged in time. Fluorinated silicon nitride films show a decrease in refractive index compared to unfluorinated silicon nitride films.

123 Modeling and Simulation of Plasma Enhanced Chemical Vapor Deposition of Silicon Nitride: *M. Mazhar IslamRaja*, Center for Integrated Systems, Stanford University, Stanford, CA 94305, *A. J. Bariya*, National Semiconductor Corp., Santa Clara, CA 95052, *J. P. McVittie*, Center for Integrated Systems, Stanford University, Stanford, CA 94305, *M. A. Cappelli*, Dept. of Mechanical Engineering, Stanford University, Stanford, CA 94305, *K. C. Saraswat*, Center for Integrated Systems, Stanford University Stanford, CA 94305, *L. Moberly* and *R. Lahri*, National Semiconductor Corp., Santa Clara, CA 95052

An analytical model has been developed to simulate profile evolution during plasma enhanced chemical vapor deposition (PECVD) of silicon nitride. The model takes into account adsorption/re-emission at the surface and a spatially varying sticking coefficient (reaction probability) of the rate limiting precursor. The sticking coefficient is modeled as a linear function of the incident ion energy flux, having a minimum value of 0.2 and a maximum value of 0.28. This model accurately predicts the experimental profile evolution in structures of different geometries.

124 Characterization of PECVD Nitride Films Used in VLSI Applications: *A. K. Stamper, S. L. Pennington,* and *G. Bazan*, IBM General Technology Div., Essex Junction, VT 05495

Several PECVD SiN_xH_y processes used in VLSI applications are discussed. Films have been deposited in an Applied Materials AME5000 cluster CVD/etch tool. The processes are characterized in terms of deposition rates, uniformity across 200 mm silicon wafers, conformality over metal lines, density, etch rates, stress, index of refraction, and stoichiometry. PECVD nitride processes with high deposition rates and good conformality are presented along with processes with etch rates comparable to LPCVD nitride films.

125 Deposition of Silicon Nitride Films by ECR-Enhanced CVD: *J. D. Chapple-Sokol* and *D. E. Kotecki*, IBM Semiconductor Research and Development Center, Hopewell Junction, NY 12533

Silicon nitride films were deposited by microwave/ECR deposition from NH_3 and SiH_4 or Si_2H_6. Dependence of film properties on deposition conditions was studied. Films deposited at less than ~500°C had about twice the bonded hydrogen content of those deposited at 500°C. With increasing temperature, an increase in refractive index was observed. Increasing microwave power caused an increase in deposition rate and a decrease in refractive index. Intrinsic stress in films was tensile, and wet etch rates were comparable to those of LPCVD nitride.

126 Plasma Deposition and Characterization of Fluorinated Silicon Nitride: *S. V. Nguyen, D. Dobuzinsky, R. Gleason,* and *M. Gibson*, IBM General Technology Div., Essex Junction, VT 05452

Fluorinated silicon nitride films were deposited in a single wafer plasma-enhanced chemical vapor deposition system (13.6 MHz) using silane (SiH_4), silicon tetrafluoride (SiF_4), and nitrogen as reactant gases. The fluorinated silicon nitride films, formed at 300°-400°C and SiF_4/SiH_4 greater than 1, have good thickness control and uniformity, good step coverage on silicon surface, and are stable in air ambient and after annealing at 900°C in nitrogen. Compositional analysis shows that up to 17 atomic percent of fluorine can be incorporated into the films without causing degradation in subsequent long term air exposure. The film's MOS electrical properties, plasma RIE, and wet etch rates are also studied in detail.

127 Modeling of PECVD TEOS Oxide Step Coverage Using an Overhang Structure: *C. Chang, J. P. McVittie,* and *K. C. Saraswat*, Center for Integrated System, Stanford University, Stanford, CA 94305

PECVD TEOS oxide deposition on an overhang structure has been performed. Comparisons of experimental and simulated profiles have determined effective values for the precursor sticking coefficient, S_r, and the ion distribution factor K_d. The PECVD process was modeled as a linear combination of a neutral precursor and ion energy limited growth components. Simulation based on such a model indicates that (*i*) the neutral precursor/LPCVD component accounts for 80% of the deposition on the top of the overhang structure and the underside profiles are characterized by a S_r of 0.15, and (*ii*) the ion angular distribution is characterized by K_d = 1.3 and the ion enhancement component is responsible for 20% of the deposition on top and 0% in the shadowed regions.

128 Low Temperature Deposition of SiO_2 by DECR-PECVD: *B. Agius*, Institut Universitaire de Technologie, Université de Paris Sud (XI), Plateau du Moulon, 91403 Orsay Cedex, France

Thin films of SiO_2 have been deposited on Si and InP substrates by SiH_4-N_2O or SiH_4-O_2 plasmas. A new type of microwave excitation, the distributed electron cyclotron resonance (DECR) inducing the formation of high density plasma (≈10^{11} cm^{-3}) of low energy ions (≈20 eV) has been used. Combining ellipsometry and nuclear microanalysis, we have studied the relationship between the optical properties and the atomic composition of the film. Moreover, we have shown that high resistivity thin films (>4 10^{15} Ω · cm) can be deposited at low temperature (<120°C) and a low in-

terface state distribution (2×10^{11} $eV^{-1} \cdot cm^{-2}$) can be achieved for SiO_2-InP structure.

129 Effects of RF Frequencies and Deposition Rates on the Moisture Resistance of PECVD TEOS-Based Oxide Films: *S. A. Robles, M. Galiano,* and *B. C. Nguyen,* Applied Materials Inc., Santa Clara, CA 95054

The moisture resistance of PECVD TEOS-based undoped oxide films deposited using different RF frequencies and deposition rates were investigated using IR spectroscopy, NRA hydrogen analysis, and stress-temperature analysis. The frequencies used to ignite the plasma were: 13.56 MHz only, 13.56 MHz mixed with 100-450 kHz, and 100-450 kHz only. The results obtained indicate that the oxide moisture resistance is not determined by the RF frequencies and deposition rates, but rather by the initial as-deposited film stress.

130 Formation of High Quality Tantalum Thin Films on SiO_2 by Dual-Frequency-Excitation Plasma Process: *H. Wakamatsu, S. Aoyama, J. Watanabe, N. Konishi,* and *T. Ohmi,* Dept. of Electronics, Faculty of Engineering, Tohoku University, Sendai 980, Japan

Among various methods of formation of tantalum oxide films for DRAM capacitors, we are studying the direct oxidation of tantalum films. To obtain high quality dielectrics in such an oxidation approach, it is needed to prepare high quality and high crystallinity tantalum films prior to oxidation. We have developed dual-frequency-excitation plasma process equipment of multichamber construction. In this work we investigate the effects of ion flux density and ion bombardment energy on the Ta film formation process on SiO_2. We have obtained high crystallinity Ta films on SiO_2 when Ta film were formed under relatively high ion bombardment energies (several tens of eV) with sufficient ion flux density which were conducted after SiO_2 film baking and *in situ* substrate surface plasma cleaning.

131 Control of Stress, Stability, and Mechanical Properties of PECVD Dielectric Films for GaAs and Si Applications: *T. H. Wu* and *L. A. Schneggenburger,* Motorola Inc., Tempe, AZ 85282, *B. van Schravendijk, B. Sparks, A. S. Harrus,* and *D. G. Hemmes,* Novellus Systems, Inc., San Jose, CA 95113

Plasma enhanced deposited dielectrics (nitrides and oxides) are widely used in advanced silicon-based VLSI manufacturing. The development of dual frequency plasmas has allowed precise stress control of these films on both Si and semi-insulating GaAs substrates. We present a comprehensive characterization of the film properties (nitrides and oxides) on both substrates. Results of stress *vs.* temperature measurements as a function of the initial stress values are presented and correlated to mechanical properties of the films and their composition (FTIR, Auger, R.I., etc.). The stability of these films over time and during temperature cycle is directly related to as-deposited film stress.

132 Formation and Characterization of Zirconia Films by Plasma-Enhanced Chemical Vapor Deposition: *C. C. Chen, M. M. Nasrallah,* and *H. U. Anderson,* University of Missouri-Rolla, Ceramic Engineering Dept., Rolla, MO 65401, *W. J. James,* University of Missouri-Rolla, Materials Research Center, Rolla, MO 65401

Zirconia (ZrO_2) films have been fabricated from zirconium tetra t-butoxide using plasma-enhanced chemical vapor deposition (PE-CVD) technique. The effect of deposition parameters: plasma power, substrate temperature, and reactive gas flow, on the film structure is presented. The fabricated films were dense and transparent. The development of structure from amorphous to crystalline and the effect of post annealing are discussed. The in-depth profiles of composition were investigated using AES. Stoichiometric cubic ZrO_2 films were successfully deposited on Si substrates. Attempts are underway to deposit dense films on porous substrates.

SECOND INTERNATIONAL SYMPOSIUM ON REDUCED-THERMAL-BUDGET PROCESSING FOR THE FABRICATION OF MICROELECTRONIC DEVICES

Dielectric Science and Technology/Electronics

133 Defect-Free Rapid Thermal Processing: *Z. Nenyei, H. Walk,* and *T. Knarr,* AST Elektronik GmbH, Science Park 7900-Ulm, Germany

A new approach to the reduction of transient thermal nonuniformities during the rapid thermal processing is described. The approach utilizes the digital control of heating lamps during the processing cycle. The power absorbed by the wafer in any time period of processing can be controlled according to a defined recipe. This feature allows elimination of any transient temperature nonuniformities, especially during heating-up. The power control, together with the proprietary back-radiant silicon ring, allows slip free processing.

134 The Impact of the Wafer Back Side on RTA Processing: *B. Lojek,* Motorola Inc., Advanced Technology Center, Mesa, AZ 85202

The emissivity of silicon wafer varies not only with temperature and wavelength, but also with the back-side roughness of wafer. In production environment, the back side of the wafer is subject to wide variations which is not easy to control. In order to define the optical properties of the back side of the wafer, quite often the back-side etch is used. Unfortunately, this is not very good practice because the wafer shows slip more easily. In addition, there is direct correlation between the warpage and etching of the back side. The experiments leading to this identification are described and mechanism for the phenomenon are discussed.

135 Oxidation of Polycrystalline Silicon during Wafer Heating Up: *K. Yamabe, K. Imai, J. Shiozawa, Y. Suizu,* and *K. Okumura,* ULSI Research Center and Semiconductor Group, Toshiba Corp., 1, Komukai Toshiba-cho, Saiwai-ku, Kawasaki 210, Japan

To form shallow p-n junction, in each process step after the impurity doping, thermal budgets have to be decreased. The thermal budgets of the heating-up duration are obtained by measuring the thickness of the oxide grown on polycrystalline Si during the heating-up step. And then, the high rate heating-up causes the thermally grown SiO_2 films to have low leakage current.

136 An Estimation of Thermal Budget for Wafer Cooling Down from Impurity Diffusion: *K. Yamabe, K. Imai, H. Kawaguchi, Y. Suizu,* and *K. Okumura,* ULSI Research Center and Semiconductor Group, Toshiba Corp., 1, Komukai Toshiba-cho, Saiwai-ku, Kawasaki 210, Japan

As wafer size increases, heating-up and cooling-down durations become a larger fraction of total process time. Here, we estimate the thermal budget of the cooling duration as a function of the cooling rate from 1000° to 800°C by using the experimental boron and arsenic profiles and the computer simulation. The effective diffusion time at 1000°C is approximately in inverse proportion to the cooling rate over the whole range of the cooling rate of 2°-60° C/min.

137 Reliability Characterization of RTO and O_2-Diluted Thin Gate Oxides: *L. A. Fonseca** and *F. Campabadal,* Centro Nacional de Microelectrónica, Universidad Autónoma de Barcelona, 08193 Bellaterra, Spain

RTO and O_2-diluted thin oxides have been electrically characterized. C-V analysis and barrier values around 3 eV for FN tunneling conduction reflected good interface quality and structural properties in both cases. Superior storage time of RTO capacitors showed that no serious damage was produced in the substrate in spite of aggressive thermal cycling. TZDB and TDDB experiments were also performed, RTO oxides resulting in superior reliability terms, presented a slightly larger dielectric strength and significantly larger Qbd.

138 A Study of the Effect of Deposition Parameters on the Growth Rates and Microstructure of Silicon Homoepitaxial Films Grown by ArF Laser-Enhanced Chemical Vapor Deposition: *S. Krishnan, S. Lian, B. Fowler, L. Jung, C. Li, D. Samara, I. Manna,* and *S. Banerjee,* Microelectronics Research Center, University of Texas, Austin, TX 78712

The effect of deposition parameters on the growth rate and microstructure of Si homoepitaxial films, grown by ArF excimer laser-enhanced photodissociation of Si_2H_6 has been studied. The growth is performed in an ultra-high vacuum chamber with the laser beam shining parallel to the substrate whose temperature is held at 300°C. The deposition pressure, when varied in the range of 600-1200 mTorr, does not have a significant effect on the growth rate as long as the Si_2H_6 partial pressure is held constant at 10 mTorr, though the crystallinity improves with increasing deposition pressure, as confirmed by *in situ* RHEED analysis. For a constant deposition pressure, the growth rate falls with increasing distance between the substrate and the laser beam, when it is varied from 0-15 mm, since fewer precursors are able to reach the substrate. The growth rate is independent of the repetition rate of the laser as long as the average power is held constant. On the other hand, it linearly increases with the repetition rate when it is varied in the range of 2-80 Hz, keeping the energy per pulse constant. The crystallinity is preserved even at 2 Hz.

139 A Green's Function Approach to a Growth Kinetic Model for Low Temperature Si Homoepitaxy by ArF Excimer Laser-Enhanced Photo Chemical Vapor Deposition Using Disilane: *S.Lian, B. Fowler, S. Krishnan, L. Jung, C. Li, D. Samara, I. Manna,* and *S. Banerjee,* Microelectronics Research Center, University of Texas, Austin, TX 78712

Low temperature Si homoepitaxy by ArF excimer laser-enhanced photo chemical vapor deposition (PCVD) using disilane in an ultra-high vacuum (UHV) deposition chamber has been successfully achieved at temperatures as low as 250°C. A Green's function based growth kinetic model has been developed based on the gas phase reactions of the primary photolysis products, diffusion of silicon-bearing radicals to the growth surface, and experimental data. The growth rate $g = J \alpha n' H \Omega \omega \delta \exp(-x_0^2/\sigma^2 + 4DT_1)(\sigma^2 + 4DT_1)^{1/2} \exp(E_a/\kappa T)/2\rho x_0$ where J is laser intensity in photons/pulse · cm², α is the absorption cross section of Si_2H_6 at 193 nm, n is the concentration of growth precursors, ω is the photofragment yield from excited disilane, and δ is the sticking coefficient. All the parameters in the above equation are either known or are measurable except for ω and δ. From the growth data, $\omega\delta$ is estimated to be 0.075 which is consistent with the value from other researchers $\omega = 0.05$, $0.1 < \delta < 0.26$. The linear depen-

dence of growth rate on laser intensity and disilane partial pressure indicates that the rate limiting step is the photo-dissociation generation rate of the growth precursors.

140 A Novel Solid Phase Epitaxy by SR Irradiation and Its Electrical Characterization: *K. Goto, F. Sato, I. Fujimoto,* and *T. Tajima,* NHK Science and Technical Research Laboratories, 1-10-11, Kinuta, Setagaya-ku, Tokyo 157, Japan

Solid-phase epitaxy by x-ray irradiation (SPEXI) technique using synchrotron radiation has been applied to the post-annealing of amorphized silicon surface layers by the implantation of phosphorus. By spreading-resistance and SIMS measurements it was found that by SPEXI, the higher electrical activation of implanted phosphorus can be achieved at much lower temperatures than by conventional furnace annealing. NMOS FET's fabricated on non-doped SPEXI films also showed almost the same characteristics as those on single crystal wafers.

141 A Low Resistivity Polysilicon Film Fabricated with a Si_2H_6/B_2H_6 Mixture at 350°C: *J. Shiozawa, K. Yamabe, Y. Kasai, S. Miyazaki,* and *Y. Mikata,* ULSI Research Center and Semiconductor Group, Toshiba Corp., 1, Komukai Toshiba-cho, Saiwai-ku, Kawasaki, 210, Japan

The preparation of boron-doped polysilcon films such as to provide low resistivity films in conjunction with well-uniformity of doping has been proposed. Typical parameters of the process are as follows; deposition temperature of 350°C, source gas of Si_2H_6 heavily mixed with B_2H_6, crystallization temperature of 600°C and so forth, and 1.7 mΩ · cm poly-Si films have been obtained.

142 Deposition and Characterization of Crystallized LPCVD Si-Films Obtained by Low-Temperature Pyrolysis of Disilane: *A. T. Voutsas* and *M. K. Hatalis,* Sherman Fairchild Laboratory, Lehigh University, Bethlehem, PA 18015

The deposition of silicon films from a 5% disilane in He gas was studied over a wide range of deposition conditions. Different deposition temperatures, pressures, gas flow rates, and wafer spacings were utilized. The deposition rate ranged between 1 and 4 nm/min, depending upon the operating conditions. The as-deposited amorphous films were crystallized at 600°C for various annealing times. The final grain size of the films was related to the combination of two nucleation mechanisms, which were shown to depend upon the deposition conditions.

143 Photo-Enhanced Reaction during Chemically Vapor-Deposition of Tantalum Pentoxide with Low Leakage Current: *S. Tanimoto, M. Matsui, N. Shibata, K. Kamisako, K. Kuroiwa,* and *Y. Tarui,* Tarui Laboratory, Dept. of Electronic Engineering, Tokyo University of Agriculture and Technology, 2-24-16, Nakamati, Koganei, Tokyo 184, Japan

This paper sheds some light on molecular-chemical reactions, especially photo-enhanced reactions occurring on substrates during LPCVD of Ta_2O_5 films with very low leakage current. For this purpose, we introduce a modified photo-CVD with cyclic injection of $TaCl_5$ vapor and O_2, and periodic UV irradiation synchronized with the vapor injections. We show that the activation of $TaCl_5$ adsorbing on the substrate virtually dominates the growth rate and that the growth rate is greatly enhanced by a relatively small amount of UV flux.

144 Low-Thermal-Budget Emitter Formation Using *In Situ* Phosphorus-Doped TAS (Thermally Deposited Amorphous Silicon): *H. Miyata, A. Tsukune, F. Mieno, Y. Furumura, H. Tsuchikawa, A. Shimizu, I. Namura,* and *T. Ono,* Process Development Div., Fujitsu Ltd., 1015 Kamikodanaka Nakahara-ku, Kawasaki 211, Japan

We have successfully developed *in situ* phosphorus doped TAS (thermally deposited amorphous silicon) using a single-wafer reactor. *In situ* phosphorus doped TAS film has a good coverage and a flat surface, and achieves low-resistivity by low-temperature annealing below 800°C. We tried to form emitter using *in situ* phosphorus doped TAS film. Transistors with 750°C annealed emitter showed right characteristics. Its V_{CEO} was 5 V and h_{FE} was 100 to 120 in emitter common mode. This technology promises a reduction of thermal-budget for device fabrication.

145 A Highly Reliable Rapid Thermal Sintering Process for Aluminum Alloy Metallization: *A. Husain,* L. S. I. Logic Corp., Milpitas CA 95035

Silicon precipitation during the post Al/Si or Al/Si/Cu metallization is considerably altered using silicon specific lamp for the rapid thermal sintering process. A significant increase (~10%) in the post assembly test yield and an improvement by factor of 2.5 in long term reliability are shown. Moreover, reduction of Si precipitate size and hillocks density is shown. Reduction of stress voids and an increase in the electromigration resistance for the metal lines are discussed.

146 Thermal Stability of Thin Submicrometer Lines of $CoSi_2$: *Q. Wang* and *C. A. Canovai,* Dept. of Electrical and Computer Engineering, North Carolina State University, Raleigh, NC 27695, *C. M. Osburn, P. L. Smith,* and *G. E. McGuire,* MCNC, Center for Microelectronics, Research Triangle Park, NC 27709

The thermal stability of submicron $CoSi_2$ lines on Si substrates was investigated using electrical, *in situ* TEM, RBS, and SEM measurements. The as-formed silicide was thinner at the edges of features, giving rise to an apparent difference in the electrically equivalent linewidth and its physical size. The 45 nm silicide films started to degrade above 1000°C. However, no line width dependence of this resistance degradation was observed up to 1000°C for linewidths down to 0.45 μm.

147 Effects of Dopants in Polysilicon on Titanium Silicide Degradation: *T. Koch,* Integrated Circuits Business Div., Hewlett-Packard, Corvallis, OR 97330

The effects of polysilicon dopants on the titanium silicide formed by rapid thermal processing were studied as a function of linewidth down to 1 μm. Significant degradation of the $TiSi_2$ during PSG densification at temperatures between 800 and 900°C was observed for patterned polysilicon near 1 μm linewidth due to unintended implanting of molybdenum during the BF_2 source/drain implant. The affects of other dopants in polysilicon including thermal doping with $POCl_3$ and implanted arsenic and phosphorus on the titanium silicide high temperature compatibility are also discussed. The investigation techniques included sheet resistance measurements, elemental depth profiling, scanning and transmission electron microscopy.

148 Low Temperature Sub-Atmospheric CVD USG/PSG for Gap Filling and Planarization of Advanced Submicron Memory Devices: *D. Cote, H. Nobel,* and *C. Basa,* Advanced Semiconductor Technology Center, Hopewell Junction, NY 12533, *K. Kwok, E. Yuh,* and *B. C. Nguyen,* Applied Materials Inc., Santa Clara, CA 95054, *B. Neureither,* Siemens Components Inc., Iselin, NJ 08830

A low temperature sub-atmospheric (SACVD) $TEOS/O_3$ process has been developed to deposit undoped and P-doped glasses as the dielectric insulator between the polycide gate conductor and the first level metal for advanced submicron DRAM applications. The PSG films can fill 0.3 μm spaces with aspect ratio greater than 2:1 without any physical voids. The effects of process conditions on the film properties, gap filling capability, and planarization properties of these glasses are presented.

149 Water Trapping and Detrapping in Thin Film Dielectrics: Temperature Dependence and Water-Trap Dynamics: *J. N. Cox, J. Z. Ren,* and *J. M. Van Horn,* Intel Corp., Santa Clara, CA 95052-8126, *K. W. Kwok,* Applied Materials, Santa Clara, CA 95054

Reduced-thermal-budget processes often eliminate high-temperature annealing steps, which normally serve to stabilize dielectric films by removing trapped water and other contaminants. Regarding trapped water, data collected by Fourier transform infrared spectrophotometry (FTIR) show that, when the water-traps in a film are filled, the water is present either as "isolated silanol" or as "associated silanol." Moisture evolution analysis (MEA), however, reveals that there can be more than one type of water-trap present which is filled by associated silanol. These different water-traps empty at distinct temperatures in the 100-500°C regime. FTIR at static temperatures cannot delineate this substructure of water-traps. While results for several types of films are presented, an emphasis is given to data for films produced by thermal-TEOS CVD, since it best illustrates the dynamics of the water-traps.

150 Characterization of Remote Plasma Enhanced CVD ONO Structures Using Electron Holography and Energy Loss Microscopy: *G. L. Waytena,* 9230 Valley Stream Road, Clarence, NY 14031, *P. Rez, J. K. Weiss,* and *W. J. DeRuijter,* Center for Solid State Science, Arizona State University, Tempe, AZ 85287-1704, *S. V. Hattangady* and *G. G. Fountain,* Research Triangle Institute, Research Triangle Park, NC 27709-2194

Oxide-nitride-oxide layered structures with oxide layers 1-3 nm wide were deposited by remote plasma enhanced chemical vapor deposition at 300°C. These films were characterized by electron holography and high resolution transmission electron microscopy and electron energy loss spectrometry. Our results show that the first oxide layer varies in thickness between 0.4 and 1 nm and there is mixing between the nitride and the second oxide layer. We show the power of holography in characterizing thin light element amorphous layers.

151 BPSG's Viscosity Determination for Rapid Flow Annealing Optimization: *A. Tissier,* Centre National d'Etudes des Télécommunications (CNET), Group, TCI/IIP, 38243 Meylan, France, *J.-F. Teissier,* SEI, 38110 La Tour du Pin, France, *A. Poncet,* CNET, Group, CCI/MDT, and *D. Sanchez,* CNET, Group, TCI/FAB, BP98-38243 Meylan, France

An original method for the determination of the borophosphosilicate glasses (BPSG) viscosity is described which associates numerical models for RTP and *in situ* characterization of the flow rate using light diffraction over regular test patterns. Thanks to the linearity of the model, and constant surface coefficient being assumed, it turns out that viscosity fitting is very similar to a time scaling. The influence on the viscosity of the major parameters, temperature boron concentration, and DVD conditions, are analyzed. Decisive implications on complimentary metal oxide semiconductor processes are shown.

152 Autodoping of Boron from BSG Glass: *K. D. Beyer, G. Fitzgibbon,* and *P. A. Ronsheim,* IBM General Technology Div., East Fishkill Facility, Hopewell Junction, NY 12533

During heat-treatments required for trench isolation using BSG as a trench fill, thin SiO_2 layers are sufficient to mask the diffusion of boron from BSG. The transfer of boron from unprotected BSG surfaces onto silicon was investigated in liquids and gaseous ambients. Depletion of boron from BSG was found after immersions into boiling water. Prolonged rinsing in deionized water removed the boron contamination incurred during immersions of bare silicon surfaces. Dry O_2 and N_2 cause negligible out-diffusion of boron from BSG at elevated temperatures, while steam produces a measurable loss of boron.

FIFTH INTERNATIONAL SYMPOSIUM ON SILICON-ON-INSULATOR TECHNOLOGY AND DEVICES

Electronics/Dielectric Science and Technology

153 Silicon-on-Insulator Technology and Devices: H. H. Hosack, Texas Instruments, Inc., Dallas, TX 75265

Silicon-on-insulator (SOI) technology has been shown to have significant performance and fabrication advantages over conventional bulk processing for large scale IC applications. Even with these advantages, the commercialization of this technology has been paced by the availability of SOI material meeting the price and quality requirements necessary for volume IC production. In this paper the advantages and current status of both SOI materials and devices are described, and the potential for meeting the promises of SOI in volume production is considered.

154 Manufacturing of VLSI CMOS on SIMOX Substrates: *J. Yue,* B. Urke, J. Kueng, R. Roisen, P. Fechner, G. Dougal,* and *M. Liu,* Solid State Electronics Center, Honeywell Inc., Plymouth, MN 55441

There has been significant improvement in the level of understanding of SIMOX (separation by implementation of oxygen) process control in the past few years. Concerns such as defect density, contamination in the top silicon layer, and pinholes in the buried oxide have been reduced drastically compared to 5 years ago. This improved SIMOX material, which is fully compatible with silicon processing, has been used to fabricate VLSI circuits with consistent functional yields comparable to bulk processes. This paper discusses the manufacturability, performance, and reliability aspects of both 1.2 and 0.8 μm CMOS technologies on SIMOX substrates.

155 High Performance Submicron CMOS/SOI for Logic and SRAM Applications: *N. Haddad,** IBM Federal Sector Div., Manassas, VA 22110, *L. K. Wang,* IBM Research Div., T.J. Watson Research Center, Yorktown Heights, NY 10598

A submicron CMOS/SOI technology is developed as an extension of a 0.5 μm bulk CMOS manufacturing technology for both memory and logic circuits. Circuit performance as well as the soft error immunity are improved to the existing designs by using SOI substrates and limited process modification. Comparison of the process complexity, circuit performance, and chip yield is presented.

156 The Implementation of a Commercial Thick Film SOI Process: *K. Yallup,* Analog Devices BV, Raheen Industrial Estate, Limerick, Ireland

SOI is an emerging technology that is ready for application to commercial integrated circuits. This paper describes one of the first uses of thick film SOI in combination with deep trench isolation for commercial dielectric isolation applications. Some of the solutions to the technological difficulties encountered while developing the dielectric isolation process and the use of such a substrate to support a 30 V CMOS process are discussed.

157 Body-Contacts for SOI MOSFETs: *M. Matloubian,* Hughes Aircraft Co., Carlsbad, CA 92009

The body region of SOI MOSFETs is floating. This leads to desirable features such as higher drive current and sleep subthreshold slope, and severe problems such as premature drain-to-source breakdown. A body-contact can be used to hold the SOI MOSFET body at a fixed potential and suppress the floating-body effects. Various types of body-contact for SOI MOSFETs are reviewed, and their effectiveness and limitations are discussed.

158 A 0.5 μm CMOS/SOI Technology Using Accumulation Mode Device Design: *L. K. Wang,** IBM Research Div., T.J. Watson Research Center, Yorktown Heights, NY 10598, *J. Seliskar, A. Edenfeld, O. Spencer,* and *N. Haddad,* IBM Federal Sector Div. Manassas, VA 22110

CMOS VLSI fabricated on thin silicon on insulator has very attractive device properties such as improved circuit performance, temperature stability, and radiation immunity. Using a fully depleted FET design on thin SOI film eliminates the "kink effect" and anomalous subthreshold current caused by the floating substrate. In addition, it can also provide higher transconductance, ideal subthreshold slope and an improvement in the short channel effect. However for a conventional device design, the device threshold voltages of the fully depleted MOSFETs would be too low for any practical applications. In this paper we report a 0.5 μm CMOS/SOI technology using reverse gate type (N+ poly/p-channel, P+ poly/n-channel) accumulation mode MOSFET design.

159 An Intelligent 500 V Power Vertical DMOS on SIMOX Substrate: *F. Vogt,* B. Mütterlein,* and *H. Vogt,* Fraunhofer-Institute für Mikroelektronische Schaltungen und Systeme, D-4100 Duisburg 1, Germany

High voltage smart power ICs need dielectric insulation to make high voltage switching possible without influencing the low voltage part. Locally applied SIMOX is used to insulate a 2 μm CMOS process from a vertical 500 V DMOS transistor. The on-state resistance of the VDMOS transistor is 0.5 Ω. Self-protecting functions are realized on the chip. A 14 mask process gives circuits for motor control or off-line applications.

160 Parasitic Capacitances of SOI MOSFETs: *J. Chen* and *R. Solomon,** Intel Corp., Santa Clara, CA 94050, *T.-Y Chan,* Cypress Semiconductor, San Jose, CA 95134, *P. K. Ko* and *C. Hu,* Dept. of Electrical Engineering and Computer Sciences, UC Berkeley, Berkeley, CA 94720

One of the major advantages of SOI MOSFET is that the parasitic capacitances are much reduced compared to those in bulk technology. Parasitic capacitances of SOI MOSFETs are important for device modeling and circuit design. In this paper, parasitic capacitances of CMOS SOI MOSFETs have been characterized. From the measurements, buried oxide thickness, and parasitic capacitances due to different sources can be extracted.

161 Transient Behavior of SOI NMOSTs at Liquid Helium Temperatures: *C. Claeys** and *E. Simoen,* IMEC, Kapeldreed 75, B-3001 Leuven, Belgium

In this paper, the threshold voltage (V_t) instability of SOI NMOSTs, observed at low temperatures is investigated in detail and explained in view of our present understanding of capture/ionization in frozen-out silicon. Particular emphasis is on the hot-carrier induced anomalous reduction of V_t, which results in a metastable low state at 4.2 K and gives rise to a pronounced hysteresis/transient behavior, for the first time reported here. This hot-carrier stress effect is investigated for different substrate types and gate-lengths. Finally, it is demonstrated that similar effects are observed for the back-gate transistor.

162 Improved Physical Modeling of Bipolar Effects in SOI Transistors: *G. A. Armstrong* and *W. D. French,* Dept. of Electrical and Electronic Engineering, Queen's University Belfast, Belfast, N. Ireland

To model bipolar snapback in thin film SOI transistors correctly, it is necessary to include bandgap narrowing in the heavily doped source region and to employ a nonlocal ballistic model of impact ionization at the drain. This improved model has been incorporated in a two-dimensional device simulator and used to give a more accurate prediction of the bipolar holding voltage in an n-channel transistor. Application of the model suggests that an ultrathin highly doped SOI film when combined with an optimized LDD should be used to maximize the bipolar holding voltage.

163 A Simple Subthreshold Model for Floating Body SOI MOSFETs: *G. Liu,* Dept. of Electrical and Computer Engineering, University of California, Irvine, CA 92717, *P. Liu,* Rockwell International Corp., Newport Beach, CA 92660, *Y. H. Chang,* and *G. P. Li,* Dept. of Electrical and Computer Engineering, University of California, Irvine, CA 92717, *J. White,* Rockwell International Corp., Newport Beach, CA 92660

A simple subthreshold model, incorporating the interaction between nonlinear feedback mechanisms of carrier generation and parasitic bipolar action, is presented here. Simulated results using this model show very good correlation with experimental data. Abrupt device transition from subthreshold to saturation explains the steep subthreshold I-V characteristics.

164 Voltage Limitations of Submicron CMOS on Thin SOI: *J. Seliskar** and *F. Brady,* IBM Federal Sector Div., Manassas, VA 22110, *L. K. Wang,* IBM Research Div., T.J. Watson Research Center, Yorktown Heights, NY, 10598, *N. Haddad,* IBM Federal Sector Div., Manassas, VA 22110

Device characteristics of 0.5 μm CMOS/SOI using both accumulation mode and enhancement mode designs are compared in terms of the short channel effect as well as the floating substrate induced drain current instability. Although the accumulation mode devices show better performance by using lighter doped substrates; the drain current instability characteristics are essentially the same for both types of devices. Yet the short channel effect for either of these two types of SOI devices are worse than the bulk CMOS at the same channel length.

165 Study of the Kink-Related Excess Low-Frequency Noise in SOI NMOSFETs at Room Temperature and 77 K: *C. Claeys* and *E. Simoen,* IMEC, Kapeldreef 75, B-3001 Leuven, Belgium

In this paper, the low-frequency noise overshoot, related to the kink in SOI NMOSTs is investigated at room temperature and at 77 K. It is demonstrated that there exists a close correlation between the impact-ionization generated holes, injected in the film and the excess noise. This overshoot increases drastically upon cooling and is strongly depending on substrate type, bias conditions, etc. These observations are explained by a model, which considers the recombination of the excess holes in the film. Finally, it is demonstrated that there exists a close relation with the

low-temperature transient behavior in SOI NMOSTs, which is very similar to the case of the kink-related excess noise in bulk transistors at liquid helium temperatures.

166 Advantages and Limitations of Thin Film SIMOX MOSFETs: Rehability Aspects: *J. Gautier* and *G. Reimbold,* DIA-LETI, CENG, 38041 Grenoble Cedex, France

In this paper, we review the advantages and limitations of SIMOX MOSFETs. Partially depleted, fully depleted, and deep depleted architecture are considered, in the case of thin silicon film, with stressing on floating substrate related effects: single latch, transient, hysteresis. We also discuss some reliability aspects, especially hot carriers effects, that are presented through a comparison between bulk and SOI technologies.

167 Hot-Carrier-Induced Degradation in Partially and Fully Depleted SIMOX MOSFETs: *S. M. Gulwadi,** ECE Dept., George Mason University, Fairfax, VA 22030, *S. Cristoloveanu,* LPCS, ENSERG INPG, BP257, 38016 Grenoble Cedex, France, *D. E. Ioannou,* ECE Dept. George Mason University, Fairfax, VA 22030, *G. Campisi* and *H. L. Hughes,* Naval Research Laboratory, Washington, DC 20375

A comparative study of hot-electron degration of the front and the back channels of partially depleted (PD) and fully depleted (FD) SIMOX MOSFETs was carried out. The back channel degraded much more than the front channel in both cases. FD transistors (film thickness > 100 nm) degraded much less than PD ones. The degradation was induced in the channel under stress, but for FD devices the properties of the opposite channel were also affected through interface coupling.

168 Back-Channel Hot-Electron Effect on the Drain Breakdown Voltage in Thin-Film SOI MOSFETs: *B. Zhang** and *T. P. Ma,* Center for Microelectronic Materials and Structures, and Dept. of Electrical Engineering, Yale University, New Haven, CT 06520-2157

The front-channel drain-source breakdown behavior in thin-film SOI MOSFETs has been studied before and after back-channel electron stress. The breakdown voltage increases significantly in the reverse mode (with source and drain interchanged) as stress time increases. The change in the breakdown behavior can be attributed to the increased barrier height of the drain-body junction resulting from the localized electron trapping near the drain in the buried oxide.

169 Numerical Analysis of Short-Channel and Drain Engineering Effects for Fully Depleted SOI MOSFETs in a Radiation Environment: *J. H. Smith** Center for Electronic Materials and Processing, Pennsylvania State University, University Park, PA 16802, *R. Lawrence,* ARACOR, Oxon Hill, MD 20745, *G. Campisi,* Naval Research Laboratory, Code 6816, Washington, DC 20375

SOI MOSFETs exhibit resistance to dose rate and single event upset radiation effects, but are susceptible to total dose effects. These total dose effects are enhanced by high electric fields in the buried oxide of these structures. A numerical device model is applied to the task of designing drain structures to decrease the electric fields present in a device as a function of channel length in order to minimize both radiation and hot electron effects.

170 Device-Based Electrical Characterization for SOI Technology Development: *D. E. Ioannou,* Dept. of Electrical and Computer Engineering, George Mason University, Fairfax, VA 22030

A review is given of the electrical characterization methods most frequently used to assess the quality of the silicon film and the buried and gate SiO_2/film interfaces, and provide feedback for the further development of SOI technology. A general evaluation is made by studying the static $I_D(V_D,V_G)$ characteristics of test MOSFET's. Bulk traps in the film are studied by current DLTS, and carrier generation by the dual-gate Zerbst-like and generation DLTS techniques. The interfaces are studied by the dynamic transconductance and charge pumping techniques. Versions and procedures for the application of these technique exist for both partially depleted (PD) and fully depleted (FD) MOSFETs, and for simpler, gated and PIN diode and capacitor structures.

171 Evaluation of ZMR SOI Films for BICMOS Application by Low Frequency Noise Investigations: *B. Tillack, R. Banisch,* and *F. Januschewski,* Institute of Semiconductor Physics, D-O-1200 Frankfurt (Oder), Germany, *A. Chovet,* Laboratoire de Physique des Composants a Semiconductors, ENSERG, 38016 Grenoble, France, *K. Hoeppner* and *H. H. Richter,* Institute of Semiconductor Physics, D-O-1200 Frankfurt (Oder), Germany

Due to the high sensitivity to traps and defects in the semiconductor material as well as near the oxide interface, low frequency noise investigations were used for the evaluation of ZMR SOI films and epitaxial films grown on them with regard to a BICMOS application. The results were supported by an electrical characterization using bipolar transistors and by crystallographic investigations using TEM and SEM.

172 Measurements and Analysis of Random Telegraph Signals in Small Area SOI MOSFETs: *O. Roux dit Buisson, G. Ghibaudo,* and *J. Brini,* LPCS/ENSERU, 38016, Grenoble, France, *T. Ouisse,* Thomson TMS, 38521, St. Egreve, France.

The purpose of this work is to present, for the first time, experimental RTS results obtained on SOI MOS devices. Small area SOI MOS devices operated at the back interface show considerably large RTS amplitude due to the large thickness of the back insulator. The RTS fluctuations at the front interface are not so large, and are not influenced by those of the back interface, while the front and back interface coupling is weak. However, in the case of strong front and back interface coupling, *i.e.,* for thin-film SOI technology, the RTS fluctuations of the back interface may propagate to the front interface and, therefore, could result in a large parasitic source of low frequency noise in such devices.

173 A New Transient Drain Current Technique for Interface Characterization in SOI MOSFETs: *S. Cristoloveanu,* LPCS, ENSERG, 38016 Grenoble Cedex, France, *H. Haddara,* Electronics and Computer Engineering Dept., Ain-Shams University, Abbasia, Cairo, Egypt, *M. T. Elewa,* Electrical Engineering Dept. Zagazig University, Shobra, Cairo, Egypt

A new technique for the characterization of interface traps in SOI MOSFETs is proposed. This technique is based on a novel analytical transient drain current model in the weak inversion regime. The method is capable of providing the same information as charge pumping but with much higher sensitivity. Measurements were carried out on partially depleted five terminal SIMOX transistors. Experimental measurements are in agreement with the model and the obtained results for the average interface trap density are in the same order as that obtained from the subthreshold slope of the drain current.

174 Defects in SIMOX Structures: Characterization and Some Formation Mechanisms: *J. Margail** and *J. M. Lamure,* CEA/DTA/LETI, Grenoble Cedex, France, *J. Stoemenos,* University of Thessaloniki, 54006 Thessaloniki, Greece, *A. M. Papon,* CEA/DTA/LETI, Grenoble Cedex, France

In this paper, dislocation and buried oxide discontinuities density measurements on SIMOX material, using chemical etching methods, are presented and discussed. The quality status of standard LETI material based on statistical analysis is given. We also show that slight changes in the material fabrication process (*e.g.,* implantation through a 250 nm thick screen oxide) can severely degrade the crystallinity of the top silicon film. (An increase of dislocation density from 10^5 to 10^9 cm^{-2} has been observed.)

175 Effect of Thermal Ramping Conditions on Defect Formtion in Oxygen Implanted Silicon-on-Insulator Material: *S. Krause, J. D. Lee,* and *J. C. Park,* Chemical, Bio and Materials Engineering, Arizona State University, Tempe, AZ 85287, *P. Roitman,* Semiconductor Electronics Div., NIST, Gaithersburg, MD 20899, *M. El-Ghor,* Texas Instruments, Inc., Central Research, Laboratory, Dallas, TX 75265

The effects of intermediate thermal processing steps on the microstructure of oxygen implanted silicon-on-insulator (SIMOX) material were studied with cross-section and plan view transmission electron microscopy. Intermediate, 2 h isothermal annealing cycles eliminated as-implanted defects (stacking faults, multiply faulted defects, and {113} defects) at 1000°C. New defects (stacking faults and a polygonalized dislocation network) formed near the upper and lower interfaces of the buried oxide, but the defect size and defect density were reduced at 1100°C and eliminated at 1200°C. At 1300°C a defect density of 10^6 cm^{-2} was found. When an as-implanted sample was rapid thermal annealed at 1300°C for 1 min, the top third of the top Si layer had a "denuded" zone which was preciptate free, but many dislocations extending to the surface had formed. In a subsequent standard anneal for 5 h at 1300°C the dislocations were not removed and a defect density of 10^9 cm^{-2} was found. The results show that intermediate thermal processing steps, including intermediate isothermal annealing and rapid thermal annealing, strongly affect the final microstructure of SIMOX material.

176 Screen Oxide Effects on the SIMOX Material Quality Observed by Raman Microprobe Measurements: *A. Perez-Rodriguez** and *J. R. Morante,* LCMM, Dept. Fisica Aplicada i Electronica, Universitat de Barcelona, 08028-Barcelona, Spain, *E. Martin* and *J. Jimenez,* Dept. Fisica de la Materia Condensada, Universidad de Valladoled, 47011 Valladoled, Spain, *J. Margail* and *A. M. Papon,* CEA, DTA, LETI, Grenoble Cedex, France

In this work we present the structural analysis of SIMOX samples implanted through different thicknesses of screen oxide by Raman microprobe measurements. The spectra obtained from as implanted and annealed samples have been correlated with TEM observations. The results obtained, in terms of strain, disorder, and thermal effects distributions, show a strong dependence of the top Si layer structure on the thickness of the screen oxide, which corroborates the key role of the surface conditions on the sample structure.

177 Kinetics of Oxygen Precipitation in Low Fluence SIMOX: *L. Meda, C. Spaggiari, G. F. Cerofolini,* and *S. Bertoni,* IGD Enichem, 20097 S. Donato-Mi, Italy, *R. Canteri,* IRST Div. Scienza Mat., 38100 Povo-Tn, Italy

The aim of this work is the study of precipitate formation after proper thermal treatments in low fluence oxygen-implanted samples. The precipitates and the extended defects behave as a well for oxygen and are the nuclei for the subsequent precipi'ate

growth; so that it is possible to deplete oxygen from regions where large precipitates are not formed and accumulate oxygen in special perturbed sites, because the oxygen diffusion against concentration gradient takes place. The kinetics of precipitate formation is followed at increasing fluences (in the range 10^{15}–10^{17} O/cm^2) in the temperature range 450°-800°C, starting from an initial condition obtained by implanting at low current density to maintain cool the sample. Cross-section and plain view micrographs have been obtained by TEM and HREM and oxygen profiles have been obtained by SIMS.

178 Novel Approach to Defect Etching in Thin Film SOI: *H. Gassel,* J. Peter-Weidemann* and *H. Vogt*, Fraunhofer-Institut für Mikroelektronische Schaltungen und Systeme D-W4100 Duisburg, Germany

A new etch process including three sequential etch steps was developed to measure low defect densities in thin SOI silicon films. It allows for a fast, simple, and cost effective measurement of defect densities in a range of about 10^3–10^9 cm^{-2}. Dependence of defect density on the implanted oxygen dose has been studied for SIMOX wafers. The experiment shows an exponential increase of defect density with the dose. A comparison with plan view TEM results is under investigation. Main advantages of this approach compared to earlier ones are independence of defect density and improved simplicity in addition to a better image contrast.

179 Correlation Between X-Ray Moiré Pattern and Dislocation Density in SIMOX: *M. K. El-Ghor* and *K. A. Joyner*, Texas Instruments, Inc., Dallas, TX 75265, *G. A. Rozgonyi*, Dept. of Materials Science and Engineering, North Carolina State University, Raleigh, NC 27695-7916

Singly and multiply implanted SIMOX wafers were evaluated using Lang transmission x-ray topography as well as chemical etching. Moiré patterns were clearly observed in the multiple implanted material and some areas in the single implanted ones. It is found that wafers having dislocation densities greater than 8 x 10^4/cm^2, exhibited no moiré patterns. Strong moiré fringes were seen for densities less than 10^3/cm^2. This indicates the capability of XRT to screen SIMOX material for dislocations.

180 Raman Scattering and FTIR Spectroscopy as Characterization Techniques of SIMOX Structures: *J. Samitier,* A. Perez-Rodriguez*, and *J. R. Morante*, LCMM, Dept. Fisica Aplicada i Electronica, Universitat de Barcelona, 08028-Barcelona Spain, *E. Martin*, and *J. Jimenez*, Dept. Fisica de la Materia Condensada, Unversidad de Valladolid, 47011 Valladolid, Spain, *P. L. F. Hemment*, Dept. of Electronic and Electrical Engineering, University of Surrey, Guildford, Surry, England GU2 5XH

The characterization of SIMOX obtained by different processes has been performed by Raman scattering for the top Si layer and FTIR for the buried oxide one. Raman spectra obtained from the whole structures and from beveled samples at different excitation powers show significant differences related to the technological processes, determined by the strain distribution and thermal conductivity in the Si layers. Structural differences are also observed from FTIR spectra, which indicate the existence of different values of the disorder effects and residual stresses in the buried oxides. The ability of both techniques for the SIMOX structural characterization is demonstrated.

181 Electro-Optical Characterization of SIMOX Structures by Photoconductive Based Techniques: *J. Macia,* A. Perez-Rodriguez*, and *J. R. Morante*, LCMM, Dept. Fisica Aplicada i Electronica, Universitat de Barcelona, 08028-Barcelona, Spain, *M. A. Lourenco, P. L. F. Hemment*, and *K. P. Homewood*, Dept. of Electronic and Electrical Engineering, University of Surrey, Guildford, Surrey, England GU2 5X4

The characterization of SIMOX structures is performed by the combination of photoconductive frequency resolved spectroscopy (PCFRS) and photo induced current transient spectroscopy (PICTS). PCFRS shows the existence of an exponential recombination behavior with a lifetime in the range 10-100 μs. However, in some cases values of the ambipolar mobility in the range of 60 cm^2/Vs are found. These have been correlated with PICTS spectra, which show a density of Si/SiO_2 interface defects above 10^{12} cm^{-2} eV^{-1}. The analysis carried out confirms the suitability of the combined PCFRS and PICTS techniques for the electrical evaluation of SIMOX structures.

182 The Effects on Carrier Lifetime of SIMOX Anneal Process Parameters: A Designed Experiment: *K. A. Joyner*, Texas Instruments, Inc., Dallas TX 75265

A designed study of the effects of high temperature anneal process variables on the properties of SIMOX films was conducted. In this study, the effects of the anneal variables were examined, and coefficients for a linear model were derived. Modeling of the minority carrier lifetime produced quantitative results and revealed a strong effect of HCl incorporation, temperature, and anneal time. Higher HCl concentrations, lower temperatures, and shorter anneal times resulted in longer carrier lifetimes.

183 Nondestructive SOI Process Evaluation Using Recombination Lifetime Measurements: *A. Buczkowski,** and *F. Shimura*, Dept. of Materials Science and Engineering, North Carolina State University, Raleigh, NC 27695-7916, *B. Cordts*, IBIS Technology Corp., Danvers, MA 01923, *G. A. Rozgonyi*, Dept. of Materials Science and Engineering, North Carolina State University, Raleigh, NC 27695-7916

The properties of the buried $Si-SiO_2$ interface, the concentration of structural defects, and the level of contamination have been monitored nondestructively via their effect on the surface and bulk components of recombination lifetime by a laser/microwave photoconductance technique. It has been found for single implant/anneal SIMOX material that the bulk recombination lifetime decreased from 1 ms, characteristic of origin substrates, to 35 μs or to 8 μs if the annealing alone (no implantation), or both implantation and annealing processes have been applied, respectively. Moreover, the $Si-SiO_2$ interface still contains a very high density of electrical defects even after the structural damage removing/oxide forming high temperature treatment. This defect density results in a surface recombination velocity on the order of 1000 cm/s, two or three orders of magnitude more than a surface subjected to annealing alone (without implantation), and only one order less than material implanted, but nonannealed.

184 Investigation of Local Isolation Structures on SIMOX Substrates with Micro-Raman Spectroscopy and Correlation with XTEM: *I. De Wolf,** Interuniversity Micro-Electronics Center (IMEC), Kapeldreef 75, B-3001 Leuven, Belgium, *A. Romano-Rodriguez*, LCMM Department de Física Aplicada i Electrònica, University of Barcelona, Diagonal 645, E-08028 Barcelona, Spain, *J. Vanhellemont*, Interuniversity Micro-Electronics Center (IMEC), Kapeldreef 75, B-3001 Leuven, Belgium, *H. Norström*, Swedish Institute of Micro-Electronics, S-16421 Kista, Sweden, *H. E. Maes*, Interuniversity Micro-Electronics Center (IMEC), Kapeldreef 75, B-3001 Leuven, Belgium

LOCOS structures on SIMOX wafers were studied with cross-sectional transmission electron microscopy and with micro-Raman spectroscopy (μRS). Prolonged field oxidation results in considerable oxidation of the active silicon film, giving rise to a curved interface. μRS showed that the local mechanical stress variations in LOCOS on SIMOX wafers are similar to the ones observed in LOCOS structures on conventional substrates. Field oxidation for longer times results in increased stress levels.

185 Dislocation-Free SIMOX Substrates: *A. Yoshino*, Becton Center, Yale University, New Haven, CT 06520-2157

This is the first report of dislocation-free SIMOX substrates. We present experimental results showing the effects of various process parameters on the dislocation density in SIMOX substrates. Comparing the results for the samples formed by single-implant with those formed by double-implant, together with the data from RBS, optical microscope, SEM and TEM measurements and wafer warp evaluation, the possible origin of the dislocation formation mechanism is discussed.

186 Effects of High Temperature Anneal Variables on SIMOX Films: *K. A. Joyner,* M. K. El-Ghor*, and *H. H. Hosack*, Texas Instruments, Inc., Dallas, TX 75265, *A. K. Rai*, Universal Energy Systems, Dayton, OH 45432

A study of the effects of high temperature anneal process variables on the properties of SIMOX films was conducted. The study was structured as a designed experiment with seven variables, each at three levels. Modeling of the dislocation density produced quantitative results and revealed a strong effect of temperature and measurable effects of time and ramp rate. Higher temperatures, lower ramp rates, and longer anneal times resulted in lower dislocation densities.

187 The Effects of HCl in SIMOX Annealing: A Time Series Experiment: *K. A. Joyner** and *G. A. Brown*, Texas Instruments, Inc. Dallas, TX 75265

A study of the effects of HCl inclusion in the SIMOX high temperature annealing ambient on tube self-contamination and radiation immunity was conducted. Contamination was studied by measurement of minority carrier lifetime and radiation immunity by MOS capacitor C-V curve shift. Inclusions of 5% HCl at a temperature of 1000°C was sufficient to restore furnace cleanliness. Neither the moderate levels of contamination nor the presence of HCl had any effect on radiation hardness.

188 Post-Oxygen-Implant Anneal Effects on SOI Transistor Electrical Characteristics: *G. V. Rouse* and *R. D. Cherne*, Harris Semiconductor, Melbourne, FL 32902, *W. A. Krull*, IBIS Corp., Danvers, MA 01923

The relationship between SIMOX anneal temperature and CMOS transistor characteristics are investigated. Post-oxygen implant anneal temperatures from 1150 to 1320°C were used in an Ar/O_2 atmosphere with a minimum of three wafers per test. Back-channel threshold voltage increases while snap-back sustaining voltage decreases with increasing anneal temperature. Transistor off-leakage current was found to be independent of anneal temperature.

189 A High-Quality SIMOX Wafer and Its Application to Ultrathin-Film MOSFETs: *S. Nakashima, Y. Omura*, and *K. Izumi*, NTT LSI Laboratories, 3-1 Morinosato Wakamiya, Atsugi 243-D1, Japan

A high-quality SIMOX wafer with extremely low dislocation densities of less than 300 cm^{-2} and an 80 nm buried oxide layer is introduced. Employing the SIMOX wafer to fabricate an 0.085 μm

gate, n and pMOSFET demonstrates that SIMOX has excellent potential for future ULSI applications.

190 The Effects of Dose and Target Temperature on the Low Energy (70 keV) SIMOX Layers: *Y. LI,* J. A. Kilner,* and *R. J. Chater,* Dept. of Materials, Imperial College, London, England SW7 2BP, *P. L. F. Hemment, A. Nejim, A. K. Robinson,* and *K. J. Reeson,* Dept. of Electronic and Electrical Engineering University of Surrey, Guildford, Surrey, England GU2 5XH, *C. D. Marsh* and *G. R. Booker,* Dept. of Materials, University of Oxford, Oxford, England OX1 3PH

The dislocation density and the density of silicon islands in annealed (70 keV) SIMOX layers are found to be strongly dependent upon the oxygen dose. The critical dose required to form a continuous buried stoichiometric oxide layer either during implantation, Φ_c^I, or after implantation and annealing, Φ_c^A were estimated to be $\approx 7 \times 10^{17}$O$^+$/cm^2 and $\approx 3 \times 10^{17}$O$^+$/cm^2, respectively. Good quality, thin film SIMOX layers (with a low threading dislocation density in the silicon overlayer and low density of silicon islands in the buried SiO_2 layer) have been produced by implantation of both 3.3×10^{17}O$^+$/cm^2 at 680°C and 3×10^{17}O$^+$/cm^2 at 550°C.

191 Etch-Stop Layer in Silicon Produced by Implantation of Electrically Inactive Impurities: *Q.-Y. Tong,* G. Cha, H.-M. You,* and *U. Gösele,* Dept. of Mechanical Engineering and Materials Science, Duke University, Durham, NC 27706, *D. Feijoo,* AT&T. Reading, PA 19612-3396

The etch stop performance of carbon implanted layer in silicon was found to be not only dependent on carbon concentration but also related to the etchant used and the structural properties of the layer. Thermal annealing reduces the damage and defects resulting in degraded etch stop performance. Silicon self-implantation and germanium implantation also show etch stop function resulting from formation of amorphized layer and inisotropic etch character of etchant used.

192 SIMOX: An Efficient Etch-Stop to Fabricate Silicon Membranes with Well-Defined Thickness: *H. Gassel,* H. G. Dura, W. Mokwa,* and *H. Vogt,* Fraunhofer-Institut für Mikroelectronische Schaltungen und Systeme, D-4100 Duisburg, Germany

This paper shows that SIMOX wafers with an epitaxial silicon layer are an excellent material for the production of homogeneous silicon membranes with well-defined thicknesses. Due to the very high selectivity of TMAH as etch solution, a four times lower oxygen dose than for standard SIMOX production is sufficient to form a good etch stop layer. This technique allows for a simple and very cost effective batch process production in addition to a large improvement of the silicon film quality.

193 Reactive Ion Etching of SOI (ZMR and SIMOX) Silicon in $CF_4 + O_2$ and $SF_6 + O_2$ Plasmas: *O. W. Purbo* and *C. R. Selvakumar,* Dept. of Electrical and Computer Engineering, University of Waterloo, Waterloo, Ont. Canada N2L 3G1, *D. Misra,* Dept. of Electrical and Computer Engineering, New Jersey Institute of Technology, University Heights, Newark, NJ 07102

The results of a comparative study of the etch rates and selectivities of bulk-silicon and SOI samples (SIMOX and ZMR) using $CF_4 + O_2 + N_2$ and $SF_6 + O_2 + N_2$ plasmas are reported. The N_2 addition increases etch rates in both plasmas and, thus, increases selectivities (11-45%). The etch rate enhancement due to N_2 addition in CF_4 plasma (45-140%) is more than in SF_6 plasma (2-7%).

194 Gettering of Bonded SOI Layers: *H.-D. Chiou,* F. Secco d'Aragona,* and *E. Strickland,* Discrete and Materials Technology Group, Motorola Inc., Phoenix, AZ 85005

Thin SOI layers created by bonding two oxidized wafers lack IG ability and are consequently susceptible to defect formation during processing. This is because during bonding, oxygen diffuses towards the middle oxide layer leading to a denuded zone (DZ) in proximity of the oxide. SOI layers ≤ DZ if oxidized will show microdefects in the shape of OISF. To improve the gettering ability of SOI layers we implanted different doses of boron, phosphorus, or oxygen in selected areas of the SOI layers with different size of patterns before or after wafer bonding. The results of the lateral gettering for the various implanted species are reported.

195 50 nm Thick SOI Fabrication by Advanced ELO: Tunnel Epitaxy: *A. Ogura,* A. Furuya,* and *R. Koh,* NEC Corp., Microelectronics Research Laboratories, 34 Miyukigaoka, Tsukuba, Ibaraki 305, Japan

ELO is well known as an SOI fabrication technique with good crystalline quality. However, conventional ELO is not applicable for thin SOI fabrication which is considered to have great potential for future nano-structure devices. We present an advanced ELO technique called tunnel epitaxy, in which the lateral epitaxy is grown in a small gap between the upper and the lower SiO_2. Therefore, the fabricated SOI thickness can be precisely controlled by the gap height. Thin SOI films with thicknesses of 50-200 nm were fabricated using this technique.

MATERIALS AND PROCESSING ISSUES FOR LARGE SCALE INTEGRATED ELECTRONIC AND PHOTONIC ARRAYS

Electronics/Dielectric Science and Technology

196 Full Wafer Technology for Large Scale Laser Fabrication and Integration: *P. Vettiger,* IBM Research Div., Zurich Research Laboratory, 8803 Ruschlikon, Switzerland, *M. K. Benedict,* IBM Corp., Kingston, NY 12401, *G. L. Bona* and *P. Buchmann,* IBM Research Div., Zurich Research Laboratory, 8803 Ruschlikon, Switzerland, *N. Cahoon,* IBM East Fishkill, Hopewell Junction, NY 12533, *K. Datwyler, H. P. Dietrich, A. Moser,* and *H. K. Seitz,* IBM Research Div., Zurich Research Laboratory, 8803 Ruschlikon, Switzerland, *O. Voegeli,* Almaden Research Center, San Jose, CA 95120, *D. J. Webb* and *P. Wolf,* IBM Research Div., Zurich Research Laboratory, 8803 Ruschlikon, Switzerland

Semiconductor laser applications for consumer products (primarily for compact disk players) increased the worldwide demand for lasers to several tens of millions of devices per year. However, today's manufacturing technologies cannot accommodate this steadily increasing demand since fabrication and testing of semiconductor lasers are still on the level of discrete devices as was the case in the early days of transistor fabrication. This is in marked contrast to the current technology used to fabricate VLSI circuits. A new concept/technology is presented called full wafer (FUWA) fabrication and testing that produces high-quality semiconductor lasers. It features an excellent potential for high processing yield and testing throughput. In addition to large-scale fabrication, the etched mirror technology offers the capability of integrating new functions and other opto-electronic devices. FUWA technology is well suited for lasers used in such applications as optical storage and interconnects.

197 Microfabrication of Ultra-Small Optical Cavities: *A. Scherer, E. Yablonovich, J. L. Jewell, B. P. Van der Gaag,* and *E. D. Beebe,* Bellcore, Red Bank, NJ 07701

High-resolution microfabrication allows us to define small three-dimensional optical cavities which can reduce the threshold power required for switching or lasing. To demonstrate this, we have measured the lasing behavior in 0.4 μm wide surface-emitting microlasers. We have also fabricated completely three-dimensional "photonic bandgap" structures which can be incorporated to define optical cavities in future surface emitting lasers. These fabrication methods are expected to be used to substantially reduce the threshold currents of future surface-emitting lasers.

198 Surface Emitting Laser-Lasing Characteristics and Its Functional Operations: *F. Koyama* and *K. Iga,* Tokyo Institute of Technology, P&I Lab., 4259 Nagatsuta, Midori-ku, Yokohama 227, Japan

The surface emitting (SE) laser is rapidly attracting a current research looking forward to future parallel optoelectronics, including optical interconnects and optical parallel processing. We review our recent work on GaAlAs/GaAs and GaInAsP/InP SE lasers, especially focusing on lasing characteristics such as polarization characteristics and quantum noises. The future prospects and basic technologies for SE lasers are also addressed. In addition, a possibility of a polarization independent and low power consumption active filter based on the SE laser is presented.

199 Laser and Photoreceiver Arrays for Parallel Optical Data Link Applications: *N. K. Dutta* and *P. R. Berger,* AT&T Bell Laboratories, Murray Hill, NJ 07974

Very low threshold ($I_{th} \sim 1$ mA) lasers emitting near 1.3 μm have been fabricated using multiquantum well active region, short cavity length, and high reflectivity facet coatings. A laser array transmitter utilizing these lasers can be operated with prebias, and has negligible skew for 1 Gb/s operation. No crosstalk is observed when adjacent elements of the laser array are modulated. A PIN-MODFET photoreceiver array comprised of a p-i-n InGaAs photodiode integrated with an InGaAs/InAlAs MODFET using MBE has been fabricated. The MODFET has a transconductance of 560 ms/mm and f_T and f_{max} of 57 and 66 GHz, respectively. The p-i-n photodiode has a responsivity of 0.3 A/W and bandwidth of >10 GHz.

200 An Individually Addressed Dense 102-Laser Array: *T. Kobayashi, H. Narui, M. Dohsen, O. Matsuda,* and *Y. Mori,* Sony Corp., Research Center, 174, Fujitsuka-cho, Hodogaya-ku, Yokohama 240, Japan

We have successfully fabricated a very dense one-dimensional semiconductor laser array using separated double heterostructure (SDH) lasers. The array consists of 102 lasers, each of which can be addressed individually. The pitch of the lasers is 4.5 μm. Typical threshold current and output power were 2 mA and 3 mW/facet (I = 10 mA) for a laser under continuous wave operation at room temperature. The density and the number of lasers are the highest ever reported.

201 Anisotropic Photoetching of GaAs: *E. Mannheim, R. L. Sani,* and *R. C. Alkire,* Dept. of Chemical Engineering, University of Illinois, Urbana, IL 61801

A two-dimensional mathematical model was used to obtain the current and potential distribution near the illuminated region of a semiconductor during photoetching. The potential distribution was described by Poisson's equation. Electron and hole transport equations included generation, diffusion, migration, and recombination terms. A commercial finite element fluid dynamics code, FIDAP, was modified to numerically solve the model equation. The sensitivity of the process with respect to the important parameters was investigated.

202 Two-Dimensional Vertical to Surface Transmission Electro-Photonic Device Array for Optical Interconnection: *K. Kasahara,* Opto-Electronics Research Laboratories, NEC Corp., 34, Miyukigaoka, Tsukuba, Ibaraki 305, Japan

The vertical to surface transmission electro-photonic device (VSTEP) is a concept proposed to allow functional optical interconnection. This paper focuses primarily on the laser-mode VSTEP. The design of vertical-cavity VSTEPs and their fabrication using MBE-grown epitaxial structures is described and their characteristics are discussed. A 4 × 4 optical self-routing switch, fabricated using vertical-cavity VSTEPs is described.

203 Long Wavelength Infrared 128 × 128 Starring Array from AlGaAs/GaAs Multiquantum Well Detectors-Growth, Processing, and Array Performance: *V. Swaminathan,* AT&T Bell Laboratories, Breinigsville, PA 18031

Quantum well infrared photodetectors (QWIPs) utilizing intersubband transitions in AlGaAs/GaAs multiquantum well structures have emerged as an attractive alternative to HgCdTe for long wavelength infrared applications. Recently, a first generation (128 × 128) AlGaAs/GaAs QWIP focal plane starring array with excellent imaging performance and a noise equivalent temperature of 10 mK has been demonstrated. In this paper, we discuss the principles of operation of QWIP, design and fabrication of the array, and the results from the imaging demonstration.

204 Be^+ Ion Implantation in Ga(Al)Sb Layers: Radiation Damage: *M. Perotin, H. Luquet, L. Gouskov,* and *A. Sabir,* Centre d'Electronique de Montpellier, Universite Montpellier II, 34095 Montpellier Cedex, France, *A. Perez,* Laboratoire de Physique des Materiaux, Universite Claude Bernard, Lyon I, 69622 Villeurbanne, France

For the first time, study of Be^+ ions implantations is carried out in G(Al)Sb compounds. Be^+ ions are implanted into low doped Te $Ga_{0.96}Al_{0.04}Sb$ epilayers grown by liquid phase epitaxy. Low damaging level is found to occur in the G(Al)Sb layers in relation with the weak mass of the beryllium ions, a quasi total restoration being performed through some annealings. A complete activity of the Be-implanted ions is measured in the annealed implanted layers. Double Be^+ implant in Ga(Al)Sb layers leads to abrupt junctions of good quality.

205 Integrated Optoelectronic Device Technology: *S. R. Forrest,* Dept. of Electrical Engineering and Materials Science, University of Southern California, Los Angeles, CA 90089-0241

The field of integrated optoelectronics has faced numerous bottlenecks since the first devices were demonstrated more than 10 years ago. However, as photonic systems have advanced in both sophistication and performance, the level of integration required for these advances has not kept pace. We are now at a critical point in the short history of this technology where it is essential that practical integrated devices with clear advantages in performance, functionality, and cost are demonstrated over competitive hybrid technologies. The means for achieving these devices has been to develop materials growth and fabrication processes which lead to the simplified fabrication of highly complex integrated structures. These processes include use of selective etchants and sacrificial materials layers, hybrid growth (*e.g.*, GaAs on Si) and packaging technologies (*e.g.*, graphoepitaxy), and clever design of multifunctional materials and device structures. In this paper we address many of the bottleneck issues now confronting advanced integrated optoelectronic circuit technology.

206 Devices and Processes for Integrated Photoreceivers on InP: *A. Scavennec, L. Giraudet, P. Blanconnier, G. Post J. P. Praseuth,* and *A. Temmar,* CNET-Laboratoire de Bagneux, 92220 Bagneux, France

Monolithic photoreceivers or photoreceiver arrays with good sensitivity, produced at low cost, are expected to contribute in opening new application areas such as distributive telecom services, broadband switching, etc. The fabrication of such monolithic photoreceivers on InP has been faced with basic problems, such as insufficient performances of InP-based FETs at moderate frequency, processing compatibility of transistors and photodetectors, and immature development of the InP technology. In recent years major progress has been made in these different areas, and is illustrated by recent developments at CNET on pin-FET front ends and metal-semiconductor-metal photodiode arrays.

207 GaAs-on-InP, Receiver Transmitter Optoelectronic Integrated Circuit: *P. J. O'Sullivan* and *D. A. Allan,* BT Laboratories, Martlesham Heath, Ipswich, England IP5 7RE

Long wavelength optoelectronic integrated circuits (OEICs) are expected to be important components for future communication systems, *e.g.*, as nodes on high speed optical networks. This paper reports the fabrication of a monolithic GaAs-on-InP, long wavelength, optical regenerator integrating an optical detector and transmitter together with digital and analog electronics (a total of 123 components). This is, to our knowledge, the highest functionality, long wavelength, transceiver OEIC yet demonstrated.

208 Computer Simulation and Characterization of MBE Growth of AlGaAs/GaAs Heterostructures: *P. E. Kosel* and *T. R. Krishna,* University of Cincinnati, Cincinnati, OH 45221

A computer simulation program (MBESIM) has been developed for the simulation of growth of complex materials in the AlGaAs/GaAs material system. MBESIM has been applied (*i*) in determining the sensitivity of a device structure to growth perturbations in a given MBE system, (*ii*) for devising growth recipes for novel material structures, and (*iii*) for providing fine structure information about grown materials for use in device simulators. MBESIM takes account of the major known features of MBE growth and the system in which the growth is performed. These include (*i*) the 3D nature and distribution of the effusion cells, (*ii*) the characteristics of the melt and crucible wall surfaces, (*iii*) the sticking and re-evaporation coefficients of the host and dopant species, and (*iv*) the diffusion and segregation properties of dopants in the growing host material. Interface roughness is incorporated through a semi-empirical model to account for the effects of growth interruptions at interfaces. MBESIM has been applied to the prediction of spread in material characteristics for HEMT devices and heterojunction CCDs and NIPI superlattices. This paper will report on the application of MBESIM to the study of HEMT electrical performance variations caused by MBE process variations.

209 Formation of Epitaxial $CoSi_2$ Films on (001) Silicon Using Ti-Co Alloy and Bimetal Source Materials: *S. L. Hsia, T. Y. Tan, P. L. Smith,* and *G. E. McGuire,* Microelectronics Center of North Carolina, Research Triangle Park, NC 27709

Using a Ti-Co bimetallic layer as a reaction source with Si substrates, epitaxial $CoSi_2$ films have been grown on (001) Si via rapid thermal annealing. The films' resistivity and thermal stability are excellent. The epitaxial $CoSi_2$ layers are single crystal films containing anti-phase domains. Models of the $CoSi_2$/Si interfacial structure have been constructed for [001] and [111] orientations. These models reveal that anti-phase boundaries serve the role of relieving the lattice mismatch between the epitaxial $CoSi_2$ film and the Si substrate.

SECOND INTERNATIONAL SYMPOSIUM ON THE PHYSICS AND CHEMISTRY OF SiO_2 AND THE Si-SiO_2 INTERFACE

Electronics/Dielectric Science and Technology

210 Silicon Oxides and Silicon Oxidation: *A. M. Stoneham,* AEA Industrial Technology, Harwell Laboratory, Didcot, Oxon, England OX11 0RA

Needs for thinner oxides and higher quality raise processing problems and demand better understanding of the silicon/oxide interface. This paper reviews the theory of (*i*) the evidence for a modified near-interface oxide, and its characteristics (stoichiometry, reactivity, structure, and structural evolution), (*ii*) the role of roughness and of electrostatics, (*iii*) the implications of electrical noise and breakdown data, and (*iv*) the localized electronic processes which might be involved and their relationship to bulk SiO_2 data.

211 Use of ^{18}O Labeling to Study Growth Mechanisms in Dry Oxidation of Silicon: *I. Trimaille, J.-J. Ganem,* and *S. Rigo,* Université Paris 7, Groupe de Physique des Solides, 75251 Paris Cedex 05, France, *S. I. Raider* and *N. A. Penebre,* IBM Research Division, T.J. Watson Research Center, Yorktown Heights, NY 10598

Oxygen fixation during dry oxidation of silicon was investigated using ^{18}O labeling. We showed that the variation of the amount of oxygen fixed near the external surface of the oxide as a function of oxide thickness was not related to the variation in the oxidation rate at the Si-SiO_2 interface. To show this, we oxidized in $^{18}O_2$ nitrogen-implanted SiO_2 structures for which interfacial oxidation is inhibited and compared with $Si^{18}O_2$ films of same thicknesses.

212 Strain Dependent Diffusion during Dry Thermal Oxidation of Crystalline Si: *C. H. Bjorkman* and *G. Lucovsky,* Dept. of Physics, North Carolina State University, Raleigh, NC 27695-8202

The effect of strain on the rate of dry thermal oxidation of silicon has been investigated. Local atomic strain in SiO_2 films, grown in two steps separated by an intermediate anneal, was determined by infrared spectroscopy. The results support an oxidation model based on strain dependent diffusion of oxygen to the growth interface. In this interpretation, the intermediate annealing step enhances the diffusion of oxygen through the oxide grown before the anneal, and therefore increases the oxidation rate.

213 Oxidation of Silicon in Oxygen: Measurement of Film Thickness and Kinetics: *S.-C. Kao* and *R. H. Doremus,* Rensselaer Polytechnic Institute, Materials Engineering Dept., Troy, NY 12180-3590

Ellipsometry, transmission electron microscopy (TEM), and step-profile measurement are used to study the dry oxidation kinetics of silicon at temperatures from 750 to 1100°C. For oxide film thicker than 80 nm, all three thickness measurements agree within experimental error. For oxide film thinner than 35 nm, the ellipsometry gives higher thickness values than the TEM measurements. Thickness measurements by TEM below 50 nm were combined with measurements on thicker films by all three measurements and fitted by a linear-parabolic relationship throughout the measured thickness range. Previous deviations from linear-parabolic behavior result from inaccurate thickness measurements by ellipsometer for film thinner than 30 nm.

214 Modeling Process-Dependent Thermal Silicon Dioxide (SiO_2) Films on Silicon: *H. Wei* and *A. K. Henning,* Thayer School of Engineering, Dartmouth College, Hanover, NH 03755, *J. Slinkman* and *J. Rogers,* IBM General Technology Div., Essex Junction, VT 05452

This study models the process-dependent SiO_2 film microstructure and associated high frequency dielectric constants. For Si-device dielectric thicknesses under 200 Å, the correct understanding of bulk SiO_2 and interlayer film thicknesses is essential to device physics studies, such as accurate CV data interpretation, proper image charge accounting, spectral reflectance data reduction, and hot-carrier reliability analysis. We demonstrate the need for a two-layer model by exploring the characteristic signature of ellipsometric data reduced using a one-layer model, and comparing it to a two-layer model. We conclude with extraction of index of refraction data for both interfacial and bulk portions of the oxide films, using the two-layer model, as a function of processing temperature.

215 New Approach to Chemically Enhanced Oxidation—A Review: *R. J. Jaccodine,* Lehigh University, Sherman Fairchild Laboratory, Bethlehem, PA 18015

A new approach to the technology of silicon oxidation involves the use of very low concentrations (ppm) of an appropriate fluorine compound to the oxidant stream. This paper reviews the role of fluorine as an additive to the oxidation process and some of the related studies that indicate its advantage over present state-of-the-art oxidation practice. The work is discussed by considering experimental techniques and growth kinetics, along with stacking faults annealing, OED/ORD, and MOS characterization.

216 Kinetics of Oxidation of Silicon by Electron Cyclotron Resonance Plasma: *J. Joseph,* Ecole Centrale de Lyon, Ecully, France; *Y. Z. Hu* and *E. A. Irene,* Dept. of Chemistry, University of North Carolina, Chapel Hill, NC 27599-3290

The electron cyclotron resonance, ECR, plasma oxidation of silicon was investigated using *in situ* during process static spectroscopic ellipsometry and dynamic real time ellipsometry. Through the use of a temperature independent photon energy fast dynamic oxidation kinetics measurements were performed. Along with spectroscopic ellipsometric measurements, the kinetics are interpreted in terms of an electric field assisted model where ionic species dominate the kinetics. Interface damage was also assessed.

217 Mechanisms of Oxidation Rate Enhancement in Negative-Point Oxygen Corona Discharge Processing of SiO_2 Films on Si: *L. M. Landsberger,* Dept. of Electrical and Computer Engineering, Concordia University, West Montreal, Que., Canada H3G 1M8

Negative-point oxygen corona discharge processing at 600-900°C dramatically enhances the oxidation rate, while creating SiO_2 films with the refractive indexes and oxygen transport characteristics normally found in films dry-thermally grown at 1000-1200°C. By an analysis of the atomic mechanisms affecting the corona-treated region, features of the film thickness enhancement profile are quantitatively explained by additive components: fieldaided O ion flux, enhanced oxygen diffusion, and relaxed oxide density differential.

218 High Pressure, Low Temperature Oxidation of $Si_{1-x}Ge_x$: Promise for MOS-Quality Passivation: *C. Caragianis, Y. Shigesato,* and *D. C. Paine,* Div. of Engineering, Brown University, Providence, RI 02912

Thermally grown SiO_2 on Si is technologically essential since it provides high quality electronic passivation of surfaces and junctions in Si-based microelectronics. Such a simple method of producing device quality passivation does not exist, however, for other potentially useful semiconductor systems such as $Si_{1-x}Ge_x$. Conventional oxidation of $Si_{1-x}Ge_x$ produces oxides which, due to selective oxidation of Si, are useless for device applications. We have recently demonstrated a method for producing compositionally congruent oxides from alloys of $Si_{1-x}Ge_x$ at low process temperatures. To accomplish this, extremely high pressure oxygen (>700 atm) was used at low process temperatures (<550°C). In this paper we report AES, FTIR, Raman, ESCA, and HREM results which demonstrate both hydrothermal (wet) (510 atm, 550°C) and dry high pressure (700 atm, 550°C) can be used to provide high quality passivation for $Si_{1-x}Ge_x$ (x = 10 a/o). The suitability of these oxides to MOS-device applications was evaluated using MOS-CV quasistatic and high frequency measurements.

219 A New Ellipsometry Technique for Interface Analysis: Application to Si-SiO_2: *E. A. Irene,* Dept. of Chemistry, The University of North Carolina, Chapel Hill, NC 27599-3290, *V. A. Yakovlev,* Institute of Crystallography, Academy of Science, USSR, Moscow 117333 USSR

In this paper we report a new spectroscopic ellipsometry technique that overcomes the ambiguity associated with measuring an interface under a film. In this technique we match the refractive index of the overlayer with an immersion liquid and then perform spectroscopic ellipsometry at several angles of incidence. Essentially, the overlayer is optically (not physically) removed, thereby rendering the ellipsometric measurement sensitive to the interfacial layer which is known to be optically and chemically different than either Si or SiO_2.

220 Infrared-Dichroism on a Thin Silicon Oxide Layer: *S. Fujimura, K. Ishikawa,* and *T. Ogawa,* Fujitsu, Ltd., Process Development Div., 1015 Kamikodanaka, Nakahara-ku, Kawasaki 211, Japan

Infrared-dichroism of thermally grown thin silicon oxide films is found using Fourier transform infrared reflection absorption spectroscopy. Two types of peaks were observed at 1250 cm^{-1} only on the IR spectra using infrared rays polarized parallel to the plane of incidence: one projected upward and another projected downward. Between these two peaks, the upward peak did not increase linearly with oxide thickness, and was considered to appear even on a very thin oxide film. Thus we believe that the upward peak reflects the chemical structure of the Si/SiO_2 interface.

221 Deconvolution of Thickness-Averaged Structural and Optical Properties of Thermally Grown and RPECVD SiO_2 Films: *C. E. Shearon, Jr., C. H. Bjorkman,* and *G. Lucovsky,* Dept. of Physics, North Carolina State University, Raleigh, NC 27695-8202

The local atomic strain and index of refraction of SiO_2 films that were thermally grown or deposited at remote plasma-enhanced chemical-vapor deposition, were determined by IR spectroscopy and ellipsometry, respectively. The films were etched back in 100 Å increments and examined at each thickness. These thickness averaged values were then deconvolved providing continuous plots of the index of refraction and the frequency of the dominant bond-stretching vibrational mode as a function of the oxide thickness.

222 TEM Investigations of the Oxidation Kinetics of Amorphous Silicon Films: *M. Reiche,* Institut für Festkörperphysik und Elektronenmikroskopie, Weinberg 2, D-04050 Halle/S., Germany

Thin SiO_2 films (10 nm ≤ d ≤ 100 nm) were prepared by dry oxidation (T = 960°C) of amorphous deposited silicon (a-Si) layers. The film thickness d *vs.* the oxidation time and the development of the interface roughness Δd were measured by X-TEM. The oxidation kinetics are described on the basis of Deal and Grove's model; differences have occurred as a function of the phosphorus doping (by ion implantation) of the a-Si layers. In addition, Δd was found to vary also with the dopant concentration. Comparisons clearly show that the oxidation of a-Si layers differs from that of polycrystalline deposited ones. This is especially true of the preparation of ultrathin SiO_2 films (d < 20 nm).

223 Thermal and X-Ray Production of Point Defects in Vitreous SiO_2: *F. L. Galeener,* Dept. of Physics, Colorado State University, Fort Collins, CO 80523

The concentrations of E', NBOHC, and PROHC defects in vitreous SiO_2 are reported as a function of x-ray dose and photon energy, as well as hydroxyl concentration and fictive temperature. The concentration *vs.* dose curves for electron spin resonance and x-radioluminescence are highly nonlinear, but are fit well be a model involving creation, activation, annihilation, and deactivation. The photon energy studies demonstrate that the spin active defects are caused by electrons ejected by photoabsorbed x-rays.

224 Nonstoichiometry and Defects in Bulk a-SiO_2: *H. Kawazoe,* Research Laboratory of Engineering Materials, Tokyo Institute of Technology, Nagatsuta, Midori-ku, Yokohama 227, Japan, *K. Awazu,* Electrotechnical Laboratory, 1-1-4 Umezono, Tsukuba, Ibaraki 305, Japan

Effects of nonstoichiometries and impurities on the type and concentration of the structural imperfections present in synthetic and bulk a-SiO_2 were studied. O_2 molecules dissolved in the glasses were found as oxygen excess type defects. The O_2 molecules were found to have an optical absorption band above 7 eV and to show the photochemical reactions similar to those of O_2 molecules in the gas phase.Divalent Si dissolved in glass network and small Si cluster are the oxygen deficient type defects found in the glasses.

225 The Paramagnetic Defects in Crystalline SiO_2: *J. A. Weil, R. J. McEachern,* and *M. M. Mombourquette,* Dept. of Chemistry, University of Saskatchewan, Saskatoon, SK, Canada S7N 0W0

The so-called point defects in crystalline silicon dioxide are multitudinous, and form a basis for the understanding of such defects in fused quartz and silica glasses. More than fifty of the paramagnetic species in α-quartz are now known, most characterized in detail by electron paramagnetic resonance spectroscopy. A review of the latter defects is presented, including a discussion of recent work on generating powder/glass epr lineshapes from the single-crystal parameters.

226 Formation of Si/SiO_2 Heterostructures by Low-Temperature, Plasma-Assisted Oxidation and Deposition Processes: *G. Lucovsky, Y. Ma, T. Yasuda,* and *S. Habermehl,* Dept. of Physics, North Carolina State University, Raleigh, NC 27695-8202

Conventional techniques for fabricating Si/SiO_2 structures combine Si/SiO_2 interface formation with growth, or deposition of the bulk oxide. We describe a new low-temperature process in which interface formation and oxide deposition are separately controlled. This technique includes oxidation of Si by remotely generated O-atoms, following an RCA clean that concludes with a rinse in dilute HF, and deposition of an oxide, or a multilayer dielectric (ON or ONO) by remote plasma-enhanced CVD.

227 Growth and Characterization of SiO_2 Thin Films Deposited by DECR-PECVD at Low Temperature: *B. Agius, M. C. Hugon,* and *N. Jiang,* Institut Universitaire de Technologie, Universite de Paris Sud (XI), 91403 Orsay Cedex, France, *M. Puech* and *G. Ravel,* Alcatel SDG, PAE les Glaisins, 74009 Annecy Cedex, France, *F. Plais,* Thomson-CSF LCR, Domaine de Corbeville, 91404 Orsay Cedex, France

Silicon dioxide films have been deposited, at low temperature, by the DECR-PECVD technique, using pure silane and oxygen gases on Si substrates. This paper reviews the physical, optical, and electrical properties of these films and their dependence on deposition conditions. High density films with a stoichiometry closed to thermal oxide one and low hydrogen contamination can be obtained by judicious choice of pressure (0.1 Pa), microwave power (800 W), total gas flow (20 sccm), and oxygen flow to silane flow ratio (9).

228 Low Temperature Synthesis and Characterization of Silicon Dioxide Films: *G. S. Chakravarthy, R. A. Levy,* and *J. M. Grow,* New Jersey Institute of Technology, Newark, NJ 07102

Diethylsilane (DES) has been used as a precursor to produce silicon dioxide films by low pressure chemical vapor deposition. The growth rate of the deposited glass films in the temperature range of 375-475°C was observed to follow an Arrhenius behavior yielding an activation energy of 10 kcal/mol. The growth rate was also observed to increase with higher pressure and to vary as a function of the square root of the DES flow rate and O_2/DES ratio. In both the pressure and the O_2/DES ratio studies, there were points of abrupt cessation in deposition. The density of the films was measured to be close to 2.2 g/cm^3 regardless of deposition conditions. IR spectra of the films showed peaks centered at 1060, 810, and 440 cm^{-1} indicating the presence of Si-O stretching bonds. The refractive index of the films was found to be at 1.46, independent of deposition temperature. The P-etch rate of the films deposited at 450 C was measured to be 90 nm/min at 25°C.

229 Fundamental Spectroscopic Studies of SiO_2 Deposition from TEOS: *J. E. Crowell, H.-C. Cho,* and *L. L. Tedder,* Dept. of Chemistry, University of California, San Diego, La Jolla, CA 92093-0314

We have studied the reaction of tetraethoxysilane (TEOS) with Si and SiO_2 surfaces using AES, XPS, TPD, and transmission IR spectroscopy. We have also examined the role of phosphorus in catalyzing the SiO_2 deposition process, and its deposition from PH$_3$. We have delineated the nature of the TEOS adsorption reaction and its dependence on adsorption site by varying the surface hydroxyl concentration and the chemical nature of the oxide surface. Our temperature dependent studies in UHV and at milliTorr conditions have permitted us to determine and compare the mechanism by which TEOS reacts and decomposes on Si and SiO_2 surfaces. We present reaction mechanisms for SiO_2 and PSG deposition, and we discuss modeling of the surface reactions using ethanol

230 Native Oxide Growth and Hydrogen Bonding Features on Chemically Cleaned Silicon Surfaces: *M. Hirose, M. Takakura, T. Yasaka,* and *S. Miyazaki,* Dept. of Electrical Engineering, Hiroshima University, Higashi-Hiroshima 724, Japan

Ultra thin oxide (<13 Å) grown in pure water after HF or BHF treatment contains a wide variety of hydrogen bonds as revealed by FT-IR-ATR. An appreciable amount of SiH_2 bonds is existing in the SiO_2/Si(100) interface. Correspondingly, the Si^{2+} XPS signal is hardly observable in the interface and appears after 500°C annealing in vacuum as a consequence of hydrogen desorption from the matrix.

231 Understanding the Surface Chemical and Structural Implications of HF Solution Cleaning of Silicon: *G. S. Higashi,* AT&T Bell Laboratories, Murray Hill, NJ 07974-0636

Ab-initio molecular orbital calculations show that the mechanism responsible for H-termination subsequent to HF treatment of Si surfaces involves bond polarization and subsequent HF attack. This leads to the dissolution of polar molecular species, leaving nonpolar silicon hydrides behind. Infrared spectroscopy finds these H-terminated surfaces to be atomically rough when HF solutions of low pH are employed, and are composed of mono-, di-, and tri-hydride Si species. High pH HF solutions form (111) facets on Si(100) but allow the formation of single-domain mono-hydride terraces on Si(111). Scanning tunneling microscopy confirms that atomically perfect Si(111) surfaces can be realized using HF solutions with a pH ~ 8

232 Pre-Gate Oxide Si Surface Control: *M. Morita* and *T. Ohmi,* Dept. of Electronic Engineering, Faculty of Engineering, Tohoku University, Sendai 980, Japan

Very thin oxide films with high electrical insulating performance and high reliability are formed by controlling the preoxide growth on Si surfaces during the temperature ramp-up right before thermal oxidation using ultraclean oxidation systems. The barrier height at the Si-SiO_2 interface for electrons tunneling from Si to SiO_2 for the ultraclean oxide is little decreased as the thickness is thinner, while the height for the conventional dry oxide including thicker preoxide is drastically decreased.

233 Chemical Structures of Native Oxides Formed during Wet Chemical Treatments on Atomically Flat Si(111) Surface: *H. Ogawa* and *T. Hattori,* Dept. of EEE, Musashi Institute of Technol., Tamazutsumi, Setagaya-ku, Tokyo 158, Japan

The infrared and photoelectron spectra arising from Si-H bonds at and near the native oxide/silicon interface could be extracted without deconvolution using reference spectra obtained for native oxide formed in H_2SO_4-H_2O_2 solution, which was found to contain negligible amount of Si-H bonds at and near the native oxide/silicon interface.The native oxides studied using FT-IR-ATR and XPS were formed during wet chemical treatments on H-terminated atomically flat Si(111) surfaces.

234 Silicon Surface Analysis and Very Thin Silicon Oxide Characterization after HF/Ethanol Preoxidation Silicon Cleaning: *J. R. Morante, B. Garrido,* and *J. Samitier,* LCMM Dept. Física Aplicado i Electrònica Univ. de Barcelona, Diagonal 645-647, 08028 Barcelona, Spain, *F. Gessin, J. L. Prom,* and *G. Sarrabayrouse,* LAAS, CNRS 7, 31077 Toulouse Cedex, France

A comparison between the silicon HF/ethanol cleaning and the HF/H_2O one has been performed. Ellipsometric measurements show the presence of an overlayer 0.3 nm thick *vs.* the 0.6-0.7 nm in the HF/H_2O case. Atomic force microscopy shows a drastic reduction of the surface roughness. The subsequently thermally grown SiO_2 layers (<100 Å) analyzed by IR absorption show an increased percentage of high bond angles in HF/ethanol case.

235 Effects of Metallic Impurities upon Thin Gate Oxide Integrity and Related Bulk Electrical Properties in CZ Si: *K.-C. Cho, J.-G. Park, Y.-S. Kwok, D.-J. Lee, C.-S. Lim,* and *C.-K. Shin,* Samsung Electronics, Quality Control Div., Kihung Plant, Kihung-Eup, Kyungki-Do, Korea, *S. Hahn,* Dept. of Materials Science and Engineering, Stanford University, Stanford, CA 94305

We investigated effects of various well-known metallic impurities such as Fe, Cu, Al, and Au (contaminated by a spin coating method with concentration levels ranged from 1E10 to 1E15 atoms/cm^2) upon: (*i*) thin gate oxide (thickness ~23 nm) integrity: (*ii*) total oxide charges; and (*iii*) various bulk electrical and structural defects. Based upon our oxide integrity and bulk electrical and structural characterization data, we conclude that Fe is the most harmful metallic impurity among the four metallic elements investigated in this study.

236 Carbon Impurities at Si-SiO_2 Interfaces: *S. I. Raider,* IBM T.J. Watson Research Center, Yorktown Heights, NY 10598

An interfacial oxidation reaction is identified in which chemically reactive carbon impurities in a Si substrate are oxidized by SiO_2 at a Si-SiO_2 interface during thermal annealing in inert ambients. The electrical properties of MOS devices are degraded during the initial stages of this SiO_2 decomposition reaction. The presence of oxidizable carbon species at a Si-SiO_2 interface provides a reaction path that can proceed in parallel with Si oxidation during thin (<20 nm thick) SiO_2 growth. The similarity between degradation of MOS electrical properties after inert ambient annealing and standard processing indicates that oxidation of carbon impurities at a Si-SiO_2 interface is of technological significance.

237 Microscopic Structure of the Si/SiO_2 Interface: *F. J. Himpsel,* IBM T.J. Watson Research Center, Yorktown Heights, NY 10598

The distribution of oxidation states at the Si/SiO_2 interface is determined using high-resolution Si2p core level spectroscopy with synchrotron radiation. The dependence on crystallographic orientation, substrate roughness, and growth temperature was investigated, and is discussed in view of current structural models for the interface.

238 High Resolution Transmission Electron Microscope Image of the SiO_2/(001)Si Interface: *H. Akatsu,* IBM Tokyo Research Laboratory, Sanbancho 5-19, Chiyoda-ku, Tokyo 102, Japan, and *Y. Simi* and *I. Ohdomari,* School of Science and Engineering, Waseda University, Ohkubo 3-4-1, Shinjuku-ku, Tokyo 169, Japan

Cross-sectional HRTEM observation of the SiO_2/(001)Si interface prepared by thermal oxidation reveals that there is a thin layer exhibiting 110 period image at the interface. Simulation using simple interface model shows that the interface roughness modifies the c-Si lattice image so as to exhibit the 110 period image. A tridymite/(001)Si interface also exhibits the 110 period image but a number of planar defects have to be introduced in this case.

239 Dependence of Surface Microroughness on Types of Silicon Substrates: *T. Ohmi, T. Tsuga,* and *J. Takano,* Dept. of Electronics, Faculty of Engineering, Aza-Aoba, Aramaki, Aobaku, Sendai 80, Japan

The dielectric breakdown field intensity is affected by the surface microroughness of silicon substrate. It has been found that the increase of surface microroughness due to the APM cleaning varies among the wafer types such as CZ, FZ, and EPI. The surface microroughnes is caused by the point defect such as vacancy. In the case of the n type CZ wafer, the suface microroughness is increased even in the dilute HF cleaning, however this problem is perfectly resolved by injecting H_2O_2 into the dilute HF.

240 The Effect of Surface Roughness on Gate Oxide Leakage Currents: *M. Chonko*, Motorola Inc., Advanced Products Research and Development Laboratory, Austin, TX 78721, *V. Kaushik*, Motorola Inc., Surface Analysis Laboratory, Microprocessor and Memory Technology Group, Austin, TX 78721

We have studied the effects of silicon surface roughness on 150 Å gate oxide characteristics. Varying degrees of roughness were induced by timed wet silicon etches. For short etch times, the initial roughness is reflected at the top oxide surface while the substrate/oxide interface is smoothed. This results in increased current injection from the poly/oxide interface. The substrate injection remains at its initial level. The poly/oxide interface rapidly degrades with increasing roughness (etch time). At longer times, the substrate/oxide interface begins to retain some of the etch-induced roughness, and injection characteristics from this interface also begin to degrade.This nonsymmetric degradation of IV characteristics can be used to qualitatively evaluate process-induced suface roughness. The potential of two common oxide etching solutions to roughen the Si suface are compared using this technique.

241 A Double Sacrificial Oxide Process for Smoother 150 Å SiO Gate Oxide Interfaces: *H.-H. Tseung** and *P. J. Tobin*, Motorola Inc., Advanced Produces Research and Development Laboratory, Austin, TX 78721

We have found that a double sacrificial oxide process provides a smoother active surface than the single sacrificial oxide process. The onset of Fowler-Nordheim tunneling (injected from a polysilicon/gate oxide interface) for gate oxide grown using a double sacrificial oxide process occurs at a higher field than that for the single sacrificial oxide case. This implies that the double sacrificial oxide process results in a smoother polysilicon/gate oxide interface. Further, the interface state density of the gate oxide/substrate interface is reduced for the double sacrificial oxide process.

242 Effect of Solidification Induced Defects in CZ-Silicon upon Thin Gate Oxide Integrity: *H. Suga, H. Abe, H. Koya, T. Yoshimi, I. Suzuki, H. Yoshioka*, and *N. Kagawa*, Mitsubishi Materials Silicon Corp., 314 Kanauchi, Nishi-sangao Noda-shi, Chiba-ken 330, Japan

Thin gate oxide in VLSI devices is clarified to be correlated inherently with crystal growth conditions in the Czochralski method; especially, the growth rate increase consistently degenerates the dielectric breakdown voltage of thermal gate oxide. Experimental results show that the density of freezed-in defects associated with faster pull rate affects the occurrence of weak spot breakdown of thin gate oxide. This feature is not affected by doping, oxygen incorporation, thermal history below 1250°C.

243 Effects of D-Defects in CZ Silicon upon Thin Gate Oxide Integrity: *J.-G. Park, S.-P. Choi, G.-S. Lee, Y.-J. Jeong, Y.-S. Kwak*, and *C.-K. Shin*, Samsung Electronics, Quality Control Div., Kihung Plant, Kihung-Eup, Kyungki-Do, Korea, *S. Hahn*, Dept. of Materials Science and Engineering, Stanford University, Stanford, CA 94305, *P. Mascher*, Dept. of Engineering Physics, McMaster University, Hamilton, Ont., Canada L8S 4M1

We investigated the effects of D-defects upon oxide breakdown field strength and time-dependent-dielectric breakdown characteristics of 23 nm thick thermally grown gate oxide and the nature of these defects by Secco etching/cross-section optical microscopy, thermal wave imaging, and positron annihilation spectroscopy. Our data show that: (*i*) D-defects in Si substrate indeed degrade breakdown field strength and time-dependent-dielectric breakdown characteristics; and (*ii*) D-defects are definitely not of interstitial nature, and are most likely vacancy-related defects.

244 Oxidation-Induced Changes in the Si Surface Microroughness: *V. Nayar, A. J. Pidduck*, and *C. Pickering*, DRA Electronics Div., (RSRE), Malvern, Worcs., England WR14 3PS

The roughness of SiO_2 surfaces and interfaces resulting from different oxide growth conditions and to different thicknesses has been studied over a wide range of length scales using spectroscopic ellipsometry, scanning optical microscopy in differential phase contrast mode, and atomic force microscopy. A comparison of wet and dry oxidations revealed an increase of roughness at both the oxide interfaces relative to the starting surface. The interface topography was observed to evolve and become significantly different from that of the starting wafer for increasing oxide thickness.

245 Properties of SIMOX and Related Systems: *S. Cristoloveanu*, LPCS, Enserg, 38016 Grenoble Cedex, France

The flexibility and quality of the SIMOX process are addressed by referring to the electrical properties of the silicon film, buried oxide, and interfaces. The most reliable methods of characterization are described. Interface coupling, floating body, and transient effects are shown to be typical effects in thin film SIMOX devices. The nature of the buried oxide is revealed by hot carrier injection and irradiation experiment.

246 Reoxidized Nitrided Oxide Gate Dielectrics for Advanced CMOS: *G. J. Dunn*, M.I.T. Lincoln Laboratory, Lexington, MA 02173

The advantages of reoxidized nitrided oxide (RNO) gate dielectrics for advanced CMOS applications are reviewed. RNO n-MOSFETs exhibit greatly improved resistance to channel hot carrier stress, due to the suppression of interface trap and bulk electron trap generation. However, RNO p-MOSFETs exhibit reduced resistance to stress, due to background trapping on nitridation-induced bulk traps. As dielectric thickness approaches ~5 nm, background trapping will diminish in importance relative to trap generation.

247 Interface Properties and Device Reliability of High Quality PECVD Oxide for MOS Applications: *L. K. Wang, C. C-H. Hsu*, and *W. Chang*, IBM Research Div., T.J. Watson Research Center, Yorktown Heights, NY 10598

Low temperature deposited high quality thin plasma enhanced CVD oxides have been used as gate dielectric to investigate the interface characteristics. From the comparison of the CMOS device using PECVD gate oxide and thermally grown gate oxides, the PECVD oxide properties are not much divergent from the thermally grown gate oxides. The oxide reliability is examined by using high field tunneling, channel hot carrier stress, and buried junction injection. The results suggest that although the oxide trapping density is comparable to the thermal grown gate oxides, the Si-SiO_2 interface strength is still slightly weaker.

248 Charge Trapping in an ONO Gate Dielectric: *R. B. Klein*, SFA, Inc., Landover, MD 20785, *N. S. Saks*, Code 6813, Naval Research Laboratory, Washington, DC 20375

The capture cross section σ_t and density N_t of intrinsic electron traps in a composite ONO (oxide-nitride-oxide) dielectric were measured using low-field substrate hot electron (SHE) injection. We find that $N_t = 5.4 \times 10^{18}$ cm^{-3} and $\sigma_t = 1.2 \times 10^{-13}$ cm^2, characteristic of a Coulomb-attractive trap. Radiation experiments performed after SHE injection reveal hole traps with the same cross section. These results are discussed in light of our current understanding of electron and hole traps.

249 Interface Trap Density Reduction and Oxide Profiling for Fluorinated MOS Capacitors: *D. Kouvatsos** and *R. J. Jaccodine*, Sherman Fairchild Center for Solid State Studies, Lehigh University, Bethlehem, PA 18015, *F. A. Stevie*, AT&T Bell Laboratories, Allentown, PA 18103

The effect of fluorine incorporation on the as-grown interface trap density was investigated using MOS capacitors with fluorinated oxide dielectrics as test structures. A clear reduction of the interface trap density was shown for NF_3 additions in the ppm range as compared to dry oxides. The fluorine incorporation in the oxide was investigated by means of SIMS profiling. A tendency of fluorine to be partially immobilized in the oxide at the time of its incorporation was observed.

250 Physics of Extreme Quantum Confinement Examplified by Si/SiO_2 System: *R. Tsu*, University of North Carolina at Charlotte, Charlotte, NC 28223

The physics of extreme quantum confinement involves considerations beyond present day treatment of superlattices and quantum well structures. Apart from retaining the effective mass approximation, a constant dielectric constant cannot be assumed. Interface strain plays a major role in determining reaction rate. Oxide growth as a barrier for confinement in a nanocrystal of silicon involves processes similar to the strain-layered superlattices with a lowering of defect density at the interface. Therefore, a better barrier consists of a Si/SiO_2 composite. Some new insights in the physics of extreme quantum confinement are discussed.

251 Integrity of Very Thin Silicon Films Deposited on SiO_2: *M. Chonko** Motorola Inc., Advanced Product Research and Development Laboratory, Austin, TX 78721, and *D. Keitz*, Motorola Inc., MOS 11 Wafer Fabrication Facility, Austin, TX 78735

The physical integrity of very thin LPCVD silicon films has been studied as a function of deposition temperature and pressure. Integrity was defined as the ability of the film to protect an underlying oxide film from an HF etch. We have found that polycrystalline films deposited at temperatures close to 600°C are not continuous. Films deposited in the amorphous phase protect the underlying oxide and therefore must be continuous.

252 Researches of SiO_2 on InP and GaAs MOS Structure: *Y. K. Su* and *C. J. Hwang*, Dept. of Electrical Engineering, National Chang Kung University, Tainan, Taiwan, China

The high quality SiO_2 layer has been deposited on GaAs and InP by direct photo-CVD using deterium lamp. Its refractive index is 1.462 at $SiH_4/N_2O = 0.25$. The FTIR data show that Si-O bonds are dominant in this film. XPS and AES measurements show that a good interface and bulk layer are attained. The high frequency (1 MHz) C-V of the *n*-InP MOS diode has been measured, and a minimum interface state density (D_{it}) of 2×10^{11} cm^{-2} eV^{-1} was derived by Terman's method. DLTS measurement was applied to *n*-GaAs MOS diode and a maximum surface state density (N_{ss}) of 6×10^{13} cm^{-2} eV^{-1} at $E_c \times 0.4$ eV was detected.

253 Generation of Telegraph Noise via Single Interfacial Defects: *M. J. Uren*, DRA Electronics Div., RSRE Malvern, Worcs., England, WR14 3PS, *D. H. Cobden*, Semiconductor Physics, Cavendish Laboratory, Cambridge CB3 OME, England

This paper reviews the information that has been deduced about the SiO_2 slow states from the study of Random Telegraph Signals. New results on the interpretation of the entropy change on capture into the defect, and the measurement of an RTS due to an oxide two-level-system are presented.

254 Single Electron Transfer from the Channel in Sub-μm MOSFETs to an Individual Interface Trap: *M. Schulz* and *A. Pappas*, Institute of Applied Physics, University of Erlangen, D-8520 Erlangen, Germany

Random telegraph switching (RTS) of only a single interface trap in the active gate area of a sub-μm sized MOSFET is reported. The usual 1/f noise at low frequencies generates in this case a pure Lorentzian frequency spectrum. The trapping rate constants for capture and emission are analyzed over 5 orders of magnitude as a function of the gate bias voltage, the temperature, and for the first time of the substrate bias voltage. From the experimental data, we can evaluate the level energy 150 meV, the image charge energy lowering 45 meV, and the free energy 170 meV of the Coulomb blockage in the transfer rate.

255 ^{17}O Hyperfine Study of the P_b Center: *J. H. Stathis*, IBM Research Div., T.J. Watson Research Center, Yorktown Heights, NY 10598, *S. Rigo* and *I. Trimaille*, Group de Physique des Solides, Universite Paris VII, 75251 Paris Cedex 05, France

We have measured the ^{17}O hyperfine structure of the P_b center in order to learn something about the oxide structure around the defect. To enhance the concentration of ^{17}O (I = 5/2, natural abundance 0.037%) oxides were grown in 55.65% isotopically enriched oxygen. By deconvolution of the ^{17}O hyperfine-broadened spectrum, we are able to ascertain that the unpaired electron on the P_b center interacts weakly with only a single oxygen atom in the SiO_2. Within the resolution of our analysis, the position of this oxygen atom relative to the dangling bond is not unique, but varies randomly from site to site. The number of oxygen atoms, however, is the same at every site.

256 The Influence of Crystal Orientation and Processing Conditions on the Energy Distribution of Traps at the Si-SiO_2 Interface: *C. H. Bjorkman, Y. Ma, T. Yasuda*, and *G. Lucovsky*, Dept. of Physics, North Carolina State University, Raleigh, NC 27695-8202

We have studied the local atomic strain as a function of crystal orientation and processing conditions, and its relationship to the energy distribution of interface traps in the Si bandgap. For example, for oxides grown on Si(100) surfaces, an increase in oxidation temperature promotes strain relaxation and reduction of interface states at energies above 0.4 eV in the Si bandgap, but not at energies between 0.2 and 0.4 eV.

257 Charge Trapping and Degradation of Thin Dielectric Layers: *M. M. Heyns, A. v. Schwerin* (Present address: Siemens, Corporate R&D, D-8000 Munchen 83, Germany), *S. Verhaverbeke*, and *A. Kelleher* (Present address: NMRC, University College, Lee Meltings, Cork, Ireland), Interuniversity Microelectronics Centre (IMEC), 3001 Leuven, Belgium

The injection of charges in the gate oxide is a potential reliability problem due to the charge build-up in the SiO_2 layer and the degradation of the Si/SiO_2 interface which follows from it. In this work a detailed study is made on the charge trapping and trap generation during injection of electrons and holes using homogeneous injection at varying oxide field. Beside this the effect of the addition of Cl and F in the oxide layer and the effect of rapid thermal nitridation and re-oxidation on the oxide trapping characteristics is also discussed.

258 Charging and Discharging Properties of Electron Traps Created by Hot-Carrier-Injections in Gate Oxide of n-MOSFET: *D. Vuillaume*, URA253 CNRS, ISEN, 59046 Lille, France

We have analyzed the capture and emission properties of oxide defects induced by hot-carrier-aging of MOSFET. The changes of the charge states of the traps have been monitored by the time-evolution of the very low level gate current measured by the floating-gate technique. A large capture cross section (~10^{-14} cm^2) has been found for electron traps which has been correlated with optical properties. According to these optical properties, the hot-carrier-induced defects should be an acceptor-like defect at ~1.7 eV below the CB with a large lattice relaxation (photoionization energy of ~3 eV). A possible relation with the $O_3 \equiv Si$ defect in the oxide is assessed by comparison with theoretical calculations.

259 Optically Induced Nitrogen Dangling Bonds in Amorphous Silicon Nitride Thin Films: *W. L. Warren* and *P. J. McWhorter*, Sandia National Laboratories, Albuquerque, NM, 10598, *J. Kanicki*, IBM T.J. Watson Research Center, Yorktown Heights, NY 10598, *E. H. Poindexter*, Electronics Technology and Devices Laborartory, Fort Monmouth, NJ 07703

Using X-band and Q-band electron paramagnetic resonance microwave frequencies, we have confirmed a model for the two-coordinated N dangling bond in stoichiometric and N-rich silicon nitride. Our results further suggest that the creation of the N dangling bond is related to H evolution from the films, and that the N dangling bond is an electrically active point defect.

260 Impact Ionization and Positive Charges in SiO_2: *D. J. DiMaria,* D. Arnold*, and *E. Cartier*, IBM Research Div., T.J. Watson Research Center, Yorktown Heights, NY 10598

Impact ionization and positive charge formation in silicon dioxide have been controversial issues for many years. In this study, bandgap ionization due to the development of a high energy tail on the hot-electron energy-distribution is shown to occur in films thicker than 20.0 nm at fields higher than 8 MV/cm. This process is demonstrated to account for hole currents in the substrate circuit of n-channel FETs and for the observation of positively trapped-charges accumulating at the silicon-silicon dioxide interface at low injected-carrier-fluencies (less than 0.01 C/cm^2).

261 Hot-Electron Dynamics in SiO_2 Studied by Photo-Induced Electron Transmission Through Thin Films: *E. Cartier, E. A. Eklund, D. Arnold, D. J. DiMaria*, and *F. R. McFeely*, IBM Research Div., T.J. Watson Research Center, Yorktown Heights, NY 10598

Internal photoemission in combination with semiclassical Monte Carlo simulations was used to measure energy dependent absolute electron-phonon scattering rates and impact ionization rates in SiO_2 at electron energy from 1 to 20 eV. At low energy, our results are consistent with the standard model for electron-phonon interaction. At high energies, strong deviations from this model are observed. Using the measured rates as empirical parameters, we are able to quantitatively explain hole generation in n-channel MOSFETs.

262 Constant Current Stress Breakdown in Ultrathin SiO_2 Films: *T. Kubota* (Permanent address: NEC Corp., 1120 Shimokuzawa, Sagamihara, Kanagawa 229, Japan), *P. Apte* and *K. C. Saraswat*, Center for Integrated Systems, Stanford University, Stanford, CA 94305

We have characterized the charge-to-breakdown (Q_{bd}) in ultrathin oxides as a function of stress current density (J_{ox}), oxide thickness and temperature, using constant current stress Q_{bd} decreases with increasing J_{ox} for different oxide thicknesses and the differences in the slope for each thickness are indicative of different breakdown mechanisms. Q_{bd} is also seen to decrease with temperature and thickness for a fixed J_{ox}. We explain these trends qualitatively in a self-consistent manner utilizing existing models and some new concepts.

263 Radiation-Induced Interface Traps in MOS Devices: *N. S. Saks* and *D. B. Brown*, Naval Research Laboratory, Washington, DC 20375

Creation of interface traps in MOS devices has been studied as a function of time following a short irradiation pulse. Measurements have been made as a function of oxide field, oxide thickness, and other variables. A new model based on dispersive H^+ transport has also been developed. We find excellent qualitative and quantitative agreement between the data and this H^+ model.

264 Hydrogen Related E' Centers and Positive Charge In Irradiated Oxide Films: *M. E. Zvanut,*,† R. E. Stahlbush, W. E. Carlos*, and *H. L. Hughes*, Naval Research Laboratory, Washington, DC 20375

Electron paramagnetic resonance and capacitance-voltage results indicate that oxygen vacancy related defects (E') in hydrogen-treated oxide films occur in concentrations ten times that found in nonhydrogen treated films and, unlike their counterparts in nonhydrogen treated films, they are not associated with an increase in irradiation-induced positive charge. We deduce that this hydrogen-related E' type oxide defect is formed from an SiH precursor rather than from a standard oxygen vacancy precursor.

†NRC/NRL Postdoctoral Research Associate.

265 Molecular Orbital Studies of Oxygen-Related Hole Traps and of Their Interactions with Hydrogen Atoms and Molecules: *A. H. Edwards*, Dept. of Electrical Engineering, UNC-Charlotte, Charlotte, NC 28223

We report recent theoretical studies of several models for defects that could transform dissolved H_2 into H^+. The models considered are the E' center, the nonbridging oxygen hole center, the self-trapped hole, and two new variants we call the strained-bond and broken-bond self-trapped hole. Based on the calculated energies of reaction and activation energies, the most likely candidates are the last two. For the STH defects, the activation energy for H_2 dissociation is a function of local network strain and is in a range of 0.6 to 1.1 eV. Our calculation of the self-trapped hole agrees very well with Griscom's ^{29}Si hyperfine results for STH1. We discuss the variation of these parameters with network strain.

266 Removal of Traps in Process-Damaged MOS Structures by Room-Temperature Hydrogenation: *S. Kar*, Dept. of Electrical Engineering, Indian Institute of Technology, Kanpur-208016, India

The aim of this investigation was to examine the efficacy of room temperature hydrogenation [by a 400 eV hydrogen beam from a Kaufman source] in the removal of electronic defects in SiO_2, at the Si-SiO_2 interface, and the Si sub-surface by exposure to a beam of 16 keV Si ions. Upon hydrogenation, profound changes were observed in the trap parameters as well as in the admittance characteristics of the MOS structures. There was significant decrease in the trap density and the oxide leakage current.

267 Hot-Electron Induced Hydrogen Redistribution in SiO_2: *D. A. Buchanan*, IBM East Fishkill, Hopewell Junction, NY 12533, *A. Marwick*, IBM T.J. Watson Research Center, Yorktown Heights, NY 10598, *L. Dori*, C.N.R.-Lamel-Institute, Bologna, Italy, *D. V. DiMaria*, IBM T.J. Watson Research Center, Yorktown Heights, NY 10598

Hot electron induced hydrogen redistribution in Al-gate MOS capacitors has been observed using electron injection by internal

photo-emission together with hydrogen concentration profiling by ion beam nuclear reaction analysis. After injection, the hydrogen profile was measured with the gate in place. Initially, most of the hydrogen in the capacitors, ~2×10^{15} H/cm^2, was found to be at the Al/SiO_2 interface, probably as a result of water contamination of the SiO_2. After injection, this peak was reduced in size, while depending on the injection dose and the polarity of the bias a substantial buildup of hydrogen at the Si/SiO_2 interface was observed. This was found to increase with electron fluence, reaching ~2×10^{14} H/cm^2 at a fluence of 5 C/cm^2 under negative bias. Clear evidence was obtained for slow H diffusion into the SiO_2 layer from the Al/SiO_2 interface under positive gate bias. However for moderate fluences the hydrogen concentration in the bulk of the SiO_2 changed only slightly as the interface peak grew. These results show that hydrogen at the Al/SiO_2 interface acts as a source for the hot electron induced redistribution. They are discussed in terms of current models of hot electron induced defect generation.

268 H_2 Cracking in Irradiated MOSFETs and H^+ Formation: *R. E. Stahlbush*, Naval Research Laboratory, Washington, DC 20375 and *A. H. Edwards*, University of North Carolina, Charlotte, NC 28223

Molecular hydrogen introduced into irradiated MOSFETs causes the buildup of interface states and decrease of trapped positive charge. Results are explained by the sequence in which H_2 is cracked to form H^+, and H^+ causes interface state creation. New molecular orbital calculations model the cracking process. Comparing cracking by E' centers and broken Si-O bonds, the latter is more likely. It is also argued that H^+ is a small polaron.

JOINT GENERAL SESSION

Electronics/Dielectric Science and Technology

269 Suppression of WSi_x Peeling in 0.8 μ BiCMOS Technology: *B. L. Mantha* and *C. S. Wang*, VLSI Technology Inc., San Jose, California 95131

Tungsten silicide on top of arsenic-implanted polysilicon has been employed in a 0.8 μ BiCMOS technology to serve as a gate material for MOS transistors, and as emitters for bipolar transistors. We have observed peeling of the tungsten silicide film after contact reflow. Dependence of tungsten silicide peeling on arsenic implant dose and anneals before contact reflow has also been studied. We found that it is safe to use up to 1.2E16/cm^2 arsenic implant dose without peeling if an anneal step is included before reflow. An anneal step at 950° C for 60 min in nitrogen is required to completely suppress tungsten silicide peeling.

270 Characterization of WSi_x Films Deposited by Dichlorosilane Reduction Process for MOS VLSI: *A. Ookawa*, Semiconductor Design and Development Center, Hitachi, Ltd., 111 Nishiyokote-Machi, Takasaki-shi, Gunma-ken 370, Japan, *S. Moribe*, *S. Morita*, and *A. Koike*, Hitachi, Ltd., 5-20-1 Josuihon-cho, Kodaira-shi, Tokyo 187, Japan

A new LP-CVD technique for WSi_x deposition using dichlorosilane in a cold wall system was developed. Film properties such as adhesion, resistivity, density, and thermal stability were studied. These films characterized better adhesion and thermal stability due to the stable as-deposited crystal structure. The ratio of the sheet resistance on a memory cell pattern (with many steps) and on a planar pattern (no steps) was lower than that in the case of the conventional monosilane-reduction CVD WSi_x.

271 Effect of Underlying TiW Thickness on the Electromigration of Vias: *D. Pramanik* and *V. Jain*, VLSI Technology Inc., San Jose, CA 95131

The effect on the reliability and electrical parameters of a double metal circuit, due to a TiW layer deposited under the Al-1% Cu, comprising the second level of interconnect metal has been studied as a function of the thickness of the TiW. Metal line resistances were not affected but the resistance of the vias increased with increasing TiW thickness due to degradation of the aluminum step coverage in the vias. At the same time the electromigration of the vias improved dramatically with increasing TiW thickness. The optimum thickness for the TiW which gives acceptable via resistance and enhanced reliability is 200 nm.

272 Microstructure Control and Thermal Stability of Titanium Silicide: *R. W. Mann* and *C. Racine*, IBM General Technology Div., Essex Junction, VT 05452

Understanding factors governing the thermal stability of thin film titanium silicide is essential to the extendability of this material for sub-half-micron VLSI technologies. It is demonstrated that the silicide microstructure can be an important variable in determining the thermal stability of titanium silicide. Using higher formation temperature and/or a silicon implant through the titanium film are explored as methods to tailor the silicide microstructure and improve the thermal stability of the low resistance C54 (oF24) phase film.

273 The Direct Observation of Atom Column Defects in $MoSi_2$ and WSi_2: *K. M. Pollack* and *P. Fraundorf*, University of Missouri at St. Louis, St. Louis, MO 63121, *D. S. Schwartz*, McDonnell Douglas Research Laboratories, St. Louis, MO 63166, *T. C. Bryant*, Micron Technologies, Boise, ID 83706-9698

Molybdenum and tungsten disilicides show promise as a complement to polysilicon in VLSI gate electrode and interconnect applications, and in high temperature structural alloy applications as well. We show here, theoretically and experimentally, that the lattice of these structures down their tetragonal <100> direction consists of monatomic columns sufficiently separated to be resolvable in <0.2 nm-resolution HREM images. HREM imaging of polycrysalline Mo or W disilicide VLSI structures may thus prove efficient for getting atom-scale information on grain interconnects.

274 Poly-Void Formation in Poly Buffer LOCOS Process: *H. S. Yang*, *C. S. Han*, *W. G. Lee*, *K. M. Lee*, *H. S. Park*, and *K. H. Oh*, Semiconductor R & D Center, HYUNDAI Electronics Ind. Co., Ltd., Ichon-kun, Kyoungki-do, 467-860, Korea

This paper describes etch pits or poly-voids which have been observed in the poly layer using SEM and TEM right after the nitride strip step for poly buffer LOCOS process of the semiconductor IC fabrication. Various process parameters have been examined to find the causes of the poly-void formation. In this study, it may be concluded that the poly-void formation is quite closely related to the oxidation-induced stress, grain boundaries of the polysilicon layer, and field oxidation temperature.

275 Influence of Field Isolation Stress on Gate Oxide Reliability: *K. Shiozaki*, *K. Shimanoe*, *K. Kato*, and *J. Nakano*, ME Div., Toyota Motor Corp., 456, Kirigahora, Nishihirose-cho, Toyota-shi, Aichi 471-03, Japan

Reliability of the gate oxide with the field isolation edge was investigated. It was found that the degradation of the gate oxide is strongly associated with the stress of isolation edge. And the stress can be controlled with the processing condition. The stress at the isolation edge is an important indicator to evaluate gate oxide reliability. The stress control at field isolation edge promises a highly reliable gate oxide in future LSIs.

276 A Comparison of Interstitial Oxygen Calculated by Different Techniques: *J. W. Medernach* and *J. O. Stevenson*, Sandia National Laboratories, Albuquerque, NM 87185-5800

A FORTRAN software package was developed to provide an estimate of interstitial oxygen (O_i) from FTIR absorption in silicon by three separate methods. We report on a comparison of calculation methods, which include the ASTM standard test F1188-88, the short baseline (SBL) and the curve baseline (CBL) methods. Reproducible O_i results are obtained for the SBL and CBL techniques, although the CBL values are systematically lower. A FTIR-SIMS calibration is given for both lightly and heavily doped silicon, where selective electrochemical thinning was used to enable the FTIR absorption measurements.

277 The Warpage of As-Received and Oxygen Precipitated CZ Silicon Wafers: *J. Jeong* and *H.-D. Chiou*, Discrete and Materials Tech. Group, Motorola Inc., Phoenix, AZ 85008

Various types of as-received and CMOS thermal processed 100 mm diam wafers were used for warpage study under different furnace operations. The results indicate that as-received wafers showed very little increase in bow and warp up to 1000°C furnace temperature and 24 in./min insertion rate. For the CMOS thermal processed wafers, both the prior amount of oxygen precipitation and the bulk microdefect morphology affect warpage.

278 Modeling of Phosphorus Precipitation: *S. Dunham*, Boston University, Boston, MA 02215

The deactivation of dopants at high concentrations can be accounted for by considering aggregation of the dopant into precipitates. In this work, we model phosphorus precipitation as a function of time and temperature by simulating the evolution of the distribution of precipitate sizes using discrete rate equations and the Fokker-Planck equation. We compare the results to observations of dopant deactivation of laser-annealed implants in the temperature range 300-1000°C as measured by Nobili and coworkers.

279 Accurate and Computationally Efficient Modeling of BF_2 Implants into Single-Crystal Silicon: *S. J. Morris*, *V. Do*, *P. Gupta*, *S.-H. Yang*, *C. Park*, *K. M. Klein*, and *A. F. Tasch*, Microelectronics Research Center, The University of Texas, Austin, Texas 78712, *R. B. Simonton*, Eaton Corp., Austin, TX 78758, *G. E. Lux*, Charles Evans and Assoc., Redwood City, CA 94063

We have developed a new model for accurate and comprehensive simulation of BF_2 implants into single-crystal silicon. This model simulates the boron concentration profiles resulting from BF_2 implants in silicon, and it takes into account the effects of tilt and rotation angles as well as the effects of implant energy and dose. The model covers the following ranges of implant conditions: energies of 15-65 keV, doses of 1×10^{12} cm^{-2}-1×10^{16} cm^{-2}, tilt angles of 0°-10°, and rotation angles of 0°-360°. This model can be easily implemented into existing process simulation codes such as SUPREM.

280 Investigation of Ion-Surface Interaction in Ar Plasma Etching of Si and PECVD of SiO_2 Film by High-Frequency C-V Method: *C. Pavelescu*, Stanford University, Staford, CA 94305, *J. P. McVittie*, Center for Integrated Systems, Standford University, Stanford, CA 94305, *C. Chang*, Stanford University, Stanford, CA 94305, *K. C. Saraswat*, Center for Integrated Sys-

tems, Stanford University, Stanford, CA 94305, and *J. Y. Leong*, Applied Materials, CVD Product Div., Santa Clara, CA 95054

The behavior of HF C-V curves of Al-CVD SiO_2-Si MOS capacitors prepared by PECVD (TEOS-O_2) and medium pressure CVD (TEOS-O_3) *vs.* processing parameters was interpreted in terms of changes induced at Si-SiO_2 interface due to native oxide growth and ion-surface interaction involved in Ar plasma clean of Si wafers and in initial stage of PECVD SiO_2 deposition process. Ion implantation in silicon substrate at low energy of O, C, and H atoms (originating from TEOS-O_2 plasma) and of Ar atoms (from Ar plasma) was considered responsible for the increase of positive fixed charge at Si-SiO_2 interface.

281 Trace Moisture Analysis in Monosilane-Hydrogen Mixtures at Atmospheric Pressure and Ion-Molecule Reactions: *T. Irie, S. Iijima,* and *Y. Mitsui,* Central Research Laboratory, Hitachi, Ltd., Kokubunji, Tokyo 185, Japan

Atmospheric pressure ionization mass spectrometer has been used for analyzing trace moisture contained in gaseous mixtures of monosilane and hydrogen for semiconductor fabrication processes. Trace moisture can be evaluated from the intensities of cluster ions, such as SiH_3H_2O and $SiH_3(H_2O)_2$, at several percent of monosilane concentrations. SiH_3H_2O may result from Si_2H_7 reacting with H_2O through proton-transfer and/or switching processes, where collisional stabilization plays an important role.

282 Chemical Foundations in Understanding the Step Coverage Problem in CVD Using the Silane Chemistry: *C. Pavelescu* and *K. C. Saraswat,* Center for Integrated Systems, Stanford University, Stanford, CA 94305

The correlations between the deposition kinetics and the step coverage problem in CVD using the silane chemistry are investigated. For LPCVD of polysilicon, the near 1 value of the step coverage is consistent with a near zero surface reaction order with respect to silane, which indicates the surface saturation with silicon containing species, and a low value of reaction probability (sticking coefficient), K_s, is predicted. Although LPCVD and PECVD processes for SiO_2 deposition in a trench of dimensions around 1 μm are characterized by a free molecular flow regime, while APCVD is described by a transitional flow regime, the step coverage of SiO_2 thin films in all these processes presents similar poor values. This behavior can be interpreted in terms of the surface reaction kinetics described by a reaction order around 0.5 with respect to silane, which suggests that the film surface is not saturated with silicon containing species, and higher values of K_s are predicted for these CVD processes.

283 Characterization of Band-Pattern Polishing Marks Induced during Waxless/Wax Polishing Process Using Magic Mirror Method: *K. H. Cho* and *H. Y. Cho,* Siltron Inc., Gumi, Kyungsangbukdo 730-350, Korea, *S. Hahn,* Dept. of Materials Science and Engineering, Stanford University, Stanford, CA 94305, *D. Feindel* and *F. Mason,* Zygo Corp., Middlefield, CT 06455-0448, *P. R. Blaustein,* Hologenix Inc., Torrance, CA 90503, *K. W. Kim,* Dept. of Electronics, *Kyungpook National University, Taegu 702-701,* Korea

In this study, we investigated various properties of band-pattern (one of the most commonly observed surface flaws) induced during waxless/wax polishing process using the magic mirror method. In order to understand the origin of this pattern and its effects upon various physical properties of the Si wafer, total thickness variation (TTV) mapping with automatic sorter, strain/damage measurement by x-ray double crystal rocking curve method, thermal wave modulated reflectance measurement (TW) and photo-acoustic displacement measurement (PAD), microsurface roughness measurement by laser surface interferometry, and electrical parameter measurements such as oxide breakdown strength and time dependent dielectric breakdown have been performed.

284 Highly Reliable Electrostatic Chucks Employing Plasma-Sprayed Aluminum-Oxide Coating for Advanced Semiconductor Processing: *H. Uetake, K.Morizuka,* and *T. Ohmi,* Dept. of Electronics, Faculty of Engineering, Tohoku University, Sendai 980, Japan

A highly reliable electrostatic chuck for the advanced semiconductor manufacturing equipment has been developed by plasma sprayed aluminum oxide coating. Fabrication procedure is shown. Furthermore, the stable attraction force in the low temperature range has been realized by mixing of TiO_2 to aluminum oxide in the plasma spray step. Some fundamental evaluations are described. Excellent thermal contact between the wafer and the wafer stage, as well as the electric potential control, has been established by applying the electrostatic chuck developed here.

285 Investigation of Single-Layer p-SnS:M and Double Layer p-SnS:M/n-MS:Sn (M = Zn or Cd)-Based Photoconductive Cells Produced by a Combined Chemical Bath Deposition/Ion Exchange Process: *R. Engelken, C. Brinkley, L. N. Chang,* and *L. Yu,* Dept. of Engineering, Arkansas State University, State University, AR 72467

We report investigation of photoconductive cells sensitive to the entire visible spectrum and comprising a p-SnS:M layer or a p-SnS:M/n-MS:Sn (M = Zn or Cd) bilayer deposited between two intertwined comb-like copper contacts on fiberglass. The semiconductor is formed by chemical-precipitation deposition of ZnS or CdS via thiourea-metal salt baths followed by immersion in an ethylene glycol bath of $SnCl_2$. The Sn(II) ion exchanges with the M(II) lattice cation and forms a partial or complete (depending on immersion time) SnS layer containing residual Zn or Cd which fills tin vacancies and reduces the native p-nature of the SnS. The cells offer effective, low cost, minimally toxic detection of the entire visible spectrum and an alternative to PbS and CdS whose performance is less than optimum in the near infrared, red, and orange portion of the spectrum.

286 Mix-Cation Oxide Powders via Resin Intermediates Derived from Water Soluble Polymers: *L.-W. Tai** and *H. U. Anderson,* Ceramic Engineering Dept., University of Missouri-Rolla, Rolla, MO 65401

Polymeric synthesis of mix-cation oxides via a liquid-mix (LM) process is described. Two types of polymeric gels have been developed to form fluffy resin intermediates which were calcined to form oxides powders at relatively low temperatures. In addition to an optimized precursor made of critic acid and ethylene glycol, a new water-soluble polymer prepared from starch derivatives was utilized in LM process. $La_{1-x}Sr_xCo_{1-y}Fe_yO_{3-\delta}$ and others were prepared having a single phase, fine particles, soft agglomerates, and thus a superior sinterability.

287 A Novel Evaluation Technique of Carrier Concentration by Noncontact Eddy Current Measurement: *S. Washizuka,* Semiconductor Material Engineering Dept., Toshiba Corp., 72, Horikawacho, Saiwai-ku, Kawasaki, Kanagawa, 210, Japan, *Y. Yoneda, A. Watanabe,* and *T. Ohta,* ULSI Process and Material Laboratory, Toshiba Microelectronics Corp., 25-1, Ekimaehoncho Kawasaki-ku, Kawasaki, Kanagawa, 210, Japan

A novel evaluation technique of III-V semiconductor materials, such as GaP, GaAs, has been attained using a newly developed noncontact wafer carrier concentration inspection system by eddy current measurement. The validity of this system is demonstrated in comparison with van der Pauw method for wafers with carrier concentration over the range of 10^{14} to 10^{19} cm^{-3}. The correlation factor is 0.99 and the discrepancy between the two is the maximum limit within ±7%. This technique is accurate enough for practical usage in production line.

288 ZrO_2-CeO_2 Spherical Powders Prepared by Sol-Gel Process: Synthesis, Sintering, and Characterization: *F. Croce* and *M. Carewska,* Dept. of Chemistry, University of Rome "La Sapienza," P. le A. Moro, 5-00185 Rome, Italy, *A. Deptula,* Institute of Nuclear Chemistry and Technology, Dept. of Structural Research, Sol-Gel Lab., Dorodna 16-03-195 Warszawa, Poland

The IChTJ[1] Sol-Gel process has been utilized to prepare spherical powders of zirconia-ceria hydroxide-gels (with mean diameter less than 100 μm). Some preparations were stabilized with nitrate or chloride. The resulting amorphous powders were calcined at 400, 600, and 800°C in order to obtain the crystalline forms, and subsequently pressed at various pressures. The so obtained compact greens were sintered for 8 h at 1700°C. The sintered pellets had relatively high geometric density (in many cases >95% of the theoretical density -t.d.) and showed both tetragonal and/or cubic x-ray phases. The density values of these ceria doped zirconia samples are much higher than those obtained for the CaO or Y_2O_3 doped zirconia samples prepared by the same process. This probably happens through the agency of the cerium reduction due to the carbonic impurities in the gels and the subsequent high temperature reoxidation by the air oxygen.

289 A Characterization of the Effect of Deposition Temperature on Polysilicon Properties: Morphology, Dopability, Etchability, and Polycide Properties: *E. Ibok* and *Shyam Garg,* Advanced Micro Devices, Inc., Austin, TX 78741

Low pressure chemical vapor deposition polysilicon deposition was studied from 525 to 650°C. The poly appears to be amorphous with a smooth surface to 550°C and completely crystalline above 600°C. The transition region is from 560 to 590°C. The smooth surface morphology is preserved after $POCl_3$ doping and a 1000°C oxidation. However, an *in situ* anneal of amorphous silicon at 610°C results in large, coarse crystals with rough surface morphology. The smooth morphology of the 550°C silicon is transmitted through subsequent polycide structure layers. The deposition temperature is found to affect poly etch rate and resistivity. A mechanism is proposed.

290 Effect of Back-Surface Polycrystalline Silicon Layer on Oxygen Precipitation in CZ Silicon Wafer: *M. Kadoi,* Mitsubishi Materials Silicon Co. Ltd., 314 Kaneuchi, Nishisangao, Noda, Chiba 278, Japan, *H. Furuya* and *T. Shingyouji,* Central Research Institute, Mitsubishi Materials Corp., 1-297 Kitabukuro, Omiya, Saitama 330, Japan, *Y. Shimanuki,* Mitsubishi Materials Silicon Co. Ltd., 314 Kaneuchi, Nishisangao, Noda, Chiba 278, Japan

We have investigated the formation of oxygen precipitates in CZ silicon wafers covered by polycrystalline silicon (polysilicon) film. We examined the size and densities of oxygen precipitates in the wafers annealed at various conditions. The result indicated that the oxygen precipitation was enhanced in the region near the back side of the wafer, but the size of oxygen precipitates in the back-side region was not different from that in the other region. The result also indicated that the nucleation near the back side

would not have occurred during annealing for oxygen precipitation. From these results, it was assumed that the strain field induced by polysilicon film would affect the stability of nuclei existing in the wafers.

291 HfN/$Hf_xO_yN_z$ Thin Films by LPCVD: *C. Orfescu, A. J. Fortini, R. La Ferla, A. J. Sherman,* and *E. H. Liu,* Ultramet, Pacoima, CA 91331

A low-pressure chemical vapor deposition (LPCVD) process was developed for depositing thin films of hafnium nitride/hafnium oxynitride (HfN/$Hf_xO_yN_z$), based on the overall reaction ($HfCl_4 + NH_3 + 1/2\ H_2 \rightarrow HfN + 4HCl$). A total of 24 experiments were performed to deposit HfN/$Hf_xO_yN_z$ layers onto graphite substrates in a LPCVD reactor, and the effects of deposition temperature on microstructure, composition, and microhardness were evaluated. HfN/$Hf_xO_yN_z$ crystals tended to grow in a columnar manner, although deposits made at higher temperatures were fine-grained. X-ray diffraction (XRD) measurements showed $Hf_xO_yN_z$ to be the major phase at 1050 and 1200°C, and HfN the major phase at 1350°C. Vickers microhardness values were measured at 1600 kg/mm² for the materials deposited at 1050 and 1200°C, and 2000 kg/mm² at 1350°C.

292 Damage and Its Rapid Thermal Annealing Kinetics in Ar^+ Ion Implanted CZ Silicon: *Y.-K. Kwon, K.-I. Kim, Y.-H. Bae,* and *W.-J. Chung,* Semiconductor Research Laboratory, RIST, Pohang 790-600 Korea, *E. K. McIntyre, Jr.,* Semiconductor Equipment Div., Eaton Corp., Beverly, MA 01915, *T. Hara, H. Hagiwara,* and *H. Suzuki,* Dept. of Electrical Engineering, Hosei University, Kajinocho, Koganei, Tokyo 184, Japan, *W. L. Smith,* ThermaWave, Inc., Fremont, CA 94539, *S. Hahn,* Dept. of Materials Science and Engineering, Stanford University, Stanford, CA 94305, *L. Larson,* Sematech, Austin, TX 78741, *C. B. Yarling,* Ion Implant Services, Sunnyvale, CA 94086, and *R. Meinecke,* AG Associates, Sunnyvale, CA 94089

In this study, damage induced by medium (100 keV) and high (1 MeV) energy Ar^+ ion implantation and its annealing behavior during rapid thermal annealing for 10 s at temperatures between 575 and 1100°C were investigated by thermal wave modulated optical reflectance, deep level transient spectroscopy, reflection high energy electron diffraction, Rutherford backscattering aligned spectra and transmission electron microscopy. Our data show that: (*i*) thermal wave signal and its variation with respect to rapid thermal anneal temperature strongly depend upon implant dose and anneal temperature; (*ii*) regardless of implant dose and energy, four distinctive deep trap levels are induced; and (*iii*) these traps evolve during rapid thermal annealing.

293 Low Resistance Molybdenum Silicide–Molybdenum Thin Films: *S. Vasile,* Radiation Monitoring Devices Inc., Watertown, MA 02172, *D. Nicolaescu,* ICCE, Bucharest, Romania 72996

The electrical, optical, and plasma etch properties of 460 nm molybdenum silicide/molybdenum thin films, obtained by the thermal reaction of vacuum deposited silicon on molybdenum, have been reported. The sheet resistance of 900°C annealed films was as low as 0.40 Ω/square and proved a good stability when stored at 400°C temperature under oxidizing atmosphere. The resistivity of the formed silicide was in good agreement with that obtained by Mo-single crystal silicon thermal reaction. The plasma etch rate of the silicide was about 5 times lower than that of annealed molybdenum. Plasma etch profiling of the silicide/molybdenum films showed a well-defined transition region from silicide to molybdenum. The formed 70 nm molybdenum silicide was transparent within visible optical range, and behaved as a good antireflecting layer on molybdenum.

SURFACE PROCESSING IN ENERGY TECHNOLOGIES

Energy Technology

294 Photoelectrochemical and Electrochemical Polishing of Epi ß-SiC and CVD: *R. D. Rauh, T. H. Nguyen, M. M. Carrabba,* and *D. Plante,* EIC Laboratories, Inc., Norwood, MA 02062

The feasibility of using a photoelectrochemical or electrochemical process to polish extremely hard n-type SiC material has been evaluated. Statistical experimental designs have been used to identify and define the etching conditions which would lead to a supersmooth SiC surface. Statistical analysis of the experimental results show that (F^-) concentration, solution pH, and applied potential profoundly influence the morphology of the etched SiC surface. Extremely smooth SiC surfaces have been obtained with photoelectrochemical and electrochemical polishing at a very fast rate compared to conventional mechanical polishing.

295 Characterization of Electrocatalytically Active Ni-Co Amorphous and Crystalline Alloys: *K. Lian, D. W. Kirk,* and *S. J. Thorpe,* Dept. of Metallurgy and Motorola, Science and Chemical Engineering and Applied Chemistry, University of Toronto, Toronto, Ont., Canada M53 1A4

The electrocatalytic activity of amorphous and crystalline Ni-Co alloys on the oxygen evolution reaction (OER) in alkaline solution has been studied. The surface electrochemistry and chemistry were investigated by means of steady-state potentiostatic method, cyclic voltammetry, and x-ray photoelectron spectroscopy (XPS). The electrochemically oxidized (potential cycled) amorphous Ni-Co alloys showed an exceptionally high activity and excellent stability compared with their crystalline counterparts. Hydrous Ni-Co oxides, which are responsible to the enhanced catalytic activity, are believed to be formed on the surface of amorphous alloys via potential cycling process.

296 Influence of Pretreatment on the Unusual Redox Behavior of Noble Metal Electrodes: *L. D. Burke,* and *J. K. Casey,* Chemistry Dept., University College Cork, Cork, Ireland

The cyclic voltammogram for polycrystalline platinum in aqueous acid media is one of the best known features in electrochemistry. However, a considerably different, highly reproducible, response for the same system was observed recently following abrasion and extensive potential cycling. Results are presented for a similar investigation of gold; these observed novel redox transitions are of significant importance in electrocatalytic processes. The major factor influencing such transitions is the surface modification induced by the pretreatment.

297 Catalyst Layer and Interface Properties of Directly Catalyzed Polymer Electrolyte Membranes: *M. S. Wilson, T. A. Zawodzinski, T. E. Springer, J. Valerio* and *S. Gottesfeld,* Electronics Research Group, Los Alamos National Laboratory, Los Alamos, NM 87545

Low platinum loading thin film catalyst layers (approximately 5 µm thick) are applied directly to polmer electrolyte membranes. Electrode/membrane/electrode assemblies for fuel cells are prepared using several different catalyst application procedures and catalyst layer compositions. A variety of techniques are used to characterize the thin film catalyst layers. In particular, ionic and electrical conductivities and gas diffusivities within the catalyst films and ionic conductivities across the catalyst layer/membrane interfaces are studied.

298 Chemical Bath Deposition of Cadmium Sulfide Thin Films, *In Situ* Growth and Structural Studies by Combined Quartz Crystal Microbalance and Impedance Techniques: *D. Lincot* and *R. Ortega,* Laboratoire d Electrochimie, ENSCP, 75231 Paris Cedex 05, France

Chemical bath deposition (CBD) of CdS layers, using the ammonia process, have been studied for the first time by combined *in situ* quartz crystal microbalance (QCM) and electrochemical capacitance techniques. An important result is that information about the covering properties of the film, its internal structure, and the evolution during growth, have been obtained from combined experiments. The film is show to have, in general, a duplex structure, with an inner compact layer (only measured by capacitance) and an outer porous layer, growing at longer reaction times. The influence of the thiourea concentration is studied in detail. A simple columnar growth model is proposed, which accounts well for the experimental results in the coalescence range.

299 Study of the Bandedge Shifts of n- and p-type $CuInSe_2$ Semiconducting Electrodes in Varios Aqueous Electrolytes: *W. Siripale, J. Vedel,* and *D. Lincot,* Laboratoire d'Electrochimie, ENSCP, 75231 Paris, France, *D. Caben,* The Weizmann Institute of Science, 76100 Rebovot, Israel.

Impedance measurements were employed for the *in situ* determination of the flatband potential of n- and p-type $CuInSe_2$ electrodes in various aqueous electrolytes. It was observed that the flatband values could be shifted over a considerable potential range of about 0.2 to -0.8 V, depending upon the nature of the samples. Also, it was observed that the bandedges could be fixed at intermediate positions by applying necessary potentials. This could open a route for the bandedge position tailoring.

300 Highly Oriented *vs.* Microcrystalline Thick Cadmium Films Deposited on Polycrystalline Nickel from a Molten Salts Electrolyte: *R. R. Agarwal,* Dept. of Chemical Engineering, Illinois Institute of Technology, Chicago, IL 60616

Thick and large highly oriented and microcrystalline cadmium films were deposited onto polycrystalline nickel substrates from a purified chloroaluminate melt under an inert atmosphere between 175 and 115°C. These films were characterized under the SEM/EDAX with respect to their respective surface features. The shift in crystal sizes in cadmium films was caused by the phenomological solidification processes based on analysis of the chemical mechanism and rate controlling processes at the experimental conditions.

301 Surface Modification of Sintered Plates Negative Electrodes of Nickel Cadmium Battery: *S. T. Salvan, R. Sabapathi,* and *N. Venkatakrishnan,* Central Electrochemical Research Institute, Battery Div., Karaikudi 623 006 India

It is very important to consider the degradation mechanism of a Cd electrode in NiCad since its cyclability is usually affected. Out of the four organic compounds studied, the BTA-created Cd electrode proves to offer increased capacity utilization, increased life, and reduced deterioration from crystal growth. After 800 cycles, it exhibits a fairly uniform distribution of active material so as to retain 80% of its original capacity, whereas the control electrode retains only 58%.

302 Properties and Modification of Perfluorosulfonic Acid Membrane Surfaces: *T. A. Zawodzinski Jr.*, Electronics Research, Los Alamos National Laboratory, Los Alamos, NM 87545, *M. Shoichet*, Polymer Science and Engineering Dept., University of Massachusetts, Amherst, MA 01003, *N. Hamel* and *G. Gard*, Dept. of Chemistry, Portland State University, Portland, OR 97202-0751, *T. J. McCarthy*, Polymer Science and Engineering Dept., University of Massachusetts, Amherst, MA 01003, *S. Gottesfeld*, Electronics Research, Los Alamos National Laboratory, Los Alamos, NM 87545

Humidification of polymer electrolyte fuel cells is essential to maintaining adequate conductivity within the ionomeric membrane and within the polymer/C/Pt composite catalyst layer. Sorption of water by the polymer is thus a crucial element in achieving optimal fuel cell performance. Qualitative observations suggest that the surface of these perfluorinated membranes is hydrophobic. Characterization of the surface of several membranes by contact angle measurements and attempted chemical modification for enhanced hydrophilicity are described.

303 *In Situ* Study of the Chemical Bath Deposition Mechanism of Cadmium Sulfide Thin Films on Gold and Copper Indium Diselenide Substrates: *D. Lincot, R. Ortega*, and *J. Vedel*, Laboratoire d' Electrochimie, ENSCP, 75231 Paris Cedex 05, France

Chemical bath deposition of CdS layers, using the ammonia process, have been studied for the first time by *in situ* quartz crystal microbalance technique. This allowed us to monitor precisely the growth kinetic of the layer, especially in the first steps, which is not possible with classical *ex situ* methods. A detailed study of the influence of the reaction parameters is performed (concentration of precursors, pH, temperature...), giving new insights for the interpretation of the reaction mechanism. The study was also carried out on coevaporated $CuInSe_2$ layers, in direct relation with the optimization of the deposition of the CdS buffer layer entering in the structure of high efficiency $CuInSe_2$/CdS/ZnO cells.

304 Electrochemical Vapor Deposition of CeO_2 Thin Film Electrolytes for Solid Oxide Fuel Cells: *J. F. Jue* and *A. V. Virkar*, Dept. Materials Science and Engineering, University of Utah, Salt Lake City, UT 34112

Dense films of CeO_2 of a thickness on the order of 50 μm were fabricated by electrochemical vapor deposition (EVD) using $CeCl_3$ as the source of cerium. Films were deposited on zirconia and ceria substrates at 1200°C. The kinetics of film growth were observed to be parabolic in accord with Wagners oxidation theory. The measured rate constant of 3.7×10^{-8} cm/s at 1200°C is about five times larger than that reported for zirconia films.

305 Evaluation of Doped Ceria with and without Zirconia Coating for Application in Low-Temperature Solid and Oxide Fuel Cells: *K. Mehta, A. V. Virkar*, Dept. of Materials Science and Engineering, University of Utah, Salt Lake City, UT 34112

Y_2O_3-doped and Er_2O_3-doped CeO_2 solid electrolytes with and without a thin (2 μm) layer of zirconia were testeu in fuel cell mode over a range of temperatures between 600 and 700°C. Disks with zirconia coating exhibited superior performance compared to uncoated disks. Also, in cells with improved electrodes, most of the cell resistance was the electrolyte resistance. Doped CeO_2 is a potential low temperature solid electrolyte for fuel cells.

306 Kinetics of the Cadmium Electrode in Alkaline Solution: *S. Tamil Selvan, R. Sabapathi*, and *N. Venkatakrishnam*, Central Electrochemical Research Institute, Battery Div., Karaikudi 623 006, India

The purpose of this paper is to investigate the charge transfer mechanism of planar Cd electrode in KOH solution with and without organic compounds. The mechanism does not change in the presence of azole compounds, such as BTA and IDA. A Nernstian Tafel slope of 40 ± 3 mV decade^{-1} is obtained as a result of PVA/CMC addition to the electrolyte. Furthermore the results suggest that organic compound-modified Cd surface is formed which results in enhanced kinetics of the $Cd/Cd(OH)_2$ electrode reaction

307 Evaluation of Electrodeposited Electrocatalytic Composite Metal Film Coatings for Cathodic H_2 Evolution in Water Electrolyzers: *B. E. Conway, R. Simpraga, R. Brousseau*, and *L. Gao*, Dept. of Chemistry, University of Ottawa, Ottawa, Ont, Canada K1N 6N5

Electrocatalytic coatings are required for minimization of overvoltage and electric power loss at electrolyzer cathodes in water electrolyzers, and for cathodes used in the chlor-alkali and F_2 production (from KF · 2HF) processes. Results are reported for Ni-Mo-Cd, Ni-W, and Ni-V composite films electrodeposited on Fe, based on studies of Tafel polarization relations and particularly on determinations of the coverage by the "overpotential-deposited" H intermediate involved in electrocatalysts of the cathodic H_2 evolution process. Inclusion of a complement of Cd (1-2 a/o), codeposited with the transition metals, leads to substantial enhancement of activity, possibly due to changes of microstructure of the deposit and/or electronic band-structure changes.

FRACTALS IN ELECTROCHEMISTRY

Energy Technology/Physical Electrochemistry/Corrosion

308 Effects of Anisotropy on Pattern Formation in Electrochemical Deposition: *F. Family* and *K. C. B. Chan*, Dept. of Physics, Emory University, Atlanta, GA 30322

We have studied the effect of anisotropy on electrochemical deposits grown from solutions of copper sulfate in thin cells. The cell consists of two parallel plates and anisotropy is introduced by machining a 1 mm square grid of grooves on one of the plates. The effects of anisotropy on the growth are discussed and new results for the size distribution and fractal analysis of the anisotropically grown electrochemical deposition patterns are presented and compared with simulations and theory of diffusion-limited aggregation with anisotropy.

309 Interfacial Dynamics and Induced Convective Transport in Electrodeposition: *D. P. Barkey*, Chemical Engineering Dept., University of New Hampshire, Durham, NH 03824-3591

Application of pattern-forming theory to electrodeposition is reviewed. The critical role of interfacial dynamics in velocity and morphology selection is emphasized. Experimental studies of deposition from unsupported electrolyte are reported. The presence of induced convection at the growth front is demonstrated, and the resulting concentration field is imaged. This spontaneous convection is shown to be coupled to morphology development.

310 Diffusion to Patterned Electrodes: *Y. Dassas* and *P. Duby*, Henry Krumb School of Mines, Columbia University, New York, NY 10027

Diffusion to patterned electrodes has been investigated by potential step and current step techniques. We have confirmed the findings of Pajkossy and Nyikos, *i.e.*, the current on an electrode with a photoresist coverage of fractal dimension d decays with the $-(d-1)/2$ power of time during a potentiostatic test. We have demonstrated experimentally that the same relationship applies to the current density *vs.* transition time under galvanostatic conditions. We have also observed a similar effect with nonfractal patterned electrodes.

311 Electro-Convection Around Two-Dimensional Ramified Copper Aggregates: *V. Fleury, J.-N. Chazalviel*, and *M. Rosso*, Laboratoire de Physique de la Matière Condensée, Ecole Polytechnique, 9128 Palaiseau, France

We propose a model for the electrochemical deposition of ramified copper aggregates from copper sulfate, without supporting electrolyte in the régime of fast growth (current density > 50 mA/cm^2). This model takes into account the electro-convective motion of the fluid. It predicts the existence of a virtual interface in the vicinity of the tips of the deposits. This interface separates a zone free of ions of both kinds and a zone of constant concentration. Preliminary experimental observations are well accounted for by the model.

312 Electrochemical Aspects of Fractal Zinc Electrodeposition: *F. Sagues, J. Claret, L. Lopez-Tomas, J. Mach, F. Mas*, and *P. P. Trigueros*, Dpt. Quimica Fisica, Universitat de Barcelona, 08028 Barcelona, Spain

Experiments on quasi-two-dimensional zinc electrodeposition have been conducted mainly with a parallel or strip geometry. Morphological changes have been observed when varying the cell dimensions with pronounced effects leading to morphological transitions under high current conditions. In addition, the growth probability distributions of the electrodeposits have been computed and analyzed in terms of multifractal concepts. Finally, the generalization of classical Cottrell-like laws, to include the fractal roughness of the experimental electrodes, have been also tested.

313 Morphology Transitions in Rapid Electrodeposition: *L. M. Sander*, Dept. of Physics, The University of Michigan, Ann Arbor, MI, 48109-1120

Electrochemical deposition in extreme overpotential conditions provides an opportunity to directly examine the correlation between microstructure and large-scale structure in a controlled system: it is representative of a large class of interfacial pattern formation problems. We discuss how long-range order can spontaneously reemerge as growth is driven further from equilibrium. We discuss both the mechanisms for this reordering, including the discovery of a metastable crystalline form of zinc.

314 Columnar Growth and Kinetic Roughening in Electrochemical Deposition: *P.-z. Wong, G. L. M. K. S. Kahanda, X.-q. Zou*, and *R. Farrell*, Dept. of Physics and Astronomy, University of Massachusetts, Amherst, MA 01003

We report a series of electrochemical deposition experiments of copper from $CuSO_4$ solutions in a quasi-two-dimensional cell. They performed at very slow rates (0.1-0.2 mm/h) so that local growth effects can compete with the nonlocal Laplacian effects. In the early stage of growth, we observed a behavior consistent with the conventional Mullins-Sekerka instability. This is followed by coarsening and roughening of the surface which lead to a columnar structure with deep and narrow crevices. The surface roughness for length scales below the typical column width may be approximated by a power-law with an exponent $\alpha = 0.57 \pm 0.05$. These results indicate that while nonlocal growth effects are more dominant at long length scales and local effects such as stochastic noise controls the surface roughness at short length scales.

315 Evidence for a Kosterlitz-Thouless Transition in the Threshold Screening Model: Critical Region of Fractal Growth: *J. H. Kaufman* and *O. R. Mclroy*, IBM Almaden Research Center, San Jose, CA 95120-6099

We report evidence for a Kosterlitz-Thouless transition in a 2-d model of fractal pattern formation. The threshold screening model is used to produce patterns on both a square lattice and hexagonal lattice. In both cases, the fractal dimension varies from one to two as the screening strength is decreased. The pattern forming process on the square lattice passes through a single critical point as a function of temperature or field where the spatial pattern is characterized by a nontrivial fractal dimension. On a hex lattice, the data suggest the existence of a critical region as a function of temperature and field. We draw an analogy to XY models on square and triangular lattices ($p = 4$ and $p = 6$ clock models) where similar critical behavior is observed. Possible point defects, analogous to the vortices in the *xy* model, are described.

316 Probing Electrocrystallization Mechanisms of Molecular Solids: *A. C. Hillier* and *M. D. Ward*, Dept. of Chemical Engineering and Materials Science, University of Minnesota, Minneapolis, MN 55455

Molecular crystalline solids based on organic and organometallic components exhibit electronic phenomena ranging from electrical conductivity, superconductivity, nonlinear optical behavior and ferromagnetism. While structure-function relationships in these materials have been and continue to be studied extensively, relatively little attention has been paid to the fundamental aspects of the crystallization of these materials, which is commonly accomplished by electrochemical methods. Investigations involving the electrocrystallization of $TTFBr_{0.7}$ (TTF = tetrathiafulvalene) and TMTSF charge transfer salts (TMTSF = tetramethyltetraselenafulvalene) under conditions in which diffusion limited aggregation is operative were performed. Results indicate the relationship between mass transfer and the probability of growth along different crystallographic directions, as controlled by molecular level interactions between crystal faces and solute molecules and aggregates.

317 Multifractal Fluctuations in Diffusion in Disordered Systems: *S. Havlin*, Dept. of Physics, Bar-Ilan University, Ramat-Gan 52900, Israel

The multifractal features which appear in the fluctuations of diffusion in several random fractal systems are discussed. It is shown that the moments of the probability density, $P(r, t)$, for a random walker to be at distance r at time t behave as $\langle P^q \rangle \sim \langle P \rangle^{\tau(q)}$, where $\tau(q) > q$, and $\gamma < 1$, $(q > 0)$. Due to the structural disorder the distribution of P for a given r and t is anomalously broad. Similar multifractal distributions have been obtained for diffusion in stratified media with random velocity fields, which is a model for ground water flow.

318 Fractals in Electrochemical Photovoltaics: *A. J. McEvoy* and *M. Gratzel*, Institute de Chimie Physique, Ecole Polytechnique Fédérale de Lausanne, CH-1015 Lausanne, Switzerland

A wide bandgap n-type semiconductor sensitized to visible light by chemisorption of a charge-transfer dye is the photoanode of a novel photovoltaic cell. A very rough high surface area morphology is required at the semiconductor-electrolyte interface for efficient light absorption and charge transfer. Fractal concepts have been applied for its characterization, using diffusion and impedance spectroscopy data. A fractal dimensionality was determined, and the interpretation confirmed by electron microscopy.

319 Morphology and Kinetics of Fractal Growths: *D. B. Hibbert* and *S. N. Atchison*, University of New South Wales, Kensington, Sydney 2033, Australia

Various metals (copper, zinc, and silver) were electrodeposited in two dimensions and in both a linear and circular geometry, with and without a variety of support. These supports were found to have a profound effect on the resulting morphologies of the growths. The velocity of the growth varies with the transport number of the anion, in accordance with the theory herein, as well as concentration and voltage. XPS maps of codeposited metals allows a detailed study of the interface.

320 Photocatalysis on Porous Substrates: *M. Tomkiewicz* and *H. Wang*, Dept. of Physics, Brooklyn College of CUNY, Brooklyn, NY 11210

Some of the recent work in the area of photocatalysis on semiconducting powders and porous structures which correlates the morphology of the catalyst with its activity are reviewed. Computer simulations of the photocatalytic processes are used to compare the kinetics on porous photocatalysts, with various morphologies, with that of a smooth one.

321 Equivalent Circuit Study of Fractal Electrodes: *B. Sapoval*, Laboratoire de Physique de la Matière Condensée, Ecole Polytechnique, 91128 Palaiseau, France

We present an equivalent circuit study which permits through iteration of impedance complex functions to find the response of 2d self-similar electrodes. Such iteration gives an algebraic expression for the impedance, the constant phase angle exponent and the frequency range in which a CPA response exists. The admittance of a real electrode of macroscopic size L and thickness h is

$$Y_L \approx Lb\rho^{\eta-1}(\gamma\omega)^{\eta}a^{\eta-1} \text{ with } \eta = 1/D$$

where a is the smaller feature size of the fractal, ρ the electrolyte resistivity and γ the capacitance per unit surface of the electrode. The CPA frequency range is found to be equal to $(L/a)^D$ that is to the total length of the fractal.

322 The Double Layer Impedance: Effects of Electrode Roughness: *T. C. Halsey*, The James Franck Institute, The University of Chicago, Chicago, IL 60637

This paper presents the results of a numerical study of the double layer impedance of various self-similar electrodes in two and three dimensions. Our numerical method makes use of the formal relationship between the double layer impedance at a rough electrode, and the behavior of random walks reflected from the surface of that electrode. We find the behavior of the impedance is determined by the "multifractal" properties of the surface.

323 Theory of Interfacial Constant Phase Element in Electrode-Electrolyte Systems: *S. H. Liu*, Oak Ridge National Laboratory, Solid State Div., Oak Ridge, TN 7831-6032

In this paper we review theoretical and experimental evidence that the fractal nature of the electrode-electrolyte interface is the source of the constant phase element seen in the impedance spectra of electrolytic cells. The fractal geometry gives rise to a complex distribution of parallel current paths, and the competition between these paths results in the fractional power law frequency dependence of the impedance across the interface. The frequency exponent is shown to be not simply related to the fractal dimension of the interface.

324 Noise Analysis Applied to Electrochemical Systems: *U. Bertocci*, National Institute of Standards and Technology, Metallurgy Div., Washington, DC 20899

Random fluctuations of the electrical quantities (electrode potential and cell current) in electrochemical systems, are commonly referred to as electrochemical noise. The paper describes the main sources of noise, the experimental methods used for its measurement, and some of the schemes for its analysis, with particular emphasis to corrosion applications.

325 Surface Morphology Characterization with X-Ray Scattering: *C. Thompson*, Dept. of Physics, Polytechnic University, Brooklyn, NY 11201

Conventional x-ray reflectivity techniques can describe the characteristic root-mean-square width of the surface roughness profile. Extensions of the x-ray reflectivity technique are applied to probe in-plane height-height correlation functions for surface films. This technique is sensitive to the texture of the surface and to changes in the in-plane arrangement of surface structure constituting film roughness.

326 Electrochemical Fractal Dimension Measurement on Rough Surfaces: *T. Pajkossy*, *A. Imre*, and *L. Nyikos*, Central Research Institute for Physics, Budapest 114, H-1525, Hungary

Based on the analysis of the time dependence of the diffusional flux to a surface, an electrochemical method is described for the accurate ($\leq \pm 0.02$) determination of the fractal dimension of rough surfaces in the 1 to 10 μm range. We apply this method for the measurement of the fractal dimension of fractured steel surfaces.

ELECTROCHEMICAL CHARACTERIZATION OF THIN SOLID FILMS

Energy Technology/Physical Electrochemistry/Dielectric Science and Technology

327 *In Situ* Infrared Spectroscopy of Corrosion Processes at Lacquer Coated Metals: *S. N. Port* and *A. Bewick*, Dept. of Chemistry, University of Southampton, Southampton, England S09 5NH, *J. Casper*, ICI Paints, Research Dept., Slough, Berkshire, England SL2 5DS

Degradation and corrosion processes occurring at polymeric lacquer coated iron and gold in aqueous electrolytes have been investigated using *in situ* infrared spectroelectrochemical methods supplemented by voltammetry and impedance measurements. Initial measurements were made to determine the adsorption behavior and orientation of model molecules related to the monomer units of the polymer. Spectra from the coated metals at controlled potentials allowed the degradation and corrosion processes to be elucidated and monitored.

328 Coulometric Reduction of Thin Tarnish Films Formed on Copper: *B. I. Rickett* and *J. H. Payer*, Dept. of Materials Science and Engineering, Case Western Reserve University, Cleveland, OH 44106

Upon exposure to ambient air, copper develops a native cuprous oxide film which serves to protect copper from further oxidation in nonaggressive environments. Yet, the combination of relative humidity and low part per billion concentration levels of pollutants creates a corrosive adlayer, which then destroys the protective nature of the initial oxide film. Coulometric analysis (chronopotentiometry), in conjunction with x-ray photoelectron spectroscopy (XPS), allows compositional characterization and thickness determination for the thin tarnish films formed during these environmental exposures. This paper presents the results of thin film analysis for Cu-O-S compounds on a copper substrate.

329 Impedance Characterization of Polypyrroles: *P. G. Pickup, G. L. Duffitt,* and *X. Ren,* Dept. of Chemistry, Memorial University of Newfoundland, St. John's, Newfoundland, Canada A1B 3X7

Thin films of polypyrrole, poly-[1-methyl-3-(pyrrol-1-ylmethyl)pyridinium]$^+$, and poly-(3-methylpyrrole-4-carboxylic acid) have been electrochemically characterized by impedance spectroscopy. Results are incompatible with a diffusion model, and have therefore been interpreted in terms of a transmission line consisting of the ionic and electronic resistances of the film coupled by its capacitance. The dependence of ionic conductivities on potential, solvent, electrolyte concentration, and electrochemical cycling reveals significant differences between the three polymers. The origins of these different behaviors are discussed in terms of polymer film structure and solvation.

330 Electrochemical Observation of Intermediates during the Formation of Conducting Polypyrrole: *D. J. Harrison* and *D. E. Raymond,* Dept. of Chemistry, University of Alberta, Edmonton Alta., Canada T6G 2G2

Conducting polypyrrole is formed by electrochemical oxidation of pyrrole, leading to growth of a film on the electrode surface. Electrochemical characterization of the polymerization process is severely hampered by the electrochemistry of this film. Using the rotating ring disk electrode we have observed intermediates formed during the polymerization. The product bipyrrole is clearly observed, and evidence suggests the radical cation can also be observed. By following these species during polymerization, it is possible to gain insight into the effect of solution conditions on the films formed.

331 Electrochemical Quartz Crystal Microbalance Studies of Electroactive Polymer Bilayers: *A. R. Hillman* and *A. Glidle,* School of Chemistry, Bristol University, Bristol, England BS8 1TS

The electrochemical quartz crystal microbalance has been used to study ion motion accompanying charge trapping and untrapping at poly(bithiophene)/poly(xylylviologen) bilayers. On the time scale of slow scan cyclic voltammetry, anion ejection is the primary mobile species transfer accompanying the injection of electronic charge. Relatively little inner layer reduction is required to mediate charge transfer to the outer layer. A similar conclusion is reached for re-oxidation of the bilayer. Charge is primarily removed from (and anions enter) the outer layer before the inner layer.

332 Modeling of the $GaInP_2$/Aqueous Electrolyte Interface Utilizing Electrochemical Impedance Spectroscopy: *S. S.Kocha* and *B. E. Liebert,* Materials Research Laboratories, Dept. of Mechanical Engineering, University of Hawaii, Honolulu, HI 96822

The $GaInP_2$/aqueous electrolyte interface was investigated utilizing electrochemical impedance spectroscopy. The interface was modeled in terms of two time constants: one for the space charge layer and the other for an oxide film. The conduction bandedge was found to be 400-500 meV negative to the hydrogen redox level. The valence bandedge was either slightly negative or very close to the oxygen redox level. The flatband potential was found to vary by 60 mV/pH.

333 The Effect of Preparation Conditions on the Ion Diffusion and Electrochromic Properties of Li_xWO_3: *J.-G. Zhang, C. E. Tracy,* and *D. K. Benson,* National Renewable Energy Laboratory, Golden, CO 80401

Porous films of WO_3 were prepared by vacuum thermal evaporation in different partial pressures of air and H_2O. Their electrochemical potentials (emf), Li^+ ion diffusion coefficients (D) and changes in optical densities ($\Delta O.D.$) were measured as functions of porosity and lithium insertion concentration (x in Li_xWO_3). D increases with porosity and follows a $1/x^2$ relationship for $x < 0.035$. An enhanced diffusion rate is observed at values of x around 0.1, shifting to lower values of x in the more porous films.

334 Electrode Surface Modification with ZnO and ZnO-CdS Semiconductor Colloidal Particles: *P. V. Kamat,* Radiation Laboratory, University of Notre Dame, Notre Dame, IN 46556, *S. Hotchandani,* Centre de Recherche en Photobiophysique, Université du Québec à Trois Rivières, Trois-Rivières, Qué., Canada G9A 5H7

The surface modification of an optically transparent electrode has been carried out with colloidal particles of ZnO and CdS. The particulate films of ZnO and ZnO-CdS exhibit excellent photoelectrochemical properties with an incident photon to current conversion efficiency of ~15% at 320 and 400 nm, respectively. The chlorophyll-*a* electrodeposited on these modified electrode surfaces is capable of injecting electrons from its excited sate into the conduction band of the semiconductor. Photochemical and photoelectrochemical properties of these modified surfaces have been elucidated.

STABILITY OF REFRACTORY MATERIALS

High Temperature Materials

335 The Performance of W Single Crystal Faceted Coating Surface Having (110) Preference Orientation of TEC Cylindrical Electrodes: *R. V. Sarvov, A. V. Vizgalov, V. I. Yarygin,* and *Z. B. Skrebova,* Institute of Physics and Power Engineering, Obninsk, USSR

The investigation of crystallographic orientation and electron work function distribution of W crystal faceted coating deposited by special CVD technology on TEC cylindrical emitter was carried out by HRTCS, RFM, and AES methods. It was found that facet plane orientation is close to (110) direction. As a result, work function distribution is smoother and average work function is close to highest possible value for W(110) $\phi \sim 5.35$ eV. The investigation of the coating after 6460 h TEC test demonstrates its high stability.

336 Ionic Conductivity and Phase Transformation in Gd_2O_3-Stabilized Bi_2O_3: *P. Su* and *A. V. Virkar,* Dept. of Materials Science and Engineering, University of Utah, Salt Lake City, UT 84112

Samples containing 14 m/o Gd_2O_3 and 86 m/o Bi_2O_3 were annealed at many temperatures for several days. During isothermal anneal, ionic conductivity exhibited four regimes which were interpreted in terms of the volume fractions of the cubic and rhombohedral phases.Kinetics of phase transformation were investigated using conductivity measurements, x-ray diffraction, and optical microscopy.

337 Platinum-Tungsten and Rhodium-Tungsten Alloys for AMTEC Electrodes: *M. A. Ryan, R. M. Williams, B. Jeffries-Nakamura, M. L. Underwood,* and *D. O'Connor,* Jet Propulsion Laboratory, Pasadena, CA 91109

Two alloys for electrodes for the alkali metal thermal to electroc converter (AMTEC), platinum-tungsten and rhodium-tungsten, are discussed. Both alloys have been operated as electrodes in AMTEC cells or under simulated AMTEC conditions for several hundred hours, and lifetimes for these electrodes are projected to be tens of thousands of hours. Compositions of PtW ranging from Pt_2W to Pt_5W have been tested to find the optimum Pt/W ratio. Sodium transport through the electrode and its effect on electrode performance is discussed.

338 The High Temperature Work Function of Sintered Dilute Solution Tungsten, Iridium Alloys: *L. A. D'Cruz, D. R. Bosch,* and *D. L. Jacobson,* Department of Chemical, Bio and Materials Engineering, Arizona State University, Tempe, AZ 85287-6006

In this study, iridium-added tungsten powder mixtures were cold-compacted and sintered to produce a range of tungsten, iridium electrodes. An electron emission study was subsequently carried out in order to evaluate the work function behavior of the consolidated alloys. The work function was obtained by the thermionic method and was found to be temperature and composition dependent. SEM and EPMA was used to characterize the topography and composition near the surface of each tested alloy. SIMS (elemental images) and TEM of the surface regions were also carried out.

339 Dispersion Particle Strengthening in Tungsten at High Temperatures: *A. Luo* and *D. L. Jacobson,* Dept. of Chemical, Bio and Materials Engineering, Arizona State University, Tempe, AZ 85287-6006

The mechanical properties of tungsten and a W-3.6Re-0.26HfC alloy were determined from 1950 to 2980 K in a vacuum below 10^{-5} Pa. HfC particle strengthening was effective in a dilute tungsten-rhenium matrix to a temperature of approximately 2700 K. The addition of HfC to tungsten increased both the strain-hardening exponent and the temperature sensitivity of tungsten at high temperatures. An increase in the growth rate of HfC particles occurred at temperatures greater than 2450 K. The yield strength of W-3.6Re-0.26HfC, calculated based on the dislocation pinning and the particle statistical distribution, was in good agreement with the experimental data over the entire temperature range.

340 High Temperature Electron Emission and Vaporization of Tungsten-Iridium Alloys: *R. N. Wall,* IBM East Fishkill Facility, Hopewell Junction, New York 12533, *D. L. Jacobson* and *D. R. Bosch,* Dept. of Chemical, Bio and Materials Engineering, Arizona State University, Tempe, AZ 85287-6006

The effective work function of tungsten-iridium alloys was studied. The work function of W-1%Ir and W-3%Ir decreased substantially with increasing temperature, whereas, W-7%Ir showed a slight increase as the temperature was raised. The highest observed work function (5.11 eV) was obtained at low temperature (1900-2100 K) from the W-3%Ir sample. The decrease in the work function of W-1%Ir and W-3%Ir with increased temperature was attributed to depletion of surface iridium. The work functions obtained here by alloying small quantities of iridium in tungsten are among the highest of any conducting material.

SYNTHESIS AND PROCESSING FOR HIGH TEMPERATURE MATERIALS FOR THE YEAR 2000

High Temperature Materials/Dielectric Science and Technology

341 Materials Research in the U.S.: The Development of a National Agenda: *L. H. Schwartz,* Materials Science and Engineering Laboratory, National Institute of Standards and Technology, Gaithersburg, MD 20899

The comprehensive study on materials science and engineering (MS&E) published in 1989 by the National Research Council (NRC) set the stage for a National Agenda. What is the Federal response and how is it being orchestrated? This charge resides with

the Office of Science and Technology Policy (OSTP). Through its committee structure, OSTP is identifying policy issues, developing an inventory of government activities and recommending a Federal strategy and a R&D plan responsive to national needs. The plan, still in the evolutionary stage, focuses on advanced materials and materials processing and an increased interaction between government, universities, and industry.

342 Expanding Horizons for Chemical Vapor Deposition Synthesis: *K.E. Spear*, Materials Science and Engineering, The Pennsylvania State University, University Park, PA 16802

Extrapolations of trends in CVD history show that chemical vapor deposition (CVD) will play an expanded and critical role as a synthesis technique in the next century. New areas continue to be developed for utilizing CVD techniques for high temperature materials applications. Increasing technology requirements for high quality, reproducible coatings are driving research on the fundamentals of deposition processes. Thus, theoretical modeling of CVD systems will also become quite sophisticated in the next century.

343 Chemical Vapor Deposition Process Aspects for the year 2000: *J.-O. Carlsson*, Dept. of Chemistry, Uppsala University, S-751 21 Uppsala, Sweden

Chemical vapor deposition (CVD) plays an important role in science and technology today. There is an increased demand of tailor-made, well-defined, and high-purity materials. CVD, with its ability to produce films of uniform thickness and properties even on complicated shaped substrates, will play a key role in the development of the next generation of thin film materials. For the year 2000 the fundamental process related research and development has to focus on some important areas. Precursor design, a deeper knowledge of surface processes (including nucleation), and positioning of surface reactions or selective growth on unpatterned and patterned substrates are examples of such areas.

344 Computational Analysis of Fluid Flow and Chemical Kinetics in Chemical Vapor Deposition: *R. J. Kee, G. H. Evans*, and *M. E. Coltrin*, Sandia National Laboratories, Albuquerque, NM 87185

Chemical vapor deposition (CVD) processes involve the complex interaction of fluid-mechanical transport, molecular diffusive transport, gas-phase chemical reaction, and heterogeneous chemical reaction at the deposition surface. Computational simulation plays an important role in developing an understanding that facilitates optimal reactor design and operation. Drawing on work in silicon, silicon-nitride, gallium-arsenide, and diamond CVD, this paper uses specific examples to illustrate the application of modeling to practical reactor design and operation. The paper also discusses a new and general software capability that facilitates coupling of gas-phase chemistry and transport with heterogeneous chemistry at gas-surface interfaces.

345 Processing and Fabrication of Ceramic Composites in the 21st Century: *R. W. Rice*, W. R. Grace & Co.-Conn., Columbia, MD 21044

The methodologies of processing (*i.e.*, forming a solid piece of material) and fabrication (*i.e.*, achieving the size, shape, and dimensional accuracy of components) are reviewed. These include the array of powder-based processing and fabrication, polymer-based processes, and chemical vapor deposition, and coupling this with the introduction of the dispersed phase, including fiber handling. The needs and opportunities of these are assessed based on the properties, sizes, shapes, and costs achievable relative to expected application needs.

346 Chemical Vapor Infiltration: *T. M. Besmann, D. P. Stinton*, and *R. A. Lowden*, Oak Ridge National Laboratory, Oak Ridge, TN 37831

Continuous filament ceramic composites are enabling new, high temperature structural applications. Chemical vapor infiltration methods for producing these composites are being studied, with the complexity of filament weaves and deposition chemistry merged with standard heat and mass transport relationships. Silicon carbide-based materials are, by far, the most advanced, and are already being used in aerospace applications. This paper address is the state-of-the-art of the technology and outlines current issues.

347 High-Tech Fibers: *G. G. Tibbetts*, Physics Dept., General Motors Research Laboratories, Warren, MI 48090-9055

Modern, high-tech fibers offer the materials engineer a broad choice of properties for ceramic composites. Fibers may be variously produced by spinning a precursor polymer into a thread, melt spinning, whisker growth in the gas phase, vapor deposition on a pre-existing fiber, or sol-gel processing. Properties of some fibers useful for ceramic reinforcement are compared, and some of the complications of engineering a fiber-matrix system are aired.

348 Processing of Advanced Ceramic Materials: Need for Short-Range Interparticle Potentials: *F. F. Lange*, Materials Dept., University of California, Santa Barbara, Santa Barbara, CA 93106

Interparticle potentials play a dominate role in governing the slurry viscosity, maximum particle packing density, and the rheology of the consolidated body. These roles are reviewed with the objective of understanding how damage-free bodies can be consolidated from slurries to increase the structural reliability of ceramics and their composites. Recent results have shown that short-range (<4 nm) repulsive potentials that produce an attractive, but nontouching, particle network are most remarkable and desirable for developing new shaping methods for advanced ceramic systems.

349 Synthesis and Processing of Nanostructured Materials: *H. Hahn*, Dept. of Materials Science and Engineering, Rutgers University, Piscataway, NJ 08855

Nanostructured materials are synthetic metastable materials with ultrafine microstructures, typical less than 100 nm. It has been demonstrated that these materials have interesting properties such as sintering and superplastic deformation at low temperatures in nanostructured ceramics and high hardness, ductility and fracture strength in nanostructured ceramic-metal composites. Expectations are that these novel properties will lead to technological applications. A wide variety of techniques such as MBE, CVD, spray conversion, hydrolysis, laser pyrolysis, mechanical attrition, sol-gel and gas condensation has been used to synthesize nanostructured materials. The paper presents the various techniques and discusses their advantages and limitations for basic research and potential technological applications.

350 Microwave Processing of Ceramics: Promises and Challenges: *D. L. Johnson*, Dept. of Materials Science and Engineering, Northwestern University, Evanston, IL 60208-3108

The hope of high speed processing, uniform heating, energy efficiency, and precise control of heat application has spurred a recent flurry of activity in attempts to exploit microwave heating for the processing of ceramics. Significant reductions in sintering temperature have been reported. However, difficulties with microwave heating arise from the nature of the interaction of microwave energy with materials. Low loss materials are difficult to heat, and heating, once begun, can be difficult to control.

351 Microwave Surface Modifiction and Sintering: *D. E. Clark, Z. Fathi*, and *D. Folz*, Dept. of Materials Science and Engineering, University of Florida, Gainesville, FL 32611

We have processed technically important ceramics and glasses in both microwave and conventional ovens. Comparison of microstructures, hardness, and toughness of alumina samples sintered by the two methods indicate that microwave processing offers distinct advantages; more uniformity is obtained in the microwave processed samples. Surface modification of glasses and ceramics have been achieved using microwave energy. Soda-alumina-silicate glasses have been treated in a molten KNO_3 solution. A greater degree of control over the surface chemistry and depth of surface modification can be achieved in the microwave oven. A K penetration depth of 100 μm requires only 30 min as opposed to many hours using the conventional method.

352 Mathematical Modeling Issues in Plasma Synthesis: *J. Szekely*, Massachusetts Institute of Technology, Cambridge, MA 02139

Plasma systems may provide an ideal vehicle for the synthesis of fine ceramic and metallic powders because of the high temperatures and the controllable exposure times. A critical issue in the operation of these systems is to control the transport phenomena, that is the intermixing of the reactants, and if necessary, the efficient quenching of the product. We review the progress made in the modeling of these systems and address the problems that still need attention.

353 Thermal Plasma Synthesis of Fine Powders: *E. Pfender*, Dept. of Mechanical Engineering, University of Minnesota, Minneapolis, MN 55455 and *P. Kong*, INEL, EG&G Inc., IRC, Idaho Falls, ID 83415

Thermal plasmas suitable for the synthesis of fine powders are primarily produced by means of high intensity arcs or by high frequency discharges. Synthesis of fine powders in such plasmas may proceed from gaseous, liquid, or solid precursors resulting in powders of a wide array of high temperature materials, including carbides, refractory oxides, nitrides, borides, and oxide superconductors. In this paper recent advances in thermal plasma synthesis of fine powders are summarized with emphasis on novel plasma reactor designs.

354 Plasma Sintering of Ceramics: *D. L. Johnson*, Dept. of Materials Science and Engineering, Northwestern University, Evanston, IL 60208-3108

Several ceramic materials have been successfully sintered in plasmas generated by various means. Generally, plasma sintering results in enhanced densification rates, finer grain size, and greater strength than for materials sintered conventionally at the same temperatures. Recent parallel experiments in which alumina specimens were heated conventionally or in a plasma over identical temperature excursions have indicated significant enhancement of the grain boundary diffusion coefficient, probably through enhanced aluminum interstitial concentration in the plasma heated specimens.

HIGH TEMPERATURE SENSORS

High Temperature Materials/Sensor/Battery

355 Sensor Applications of Oxygen Pumping with ZrO_2 Electrochemical Cells: *E. M. Logothetis,* J. H. Visser, R. E. Soltis,* and *L. Rimai,* Ford Motor Co., Physics Dept., Dearborn, MI 48121-2053

Oxygen sensors based on ZrO_2 electrochemical cells have found extensive use in many applications. The most sensitive of these sensors employ the oxygen pumping principle with ZrO_2 cells. Oxygen pumping, however, can also be used to generate other chemical and also physical sensors. This paper discusses several of these sensors, *e.g.*, sensors for measuring CO, H_2, H_2O, hydrocarbons, gas flow, and gas pressure, and presents results of studies of the properties of some of these devices.

356 Kinetics of the Electrode Reaction at the H_2-H_2O, Porous Pt/Stabilized Zirconia Interface: *J. Mizusaki* and *H. Tagawa,* Institute of Environmental Science and Technology, Yokohama National University, 156 Tokiwadai, Hodogaya-ku, Yokohama 240, Japan, *K. Isobe, M. Tajika, I. Koshiro, H. Maruyama,* and *K. Hirano,* Shibaura Institute of Technology, Shibaura, Minato-ku, Tokyo 108, Japan

Steady-state and ac impedance measurements were made on the electrode reaction at the H_2-H_2O, porous Pt/YSZ interface as functions of H_2 and H_2O partial pressures and temperature. The reaction rate was compared with that under CO-CO_2 and O_2 gas and the possible reaction kinetics at the triple phase boundary of gas/Pt/YSZ are discussed. It is shown that the reaction rate in the H_2-H_2O gas is about 10^2 times larger than that in CO-CO_2.

357 Mixed Potential Gas Sensors: *P. T. Moseley** and *R. Peat,* AEA Industrial Technology, Harwell Laboratory, Didcot, Oxon, England OX11 0RA

Potentiometric gas sensors, in which identical electrodes are brought into equilibrium with a major constituent of separated test and reference atmospheres, have been known since the pioneering work of Nernst at the turn of the century. In recent years an alternative configuration for potentiometric sensors, in which there is no separation of atmospheres, has been explored. In this instance the measured potential of the device arises from the distinct interactions of a minority component of the atmosphere with the two different materials which comprise the electrodes. The range of applications of this configuration, both at ambient and at elevated temperatures, is reviewed.

358 New Ideas, How to Use Mixed Ionic Electronic Conductors, Instead of Solid Electrolytes, in Potentiometric Sensors: *I. Riess,* Physics Dept., Technion-IIT, Haifa 32000, Israel

A new method is suggested for determining chemical potentials by potentiometric measurements. It allows the use of mixed ionic electronic conductors, MIECs, instead of solid electrolytes, SEs. The galvanic cell includes the sample, a reference electrode, two MIECs, a power supply, and two voltmeters. The procedure of measurement is different from the usual potentiometric one. The possibility to replace SEs by MIECs should extend the range of application of the potentiometric method.

359 A Study on Properties of Electrode Materials for Oxygen Sensors: *H. Arai, K. Eguchi,* and *T. Inoue,* Dept. of Materials Science and Technology, Kyushu, University, 6-1 Kasugakoen Kasuga-shi, Fukuoka 816, Japan

The lowest limit of operation temperature from the oxide solid electrolyte oxygen sensors was effected by the electrode materials. The sensor with perovskite-type oxide electrode exhibited theoretical electromotive force at lower temperature than those with Pt electrodes. In particular, the sensor with $La_{0.6}Sr_{0.4}Co_{0.98}Ni_{0.02}O_3$ attained theoretical electromotive force even at 200°C. The electrode materials operative at low temperatures tend to have large electrode conductivity and oxygen isotopic exchange reaction rate.

360 Novel Solid Electrolyte CO_2 Sensor Using Sodium Ion Conductor and Lithium-Based Carbonate Electrode: *N. Yamazoe, S. Yao, Y. Shimizu,* and *N. Miura,* Dept. of Material Science and Technology, Kyushu University, Kasuga-shi, Fukuoka 816, Japan

An electrochemical cell combining an Na^+ conductor and an Li-based binary carbonate auxiliary electrode (Li_2CO_3-MCO_3 (M = Ca, Ba) showed excellent performance in CO_2 sensing. Its responses to CO_2 followed a Nernst equation over a broad dynamic range of 10^2-10^5 ppm CO_2 even under humid condition. The Nernst's slope coincided with a 2-electron reaction of CO_2. On the other hand, the responses were almost independent of PO_2 at higher temperatures above 450°C, while at 305°C and below the responses depended on PO_2 in coincidence with a 2-electron reaction of O_2.

361 Development of Solid-State Electrochemical Sensors Measurement of Elements in Molten Metals: *R. V. Kumar* and *D. J. Fray,* Dept. of Mining and Mineral Engineering, University of Leeds, Leeds, England LS2 9JT

The industrial applications of solid-state electrochemical sensors for measurement of elements in molten metals have mainly been confined to those species which are ionically transferred in the solid electrolyte. It has been possible to extend the range of elements by the use of auxiliary phases such that there is a chemical coupling between the element being measured and the element ionically mobile in the electrolyte. Devices for sensing phosphorus, silicon, and sulfur have been developed and their applications in metal refining are presented.

362 Miniaturization of a High Temperature Oxygen Sensor Employing Film Electrolyte and Electrodes: *E. B. Makovos, F. W. Montague, M. A. Stuczynski,* and *C. C. Liu,* Electronics Design Center, Case Western Reserve University, Cleveland, OH 44106

High degree of miniaturization in actively operated oxygen sensors may be achieved with a substitution of thin films for all of their components. A viable sensor has been constructed by using ion beam deposited ceramic electrolyte and platinum electrodes on a silicon substrate insulated by SiO_2. Thin film electrolyte of sufficient conductivity has been formed from a yttria-doped zirconia source in an oxygen-containing atmosphere. Continuous operation of up to 2 weeks at 1200 K is possible.

363 Humidity Sensor for High Temperature Usng a Limiting Current Type Plane Oxygen Sensor: *H. Yagi,* Research and Development Center, NGK Spark Plug Co., Ltd., 2808, Iwasaki, Komaki-shi, Aichi, Japan

A limiting current type plane oxygen sensor with a unique structure has been developed. This sensor has cathode and anode of Pt on the same plane of ZrO_2 electrolyte, and the cathode also serves as a hole to limit gas diffusion. It detects humidity linearally proportional to a water vapor pressure of 0-500 mm Hg in a wide operation temperature range from 20 to 300°C. No deterioration was observed after 10,000 h life test.

364 The Relationship Between Microstructure and Properties of Native Insulators Used in High Temperature-Thin Film Sensor Applications: *A. S. Lawing* and *O. J. Gregory,* Dept. of Chemical and Materials Engineering, University of Rhode Island, Kingston, RI 02881, *S. Mina,* Allied Signal Aerospace Co. Garrett Engine Div., Phoenix, AZ 85010

High temperature-thin film sensors are currently being investigated for temperature and strain measurements on gas turbine engine components. The electrical properties of the native insulating layer formed on the surfaces of these components is critical to device performance. The relationship between the microstructure and electrical properties of the native oxide layers was investigated. The formation of a high quality dielectric was achieved by minimizing the degree of internal oxidation within the bond coat layer and maximizing external oxide scale growth.

365 A Novel Polymer Blend for Solid-State Ammonia Sensor: *R. D. A. Paulmer, R. S. Srinivasa,* and *A. R. Kulkarni,* Materials Science Centre, Indian Institute of Technology, Powai, Bombay-400076, India

A new polymer electrolyte with three orders of magnitude higher sodium ion conductivity at room temperature, than the hitherto reported polymer based electrolytes is presented here. The electrolyte comprises of poly(propylene glycol), (PPG), poly(ethylene oxide), (PEO), and NaI. The films were obtained by conventional solvent casting technique. The material was found to be completely amorphous. This has been confirmed by XRD studies and supplemented by DSC. The blend was found to be a sodium ion conductor. The effect of concentration of PPG and varying sodium ion concentration (different O/Na ratios) on ionic conductivity in the blends were studied. An optimized concentration of PPG, and O/Na ratio gave a maximum conductivity of 6.0×10^{-4} $(\Omega\ cm)^{-1}$ at room temperature. This blend is completely amorphous. Studies on ionic conductivity varying the partial pressure of ammonia show that conductivity has a logarithmic relationship with partial pressure of ammonia. The effect of compositional changes and various temperature on change in ionic conductivity at various partial pressure of ammonia are presented. The results suggest the applicability of polymer electrolyte as solid-state ammonia sensor.

ELECTROCHEMISTRY IN MINERAL AND METAL PROCESSING III

Industrial Electrolysis and Electrochemical Engineering

366 Requirements for Industrial Collectorless Flotation: *N. Arbiter,* Nathaniel Arbiter Associates, Inc., Vail, AZ 85641, *J. E. Gebhardt,* Control International, Inc., Salt Lake City, UT 84108

Many sulfide minerals can be floated without collector in controlled laboratory chemical-electrochemical environments. Whether collectorless sulfide mineral flotation is commercially feasible and under what conditions are critically examined. Since molybdenite floats with frother and hydrocarbon and laboratory collectorless flotation of chalcopyrite is relatively simple, a favorable example for collectorless flotation should be chalcopyrite ores containing byproduct molybdenite. Actually, the need to consider ore geology and to control water quality and redox environments during grinding, conditioning, and flotation make commercial-scale collectorless flotation difficult, if not impossible.

367 Surface Electron Structures of Galena and Pyrite Related to Collectorless Flotation: *S. Sun, D. Wang,* and *B. Li,* Dept. of Mineral Engineering, Central South University of Technology, Changsha, Hunan, 410083, China

The electron energy level of galena surface is higher, which determines that the addition of sodium sulfide obviously reduces the platinum electrode potential of galena and depresses the collectorless flotation of galena pulp. On the other hand, pyrite surface has a lower electron energy level. It electrochemically catalyzes the oxidation of HS^- ion to neutral sulfur. The presence of Na_2S improves the collectorless flotation of pyrite. The collectorless flotation separation of galena from pyrite is possible using Na_2S as modifier.

368 Electrochemical Aspects of Cast Iron Grinding Media Wear and Its Effect on Flotation: *I. Iwasaki** (Present address: Central Research Institute, Mitsubishi Materials Corp., 1-297 Kitaburocho, Omiya, Saitama 330, Japan) and *V. Rajagopal*, Dept. of Civil and Mineral Engineering, University of Minnesota, Minneapolis, MN 55455-0220

The electrochemical and wear behavior of a series of chromium-containing cast iron balls with Cr contents ranging from 0 to 29% were investigated with regard to their abrasion and corrosion properties as well as their effects on the flotation behavior of pyrrhotite. The matrix Cr contents were related to the general and/or pitting corrosion behavior of ball materials under abrasive and static conditions. The passivation behavior of ball materials was in direct correlation with the flotabilities of pyrrhotite ground under a nitrogen or oxygen atmosphere.

369 An Electrochemical Study of Sulfide Mineral-Grinding Medium Contact and Its Relevance to Flotation: *X. Li*,* Allied-Signal Inc., Morristown, NJ 07962, *I. Iwasaki*, Central Research Institute, Mitsubishi Materials Corp., 1-297 Kitaburocho, Omiya, Saitama 330, Japan

A cathodic decomposition model for chalcopyrite in a neutral pH solution, simulating the conditions in wet grinding mills, is proposed through open-circuit potential and combination potential measurements, linear potential sweep technique, chronoamperometry and chronocoulometry, and surface analysis methods. Chalcopyrite contacted with steel grinding media undergoes a reduction reaction and the mineral surface becomes covered with a layer consisting of $Fe(OH)_2$ and Cu_2S. The $Fe(OH)_2$ layer adversely affects the flotability of chalcopyrite. The role that oxygen plays in the collectorless flotation of cathodically polarized chalcopyrite is discussed.

370 Mechanism of Thionocarbamate Interaction in Flotation Systems: *R. H. Yoon* and *C. I. Basilio*, Virginia Center for Coal and Minerals Processing, Virginia Polytechnic Institute and State University, Blacksburg, Virginia 24061-0258

The adsorption mechanism of thionocarbamate interaction in flotation systems has been investigated. Voltammetry suggests that the adsorption of thionocarbamate is probably a result of a coupled reaction of the EC-type, involving an initial electron transfer step (E), followed by a chemical reaction (C). Thus, the adsorption is controlled by both the E_h and pK of the system. *In situ* FTIR spectroscopy and contact angle measurements support the mechanism suggested for thionocarbamate interaction.

371 The Role of Pulp Redox Potentials and Modifiers in Complex Sulfide Flotation with Dithiophosphinates: *A. Gorken, D. R. Nagaraj*, and *P. J. Riccio*, American Cyanamid Co., Stamford, CT 06904

The effect of pulp redox potentials and pH on the flotation response of sulfides with dialkyl dithiophosphinate was investigated for several Cu/Pb/Zn ores in the presence of various modifiers. Flotation response of sulfides was found to be strongly dependent on pulp potential. Galena and chalcopyrite flotation was optimum in the range of -100 to +60 mV (Ag/AgCl ref.). The optimum in zinc and iron sulfides flotation occurred at slightly different potentials (under more reducing conditions, for example, for iron sulfides).

372 Mechanism of Sulfide Depression with Functionalized Synthetic Polymers: *D. R. Nagaraj*, American Cyanamid Co., Stamford, CT 06904, *C. S. Basilio* and *R. H. Yoon*, Dept. of Mining and Minerals Engineering, Virginia Polytechnic Institute, Blacksburg, VA 24061

Polymeric depressants can offer several advantages over the commonly used depressants in sulfide mineral flotation. Their use is, however, limited to polysaccharides for a few specific applications. Functionalized, synthetic polymers or modified natural products such as xanthates of polysaccharides have remained largely a laboratory curiosity. Several synthetic polymeric depressants have been developed recently by American Cyanamid. The mode of action of one such polymer containing a thiourea functionality in Cu-Mo separation, and the significant role of redox potentials (modified by NaHS) in achieving selectivity are discussed.

373 Interaction of Ethyl Xanthate with Silver and Silver/Gold Alloys: *R. Woods*,* CSIRO Div. of Mineral Products, Port Melbourne, Victoria 3207, Australia, *C. I. Basilio, D. S. Kim*, and *R. H. Yoon*, Virginia Center for Coal and Mineral Processing, Virginia Polytechnic Institute and State University, Blacksburg, VA 24061

The interaction of ethyl xanthate with silver and silver/gold alloys has been investigated by voltammetry, FTIR spectroscopy, UV/Vis spectroscopy, and measurements of contact angle. Chemisorption of xanthate occurs on the silver and alloy surfaces prior to silver xanthate formation and renders the surfaces hydrophobic. Coverage of chemisorbed xanthate was found to obey a Frumkin isotherm. Eh-pH diagrams have been constructed that include chemisorption in addition to silver xanthate and dixanthogen formation.

374 Interpretation of Electrode Responses with the Help of a Multivariate Technique: *B. I. Pålsson* and *E. Öberg*, Div. of Mineral Processing, Luleå University of Technology, S-951 87 Luleå, Sweden

Simultaneous laboratory measurements in flotation pulps with different electrodes under conditions of varying pulp chemistry are reported. It is found that the redox potential as measured with a glassy carbon electrode correlates better with the response of an oxygen probe, than the traditional Pt-foil redox electrode. The glassy carbon electrode also behaves in a way which averages the responses of mineral electrodes of pyrite, galena, and to some extent chalcopyrite.

375 Voltammetric Determination of Surface Species on Sulfide Minerals in Flotation Pulps: *L. Griffin* and *N. W. Johnson*, Mineral Processing Research, Mount Isa Mines Limited, Mount Isa, Queensland, Australia 4825, *D. F. A. Koch* and *Y. Ramprakash*, Dept. of Chemical Engineering, Monash University, Clayton, Victoria, Australia 3168, *R. Woods*, CSIRO Div. of Mineral Products, Port Melbourne, Victoria, Australia 3207

Voltammetry has been used to determine the products of interaction of sulfide minerals with iron(II), cyanide, sulfide, and xanthate ions in flotation pulps. A multilayer of sulfur was shown to form on pyrite and chalcopyrite when present in a flotation pulp containing cyanide and sulfide ions, but this resulted in a flotation recovery of these minerals of no more than 10%. The presence of a collector was necessary for efficient flotation in this system.

376 Pulp Chemistry in Pyrite Pre- and Reverse Flotation: *M. Xu* and *J. A. Finch*, Dept. of Mining and Metallurgical Engineering, McGill University, Montreal Que., Canada H3A 2A7

The McGill mobile pilot flotation facility, and the on-line system for measuring pH, DO, and Ep, is described. The effect of gas composition (O_2, N_2, and air), lime, SO_2, and temperature on the pulp chemistry was determined in pyrite pre- and reverse-flotation in a Zn flotation circuit. The interrelation between pH, DO, and Ep is examined. It is shown that pulp potential is correlated with metallurgical performance.

377 The Interaction of Ethyl Xanthate with Pyrite: *J. Ralston** and *D. Fornasiero*, School of Chemical Technology, University of South Australia, The Levels, S.A. 5095 Australia

The interaction of ethyl xanthate with pyrite is shown to be controlled by redox processes and surface chemistry. In the latter case the distribution of positive and negative surface sites permits both a kinetic description of the decomposition of ethyl xanthate as a function of pH to be obtained, as well as a quantitative explanation of the pH dependence of pyrite flotation. This behavior has hitherto eluded an oveall quantitative interpretation.

378 The Effect of EDTA on Collectorless Flotation of Pyrite: *S. Chander* and *J. Pang*, Mineral Processing Section, Pennsylvania State University, University Park, PA 16802

It is generally recognized that flotation of pyrite can be modulated by adding chelating agents, but the mechanism is not fully understood. To determine the flotation mechanism, several electrochemical and wetting studies were made in the pyrite-ethylenediamine tetraacetic acid (EDTA) system. The results show that EDTA interacts with pyrite surface through several reactions involving dissolution, complexation, and adsorption. The flotation response depends on the extent of these reactions which is a function of the reagent concentration and the rate and severity of pyrite oxidation.

379 An Electrochemical Study of Selective Deactivation/Depression of Cu(II)-Activated Pyrite and Arsenopyrite: *X.-H. Wang* and *C.-L. Jiang*, Dept. of Mining Engineering, University of Kentucky, Lexington, KY 40506, *D. Z. Xuan*, Beijing General Research Institute of Mining and Metallurgy, Beijing, China, *E. Forssberg*, Div. of Mineral Processing, Lulea University of Technology, S-951 87 Lule, Sweden

Two new effective methods were developed for selective separation of pyrite from arsenopyrite. Pyrite and arsenopyrite, when activated with Cu(II) ions, exhibit similar floatability in alkaline solutions when xanthates are used as collectors. The first separation method involves selective deactivation of pyrite. When the flotation pulp containing pyrite and arsenopyrite which were activated with Cu(II) ions at pH = 11 is acidified to pH around 6, selective deactivation of pyrite takes place, while no effect exerts on the arsenopyrite. In the second method, alkali-earth metal ions were used to selectively depress Cu(II)-activated arsenopyrite. In the presence of Sr^{2+} and Ba^{2+}, arsenopyrite is completely depressed at pH above 8.5, while the flotability of pyrite remains unaffected. The principles involved in the processes were studied using electrochemical techniques and ESCA surface analysis.

380 Surface Layer Structure of Sulfide Mineral Treated in Thiol Collector Solutions: *E. Suoninen** and *K. Laajalehto*, University of Turku, Laboratory of Materials Science, Itäinen Pitkäkatu 1, SF-20520 Turku, Finland, *S. Heimala*, Outokumpu Research Oy, SF-208101 Pori, Finland

By employing a method designed to preserve volatile components of the surface adsorption layer prepared in aqueous solution, existence of ethyl dixanthogen has been concluded from XPS measurements of pyrite surfaces treated in potassium ethyl xanthate solution within a certain range of combinations of pH and E_h. Voltammetric measurements of similar samples are in agreement with the XPS results. Flotation tests indicate increase of surface hydrophobicity due to presence of dixanthogen in the adsorption layer.

381 The Interaction of *Diethyl Dithiophosphate* with Freshly Exposed Galena and Chalcocite Surfaces: *A. N. Buckley*, CSIRO Div. of Coal and Energy Technology, North Ryde, NSW 2113, Australia, *R. Woods*, CSIRO Div. of Mineral Products, Port Melbourne, Victoria 3207, Australia

Interaction of diethyl dithiophosphate (DTP) with galena at pH 5 and chalcocite at pH 9 has been investigated by electrochemical and electron spectroscopic techniques. Adsorption of DTP on galena was very slow. The S(2p) binding energy of a submonolayer was less than that expected for $Pb(DTP)_2$. Adsorption was rapid on chalcocite, with chemisorption preceding multilayer CuDTP formation. The Cu(*LMM*) Auger spectrum when only the monolayer was present was similar to that for chalcocite and different from that for multilayers.

382 Electrochemical AC Impedance and X-ray Photoelectron Spectroscopic Studies of Interaction of Phenyl Thiourea with Coal Pyrite Surface: *S. U. M. Khan* and *T. J. Farley*, Dept. of Chemistry, Duquesne University, Pittsburgh, PA 15282, *J. P. Bultrus*, US Dept. of Energy, Pittsburgh Energy Technology Center, Pittsburgh, PA 15236

Phenyl thiourea was found to behave as a better flotation agent compared to ethyl xanthate for coal pyrite and the percentage of flotation recovery was found potential dependent. AC impedance data also indicate potential dependent adsorption of phenyl thiourea. XPS results of N 1s and S 2p spectra clearly indicate the adsorption of phenyl thiourea on the coal pyrite surface and increased adsorption under potential control. These results suggest that the chemisorption of PTU renders the pyrite surface highly hydrophobic under applied potential to attain the highest degree of pyrite floatability.

383 XPS Study of the Butyl Xanthate Adsorption on the Galena Surface: *A. V. Shchukarev*, *G. N. Mashevsky*, and *T. O. Nechiporenko*, Research Analytical Complex "MEKHANOBR-ANALYT," St.-Peterburg, USSR 199026

Adsorption of butyl xanthate on the surface of *galena* (powder of flotation size 45-60 mkm) and chemical nature of species forming under different pH and xanthate concentration were studied by means of XPS. The main products of flotoreagent interaction with lead hydroxide layer on the galena are PbS, PbOHBuX, and $Pb(BuX)_2$. The forming of individual compounds depends on xanthate concentration and pH of pulp. In dilute solutions (10^{-3} M) the collector acts to a great extent like sulfidizator, giving PbS, for 10^{-1}-10^{-2} M concentrations main product of $Pb(BuX)_2$. PbOHBuX formation is preferable under more basic pH. Maximal xanthate adsorption was found under pH = 10.5.

384 Photoelectrochemical Behavior of Chalcopyrite ($CuFeS_2$) in Alkaline Solutions: *G. H. Kelsall*, Dept. of Mineral Resources Engineering, Imperial College, London, England SWZ 2BP, *F. W. H. Dean*, Dept. of Mining and Mineral Engineering, University of Leeds, Leeds, England LS2 9JT

The oxidation of chalcopyrite ($CuFeS_2$), the principal mineral source of copper, has been studied in aqueous borate electrolytes (pH 9.2) using photocurrent voltammetry and spectroscopy. In the potential range -0.2 to +0.4 V *vs.* SCE, $Fe_2O_3/Fe(OH)_3$ was formed producing photo-anodic currents, but leaving the copper and sulfur as $CuFe_{1-x}S_2/CuS_2$* in the chalcopyrite lattice. At >0.4 V *vs.* SCE, the iron-depleted film decomposed, greatly enhancing the chalcopyrite decomposition rate and forming $CuO/Cu(OH)_2$, which on reduction during a subsequent negative-going potential sweep, produced photo-cathodic currents.

385 Electrochemical Oxidation of Chalcopyrite ($CuFeS_2$) in Alkaline Solutions: *G. H. Kelsall*, Dept. of Mineral Resources Engineering, Imperial College, London, England SW7 2BP, *K. E. R. England*, *D. J. Vaughan*, and *Q. Yin*, Dept. of Geology, University of Manchester, Manchester, England M13 9PL

The mechanism and products of the oxidation of chalcopyrite ($CuFeS_2$), the principal mineral source of copper, have been studied in alkaline electrolytes (pH 9.2 and 12.7) using cyclic and potential step voltammetry, with subsequent surface analysis by x-ray photoelectron spectroscopy (XPS) and Auger electron spectroscopy (AES). At pH 9.2 and potentials <0.4 V *vs.* SCE, $Fe_2O_3/Fe(OH)_3$ was formed, leaving the copper and sulfur as CuS_2* in the chalcopyrite lattice, which remained in tact. No evidence was found for $CuFe_2O_4$. At >0.4 V *vs.* SCE, the CuS_2* film decomposed, forming $CuO/Cu(OH)_2$ and greatly enhancing the underlying chalcopyrite decomposition rate.

386 The Photoelectrochemistry of *In Situ* Fractured Pyrite Electrodes: *P. E. Richardson*, *Y. Li*, and *R.-H. Yoon*, Dept. of Mining and Minerals Engineering, Virginia Polytechnic Institute and State University, Blacksburg, VA 24061-0258

The oxidation of *in situ* fractured natural mineral pyrite electrodes has been studied using electrochemical and photoelectrochemical techniques. No photocurrent (PC) is observable on freshly fractured pyrite under steady illumination. However, with chopped illumination, an anodic PC is observed over the range of approximately -1.0 to 0.2 V, SCE at pH 9.2. The structural features of the PC as a function of electrode response reflect oxidation and reduction processs occurring on the electrodes. At cleavage, a spontaneous PC is observed, suggesting instantaneous upward band bending, probably due to fast intrinsic surface states.

387 Interfacial Electrochemistry of Semiconductor Pyrite: *K. K. Mishra*, MEMC Electronic Materials Inc., St. Peters, MO 63376, *K. Osseo-Asare*, Dept. of Materials Science and Engineering, Pennsylvania State University, University Park, PA 16802

Pyrite (FeS_2)/electrolyte interactions have been studied using both natural and synthetic pyrite samples and electrochemical, photoelectrochemical, and surface analysis techniques. Charge transfer studies across the pyrite/electrolyte junction were conducted in the presence of I^-, Br^-, $Fe(CN)_6^{4-}$, and Cl^- in an aqueous solvent, and in the presence of ferrocene and TMPD in a nonaqueous solvent system. The electrochemical behavior of pyrite is compared and contrasted with that of noble metals and other semiconductors. Finally, oxidation of pyrite is discussed in the light of these results.

388 Electrochemical Studies of Iron Sulfides in Relation to Their Atmospheric Oxidation and Prevention of Acid Drainage; Part II: *S. M. Ahmed* and *E. Giziewicz*, Canada Center for Mineral and Energy Technology, Mineral Sciences Laboratories, Ottawa, Ont., Canada K1A 0G1

Oxygen reduction on pyrite (FeS_2) and pyrrhotite (FeS) and related redox reactions have been studied using RDE and RRDE. The mechanism of charge transfer in the oxidation and dissolution of pyrite has been examined in light of the energy level diagrams and the semiconducting nature of FeS_2. The problem of the "acid mine drainage" resulting from the atmospheric oxidation of the iron sulfides has also been examined. Methods of preventing the AMD by cathodic protection and by growing passive, iron oxide films on FeS_2 and FeS (on electrodes only) have been developed.

389 Transpassive Oxidation of Pyrite: *X. Zhu*, *J. Li*, *D. M. Bodily*, and *M. E. Wadsworth*, Dept. of Metallurgical Engineering, University of Utah, Salt Lake City, UT 84112

The electrochemical behavior of mineral and coal pyrites in basic solutions was investigated using cyclic voltammetry. Emphasis was centered on transpassive oxidation, where aggressive oxidation of pyrite occurred just prior to oxygen evolution. The reaction products in this region were Fe(III) oxides and partially oxidized sulfur intermediates and sulfate ion. The Fe(III) oxides and sulfur intermediates were identified indirectly by ferrous hydroxide and ferrous sulfide formation during cathodic/anodic scan reversal, and directly by Raman spectroscopy and electron microprobe analyses.

390 Comparative Studies of Surface Properties of Pyrite from Coal and Ore Sources: *X.-H. Wang*, *C. L. Jiang*, *A. M. Raichur*, and *J. W. Leonard*, Dept. of Mining Engineering, University of Kentucky, Lexington, KY 40506, *B. K. Parekh*, Center for Applied Energy Research, University of Kentucky, Lexington, KY 40511

The electrochemical reactivity and surface properties of pyrite from coal and ore sources were investigated. The electrochemical studies indicate that an oxidation layer is rapidly formed on the pyrite surfaces even when the electrode is polished under nitrogen and with deoxygenated water. The initial process of pyrite surface oxidation is controlled by the adsorption and discharge of hydroxide ions/water molecules, independent of the solution pH, source and semiconducting properties. The results obtained from film/micro flotation and contact angle titration studies show that pyrites from different sources exhibit similar surface hydrophobicity, though the thickness of the surface oxidation layers may be different. The results are compared with surface studies by SEM to elucidate the pyrite surface oxidation mechanisms.

391 Electrochemical Kinetics of Silver Dissolution in Cyanide Solutions: *J. Li* and *M. E. Wadsworth*, Dept. of Metallurgical Engineering, University of Utah, Salt Lake City, Utah 84112

The electrochemical kinetics for anodic dissolution of silver in cyanide solutions were measured using interval potentiodynamic scanning, cyclic voltammetry, potentiostatic scanning, and impedance techniques. Coupled charge transfer, plus boundary diffusion of cyanide ions from the bulk solution to the silver surface, were found to be rate limiting. Experimental results were well correlated by kinetic expressions derived using Butler-Volmer and Levich equations. The activation energy for the charge transfer process and the coefficient for cyanide diffusion were determined. The model derived for the anodic dissolution of silver was in accord with results obtained from separate impedance measurements.

392 Thermodynamic Equilibrium Calculations on Au/Ag-Lixiviant Systems Relevant to Gold Extraction from Complex Ores: *X.-H. Wang*, Dept. of Mining Engineering, University of Kentucky, Lexington, KY 40506

Thermodynamic equilibrium calculations were performed on Au/Ag-Lixiviant systems to study the feasibility of extracting gold from complex ores using noncyanide lixiviants. A number of potential lixiviants, including chloride, bromide, iodide, thiourea, ammonia, thiosulfate, and their combinations were compared with cyanide. The results demonstrate that all these lixiviants can dissolve gold and form gold-lixiviant complexes. However, the halogen lixiviants (Cl^-, Br^-, and I^-) need much higher oxidation potential and acidic pH to dissolve gold than cyanide did. Gold and silver dissolve in thiosulfate and ammonia, as well as thiosulfate-ammonia mixture solutions, under conditions comparable to cyanide, indicating these two chemicals can be effective lixiviants for gold extraction. The electrochemical studies with gold electrode in the above lixiviant solutions confirmed the conclusions drawn from the thermodynamic calculations.

393 Gold Leaching and Recovery: The Bromide Process: *A. Dadgar** and *J. Howarth*, Great Lakes Chemical Corp., West Lafayette, IN 47906

Gold extraction and recovery for gold ores and concentrates were investigated using cyanide and bromine reagents. Gold extractions for cyanide leaching (24-48 h) and bromine leaching (4-6 h) were the same and ranged from 92 to 96%. Gold recoveries from bromine pregnant solutions using carbon adsorption, ion exchange, solvent extraction, zinc precipitation, and electrowinning methods were better than 99.6%. Commercially available undivided cells were used to generate bromine from simulated solutions. Electrolyses were performed with solutions containing different levels of bromide ion. The current efficiencies were high (80-90%) and unaffected by the bromide concentrations (over the range of 2.5-5.0%). The electrochemical module was capable of delivering 0.6 kg bromine per hour at a cost of 8.5¢ per kg. Using these figures, a detailed economic assessment for a 1000 mtpd gold ore processing plant was made. Electrolytic regeneration of bromine in a gold leach/recovery circuit dramatically improves the process economics over cyanidation.

394 Complex Technology of Electrochemical Water Treatment with Regeneration of Valuable Components in Electroplating Production: *V. A. Kolesnikov, E. A. Shalyt*, and *P. K. Aarinola*, Mendeleev Institute of Chemical Technology, Moscow 125190, USSR

The complex of techniques developed in the MChTI includes electrolysis, electrochemical correction pH, electroflotation, electrodialysis, and provides removal of impurities down to the residual concentration of 0.01 mg/l when initial concentration is not limited. Necessary exposition is about 10 min for every technique. On the basis of experimental study and computer simulation, the authors optimized apparatus design and the operation mode of techniques. The most technical ideas have been patented. Commercial modules having an output of 1-20 m^3/h operate successfully at 5 factories, and more modules are under installation. The economic benefit of one module is 100-400 thousand of roubles yearly.

395 A Comparative EIS Study on Cermet and Platinum Anodes for the Electrolytic Production of Aluminum: *C. F. Windisch, Jr.*, Pacific Northwest Laboratory, Richland, WA 99352

Electrochemical impedance spectra were obtained for NiO-$NiFe_2O_4$-Cu cermet anodes and platinum anodes during the electrolysis of alumina-saturated molten cryolite at 983°C. When the anodes were polarized above the decomposition potential for alumina, an impedance loop was obtained with a characteristic frequency of about 1 Hz. Analysis of the data suggests the loop was due to oxygen gas bubbles produced at the anodes. Features associated with charge-transfer processes were not sufficiently resolved to determine the corrosion properties of the cermet anode.

396 Solid Metal Reductive Stripping of Cerium from Tri-n-Butyl Phosphate: *T. J. O'Keefe* and *J. D. Dillon III*, Graduate Center for Materials Research, University of Missouri-Rolla, Rolla, MO 65401

Solvent extraction is used extensively in the processing of the rare earth metals. Recently, it has been shown that redox reactions are feasible in many organic extractant/inert diluent systems using metal reductants. It was demonstrated in this study that Ce(IV) could be effectively reduced to Ce(III) in a tri-n-butyl phosphate (TBP) solvent. In the reduced state, the Ce was found to be much easier to strip into the aqueous phase. Whereas Ce(IV) is difficult to strip even with concentrated (4*N*) acids, the Ce(III) was readily removed using water.

397 The Electrochemical Behavior of Group V Elements during Copper Deposition: *J. B. Hiskey*, Dept. of Materials Science and Engineering, University of Arizona, Tucson, AZ 85721, *Y. Maeda*, Nippon Mining Co. Ltd., Japan

The electrochemical behavior of copper deposition in the presence of Group V elements (arsenic, antimony, and bismuth) was investigated using several nonsteady-state techniques. Electrodeposition was carried out in cupric sulfate electrolytes containing 45 g/liter Cu^{2+} and 200 g/liter H_2SO_4 maintained at 63°C. Group V elements behave as depolarizers towards copper deposition and hydrogen evolution. Linear sweep voltammetry for the As-containing electrolyte is characterized by two reduction peaks. The first peak corresponding to copper deposition and the second to arsenic reduction at approximately -0.33 V. Cyclic voltammetry data were collected to obtain detailed information about the effect of Group V impurities on the mechanism of copper deposition.

398 Mass Transport in High-Current-Density Zinc Electrowinning: *K. J. Cathro*, Div. of Mineral Products, CSIRO, Port Melbourne, Victoria 3207, Australia

Limiting mass transfer coefficients have been measured for zinc during zinc deposition covering the ranges 50-1000 mA cm^{-2} for current density, 25-400 cm s^{-1} for flow velocity, and 30-70°C for temperature. The transfer coefficients were consistently much greater than those calculated from published correlation equations, probably due to coevolution of hydrogen. Extrapolation to zero-hydrogen conditions gave coefficient values in substantial agreement with those calculated from correlations.

399 Full-Scale Hydrogen Diffusion Anodes for Immersed Tank Electrowinning and Electroplating: *P. C. Foller, R. J. Allen*, and *R. Vora*, E-TEK, Inc., Framingham Industrial Park, Framingham, MA 01701

Immersed 1.2 m^2 hydrogen diffusion anodes have been tested in zinc electrowinning. At 500 A/m^2, 1.9 V savings are achieved vs. oxygen evolution. The electrodes were prepared by the lamination of a polymeric anti-gas percolation coating to the catalyzed surface of a heavy carbon cloth. The cloth is then laminated with carbon epoxy to a lead substrate. The coating constrains hydrogen within the cloth; it flows between the catalyst and the epoxy bond. Utilization is over 90%.

400 Cathodic Reduction of Hg(II)-Cl(I) Complex on Ag-Hg Electrode: *Q. Yin*, Dept. of Geology, University of Manchester, Manchester, England M13 9PL

The cathodic reduction mechanism of the Hg^{2+}-Cl^- complex on the Ag-Hg electrode in aqueous solution is varied with the concentration of the complex. In concentrated mercury chloride electrolyte, the reduction process is controlled by Ohm polarization; while in dilute mercury chloride electrolyte, the process is controlled by concentration polarization. For the latter process, the apparent activation energy for reduction of Hg^{2+}-Cl^- complex to mercury has been determined to be 11.631 kJ/mol and the diffusion coefficient of Hg^{2+}-Cl^- complex has been determined to be 4.388×10^{-6} cm^2/s. The cathodic reduction process is also significantly affected by the formed $Hg_2Cl_2(s)$ layer on the electrode surface, and it has been found to be 3.905×10^{-9} mol/cm^2 as the electrode is stationary and the concentration of mercury chloride is 0.05588*M*.

INDUSTRIAL ELECTRO-ORGANIC PROCESS

Industrial Electrolysis and Electrochemical Engineering

401 Organic Electrosynthesis at Extended Area Nickel Electrodes: *C. J. Brown* and *D. Pletcher*, Dept. of Chemistry, University of Southampton, Highfield, Southampton, England S09 5NH

Extended area electrodes are a good choice for electrosynthesis requiring a low current density due to slow kinetics or poor solubility of reactants. A wide variety of extended area nickel materials are commercially available for manufacture into suitable electrodes. Oxidation of various alcohols at a nickel anode in aqueous base, using an ICI FM01 parallel plate cell have been studied. Clean products with good current efficiencies are obtained.

402 Oxidation of Methanol on a Metallized Polymer Electrolyte Membrane: *R. Liu* and *P. Fedkiw*, Dept. of Chemical Engineering, North Carolina State University, Raleigh, NC 27695-7905

A study of the product distribution of the partial electrooxidation of gaseous methanol using a platinized Nafion 117 membrane has been conducted. The product distribution is found to be sensitive to the morphology of the electrode, temperature, methanol concentration, and water content in the reaction zone. The goal of this work was to manipulate the variables so to increase the selectivity of a particular partial oxidation product. Experimental conditions that produced formaldehyde, methylformate, or methylal at high selectivities (≥75%) have been obtained and are reported.

403 The Electrocatalytic Hydrogenation of Soybean Oil: *G. Yusem* and *P. N. Pintauro*, Dept. of Chemical Engineering, Tulane University, New Orleans, LA 70118

A novel electrochemical approach for hydrogenating edible oils has been developed. Such a technique offers the advantages of less severe operating conditions and improved unsaturated cis-isomer product yield. Soybean oil has been hydrogenated electrocatalytically at 70°C and 1 atmosphere pressure in a flow-through reactor using a two-phase oil-in-water emulsion and a Raney nickel powder cathode. The effects of reactor operating conditions on current efficiency and the composition of the hydrogenated product are presented.

404 Direct and Indirect Electrochemical Epoxidation of Olefins in a Sieve Plate Reactor: *C. F. Oduoza* and *K. Scott*, Dept. of Chemical and Process Engineering, University of Newcastle, Newcastle upon Tyne, England NE1 7RU

Experimental data is presented both on the direct and indirect electrosynthesis of epoxides in a batch cell and sieve plate electrochemical reactor (SPER). High current efficiency of 95.0% was achieved in the medium of halogen salts compared to 70% in alka-

line medium, which fell sharply to less than 10% with time of electrolysis. The same pattern as with SPER was obtained with a batch cell. However, the relatively higher costs of halogen salts compared to the alkali renders their use less competitive.

405 A Comparison of Some Insoluble Oxide Catalysts in the Electro-Oxidation of Thioethers in Aqueous Surfactant Suspensions: *T. C. Franklin, R. Nnodimele, and R. C. Duty,* Dept. of Chemistry, Baylor University, Waco, TX 76798-7348

Insoluble oxides were suspended with cationic surfactants in aqueous systems and electrolytically oxidized to higher oxidation states. Barium peroxide was oxidized to barium superoxide; copper (I) and copper (II) oxide to copper (III) oxide and manganese (II) oxide to manganese (III) and manganese (IV) oxides. The products and yields were obtained when these oxides reacted with diethylsulfide. The superoxide did not react; Cu (II) destroyed the compound and produced the sulfoxide; Mn (III) produced several products and Mn (IV) did not react.

406 Electrochemical Oxidation of Organic Pollutants for Waste Water Treatment: *Ch. Comninellis,* Institute of Chemical Engineering, Swiss Federal Institute of Technology, CH-1015 Lausanne, Switzerland

The possibilities of electrochemical oxidation for the treatment of organic pollutants are elucidated and the nature of organic pollutants which can be economically treated by this treatment are discussed. It is concluded that electrochemical treatment can be used as a pretreatment step (for the oxidation of the refractory organic pollutant to biodegradable organic compounds) before biological treatment.

$$\begin{bmatrix}\text{Refractory}\\ \text{organic}\end{bmatrix} \xrightarrow{\text{E.T.}} \begin{bmatrix}\text{Biodegradable}\\ \text{organic}\end{bmatrix} \xrightarrow{\text{B.T.}} CO_2 + \text{Biomass}$$

407 Proton-Exchange Membrane Reactor for Removal of Organic and Bacterial Contaminants from Reclaimed Water: *L. M. Kaba, S. Srinivasan,* and *A. J. Appleby,* Center for Electrochemical Systems and Hydrogen Research, Texas A&M University, College Station, TX 77843-3402, *G. D. Hitchens* and *O. J. Murphy,* Lynntech, Inc., Bryan, TX 77803

An electrochemical reactor that utilizes a proton exchange membrane (PEM) is being developed for the removal of organic and bacterial contaminants from reclaimed waters. The electrochemical procedure is the final step in waste water treatment prior to reuse and constitutes reducing levels of organic impurities from 100 ppm to <500 ppb by electro-oxidation. The electrochemical cell is akin to a proton exchange membrane water electrolyzer. The initial experiments were carried out with Pt-Ir and Pt coated titanium meshes for the anode and cathode, respectively. In order to enhance the energy efficiency for the process by reducing the anodic currents due to oxygen evolution, SnO_2 coated Ti anodes are currently being used. The results show that the electric energy consumption for the removal of organic contaminants was reduced by a factor of two with the SnO_2 rather than the Pt-Ir electrocatalysts.

408 Hydrodimerization of Dimethylmaleate: I. Scouting: *J. H. Wagenknecht, M. R. Bagley, E. A. Casanova, M. C. Dutton,* and *D. J. Kalota,* Monsanto Chemical Co., St. Louis, MO 63167

Butanetetracarboxylic acid (BTCA) is a replacement for currently used cross-linking agents for permanent press cotton fabric. BTCA does not release formaldehyde as currently used agents do. A process to produce BTCA involves electrohydrodimerization of dimethylmaleate (DMM) followed by hydrolysis. It has been found that hydrodimerization of DMM proceeds well in methanol containing sodium acetate in an undivided cell with graphite electrodes. This presentation describes the work leading to definition of solvent, electrolyte, electrodes, cell type, current density, etc.

409 Hydrodimerization of Dimethylmaleate: II. Process for Converting Maleic Anhydride to 1,2,3,4-Butanetetracarboxylic Acid: *D. J. Kalota, M. R. Bagley, E. A. Casanova, M. C. Dutton,* and *J. H. Wagenknecht,* Monsanto Chemical Co., St. Louis, MO 63167

Butanetetracarboxylic acid (BTCA) is a polycotton cross-linking agent that does not release formaldehyde. Its viability as a replacement for currently used agents is contingent on good performance in heat discoloration tests. This presentation describes the overall process, except for the electrohydrodimerization of dimethylmaleate, for converting maleic anhydride into an isolated BTCA product. Heat discoloration results show the effectiveness of water extraction, hydrogen peroxide treatment, and catalyst removal in producing a high quality product.

410 Hydrodimerization of Dimethylmaleate: III. Electrochemical Parameter Evaluation: *M. C. Dutton, M. R. Bagley, E. A. Casanova, D. J. Kalota,* and *J. H. Wagenknecht,* Monsanto Chemical Co., St. Louis, MO 63167

Work done by the USDA showed that 1,2,3,4-butanetetracarboxylic acid (BTCA) was an effective permanent press cross-linking agent for polycotton fabrics. The electrohydrodimerization (EHD) of dimethylmaleate to form tetramethyl-1,2,3,4-butanetetracarboxylate is a step in the process to produce BTCA. It has been found that this reaction runs well in a batch system with a bulk pH of 7 to 8. This presentation describes experiments pertaining to batch *vs.* continuous operation, pH effects, and EHD cell life.

411 The Preparation of Metal Ion Reductants via the Use of Hydrogen Diffusion Anodes: *P. C. Foller,* R. J. Allen,* and *R. Vora,* E-TEK, Inc., Framingham, MA 01701

Ti(III) has been prepared from Ti(IV) in sulfuric acid via the use of hydrogen diffusion anodes (HDAs). HDAs allow the preparation of Ti(III) sulfate free of extraneous ions as are introduced via aluminum or zinc reduction, the usual route to such reducing agents. No membrane is required, as the potential of the HDA is insufficient to re-oxidize Ti(III) once it is formed. High (95%) conversions can be obtained using multiple-pass flow. Use of the approach is foreseen in indirect organic electrochemistry.

412 An Anolyte Model of a Diaphragm-Type Chlorine/Caustic Cell: *J. W. Van Zee* and *C. T. Lee,* Chemical Engineering Dept., Swearingen Engineering Center, University of South Carolina, Columbia, SC 29208

A time-dependent anolyte model of a diaphragm-type chlorine/caustic cell, which includes the multiphase chlorine reactions, is presented. The effects of convection, migration, and gas void fraction on mass transfer of the species in the anolyte are considered. The model is formulated in terms of feed flow rates, which enables the model to be used readily for developing process control schemes for the anolyte variables in a diaphragm-type cell, and to be modified to simulate the anolyte of membrane-type chlorine/caustic cells. The predictions of the major species concentrations are shown to agree with the experimental data of a lab-scale diaphragm cell.

413 Design of a Digital Multiloop PID Control System for a Diaphragm-Type Chlorine/Caustic Cell: *C. T. Lee* and *J. W. Van Zee,* Chemical Engineering Dept., Swearingen Engineering Center, University of South Carolina, Columbia, SC 29208

A digital multiloop PID (proportional-integral-derivative) feedback control system was designed for a diaphragm-type chlorine/caustic cell using a theoretical model. The anolyte pH and the caustic effluent concentration were chosen as the controlled outputs. A feedback control simulator of the cell based on the design was also developed. The design methodology presented is general, and could be readily applied to other electrochemical processes, especially to those with nonlinear and complicated model equations. This work provides a basis of studying the effects of digital process control schemes on performance of a diaphragm-type cell.

ELECTRO-ORGANIC SYNTHESIS WITH HOMOGENEOUS AND HETEROGENEOUS CATALYSTS

Organic and Biological Electrochemistry

414 Mediated Reductive Dechlorination of PCBs in Surfactant Dispersions and Microemulsions: *I. Ul Haque, E. C. Couture, S. Zhang,* and *J. F. Rusling,* Dept. of Chemistry (U-60), University of Connecticut, Storrs, CT 06269-3060

Yields of dehalogenated products were better in dispersions and microemulsions containing didodecyldimethylammonium bromide (DDAB) than in aqueous CTAB micelles. Hg was the most efficient cathode. Using zinc phthalocyanine as mediator, 0.10 g of a commercial PCB mixture was completely dechlorinated in 18 h. Bicontinuous microemulsions of DDAB, dodecane, and water gave promising results with Pb cathodes.

415 Electrocatalytic Hydrogenation at Palladium Black Electrodes: *S. J. C. Cleghorn** and *D. Pletcher,* University of Southampton, Highfield, Southampton, England SO9 5NH

Palladium black electrodes have been prepared by electrodeposition of palladium onto graphite and nickel from an acid chloride bath. These electrodes in a methanol containing acetic acid electrolyte are suitable for the hydrogenation of many organic molecules. The mechanism involves the reversible formation of Pd(H) by reduction of acetic acid, followed by a chemical reaction between the Pd(H) and the organic reactant. Electrolysis in a FM-01 laboratory electrolyzer is described.

416 The Electrochemical Reduction of Nitroaromatic Compounds to Amines in Basic Solutions at Porous Metallic Electrodes: *J. Lessard, Y. Couture, M.-J. Lessard, A. Martel,* and *C. Roy,* Dept. de Chimie, Facultes des Sciencies, Universite de Sherbrooke, Sherbrooke, Que., Canada J1K 2R1

The electrocatalytic hydrogenation of nitrobenzoic acids (para and ortho) and nitrobenzenesulfonic acids (meta and para) at Raney nickel (RNi) and Devarda copper (DCu) electrodes in a basic aqueous medium (0.15*M* NaOH) gave the corresponding amino acids with chemical yields of 80-100% and current efficiencies of 75-100% under controlled potential or constant current conditions in a two-compartment H-cell (2 g scale). On a larger scale (~110 g) and using a flow-cell, metanitrobenzenesulfonic acid gave metanilic acid in a 85-90% yield and 60-65% current efficiency. The lifetime of the electrodes was of the order of 50 to 60 days. Other porous electrode materials made of copper were found to be as efficient as DCu for the conversion of nitrobenzene to aniline in basic aqueous methanolic solutions.

417 Role of Sulfide Ion as Mediator in the Electroreduction of Nitroaromatics: *A. Tandon, P. S. Verma, S. K. Mukerji,* and *K. N. Tandon,* Dept. of Chemistry, University of Rajasthan, Jaipur-302004, India

The sulfide ion acts as a mediator in the electroreduction of nitroaromatics in weakly basic medium at stainless steel (type 316) cathode by forming reversible sulfide-polysulfide couple. The polysulfide is reduced to sulfide at a less cathodic potential than the substrates.The sulfide mediator reduces the nitroaromatic to the hydroxylamine stage in the cold but to the aniline stage at a characteristic elevated temperature which varies from substrate to substrate. The difference in the electrolytic behavior of nitrobenzene and 1,3-dinitrobenzene is explained on the basis of their structural difference and the difference in the polarity of the two molecules.

418 Indirect Reduction of Sulfonium Salts by Means of p-Acceptor Radical Anions (in Liquid Phase) and n-Doped Electroactive Polymers (in Solid Phase) Application to Functionalization Reactions: *J. Simonet, P. Martigny, H. Le Deit,* and *J. Rault-Berthelot,* Laboratoire d'Electrochimie, Universite de Rennes I, Campus de Beaulieu, 35042 Rennes Cedex, France

The use of mediators such as anthracene, naphtalene, acenaphtylene, and benzophenone may induce the indirect reduction of onium salts in aprotic electrolyte. This paper deals with the indirect reduction of diphenylalkylsulfonium cation either by anion radicals of π-acceptors (leading to alkyldihydro relevant structures) or by n-doped polyparaphenylene type deposits on a platinum cathode (also formation of polydihydropolyalkyl structure but within a very narrow potential range).

419 On the *ipso*-Substitution in Aromatic Compounds by Electrogenerated Radicals: *H. Lund,* Dept. of Organic Chemistry, University of Aarhus, DK-8000 Aarhus C, Denmark, *K. Pang* and *Q. Chen,* Dept. of Organic Chemistry, Shenyang College of Pharmacy, Shenyang, 110015 China

Anion radicals of aromatic compounds react with alkyl halides with formation of radicals which may couple with an anion radical. When the aromatic compound is substituted with a suitable leaving group Y (*e.g.*, CN) an *ipso*-substitution followed by elimination of HY may occur. The regioselectivity in the reaction of ArY is improved compared to that of AH. Thus reduction of 4-cyanopyridine in the presence of *t*-butyl bromide and diethylamine gives 4-*t*-butylpyridine in good yield.

420 Production of Pyrene Quinone by Indirect Electro-Oxidation of Suspended Pyrene: *T. Nonaka* and *A. Yoshiyama,* Dept. of Electronic Chemistry, Tokyo Institute of Technology, 4259 Nagatsuta, Midori-ku, Yokohama, 227, Japan, *M. Wakamatsu, S. Tsuji* and *I. Okubo,* Chugaikasei Co., Ltd., 6-1 Kamirenjaku 6-Chome, Mitaka, Tokyo 181, Japan

The indirect electro-oxidation of water-insoluble solid materials such as cellulose, tetramethylbenzene, and pyrene was performed by electrolyzing their suspensions in the presence of suitable redox mediators (catalysts) dissolved in aqueous electrolytic solutions. Particularly, the oxidation of pyrene was investigated in detail using a bench-scale parallel plate flow cell from a practical aspect of the pyrene quinone production.

421 Electro-Oxidation of Propene in Aqueous Zeolite Suspensions: *J. Z. Stemple* and *D. R. Rolison,* Code 6170, Surface Chemistry Branch, Naval Research Laboratory, Washington, DC 20375-5000

Zeolite-supported metal clusters sized less than 10 nm are addressed as ultramicroelectrodes via dispersion electrolysis between two feeder electrodes. This system couples materials which, when sized on the nanometer scale, can exhibit physical and chemical properties that differ from bulk properties and zeolites which allow for molecular discrimination based on size, shape, and charge selectivity. Ultramicroelectrodes supported on zeolites, therefore, provide a unique interphase that undoubtedly will affect not only charge-transfer processes, but also interfacial chemical reactions. Accordingly, the oxidation of propene is chosen as a model reaction to study (*i*) the zeolite influence on electron transfer and subsequent chemical reactions at metallated zeolites, and (*ii*) the influence of an electric field on the inherent catalytic activity of metallated zeolites.

422 Mediated Reduction of Aryl Bromides at Tin Cathodes: *E. G. Gunderson, E. Kariv-Miller,* and *V. Svetlicic,* Dept. of Chemistry, University of Minnesota, Minneapolis, MN 55455-0431

The mediated reduction of aryl bromides at tin cathodes was investigated. The mediator was dimethylpyrrolidinium-Sn, $DMP(Sn_3)$, generated by the cathodic reduction of the electrolyte cation. The relative rate of electron transfer to the various bromides was determined by a combination of constant potential electrolysis (CPE) and anodic stripping voltammetry (ASV). It was found that the electronic nature and relative location of the substituents on the aromatic ring had a significant effect upon the rate of reaction.

423 Fluoride Ion Promoted Anodic Substitution, Regioselective Anodic Alkoxylation of Sulfides: *T. Fuchigami, H. Yano, A. Konno,* and *T. Nonaka,* Dept. of Electronic Chemistry, Tokyo Institute of Technology, Nagatsuta, Midori-ku, Yokohama 227, Japan

Anodic α-alkoxylation of sulfides was promoted in the presence of fluoride ions. When Et_3N 3HF was used as a supporting electrolyte, simple alkyl phenyl sulfides and sulfides bearing weak electron-withdrawing groups underwent anodic alkoxylation via fluorosulfonium ions as key intermediates in a unique Pummerer-type mechanism with reasonable or high yields for the first time.

424 Use of [2,2'-Ethylenebis(nitrilomethylidyne)diphenolato]-nickelate(I) as a Homogeneous and Polymer-Based Catalyst for Reduction of Organic Halides: *C. E. Dahm* and *D. G. Peters,* Dept. of Chemistry, Indiana University, Bloomington, IN 47405, *M. S .Mubarak,* Dept. of Chemistry, King Saud University, Abha, Saudi Arabia

In dimethylformamide containing tetraethylammonium perchlorate, [2,2'-ethylenebis(nitrilomethylidyne)diphenolato]nickel(II) undergoes reversible one-electron reduction at a carbon cathode to generate the corresponding nickel (I) species. In the presence of this nickel(I) species, 6-iodo- and 6-bromo-1-phenyl-1-hexyne are homogeneously and catalytically reduced to form a radical intermediate that cyclizes to yield benzylidenecyclopentane. Oxidative polymerization of the nickel(II) species at reticulated vitreous carbon in acetonitrile containing tetra-ethylammonium tetrafluoroborate produces a polymer-coated electrode that can be employed subsequently for the efficient catalytic reduction of alkyl halides.

425 Long Life Anion Radicals from ArX or RX Type Compounds: Mediators, or Ar• and R• Providing Species? Case of Ortho-bis(Alkylsulfonyl)Benzenes: *J. Simonet,* Laboratoiré d'Electrochimie, Université de Rennes I, Campus de Beaulieu, 35042 Rennes Cédex, France

Title compounds (I) lead by means of their cathodic reduction to surprisingly stable anion radicals. Bimolecular reaction of (I) anion radical either on starting material or on aliphatic organic halides in excess affords very unexpected aromatic substitutions which depend on the nature of the halide. For example:

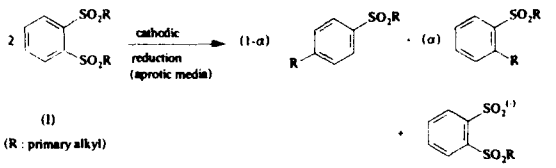

426 Conversion of isoSafrole to Piperonal Using Electrolytically Recycled Higher Oxides of Manganese: *J. Grimshaw,* Dept. of Chemistry, Queen's University, Belfast, Northern Ireland BT9 5AG, *C. Hua,* Dept. of Applied Chemistry, Beijing Institute of Chemical Technology, Beijing 100029, China

Anodic oxidation of manganese(II) sulfate in aqueous sulfuric acid of concentration less than 50% (w/w) gives a fine precipitate of nonstoichiometric manganese dioxide. This precipitate, suspended in dilute sulfuric acid, converts isosafrole to piperonal and the manganese compounds dissolve as manganese(II) sulfate. Piperonal is isolated and the manganese recycled. When the manganese dioxide is filtered, any water soluble impurities are removed in the filtrate and such a step is necessary in any process for continuous operation.

427 Mechanism of Electron Transfer Activation of Organic Substrates in the Presence of Organometallic Catalysts. Application to Homogeneous Catalysis under Reductive Conditions: *A. Jutland* and *C. Amatore,* Laboratoire de Chimie, Ecole Normale Superiere, F 7521, Paris Cedex, France, *M. Nielsen,* Dept. of General and Organic Chemistry, University of Copenhagen, DK-2100, Copenhagan, Danemark

Bidentate nickel and monodentate palladium complexes catalyze the electrosynthesis of aromatic carboxylic acids from carbon dioxide and aromatic halides. The catalysis proceeds via a succession of chemical and reductive steps involving diamagnetic and paramagnetic nickel complexes but only diamagnetic palladium complexes. The carboxylation occurs in the nickel coordination shell (via a $Ar\text{-}Ni^{I}L_2$ intermediate). Whereas in the case of palladium, carbon dioxide reacts with an aryl anion Ar^- formed from a $Ar\text{-}Pd^{0}L_2$-intermediate.

428 Electrochemistry of 9,9'-Spirobifluorene Derivates: 2,2'-Diacetyl 9,9'-Spirobifluorene: *L. Mattiello* and *L. Rampazzo,* Dept. ICMMPM, University of Rome, 00161 Rome, Italy

2,2'-Diacetyl 9,9'-spirobifluorene (*1*) is an aromatic compound with two identical orthogonal halves. The cyclic voltammogram of (*1*) shows five reduction processes, measured in dry DMF-0.1*M* $Et_4\text{-}NClO_4$, glassy carbon electrode. The first two are reversible, one-electron transfers with $E_1^{\cdot}$ + -1.75 V and $E_2^{\cdot}$ = -1.90 V (SCE); they are followed by three (apparently) irreversible reduction processes occurring at very negative potentials, E_p = -2.40, -2.67, and -2.80 V (sweep rate 0.2 V/s), related to the spirobifluorene moiety.

429 A Study of Substituted Catechols as Electron Transfer Mediators in Electrocatalytic Enzyme Reactions: *T. J. Moore* and *L. A. Coury,* Dept. of Chemistry, Duke University, P. M. Gross Laboratory, Durham NC 27706-7706

The rate constants for reduction of 13 *o*-quinones by reduced glucose oxidase are determined and found to not be correlated to either the $2e^2/2H^+$ redox potentials or the hydride transfer potentials. Results from kinetic experiments in deuterium oxide and protic water indicate that the rate-limiting step may be abstraction of the first electron. An understanding of the kinetics of this

reaction is important to the development of more effective electrochemical biosensors.

430 Electroreductive Cleavage of the C-Ce Bond of 9-Chlorofluorenes: *F. Maran* and *E. Vianello*, Dept. of Physical Chemistry, University of Padova, 35131 Padova, Italy

The electroreduction of a series of substituted 9-chlorofluorenes has been investigated in DMF by cyclic and convolution potential scan voltammetries and controlled potential electrolysis. Through the determination of the heterogeneous rate constant of the initial one-electron uptake in a wide potential range, a potential dependence of the electrochemical transfer coefficient α was found, thus pointing to a concerted electron transfer-bond breaking process. The potential dependence of α was taken into account in the kinetic analysis of the expected self-protonation reaction involving the carbanion eventually electrogenerated at the electrode. The dependence of the support rate constant on the substrate concentration as well as further evidence pointed to the occurrence of complex chemical pathways in the voltammetric time scale.

431 Electrochemical Behavior of Cytochrome c_3 Hildenborough on a Gold Electrode: *B. A.Gorecka*, Dept. of Pharmaceutical Chemistry, University of Kansas, Lawrence, KS 66045, *G. S. Wilson*, Dept. of Chemistry, University of Kansas, Lawrence, KS 66045

Electrochemical behavior of cytochrome c_3 Hildenborough in solution phase as well as adsorbed films on gold electrode has been studied by cyclic voltammetry chronocoulometry and chronoamperometry. Properties of the cytochrome c_3 films are compared with those of the redox polymer film.

432 The Anodic Oxidation of Hydrazones: *M. R. Van De Mark* and *E.-C. Lin*, Dept. of Chemistry, University of Missouri-Rolla, Rolla, MO 65401, *W. Eldefi*, University of Miami Medical School, Miami, FL 33101

The anodic oxidation of aldehyde hydrazones at a graphite anode in aqueous acetonitrile was investigated. The major products were the parent aldehyde, the caraboxylic acid, hydrazide and RCON = NAr. A proposed mechanism consistent with the products was suggested including geometry optimizing MNDO and AM1 calculations. A very good linear free energy correlation with sigma plus was found.

433 Pin Loosening in External Skeletal Fixation: *In Vivo* Electrochemical Impedance Study of the Pin Bone Interface: O A Velev, Center for Electrochemical Systems and Hydrogen Research, Texas A&M University, College Station, TX 77843, *R. H. Palmer*, Santa Cruz Veterinary Hospital, Santa Cruz, CA 95065, *P. Srinivasan*, Center for Electrochemical Systems and Hydrogen Research, Texas A&M University, College Station TX 77843, *D. A. Hulse*, Dept. of Small Animal Medicine and Surgery, Texas A&M University, College Station, TX 77843, *H. W. Sampson*, Dept. of Anatomy, College of Medicine, Texas A&M University, College Station, TX 77843, *W. H. Hyman*, Dept. of Industrial Engineering Division of Bioengineering, Texas A&M University, College Station, TX 77843

External skeletal fixation is commonly used for treatment of many orthopedic injuries and diseases in human and animal patients. Loosening of the percutaneous fixation pins within the bone affects up to 42% of such pins and remains the major complication associated with this technique. Pin-loosening results from a poorly understood cascade of inter-related mechanical and biological events. Electrical fields resulting from local mechanical strains are considered the primary signal which initiates bone remodeling. The purpose of this study was to characterize the electrochemical environment of the pin-bone interface *in vivo* during the first 43 days after implantation from open circuit potential and impedance spectroscopy measurements.

ELECTROCHEMISTRY OF HIGH TEMPERATURE SUPERCONDUCTORS

Physical Electrochemistry

434 Progress in Observing Electrochemical Processes at Superconducting Electrode/Molecular Solvent Interfaces: *S. R. Peck, L. S. Curtin, L. M. F. Tender, J. N. Richardson*, and *R. W. Murray*, Kenan Laboratories of Chemistry, University of North Carolina Chapel Hill, NC 27599-3290

This paper reports progress in our program to observe electrochemical processes at high temperature superconductor electrodes, contacted by a fluid electrolyte solution, at temperatures that span their T_c transition temperatures. In particular we have observed a change in the double layer capacity of these electrodes at T_c.

435 Low-Temperature Electrochemistry on High T_c Superconductors: *W. J. Lorenz*, Institute of Physical Chemistry and Electrochemistry, University of Karlsruhe, Karlsruhe, Germany, *G. Saemann-Ischenko*, Institute of Physics, University of Erlangen-Nürnberg, Erlangen, Germany, *M. W. Breiter*, Institute of Technical Electrochemistry, University of Vienna, Vienna, Austria

The charge transfer across superconductor/ionic conductor interfaces represents a relatively new experimental and theoretical field. This paper deals with electrochemical studies in this area. Both n-type classical super-conductor (SC) and p- and n-type high T_c superconductors (HTSC) in contact with different superionic conductors (Ag ß"-alumina, Ag^+ ion conducting glass, and $RbAg_4I_5$), which are used as solid electrolytes (SE), are considered in experiments covering the temperature range $10\ K \leq T \leq 298\ K$. The faradaic process occurring at those HTSC/SE interfaces is the silver deposition and dissolution, measured by either a transient technique in the time domain or by electrochemical impedance spectroscopy (EIS) in the frequency domain. The results show a positive admittance peak in transient measurements or a corresponding negative impedance peak in EIS-measurements around $T \approx T_c$. These findings are attributed to an enhancement of the rate of the faradaic reaction around T_c. The effect is interpreted as a quantum-electrochemical phenomenon caused by the contribution of Cooper pairs crossing the electrochemical double layer as correlated charge carriers and participating in the charge transfer step of the phase boundary reaction. A proximity-like phenomenon can be excluded.

436 Corrosion Reactivities of Various Copper Oxide and Fullerene High Temperature Superconductor Phases: *J. T. McDevitt, D. R. Riley*, and *J.-P. Zhou*, Dept. of Chemistry and Biochemistry, University of Texas at Austin, Austin, TX 78712-1167, *A. Manthiram*, Center for Materials Science and Engineering, University of Texas at Austin, Austin, TX 78712, and *D. Jurbergs*, Dept. of Chemistry and Biochemistry, University of Texas at Austin, Austin, TX 78712-1167

Before practical utilization of the high temperature superconductors is possible, a more complete understanding of their surface chemistry is necessary. In this paper, the relative reactivity of the common high-T_c phases toward water is reported. Electrochemical, x-ray powder diffraction, and scanning electron microscopy measurements are utilized to establish the corrosion trends. From this comprehensive study, the following chemical reactivity scale is established: $K_3C_{60} >> YBa_2Cu_3O_7 > Tl_2Ba_2Ca_2Cu_3O_{10} > Bi_2Sr_2CaCu_2O_8 \geq La_{1.85}Sr_{0.15}CuO_4 >> Nd_{1.85}Ce_{0.15}CuO_4 > Nd_{1.85}Th_{0.15}CuO_4$

437 Electrochemical Rate Data of Superconductor Materials and Their Lithium Insertion Compounds as Electrodes: *N. A. Fleischer* and *J. Manassen*, Dept. of Materials and Interfaces, The Weizmann Institute of Science, Rehovot 76100, Israel

The insertion of lithium into the lamellar bismuth oxide 2212 and 2201 superconductors modifies their structural chemistry and electronic properties. Electron transfer reactions were studied at electrodes made from 2212 and 2301 in the normal state and compared to their Li insertion compounds, regular perovskites, and metals. The heterogenous rate constants for several redox reactions in organic solvents decreased with increasing Li content. The insertion reaction itself was studied by cyclic voltammetry and the effective diffusion coefficient for Li in the superconductors was measured.

438 The Surface Structure and Electronic States of High-Tc Superconductors by STM: *C. M. Lieber* and *Z. Zhang*, Dept. of Chemistry, Harvard University Cambridge, MA 02138

Scanning tunneling microscopy (STM) and scanning tunneling spectroscopy (STS) have been used to characterize the structure and electronic states of the surfaces of single crystal Bi-Sr-Ca-Cu-O superconductors. STM images have been used to elucidate variations in the atomic structure and superstructure of the Bi-O layer that result from metal-substitution and oxygen doping. STS data further show how the electronic states of this material evolve with metal and oxygen doping.

439 Physical and Chemical Characterization of Electrodeposited Superconducting Bismuthates: *M. L. Norton*, Dept. of Chemistry, Marshall University, Huntington, WV 25755, *H.-Y. Tang*, Materials Science Center, National Tsinghua University, Hsinchu, Taiwan, China

Large single crystals of the bismuth based superconductors $Ba_{1-x}M_xBiO_3$ (M = K, Rb) produced by anodic electrocrystallization have been characterized. Low resolution scanning tunneling microscopy fractographs indicate the presence of a mosaic structure with a domain size of approximately 50 nm. Although significant sodium contamination was not detected in bulk analysis performed utilizing inductively coupled plasma mass spectrometry, significant subgrain boundary sodium decoration was observed using scanning ion microscopy.

440 Synthesis of Superconducting Films via an Electrochemical Pathway: *A. Weston, N. Ali*, and *S. B. Lalvani*, College of Engineering and Technology, Southern Illinois University, Carbondale, IL 62901

Precursor thin films of Y-Ba-Cu-O and Er-Ba-Cu-O superconductor were produced by potentiostatic and pulse electrodeposition from the dissolved nitrate salts of the constituent metals in dimethylformamide. The films were deposited on metal foils such as Ag-coated Cu, Ag, Zr, as well as on Ag-coated $SrTiO_3$, $CaTiO_3$, and Al_2O_3. The electrodeposited films were heat-treated in flowing O_2 in order to produce the superconducting phase. Y-Ba-Cu-O films formed on Zr had highest T_c onset at 93 K.

441 Superconductor Oxide Films via an Electrodeposition Process: *R. N. Bhattacharya, P. A. Parilla,* and *R. D. Blaugher,* National Renewable Energy Laboratory, Golden, CO 80401-3393

Superconductor oxide films were fabricated via a one-step electrodeposition process followed by short annealing in oxygen. Cyclic voltammetry was employed to investigate the reduction potentials of the metal ions and reaction mechanism. The precursors of the superconducting oxide films were codeposited from a nonaqueous solution (nitrate salts dissolved in dimethyl sulfoxide) at a constant potential of -4 V and also under a pulsed-potential condition, where the pulse cycle was 10 s at -4 V followed by 10 s at -1 V (*vs.* $Ag/AgNO_3$). The substrates used were silver-coated single crystals of $SrTiO_3$, Nb-doped $SrTiO_3$, MgO, ZrO_2, and foils and wires of Ag, Ag(25%)-Pd, and Ni. The outstanding critical current densities measured to date for polycrystalline TBCCO films are as follows: (*i*) the critical current density at 77 K for a pulsed-potential TBCCO film on silver foil was 10,000 A/cm² in zero field, (*ii*) the critical current density at 76 K for a TBCCO film deposited at constant potential on a silver-coated $SrTiO_3$ substrate was 20,000 A/cm² in zero magnetic field and 5,000 A/cm² in a 10 Koe field parallel to the film plane, and (*iii*) the critical current density of a pulsed-potential deposited TBCCO film on silver-coated $SrTiO_3$ was 56,000 A/cm² at 76 K in zero field.

442 Reactivity of Compound Superconductors: Cuprates, Bismuthates, Fullerides: *B. Miller* and *J. M. Rosamilia,* AT&T Bell Laboratories, Murray Hill, NJ 07974-0636

Recently developed materials with T_c above 23 K include an assortment of cuprates, bismuthates like $Ba_{1-x}K_xBiO_3$, and fulleride salts, such as Rb_3C_{60}. Electrochemically, each of these has a powerful driving force for interfacial reactivity; strong oxidants having nominal copper oxidation states >+2 or Bi >+3, strong reductants with C_{60}^{3} anions. We discuss the reactivity, which impacts greatly on junction formation, device stability, and means of protection.

443 Controlled Room Temperature Formation of Weak Link or Josephson Junction in Thin Film $YBa_2Cu_3O_{7-x}$: *D. Cahen* and *Y. Scolnik,* The Weizmann Institute of Science, Rehovot 76100, Israel

We show how the earlier developed methodologies of room temperature reduction and reoxygenation of samples of $YBa_2Cu_3O_7$ can be used to pattern μm-thin films at room temperature by way of selected area electrochemistry. The resulting bridge structures are characterized in terms of their I-V-T characteristics and found to show SNS junction behavior. In several cases reduction and reoxygenation can improve the homogeneity of the sample in the affected areas.

444 High Temperature Electrochemical Behavior of $XBa_2Cu_3O_x$ Electrodes on Stabilized Zirconia Solid Electrolyte: *T. M. Gur,* Center for Matls. Res., Stanford, CA 94305-4045, *R. A. Huggins,* Dept. of Matls. Sci. and Engineering, Stanford University, Stanford, CA 94305-2205

The high temperature superconducting $YBa_2Cu_3O_x$ is also a mixed-conductor with a wide range of oxygen nonstoichiometry. To evaluate its potential as an electrode material for solid oxide fuel cell applications, the $YBa_2Cu_3O_x$ powder was deposited as a contiguous layer on yttria stabilized zirconia (YSZ) solid electrolyte. A porous platinum electrode was used as the counterelectrode. The electrochemical behavior of the $YBa_2Cu_3O_x$ electrode was studied between 465 and 835°C in air by dc polarization and ac impedance spectroscopy techniques. The results indicated that $YBa_2Cu_3O_7$ may be employed as an electrode material under oxidizing conditions.

445 Electrochemical Response of $YBa_2Cu_3O_x$ as a Function of Oxygen Content: *D. R. Riley,* and *J. T. McDevitt,* Dept. of Chemistry and Biochemistry, University of Texas at Austin, Austin, TX 78712-1167

By varying the oxygen content in the high temperature superconductor phase $YBa_2Cu_3O_x$ ($6 < x < 7$), the electrical properties of this material can be manipulated from that of a superconductor to that of an insulating semiconductor. In this paper, we describe a method for preparing $YBa_2Cu_3O_x$ samples with different oxygen contents and describe a corresponding procedure for fabricating electrodes from these samples. The procedure provides a simple and systematic means of tailoring the conductive properties of electrode specimens and the response of these electrodes are discussed herein.

446 Application of High Temperature Electrochemical Techniques to $YBa_2Cu_3O_{7-\delta}$: *R. V. Kumar* and *D. J. Fray,* Dept. of Mining and Mineral Engineering, University of Leeds, Leeds, England LS2 9JT, *J. E. Evetts, H. W. Williams,* and *A. Misson,* Dept. of Materials Science and Metallurgy, University of Cambridge, Cambridge, England CB2 3QZ

High temperature solid state electrochemical techniques have been applied in the determination of oxygen nonstoichiometry and phase stability diagram of $YBa_2Cu_3O_{7-\delta}$. Much of the nonstoichiometric composition of $YBa_2Cu_3O_{7-\delta}$ is metastable, and they fall in the phase region of $YBa_2Cu_4O_8$. Under favorable conditions of temperatures and oxygen pressures, $YBa_2Cu_3O_{7-\delta}$ was electrochemically decomposed to $YBa_2Cu_4O_8$ and the corresponding phase boundary determined. Enhanced texture can also be obtained in the bulk sintered samples by electrochemical processing of $YBa_2Cu_3O_{7-\delta}$. By incorporating grains that are platelet-like with high aspect ratio as feed material into the matrix of fine-sized reactive precursor, bulk samples with good texture can be produced by the combined effect of pressure, temperature, and electrochemical potential.

GENERAL SESSION

Physical Electrochemistry

447 The Effect of Solvent on the Simultaneous Adsorption of Anions and Cations: *M. Anbu Kulandainathan** and *S. Venkatakrishna Iyer,* CECRI, Karaikudi 623 006, India

The adsorption of tetrabutylammonium chloride from water, heavy water, and DMSO on mercury electrode has been studied using capillary electrometer. Parameters like capacitance values at different potentials, potential of zero charge, Esin-Markov coefficient values, and electrosorption valency have also been calculated to characterize the simultaneous adsorption. The adsorption of TBA ions from different solvents can be explained using Virial adsorption isotherm. The amount of specifically adsorbed charge due to cations in the presence of adsorbed anions is evaluated using Saffarian and de Levie model.

448 Manipulation of Double Layer in Metal Insulator Electrolyte: *K. Ghowsi,* Dept. of Chemistry and Biochemistry, Texas Tech University, Lubbock, TX 79409-4260

The manipulation of double layer is possible at the insulator electrolyte by applying a strong field (10^5-10^6 MV/cm) across metal-insulator-electrolyte. In the proposed model for metal-insulator-electrolyte the surface ionization and specific adsorption have been combined with Stern Gouy Chapman theory. By combining the metal insulator electrolyte characteristics and the electroosmotic effect in a capillary, a novel effect called field effect electroosmosis has been proposed.

449 Molecular Recognition at Interfaces: Specific Binding of an Electroactive Tetrathiafulvalene (TTF) Derivative to Organosulfur Monolayers by Hydrogen Bonding: *L. M. Frostman* and *M. D. Ward,* Dept. of Chemical Engineering and Materials Science, University of Minnesota, Minneapolis, MN 55455

We present evidence that the monocarboxylic acid derivative of tetrathiafulvalene (TTF) binds specifically via hydrogen-bonding to -COOH terminated oganosulfur monolayers on gold. Cyclic voltammetry of these films shows TTFCOOH coverages on the order of a monolayer. These studies indicate that molecular recognition is operative on functional molecular monolayers.

450 Kinetics of Electron Hopping in Langmuir Monolayers at the Air/Water Interface: *M. Majda, D. H. Charych,* and *J. T. Orr,* Dept. of Chemistry, University of California, Berkeley, Berkeley, CA 94720

We discuss dynamic solvent effects and the distance dependence on the electron transfer kinetics. Our approach involves 2-D electrochemical measurements carried out at the air/water interface. In these experiments, a "line" microelectrode is positioned in the plane of the air/water interface, where it addresses molecules forming monolayers at that interface under the controlled surface pressure conditions of a Langmuir trough. Under these conditions, diffusion coefficients obtained in the voltammetric studies of osmium tris-diphenylphenanthroline can be interpreted in terms of the rate constant of the lateral electron hopping.

451 Effects of Monosubstituted Phenol Additives on the Conductivity of Electrochemically-Synthesized Polypyrrole: *M. Fukuyama, N. Nanai, T. Kojima, Y. Kudoh,* and *S. Yoshimura,* Matsushita Research Institute Tokyo, Inc., 3-10-1 Higashimita, Tama-ku, Kawasaki 214, Japan

We report the effects of monosubstituted phenol additives that are contained in a polymerization solution, on the conductivity of electrochemically-synthesized polypyrrole. For the case of p-nitrophenol the conductivity is 64 S/cm which is about 7 times higher than that without additives. From the elemental analysis data, mass spectra, infrared spectra, electronic absorption spectra, and laser Raman spectra, it is clear that the additives are not included in polypyrrole films but the electronic state of polypyrrole is changed.

452 Impedance and Voltammetric Characterization of Electrochemically Deposited (Poly)aniline Conducting Films: *P. Vanysek* and *G. Sandi,* Dept. of Chemistry, Northern Illinois University, DeKalb, IL 60115

Polyaniline films electrochemically deposited on Pt electrodes are characterized by semiautomated impedance spectroscopy. Repetitive measurements at varying bias potentials and concentrations are recorded and evaluated. The films are grown in several acidic solutions, with the best film obtained in sulfuric acid. Circuit analysis reveals a potential dependent constant phase element in parallel with a potential dependent resistance. These parameters are correlated with the varying conductivity of the film and with the changes of the double-layer capacitance.

453 A Cathodically Polymerized Binuclear Cobalt Complex and Its Electrocatalytic Reduction of Carbon Dioxide: *X. Ren, S. K. Mandal,* and *P. Pickup,* Dept. of Chemistry, Memorial University of Newfoundland, St. John's, Newfoundland, Canada A1B 3X7

A binuclear cobalt (II) complex with a pyrrole substituent has been cathodically deposited from CH_3CN + 0.1*M* Et_4ClO_4. The resulting polymer films are porous and exhibit reversible electrochemistry at a formal potential of -1.5 V *vs.* SSCE. They become electronically conductive and show an electrochromic color change when reduced. The immobilized Co complex catalyzes the reduction of CO_2 in acetonitrile.

454 The Electrochemical Reduction of CO_2 on Ag and Au Electrodes: The Effect of Trace Impurities: *R. Kostecki, P. Kedzierzawski,* and *J. Augustynski,* Laboratory of Electrochemistry and Applied Chemistry Université de Genève, Chimie appliquèe, CH 1211 Genéve 4, Switzerland

Electrochemical reduction of CO_2 in aqueous bicarbonate solutions has been examined with particular regard to the effect of trace metal impurities present in the solution. Deposition of such impurities at the surface of Au and Ag electrodes is apparently responsible for the progressive decrease of their electrocatalytic activity observed during prolonged electrolysis runs. Methods allowing continuous or periodic reactivation of the Au and Ag cathodes are discussed.

455 Redox Potential of N-Hexadecyl-N'-Methyl Viologen$^{(2+/+)}$ Solubilized in Cetyltrimethylammonium Chloride Micelle: *C.-W. Lee** and *M.-K. Oh,* Dept. of Chemistry, Korea University, Jochiwon, Choongnam 339, Korea

The redox potentials of N-hexadecyl-N'-methyl viologen$^{(2+/+)}$ in several different thermodynamic conditions of aqueous solution were measured, and the results show that the formal potential of the redox couple in organized molecular assembly could differ by 200 mV from that of methyl viologen $^{(2+/+)}$. Implications for useful chemical reactions using viologen moiety [ex. P.-A. Brugger, P. P. Infelta, A.M. Braun, and M. Gratzel, *J. Am. Chem. Soc.,* **103,** 320 (1981)] are presented.

456 Analytical Utility of the Iridium-Based Mercury Ultra-Microelectrode with Square Wave Anodic Stripping Voltammetry: *W. Deng* and *S. P. Kounaves,* Dept. of Chemistry, Tufts University, Medford, MA 02155

Square wave anodic stripping voltammetry (SWASV) was conducted on iridium-based mercury ultramicroelectrode (Ir-based Hg-UME) to determine Pb in the neat seawater and drinking water by using standard addition method. Unlike commonly used Pt-based Hg-UME, iridium substrate did not form intermetallic compounds with analyte metals deposited into the Hg film during the preconcentration step. The excellent linear relationship between the Pb stripping current and concentration of Pb added to the samples was obtained without stirring or adding supporting electrolyte. The application of the Ir-based Hg-UME to SWASV provides a rapid, accurate, and sensitive electrochemical method for the determination of environmentally important heavy metals.

457 Modified Cottrell Behavior for Constant-Resistance Systems: *T. M. Nahir* and *R. P. Buck,* Dept. of Chemistry, University of North Carolina, Chapel Hill, NC 27599

Using a new boundary condition, the response to a potential step of diffusion-controlled electrochemical systems with significant bulk resistance is investigated. The numerical solution, digital simulation, and analytical approximation of the current-time plots under these circumstances are presented for finite thickness systems. Comparison of theoretical predictions with experimental results for the system of plasticized PVC membranes which contain valinomycin shows good agreement.

458 Electrochemical Measurements of the Effects of Ultrasound in Solution and at Surfaces: *H. Zhang, C. R. Smith,* and *L. A. Coury, Jr.,* Dept. of Chemistry, Duke University, P. M. Gross Laboratory, Durham, NC 27706-7706

Electrochemistry is utilized as a probe to determine the effects of ultrasonically induced cavitation in liquids and at solid-liquid interfaces. The functional form of the mass transport coefficient is explored through the observation of steady-state limiting currents under a variety of solution conditions. Effects on heterogeneous electron transfer rate are examined from Tafel plots. Observed changes in electrode surfaces in different chemical environments due to interfacial cavitation are also discussed.

459 Reduction of Pd(II) at a Mercury Electrode: *R. S. Rodgers,* EG&G Princeton Applied Research, Princeton, NJ 08543-2565

The reduction of Pd(II) in 1*M* NH_3, 1*M* NH_3NO_3 at a mercury electrode has been examined. Although the chronoamperometric, normal pulse polarographic, and cyclic staircase voltammetric data appear to agree with proposed mechanism for irreversible electron transfer, square wave voltammetry clearly reveals that the process is more complicated. Only upon fitting the NPP and CV data using the COOL algorithm do these techniques reveal evidence for a more complicated process.

460 Voltammetric Studies on the Formation and Reduction of Palladium Oxides in Alkaline Media: *I.-H. Yeo* and *M.-C. Jeong,* Dept. of Chemistry, Dongguk University, Seoul 100-715, Korea, *C. H. Pyun,* Solid State Chem. Laboratory, KIST, Seoul 136-791, Korea

The formation and stripping of palladium oxides in 0.1*M* LiOH solution were studied by cyclic voltammetry. The cyclic polarization method was used to form palladium oxides on the surface of the palladium electrode. It is considered that three different types of palladium oxides are formed in alkaline solution. A higher oxidation state of palladium oxide (PdO_3) can be formed (induced) on the surface of the electrode even at low anodic potential limit, 0.6 V. Strong evidence was observed that PdO_3 can only be formed in a specific potential range. From the voltammogram obtained after long cyclic polarization time the peak in the range of -0.47 to -0.60 V could be attributed to the reduction of the dehydrated PdO.

461 Amorphous Nickel Boride as an Electrocatalyst for the Hydrogen Evolution Reaction in Alkaline Solutions: *P. Los* and *A. Lasia,* Département de chimie, Université de Sherbrooke, Sherbrooke, Qué., Canada J1K 2R1

The hydrogen evolution reaction (HER) was studied on the electrodes obtained by pressing amorphous nickel boride and nickel powders. The structure and morphology of the electrodes were studied using x-ray diffraction and scanning electron microscopy. The mechanism and kinetics of the HER were investigated by steady-state polarization and the ac impedance techniques. An influence of the composition of nickel-nickel boride powder electrodes on the electrocatalytical activity was studied in 1*M* NaOH at 70°C.

462 *In Situ* X-Ray Diffraction Study of Prussian Blue Modified Electrode: *C. G. Chen* and *Z. Q. Huang,* Dept. of Applied Chemistry, Chongqing University, Chongqing 630044, China

Subtractive x-ray diffraction method with electrochemical modulation was used for an *in situ* study of the crystal structure change of Prussian blue modified electrode on platinum (PB/Pt). The different patterns measured are basically consistent with those calculated theoretically. Results have shown that the crystal skeleton (face-centered cubic) of PB/Pt has not been changed when K^+ goes into and out of the modified film in electrochemical reaction.

463 *In Situ* Ellipsometric Spectroscopy for Redox of Prussian Blue Films on Platinum Electrode: *S. F. Xie* and *Z. Q. Huang,* Dept. of Applied Chemistry, Chongqing University, Chongqing, 630044, China

This paper describes the ellipsometric spectroscopy with V_{op} - *E* spectra of redox for Prussian blue (PB) film on Pt. The purpose is to know how wide area is applicable by this new approach. Experimental results show that the peaks on V_{op} - *E* spectra could also characterize the redox of PB. It seems that spectroellipsometry is very sensitive for studying redox on very thin film.

464 New Aspect of Ellipsometry for Studying Redox in Electrochemistry: *Z. Q. Huang* and *S. F. Xie,* Dept. of Applied Chemistry, Chongqing University, Chongqing, 630044, China

After a review of application for ellipsometry, this paper points out that the model required for calculating film thickness and optical constant are the difficulty of ellipsometry. The authors suggested a new function V_{op}, and using V_{op} - *E* obtained some peaks on V_{op} - *E* spectra to characterize the reaction processes as the same as the cyclic voltammogram. This paper summarizes our experimental results.

MICROMORPHOLOGY IN ELECTROCRYSTALLIZATION

Physical Electrochemistry/Electrodeposition

465 Study of Unidirectional Crystallization of 1-D Quantum Conductors: *A. R. Hiuman, D. C. Loveday,* and *M. Heper,* School of Chemistry, University of Bristol, Bristol, England B58 1TS

Partially oxidized 1-D cyanoplatinate compounds are of interest because of their high and anisotropic electrical conductivities. The Pt atoms form "chains" with short metal-metal separations within the chain, effectively confining electron transport to one dimension. We describe the electrochemical synthesis and characterization of partially oxidized tetracyanoplatinate (POTCP) complexes. The electrochemical quartz crystal microbalance has been used to monitor the nucleation and growth processes of cation and anion deficient POTCP salts. Morphological characterization employed scanning electron microscopy.

466 Electrodeposition of Epitaxial Films of $Ag(Ag_3O_4)_2NO_3$: *B. E. Breyfogle* and *J. A. Switzer,* Graduate Center for Materials Research, University of Missouri-Rolla, Rolla, MO 65401

The conducting oxysalt $Ag(Ag_3O_4)_2NO_3$ has been electrodeposited on highly oriented conducting oxide substrates of Tl_2O_3 and $Pb_aTl_bO_c$. $Ag(Ag_3O_4)_2NO_3$ has an fcc Bravais lattice with four formula units per unit cell. It belongs to the cubic space group Fm3m with a = 0.989 nm. The orientation of the $Ag(Ag_3O_4)_2NO_3$ crystals with respect to the substrate surface was determined by x-ray diffraction. It was found that the cubic oxides Tl_2O_3 and $Pb_aTl_bO_c$ have a strong epitaxial influence on the cubic $Ag(Ag_3O_4)_2NO_3$ crystals.

467 *In Situ* Characterization of p-Type Copper Thiocyanate Films by Raman Spectroelectrochemistry: *Y. Son, N. R. de Tacconi,* and *K. Rajeshwar,* Dept. of Chemistry, The University of Texas, Arlington, TX 76019-0065

The anodic formation of copper thiocyanate films on Cu electrode in acidic KSCN solution was studied *in situ* by Raman spectroelectrochemistry. A restricted potential domain was used to promote nucleation and growth of copper thiocyanate and to avoid oxide formation. At -0.37 V (*vs.* Ag/AgCl reference) a sharp Raman band at 2172 cm^{-1} was assigned to the υ(CN) mode of a bridged structure of α-CuSCN. Another band at 2120 cm^{-1} at open-circuit peaks in intensity during the electroreduction of the α-CuSCN film. A mechanism including $(CuSCN)_z$ aggregates is proposed to explain the chemical and electrochemical behavior.

468 Electrochemical Architecture of Nanomodulated Tl-Pb-O Superlattices: *J. A. Switzer, R. J. Phillips,* and *R. P. Raffaelle,* University of Missouri-Rolla, Graduate Center for Materials Research, Rolla, MO 65401

Electrochemical deposition was used to produce superlattices based on the Tl-Pb-O system with layers as thin as 3 nm. The composition was modulated using square-wave current pulses. The oxides are degenerate semiconductors with a band-to-band transition in the 1.4-1.8 eV range, and a free-electron plasma edge in the near-IR. The oxides adopt a bcc bixbyite structure at low lead contents, but show the fcc fluorite structure for lead contents greater than about 35 atomic percent.

469 Electrosynthesis, Characterization, and Modeling of Highly Efficient Polypyrrole/Pt Nanocomposite Catalysts: *C. S. C. Bose,* C. C. Chen,* and *K. Rajeshwar,* Dept. of Chemistry, University of Texas, Arlington, TX 76019

Polypyrrole films containing nanometer-sized Pt particles (ppy/Pt) were electrosynthesized at glassy carbon and gold electrode surfaces. This was done either by voltammetric cycling between +0.95 and -0.80 V (*vs.* Ag/AgCl) or via a potential step technique in solutions containing colloidal Pt^0 particles. A chloroplatnate medium with a citrate reducing/protection agent was employed for generating the colloids.The growth of the ppy/Pt films was studied by combined voltammetry-electrochemical quartz crystal microgravimetry. These films exhibited unusually high catalytic activity towards the hydrogen evolution reaction and O_2 reduction. The rate does not saturate with increasing film thickness for these 3-D array of polymer confined-Pt^0 particles contrasting surface-confined catalyst situations. Finally, a model is presented for ppy/Pt based on hydrodynamic voltammetry data.

470 Electrodeposition of Metals on Polypyrrole Coated Au/Quartz Piezoelectrodes: *M. Hepel** and *S. Perkins,* Dept. of Chemistry, Potsdam College of SUNY, Potsdam, NY 13676, *T. Hepel,* ELCHEMA, Potsdam, NY 13676

Electrodeposition of various metals at polypyrrole (PPy) coated Au electrodes evaporated onto a quartz crystal have been investigated using the electrochemical quartz crystal microbalance (EQCM) and scanning electron microscopy (SEM). The effect of pH, type of anions, different organic additives, and the morphology of the polypyrrole substrate on the electrodeposition of Cu, Ni, Pb, Sn, and Cd have been studied. The nucleation density has been determined from SEM experiments and has been correlated with the current-time and frequency-time transients. The effect of ohmic potential drop in partially reduced PPy film has been taken into account in numerical simulation of the nucleation and growth processes.

471 Localized I/V and I/Z Measurements on Conductive Poly-n-methyl Pyrrole Thin Films Performed with a Scanning Tunneling Microscope: *S. Creager,* Dept. of Chemistry, Indiana University, Bloomington, IN 47405

Current *vs.* tip displacement measurements obtained on oxidatively doped poly-N-methyl pyrrole films reveal that the STM tip is buried up to 100 Å deep in polymer. STM images are very noisy, a consequence of the tip plowing through polymer while imaging. Current *vs.* bias potential measurements are interpreted in terms of an electric-field-driven electron hopping model of the electronic conductivity.

472 Factors Affecting Electrochemical Metallization of Insulating Substrates Precoated by Conducting Polymer Films: *F. A. Uribe, A.J. Rudge,* and *S. Gottesfeld,* Electronics Research, Los Alamos National Laboratory, Los Alamos, NM 87545

Chemically deposited conducting polymer (*e.g.*, polypyrrole) films have been used as a precoat for surface metallization of insulator materials. Metal electroplating onto thin conducting polymer films is discussed. Scanning electron microscopy and cyclic voltammetry show that Cu electrodeposition onto polypyrrole proceeds by a nucleation and an island dendritic growth mechanism. The electrochemical growth and propagation of Cu films on conducting polymers of various thickness, conductivities, and dopants are described. The effect of current densities and potentials on the same process is also discussed.

473 When Anodic Polymerization of Dibenzo-18-Crown-6 Leads to a New Artificial Membrane: Changes of Micromorphology Upon Different Modes of Doping: *J. Simonet, J.Rault-Berthelot, V Questaigne,* and *L. Angely,* Laboratoire d'Electrochimie, Universite de Rennes I, Campus de Beaulieu, 35042 Rennes Cedex, France

Dibenzocrown ethers lead by means of anodic oxidation to p-doped resins possessing the structure of polytriphenylenes. Great changes of structure (followed by conventional physical methods) can be obtained when reducing those resins. Their capability to extract (fast) certain inorganic cations from aqueous solutions is presented. Some use of those membranes are also discussed.

474 Formation and Removal of p-SnS Patterns and Characters on Transparent Conductive Oxide Glass by Mask-Defined Photoelectrodeposition and Dissolution: *R. D. Engelken, C. Brinkley, L. N. Chang,* and *L. Yu,* Dept. of Engineering, Arkansas State University, State University, AR 72467

We report formation of photomask delineated patterns/characters of orange-brown to gray SnS electrodeposited under illumination on In_2O_3:Sn glass cathodes. By electrodepositing at low currents (~10 $\mu A/cm^2$) at voltages just positive of the dark SnS reversible potential in the ethylene glycol/$SnCl_2$ solution, the electrode reaction is driven cathodic under illumination through mask openings but anodic in the dark regions blocked by the mask. This produces no deposition in the dark regions and SnS film "negatives" of/through the illuminated mask openings. The technique has potential as a means to form mask defined photoconductor patterns for optoelectronics, printing, memory, and imaging applications.

475 *In Situ* Studies of Shape Evolution during Copper Electrodeposition Using Atomic Force Microscopy: *R. M. Rynders* and *R. C. Alkire,* Dept. of Chemical Engineering, University of Illinois, Urbana, IL 61801

Electrodeposition of copper films with properties suitable for electronic applications requires use of organic additives to control the deposit morphology. An improved fundamental understanding of how additives influence the film structure is needed. The purpose of this work was to study the shape evolution of copper deposits in the presence of benzotriazole (BTA) by using *in situ* atomic force microscopy. Copper was deposited onto polycrystalline copper from 0.5*M* $CuSO_4$ in 1*N* H_2SO_4 with various BTA concentrations ranging from 0 to 1 mM. The crystalline growth in the absence of BTA and the amorphous growth in the presence of BTA was observed. When BTA was present, it was found that there was an effect from the imaging process that must be considered in the experimental procedure.

476 Electrochemical Behavior of an Amorphous Pd-Ni-Si Alloy in Aqueous Solutions: *A. Zhang* and *V. Birss,* Dept. of Chemistry, University of Calgary, Calgary, Alta., Canada T2N 1N4

In the present work, an amorphous $Pd_{35}Ni_{45}Si_{20}$ alloy was studied electrochemically in aqueous solutions. In alkaline solutions, both Ni and Pd oxide films can be formed on the alloy surface, with the Ni oxide characteristics being indicative of hydrous oxide film formation. In acidic solutions, Pd oxide is the principal surface product. Effort has also focused on the controlled modification of electrochemical properties of the alloy, *e.g.*, on the hydrogen adsorption/desorption and evolution reactions, particularly by controlling/altering the potential in various solutions.

477 Electrodeposition of Fe-Ni-Cr-P-C Alloys: *J.-C. Kang,* Mechanical Engineering and Energy Processes, Southern Illinois University, Carbondale, IL 62901, *C. A. Melendres,* Materials Science and Chemical Technology Div., Argonne National Laboratory, Argonne, IL 60439-4837, *S. B. Lalvani,* Mechanical Engineering and Energy Processes, Southern Illinois University, Carbondale, IL 62901

Amorphous alloys of Fe, Ni, Cr, P and C were prepared by electrodeposition from aqueous solutions and found to have excellent corrosion resistance in 0.9 w/o NaCl. The alloy composition, thickness and current efficiency for deposition for Fe-Ni-Cr-C, Fe-Ni-Cr-P, and Fe-Ni-Cr-P-C were determined as a function of the curent density. Addition of phosphorus was found to lower the cracking in the deposits. Crack-free Fe-Ni-Cr-P-C alloys were obtained.

478 Application of Pulse Current Process to Plated-Through-Holes: *A. S. Woodman, E. J. Taylor, N. R. K. Vilambi Reddy,* and *E. B. Anderson,* PSI Technology Co., 20 New England Business Center, Andover, MA 01810, *G. L. Fisher,* Shipley Co., Inc., Newton, MA 02162-1469

We investigated several rectangular current waveforms as applied to uniform through-hole plating. These waveforms included: cathodic pulse current, anodic pulse current, cathodic direct current followed by anodic direct current (DC-DC), cathodic direct current followed by anodic pulse current (DC-PC), cathodic pulse current followed by anodic pulse current (PC-PC), and pulse reverse current (PRC). These experiments were conducted in inorganic nonadditive baths. The most promising results were obtained using the PRC waveform.

479 Potential Step Probes of Epitaxial Growth in Electrodeposited Ceramic Superlattices: *R. J. Phillips, R. P. Raffaelle,* and *J. A. Switzer,* Graduate Center for Materials Research, University of Missouri-Rolla, Rolla, MO 65401

Epitaxy is the growth of crystals on a crystalline substrate that determines their orientation. Epitaxy between layers must be maintained for superlattice growth. This work focuses on the analysis of current time transients resulting from single potential steps as an *in situ* probe of epitaxy in the $Pb_aTl_bO_c$ mixed oxide superlattice system. A reduction in the induction time and elimination

of the growth segment of the transient results in an epitaxial film as demonstrated by x-ray diffraction.

480 Mass Sensitivity Mapping of the Quartz Crystal Microbalance in Liquid Media: *A. C. Hillier* and *M. D. Ward*, Dept. of Chemical Engineering and Materials Science, University of Minnesota, Minneapolis, MN 55455

The quartz crystal microbalance (QCM) utilizes the mass-frequency relationship of an oscillating AT-cut quartz resonator, consisting of a thin quartz wafer sandwiched between two excitation electrodes, to examine interfacial mass changes that occur at one of the excitation electrodes. Accurate application of the QCM as a mass sensor, particularly in the presence of nonuniform mass deposits, requires knowledge of the radial and angular dependence of the QCM mass sensitivity. The mass sensitivity distribution, $S(r, \theta)$, was determined for plano-plano and plano-convex AT-cut quartz resonators *in situ* using scanning electrochemical methods. Complete closed form mathematical descriptions of $S(r, \theta)$ were obtained under conditions typically encountered in QCM experiments. Results illustrate the influence of crystal contouring and the extent of field fringing on the mass sensitivity distribution.

481 Electrochemical Preparation of Platinum Nanoparticules: *R. Durand* and *K. Louhab*, Crem-GP, Enseeg, 38402 Saint-Martin d'Heres, France

Electrochemical nucleation and growth of platinum particles in the nanometer range have been studied on various substrates (graphite plates, carbon fibers, and powders) with short potentiostatic (or galvanostatic) pulses, from $PtCl_6^{2-}$ and $Pt(NH_3)_4^{2+}$ solutions. The processes were characterized by TEM, STM, and transient recording. The nucleation is progressive or instantaneous, depending on potentials and activations. We demonstrate that electrochemical deposition of nanoparticles inside preformed volumic electrodes is one of the most Pt-saving preparation of fuel cell electrodes.

EIGHTH INTERNATIONAL SYMPOSIUM ON MOLTEN SALTS

Physical Electrochemistry/High Temperature Materials

482 On Charging Palladium in an Al/LiCl-KCl Eutectic, Excess LiH(D)/Pd Cell: *B. Y. Liaw* and *P.-l. Tao*, Hawaii Natural Energy Institute, School of Ocean Earth Science and Technology, University of Hawaii, Honolulu, HI 96822, *B. E. Liebert*, Dept. of Mechanical Engineering, College of Engineering, University of Hawaii, Honolulu, HI 96822

An anomalous heat effect was found during high-current-density charging of an Al|LiCl-KCl eutectic with excess LiD|Pd cell at elevated temperatures. The principle regarding electrochemical and calorimetric behavior of this molten salt approach is presented. The thermochemical aspects of the reactions at each charging stage are discussed to seek a possible explanation for the anomalous heat. We were unable to identify any conclusive chemical nature of the anomalous phenomenon. The phenomenon is quite irreproducible, because of several materials problems and the lack of understanding of the predominant electrochemical reactions during the excess power excursion.

483 Structure of Molten Iron Chloride: *D. L. Price* and *M.-L. Saboungi*, Materials Science Div., Argonne National Laboratory, Argonne, IL 60439, *S. C. Moss*, Dept. of Physics, University of Houston, Houston, TX 77004, *S. Hashimoto*, Institute for Materials Research, Tohoku University, Sendai 980, Japan

The structure of molten $FeCl_3$ at 320°C has been measured with neutron diffraction at the intense pulsed neutron source. After subtraction of the paramagnetic scattering, the structure factor exhibits a three-peak structure with a first sharp diffraction peak at wave vector $Q = 1.0$ Å^{-1}. The first peak in the radial distribution function can be fitted by two gaussians centered at 2.17 and 2.32 Å, slightly larger than the two Fe-Cl distances observed for Fe_2Cl_6 molecules in the vapor. The results indicate that melting in $FeCl_3$, associated with a large (63%) volume change, is accompanied by a change in local structure from the octahedral environment of the Fe^{3+} in the solid to an Fe_2Cl_6 molecular liquid. (This work was performed under the auspices of the U.S. Department of Energy, Division of Materials Science, Office of Basic Energy Sciences, under Contract W-31-109-ENG-38.)

484 Electronic Conduction in Molten KBr-K Solutions: *G. M. Haarberg*, Laboratories of Industrial Electrochemistry, University of Trondheim, 7034 Trondheim, Norway, *J. J. Egan*, Brookhaven National Laboratory, Upton, NY 11973

The electronic conductivity of molten KBr-K solutions was determined as a function of the activity of potassium at various temperatures by using the Wagner polarization technique. The diffusion coefficient of electrons was obtained from potential step measurements. The concentration of defects in the salt was calculated as a function of the K activity by applying a thermodynamic model.

485 Electronic Polarizabilities of LiCl-CsCl, LiI-KI, and LiI-CsI Bindry Melts: *M. Endo*, *Z. Hongmin*, *Y. Sato*, and *T. Yamamura*, Dept. of Metallurgy, Faculty of Engineering, Tohoku University, Sendai 980, Japan

Refractive indexes and densities of LiCl-CsCl, LiI-KI, and LiI-CsI binary melts have been measured. The electronic polarizabilities of the melts have been determined from the measured refractive indexes and densities by the Clausius-Mossotti equation. The correlation between the electronic polarizability and the structure of the salts has been examined. The electronic polarizabilities of the melts have the positive temperature dependence and those of the binary melts negatively deviate from the additive rule. Factors which affect the electronic polarizabilities of the melts have been investigated.

486 Computer Assisted Data Acquisition and Analyses of Brillouin Spectra of $ZnCl_2$ Single and $ZnCl_2$-NaCl Binary Melts: *Z. Hongmin*, *Y. Sato*, *T. Yamamura*, and *K. Sugimoto*, Dept. of Metallurgy, Faculty of Engineering, Tohoku University, Sendai, Japan

Brillouin scattering experiment has been carried out for single $ZnCl_2$ and $ZnCl_2$-NaCl binary melts. The sample used was carefully refined to avoid the spikes caused by inclusion. Brillouin spectra were obtained at scattering angles of 45, 90, and 140°, over full frequency range. The spectra were found to be nonLorentzian, indicating the presence of the relaxation of the sound wave propagation. The spectra obtained by a computer assisted retrieval system were analyzed on the basis of a single relaxation theory. The sound velocities at low and high frequencies, and the relaxation time, were determined.

487 Preparation, Vapor Pressure, and Thermochemistry of Tin(II) Bromide: *T. R. Brumleve* and *S. R. Walston*, APL Engineered Materials, Inc., Urbana, IL 61801, *S. A. Mucklejohn* and *N. W. O'Brien*, GE Thorn Lamps Ltd., Lamp Research, Leicester, England LE4 7PD

The synthesis of high-purity tin(II) bromide from the elements is outlined. The vapor pressure of liquid $SnBr_2$ from 576 to 923 K is measured by the quasi-static method. Previous Knudsen effusion mass spectrometric studies are reviewed. A critical evaluation of the literature values for melting temperature and enthalpy of fusion is presented. The molar heat capacities of $SnBr_2$(s) and $SnBr_2$(l) are evaluated, and an expression for the molar heat capacity of $SnBr_2$(g) is derived from spectroscopic constants and structural data. A complete set of thermochemical data useful in the modeling of discharge arcs containing $SnBr_2$ is derived from the vapor pressure measurements.

488 Development of Raman Spectroscopic Sensors for the Determination of Magnesium in a Molten Salt System: *G. Mamantov* and *S. Dai*, Dept. of Chemistry, University of Tennessee, Knoxville, TN 37996-1600, *G. M. Begun*, Chemistry Div., Oak Ridge National Laboratory, Oak Ridge, TN 37831, *J. P. Young*, Analytical Chemistry Div., Oak Ridge National Laboratory, Oak Ridge, TN 37831, *J. E. Coffield*, Dept. of Chemistry, University of Tennessee, Knoxville, TN 37996-1600

A study of the Raman spectra of the soluble magnesium species in melts such as NaCl-KCl-$CaCl_2$ (41-41-18 m/o) has been carried out. Over the range of 0-25 m/o $MgCl_2$ in NaCl-KCl-$CaCl_2$ at 700°C, the intensity of the $MgCl_4^{2-}$ Raman band near 250 cm^{-1} was found to vary linearly with Mg(II) concentration. A new normalization procedure has been developed to generate these results. An all silica fiberoptic probe has also been developed to carry out these measurements. Details of these studies are discussed.

489 Structural Properties of Zinc Halide Melts: *E. A. Pavlatou* and *G. N. Papatheodorou*, Institute of Chemical Engineering and High Temperature Chemical Processes and Dept. of Chemical Engineering, University of Patras, GR 261 10 Patras, Greece

Vibrational Raman spectroscopy has been used to identify and determine the structure of species formed in $ZnCl_2$, $ZnBr_2$ and in the binary mixtures ACl-$ZnCl_2$ (A = Cs,Li) and $ZnCl_2$-$ZnBr_2$. The data indicate that the network-like structure of the zinc halide melts breaks up with the addition of alkali metal halide and with increasing temperature. The tetrahedral structure around the Zn is preserved but one, two, three, or four "terminal" halogen atoms having A$^+$ as nearest neighbors are formed.

490 Structural Investigation of Molten Lithium Bromide: *S. Itoh*, The Nishi-Tokyo University, Uenohara, Kitatsurugun, Yamanashi 409-01, Japan

The structural properties of molten LiBr were investigated by the molecular dynamics simulation method. The temperature dependence of the partial pair distribution functions, the distribution of the coordination numbers, the angular distribution functions were examined at 850, 1000, 1200, and 1500 K. On increasing the temperature, the first peak position and the second peak position of the g(r) of the Li and Br interaction shift to shorter distance and longer distance, respectively.

491 Use of Raman Spectroscopy for Determining the Corrosion of Ceramics in Molten Fluorides: *C. G. Kontoyannis* and *N. S. Tziafos*, Institute of Chemical Engineering and High Temperature Chemical Processes, GR 261 10 Patras, Greece

Laser Raman spectroscopy was employed in a semi-quantitative way in order to probe the changes caused in the crystal structure of partially and fully stabilized zirconia ceramics after their immersion in the abrasive environment of molten LiF, NaF, KF(FLINAK) eutectic for different periods of time. From the test-

ed ceramics, ZrO_2-8 m/o Y_2O_3 exhibits the best resistance to the corrosive influence of molten FLINAK.

492 Raman and Infrared Spectroscopic Studies of the Platinum Electrode-Molten Nitrates Interface: *M. M. Gaphurov*, Institute of Physics, Academy of Science of the USSR, 367003, Makhachkale, USSR, *V. D. Prisyaznhyi*, Institute of General and Inorganic Chemistry, 252601, Kiev, USSR

We present the results of the Raman and reflectance-absorbance infrared spectroscopy (RAIRS) study of the molten lithium, sodium, and potassium nitrates-platinum electrode interface. The constructions of the high temperature spectroelectrochemical cells which are used for obtain vibrational spectra of interfacial species are described. The variations of the nitrate ion NO_3^- internal vibrational spectra upon change in the electrode potential have been investigated.

493 Selective Precipitation of Oxide Superconductors from Molten Hydroxide and Molten Nitrate: *A. M. Stacey, S. L. Stoll, L. N. Marquez*, and *S. W. Keller*, Dept. of Chemistry, University of California, Berkeley, CA 94720

Copper and bismuth oxide superconductors generally have been prepared by solid-state reactions at temperatures above 800°C. Unfortunately, there are many disadvantages with the use of solid-state reactions, several of which are especially detrimental to the performance of the oxide superconductors. Here we report the synthesis of three classes of oxide superconductors by selective precipitation from molten salts at substantially lower temperatures than have been reported previously. Specifically, $La_{2-x}M_xCuO_4$ (M = Na, K) and $EuBa_2Cu_3O_7$ were precipitated from molten NaOH and/or KOH at 320 and 450°C, respectively, and $Ba_{1-x}K_xBiO_3$ was obtained from molten alkali metal nitrates at 260°C.

494 A New Series of Complex Metal Oxides: Crystallization of AB_3MO_8 (A = Na, Li: B = Ba, Sr; M = Bi, Sb) from Hydroxide Melts: *V. A. Carlson* and *A. M. Stacy*, Dept. of Chemistry, University of California, Berkeley, CA 94720

Molten hydroxides are excellent solvents for the synthesis of new complex metal oxides. Five new materials with the structure type AB_3MO_8 ($NaBa_3BiO_8$, $NaSr_3BiO_8$, $LiSr_3BiO_8$, $NaSr_3SbO_8$, and $LiSr_3SbO_8$) have been crystallized from mixtures of alkali and alkaline earth metal hydroxides at 550°C. In this paper we discuss the synthetic method, as well as the crystal structure and properties of these highly oxidized products.

495 Investigation of a Molten Salt Extraction/Electrolysis Process for Converting Ilmenite to Iron and a High Grade TiO_2 Feedstock: *K. J. Leary*, E. I. du Pont de Nemours & Co., Inc., DuPont Chemicals, Iler Research Center, New Johnsonville, TN 37134

The feasibility of using a molten salt extraction/electrolysis process to convert ilmenite ore to a high grade TiO_2 feedstock and a salable iron product was investigated. Several salt systems were examined, including LiCl-KCl, NaOH-KOH, $LiBO_2$-KBO_2, and LiCl-KCl-$LiBO_2$. It has been demonstrated that iron oxide can be extracted from ilmenite and converted to metallic iron at the cathode and CO/CO_2 at a carbon anode.

496 New Principles for the Processing of Carnallitites in the Domain of Molten Salt Hydrates: *H.-H. Emons*, Central Institute for Inorganic Chemistry, Berlin-Adlershof, Germany, *T. Fanghanel*, Nuclear Research Center, Karlsruhe, Germany

Based on the phase diagram of KCl-$MgCl_2$-H_2O (up to 250°C) and structural models of molten salt hydrates, new principles for the processing of carnallitites are discussed. Basic ideas are the recovery of KCl and $MgCl_2 \cdot 4H_2O$ from carnallite via corresponding molten hydrates as well as the direct separation of a magnesium chloride hydrate from complex mixtures. Despite the increased temperature range, all stages of the process are realized at pressures below or equal to 0.1 MPa.

497 Molten Carbonate Fuel Cell Reaction Mechanisms: *K. Hemmes, R. C. Makkus, R. Weewer*, and *J. H. W. de Wit*, Delft University of Technology, Faculty of Chemical Technology and Materials Science, Laboratory of Materials Science, Div. of Corrosion Technology and Electrochemistry, 2628 AL Delft, The Netherlands

An overview is presented of our research on the reaction mechanisms in a molten carbonate fuel cell of the last four years. Chronoamperometry and impedance measurements were performed on gold, Ni, and Cu flag electrodes in a half-cell setup and on porous anodes and cathodes in a small laboratory-scale fuel cell. The gas composition was varied over a wide range to determine the reaction orders accurately. The research is described in detail in two theses.

498 IMHEX® Molten Carbonate Fuel Cell Program Status: *G. L. Reznikov* and *R. Donelson*, M-C Power Corp., Burr Ridge, IL 60521

The results of MCFC component development and a 70-cell internally manifolded (IMHEX®) subscale (1000 cm^2) stack test are reported. The test confirmed "stackability" and the absence of carbonate migration in IMHEX® MCFC stacks. Specific power 103 mW/cm^2 was obtained at current density 160 mA/cm^2 and 75% fuel utilization. The stack operated 1500 h with average power output of 5.5 kW. Maximum stack power exceeded 9.0 kW. A 20 kW full-area (1 m^2) stack will be tested in the beginning of 1992.

499 A Comparative Study of Electrochemical Systems of Oxygen in Molten Alkaline Carbonates at 500-750°C: *J. Devynck, G. Moutiers, M. Cassir*, and *B. Tremillon*, Laboratoire d'Electrochimie, Ecole Nationale Supérieure de Chimie de Paris, F75231 Paris Cedex 05, France

Electrochemical properties of oxygen species have been studied in molten sodium-potassium-lithium carbonates between 500 and 750°C by means of voltammetry and other electrochemical techniques at gold electrodes. Relative stability of the reduced forms: peroxide and superoxide was examined as a function of the alkaline cations and of the oxoacidity of the media. The solubility of alkaline oxides and peroxides was determined. Experimental values are compared with theoretical results calculated from thermochemical data. The choice of suitable media for applications in catalytic oxidations is discussed.

500 High Temperature Corrosion of Nickel Coated with Molten Alkali Carbonates: *K.-i. Oto,* B.-u. Kim, H. Yoshitake*, and *N. Kamiya*, Dept. of Energy Engineering, Yokohama National University, 156 Tokiwadai, Hodogaya-ku, Yokohama 240, Japan

The high temperature corrosion of nickel with molten alkali carbonate coating has been studied in CO_2/O_2 atmosphere. The reaction obeyed the parabolic rate law except the low pressure of CO_2 at 1073 K with $(Li_{0.62}K_{0.38})_2CO_3$ coating. The parabolic rate constant decreased with the increase of temperature at $P_{CO_2} = 0.66$ atm with $(Li_{0.62}K_{0.38})_2CO_3$ coating. The accelerated oxidation was observed at low pressures of CO_2 at 1073 K. These results were affected by the solubility of NiO that was formed on the metal.

501 Galvanic Corrosion of Coupled Pt-Ni System in Molten Na_2CO_3 at 1173 K: *Y. Shinata* and *M. Hara*, Mining College, Akita University, 1-1 Tegata Gakuen-Cho, Akita 010, Japan, *S. Hashimoto*, TDK Co. Ltd., 1-13-1 Nihonbashi, Chuo-Ku, Tokyo 103, Japan

To discuss corrosion mechanism of metals in molten Na_2CO_3 at high temperature, galvanic corrosion behavior of Pt and Ni electrodes was examined at 1173 K in flowing Ar, CO_2, and O_2 gases. In Ar atmosphere, there was little corrosion. In CO_2, a little mass-loss of Ni with NiO formation was observed. Whereas in O_2, mass-gain of Ni anode by oxide formation and severe corrosion of Pt cathode were observed.

502 Development of Cathodes for an Aluminum-Chlorine Fuel Cell in High Temperature Chloride Melts: *T. Ishikawa, T. Sasaki*, and *S. Konda*, Dept. of Metallurgical Engineering, Faculty of Engineering, Hokkaido University, Sapporo 060, Japan

An aluminum-chlorine fuel cell to be used in the production of high-purity aluminum from scrap aluminum is proposed. The output voltage drop due to the chlorine reduction reaction of the fuel cell was investigated in a mixture of $MgCl_2$ 25 m/o NaCl 75 m/o by using various electrodes with different hole sizes and numbers. The reaction resistance decreased with the decrease in hole diameter and had minimum values when the hole size was about 3 mm.

503 Application of Molten Salts in Pyrochemical Processing of Reactive Metals: *B. Mishra* and *D. L. Olson*, Dept. of Metallurgical and Materials Engineering, Colorado School of Mines, Golden, CO 80401, *W. A. Averill*, EG&G Rocky Flats, Inc., Rocky Flats Plant, Golden, CO 80402

Various mixes of chloride and fluoride salts are used as the media for conducting pyrochemical processes in the production and purification of reactive metals. These processes generate a significant amount of contaminated waste that has to be treated for recycling or disposal. Molten calcium chloride based salt systems have been used in this work to regenerate calcium metal for the *in situ* reduction of reactive metal oxides. The recovery of calcium is characterized by the process efficiency to overcome back reactions in the electrowinning cell. However, it has been possible to potentially combine the two processes of reduction and electrowinning. Theoretical treatment of the reaction rates has been presented to determine the temperature and current density for the combined process which must be maintained to carry out the *in situ* reduction of metal oxides by the electrowon calcium. The formation and behavior of double layers adjacent to the electrodes has also been analyzed.

504 Investigations at Los Alamos National Laboratory of Calcium Chloride Based Molten Salts Systems: *S. D. Ownes, K. M. Axler*, and *G. D. Bird*, Los Alamos National Laboratory, Los Alamos, NM 87545, *G. L. DePoorter*, Colorado School of Mines, Metallurgy Dept., Golden, CO 80401

Calcium chloride has been in service as a media for the reduction of plutonium oxide to metal and for the molten salt extraction of americium from aged plutonium metal. To provide data for the optimization of plutonium oxide reduction, the solubility of calcium metal has been measured in solutions comprised of varying amounts of calcium oxide in calcium chloride. Additionally, recent work has demonstrated the viability of calcium chloride as an electrolyte for plutonium electrorefining.

505 Voltammetric Study of a Planar Electrode with Supermeniscus Film in Molten Carbonate: *G. L. Lee* and *J. R. Selman*, Dept. of Chemical Engineering, Illinois Institute of Technology, Chicago, IL 60616

Cyclic voltammetry with a variable scan window was applied to study the mechanism of oxygen reduction at a flag electrode in molten carbonate. To account for the effect of supermeniscus film formation, a modeling approach was combined with oxide addition and linear potential scanning at a wire electrode. Characteristic peaks are observed in the -0.3 to -0.5 V range, which are due to a different reaction (most likely the reduction of superoxide) than that producing CV peaks at -0.1 to -0.3 V.

506 Material-Deposition Processes in the Separator of Li-Alloy/Fe/S_2 Thermal Cells: *M. C. Hash* and J. A. Smaga*, Electrochemical Technology Div., Argonne National Laboratory, Argonne, IL 60439, *R. A. Guidotti* and *F. W. Reinhardt*, Battery Development Div., Sandia National Laboratories, Albuquerque, NM 87185-5800

The deposition of Li_2S and Fe in the separator layer of Li-alloy/FeS_2 thermal cells during discharge was studied. The parameters having the most impact included: anode activity, catholyte treatment (fused *vs.* unfused, lithiated *vs.* unlithiated), and electrolyte composition. The quenched cells were subjected to detailed postmortem examination by optical microscopy to measure the distribution and amount of deposition products in the separator layer. Complementary examination of select cells was also conducted using scanning electron microscopy and energy dispersive spectroscopy.

507 Performance of a Sodium/Selenium(IV) Molten Chloroaluminate Cell for an Electric Vehicle: *M. Matsunaga, M. Morimitsu, G. Mori, S. Obata, T. Kitazaki*, and *K. Hosokawa*, Dept. of Applied Chemistry, Faculty of Engineering, Kyushu Institute of Technology, 1-1 Sensui-cho, Tobata, Kitakyushu 804, Japan

The discharging behavior of Nb/β"-alumina/Se(IV) in a basic $AlCl_3$-NaCl melt has been studied to develop the new battery for an electric vehicle. This cell shows the quick response to high current pulses even at 160°C. The resistivity of this cell was improved to be 3.8 Ω · cm^2-β" at 200°C. The current distribution in the positive current collector is also discussed.

508 The Modification of Flemion Membranes for Use in Energy Generating Devices: *D. S. Newman,** Dept. of Chemistry, Bowling Green State University, Bowling Green, OH 43403, *S. Li*, Dept. of Pharmaceutical Chemistry, Kansas, Lawrence, KS 66045, *T. Howard*, Dept. of Chemistry, Morehead State University, Morehead, KY 41465

Flemion is a perfluorocarboxylated polymer, somewhat similar to Nafion, which allows Na^+ ions to pass through it while excluding OH and Cl ions. This membrane was modified by first converting the carboxyllic ester to an acyl group and then acylating dibenzo-18-cr-6 using the ambient temperature molten salt pyridinium heptachloroaluminate as the Friedel-Crafts catalyst. Crown ether containing Flemion was complexed with LiCl forming an electrolyte with a Cl ion transference number of 0.39 and a Li^+ transference number of 0.61.

509 Molten Salt Regular Mixture Theory Applied to Ion Exchange Membranes: *K. S. Forland* and *S. K. Ratkje*, Div. of Physical Chemistry, Norwegian Institute of Technology, N-7034 Trondheim-NTH, Norway, *T. Okada*, Industrial Products Research Institute, 1-1-4 Higashi, Tsukuba, Ibaraki 305, Japan

Ion exchange membranes are increasingly important in chemical technology. We show that membranes can be compared to mixtures of molten salts. Exchange equilibria between a cation exchange membrane and an aqueous solution of two alkali salts were studied. When the difference in cation size is small, the membrane behavior is nearly ideal. For larger differences, the membrane is described as a regular mixture. A new method for analysis of data gave thermodynamic values, *e.g.*, activity coefficients.

510 Theory of Thermocells: Transported Entropies and Heat of Transfer in Ag_2SO_4-Li_2SO_4: *A. Grimstvedt* and *S. K. Ratkje*, Div. of Physical Chemistry, Norwegian Institute of Technology, N-7034 Trondheim-NTH, Norway

New expressions for determination of thermoelectric powers from thermopotential measurements are presented. These expressions include the transported entropies variation with temperature (Thomson effects). Transported entropies and heats of transfer are calculated from thermopotential measurements in the nonisothermal cell $Ag(T_1)|Ag_2SO_4$-$Li_2SO_4|Ag(T_2)$. Models for transported entropies and heats of transfer are discussed and compared with experimental results.

511 The Nature of Proton in Ambient-Temperature Chloroaluminate Molten Salts: *R. A. Osteryoung*, Dept. of Chemistry, State University of New York at Buffalo, Buffalo, NY 14214, *P. C. Trulove*, Frank J. Seiler Research Laboratory, U.S. Air Force Academy, CO 80840

Proton is an ubiquitous contaminant in ambient-temperature molten salts composed of mixtures of aluminum chloride and 1-ethyl-3-methylimidazolium chloride (ImCl). FTIR, NMR, and electrochemistry have been used to study the nature of proton in these ionic liquids. In oxide-free basic melts (excess ImCl) there exist two forms of proton, HCl and HCl_2^-, in equilibrium, while in acidic melts (excess $AlCl_3$) only HCl is present. Implications of this composition dependent proton speciation with respect to proton chemistry and melt purification are discussed.

512 The Chemistry of Proton in Ambient-Temperature Chloroaluminate Molten Salts: *P. C. Trulove*, Frank J. Seiler Research Laboratory, U.S. Air Force Academy CO, 80840, *R. A. Osteryoung*, Dept. of Chemistry, State University of New York at Buffalo, Buffalo, NY 14214

In basic molten salts composed of aluminum chloride and 1-ethyl-3-methylimidazolium chloride, proton is partitioned between HCl and HCl_2^-. The equilibrium between these two species was studied using ^2H and ^1H NMR and values for the equilibrium constant at various temperatures and the heat of reaction were obtained. In acidic melts proton is a Brønsted superacid which exists primarily as HCl. ^2H NMR and FT-IR were used to show that ^2HCl in the acidic melts exchanges rapidly with the imidazolium cation ring hydrogens at the 4,5 position. The kinetics of this exchange have been examined with respect to changes in the acidic melt composition.

513 Ionic Equilibria in Ambient Temperature Molten Salts: *J. L. E. Campbell** and *K. E. Johnson*, Dept. of Chemistry, University of Regina, Regina, Saskatchewan, Canada S4S 0A2

$ImHCl_2$ ($0.38 < X_{HCl} < 0.67$) and $ImAlCl_4$ ($0.33 < X_{AlCl_3} < 0.67$) ionic liquids (IM ≡ 1-ethyl-3-methyl-1H-imidazolium) have been investigated by 200 MHz ^1H-NMR spectroscopy. It is widely believed that the protic species formed upon addition of HCl to these liquids, is the hydrogen dichloride anion, HCl_2^-. Our investigations, however, indicate the presence of other protic species in significant quantities. Molecular HCl does not contribute significantly to the total HCl content of these liquids. The probable identity of the protic species present in acidic chloraluminate melts has been determined and the equilibrium constants governing the concentrations of protic species in $ImHCl_2$ and $ImAlCl_4$ liquids have been evaluated.

514 Dual Spin Probe NMR Relaxation Studies of Microdynamics in Chloroaluminate Melts: *W. R. Carper* C. E. Keller*, and *P. A. Shaw*, Dept. of Chemistry, Wichita State University, Wichita, Kansas 67208, *M. Parrish* and *J. S. Wilkes*, Frank J. Seiler Research Laboratory, USAF Academy, CO 80840-6528

The microdynamics of room temperature chloroaluminate melts consisting of 1-methyl-3-ethylimidazolium chloride (MEICl), $AlCl_3$ and $EtAlCl_2$ has been investigated by ^{13}C and ^{27}Al NMR relaxation methods over the temperature range of 0-70°C. These studies support the existence of $EtAl_2Cl_6^-$ species in addition to $AlCl_4^-$ and other complex ions. The dual spin probe method (DSP) has been used to establish the existence of interactions between $EtAlCl_2$ and MEICl and to determine the liquid state quadrupolar coupling constant (QCC) for $EtAlCl_2$ and $AlCl_4^-$ in various melt compositions. Determination of the QCC as a function of melt composition provides information concerning the symmetry of these complex species.

515 NMR Measurements in Solutions of Dialkylimidazolium Haloaluminates: *S. Takahashi, J. Rathke*, and *M.-L. Saboungi*, Argonne National Laboratory, Argonne, IL 60439

Measurements of ^{27}Al and ^{35}Cl NMR spectra were carried out on different compositions of $AlCl_3$-EMIC solutions ranging from basic to acidic regime. The temperature was varied to improve the resolution of ^{35}Cl spectra and to gain a better understanding of the kinetics of the exchange reactions. At room temperature, for each of the 46, 50, 60, 67 m/o $AlCl_3$, only one ^{27}Al resonance was observed. At 50 m/o $AlCl_3$ mixture, only one ^{35}Cl resonance was obtained, while another ^{35}Cl resonance appeared with increasing $AlCl_3$ for acidic melts.

516 The Electrochemistry of Aluminum and Protons in Room Temperature Chloroaluminate Molten Salts Buffered with Sodium Chloride: *T. L. Riechel* and *J. S. Wilkes*, The Frank J. Seiler Research Laboratory, United States Air Force Academy, USAF Academy, CO 80840-6528

Lewis neutral room temperature chloroaluminate molten salts made by mixing 1-methyl-3-ethyl-imidazolium chloride (MEIC) and aluminum chloride are being investigated as battery electrolytes because of their wide voltage windows, about 4.4 V. To maintain this voltage window, the electrolyte must be Lewis buffered by NaCl. In this paper we present a detailed investigation of the electrochemistry of NaCl-buffered MEICl/$AlCl_3$ melts at W and Pt electrodes. Based on the electrochemistry and SEM examination of the electrode surfaces, it appears that when a melt is buffered with NaCl, it remains slightly Lewis acidic, and Al can be plated and stripped from these electrodes. At a Pt electrode, residual protons are also active. The currents resulting from these processes are small, and do not limit the voltage widow of the electrolyte, but may result in unwanted side reactions in an operating battery.

517 Reduction Potentials for Lithium and Sodium in Ambient-Temperature Chloroaluminate Molten Salts: *R. T. Carlin* and *C. Scodilis-Kelley*, Dept. of Chemistry, University of Alabama, Tuscaloosa, AL 35487

By adding protons to a LiCl buffered neutral $AlCl_3$:MEIC (1-methyl-3-ethylimidazolium chloride) molten salt, elemental lithium can be deposited and stripped at a tungsten microelectrode. By measuring the open-circuit potential of lithium deposited from melts having different Li^+ concentrations, the standard reduction potential for the Li^+/Li couple was determined to be -2.074 (±0.010) V (*vs.* Al(III)/Al). By employing proton-containing buffered neutral $AlCl_3$:DMPIC (1,2-dimethyl-3-propylimidazolium chloride) melts, both lithium and sodium can be deposited and stripped well within the electrochemical window. Lithium and sodium deposits in the DMPIC melt system exhibit open-circuit potentials of -2.106 and -2.107 V, respectively. *In situ* optical studies confirm the deposition of elemental lithium and sodium which are stable in the melts for several minutes.

518 Physico-Chemical Behavior and Liquid Crystalline Properties of Molten Alkali Metal Alkanoates: *T. A. Mirnaya* and S. V. Volkov*, Institute of General and Inorganic Chemistry, 32-34 Prospect Palladina, 252680 Kiev-142, Ukraine

The electrical conductivity, ionic mesophase stability, and ^1H NMR spectra of binary molten alkali metal n-alkanoate systems with common anion are discussed in connection with their phase diagrams. As increasing the difference in radii of uncommon cations of the melts it is found: (*i*) increasing of physico-chemical properties deviations from additivity, (*ii*) enhancement of tendencies to ion associate formation, and (*iii*) enhancement of the reciprocal orientational ordering of n-alkanoate anions along their main axes of symmetry. Elongation of the n-alkanoate anion chain gives rise to enhancement of ion association and ordering and promotes liquid crystal formation in the salt melts.

519 Low Temperature Molten Salt Electrolytes Based on Quaternary Alkylphosphonium Salts: *G. E. Blomgren*, and *S. D. Jones*, Eveready Battery Co., Inc., Technology Laboratory, Westlake, OH 44145

A new room temperature molten salt comprised of a 1:2 mixture of quaternary alkylphosphonium chloride and aluminum chloride has been discovered. Formation of a room temperature melt was unexpected due to the high melting point of tetramethylphosphonium chloride and the absence of an inversion vibration. The melt has good conductivity and also has higher stability toward electrochemical reduction than any previously studied room temperature melt. Aluminum metal can be reversibly plated and stripped from the melt.

520 New, Stable, Ambient-Temperature Molten Salts: *E. I. Cooper* and *E. J. M. O'Sullivan*, IBM, T.J. Watson Research Center, Yorktown Heights, NY 10598

New ambient-temperature organic molten salts are described. They are easily prepared (usually in one step) and consist of alkyl-substituted aromatic heterocyclic cations and triflate or methanesulfonate anions. For example, 1-ethyl-3-methylimidazolium trifluoromethanesulfonate melts at ≈-10°C, σ = 0.0093 S/cm at 25°, and loses <2 w/o at 350°C in N_2. Interesting differences between triflates and methanesulfonates are discussed. The thermal and chemical stability, wide "electrochemical window" and good conductivity of the new salts make them promising electrolytes and antistats.

521 Mixed Chloroborate and Chloroaluminate Room Temperature Melts: *R. J. Gale* and *J. Liu*, Dept. of Chemistry, Louisiana State University, Baton Rouge, LA 70803

Tetrachloroborate salts of *n*-butylpyridinium or methyl-3-ethyl imidazolium chloride are known to be viscous melts at room temperature. It is of interest for battery electrolyte development to see if mixed chloroaluminate/chloroborate systems might be useful for reversible Al deposition, and if mixed complex species of type $[BAlCl_7]^-$ form, since boron compounds would minimize electrolyte density. Our studies indicate, however, that addition of Al_2Cl_6 to a tetrachloroborate melt tends to displace volatile BCl_3, although an excess of the Lewis acid Al_2Cl_6 seemed to permit reduction of boron species. Aluminum generally bonds more strongly to chlorine then boron does, and thus Al species are likely to be the stronger Lewis acids.

522 Electrochemistry of 9,10-Anthraquinone in the Presence of Proton and Tetrachloroaluminate in Ambient Temperature Molten Salts: *M. T. Carter* and *R. A. Osteryoung*, Dept. of Chemistry, State University of New York at Buffalo, Buffalo, NY 14214

The electrochemistry of 9,10-anthraquinone (AQ) in a basic room-temperature molten salt composed of $AlCl_3$ mixed with 1-ethyl-3-methylimidazolium chloride (ImCl) is described. AQ is reduced via a quasi-reversible two electron transfer to $AQ(AlCl_3)_2^{2-}$ in the absence of a proton source. Addition of proton as imidazolium hydrogen dichloride ($ImHCl_2$) causes the reactions coupled to electron transfer to shift from solvent leveling of reduced AQ by $AlCl_4^-$ to more facile protonations. The hydroquinone formed, AQH_2, is unstable in the $AlCl_3$:ImCl melt, but is stable on the voltammetric time scale in neat $ImHCl_2$. The AQ/AQH_2 redox couple is quasi-reversible under these conditions. Experiments in molten ImCl, at 90°C, show that AQ^- and AQ^{2-} are stable only under conditions where no Lewis acid is available for adduct formation.

523 Electrochemical Reduction of Aromatic Ketones in a Room-Temperature Molten Salt: *G. T. Cheek*, Dept. of Chemistry, United States Naval Academy, Annapolis, MD 21402-5026

The electrochemical behavior of fluorenone and benzophenone in the aluminum chloride:1-methyl-3-ethylimidazolium chloride molten salt system has been investigated. Reduction of fluorenone in the acidic melt produces an anion radical which couples to form the pinacolate. This latter species can exist in two conformations, the cis form undergoing oxygen abstraction to produce difluorenylidene and fluorenone pinacolone. The benzophenone anion radical is much more stable under these conditions, and products analogous to those found for fluorenone reduction have been identified.

524 Studies on Characteristics of Room Temperature Molten Salts $AlCl_3$-1-butylpyridinium Chloride: *N. Koura, K. Ueda*, and *K. Takeishi*, Dept. of Industrial Chemistry, Faculty of Science and Technology, Science University of Tokyo, 2641 Yamazaki, Noda 278, Japan

The changes of an Al plating surface, an Al/Polyaniline cell performance, and ion species in the bath with $AlCl_3$ concentration and with temperature were investigated to study the characteristics of the room temperature molten salts $AlCl_3$-1-butylpyridinium chloride (BPC) at 30-80°C and at 42.0-66.7 m/o $AlCl_3$ content. Viscosity, conductivity, and EMF of the bath changed at 50 m/o $AlCl_3$ and 60°C. Ion species in the bath were also discussed from the ^{27}Al and ^1H NMR spectra.

525 Electrodeposition of Metals from Room-Temperature Chloroaluminate Molten Salts: *X. Xu* and C. L. Hussey*, Dept. of Chemistry, University of Mississippi, University, MS 38677

The electrodeposition of lead, silver, and gold was studied in the aluminum chloride-1-methyl-3-ethylimidazolium chloride rom-temperature molten salt. Evidence for the underpotential deposition of silver was found at polycrystalline gold in acidic melt. The electrodeposition of silver on tungsten and glassy carbon involves instantaneous and progressive three-dimensional nucleation, respectively, with hemispherical diffusion-controlled growth of the nuclei. The electrodeposition of lead at glassy carbon in acidic melt involves a progressive nucleation process with diffusion-controlled growth similar to that found for silver. The voltammetric reduction of gold(III) at glassy carbon in basic melt produces an intermediate gold(I) species. Although the Au(I)/Au formal potential is more positive than that of Au(III)/Au(I), this intermediate is observed because the electrodeposition of gold at glassy carbon is impeded by a large nucleation overpotential.

526 Electrodeposition of Palladium onto Electrodes from Acidic, Neutral, Neutral-Buffered, and Basic MEIC-$AlCl_3$ Molten Salts: *H. C. DeLong* and *J. S. Wilkes*, The Frank J. Seiler Research Laboratory, U.S. Air Force Academy, CO 80840-6528

The electrodeposition of palladium onto various electrode surfaces was examined in $AlCl_3$-MEIC molten salts at room temperature. The behavior of palladium electrodeposition was markedly dependent on the mole fraction of the $AlCl_3$ in the molten salts. Shifting from basic to acidic melts, results in a 2.0 V shift in the potential of palladium. Mole fractions from 0.33 to 0.67*N* $AlCl_3$ were examined. Large nucleation potentials were evident in the basic melts, but not the acidic and neutral melts.

527 Nucleation and Morphology Studies of Aluminum Deposited from an Ambient-Temperature Chloroaluminate Molten Salt: *R. T. Carlin, W. Crawford*, and *T.-L. Liu*, Dept. of Chemistry, University of Alabama, Tuscaloosa, AL 35487, *M. Bersch*, School of Mines and Energy Development, University of Alabama, Tuscaloosa, AL 35487

Aluminum deposition from $AlCl_3$:MEIC (1-methyl-3-ethylimidazolium chloride) was studied employing an inverted optical microscope to perform *in situ* optical observations during the deposition process at a 250 μm tungsten microelectrode. Thin, continuous aluminum coatings were produced from a 1.1:1.0 $AlCl_3$MEIC molten salt using constant potential deposition at potentials ≤ -2V. At less negative potentials, the deposits displayed a grainy appearance. Analysis of chronoamperograms indicated that the deposition process consisted of instantaneous nucleation followed by diffusion-controlled growth of the three-dimensional centers. Calculated nuclear site densities and grain sizes were in agreement with the optical and electron microscope images.

528 Ionic Conductivity, Thermodynamics and IR-Spectroscopy of Tetra-n-Pentylammonium Thiocyanate-Benzoic Acid System: *A. M. Elias* and *M. E. Elias*, Dept. of Chemistry, Lisbon University, Camp Grande CL-5°, 1700 Lisbon, Portugal

Electrical conductivities were measured for the binary system tetra-n-pentylammonium thiocyanate ($Q_{5555}SCN$) with benzoic acid in the range of temperatures from 30 to 180°C and theoretical glass transition temperatures, T_o, were derived using VTF equation. Electrical conductivities decrease as the acid content increases in the mixtures and the opposite happens to T_o and T_g. A partial phase diagram of the system is presented, revealing an incongruent melting point compound. The infrared study of the systems, particularly in the range 1025-1150°C cm^{-1} also gives support to the formation of that organic complex.

529 Max Bredig Award Address: Through the Years and Temperatures: Adventures in Molten Salt Land: *R. A. Osteryoung*, Dept. of Chemistry, State University of New York, Buffalo, NY 14214

A retrospective of the author's tour through the molten salt vineyards is presented. Initial work was performed in molten $BaTiO_3$ at very high temperatures; studies in KCl-LiCl and metal-metal salt solutions, at blissfully lower temperatures, were followed by forays into molten nitrates and alkali metal chloroaluminates, at still lower temperatures. Finally, work has been carried out at ambient temperature in organochloroaluminates. The work in the chloroaluminate area has been supported by the Air Force Office of Scientific Research, to whom much gratitude is owed.

530 Synthesis of Molybdenum-Doped Alkaline Metal Vanadium Bronzes by Molten Salts Electrolysis: *Y. Kaneko, H. Ishikawa,* and *H. Kojima,* Faculty of Engineering, Yamanashi University, Kofu, Yamanashi 400, Japan

Molybdenum doped vanadium bronzes were synthesized by electrolysis of molten mixtures of V_2O_5 and M_2MoO_4 at 650-750°C using platinum wire as the cathode and carbon rod as anode in a platinum crucible. The crystals of ß-$Li_{0.29}V_{1.82}Mo_{0.18}O_5$ and ß-$Na_{0.29}V_{1.82}Mo_{0.18}O_5$ were obtained by electrolysis of V_2O_5 melts containing 25 m/o Li_3MoO_4 and Li_3MoO_4, respectively. The activation energy of conductivity for Mo-doped lithium vanadium bronzes was less than the non Mo-doped bronzes.

531 Electrodeposition of Molybdenum and Molybdenum Carbide Coatings from Oxide-Based Molten Salts: *J. R. Selman, B. Aladjov,* and *D. Topor,* Dept. of Chemical Engineering, Illinois Institute of Technology, Chicago, IL 60616

Dense, well-adherent molybdenum and molybdenum carbide coatings have been deposited on mild steel substrates by electrochemical deposition from a Na_2WO_4-K_2WO_4 molten bath containing alkali molybdates and carbonates. Coatings with a thickness of up to 30 µm have been prepared at current densities between 20 and 80 mA · cm^{-2} under air as ambient atmosphere. The coating morphology depends strongly on melt composition, temperature, and moisture content. Addition of $Na_2B_4O_7$ to the basic nonlithium bath composition causes significant morphology and quality improvements.

532 A Novel Pulsating Current Technique Used in the Study of Platinum and Molybdenum Electrodes in Molten Silicates, Borates, and Phosphates: *J. K. Higgins,* 8 Delph Top, Greetby Hill, Ormskirk, Lancs., England L39 2DX

Comparisons are made between platinum and molybdenum electrodes, between electrolytes, with single pulse methods. Parameters measured included the following: time to oxygen evolution, double layer capacity, initial potential of oxide film formation, thickness of oxide film, oxygen evolution potential. In silicate melts at Pt the formation of a monolayer of PtO_2 delays the onset of oxygen evolution every cycle, but this does not occur at Mo; salt films are found at Pt in phosphates.

533 Anodic Reaction on Nickel in a Molten CsF-NH_4F-HF System: *A. Tasaka, K. Mizuno, K. Miki, A. Kamata, H. Teruta, W. Sato,* and *K. Yanagawa,* Dept. of Applied Chemistry, Doshisha University, Imadegawa, Karasuma, Kamigyo-ku, Kyoto 602, Japan

The electrochemical behavior of nickel was investigated at 50°C in molten CsF · NH_4F · 4HF. Anodic reaction on nickel seemed to vary with increasing the potential, permitting division into four regions stated as follows: Anodic dissolution of nickel in region I (0 ~ 1 V *vs.* H_2), formation of nickelous compound on nickel in region II (1 ~ 3 V), oxidation of nickelous film to Ni(III) and/or Ni(IV) compounds in region III (3 ~ 5 V), and electrofluorination in region IV (more than 5 V). The current losses caused by nickel dissolution at 5 ~ 7.6 V were only 1.3%.

534 Electrochemical Formation of Thin Carbon Film from Molten Chloride System: *Y. Ito, T. Shimada,* and *H. Kawamura,* Dept. of Nuclear Engineering, Faculty of Engineering, Kyoto University, Sakyo-ku, Kyoto 606, Japan

A novel electrochemical process has been proposed. The process contains the following two steps. First, CO_2 gas is bubbled into molten halides containing oxide ion, to form carbonate ion. And then, by electrolysis, cathodic reduction of carbonate ion takes place to form various types of carbon film on the cathode, depending on the electrolytic conditions. This paper describes the results of experiments conducted by using LiCl-KCl eutectic melt containing carbonate ion, which exemplified the possibility of the second step of the above process. Especially, dense and adherent carbon film could be obtained on the aluminum plate cathode.

535 Melting Behavior for Powder/Hydrated Melt ($CaCl_2$ · nH_2O n:6.00, 7.35) Coexisting Systems: *S. Deki, M. Mizuhata, A. Kajinami,* and *Y. Kanaji,* Dept. of Industrial Chemistry, Faculty of Engineering, Kobe University Rokkodai, Nada, Kobe 657, Japan

The melting behavior of $CaCl_2$ hydrate melt coexisting with a-Al_2O_3 or a-SiC was investigated to be measured with DSC. For a-Al_2O_3 powder/$CaCl_2$ · 6.00 H_2O hydrate melt coexisting system, m.p. of the $CaCl_2$ · 6.00 H_2O lowered and ΔH_m decreased with both the decrease of the liquid content and the increase of the specific surface area of the powder. The nonfrozen liquid phase was observed near the solid surface. The relationship between the amount of the nonfrozen liquid, ϕ_{NFL}, and the electrical conductivity was observed. For a-SiC powder/$CaCl_2$ · 6.00 H_2 Ohydrate melt coexisting system, m.p. and ΔH_m were constant. These behaviors led to the conclusion that the phase transition of hydrate melt near the surface of the solid phase was influenced by the hydrophilicity of solid phase surface.

536 Transference Numbers in Molten Fluorides by an Operationally Defined EMF-Method: *T. Førland, S. K. Ratkje,* and *H. Rajabu,* Div. of Physical Chemistry, Norwegian Institute of Technology, N-7034 Trondheim-NTH, Norway

A practical procedure for determination of transference numbers from EMF measurement is proposed, using an operationally defined method. The procedure is applied to molten fluorides using literature data. We show that EMF measurements with NaF-AlF_3 are incorrect; results with NaF have no thermodynamic significance. Data for the system NaF-AlF_3-Al_2O_3 give only the movement of one ion with respect to the others, and t_{Na^+} is discussed with F^- as a reference.

537 Thermodynamics of Li_2O-LiF-CaF_2 Melts: *R. G. Reddy, S. T. G. Sampath Kumar,* and *A. Narayan,* Dept. of Chemical and Metallurgical Engineering, University of Nevada, Reno, NV 89557

Processing of aluminum-lithium alloys by an electrochemical method was investigated. Thermodynamics of solubility of lithium oxide in Li_2O-LiF-CaF_2 melts was studied as a function of temperature and composition; and the solubility of Li_2O was found to increase from 10.6 weight percent (w/o) at 1058 K to 14.8 w/o at 1133 K. The liquidus temperature of 4LiF · CaF_2 + Li_2O (sat.) melt was determined to be 1004.5 ± 2.5 K. The equilibrium phase and activity of Li_2O in the melts as a function of temperature was determined.

538 Predominance Area Diagram of Niobium Species in Molten LiCl + KCl Eutectic: *G. S. Picard** and *P. Bocage,* Laboratoire d'Electrochimie Analytique et Appliquée Unité associée au C.N.R.S. (URA No. 216), Ecole Nationale Supérieure de Chimie de Paris, 75231 Paris Cedex 05, France

Redox and acidic properties of dissolved niobium chlorides in the molten LiCl + KCl eutectic melt at 450°C have been investigated. Niobium is stable in the eutectic melt under four oxidation states: 0, III, IV, and V in oxoacidic media. The standard potentials of the corresponding electrochemical systems have been determined *vs.* the standard chlorine-chloride reference electrode. In oxobasic media (lithium oxide containing melt), the niobium(II) is stable under the form of NbO(s). This oxide disproportionates in acidic media leading to the formation of metallic niobium and niobium(III). In very basic media, NbO_2(s) disproportionates into lithium niobiate and niobium monoxide. The solubility products of oxides and oxychlorides have been also determined. An equilibrium potential-oxoacidity diagram of niobium is given.

539 Thermogravimetric Study of the 800°C Reaction of Zirconia Stabilizing Oxides with SO_3-$NaVO_3$: *R. L. Jones,* Code 6170, Naval Research Laboratory, Washington, DC 20375-5000

The reaction of the zirconia stabilizing oxides, Y_2O_3, MgO, Sc_2O_3, and In_2O_3, with molten $NaVO_3$ at 800°C under SO_3 partial pressures of 10^{-3} to 10^{-8} atm was studied by thermogravimetry. The difference in tendency for reaction with SO_3-$NaVO_3$ for the individual oxides could be clearly distinguished. Certain information concerning activity coefficients and other thermodynamic data for the SO_3-$NaVO_3$ melt system was also revealed.

540 Electroanalytical Study of the Reduction of K_2WCl_6 in Molten LiCl-KCl Eutectic: *C. A. C. Sequeira,* Instituto Superior Técnico, Technical University of Lisbon, 1096 Lisboa Codex, Portugal

The mechanism of the reduction of K_2WCl_6 in molten LiCl-KCl eutectic was studied using cyclic voltammetry, chronopotentiometry, and controlled potential coulometry over a temperature range of 400-500°C and a WCl_4^{2-} concentration of 0.0005-0.005 mol/liter. A single irreversible wave attributed to the reduction of W(IV) to W(III) was observed. The experimental results further indicated the process to be diffusion controlled with $n \cong 1.3$ and α ranging from 0.85 to 0.95. W(III) is soluble at 500°C and insoluble, but still electroactive, below 460°C.

541 Electrochemical Behavior of Tantalum in Halide Melts: *E. Polyakov* and *L. Polyakova,* Institute of Chemistry KSC, Apatity, Murmansk Reg., 184200 USSR

A comparative study of cathodic and anodic processes during the electrolysis of tantalum containg melts is presented. The voltammetric data indicate that the reduction of Ta(V) in CsCl-KCl NaCl-TaCl melt includes two steps: Ta(V) → Ta(IV) → Ta(0), whereas CsCl-KCl-NaCl-K_2TaF_7 melt shows the one-step reduction of Ta(V) ions. Gravimetric data as well as linear voltammetry demonstrate the appearance of Ta(IV) and Ta(V) chloride complexes during the anodic dissolution of Ta. The new wave on voltammograms, which distinguishes a chloride-fluoride melt from a chloride one is associated with the dissolution of tantalum in the form of fluoride complexes.

542 Physical Electrochemistry/High Temperature Materials Models of Alumina Dissolution in Cryolite: *F. G. Haverkamp, B. J. Welch,* and *J. B. Metson,* Dept. of Chemical and Materials Engineering, University of Auckland, Auckland, New Zealand

Two simple models for the dissolution of dispersed alumina in molten cryolite bath have been developed. The first model is one where the rate of reaction depends on only the surface area of the alumina. The dissolving alumina is regarded as shrinking hard spheres. The second model is a development of the first, where a competing reverse action is supposed to take place which is dependent on the concentration of alumina in the cryolite bath.

543 The Effects of pH and Temperature on the Structure and Properties of Molten Sn(2+) Dicarboxylates: *T. A. Ibidapo*, Dept. of Chemical and Polymer Engineering, Lagos State University, P.M.B. 1087, Apapa, Nigeria

Sn(2+) salts of dicarboxylic acids (*i.e.*, suberic, sebacic, dodecanedioic, isophthalic, propoxyterephthalic, and terephthalic) were synthesized from aqueous solution by the double decomposition reaction using various conditions of temperature (20, 50, and 98°C) and pH (6.4, 8.0, and 11.6) and then fused. The molten salts were characterized by the properties of polymeric materials. They exhibited relatively high shear rate and temperature dependent melt viscosities. They showed the Barus Effect which, along with their shear rate dependent elastic modulus, G' is an indication of their elasticity.

ELECTROCHEMICAL SENSORS IN MEDICAL SCIENCE

Sensor

544 Development of an Implantable Glucose Sensor: *G. S. Wilson* and *Y. Zhang*, Dept. of Chemistry, University of Kansas, Lawrence, KS 66045, *D. Moatti-Sirat*, *V. Poitout*, and *G. Reach*, INSERM U341, Service de Diabétologie, Hotel-Dieu, 75005 Paris, France, *D. R. Thévenot*, LABAM Université Paris Val de Marne, 94010 Creteil Cedex, France

A needle-type subcutaneous glucose sensor was developed and its performance evaluated. The sensor has an overall diameter of 0.35 mm and length of 35 mm. It can be sterilized and stored in a dry state for extended periods. Extensive *in vivo* tests were conducted in dogs and rats. The sensitivity decreases in the first few hours of implantation and then remains essentially unchanged for at least 10 days. The sensor output follows glycemia closely with a 5 min lag-time. Typical *in vivo* sensitivity was between 0.2-0.8 nA/mM. A bioassay and histological studies were also employed to evaluate biocompatibility.

545 Permeability of Glucose and Other Neutral Molecules in Nafion Films Cured at 25 and 120°C: *D. J. Harrison* and *Z. Fan*, Dept. of Chemistry, University of Alberta, Edmonton, Alta., Canada, T6G 2G2.

The permeation of neutral species through Nafion is critical to its application as a protective, selective coating on electrodes in harsh sample environments. Nafion protects glucose electrodes in whole blood, however, both glucose and O_2 must permeate it. Little is known about neutrals in Nafion, particularly solvent recast and thermally cured forms. We find neutral forms of glucose, hydroquinone, and ascorbic acid have effective diffusion coefficients of 3.4, 5.4, and 22×10^{-8} cm²/s in Nafion cured at 25°C. Curing at 120°C with dimethylformamide reduces these values 4 to 8 fold and decreases the film solubility.

546 Amperometric Glucose Sensors Based on Glucose Oxidase Immobilized in Nafion®: *T. A. Zawodzinski Jr.* and *S. Gottesfeld*, Electronics Research, Los Alamos National Laboratory, Los Alamos, NM 87545, *J. Rishpon*, Dept. of Biotechnology, University of Tel Aviv, Ramat-Aviv, 69978 Tel-Aviv, Israel

Humidification of polymer electrolyte fuel cells is essential to maintaining adequate conductivity within the ionomeric membrane and within the polymer/C/Pt composite catalyst layer. Sorption of water by the polymer is thus a crucial element in achieving optimal fuel cell performance. Qualitative observations suggest that the surface of these perfluorinated membranes is hydrophobic. Characterization of the surface of several membranes by contact angle measurements and attempted chemical modifications for enhanced hydrophilicity are described.

547 Development of a Transdermal Electrochemical Sensor for the Continuous Monitoring/Recording of Alcohol Vapor: *L. Swette*, *N. Kackley*, and *A. B. LaConti*, Giner, Inc., Waltham, MA 02154, *R. M. Swift*, Brown University, Providence, RI 02912

The measurement of alcohol consumption over long time periods is important for monitoring treatment outcome and for research applications. Giner, Inc., has developed a small wearable device that senses ethanol vapor at the skin surface, and stores several days of data recorded at 2 to 5 min intervals. The sensor is an electrochemical cell that generates a continuous current proportional to ethanol concentration. This paper describes the concept of electrochemical transdermal ethanol measurement and presents some of the clinical data collected in support of the electrochemical sensor/recorder development.

548 Progress in the Development of Amperometric Sensors for Measuring the Partial Pressure of Oxygen in Blood: *J. S. Foos*, Ciba Corning Diagnostics, Medfield, MA 02052

The partial pressure of oxygen in blood is measured routinely in medical laboratories. For some time this measurement has been made using variations of the amperometric Clark sensor. Over the years the requirements of commercial blood instruments have become increasingly stringent. The requirements for ease of use and lifetime have increased, while the need for great accuracy and precision remains. The evolution of the oxygen sensor will be addressed.

549 Moving Sensors from the Journal to the Clinical Lab: Some Real World Considerations: *R. W. Mason*, Ciba Corning Diagnostics, Medfield, MA 02052

There is much to be learned from today's many journal publications dealing with sensors. Unfortunately the tendency has been for authors to report some of the science, and not to consider the implementation of that science as successful products for the medical community. This paper presents some of the issues that must be considered in the translation of sensors from research articles to useful clinical laboratory tools.

550 Improved Adhesion of Hydrophilic Membranes on Planar Silicon Based Oxygen Sensors: *E. Aw*, *J. Lee*, *C.-Y. Aw*, and *J. C. Patton*, Microsensor Technology Center, Washington Technology Center, University of Washington, Seattle, WA 98195

Structurally firm electrolyte containing hydrophilic polyvinyl alcohol (PVA) membranes were successfully spin-coated onto p-type Si-SiO_2 wafers using silicon processing techniques. A silane coupling agent was applied to improve the adhesion between the silicon device and the electrolyte-carrying membrane. The performance of the novel polarographic solid-state oxygen sensors based on this technology is shown in this paper. From the preliminary study we have demonstrated the possibility of mass production of Clark-type oxygen electrode based miniaturized biosensors.

551 A Thin Platinum Island Film Glucose Sensor: *B. Kasapbasioglu*, *P. J. Hesketh*, *W. C. Hanly*, and *J. Maclay*, Dept. of EECS and Microbiology and Immunology, The University of Illinois at Chicago, Chicago,IL 60680

A 25 Å platinum thin film glucose sensor has been developed. The island design of the metal film allowed the immobilization of the glucose oxidase on the SiO_2 surface in a thin layer adjacent to the metal islands. The impedance of the 25 Å Pt thin film was measured over a frequency range of 100 Hz to 1 MHz. The series capacitance component of the RC equivalent circuit impedance changed by 50% at 100 Hz with 560 mM of glucose. The rate of change in the film impedance at 1 kHz with time exhibited a rapid response.

552 Evaluation of Sensing Surfaces for Use in LAPS-Based Biosensor Devices: *L. Bousse*, Molecular Devices Corp., Menlo Park, CA 94025, *B. van der Schoot* and *N. F. de Rooij*, Institut de Microtechnique, Université de Neuchâtel, CH-2000 Neuchatel, Switzerland

Light-addressable potentiometric sensors in microvolumes can be used as sensitive immunoassays, and for the rapid measurement of metabolic rates of small numbers of cells. The sensitivity and precision of detection depend on the properties of the pH sensing surface used. To optimize these characteristics, we have compared three insulators: Si_3N_4, Ta_2O_5, and Nb_2O_5. The best pH response was obtained with Ta_2O_5, although long-term drift appeared higher than with Si_3N_4. Nb_2O_5 has the highest pH response, but suffers from some drift, presumably caused by current leakage through the insulator.

553 Design, Fabrication and Testing of Flexible Ion Microsensors for Cardiovascular Applications: *R. P. Buck*, *E. Lindner*, and *V. V. Cosofret*, Dept. of Chemistry, University of North Carolina, Chapel Hill, NC 27599-3290, *R. P. Kusy*, Dept. of Orthodontics and Biomedical Engineering, University of North Carolina, Chapel Hill, NC 27599, *T. A. Johnson*, School of Medicine, Dept. of Cardiology, University of North Carolina, Chapel Hill, NC 27599, *M. P. Newman*, Dept. of OB/GYN, MetroHealth Medical Center, Cleveland, OH 44109

New, flexible microsensor arrays on Kapton using aminated poly(vinylchloride) or high molecular weight neutral carriers prove to yield sensors rivaling glass pH sensors. Special redox inner reference electrodes provide greater stability of responses than electrodes of the second kind. Results of both *in vivo* and *in vitro* testing, and biocompatibility studies show recent advances toward the goal of effective sensors for cardiology and perfusion measurements.

554 Measurement of Guinea-Pigs Heart Intracellular Potassium Ion Concentration with Potassium Microelectrodes: *Y. M. Liu* and *Z. Q. Huang*, Dept. of Applied Chemistry, Chongqing University, Chongqing 630044, China, *J. S. Xiao* and *S. Z. Yan*, Dept. of Physiology, the Third Military Medical College, Chongqing 630044, China

Potassium ion selective microelectrodes (K^+-ISE) were used to measure the K^+ content in myocardial cells of normal and early burn injured guinea-pigs. The results proved that during early burn injury, myocardial cellular resting potential is decreased, and the intracellular K^+ concentration also decreases, which suggests that during early burn injury, the decrease of myocardial cellular K^+ concentration may be one of the important factors causing the functional reduction of heart-pump.

555 Carrier Based Optodes: *K. Seiler* and *W. Simon*, Swiss Federal Institute of Technology (ETH), Dept. of Organic Chemistry, CH-8092 Zürich, Switzerland

New optical chemical sensors (optodes) selective for many different analytes have been realized using plasticized poly(vinyl chloride) membranes. They incorporate specially designed chromoionophores allowing the optical transduction together with conventional ion-selective neutral carriers. Such bulk optode membranes exhibit the theoretically expected response behavior. They have shown practical reliability for the determination of clinically relevant ions in diluted blood plasma samples, as well as several electrically neutral analytes in different media.

556 Towards Reversible Sensors Based on Photochemical-Electrochemical Switching: *M. J. Preigh* and *S. G. Weber*, Dept. of Chemistry, University of Pittsburgh, Pittsburgh, PA 15260

The reversible isomerization of photochromic spiropyrans and spiro-oxazines potentially provides a means for remote modulation of sensor activity. The ability to switch a sensor photochemically and fix it electrochemically would solve many serious problems concerning sensor reversibility. We have performed the first investigation of spiropyran voltammetry and discuss the electrochemical mechanism as it relates to the photochemical isomerization of spiropyrans and the development of reversible metal-ion sensors.

557 Electrochemical Methods for Quantitation of Peroxidase and Alkaline Phosphatase: *H. Song* and *D. G. Hafeman*, Molecular Devices Corp., Menlo Park, CA 94025

Electrochemical methods have been developed for ultrasensitive quantitation of the enzymes alkaline phosphatase (ALP) and horseradish peroxidase (HRP). The products of each enzyme-catalyzed reaction are coupled to redox mediators that are detected potentiometrically at an inert metal electrode. Quantitation of ALP at pH of 10.0 is accomplished via the ALP-catalyzed hydrolysis of 5-bromo-4-chloro-indolylphosphate to the corresponding indole derivative and phosphate; the indole derivative is oxidized by a tetrazolium mediator, the reduction of which is detected potentiometrically. Quantitation of HRP at pH 5.5 is accomplished via HRP-catalyzed tetramethylbenzidine (TMB) oxidation by hydrogen peroxide; the oxidation product of TMB is reduced by ferrocyanide, the oxidation of which also is detected potentiometrically. In solid phase enzyme-linked immunoassays, enzyme bound to a solid phase may be quantitated with these electrochemical methods. In a small volume detection cell, the assays have extremely high sensitivity and precision. Detection limits of 912,000 molecules of ALP (1.5 attomoles) and 3.8 million molecules of HRP (6.25 attomoles) were observed.These electrochemical quantitation methods promise to have greater precision compared to optical detection methods, *e.g.*, fluorescence or chemiluminescence, because of the absence of interferences from optically dense substances.

558 Bienzyme Amperometric Sensors Using a Polymeric Electron Transfer Mediator: *A. C. Michael* and *M. G .Garguilo*, Dept. of Chemistry, University of Pittsburgh, Pittsburgh, PA 15260

A bienzyme amperometric sensor for choline can be prepared with a combination of choline oxidase and horseradish peroxidase immobilized onto an electrode surface in a redox polymer gel. Detection limits in the low micromolar range are obtained and the sensors exhibit subsecond response times. Microsensors based on this approach will be suitable for *in vivo* studies of cholinergic neurotransmission. Incorporation of acetylcholine esterase will allow detection of acetylcholine directly.

559 Glutamate Electrodes: Construction, Function, and Applications: *J. R. Woodward** and *R. B. Spokane*, Yellow Springs Instrument Co., Yellow Springs, OH 45387, *S. Parker*, *T. D. Gibson*, and *J. N. Hulbert*, Dept. of Biochemistry and Molecular Biology, University of Leeds, Leeds, England LS2 9JT, *L. C. Clark, Jr.*, The Kettering Building, Antioch College, Yellow Springs, OH 45387

Two types of glutamate membrane have been constructed; one by the creation of a membrane sandwich using glutamate oxidase, the second by NMP-TCNQ mediated direct coupling of glutamate oxidase to a carbon electrode. The enzyme electrodes have been shown to be stable, linear up to 15 mM glutamate and capable of long term storage without significant loss of activity. The sandwich membranes have been used in experiments to monitor glutamate on the surface of the rabbit brain cortex after intravenous injection of glutamate.

560 Glutamate Dehydrogenase-Modified Carbon Fiber Microelectrodes with Millisecond Response Times: *W. G. Kuhr* and *P. Pantano*, Dept. of Chemistry, University of California, Riverside, CA 92521

Recently we reported the construction of an enzyme-modified carbon-fiber microelectrode that has the size, speed, and sensitivity required for dynamic measurements of *in vivo* biochemical processes. The covalent attachment of the enzyme to the carbon surface through a hydrophillic tether employing biotin-avidin technology allows the surface coverage of enzyme to be closely controlled and subject to electrochemical and spectroscopic characterizations. The biotin-avidin "molecular sandwich" permits the enzyme to be closely attached to the carbon surface. The major virtue of the biotin-avidin coupling scheme is that it permits the selectivity of the electrochemical measurement to be easily changed. The possibility for fabricating a series of single-component-selective ultramicroelectrodes with millisecond response times is demonstrated here as the selectivity of the electrode ensemble is changed by incorporating glutamate dehydrogenase into the derivatization procedure.

561 Application of ω-Thiocarboxylic Acid Monolayers for the Detection of Dopamine in the Presence of High Concentration of Ascorbic Acid: *D. Mandler* and *F. Malem*, Dept. of Inorganic and Analytical Chemistry, The Hebrew University of Jerusalem, Jerusalem 91904, Israel

Self-assembled monolayers of ω-thiocarboxylic acids, $HS-(CH_2)_nCO_2H$ (n = 2, 5, 10) on gold electrodes were used as a means to induce electrochemical differentiation between a neurotransmitter, dopamine, and ascorbic acid. The optimum differentiation was found for n = 5, and it is attributed to a compromise between a well-organized system (requires to increase n) and a reasonable rate of electron transfer (requires to reduce n).

562 Controlled Binding and Electrorelease of Metal Ions, Drugs, and Neurotransmitters from Cation Gate Composite Polymer Films Studied by Piezoelectric Sensor Technique: *M. Hepel** and *L. Dentrone*, Dept. of Chemistry, Potsdam College of SUNY, Potsdam, NY 13676

New composite polypyrrole films with cation gating properties containing Adenosine 5'-triphosphate (ATP) or flavin adenine dinucleotide (FAD) have been prepared. The use of the electrochemical quartz crystal microbalance (EQCM) technique allowed us to follow polymerization process and interactions of these films with metal ions, drugs, and neutrotransmitters. The uptake and release of metal ions, (*e.g.*, Ca^{+2}, Mg^{+2}, Zn^{+2}, Cd^{+2}, K^+, Na^+), neuroleptic drugs (*e.g.*, chlorpromazine, thioridazine) and neutransmitters (*e.g.*, dopamine) from these composite polymer films have been investigated. We have found considerable differences in ion dynamics for different cations.

563 The Effect of Overoxidation on the Electrochemical Behavior of Polypyrrole Films Doped with Various Anionic Species: *D. Belanger* and *F. Provencher*, Dépt. de chimie, Université du Québec à Montréal, Montréal, Qué., Canada H3C 3P8

Polypyrrole film electrodes doped with various anions and the enzyme glucose oxidase, GOD, were prepared on platinum electrode by oxidative electropolymerization of pyrrole in an aqueous solution also containing the enzyme and one of the following anionic species: chloride, pentanesulfonate, polyvinylsulfate or poly(4-styrenesulfonate). The cyclic voltammetry behavior of all these composite electrodes was investigated in aqueous 0.1*M* KCl and in the same aqueous solution containing electroactive redox species such as $Fe(CN)_6^{-3}$ and hydroquinone. Following overoxidation of these composite electrodes at 1.2 V in 0.1*M* KCl, the voltammetric responses changed dramatically. The electroactivity of polypyrrole was lost in all cases. The voltammetric responses of the overoxidized polymer electrodes in the presence of hydroquinone may suggest that the electrochemical oxidation of the latter occurs at a polypyrrole surface instead of the underlying platinum electrode.

564 Polypyrrole-Enzyme Film Electrode Mediated by Electropolymerized Catalytic Polymer Film: *H. Tachikawa*, *Z. Sun*, and *H. Ge*, Dept. of Chemistry, Jackson State University, Jackson, MS 39217-0510

A bilayer thin-film conducting polymer has been prepared on a glassy carbon (GC) electrode by successive electrochemical polymerizations of two different polymers: Catalytic polymer and enzyme polymer. Either a polymetallophthalocyanine (PMePc) or a polymetalloporphyrin (PMePr) was used as a catalytic polymer and an enzyme (glucose oxidase) doped polypyrrole film (PPy-GOD) was used as an enzyme polymer. Both the GC/PMePc/PPy-GOD and GC/PMePr/PPy-GOD films show good catalytic behaviors which include a reduced oxidation potential and an enhanced amperometric response with a substrate.

INDEX TO AUTHORS

FUTURE SOCIETY MEETINGS

**182nd MEETING—TORONTO, ONTARIO, CANADA—
OCTOBER 11-16, 1992—HEADQUARTERS AT THE ROYAL YORK HOTEL**

The final program will be published in the August 1992 issue of the **Journal of The Electrochemical Society.**

Planned symposia for the Toronto Meeting include the following: Electric Vehicle Batteries and Fuel Cells. Environmental Aspects of Batteries. Lithium Batteries. Battery General Session. High Temperature Batteries. Solid Polymer Electrolyte Fuel Cells. Battery, End-of-Charge, and State-of-Charge Sensors. Corrosion General Session. Oxide Films on Metals and Alloys. Corrosion and Reliability of Electronic Materials and Devices. Microscopic Models of Electrode/Electrolyte Interfaces. Isolation and Trench Technology. Silicon Nitride and Silicon Dioxide Thin Insulating Films. Thin Film Transistor Technologies. Dielectric Science and Technology/Electronics Joint General Session. Dielectric Science and Technology/Electronics Joint Recent News Paper Session. Autocatalytic Deposition. Electrodeposited Contacts and Interconnects. Structure and Properties of Electrodeposited Protective Coatings. Electrodeposition General Session. Simulation of Electrodeposition Processes. Contamination Control and Defect Reduction in Semiconductor Manufacturing I. High Purity and High Resistivity Silicon II. Logic and Functional Devices for Photonics. State-of-the-Art Program on Compound Semiconductors XVII. Third International Symposium on Focused Ion Beam Technology. Environmental, Health, and Safety Aspects of Energy Systems. Energy Technology General Session. Power Sources for Underwater Applications. Characterization of Semiconductor Thin Films and Interfaces. Hydrogen Energy Systems. Advances in High Temperature Interface Chemistry. Lighting, Display and Imaging Technology. Nonlinear Optics and Materials. Physics and Chemistry of Luminescent Materials. Optoelectronic Device Materials and Processing. Scanning Probe Microscopy and Fabrication. Physical Electrochemistry General Session. Electrochemistry of Biomaterials. Charge Transfer Process at Liquid-Liquid Interfaces. Sensor General Session. Piezoelectric Sensors. Recycling and Recovery for Industrial Electrochemical Processes....

HONOLULU, HAWAII—MAY 16-21, 1993—HEADQUARTERS AT THE HILTON HAWAIIAN VILLAGE

183rd Meeting of The Electrochemical Society, Inc. Cosponsored by The Electrochemical Society of Japan and with the cooperation of The Japan Society of Applied Physics

The final program will be published in the March 1993 issue of the **Journal of The Electrochemical Society.**

Planned symposia for the Honolulu Meeting include the following: Advanced Engineering of Luminescent Materials and Its Impact on Future Devices. Batteries and Fuel Cells for Stationary and Electric Vehicle Applications. Battery/Energy Technology Joint General Session. Carbonate Fuel Cell Technology—Third International Symposium. Chemical Sensors. Chemical Vapor Deposition—Twelfth International Conference. Chemistry, Structure, and Stochastic Processes in the Breakdown of Passivity. Chlor-Alkali and Chlorate Production. Conduction Processes in Disordered Materials. Conductive Polymers and Surface Modified Electrodes. Corrosion. Electrochemistry and Catalysis of Metastable Metals and Intermetallics. Corrosion General Session. Corrosion Protection by Coatings and Surface Modification. Diamond Materials—Third International Symposium. Electrocatalysis. Electrochemical Processing of Tailored Materials—Second International Symposium. Electrochemical Technology Applications in Electronics—Second International Symposium. Electrochemically Deposited Thin Films. Electrochemistry of Cells and Organelles. Electron Transfer in Organic Colloidal Systems II. Electronic Materials Technologies for the 21st Century. Electronics/Dielectric Science and Technology Joint General Session. Electronics/Dielectric Science and Technology Joint Recent News Paper Session. Environmental Aspects of Electrochemistry and Photoelectrochemistry. Fundamentals of Solid Polymer Electrodes and Electrolytes. High Temperature Materials Chemistry VI. Intercalation Chemistry and Intercalation Electrodes. Low Temperature Electronics and High Temperature Superconductivity. Luminescence and Display Materials General Session. Mechanistic Aspects of Microbiology Influenced Corrosion—MIC. Metallized Plastics: Fundamental and Applied Aspects IV. Molten Salt Chemistry and Technology—1993—International Symposium. New Mathematical and Computational Methods in Electrochemical Engineering. New Sealed Rechargeable Batteries and Supercapacitors. Physical Electrochemistry General Session. Polymers for the 21st Century. Quality Management in Industrial Electrochemistry. Redox Mechanisms and Interfacial Properties of Molecules of Biological Importance—Fifth International Symposium. Semiconductor Wafer Bonding: Science, Technology, and Applications—Second International Symposium. Solar Energy Conversion Using Solid/Solid and Solid/Liquid Interfaces. Solid Oxide Fuel Cells—Third International Symposium. State-of-the-Art Program on Compound Semiconductors XVIII. Surface Analytical Methods and New Techniques for *In Situ* Measurements. The Role of Electrochemistry in Organic Synthesis and Organometallic Chemistry. Ultra Large Scale Integration Science and Technology—Fourth International Symposium: (1) Process Physics and Modeling in Semiconductor Technology—Third International Symposium; (2) Contamination Control and Defect Reduction in Semiconductor Manufacturing II; (3) Fine-Line Lithography and Pattern Technology; (4) Highly Selective Dry Etching and Damage Control; (5) Interconnects, Contact Metallization and Multilevel Metallization; (6) Reliability of Semiconductor Devices, Interconnects and Thin Insulator Materials.

EXTENDED DEADLINE SYMPOSIA

STATE-OF-THE-ART PROGRAM ON COMPOUND SEMICONDUCTORS XVI

• Sponsored by The Electronics/Dielectric Science and Technology Divisions

Abstracts 565 SOA - 588 SOA

QUANTUM CONFINEMENT

• Sponsored by The New Technology Subcommittee/Electronics/Dielectric Science and Technology Divisions

Abstracts 589 QUA - 595 QUA

MICROMACHINING AND MICROSTRUCTURES

• Sponsored by The New Technology Subcommittee/Sensor Group/Electronics/Dielectric Science and Technology Divisions

Abstracts 596 MIC - 612 MIC

FULLERENES: CHEMISTRY, PHYSICS AND NEW DIRECTIONS

• Sponsored by The Physical Electrochemistry/Dielectric Science and Technology/Electronics Divisions

Abstracts 613 FUL - 697 FUL

JOINT RECENT NEWS PAPER SESSION

• Sponsored by The Electronics/Dielectric Science and Technology Divisions

Abstracts 698 RNP - 709 RNP

181st Meeting of The Electrochemical Society, Inc.
Adam's Mark Hotel, May 17-22, 1992

Extended Deadline Symposia Programs and Abstracts

STATE-OF-THE-ART PROGRAM ON COMPOUND SEMICONDUCTORS (SOTAPOCS XVI)

Electronics/Dielectric Science and Technology

Room 43, 4th Level

SOA

TUESDAY, MAY 19, 1992

V. Swaminathan, Chairman; N. Buckley, Vice-Chairman

2:00	OEIC Technological Compatibility: Some Examples for Photoreceiver Applications - D. Decoster	565 SOA
2:40	Technological Aspects of Prime Importance for Performances of Microwave Devices - M. Francois and J. Vanbremeersch	566 SOA
3:20	Novel $In_yGa_{1-y}As/GaAs$ Graded Superlattice Channel ($0.2 \leq y \leq 0.4$) for Pseudomorphic $Al_xGa_{1-x}As/In_yGa_{1-y}As$ HFET - J. Kraus, H. Meschede, Q. Liu, W. Prost, and F. J. Tegude	567 SOA
3:40	Frequency Resolved Admittance Measurements on InAlAs/InGaAs/InAlAs Single Quantum Wells Applied to Determine the Conduction Band Offset and the Capture Time Constant - J. M. Lopez-Villegas, P. Roura, J. Bosch, J. R. Morante, A. Georgakilas, and K. Zekentes	568 SOA

WEDNESDAY, MAY 20, 1992

T. Kamijoh, Chairman; J. P. Vilcot, Vice-Chairman

9:00	Material and Process Considerations in the Manufacture of GaAs Electronic Devices - C. L. Reynolds	569 SOA
9:40	Growth Temperature Optimization for InAlAs Molecular Beam Epitaxy - A. Georgakilas, A. Christou, G. Halkias, K. Zekentes, N. Kornilios, A. Dimoulas, F. Peiro, A. Cornet, A. Tabata, T. Bonyattou, and G. Guillot	570 SOA
10:00	Atomic Layer Epitaxy Growth and Characterization of InP/GaAs - L. Lazzarini, D. Bertone, P. Franzosi, C. E. Norman, and G. Salviati	571 SOA
10:20	Ten-minute intermission	
10:30	Plasma Assisted Epitaxy of Compound Semiconductors - T. Hariu	572 SOA
11:10	Low Pressure MOVPE of GaInP/GaAs Heterojunctions - Growth Interruption Studies Using EDMI and TEG - K. Chou, B. Pathangey, and T. Anderson	573 SOA
11:30	The Effect of the Sulfur Partial Pressure on the Growth of $CuInS_2$ Single Crystals - M. L. Fearheiley, M. Kanis, and S. Fiechter	574 SOA
11:50	Thermal Decomposition of Copper Acetylacetonate Studied by Using Fourier Transform Infrared Spectroscopy - Y. Chang	575 SOA

WEDNESDAY, MAY 20,1992

G. Valco, Chairman; A. Katz, Vice-Chairman

2:00	Gas-source MBE of (Ga,Al)As Using Only Gaseous Sources for HBT Applications - T. Fujii, H. Ando, A. Sandhu, N. Okamoto, S. Yamaura, T. Takahashi, and N. Yokoyama	576 SOA
2:40	Strain Release in MBE Grown InGaAs/GaAs Superlattices - C. Ferrari, M. R. Bruni, M. G. Simeone, F. Martelli, L. Lazzarini, L. Nasi, C. E. Norman, and G. Salviati	577 SOA
3:00	Formation of Quasi-Quantum-Wires by Strain Induced Lateral Layer Ordering Process - K. Y. Cheng and K. C. Hsieh	578 SOA
3:20	Ten-minute intermission	
3:30	Surface Modification and Stabilization in GaAs and InP - J. Shirafuji and T. Sugino	579 SOA
4:10	Achievement of the Theoretical Resolution of Electron Beam Lithography on Thick GaAs Substrates - S. A. Dickey, T. McCormick, and A. Majerfeld	580 SOA
4:30	Speculation on the Effects of the Interaction Between HCl and HNO_3 on the Etching of Illuminated n-GaP in HCl/HNO_3 - H. F. Hsieh and H. C. Shih	581 SOA

THURSDAY, MAY 21, 1992

C.L. Reynolds, Chairman; D. Decoster, Vice-Chairman

9:00	Wafer Level Characterization of InP and GaAs Based Devices - G. E. Carver and R. W. Heebner	582 SOA
9:40	Nondestructive Evaluation of AlGaAs/GaAs Heterojunction Structures by Photoluminescence Spectroscopy - Z. H. Lu, M. C. Hanna, E. G. Oh, E. Mao, B. W. Kim, A. Majerfeld, P. D. Wright, and L. W. Yang	583 SOA
10:00	Very High Quality GaAs/AlGaAs Multiple Quantum Well Structures Grown by Atmospheric Pressure MOVPE - E. Mao, Z. H. Lu, B. W. Kim, T. McCormick, E. G. Oh, and A. Majerfeld	584 SOA
10:20	Ten-minute intermission	
10:30	AlAs/GaAs Lattice Parameter Measurement by High Resolution X-Ray Diffraction - C. Ferrari, C. Bocchi, P. Franzosi, A. Bosacchi, and S. Franchi	585 SOA
10:50	X-Ray Diffraction and Electron Microscopy Characterization of H_2 Implanted InP Single Crystals - P. Franzosi, C. Bocchi, L. Gastaldi, L. Lazzarini, and G. Salviati	586 SOA
11:10	Structural Characterization by TEM of Strained InGaAs/InAlAs Quantum Well Structures - F. Piero, A. Cornet, J. R. Morante, A. Georgakilas, and G. Halkias	587 SOA
11:30	Spectral Decomposition of Mapped PIMR Semiconductor Wafer Characterization Data Using Numerical Frequency Domain Methods - E. R. Atwood and R. J. Gutmann	588 SOA

Abstracts

565 SOA OEICs Technological Compatibility: Some Examples for Photoreceiver Applications: *D. Decoster*, Centre Hyperfrequences et Semiconducteurs U.A. CNRS 287, Universite des Sciences et Techniques de Lille Flandres Artois, F-59655 Villeneuve, D'Ascq Cedex, France

III-V Optoelectronic integrated circuits (OEICs) require the monolithic fabrication of different components, each with its own material and structure parameters. Optimum performance can then be attained if each device can be designed with ideal thicknesses and doping levels of the various epilayers. Unfortunately, a multilayer structure that can be optimum for one particular device, for example a photodetector, cannot be optimum for a transistor, or an optical waveguide. Such a problem explains the technological difficulties for the fabrication of OEICs. In this paper, we present and discuss recent advances on monolithic integration of photodetectors with field effect transistors or optical waveguides. Various types of photodetectors are investigated (photoconductors, MSM, ...) and emphasis is made on the use of large lattice mismatch materials and selective epitaxy to combine independently on the same substrate, the various epilayers needed for each function whatever the substrate is (Si, GaAs, ...).

566 SOA Technological Aspects of Prime Importance for Performances of Microwave Devices: *M. Francois* and *J. Vanbremeersch*, Centre Hyperfréquences et Semiconducteurs, Universite des Sciences et Technologies de Lille, F-59655 Villeneuve d'Ascq Cedex, France

In this paper, we present an overview of our recent technological improvements applied to microwave devices such as: MESFET, HEMT, HFET, resonant tunneling diode, etc. Epitaxial structure and technological process directly acting on the device intrinsic performances and parasitics are of prime importance for their microwave behavior. Effects such as parasitic capacitances and resistances and gate position strongly influence the cutoff frequency, transconductance of FETs, and noise level. Special emphasis is made on new techniques such as Y and T shaped GaAs FET gate. Also discussed are some more techniques such as air bridges. As an example, we have recorded a transconductance of 1.4 S/mm and a cutoff frequency of 100 GHz for a GaAs MESFET. We discuss particularly the connection between the material (MBE growth in our laboratory), the technology, and the performances of these devices.

567 SOA Novel $In_yGa_{1-y}As/GaAs$ Graded Superlattice Channel ($0.2 \leq y \leq 0.4$) for Pseudomorphic $Al_xGa_{1-x}As/In_yGa_{1-y}As$ HFET: *J. Kraus, H. Meschede, Q. Liu, W. Prost*, and *F. J. Tegude*, Solid State Electronics Dept., University-GH-Duisburg, Sonderforschungsbereich 254, D-4100 Duisburg, Germany

In order to improve the high frequency performance of $Al_xGa_{1-x}As/In_yGa_{1-y}As$ HFET devices a graded $In_yGa_{1-y}As/GaAs$ superlattice as active channel layer is introduced. Concerning the limiting factors, critical thickness and surface roughness, our new approach permits the use of higher indium composition. Layers were grown by MBE under optimized $In_yGa_{1-y}As$ growth conditions evaluated from RHEED measurements. The superlattice is designed to utilize high indium concentration (>30%) at the location of maximum probability density of electrons, only. Starting with 12 monolayers $In_{0.4}Ga_{0.6}As$ at the bottom interface the indium content was increased up to 40% in 3 steps interrupted by 4 monolayers of GaAs. These barriers are transparent to the electrons according to photoluminescence measurements leading to an estimated carrier concentration of $n_s = 2 \cdots 10^{12}$ cm^{-2}. Regarding screening effects sufficient mobilities of $\mu_{300K} = 4{,}200$ cm^2/Vs and $\mu_{77K} = 20{,}000$ cm^2/Vs were measured by magnetotransconductance profiling. Devices with gate length $L_G = 0.5$ μm and width $W_G = 2 \cdots 20$ μm were processed using optimized optical lithography. A maximum transconductance of $g_m = 410$ mS/mm could be achieved. From on-wafer RF measurements an intrinsic current gain cutoff frequency of $f_t = 86$ GHz can be extracted leading to an average carrier velocity of $v = 2.7 \cdot 10^7$ cm/s. These values represent a distinct increase of about 40% compared to homogen $In_{0.4}Ga_{0.6}As$ channel HFET with same dimensions.

568 SOA Frequency Resolved Admittance Measurements on InAlAs/InGaAs/InAlAs Single Quantum Wells Applied to Determine The Conduction Band Offset and the Capture Time Constant: *J. M. Lopez-Villegas, P. Roura, J. Bosch*, and *J. R. Morante*, LCMM Dept. de Fisica Aplicada i Electrònica, Univ. de Barcelona, Diagonal 647, E-08028 Barcelona Spain, *A. Georgakilas* and *K. Zekentes*, FORTH, Heraklion, Crete, Greece

The frequency resolved admittance measurements have been used to determine the conduction band offset and the capture time constant of $In_{0.53}Al_{0.47}As/In_xGa_{1-x}As/In_{0.53}Al_{0.47}As$ single quantum well structures (SQW). A theoretical analysis of the SQW admittance which takes into account nonparabolicity of the conduction band has been performed. The deduced expressions of the capacitance and the conductance as a function of both bias and frequency have been used to fit the experimental data. So, the conduction band offset and the capture time constant have been obtained. Two different well compositions, $x = 0.53$ lattice matched and $x = 0.60$ strained, have been studied. In both cases the well width is 5 nm. Our results indicate that the conduction band offset at room temperature are $\Delta E_c = 0.50 \pm 0.02$ eV for $x = 0.53$ and $\Delta E_c = 0.55 \pm 0.02$ eV for $x = 0.6$. The capture time constant is found to be in the range of 10^{-11}–10^{-10} s in both cases. A discussion of the obtained values is reported.

569 SOA Material and Process Considerations in the Manufacture of GaAs Electronic Devices: *C. L. Reynolds, Jr.*, AT&T Bell Laboratories, Reading, PA 19612

The use of GaAs for the fabrication of microwave devices and high speed integrated circuits has led to considerable expansion of production facilities. While the main focus has been on improved materials growth and the development of suitable process techniques, the need for higher performance and yield provides the driving force for more uniform growth and control of wafer processing. An understanding of the relationship between materials characteristics and device performance and the interaction between growth structures and processing is crucial to success. In this talk we address some of the material and process issues which arise during the fabrication of self-aligned refractory gate integrated circuits using complex heterostructures. In particular, the role of interfacial impurities on carrier depletion and the mobility of the two-dimensional electron gas in selectively doped heterostructure transistor wafers are discussed. It is found that C and Si impurities at the interface can dramatically influence the threshold voltage of depletion-mode field effect transistors. High temperature activation of ohmic implants in a self-aligned process can result in Si dopant outdiffusion with subsequent layer disordering of the heterostructure, which also affect the two-dimensional electron gas. These and other topics are elaborated.

570 SOA Growth Temperature Optimization for InAlAs Molecular Beam Epitaxy: *A. Georgakilas* and *A. Christou*, University of Maryland, CALCE Center for Electronics, College Park, MD 20742, *G. Halkias, K. Zekentes, N. Kornilios*, and *A. Dimoulas*, Foundation for Research and Technology, I.E.S.L., 711 10 Heraklion, Crete, Greece, *F. Peiro* and *A. Cornet*, Universitat de Barcelona, Av. Diagonal 647, E-08028 Barcelona, Spain, *A. Tabata, T. Bonyattou*, and *G. Guillot*, INSA de Lyon, LPM Bat. 602, 69621 Villeurbanne Cedex, France

There are a considerable number of publications dealing with the properties of InAlAs grown by molecular beam epitaxy (MBE) and their correlation to the MBE growth conditions. However, the determination of temperature and growth conditions of MBE InAlAs remains a problem. Thus, we have undertaken a systematic study of InAlAs MBE. Choosing a stable As_4: (Ga + In) equivalent beam flux pressure ratio of 25, we varied the growth temperature between 300 and 590°C, growing undoped or Si-doped samples. Structural (TEM, SEM) optical (PL, PR) and electrical (Hall, CV, DLTs) characterization techniques have been used to assess the properties of the films. The results indicate that acceptable quality of InAlAs for most applications can be grown at a growth temperature around 530°C. This temperature can be calibrated in respect to RHEED transitions appearing before growth initiation for the As stabilized InP surface. Our conclusions are in agreement with Welch *et al.* [APL, **46**, 169 (1985)] who had found an optimum growth temperature of 510°C for InAlAs optical properties. Additionally, we addressed both structural and electrical aspects of the material obtaining an understanding about their interrelation. We discuss our results as well as the implications in FETs performance.

571 SOA Atomic Layer Epitaxy Growth and Characterization of InP/GaAs: *L. Lazzarini*, C.N.R.-MASPEC Institute, Parma, Italy, *D. Bertone*, CSELT, Torino, Italy, *P. Franzosi, C. E. Norman*, and *G. Salviati*, C.N.R.-MASPEC Institute, Parma, Italy

The study of the InP/GaAs system is interesting as an intermediate step to growth of InP/Si because of the intermediate lattice mismatch (≈ 4%) and thermal expansion coefficient of GaAs with respect to InP and Si. The samples were grown by atomic layer epitaxy at 340°C in a low-pressure metallorganic chemical vapor deposition system using a pulsed flow of TMIn and PH_3 in an argon atmosphere, with a thickness, t, ranging between 5 and 150 nm. The structural quality of the layers was investigated by double crystal diffraction (DCD) and electron microscopy techniques. DCD rocking curves evidenced different amounts of strain release in layers of different thickness; in particular the layer with $t = 150$ nm was completely relaxed whereas the specimen with $t < 5$ nm was almost completely strained. Further, the x-ray peak full-width-half-maximum decreased by increasing the layer thickness. Cross-section transmission electron microscopy investigations in the high resolution (HREM) mode revealed misfit dislocations at the InP/GaAs heterointerface and stacking faults in the bulk epilayers. No threading dislocations were observed. The InP quality improved by increasing the layer thickness and the defect density decreased beyond ≈ 100 nm from the heterointerface. Both 90° and 60° type dislocations were evidenced by the

*** An asterisk by a name indicates which author will present the paper.**

Burgers vector analysis in the HREM mode. Finally, the influence of different annealing conditions on the layer structural quality as also studied by DCD and HREM investigations.

572 SOA Plasma-Assisted Epitaxy of Compound Semiconductors: *T. Hariu*, Dept. of Electronic Engineering, Tohoku University, Sendai 980, Japan

Plasma-assisted epitaxy (PAE) has been developed for low temperature epitaxial growth of semiconductors including surface cleaning of substrates in view of its fundamental advantage that internal energy for enhanced chemical reaction and kinetic energy for enhanced migration over the growing surface can be both given to supplied species in plasma. Design consideration of growth chamber and plasma diagnostics including optical emission spectroscopy to detect active species and the results of low-temperature epitaxial growth of compound semiconductors (III-V and II-VI) mainly on GaAs and Si are reviewed. Hydrogen plasma treatment has been found to be effective in removing native oxide at a lower temperature of GaAs (~270°C) and Si (~450°C). The successful epitaxial growth of InSb, InAs, GaSb, GaAs, (In, Ga) As, (In, Ga) Sb, In (As, Sb), and ZnSe has been achieved at lower temperatures than the growth without plasma. It is also shown that such growth conditions as RF power applied to plasma and supply ratio V/III or VI/II should be optimized because the electronic property and surface morphology depend much more critically upon them at a lower growth temperature. Optical emission spectroscopy revealed that one of the important advantages of PAE is the enhanced chemical reactivity of group V elements by plasma-cracking of their molecules supplied by evaporation into excited atoms.

573 SOA Low Pressure MOVPE of GaInP/GaAs Heterojunctions: Growth Interruption Studies Using EDMI and TEG: *K. Chou,* B. Pathangey*, and *T. Anderson*, Dept. of Chemical Engineering, University of Florida, Gainesville, FL 32611

A wide range of nanostructure devices such as optical thyristors, quantum well lasers, and superlattice photodetectors with high speed capabilities are currently being grown by molecular beam epitaxy (MBE) and organometallic vapor phase epitaxy (OMVPE) techniques. The performance of such devices depend on the quality of the interfaces between two different compound semiconductors. Atomic scale structural disorder at the growth surface creates interfacial compositional variations that result in the poor device performance. This problem can be alleviated by scheduling growth interruptions to give interface stabilization for a specific growth system. Growth of GaInP/GaAs heterostructures require simultaneously switching the arsenic, phosphorus and indium supply to the interfaces. Single and multiple quantum well structures of nominally lattice matched GaInP/GaAs with equal and variable well sizes were grown in a low pressure OMVPE reactor. The influence of varying the duration of growth interruptions on the interfacial abruptness and compositions were examined using the *ex situ* characterization techniques: high resolution x-ray diffraction (FWHM and intensity of primary and satellite peaks), low temperature photoluminescence (FWHM and energy shifts due to quantum confinement), and high resolution transmission electron microscopy (well thickness and interface disorders). Under conditions of continuous growth front (without interruptions), the interface was found to contain regions of altered growth compositions resulting from the incorporation of phosphorus and indium in GaAs layers. For longer interruptions, the growth front tends to become rough due to highly strained interfacial regions. The optimal lengths of interruptions at both GaInP-to-GaAs and GaAs-to-GaInP interfaces have been found to vary with the growth temperatures as well as the molar V/III ratio for the well layers.

574 SOA The Effect of the Sulfur Partial Pressure on the Growth of $CuInS_2$ Single Crystals: *M. L. Fearheiley, M. Kanis*, and *S. Fiechter*, Hahn-Meitner-Institut-Berlin, Bereich Photochemische Energieumwandlung, 1000 Berlin 39, Germany

The chalcopyrite $CuInS_2$ has an optimum bandgap for the direct conversion of solar energy. However the optimization of this material has not progressed very rapidly. One reason is due to the fact that the growth from stoichiometric melts of large, high quality single crystals of $CuInS_2$ have been inhibited by the presence of two solid-state phase transformations which induce cracking of the material. Recently we have shown that it is possible to produce single crystals of moderate size with the gradient freeze technique, but only under elevated pressures. To determine the optimum conditions for the growth of large, homogeneous single crystals, different vapor pressures of sulfur have been used with and without argon overpressures. We discuss the best conditions for single crystal growth. A comparison of the material properties, obtained by EDX, Hall measurements, and photoluminescence, with growth conditions is presented.

575 SOA Thermal Decomposition of Copper (acetylacetonate) Studied by Using Fourier Transform Infrared Spectroscopy: *Y. Chang*, Dept. of Chemical Engineering, Iowa State University, Ames, IA 50011

Thermal decomposition phenomena of copper (acetylacetonate) during the copper oxide metal organic chemical vapor deposition (MOCVD) process, was studied by gas phase transmission Fourier transform infrared spectroscopy (FTIR), differential scanning calorimetry (DSC), and thermogravimetric analysis (TGA). *Decompositions of Cu (acac)$_2$ were performed at atmospheric* pressure in either inert or oxidizing environment. FTIR spectra of the gas phase decomposed products revealed that pyrolysis patterns were affected by the temperature and the chemical nature of ambient. From 150° to 250°C, CO_2 and H_2O were the primary vapor phase species. Above 280°C, acetylacetone, the ligand of the $Cu(acac)_2$ precursor, was the primary high molecular weight specie found in the inert (He) environment. In an oxidizing environment, acetone was the primary gas phase specie. The amounts of CO_2, alkyl alcohol, and H_2O also increased significantly when oxygen was introduced into the MOCVD reactor. DSC was performed to determine the impacts of heating rate and oxygen to the decomposition of $Cu(acac)_2$.

576 SOA Gas-Source MBE of (Ga, Al)As Using Only Gaseous Sources for HBT Applications: *T. Fujii, H. Ando, A. Sandhu, N. Okamoto, S. Yamaura, T. Takahashi*, and *N. Yokoyama*, Fujitsu Laboratories Ltd., 10-1 Morinosato-Wakamiya, Atsugi 243-01, Japan

Gas-source molecular beam epitaxy (GSMBE) is a promising method for the growth of carbon-doped base GaAs/AlGaAs heterojunction bipolar transistors (HBTs). The ability to reproducibly control the doping of n-AlGaAs has been a major concern for the practical application of GSMBE for the growth of GaAs:C/AlGaAs HBTs. We have carried out extensive studies into the n-type doping of AlGaAs by GSMBE using triethylaluminum (TEA) and trimethylamine alane as aluminum sources; triethylgallium as the gallium source; cracked arsine as the arsenic source; and uncracked disilane as an n-type dopant source. Furthermore, we grew a carbon-doped base ($p = 4 \times 10^{19}$ cm^{-3}; trimethylgallium as the carbon source) GaAs/AlGaAs HBT having a silicon doped emitter layer ($n = 9 \times 10^{17}$ cm^{-3}; TEA). The emitter-base ideality factor was 1.12, indicating that an excellent junction had been formed using silicon and carbon. The dc current gain was 53 at a current density of 3×10^4 A/cm^2. Device characteristics under current stress are presented, and we discuss the implications of our results for the future development of GSMBE for device applications.

577 SOA Strain Release in MBE Grown InGaAs/GaAs Superlattices: *C. Ferrari*, C.N.R.-MASPEC Institute, Parma, Italy, *M. R. Bruni* and *M. G. Simeone*, ITSE, Monterotondo (Roma), Italy, *F. Martelli*, Fondazione U. Bordoni, Roma, Italy, *L. Lazzarini, L. Nasi, C. E. Norman*, and *G. Salviati*, C.N.R.-MASPEC Institute, Parma, Italy

Strained heterostructures are attractive because of the more flexible tailorability of their electronic properties, which arises from the competition of quantum-size effects and strain-induced effects. $In_xGa_{1-x}As/GaAs$ superlattices (SLs) ($0.065 < x < 0.194$) were grown in a conventional MBE system at 530°C both for buffers and epilayers. The structural quality of the layers has been studied by double crystal diffractometry (DCD), low temperature spectroscopic cathodoluminescence (LTSCL), room temperature panchromatic CL, and both scanning and transmission electron microscopy techniques. All the layers showed good crystal quality despite the presence of misfit dislocations parallel to the <110> directions. A broadening of the full width half maximum of both LTSCL and DCD peaks was observed with increasing In content. DCD rocking curves suggested that the structure with the lowest In concentration was fully strained despite a low concentration of dislocations (<10^4 cm^{-1}) observed using CL. Proof that this structure was in a metastable state came from CL observations of an asymmetric dislocation movement under electron beam irradiation in the scanning electron microscope. The structures with higher In content had relaxed. Cross-section transmission electron microscopy investigations showed that dislocations, which high resolution electron microscopy showed to be mainly 60° type, were present at the InGaAs/GaAs interface and in the buffer layer. No dislocations threading the layers were observed.

578 SOA Formation of Quasi-Quantum-Wires by Strain-Induced Lateral Layer Ordering Process: *K. Y. Cheng* and *K. C. Hsieh*, 311 Microelectronic Lab., University of Illinois Urbana, IL 61801

The formation mechanism of the quasi-quantum-wire structures formed in vertical $(GaAs)_n/(InAs)_n$ and $(GaP)_n/(InP)_n$ short-period-superlattices (SPS) ($n = 1$ or 2) grown on nominally (100) InP and GaAs substrates, respectively, have been investigated by examining the microstructure of the SPS grown under different column III flux ratios with transmission electron microscopy. The strain induced from the deviation in periodicity of the SPS layer (n) from an integer number of monolayers is the major driving force of the lateral modulation of the composition along the [110] direction. When the periodicity deviation is larger than 5%, both $(GaAs)_n/(InAs)_n$ and $(GaP)_n/(InP)_n$ vertical SPS layers were found to have a lateral periodic modulation of composition with periodicities as small as ~200Å. The existence of lateral two-dimensional quantum confinement in these quasi-quantum-wire structures have been confirmed by polarized photoluminescence measurements.

579 SOA Surface Modification and Stabilization in GaAs and InP: *J. Shirafuji* and *T. Sugino*, Dept. of Electrical Engineering, Faculty of Engineering, Osaka University, 2-1 Yamada-oka, Suita, Osaka 565, Japan

More improvement of Schottky barrier contacts and insulator-semiconductor interfaces of GaAs and InP necessitates the development of surface modification and stabilization techniques. Much interest is also paid on suppressing surface damage during various plasma processes such as reactive-ion-etching. This paper describes effects of PH_3 (phosphine) plasma treatment on the surface properties of GaAs and InP, including partly H_2 plasma and UV excimer-laser excited PH_3 treatment effects. The PH_3 plasma treatment makes us expect the following various effects: (*i*) Atomic hydrogen removes native oxide of GaAs or InP surface. (*ii*) Phosphorus atom substitutes for arsenic near the surface of GaAs. This may reduce elemental arsenic formation at the surface. (*iii*) Phosphorus atom fills As- and P-vacancies, if existing, near the surface of GaAs and InP, respectively. Preferential etching of phosphorus in the course of plasma processes can be suppressed in InP. (*iv*) Amorphous phosphorus layer which can be used as an insulating or a passivation layer is deposited by adjusting substrate temperature. Phosphidization of GaAs surface by PH_3 plasma treatment reduces generation of arsenic oxide and free arsenic. The release of the surface Fermi level pinning by the treatment is suggested by the observation of the metal work function dependence of Schottky barrier height. Generation of EL2 defects which are induced during Ar or H_2 plasma process is found to be suppressed in the case of PH_3 plasma due to the existence of excess phosphorus. A visual inspection reveals reduced preferential removal of phosphorus from the InP surface in the PH_3 plasma in comparison with H_2 or Ar plasma. The effective suppression of surface damage of InP during plasma process is demonstrated clearly by DLTS measurement. A combined process of PH_3 plasma treatment and Se vapor passivation shows a much improved dependence of the Schottky barrier height on the metal work function in InP.

580 SOA Achievement of the Theoretical Resolution of Electron Beam Lithography on Thick GaAs Substrates: *S. A. Dickey, T. McCormick,* and *A. Majerfeld,* Dept. of Electrical and Computer Engineering, University of Colorado, Boulder, CO 80309

We present E-beam lithography experiments performed with an atomic resolution scanning transmission electron microscope (STEM) that show that the proposed resolution limit of 10 nm for PMMA resist on thick substrates (1) can be realized. This limit is independent of beam spot size or electron beam energy. For these experiments a spot size of 2.6 nm and beam energy of 200 keV were used. It is demonstrated that clean 11.5 nm lines can be defined in single layer PMMA on thick GaAs substrates. We also observed that SEM imaging allowed accurate direct measurement of the written features in the resist at 200 keV. The dependence of feature size on dose exposure on 100 nm monolayer PMMA films on thick semiconductor substrates is discussed, as well as the fabrication of arrays of dots.

1. A. N. Broers, *IBM J. Res. Develop.*, **32**, 502 (1988).

581 SOA Speculation on the Effects of the Interaction Between HCl and HNO_3 on the Etching of Illuminated n-GaP in HCl/HNO_3: *H. F. Hsieh* and *H. C. Shih,* Dept. of Materials Science and Engineering, National Tsing Hua University, Hsinchu 30043, Taiwan, China

Some interesting phenomena were found in illuminated n-GaP in the mixture of concentrated HCl/HNO_3 solutions. No trace of reaction products has been detected by inductively coupled plasma emission spectrometry in the etching solution which was prepared by dissolving the most concentrated HCl and HNO_3 in the adequate amount of pure water followed by a uniform mix of individual solutions. However, from the qualitative observation of the way in which the surface on the sample foamed in the solution which was obtained from the mixture of the two most acidic solutions, then it was diluted to the same concentration as mentioned above. It appeared that the reaction occurred suddenly and rapidly. Knowledge of this difference is of particular importance to indicate which parameter controls the etching reactivity of the n-GaP in a mixture of hydrochloric and nitric acids. Brown fumes were observed to evolve, presumably nitrogen dioxide, when the two most acidic solutions were mixed with each other. On the contrary, no gas was evolved from the mixture of the two diluted acids. Consequently, it is revealed that etching is very susceptible to the attack and dissolution by the product of the reaction between hydrochloric and nitric acids.

582 SOA Wafer Level Characterization of InP and GaAs Based Devices: *G.E. Carver* and *R. W. Heebner,* AT&T Bell Laboratories, Princeton, NJ 08540

Micron-sized defects in GaAs and InP wafers have been detected via spatially resolved photoluminescence (SRPL). Contrast levels in SRPL scans are due to local variations in electron/hole pair recombination rates. Optical contrast is interpreted by analyzing the composition and structure of scanned areas with destructive techniques such as TEM, SIMS, and chemical etching. SRPL scans are displayed on a video monitor with a 250 by 250 micron field of view. This limited field size allows for the observation of micron-sized features, but necessitates high rate scanning such that wafer maps can be generated in reasonable lengths of time. Further, defects within video frames must be counted in real time. Color coded maps of GaAs and InP wafers separate and display the spatial distributions of bulk defect density and localized polishing damage. The impact of defects on device performance depends on the nature of the defect, the device design, and the location of the defects within the device. Wafer level maps in semi-insulating GaAs wafers have been spatially registered to regions destined to become the gates of FETs. Maps in quaternary epitaxial films on InP wafers must be registered to areas that will form the mesas in semiconductor laser structures.

583 SOA Nondestructive Evaluation of AlGaAs/GaAs Heterojunction Structures by Photoluminescence Spectroscopy: *Z. H. Lu, M. C. Hanna, E. G. Oh, E. Mao, B. W. Kim,* and *A. Majerfeld,* Dept. of Electrical and Computer Engineering, University of Colorado, Boulder, CO 80309. *P. D. Wright,* Martin Kestrel Co., Colorado Springs, CO 80921. *L. W. Wang,* Ford Microelectronics, Inc., Colorado Springs, CO 80908

We show an essentially nondestructive method of using low temperature photoluminescence (PL) spectroscopy for the evaluation of npn heterojunction bipolar transistor (HBT) wafers. The hole density in the base of carbon doped HBT structures was determined from the PL emission peak associated with the p$^+$-GaAs on the basis of significant bandgap narrowing in heavily doped GaAs. In addition, we observed physically significant correlations between the other PL emission peaks and key electrical properties of the HBTs, in particular, the quality of the emitter-base heterojunction. We applied this method to characterize HBT structures with base thickness of 75-100 nm and hole density of 10^{19}-10^{20} cm^{-3} obtaining useful insight into the performance of these devices. We also observed distinctive characteristics of PL spectrum which relate to the relative position of the p-n and the metallurgical junctions. These results show that PL analysis is a powerful tool that can provide rapid feedback for the evaluation of heterojunction structures and, therefore, it aids in the growth and design of heterojunction devices.

584 SOA Very High Quality GaAs/AlGaAs Multiple Quantum Well Structures Grown by Atmospheric Pressure MOVPE: *E. Mao, Z. H. Lu, B. W. Kim, T. McCormick, E. G. Oh,* and *A. Majerfeld,* Dept. of Electrical and Computer Engineering, University of Colorado, Boulder, CO 80309

We demonstrate, for the first time, that GaAs/AlGaAs multiple quantum well (MQW) structures grown by the atmospheric pressure metalorganic vapor phase epitaxy (MOVPE) process have state-of-the-art structural, electrical and optical properties. The 50-well MQW structures, with well thicknesses ranging from 14 to 90 Å, were grown at 720°C with trimethylgallium, trimethylaluminum, and arsine as sources. The structures were investigated by atomic resolution transmission electron microscopy (TEM), photoluminescence (PL), and deep level transient spectroscopy (DLTS) techniques. A theoretical model including both bound and virtual states in the MQWs was developed to correlate the TEM lattice imaging observations with the interband 10 K PL spectrum and intersubband infrared absorption data. This study proves that MQW structures with wells as thin as 14 Å can be grown by the MOVPE process having layer to layer thickness uniformity, interface roughness and heterojunction abruptness of only one monolayer.

585 SOA AlAs/GaAs Lattice Parameter Measurement by High Resolution X-Ray Diffraction: *C. Ferrari, C. Bocchi, P. Franzosi, A. Bosacchi,* and *S. Franchi,* C.N.R.-MASPEC Institute, Parma, Italy

The high resolution diffraction technique can be used for measuring the alloy composition in III-V epitaxial layers with an accuracy which in many cases is better than 1%. This method is based on the exact knowledge of the semiconductor lattice parameters and on the application of Vegard's law. Unfortunately the composition measurement in the GaAlAs/GaAs system is difficult because of the small lattice parameter difference between AlAs and GaAs and the poor accuracy of the AlAs parameter values reported in the literature, some of them being obtained from powder diffraction data. In this work an accurate measurement of the AlAs parameter has been performed by the analysis of the x-ray diffraction profiles of some AlAs epitaxial samples grown by the molecular beam epitaxy technique on semi-insulating GaAs substrates. X-ray topography was used to verify that no misfit dislocations were introduced during the growth. A very good fit between the experimental and simulated profiles could be obtained with an AlAs lattice parameter of 5.66203 Å if a Poisson ratio $n = 0.299$ for the elastically deformed AlAs layer and a GaAs lattice parameter of 5.6535 Å were assumed. An accurate analysis of the diffraction profiles also evidenced a small mismatch between the semi-insulating substrate and the undoped GaAs cap.

586 SOA X-Ray Diffraction and Electron Microscopy Characterization of H_2 Implanted InP Single Crystals: *P. Franzosi* and *C. Bocchi,* C.N.R.-MASPEC Institute, Parma, Italy. *L. Gastaldi,* CSELT, Torino, Italy. *L. Lazzarini,* and *G. Salviati,* C.N.R. MASPEC Institute, Parma, Italy

H_2 was implanted in n-type InP crystals grown by the liquid encapsulated Czochralski method; the ion energy as 200 KeV and the dose ranged from $5 \cdot 10^{12}$ to $5 \cdot 10^{15}$ cm^{-2}. The structural properties were studied by x-ray diffraction and transmission electron microscopy. The lattice strain was measured using both a double crystal diffractometer and a high resolution diffractometer equipped with a four crystal monochromator. Cu $K\alpha_1$ radiation,

004 symmetric and 117 asymmetric reflections were used. By means of standard simulation procedures the depth dependence of the lattice strain normal to the surface was determined. H_2 implantation has been found to produce a lattice dilation; for the highest dose ($5 \cdot 10^{15}$ cm^{-2}) a maximum strain of about $2.1 \cdot 10^{-2}$ has been obtained. The strain decreases rapidly by decreasing the dose and no strain has been observed for doses smaller than $5 \cdot 10^{14}$ cm^{-2}. The correlation between doses and distribution and nature of extended defects has been studied both by conventional and high resolution electron microscopy on both (001) plan view and (011) cross-sectional samples prepared by iodine ion milling. The defect depth distribution has been correlated to the strain depth profiles obtained from x-ray diffraction; finally, the defect nature and its influence on the strain profiles has been also studied by comparing x-ray and electron microscopy results.

587 SOA Structural Characterization by TEM of Strained InGaAs/InAlAs Quantum Well Structures: *F. Peiró, A. Cornet, and J. R. Morante*, LCMM. Dept. Física Aplicada i Electrònica, U.B., 08028 Barcelona, Spain. *A. Georgakilas* and *G. Halkias*, F.O.R.T.H., Heraklion, Crete

Lately there has been extensive research into the properties of strained structures. It is now clear that strain provides a most useful additional parameter in the design and fabrication of devices based on semiconductor superlattices and multiquantum wells. However, to date these devices are not fully developed due to the difficulties to fabricate structures with good crystalline quality. In this work we use transmission electron microscopy (TEM) to study the structural properties of strained InGaAs/InAlAs quantum well structures on InP substrates in order to improve the technological growth conditions. The first part of the work will be devoted to the study the optimization of the InAlAs buffer layer used to favor the overgrowth of the epilayer with a good crystalline quality. Finally, a structural characterization of the influence of lattice mismatch and epilayer thickness on the morphology of the single and multiple quantum well structures is presented.

588 SOA Spectral Decomposition of Mapped PIMR Semiconductor Wafer Characterization Data Using Numerical Frequency Domain Methods: *E. R. Atwood* and *R. J. Gutmann*, Dept. of Electrical, Computer and Systems Engineering, The New York State Center for Advanced Technology in Automation and Robotics and The Center for Integrated Electronics, Rensselaer Polytechnic Institute, Troy, NY 12180

Photoinduced microwave reflectometry (PIMR) is used in conjunction with image processing methods to produce spatially resolved maps of structures across semi-insulating gallium arsenide and indium phosphide substrates. Two maps of peak conductivity transient data are obtained using AlGaAs and GaAs pulsed lasers. For GaAs substrates the optical excitation is above and below bandgap, while for InP both lasers are above bandgap. Previous work has shown that for GaAs substrates the peak photo induced transient response is related to shallow acceptor and defect concentrations, while the InP peak transient response is sensitive to surface quality. A third map of conductivity (dark) is obtained without optical excitation. The mapped dark data represents variations in material conductivity, augmented by the effect of wave interactions between the microwave probe system and the wafer under test. Image processing using Fourier domain techniques allows separation of mapped photo-induced peak transient data from dark mapped data. Image processing also provides a way to separate the peak transient response from the two different optical sources into correlated and uncorrelated transient response maps. The maps yield spatial information related to carrier generation and recombination. The mapped PIMR method combined with image processing can provide an enhanced noncontacting nondestructive method for the characterization of GaAs and InP semiconductor substrates.

LATEST VOLUMES OFF THE PRESS

THE ELECTROCHEMICAL SOCIETY BOOKS IN PRINT

Proceedings Volumes from 1990-1991 Symposia

The following softbound proceedings volumes are sponsored and published by The Electrochemical Society, Inc., Orders filled at the list price given, subject to availability. Send order with payment to: The Electrochemical Society, Inc., 10 South Main Street, Pennington, NJ 08534-2896. Phone (609-737-1902) or FAX (609-737-2743) orders are accepted with bank card payment (Mastercard or Visa).

Fourth International Symposium on Silicon-on-Insulator Technology and Devices. (PV 90-6) D. N. Schmidt, Editor. A 1990 symposium. 580 pages. **$48.00 Member, $58.00 Nonmember.**

Semiconductor Silicon/1990. (PV 90-7) H. R. Huff, K. G. Barraclough, and J-i. Chikawa, Editors. A 1990 symposium. 1120 pages. **$70.00 Member, $84.00 Nonmember.**

Electrochemical Engineering and Small Scale Electrolytic Processing. (PV 90-10) C. W. Walton, J. W. Van Zee, and R. D. Varjian, Editors. A 1990 symposium. 324 pages. **$28.00 Member, $34.00 Nonmember.**

Plasma Processing. (PV 90-14) G. S. Mathad and D. W. Hess, Editors. A 1990 symposium. 800 pages. **$50.00 Member, $60.00 Nonmember.**

Twelfth State-of-the-Art Program on Compound Semiconductors and Superlattice Structures and Devices. (PV 90-15) D. C. D'Avanzo, A. T. Macrander, R. E. Enstrom, and D. DeCoster, Editors. A 1990 symposium. 480 pages. **$40.00 Member, $48.00 Nonmember.**

Seventh International Symposium on Molten Salts. (PV 90-17) C. L. Hussey, J. S. Wilkes, S. N. Flengas, and Y. Ito, Editors. A 1990 symposium. 892 pages. **$58.00 Member, $70.00 Nonmember.**

Eleventh International Conference on Chemical Vapor Deposition. (PV 90-12) K. E. Spear and G. W. Cullen, Editors. A 1990 symposium. 764 pages. **$70.00 Member, $84.00 Nonmember.**

Second International Symposium on Process Physics and Modeling in Semiconductor Technology. (PV 91-4) G. R. Srinivasan, J. D. Plummer, and S. T. Pantelides, Editors. A 1990 symposium. 820 pages. **$42.00 Member, $50.00 Nonmember.**

Molten Carbonate Fuel Cell Technology. (PV 90-16) J. R. Selman, H. C. Maru, D. A. Shores, and I. Uchida, Editors. A 1990 symposium. 542 pages. **$40.00 Member, $48.00 Nonmember.**

High Temperature Materials Chemistry—V. (PV 90-18) W. B. Johnson and R. A. Rapp, Editors. A 1990 symposium. 248 pages. **$30.00 Member, $36.00 Nonmember.**

Thirteenth State-of-the-Art Program on Compound Semiconductors and Metallization of III-V Compound Semiconductors. (PV 91-1) H. H. Lee, P. Clechet, O. Ueda, and J. M. Woodall, Editors. A 1990 symposium. 376 pages. **$40.00 Member, $48.00 Nonmember.**

Corrosion of Electronic Materials and Devices. (PV 91-2) J. D. Sinclair, Editor. A 1990 symposium. 480 pages. **$36.00 Member, $43.00 Nonmember.**

Primary and Secondary Lithium Batteries. (PV 91-3) K. M. Abraham and M. Salomon, Editors. A 1990 symposium. 456 pages. **$44.00 Member, $53.00 Nonmember.**

Automated Integrated Circuits Manufacturing. (PV 91-5) V. E. Akins and H. Harada, Editors. A 1990 symposium. 424 pages. **$36.00 Member, $43.00 Nonmember.**

High Temperature Electrode Materials and Characterization. (PV 91-6) D. D. Macdonald and A. C. Khandkar, Editors. A 1991 symposium. 304 pages. **$32.00 Member, $39.00 Nonmember.**

4/92

The Application of Surface Analysis Methods to Environmental/Material Interactions. (PV 91-7) D. R. Baer, C. R. Clayton, and G. D. Davis, Editors. A 1991 symposium. 576 pages. **$47.00 Member, $57.00 Nonmember.**

Second International Symposium on Diamond Materials. (PV 91-8) A. J. Purdes, J. C. Angus, R. F. Davis, B. M. Meyerson, K. E. Spear, and M. Yoder, Editors. A 1991 symposium. 688 pages. **$64.00 Member, $77.00 Nonmember.**

Defects in Silicon II. (PV 91-9) W. M. Bullis, U. Gösele, and F. Shimura, Editors. A 1991 symposium. 704 pages. **$66.00 Member, $79.00 Nonmember.**

Modeling of Batteries and Fuel Cells. (PV 91-10) R. E. White, M. W. Verbrugge, and J. F. Stockel, Editors. A 1991 symposium. 412 pages. **$36.00 Member, $43.00 Nonmember.**

ULSI Science and Technology/1991. (PV 91-11) J. M. Andrews and G. K. Celler, Editors. A 1991 symposium. 924 pages. **$72.00 Member, $86.00 Nonmember.**

First International Symposium on Ionic and Mixed Conducting Ceramics. (PV 91-12) T. A. Ramanarayanan and H. L. Tuller, Editors. A 1991 symposium. 264 pages. **$30.00 Member, $36.00 Nonmember.**

Fourteenth State-of-the-Art Program on Compound Semiconductors and Large Area/Scale Epitaxy for III-V Device Fabrication. (PV 91-13) D. N. Bucklev and A. T. Macrander, Editors. A 1991 symposium. 316 pages. **$45.00 Member, $54.00 Nonmember.**

Low Temperature Electronic Device Operation (PV 91-14). D. Foty, N. Saks, S. Raider, and G. Oleszek, Editors. A 1991 symposium. 256 pages. **$33.00 Member, $40.00 Nonmember.**

X-Ray Methods in Corrosion and Interfacial Electrochemistry (PV 92-1). A. Davenport and J. G. Gordon II, Editors. A 1991 symposium. 392 pages. ISBN 1-56677-000-9. **$35.00 Member, $42.00 Nonmember.**

Diagnostic Techniques for Semiconductor Materials and Devices (PV 92-2). J. L. Benton, G. N. Maracas, P. Rai-Choudhury, Editors. A 1991 symposium. 292 pages. ISBN 1-56677-001-7. **$30.00 Member, $36.00 Nonmember.**

First International Symposium on Electrochemical Microfabrication (PV 92-3). M. Datta, K. Sheppard, and D. Snyder, Editors. A 1991 symposium. 404 pages. ISBN 1-56677-002-5. **$35.00 Member, $42.00 Nonmember.**

Reliability of Semiconductor Devices/Interconnections and Dielectric Breakdown and Laser Processes for Microelectronic Applications (PV 92-4). H. S. Rathore, G. S. Mathad, and D. B. Nguyen, Editors. A 1991 symposium. 340 pages. ISBN 1-56677-003-3. **$35.00 Member, $42.00 Nonmember.**

Hydrogen Storage Materials, Batteries, and Electrochemistry (PV 92-5). D. A. Corrigan and S. Srinivasan, Editors. A 1991 symposium. 460 pages. ISBN 1-56677-006-8. **$36.00 Member, $43.00 Nonmember.**

Patterning Science and Technology II and Interconnection and Contact Metallization for ULSI (PV 92-6). W. Greene, G. J. Hefferon, L. K. White, T. O. Herndon, and A. L. Wu, Editors. A 1991 symposium. 392 pages. ISBN 1-56677-007-6. **$36.00 Members, $43.00 Nonmember.**

QUANTUM CONFINEMENT

New Technology Subcommittee/Electronics/Dielectric Science and Technology

St. Louis Ballroom F, 4th Level

WEDNESDAY, MAY 20 1992

E. H. Nicollian, Chairman; R. Tsu, Vice-Chairman

10:00	From Superlattices, Quantum Wells to Quantum Dots - R. Tsu	589 QUA
10:45	Semiconductor Nanocrystals - A. P. Alivisatos	590 QUA
11:30	$HBr/HNO_3/H_2O$ A Solution for Submicrometer III-V Compounds Etching: Diffraction Gratings, Quantum Wire and Quantum Box Applications - S. Pellegreno, L. Boschis, and P. Doste	591 QUA

WEDNESDAY, MAY 20, 1992

R. Tsu, Chairman, E. H. Nicollian, Vice-Chairman

2:00	Admittance of Silicon Quantum Dots - E. H. Nicollian	592 QUA
2:30	Two-Dimensional Carrier Confinement in GaAlAs Quantum Wire Arrays Grown by Molecular Beam Epitaxy - P. M. Petroff	593 QUA
3:00	Quantum Devices or Quantum Chaos - M. A. Reed	594 QUA
3:30	Germanium - Silicon Quantum Well Structures - J. C. Bean and R. People	595 QUA

QUA

Abstracts

589 QUA From Superlattices, Quantum Wells to Quantum Dots: *R. Tsu*, University of North Carolina, Charlotte, NC 28223

Since the introduction of superlattices and quantum well structures, it is well known that quantum mechanics plays a major role in the understanding of quantum effects. Quantum dots represent a further leap into the man-made atoms. The physics and chemistry of three-dimensional quantum confinement and its implications on quantum devices are discussed.

590 QUA Semiconductor Nanocrystals: *A. P. Alivisatos*, Dept. of Chemistry, University of California, Berkeley, CA 94720

Relatively monodisperse, high quality nanocrystals of II-VI and III-V semiconductors can be produced by colloidal chemical synthesis. Because of their finite size, these nanocrystals have many size-dependent properties, including: melting temperature, optical spectrum, electron-phonon coupling, and others. The chemical nature of the nanocrystal surface can be manipulated, so that one can control the environment of the nanocrystals. Thus, they can be bound to a metal of semiconductor surface, dissolved homogeneously in a fluid or polymer film, etc. Many interesting quantum confinement effects can be explored in these systems.

591 QUA $HBr/HNO_3/H_2O$ A Solution for Submicrometer III-V Compounds Etching: Diffraction Gratings, Quantum Wire and Quantum Box Applications: *S. Pellegrino*, ALCATEL-TELETTRA, 20059 Vimercate (mI), Italy, *L. Boschis*, CSELT, 10148 Torino, Italy, *P. Daste* (Present address: PICOGICA, F-91940 Les Ulis, France), LEP, 94451 Limeil-Brevannes Cedex, France

We have extensively characterized the $HBr/HNO_3/H_2O$ etching solutions from the point of view of their reactivity in respect to *In(GaAs)P materials. We obtained insight into the chemistry of the* solutions and on the etching mechanism. A minimum controllable 20 Å/min etching rate was measured along with a strong unselectivity with respect to the In(GaAs)P materials range. We found a large capability of tailoring the grating shape in case of diffraction gratings, and the feasibility of quantum wire and box structures was demonstrated.

592 QUA Admittance of Silicon Quantum Dots: *E. H. Nicollian*, University of North Carolina, Charlotte, NC 28223

Admittance measurements on a 200 Å thick layer of silicon microacceptabilities embedded in a matrix of SiO_2 are described. It is shown that electrically active traps at the μc-Si/SiO_2 interface are filled with electrons at gate bias values before quantum confinement occurs. Therefore, even with large electrically active trap densities, coherence is not destroyed and three-dimensional quantum confinement is observed.

593 QUA Two-Dimensional Carrier Confinement in GaAlAs Quantum Wire Arrays Grown by Molecular Beam Epitaxy: *P. M. Petroff*, Materials Dept., University of California, Santa Barbara, CA 93106-5050

Quantum wire superlattices are obtained by direct growth on a GaAs vicinal (100) surface by alternately depositing submonolayers of GaAs and AlAs. By varying linearly as a function of time the total amount deposited per GaAs-AlAs cycle, a superlattice consisting of quantum wells with parabola-shaped interfaces is formed. At the apex of each parabola, a quantum wire region is introduced. This type of superlattice is hereafter called a "serpentine superlattice" (SSL). We have used transmission electron microscopy (TEM) measurements to characterize the SSL perfection. TEM contrast studies indicate a poor segregation of the group III elements at the step edges during deposition. This in turn produces quantum wires with $Al_xGa_{1-x}As$ in the wires and nonabrupt interfaces between wire and barrier regions. Both [100] and [110] vicinal surfaces have been investigated. We find that the Al segregation at step edges is superior for growth on the [100] vicinal surfaces. Possible reasons for this result are given. Polarization dependent photoluminescence and photoluminescence excitation measurements have been used to characterize carrier confinement. A comparison of the luminescence data with calculated optical properties as a function of segregation into lateral wells and barriers, yields $Al_xGa_{1-x}As$ wells and barriers with $x = 0.11$ and 0.22, respectively, instead of the nominally intended values of 0.00 and 0.33. The optical characteristics of a GaAs-AlGaAs laser with a quantum wire array in the active region are discussed.

594 QUA Quantum Devices or Quantum Chaos?: *M. A. Reed*, Dept. of Electrical Engineering, Yale University, New Haven, CT 06520

Recent advances in nanometer scale fabrication techniques now allow the realization of quantum-confined and charge-quantized electron systems that exhibit transport phenomena dominated by quantum effects and single-electron charging effects. These systems are fascinating nanoscale laboratories to probe the limit of electron conduction and quantum effects at the one-electron level, and promise a technology for future integrated circuits with staggering density. A brief introductory survey of the physics and technology of some of these structures is presented. At present, the implementation of useful electron devices and circuits utilizing quantum-confined or charge-confined effects has not yet occurred. In addition to well-recognized problems of fabrication and tolerance that exist at this scale, there are issues that are unique to quantum devices and circuits, such as: isolation in phase-coherent structures; how to obtain gain from single-electron devices; invasive and statistically uncontrollable contacts; and architectural issues. This paper focuses on the critical issues that impede the insertion of quantum devices into useful electronic circuits, and possible solutions to these problems.

595 QUA Germanium Silicon Quantum Well Structures: *J. C. Bean* and *R. People*, AT&T Bell Laboratories, Murray Hill, NJ 07974

Ge_xSi_{1-x}/Si quantum wells have been used to fabricate modulation doped transistors, 1.3 μm avalanche photodetectors, resonant tunneling diodes, and 8-14 μm intrasubband infrared devices. Although these devices resemble III-V semiconductor analogs, strain fundamentally alters their characteristics. A strained alloy may have a bandgap one-third lower than a comparable relaxed structure. Normally degenerate conduction and valence band energy levels will be strongly split. The conduction bandedge of the alloy may move either above or below that of adjacent silicon, producing structures where electrons and holes accumulate in the same layer or are driven into adjacent layers. Finally, in even "conventional" device structures, the maintenance of defect-free strained layer growth may require individual layer thickness so small that pronounced quantum confinement effects occur. The design of Ge_xSi_{1-x}/Si quantum structures it thus significantly more complex. In certain instances, such as intrasubband absorption, it can yield a particularly broad and useful infrared device characteristic.

THE ELECTROCHEMICAL SOCIETY BOOKS IN PRINT

Proceedings Volumes from 1987-1989 Symposia

The following softbound proceedings volumes are sponsored and published by The Electrochemical Society, Inc., 10 South Main Street, Pennington, NJ 08534-2896. Orders filled at the list price given, subject to availability. Enclose payment with order, either by check or Mastercard or VISA credit card.

ULSI Science and Technology/1987. (PV 87-11) S. Broydo and C. M. Osburn, Editors. A 1987 symposium. 852 pages, **$50.00.**

Electrode Materials and Processes for Energy Conversion and Storage. (PV 87-12) S. Srinivasan, S. Wagner, and H. Wroblowa, Editors. A 1987 symposium. 660 pages, **$45.00.**

High Voltage and Smart Power Devices. (PV 87-13) P. W. Shackle, Editor. A 1987 symposium. 360 pages, **$35.00.**

History of Battery Technology. (PV 87-14) A. J. Salkind, Editor. A 1987 symposium. 296 pages, **$23.00.**

Sensor Science and Technology. (PV 87-15) B. Schumm, Jr., C. C. Liu, R. A. Powers, and E. B. Yeager, Editors. A 1987 symposium. 237 pages, **$25.00.**

Second Annual Battery Conference on Application and Advances. (PV 87-16) R. L. Das, B. M. Eliash, H. A. Frank, and D. F. Pickett, Jr., Editors. A 1987 symposium. 274 pages, **$25.00.**

Joint International Symposium on Molten Salts. (PV 87-7) G. Mamantov, M. Blander, C. Hussey, C. Mamantov, M.-L. Saboungi, and J. Wilkes, Editors. A 1987 symposium. 1080 pages, **$75.00.**

Tenth International Conference on Chemical Vapor Deposition. (PV 87-8) G. W. Cullen, Editor. A 1987 symposium. 1288 pages, **$65.00.**

Chemical Sensors. (PV 87-9) D. R. Turner, Editor. A 1987 symposium. 548 pages, **$45.00.**

Corrosion, Electrochemistry, and Catalysis of Metallic Glasses. (PV 88-1) R. B. Diegle and K. Hashimoto, Editors. A 1987 symposium. 448 pages, **$30.00.**

Electrochemical Engineering in the Chlor-Alkali and Chlorate Industries. (PV 88-2) F. Hine, R. E. White, W. B. Darlington, and R. D. Varjian, Editors. A 1987 symposium. 416 pages, **$30.00.**

Electro-Ceramics and Solid-State Ionics. (PV 88-3) H. L. Tuller and D. M. Smyth, Editors. A 1987 symposium. 244 pages, **$25.00.**

High Temperature Materials IV. (PV 88-5) Z. A. Munir, D. Cubicciotti, and H. Tagawa, Editors. A 1987 symposium. 672 pages, **$56.00.**

Primary and Secondary Ambient Temperature Lithium Batteries. (PV 88-6) J. P. Gabano, Z. Takehara, and P. Bro, Editors. A 1987 symposium. 816 pages, **$56.00.**

Dry Process. (PV 88-7) J-i. Nishizawa, M. Hirose, Y. Horiike, and K. Suto, Editors. A 1987 symposium. 356 pages, **$28.00.**

Second International Symposium on Silicon Molecular Beam Epitaxy. (PV 88-8) J. C. Bean and L. J. Schowalter, Editors. A 1987 symposium. 640 pages. **$45.00.**

Low Temperature Electronics and High Temperature Superconductors. (PV 88-9) S. I. Raider, R. Kirschman, H. Hayakawa, and H. Ohta, Editors. A 1987 symposium. 616 pages, **$55.00.**

Laser Processes for Microelectronic Applications. (PV 88-10) J. J. Ritsko, D. J. Ehrlich, and M. Kashiwagi, Editors. A 1987 symposium. 260 pages, **$25.00.**

Stationary Energy Storage: Load Leveling and Remote Applications. (PV 88-11) A. R. Landgrebe, D. J. Rand, S. L. Van Voorhees, and R. K. Sen, Editors. A 1987 symposium. 408 pages, **$40.00.**

Electroless Deposition of Metals and Alloys. (PV 88-12) M. Paunovic and I. Ohno, Editors. A 1987 symposium. 306 pages, **$25.00.**

Automated Integrated Circuits Manufacturing. (PV 88-13) J. B. Anthony, Editor. A 1987 symposium. 486 pages, **$45.00.**

Photoelectrochemistry and Electrosynthesis on Semiconducting Materials. (PV 88-14) D. S. Ginley, K. Honda, A. Nozik, A. Fujishima, N. Armstrong, T. Sakata, and T. Kawai, Editors. A 1987 symposium. 518 pages, **$56.00.**

Dielectric Films on Compound Semiconductors. (PV 88-15) V. J. Kapoor, Editor. A 1987 symposium. 340 pages, **$25.00.**

Polymeric Materials for Electronic Packaging and High Technology Applications. (PV 88-17) J. R. Susko, R. W. Snyder, and R. A. Susko, Editors. A 1987 symposium. 220 pages, **$25.00.**

Modeling and Simulation of Electrolytic Solution Processes. (PV 88-18) D-T. Chin and P. N. Pintauro, Editors. A 1987 symposium. 296 pages. **$27.00 Member, $32.00 Nonmember.**

Electrochemical Technology in Electronics. (PV 88-23) L. T. Romankiw and T. Osaka, Editors. A 1987 symposium. 798 pages, **$47.00.**

First International Symposium on BiCMOS. (PV 89-8) A. M. Saxena, Editor. A 1987 symposium. 140 pages. **$25.00.**

High Temperature Lamp Chemistry II. (PV 88-4) E. G. Zubler, Editor. A 1988 symposium. 360 pages, **$30.00.**

First International Symposium on Advanced Materials for ULSI. (PV 88-19) M. P. Scott, Y. Akasaka, and R. Reif, Editors. A 1988 symposium. 252 pages, **$32.00.**

Diagnostic Techniques for Semiconductor Materials and Devices. (PV 88-20) T. J. Shaffner and D. K. Schroder, Editors. A 1988 symposium. 296 pages. **$30.00 Member, $36.00 Nonmember.**

Electrochemistry in Mineral and Metal Processing II. (PV 88-21) P. E. Richardson and R. Woods, Editors. A 1988 symposium. 572 pages, **$35.00.**

Plasma Processing. (PV 88-22) G. S. Mathad, G. C. Schwartz, and D. W. Hess, Editors. A 1988 symposium. 408 pages, **$38.00.**

Luminescence Science and Technology. (PV 88-24) C. W. Struck, B. DiBartolo, and W. M. Yen, Editors. A 1988 symposium. 303 pages, **$45.00 Member, $54.00 Nonmember.**

Transie... Techniques in Corrosion Science and Engineering. (PV 89-1) W. H. Smyrl, D. D. Macdonald, and W. J. Lorenz, Editors. A 1988 symposium. 432 pages, **$35.00 Member, $42.00 Nonmember.**

Fourth Symposium on Automated Integrated Circuits Manufacturing. (PV 89-2) J. B. Anthony, Editor. A 1988 symposium. 320 pages, **$30.00 Member, $36.00 Nonmember.**

Packaging of Electronic Devices. (PV 89-3) P. Bindra and R. A. Susko, Editors. A 1988 symposium. 260 pages, **$28.00.**

Materials and Processes for Lithium Batteries. (PV 89-4) K. M. Abraham and B. B. Owens, Editors. A 1988 symposium. 416 pages, **$40.00 Member, $48.00 Nonmember.**

Heteroepitaxial Approaches in Semiconductors: Lattice Mismatch and Its Consequences. (PV 89-5) A. T. Macrander and T. J. Drummond, Editors. A 1988 symposium. 404 pages, **$38.00 Member, $46.00 Nonmember.**

Reliability of Semiconductor Devices and Interconnection and Multilevel Metallization, Interconnection, and Contact Technologies. (PV 89-6) H. S. Rathore, G. C. Schwartz, and R. A. Susko, Editors. A 1988 symposium. 504 pages, **$37.00 Member, $44.00 Nonmember.**

Silicon Nitride and Silicon Dioxide Thin Insulating Films. (PV 89-7) S. B. Bibyk, V. J. Kapoor, and N. S. Alvi, Editors. A 1988 symposium. 464 pages, **$48.00 Member, $58.00 Nonmember.**

Second International Symposium on ULSI Science and Technology. (PV 89-9) C. M. Osburn and J. M. Andrews, Editors. A 1989 symposium. 788 pages, **$54.00 Member, $65.00 Nonmember.**

Performance of Electrodes for Industrial Electrochemical Processes. (PV 89-10) F. Hine, B. V. Tilak, J. M. Fenton, and J. D. Lisius, Editors. A 1989 symposium. 328 pages, **$25.00 Member, $30.00 Nonmember.**

First International Symposium on Solid Oxide Fuel Cells. (PV 89-11) S. C. Singhal, Editor. A 1989 symposium. 408 pages, **$40.00 Member, $48.00 Nonmember.**

First International Symposium on Diamond and Diamond-Like Films. (PV 89-12) J. P. Dismukes, A. J. Purdes, B. S. Meyerson, T. D. Moustakas, K. E. Spear, K. V. Ravi, and M. Yoder, Editors. A 1989 symposium. 692 pages, **$48.00 Member, $58.00 Nonmember.**

Advances in Corrosion Protection by Organic Coatings. (PV 89-13) D. Scantlebury and M. Kendig, Editors. A 1989 symposium. 552 pages, **$44.00 Member, $53.00 Nonmember.**

Fuel Cells. (PV 89-14) R. E. White and A. J. Appleby, Editors. A 1989 symposium. 370 pages, **$35.00 Member, $42.00 Nonmember.**

High Voltage and Smart Power ICs. (PV 89-15) M. A. Shibib, Editor. A 1989 symposium. 530 pages. **$45.00 Member, $54.00 Nonmember.**

Patterning Science and Technology. (PV 90-1) R. Gleason, G. J. Heferon, and L. K. White, Editors. A 1989 symposium. 260 pages, **$32.00 Member, $38.00 Nonmember.**

Electrochromic Materials. (PV 90-2) M. K. Carpenter and D. A. Corrigan, Editors. A 1989 symposium. 380 pages, **$35.00 Member, $42.00 Nonmember.**

Fifth Symposium on Automated Integrated Circuits Manufacturing. (PV 90-3) V. Akins, Editor. A 1989 symposium. 296 pages, **$30.00 Member, $36.00 Nonmember.**

Nickel Hydroxide Electrodes. (PV 90-4) D. A. Corrigan and A. H. Zimmerman, Editors. A 1989 symposium. 448 pages. **$30.00 Member, $36.00 Nonmember.**

Rechargeable Lithium Batteries. (PV 90-5) S. Subbarao, V. R. Koch, B. Owens, and W. H. Smyrl, Editors. A 1989 symposium. 336 pages, **$37.00 Member, $44.00 Nonmember.**

Magnetic Materials, Processes, and Devices. (PV 90-8) L. T. Romankiw and D. A. Herman, Jr., Editors. A 1989 symposium. 780 pages, **$56.00 Member, $67.00 Nonmember.**

First International Symposium on Cleaning Technology in Semiconductor Device Manufacturing. (PV 90-9) J. Ruzyllo and R. E. Novak, Editors. A 1989 symposium. 412 pages, **$45.00 Member, $54.00 Nonmember.**

Analytical Techniques for Semiconductor Materials and Process Characterization. (PV 90-11) B. O. Kolbesen, D. V. McCaughan, and W. Vandervorst, Editors. A 1989 symposium. 372 pages, **$27.00 Member, $32.00 Nonmember.**

Ion Implantation and Dielectrics for Elemental and Compound Semiconductors. (PV 90-13) S. J. Pearton, K. S. Jones, and V. J. Kapoor, Editors. A 1989 symposium. 480 pages, **$30.00 Member, $36.00 Nonmember.**

10/90

MICROMACHINING AND MICROSTRUCTURES

New Technology Subcommittee/Sensor/Electronics/Dielectric Science and Technology

Room 29, 2nd Level

TUESDAY, MAY 19, 1992

J. N. Zemel, Chairman: P. Barth, Vice-Chairman

2:00	Recent Advances in MEMS - G. Hazelrigg	596 MIC
2:40	Vacuum Microelectronics: An Application of Micromachining and Nanostructure Fabrication - H. Gray	597 MIC
3:20	Three Dimensional Silicon Anisotropic Etching - Identification of the Key Etching Planes - P. J. Hesketh	598 MIC

WEDNESDAY, MAY 20, 1992

P. Barth, Chairman; P. J. Hesketh, Vice Chairman

9:00	Packaging and Interconnect Technologies for Solid State Microsensors - K. Najafi	599 MIC
9:40	Micromachining of Chemical Analysis and Electrophoresis Systems - D. J. Harrison, A. Manz, K. Seiler, and Z.-H. Fan	600 MIC
10:00	Multistep Anisotropic Etching Process for Producing a Three Dimensional Accelerometer - A. Koide, K. Sato, S. Suzuki, and S. Naito	601 MIC
10:20	Three Dimensional Fabrication by Precision Stacking Silicon Die - A. D. Feinerman, D. A. Crewe, and S. E. Shoaf	602 MIC
10:40	Ten-minute intermission	

P. J. Hesketh, Chairman; K. Najafi, Vice-Chairman

10:50	Aligned Au-Si Eutectic Bonding Silicon Die - S. E. Shoaf and A. D. Feinerman	603 MIC
11:10	Thermoelectric AC Power Sensor on Silicon Oxide Beam - D. Jaeggi, H. Baltes, and D. Moser	604 MIC
11:30	Thermally Excited Silicon Oxide Resonators in CMOS Technology - O. Brand, D. Moser, and H. Baltes	605 MIC
11:50	Fabrication of Novel Micromachined Magnetic Actuators - A. M. A. Hamad, W. Zhang, H. T. Henderson, and F. Radpour	606 MIC

WEDNESDAY, MAY 20, 1992

K. Najafi, Chairman; H. Baltes, Vice Chairman

2:00	Processing of Ferroelectric Materials in Micromachined Silicon-Based Structures - D. Polla	607 MIC
2:40	Microchannel Pyroelectric Anemometer - D. Yu, H. Y. Hsieh, and J. N. Zemel	608 MIC
3:00	A Fiber Optic Monitored Vertical Pressure Sensor - X.-Z. Tu and J. N. Zemel	609 MIC
3:20	Ten-minute intermission	

H. Baltes, Chairman; D. Polla, Vice-Chairman

3:30	Microfabrication of Silicon X-Ray Analyzer - H. Kasapbasioglu, P. J. Hesketh, and A. T. Macrander	610 MIC
3:50	A Thin Platinum Island Film Glucose Sensor - B. Kasapbasioglu, P. J. Hesketh, W. Carey Hanly, and J. Maclay	611 MIC
4:10	Development and Characterization of an Ultrathin Silicon Nitride for IC Sensor Applications Using Rapid Thermal Processing - R. A. Williams, L. J. Arias, and D. W. Hess	612 MIC
4:30	Late News Items	

MIC

Abstracts

596 MIC Recent Advances in MEMS: *G. A. Hazelrigg* National Science Foundation, Washington, DC 20550

The technologies of microelectronic fabrication have, over the past several years, been extended to include the fabrication of mechanical and electromechanical devices and mechanisms on a very small scale, and laying the foundations of a new field currently referred to as microelectromechanical systems (MEMS). Recently demonstrated devices include electrostatic and electromagnetic motors smaller in diameter than a human hair, gears, pumps and valves, sensors and other structures. Most recently, three-dimensional structures have been fabricated as well, including folding silicon wafers and helixes and needles grown vertical to the wafer. Together, these technologies comprise a basis for chemical processing factories-on-a-chip. This paper reviews the basic technologies of MEMS and then discusses recent advances in the field and their implications.

597 MIC Vacuum Microelectronics: An Application of Micromachining and Nanostructure Fabrication: *H. F. Gray*, Naval Research Laboratory, Washington, DC 20375

With the development of silicon field emitter arrays (FEAs) by micromachining techniques(1) and the reporting of the first vacuum transistor(2), the possibility of a new microelectronics, which we named vacuum microelectronics, was born. In addition to having the fabrication, batch processing, size, weight, integrated circuit, and unit cost advantages of solid-state devices, vacuum microelectronics based on FEAs takes advantage of vacuum electron transport. Vacuum electron transport brings with it faster carrier velocities and lower transit times than solid-state devices of comparable size, the ability to deflect the carriers to multiple collectors, the possibility of much higher voltage and higher power operation, and the promise of immunity to adverse environments, *e.g.*, very high and very low temperatures as well as high radiation environments which destroy or seriously impair solid state device operation. Benefits are even promised to scientific instrumentation because FEAs are electron sources which are essentially mono-energetic, have very high brightness, and exhibit high spatial resolution. Each cell of a FEA contains one 3-D microminiature field emitter and its monolithic extraction electron. The radius of the curvature of the field emitter is usually 100 Å or smaller, the extracture aperature is 1 μm or smaller, and the distance between extraction electrode and field emitter ground plane is about 1 μm. The nanostructure is fabricated by micromachining techniques. This paper addresses a variety of micromachining techniques which have been used throughout the world to fabricate FEAs, including orientation-dependent-etching of silicon, oxidation sharpening, beam deposition, electron beam decomposition, E-beam evaporation, plasma sputtering, reactive ion etching, and isotropic wet etching. We feel that the details of the physics and chemistry of these micromachining processes are not well understood at the present time, and that the science of micromachining of 3-D nanostructures is still in its infancy.

1. H. F. Gray, "Silicon Field Emitter Array Technology," Proceedings of the 29th International Field Emission Symposium, Goteborg, Sweden, p. 111 (1982).

2. H. F. Gray, et al, "A Vacuum Field Effect Transistor Using Silicon Field Emitter Arrays," 1986 IEDM Technical Digest, p. 776 (1986).

598 MIC Three-Dimensional Silicon Anisotropic Etching—Identification of the Key Etching Planes: *P. J. Hesketh*, University of Illinois at Chicago, Chicago, IL 60607.

A single crystal silicon sphere has been etched in aqueous solutions of potassium hydroxide and cesium hydroxide. After etching, a polyhedron-like solid with curved faces is produced with distinct vertices in the directions of the slower etching planes. The solid is twelve sided with aqueous cesium hydroxide and twenty four-sided with aqueous potassium hydroxide. The following crystal planes defined features in the structure, listed in order of ascending etch rate, (*i*) for CsOH, {111}, {100}, {311}, {110}, and, (*ii*) for KOH, {111}, {100}, {311}, {320}.

599 MIC Packaging and Interconnect Technologies for Solid-State Microsensors: *K. Najafi;* Center for Integrated Sensors and Circuits, University of Michigan, Ann Arbor, MI 48109-2122

This paper presents a review of various packaging techniques available for microsensors and the challenges that lie ahead. Hermetic packages based on micromachined silicon and glass capsules have been developed and offer a promising technique for chip-level and wafer-level batch packaging of microsensors. Nonhermetic packaging techniques based on deposited organic and inorganic films have been developed and demonstrate great promise for both microsensors and many high-speed electronic systems. Thin films of vapor deposited silicon nitride, silicon carbide and diamond-like carbon, and of polymers such as parylene are being applied in many microsensors and microsystems and have replaced conventional integrated circuit packages in many areas. For many physical sensors, the package should satisfy the added requirements of isolating the device from external physical and mechanical damage and interference, while being stable in the face of repeated exposure to such environments. Flexible multilead interconnect systems for implantable microsensors have also been developed based on silicon micromachining techniques. Silicon-based ribbon cables that are less than 5 μm thick and 100 μm wide and support a number of hermetically sealed conductors have been developed and offer the only solution to the difficult problem of interfacing with miniature implantable sensors and systems that cannot utilize a conventional package.

600 MIC Micromachining of Chemical Analysis and Electrophoresis Systems: *D. J. Harrison,* Dept. of Chemistry, University of Alberta, Edmonton, AB, Canada T6G 2G2, *A. Manz;* Central Analytical Research, Ciba Geigy, CH-4002 Basel, Switzerland, *K. Seiler,* and *Z. Fan,* Dept. Chemistry, University of Alberta, Edmonton, AB, Canada T6G 2 ;2

In this paper, we demonstrate the feasibility of miniaturizing a total chemical analysis system (μTAS) onto a planar substrate. The system utilizes electrokinetic phenomena for both sample component separation (electrophoresis) and solvent pumping (electro-osmosis flow). Using micromachining, a complex manifold of capillary channels has been fabricated in both glass and silicon substrates. Electro-osmotic pumping of the electrolyte solution within these capillaries has been achieved. However, the breakdown voltage of the silicon devices must be improved, and approaches to achieve this are discussed. In glass substrates, at a field of 300 V/cm, linear flow velocities of about 0.15 cm/s where achieved with 15 cm long channels (10 μm × 30 μm cross section). This simple structure allowed injection of samples from a side channel into the separation channel. The results show that applied potentials can be used to control the magnitude and direction of solvent flow within a manifold of channels. This eliminates the need for valves within the μTAS. On this basis, complex sample pretreatment can be effected within the channel manifold, as well as solvent pumping based on electroosmotic effects. We have also shown that separation of sample components within the glass capillary channels by electrophoresis is possible. The efficiency is exactly that predicted by theory, indicating glass is a suitable device substrate for capillary electrophoresis.

601 MIC Multistep Anisotropic Etching Process for Producing a 3-D Silicon Accelerometer: *A. Koide* and *K. Sato,* Central Research Laboratory, Hitachi Ltd, Kokubunji, Tokyo 185, Japan, *S. Suzuki,* Hitachi Research Laboratory, 4026 Kuji-cho, Hitachi-shi, Ibaraki-ken 319-12, Japan, *S. Naito,* Hitachi Ltd., Automotive Products Div., 2520 Oaza-takaba, Katsuta-Shi, Ibaraki-ken 312, Japan

A new anisotropic etching process for producing three-dimensional structures that can be applied to micromechanical silicon accelerometers is developed. Severe anisotropic etching steps are carried out sequentially. The main advantages of this process are: (*i*) a very thin cantilever can be precisely formed in the middle of the wafer; and (*ii*) a round etch profile can be made which reduces stress concentration is possible for the first time.

602 MIC Three-Dimensional Fabrication by Precision Stacking Silicon Die: *A. D. Feinerman, D. A. Crewe,* and *S. E. Shoaf;* Microfab. Appl. Lab., Dept. of Electrical Engineering and Computer Science, University of Illinois at Chicago, Chicago, IL 60680

A technique for creating three-dimensional structures with an accuracy approaching 1 μm has been developed. The immediate goal of this research is the microfabrication of a 1 cm^3 low voltage high resolution SEM. The technique combines semiconductor processing and fiber optic technology. A (100) silicon wafer is anisotropically etched to create precision v-grooves and then diced into individual die. Two methods have been developed for large and small gaps between the die. For large gaps, optical fibers are placed into the grooves then anodically bonded at 500°C. This technique presently has been used to stack up to 5 silicon die creating an electron optical column ~2.5 μm thick. The alignment accuracy between die is ~2 μm and the alignment of the top and bottom surfaces of each die is ~5 μm. The strength of the bond between the die and the fibers exceeds 1.2 lb. For small gaps, the inside of a capillary tube is metallized and then the capillaries are placed into the grooves and anodically bonded to the die.

603 MIC Aligned Au-Si Eutectic Bonding of Silicon Die: *S. E. Shoaf,* and *A. D. Feinerman,* Microfab. Appl. Lab., Dept. of Electrical Engineering and Computer Science, University of Illinois at Chicago, Chicago, IL 60680

A technique for precisely aligning structures prior to an Au-Si bond has been developed. This technique has applications to electron column fabrication and three-dimensional wafer interconnects. A (100) silicon wafer is anisotropically etched to create v-grooves around the periphery of the structure to be bonded. Gold is then deposited onto one of the wafers prior to dicing into individual die. Optical fibers serve as precision locating keys and align the die as they are assembled. The entire structure is then placed on a hot chuck at 400°C. An ultrasonic transducer aides the Au-Si bond. The fibers can be pulled out after bonding since the v-grooves are oversize. The width of the v-grooves is the 1.22*fiber diameter plus the desired tolerance. Early results have shown a maximum misalignment of 15 μm. This work will be extended to a higher accuracy and include silicon fusion and organic bonding.

604 MIC Thermoelectric AC Power Sensor on Silicon Oxide Beam: *D. Jaeggi, H. Baltes,* and *D. Moser,* Physical Electronics Laboratory, Swiss Federal Institute of Technology, CH-8093 Zurich, Switzerland

We report the first thermoelectric ac power sensor (thermoconverter) realized by industrial CMOS IC technology in combination with postprocessing micromachining. The sensor is based on a polysilicon heating resistor (47 Ω) and a polysilicon/aluminum thermopile integrated on an oxide microbridge. The thermopile sensitivity is 9.9 mV/mW. The sensor's time constant is 1.85 ms, the signal-to-noise ratio $8 \cdot 10^9$/W, and the dynamic range $5 \cdot 10^4$. The temperature coefficient is less than 1% below 1 mW heating power. The linearity error with respect to frequency is less than 0.1% below 400 MHz and less than 1% up to 1.2 GHz.

605 MIC Thermally Excited Silicon Oxide Resonators in CMOS Technology: *O. Brand, D. Moser,* and *H. Baltes,* Physical Electronics Laboratory, Swiss Federal Institute of Technology CH-8093 Zurich, Switzerland

We report thermally excited silicon oxide beam and bridge resonators realized by two different industrial CMOS processes and subsequent micromachining. We characterized the different resonators by measuring resonance frequencies, vibration amplitudes, and mode shapes using a Laser heterodyne interferometer. We investigated the acoustic transmitting and receiving efficiencies of the devices in air in order to test the possible application as ultrasound transducers for proximity sensors. The vibrations can be detected using the piezoresistive effect of polysilicon.

606 MIC Fabrication of Novel Micromachined Magnetic Actuators: *A. M. A. Hamad, W. Zhang, H. T. Henderson,* and *F. Radpour,* Dept. of Electrical and Computer Engineering, University of Cincinnati; Cincinnati, OH 45221

Trends in smart sensors and smart skins must move in the direction of micromachining and miniaturization of semiconductor devices. Tactile sensors are particularly important for robotics and related sensing as well as microactuation of valves and other electrochemical components. In this paper, the design, fabrication and the characterization of a unique micromachined solenoid coil are presented. This device is capable of converting a current signal into the mechanical motion of a plunger. The solenoids were fabricated by anisotropic etching of <100> oriented silicon in a hydrazine solution. Multilevel metalization was used to form the miniature planar coils with a 75-250 μm machined openings through the substrate, forming a guide for the magnetic plunger material. Devices were tested using an optical technique and the magnetic force was obtained using a simple model. The force was also measured using a canterlever beam technique and the magnetic force in the range of 0.02-2.3 μN was obtained. Calculations also predict that this force can be increased by several orders of magnitude using a higher permeability plunger and by stacking multiple coil layers.

607 MIC Processing of Ferroelectric Materials in Micromachined Silicon-Based Structures: *D. L. Polla,* Dept. of Electrical Engineering, University of Minnesota, Minneapolis, MN 55455

Ferroelectric thin films have been deposited on polycrystalline silicon, silicon nitride, and tungsten structures to form both piezoelectric and pyroelectric microelectromechanical devices. This work focuses on the silicon-based processing technology issues important to ferroelectric micromechanical structures. Surface micromachining techniques and sol-gel deposited $Pb(Zr_xTi_{1-x})O_3$ and $PbTiO_3$ thin films have been used to form pressure sensors, infrared detectors, and micropositioners. The measured piezoelectric coefficient d_{33} (PZT) in these structures is 180-210 pC/N. The measured pyroelectric coefficient is 85-115 $nC/cm^2{}^\circ K$.

608 MIC Microchannel Pyroelectric Anemometer: *Y. Dun,* Lab. of Semiconductor Devices, Dept. of Automatic Control, Harbin Institute of Technology, Harbin 150006, China, *H. Y. Hsieh,* and *J. N. Zemel,* Dept. of Electrical Engineering and Center for Sensor Technologies, University of Pennsylvania, Philadelphia, PA 19104

A pyroelectric ($LiTaO_3$) anemometer chip was mounted into the wall of a small micromachined channel in silicon capped by an

anodically bonded Pyrex® plate. The silicon structure was fabricated using standard micromachining technology based on a KOH crystallographically selective etch. The channel was 72 μm deep and 3 mm wide. The dimensions of the overall chip were approximately 10 mm × 15 mm. The flow response of the sensor was compared to an MKS-100 thermal flow monitor. The experimental results demonstrate that the PA chip has essentially the same flow response as a function of Reynolds number in this channel as in larger channels. Also, this structure appears to be capable of monitoring flows as small as 0.01 sccm. A discussion of the conjugate problem of simultaneous fluid and heat flow from the PA element and some of the problems associated with the analysis are presented.

609 MIC A Fiber Optic Monitored Vertical Pressure Sensor: *X.-Z. Tu* and *J. N. Zemel*, Dept. of Electrical Engineering and Center for Sensor Technologies, University of Pennsylvania, Philadelphia, PA 19104

An optical fiber pressure sensor consisting of a vertical deflectable membrane, a sealed cavity, and a channel with a single mode optical fiber for monitoring the wall deflection has been developed. The membrane, cavity, and channel all were formed within a (110) silicon wafer by using a standard KOH crystallographic micromachining etch. Membranes as thin as 4 μm have been fabricated. The cavity was anodically sealed by bonding a piece of Pyrex® glass to the etched surface of the wafer. The alignment between the fiber and the center of the membrane was realized by careful adjustments of the microfabrication process. The interference patterns obtained were clear and stable "Newton's rings." A plot of the intensity of an interference pattern *vs.* the pressure applied to the sensor is presented showing that a pressure resolution of 0.01 atm is obtained. It is expected that a minimum detectable pressure can be lower than 0.001 atm after improving the used measurement system. The temperature sensitivity of the device remains a problem. Methods for eliminating this are discussed.

610 MIC Microfabrication of Silicon X-Ray Analyzer: *H. Kasapbasioglu;* and *P. J. Hesketh*, Dept. of Electrical and Computer Engineering, University of Illinois at Chicago, Chicago, IL 60680, *A. T. Macrander*, Advanced Photon Source: Argonne National Laboratory, Argonne, IL 60439-4814

We resolved a method for the fabrication of silicon x-ray analyzer crystals. A high energy resolution of x-ray beam scattering can be obtained by Bragg scattering from perfect single crystals and focusing action can be obtained by bending the perfect crystals. Parallel and perpendicular, 1 mm spaced grooves were cut on (111) silicon wafers using a dicing saw (Microautomation Model 1006). The grooves were cut at 15° and 105° to the <110> primary flat to avoid crystallographic cleavage directions, since mechanical strength was desired. The depth of the grooves was almost 80% of the wafer thickness. The cutting parameters, progressive cutting thickness and feed rate, were optimized to reduce damage. The damage was observed by sectioning the samples along the cleavage direction and etching in Yang's etch. Optical and scanning electron microscopy revealed that the least damage occurred when two passes were used: one a light 75 μm deep and the next to the required depth. More than two passes degraded the cuts. Slow feed rates of 1-5 mm/s and fast feed rates of 40-60 mm/s produced increased damage while no edge cracks and optimal smoothness were found for 12-20 mm/s. The spindle speed was constant at 30 K rpm to minimize resonant vibration. The effect of different etchants for removing the saw damage was also investigated and the results are reported.

611 MIC A Thin Platinum Island Film Glucose Sensor: *B. Kasapbasioglu* and *P. J. Hesketh*, Dept. of Electrical and Computer Engineering, University of Illinois at Chicago, Chicago, IL 60680, *W. C. Hanly*, Dept. of Microbiology and Immunology, University of Illinois at Chicago, Chicago, IL 60680, *J. Mclay*, Dept. of Electrical and Computer Engineering, University of Illinois at Chicago, Chicago, IL 60680

A 2.5 nm thin film glucose sensor has been developed. The island design of the film allowed the immobilization of glucose oxidase on the SiO_2 surface in a thin layer adjacent to the islands. The Pt film was deposited by electron beam evaporation at 1.33×10^{-3} Pa onto a 100 nm thermal oxide on a 50 mm diameter Si wafer at room temperature. Adsorptive immobilization from a 3.1% glucose oxidase at a pH 9.3 (0.1*M* $NaHCO_3$ buffer) was used. The adsorption was allowed to proceed for about 48 h at 4°C. The sensor was then washed with a dilute non-ionic detergent (0.05% Tween 20 in 0.05*M* sodium acetate buffer, pH 5.3). For measurement of the impedance, the washed electrode was immersed in tetramethybenzidine (TMB) buffer solution, 0.04*M* sodium acetate buffer, pH 5.3 containing horseradish peroxidase (2 purpurogallin U/ml) and glucose (concentration range = 0 m*M* to 560 m*M*). The impedance and phase of the enzyme coated film was measured from 100 Hz to 1 MHz. The results of the measurements indicated that the system could be modeled with a suitable RC equivalent circuit. Glucose produced a 50% change in the series capacitance at 100 Hz because of the binding reaction. The sensitivity would be best at low frequencies. The resistance was almost independent of glucose concentration. Reaction rate constants were obtained and are discussed. The impedance returned to its original value after washing in a suitable buffer, and storage at 4°C did not affect the initial performance.

612 MIC Development and Characterization of an Ultrathin Silicon Nitride for IC Sensor Applications Using Rapid Thermal Processing: *R. A. Williams*, Dept. of Chemical Engineering, University of California; Berkeley, CA 94720, *L. J. Arias, Jr.*, Peak System Inc., Fremont, CA 94538, *D. W. Hess*; Dept. of Chemical Engineering, Lehigh University, Bethlehem, PA 18015

Rapid thermal nitridation of silicon has been investigated as an alternative to CVD silicon nitride for IC sensor applications. Ultrathin silicon nitride films have been thermally grown in ammonia and nitrogen ambients using rapid thermal processing. The effects of several process variables on the growth of thermal nitride and its material properties have been evaluated electrically (I-V behavior) and physically (etch resistance to HF). Some process conditions (longer times and higher temperatures) consistently improved nitride properties. The effect of other process variables were mixed, *i.e.*, physical etch resistance improved at the expense of electrical properties (annealing, two-step nitridation, *in situ* gaseous cleaning) or vice versa (extended purges, low-pressure nitridation). By varying these process parameters, films with etch rates as low as 0.264 nm/min in 5:1 buffered HF (BHF) were achieved. Other films required a field of 816 KV/mm to pass 1 μA through a 10^4 μm^2 structure. However, the film with the best overall physical and electrical properties had a etch rate of 0.366 nm/min in 5:1 BHF, and required a field of 509 KV/mm to pass 1 μA through a 10^4 μm^2 structure and maintained a current density of 1.2 $\mu A/mm^2$ at ≈1 V. Durable pH and glucose sensors have been fabricated using these silicon nitride films. They have demonstrated greater sensitivity than oxides or oxide/CVD nitride gate structures.

THE ELECTROCHEMICAL SOCIETY BOOKS IN PRINT

Proceedings Volumes from 1983-1986 Symposia

The following softbound proceedings volumes are sponsored and published by The Electrochemical Society, Inc., 10 South Main Street, Pennington, NJ 08534-2896. Orders filled at the list price given, subject to availability. Enclose payment with order, either by check or Mastercard or VISA credit card.

High Temperature Materials Chemistry II. (PV 83-7) Z. A. Munir and D. Cubicciotti, Editors. A 1983 symposium. 480 pages, **$30.00.**

Silicon Nitride Thin Insulating Films. (PV 83-8) V. J. Kapoor and H. J. Stein, Editors. A 1983 symposium. 522 pages, **$25.00.**

Defects in Silicon. (PV 83-9) W. M. Bullis and L. C. Kimerling, Editors. A 1983 symposium. 660 pages, **$30.00.**

Plasma Processing. (PV 83-10) G. S. Mathad, G. C. Schwartz, and G. Smolinsky, Editors. A 1983 symposium. 660 pages, **$35.00.**

Materials and New Processing Technologies for Photovoltaics. (PV 83-11) J. A. Amick, V. K. Kapur, and J. Dietl, Editors. A 1983 symposium. 512 pages, **$25.00.**

III-V Opto-Electronics Epitaxy and Device Related Processes. (PV 83-13) V. G. Keramidas and S. Mahajan, Editors. A 1983 symposium. 289 pages, **$25.00.**

Lithium Batteries. (PV 84-1) A. N. Dey, Editor. A 1983 symposium. 460 pages, **$35.00.**

Fourth International Symposium on Molten Salts. (PV 84-2) M. Blander, D. S. Newman, M.-L. Saboungi, G. Mamantov, and K. Johnson, Editors. A 1983 symposium. 776 pages, **$35.00.**

Fundamental Aspects of Corrosion Protection by Surface Modification. (PV 84-3) E. McCafferty, C. R. Clayton, and J. Oudar, Editors. A 1983 symposium. 364 pages, **$25.00.**

Advances in Battery Materials and Processes. (PV 84-4) J. McBreen, R. S. Yeo, D-T. Chin, and A. C. C. Tseung, Editors. A 1983 symposium. 320 pages, **$26.00.**

The Electrochemistry of Carbon. (PV 84-5) S. Sarangapani, J. R. Akridge, and B. Schumm, Jr., Editors. A 1983 symposium. 648 pages, **$32.00.**

Ninth International Conference on Chemical Vapor Deposition. (PV 84-6) McD. Robinson, C. H. J. van den Brekel, G. W. Cullen, J. M. Blocher, Jr., and P. Rai-Choudhury, Editors. A 1984 symposium. 824 pages, **$36.00.**

VLSI Science and Technology/1984. (PV 84-7) K. E. Bean and G. A. Rozgonyi, Editors. A 1984 symposium. 520 pages. **$30.00.**

Equilibrium Diagrams; Localized Corrosion. (PV 84-9) R. P. Frankenthal and J. Kruger, Editors. A 1984 symposium. 611 pages, **$36.00.**

Electrochemistry in Mineral and Metal Processing. (PV 84-10) P. E. Richardson, S. Srinivasan, and R. Woods, Editors. A 1984 symposium. 677 pages, **$30.00.**

Advances in the Chlor-Alkali and Chlorate Industry. (PV 84-11) M. M. Silver and E. M. Spore, Editors. A 1984 symposium. 374 pages, **$18.00.**

Computer Aided Acquisition and Analysis of Corrosion Data. (PV 85-3) M. W. Kendig, U. Bertocci, and J. E. Strutt, Editors. A 1984 symposium. 276 pages, **$17.00.**

Manganese Dioxide Electrode Theory and Practice for Electrochemical Applications. (PV 85-4) B. Schumm, Jr., R. L. Middaugh, M. P. Grotheer, and J. C. Hunter, Editors. A 1984 symposium. 696 pages, **$40.00.**

Electromigration of Metals/Multilevel Metallization and Packaging. (PV 85-6) J. R. Lloyd, R. A. Levy, J. Pierce, and R. G. Frieser, Editors. A 1984 symposium. 201 pages, **$16.00.**

Materials and New Processing Technologies for Photovoltaics. (PV 85-9) V. K. Kapur, J. P. Dismukes, and S. Pizzini, Editors. A 1984 symposium. 432 pages, **$27.00.**

Advances in Lead-Acid Batteries. (PV 84-14) K. R. Bullock and D. Pavlov, Editors. A 1984 symposium. 548 pages, **$28.00.**

Plasma Processing. (PV 85-1) G. S. Mathad, G. C. Schwartz, and G. Smolinsky, Editors. A 1984 symposium. 636 pages, **$40.00.**

High Temperature Lamp Chemistry. (PV 85-2) E. G. Zubler, Editor. A 1985 symposium. 340 pages, **$25.00.**

VLSI Science and Technology/1985. (PV 85-5) W. M. Bullis and S. Broydo, Editors. A 1985 symposium. 572 pages, **$35.00.**

Silicon Molecular Beam Epitaxy. (PV 85-7) J. C. Bean, Editor. A 1985 symposium. 455 pages, **$36.00.**

The Chemistry and Physics of Composite Media. (PV 85-8) M. Tomkiewicz and P. N. Sen, Editors. A 1985 symposium. 373 pages, **$35.00.**

Molten Salts. (PV 86-1) M.-L. Saboungi, D. S. Newman, K. Johnson, and D. Inman, Editors. A 1985 symposium. 612 pages, **$45.00.**

High Temperature Materials Chemistry—III. (PV 86-2) Z. A. Munir and D. Cubicciotti, Editors. A 1985 symposium. 346 pages, **$37.00.**

Dielectric Films on Compound Semiconductors. (PV 86-3) V. J. Kapoor, D. J. Connolly, and Y. H. Wong, Editors. A 1985 symposium. 372 pages, **$27.00.**

Engineering of Industrial Electrolytic Processes. (PV 86-8) U. Landau, R. E. White, and R. D. Varjian, Editors. A 1985 symposium. 292 pages, **$20.00.**

Reduced Temperature Processing for VLSI. (PV 86-5) R. Reif and G. R. Srinivasan, Editors. A 1985 symposium. 600 pages, **$45.00.**

Corrosion Effects of Acid Deposition and Corrosion of Electronic Materials. (PV 86-6) F. Mansfeld, V. Kucera, S. E. Haagenrud, F. H. Haynie, and J. D. Sinclair, Editors. A 1985 symposium. 400 pages, **$28.00.**

Semiconductor Silicon/1986. (PV 86-4) H. R. Huff, T. Abe, and B. Kolbesen, Editors. A 1986 symposium. 1096 pages, **$55.00.**

Fundamental Aspects of High Temperature Corrosion—II. (PV 86-9) D. A. Shores and G. J. Yurek, Editors. A 1986 symposium. 350 pages, **$22.00.**

Surfaces, Inhibition, and Passivation. (PV 86-7) E. McCafferty and R. J. Brodd, Editors. A 1986 symposium. 640 pages, **$40.00.**

Load Leveling and Energy Conservation and Industrial Processes. (PV 86-10) D-T. Chin, Editor. A 1986 symposium. 320 pages, **$23.00.**

Aluminum Surface Treatment Technology. (PV 86-11) R. S. Alwitt and G. E. Thompson, Editors. A 1986 symposium. 432 pages, **$30.00.**

Electrochemical and Thermal Modeling of Battery, Fuel Cell, and Photoenergy Conversion Systems. (PV 86-12) J. R. Selman and H. C. Maru, Editors. A 1986 symposium. 433 pages, **$22.00.**

Diaphragms, Separators, and Ion-Exchange Membranes. (PV 86-13) J. W. Van Zee, R. E. White, K. Kinoshita, and H. S. Burney, Editors. A 1986 symposium. 308 pages, **$23.00.**

Electrochemical Sensors for Biomedical Applications. (PV 86-14) C. K. N. Li, Editor. A 1986 symposium. 208 pages, **$25.00.**

Lithium Batteries. (PV 87-1) A. N. Dey, Editor. A 1986 symposium. 568 pages, **$41.00.**

Corrosion Protection by Organic Coatings. (PV 87-2) M. W. Kendig and H. Leidheiser, Jr., Editors. A 1986 symposium. 384 pages, **$23.00.**

Electrochemistry and Solid State Science Education at the Graduate and Undergraduate Level. (PV 87-3) W. H. Smyrl and F. McLarnon, Editors. A 1986 symposium. 386 pages, **$26.00.**

Multilevel Metallization, Interconnection, and Contact Technologies. (PV 87-4) L. B. Rothman and T. Herndon, Editors. A 1986 symposium. 272 pages, **$25.00.**

Sodium-Sulfur Batteries. (PV 87-5) A. R. Landgrebe, R. D. Weaver, and R. K. Sen, Editors. A 1986 symposium. 290 pages, **$23.00.**

Plasma Processing. (PV 87-6) G. S. Mathad, G. C. Schwartz, and R. A. Gottscho, Editors. A 1986 symposium. 754 pages, **$43.00.**

Silicon Nitride and Silicon Dioxide Thin Insulating Films. (PV 87-10) V. J. Kapoor and K. T. Hankins, Editors. A 1986 symposium. 560 pages, **$45.00.**

Electrodeposition Technology, Theory and Practice. (PV 87-17) L. T. Romankiw and D. R. Turner, Editors. A 1986 symposium. 764 pages, **$35.00.**

Process Physics and Modeling in Semiconductor Technology. (PV 88-16) G. R. Srinivasan, J. Plummer, and D. Antoniadis, Editors. A 1986 symposium. 312 pages, **$28.00 Member, $34.00 Nonmember.**

10/90

FULLERENES: CHEMISTRY, PHYSICS AND NEW DIRECTIONS

Physical Electrochemistry/Dielectric Science and Technology/Electronics

St. Louis Ballroom C, 4th Level

MONDAY, MAY 18, 1992

Chairman, Rodney S. Ruoff; Vice Chairman, Peter Eklund

10:00 Introductory Remarks - Rodney S. Ruoff and Karl M. Kadish

10:10 Structure and Dynamical Properties of Large Fullerenes and Other Novel Forms of Carbon by First Principles Molecular Dynamics - G. B. Adams, J. B. Page, O. F. Sankey, K. Sinha, J. Menendez, and M. O'Keeffe — 613 FUL

10:40 Synthesis and Characterization of Endohedral Metallofullerenes - J. M. Alford and R. E. Smalley — 614 FUL

11:10 Structural Studies of Organometallic Derivatives of Fullerenes - A. L. Balch, V. J. Catalano, J. W. Lee, and Maryland M. Olmstead — 615 FUL

11:40 Adsorption of 1,1,2-Trichloro-1,2,2-trifluoroethane on Fullerenes - W. L. Bell, David T. Wickham, and Amy L. Schultz — 616 FUL

MONDAY, MAY 18, 1992

Chairman, Karl M. Kadish; Vice Chairman, Ripudaman Malhotra

1:10 Quantum Molecular Dynamics Calculations for Fullerenes and *Buckytubes* - J. Bernholc, Jae-Yel Yi, Q.-M. Zhang, C. J. Brabec, E. B. Anderson, S. A. Kajihara, and B. N. Davidson — 617 FUL

1:40 Calculation of Linear and Nonlinear Microscopic Polarizabilities of C_{60} and its Doped Species - A. Rosen and E. Westin — 618 FUL

2:10 High-Resolution Transmission Electron Microscopy of Fullerenes - Peter R. Buseck and Su Wang — 619 FUL

2:40 On the Use of C_{60} or C_{70} Clusters to Nucleate Diamond Crystals - R. P. H. Chang — 620 FUL

3:10 Formation of Fullerenes from Molecular Dynamics Simulations - J. R. Chelikowsky and Xiaodun Jing — 621 FUL

3:40 Twenty-minute intermission

4:00 Molecular Dynamics Study of C_{60}, $C_{60}O$, and Alkali-Doped C_{60} - A. Cheng and Michael L. Klein — 622 FUL

4:30 Synthesis of Fullerols by Electrophilic Reactions on Fullerene Molecules - L. Y. Chiang — 623 FUL

5:00 Preparation and Characterization of C_{60} and C_{70} Crystals and Solutions - C. W. Chu, J. G. Lin, Y. K. Tao, Y. Y. Sun, R. L. Meng, and P. H. Hor — 624 FUL

5:30 Application of Real-Time SERS and STM in Studies of C_{60} and C_{70} - Y. Zhang, X. Gao, G. Edens, and M. J. Weaver — 625 FUL

6:00 Bond Breaking and Bond Making with Fullerenes - R. Malhotra, Doris S. Tse, Rodney S. Ruoff, Donald F. McMillen, and Donald C. Lorents — 626 FUL

TUESDAY, MAY 19, 1992

Chairman, Jerzy Bernholc; Vice Chairman, Brett Dunlap

8:30 The Fullerenes and Fulleroids: Preparation and Properties - F. Wudl, Q. Li, T. Suzuki, K. C. Khemani, M. Prato, and S. Shi — 627 FUL

9:00 Endohedral Complexes of the C_{60} Cluster: *Ab Initio* Electronic Structure Calculations - Jerzy Cioslowski — 628 FUL

9:30 On the Generation, Separation, Physics, and Chemistry of Large Carbon Clusters - R. N. Compton, R. L. Hettich, R. H. Ritchie, P. Britt, A. A. Puretzky, W. F. Frey, A. A. Tuinman, J. L. Adcock, P. Mukherjee, M. Diack, and G. Guichon — 629 FUL

10:00 Synthesis and Characterization Of $C_{60}O$: The First Fullerene Epoxide - Donald M. Cox — 630 FUL

10:30 Ten-minute intermission

10:40 *In-Situ* Magnetic Circular Dichroism and Fourier Transform Infrared Spectroscopy of C_{60} Species - Daniel Scherson, Ming Zhao, Sunghyun Kim, In Tae Bae, Charles Rosenblatt, Dominique Dubois, and Karl Kadish — 631 FUL

11:10 Fullerene Molecular Weight Distributions Determined by Laser Desorption/Fourier Transform Mass Spectrometry - W. R. Creasy and Jeffrey A. Zimmerman — 632 FUL

11:40 Structure and Electronic Properties of C_{60}-Based Tubules - M. S. Dresselhaus, R. Saito, M. Fujita, and G. Dresselhaus — 633 FUL

TUESDAY, MAY 19, 1992

Chairman, Donald M. Cox; Vice Chairman, David Tomanek

1:10 Symmetry for Lattice Modes in C_{60}, C_{70} and Alkali Metal Doped C_{60} - G. Dresselhaus, M. S. Dresselhaus, and P. C. Eklund — 634 FUL

1:40 Fullerenes and Fullerene Derivatives - B. I. Dunlap — 635 FUL

2:10 Ellipsometry and Optical Absorption Studies in M_xC_{60} Thin Films (x = 0, 3, 6; M = K, Rb, Cs) - Peter C. Eklund — 636 FUL

2:40 Voltammetric Studies of $[(C_6H_5)_3P]_2Pt(\eta^2\text{-}C_{60})$ and Some $([(C_2H_5)_3P]_2M)_n(\eta^2\text{-}C_{60})$ Complexes (M = Ni, Pd and Pt; n = 1, 2, 3 and 6) - Paul J. Fagan, Susan A. Lerke, and D. H. Evans — 637 FUL

3:10 Electron and Oxygen Atom Transfer to C_{60} - Formation of Oxygen Atom and 1,3-dioxolane Adducts - C. S. Foote, James W. Arbogast, Michelle Kao, Yiannis Elemes, Scott Silverman, and Chi-Min Sheu — 638 FUL

WEDNESDAY, MAY 20, 1992

Chairman, William Goddard, III; Vice Chairman, Christopher Reed

8:30 Analysis of the Raman Spectra of A_3C_{60} and A_6C_{60} - F. Negri, G. Orlandi, and F. Zerbetto — 639 FUL

9:00 Photoexcitation and Photodissociation Channels of C_{60} - Keith R. Lykke, Peter Wurz, Deborah H. Parker Michael J. Pellin, and Dieter M. Gruen — 640 FUL

9:30 The Structure and Symmetry of the Orientational Ordering of C_{60} - A. B. Harris and R. Sachidanandam — 641 FUL

FUL

10:00 Nuclear Spin Weights and Gas Phase Spectral Structure of $^{12}C_{60}$ and $^{13}C_{60}$ Buckminsterfullerene - W. G. Harter and Tyle C. Reimer 642 FUL

10:30 Charge Transfer at Fullerene-Noble Metal Interfaces - J. S. Lannin 643 FUL

11:00 Recent Results in the Synthesis and Characterization of Discrete Derivatives of C_{60} - Joel M. Hawkins 644 FUL

11:30 Molecular Structures of the Gaseous Fullerenes C_{60} and C_{70} from Electron Diffraction - Kenneth Hedberg, Lise Hedberg, D. S. Bethune, C. A. Brown, R. D. Johnson, and M. de Vries 645 FUL

WEDNESDAY, MAY 20, 1992

Chairman: Emmanuel P. Gianellis; Vice Chairman, Fred Wudl

1:10 Orientational Order in Fullerenes - P. A. Heiney 646 FUL

1:40 Structures of Carbon Cluster Ions - Gert von Helden, Paul R. Kemper, and Michael T. Bowers 647 FUL

2:10 Bandgap, Excitons and Coulomb Interaction in Solid C_{60} - R. Lof, M. van Veenendaal, B. Koopmans, H. T. Jonkman, and G. A. Sawatzky 648 FUL

2:40 Synthesis, Structure and Superconductivity of Carbon-60 Fullerides - Zafar Iqbal 649 FUL

3:10 Twenty-minute intermission

3:30 Carbon Nanotubes - Sumio Iijima 650 FUL

4:00 Solvent, Supporting Electrolyte and Temperature Effects on the Electroreductions of Buckminsterfullerene (C_{60}) in Aprotic Media - K. M. Kadish, D. Dubois, G. Moninot, W. Kutner, and M. T. Jones 651 FUL

4:30 Electron Spin Resonance Characterization of Singly, Doubly and Triply Reduced Buckminsterfullerene, C_{60}, in Aprotic Media - M. T. Jones, D. Dubois, and K. M. Kadish 652 FUL

5:00 Intercalation of Amine Functionalized C_{60} in Mica-Type Silicates - V. Mehrotra and Emmanuel P. Giannelis 653 FUL

5:30 Theoretical Studies of the Structure, Properties, and Dynamics of Fullerene, Crystals and Superconductors - W. A. Goddard III, Yuejin Guo, Guanhua Chen, and Naoki Karasawa 654 FUL

WEDNESDAY, MAY 20, 1992

Chairman, William L. Bell; Vice Chairman, Jerzy Cioslowski

7:00 Studies Related to Extraction and Separation of Fullerenes - Rodney S. Ruoff, R. Malhotra, and Don Lorents 655 FUL

7:30 ESR Studies of the Reaction of Alkyl Radicals with C_{60} - P. J. Krusic, J. R. Morton, E. Wasserman, and K. F. Preston 656 FUL

POSTER SESSION

Chairman, Karl M. Kadish; Vice-Chairman, Rodney S. Ruoff

8:00 to 10:00 Radial Vibrations of an Ion Inside Icosahedral C_{60} - J. L. Ballester and B. I. Dunlap 657 FUL

Organometallic Chemistry of Fullerenes in the Gas Phase by FTMS - Y. Huang, Q. Jiao, S. A. Lee, and B. S. Freiser 658 FUL

Solubilization of Buckminsterfullerene, C_{60}, in Water and Some Polar Organic Solvents by Cyclodextrin Inclusion Chemistry - Wlodzimierz Kutner, Pierre Boulas, and Karl M. Kadish 659 FUL

Excited State Behavior of Fullerenes (C_{60} and C_{70}) and Their Reduction in Colloidal Semiconductor Suspensions - Prashant V. Kamat and Nada M. Dimitrijevic 660 FUL

Fluorinated Buckminsterfullerenes - K. Kniaz, J. E. Fischer, J. P. McCauley, A. B. Smith, III, and H. Selig 661 FUL

Isomerism and Chirality in Bis-Metal Derivatives of Fullerene C_{60} Ligated in η-6, η-5, η-2 Fashion - V. I. Sokolov 662 FUL

Chemical Oxidation of Buckminsterfullerene (C_{60}) - D. L. Stalling, Congyuan Gao, Kenneth Kuo, and Kevin Kelly 663 FUL

MNDO Study of Silicon-Substituted Buckminsterfullerene - Xinfu Xia, James R. Bowser, Daniel A. Jelski, Thomas F. George, and Jaili Gao 664 FUL

A Systematic Study of Structures and Stabilities for Fullerenes - B. L. Zhang, C. Z. Wang, K. M. Ho, C. H. Xu, and C. T. Chan 665 FUL

Nonlinear Optical Second-Order Harmonic Generation and Suppression in C_{60} Thin Films - X. K. Wang, T. G. Zhang, W. P. Lin, Z. Y. Xu, S. Liu, M. M. Kappes, G. K. Wong, J. B. Ketterson, and R. P. H. Chang 666 FUL

Vapor Pressure and Thermal Oxidation of C_{60} and C_{70} - M. Balooch, W. J. Siekhaus, J. Abrefah, and D. R. Olander 667 FUL

Simultaneous Electrochemical Quartz Crystal Microbalance and Cyclic Voltammetry Study of Electrodeposition, Doping with Countercations, and Electrodissolution of Films of Buckminsterfullerene, C_{60}, and Its Anions in Polar Aprotic Solvents - Wonyong Koh, Dominique Dubois, Wlodzimierz Kutner, M. Thomas Jones, and Karl M. Kadish 668 FUL

THURSDAY, MAY 21, 1992

Chairman, Long Chiang; Vice Chairman, Donald Bethune

8:40 Nonlinear Optical Properties of Fullerenes in the Visible and Near-Infrared - Z. H. Kafafi, J. R. Lindle, S. R. Flom, R. G. S. Pong, and F. J. Bartoli 669 FUL

9:10 Dynamics of Free *Fullerenes in* Photophysics and Collisions - W. Kamke, E. E. B. Campbell, and I. V. Hertel 670 FUL

9:40 Thermophysical Properties of Solid C_{60}, C_{70} and Related Materials - J. L. Margrave, Chenyu Pan, M. S. Chandrasekharaiah, M. P. Sampson, and R. H. Hauge 671 FUL

10:10 Superconductivity in Metal-Doped C_{60} Solids - C. M. Lieber, C. C. Chen, Z. Zhang, and S. P. Kelty 672 FUL

10:40 Electrochemical Reactivity of Fullerenes and Their Derivatives - F. D'Souza, Ram Seshadri, R. Nagarajan, Govind Raj, V. Krishnan, and C. N. R. Rao 673 FUL

11:10 Production and ESR Spectroscopy of Fullerenes Containing Metal Atoms - Robert D. Johnson, Costantino S. Yannoni, Mattanjah S. de Vries, Jesse R. Salem, and D. S. Bethune 674 FUL

11:40 Gas-Phase Characterization of Fullerenes and Endohedral Complexes - S. W. McElvany, John H. Callahan, and Mark M. Ross 675 FUL

THURSDAY, MAY 21, 1992

Chairman, Sumio Iijima; Vice Chairman, Krishnan Ragavachari

1:10 Diamond from Fullerenes - M. N. Regueiro, P. Monceau, and J.-L. Hodeau 676 FUL

1:40 Large Fullerenes: Structures and Growth Mechanism - Yohji Achiba 677 FUL

2:10 Synthesis of a C_{60}-p-Xylylene Copolymer - D. A. Loy and R. A. Assink 678 FUL

2:40 ESR and Optical Studies of the Radical Ions of Fullerenes - Tatsuhisa Kato, Takeshi Kodama, Tadamasa Shida, Shinzo Suzuki, and Yohji Achiba 679 FUL

3:10 Twenty-minute intermission

3:30	Electronic Structures and Superconductivity of Fullerenes and Fullerides - Susumu Saito, Atsushi Oshiyama, Yoshiuyuki Miyamoto, Shin-ichi Sawada, and Noriah Hamada	680 FUL
4:00	Synthesis of Novel Fullerene Derivatives - G. P. Miller	681 FUL
4:30	Synthesis, Extraction and Characterization of Fullerenes and Metallofullerenes - Deborah Holmes Parker, Peter Wurz, Keith R. Lykke, Kuntal Chatterjee, John C. Hemminger, Michael J. Pellin, Dieter M. Gruen, and Leon M. Stock	682 FUL

THURSDAY, MAY 21, 1992

Chairman, Karl M. Kadish; Vice Chairman, Rodney S. Ruoff

7:00	Larger Fullerenes and Functionalized Fullerenes: Structures and Stabilities - Krishnan Raghavachari and Celeste M. Rohlfing	683 FUL
7:30	Coordination Chemistry with Fulleride Ions - Christopher A. Reed, Alain Pénicaud, P. Bhyrappa, and John Hsu	684 FUL
8:00 to 10:00	Open discussion/short presentations/recent news	

FRIDAY, MAY 22, 1992

Chairman, Susumo Saito; Vice Chairman, Peter W. Stephens

8:30	The Multipole Expansion of Intermolecular Forces Applied to C_{60} - G. Lasher	685 FUL
9:00	Fullerenes and Fullerides: Photoemission and Scanning Tunneling Microscopy Studies - J. H. Weaver	686 FUL
9:30	Electron-Phonon Coupling and Superconductivity in Alkali Intercalated C_{60} Solid - M. A. Schlüter	687 FUL
10:00	The Equilibrium Structure of Big Fullerenes: Spherical or Cylindrical Shape? - G. E. Scuseria	688 FUL
10:30	Twenty-minute intermission	
10:50	Mass Spectroscopic Characterization of Large Fullerenes and Metallofullerenes - Hisanori Shinohara and Yahachi Saito	689 FUL
11:20	Experimental Heat of Formation, Vapor-Phase UV Spectrum, Vapor Pressure and Heat of Sublimation of C_{60}, Buckminsterfullerene - Duane R. Kirklin, Allan L. Smith, Yiu-Wing Hui, Andrew McGhie, William J. Romanow, and George Zimmerman	690 FUL

FRIDAY, MAY 22, 1992

Chairman: Michael Schlüter; Vice Chairman, H. Nori Shinohara

1:10	Structure of Superconducting and Ferromagnetic Fullerides - P. W. Stephens	691 FUL
1:40	Isolation, Spectroscopy, and Chemical Reactions of Fullerenes - R. Taylor, Paul R. Birkett, John H. Holloway, Eric C. Hope, John G. Langley, Mohamed F. Medeine, T. John Dennis, Jonathan P. Hare, Harold W. Kroto, and David R. M. Walton	692 FUL
2:10	Collective Electronic Excitations in Fullerenes - D. Tománek	693 FUL
3:00	NMR Studies of Molecular Dynamics and Electronic Properties of Pure and Doped Buckyballs - R. Tycko, G. Dabbagh, S. E. Barrett, M. J. Rosseinsky, D. W. Murphy, R. M. Fleming, and R. C. Haddon	694 FUL
3:30	(a) Production and Characterization of Fullerene Encapsulated Metals, and (b) The Search for Fullerenes in Meteorites - M. S. de Vries, J. R. Salem, R. D. Johnson, D. S. Bethune, C. S. Yannoni, H. R. Wendt, H. E. Hunziker, K. Reihs, and M. Hoinkis	695 FUL
4:00	Light and Fullerenes: Photoconductive and Nonlinear Optical Properties - Y. Wang, J. Caspar, and L.-T. Cheng	696 FUL
4:30	Synthesis and Characterization of Exo- and Endohedral Metal Fullerides - John B. Wiley, Edward G. Gillan, Shiou-Mei Huang, Kyu Min, Marcos Alvarez, Chahan Yeretzian, Shinho Cho, Francois Diederich, Robert Whetten, Károly Holczer, and Richard B. Kaner	697 FUL

Abstracts

613 FUL Structure and Dynamical Properties of Large Fullerenes and Other Novel Forms of Carbon by First Principles Molecular Dynamics: *G. B. Adams, J. B. Page, O. F. Sankey,* K. Sinha, J. Menendez,* and *M. O'Keeffe,* Depts. of Physics and Chemistry, Arizona State University, Tempe, AZ 85287

We have used our first principles molecular dynamics method[1] to determine the minimum energy geometries and electronic structure of more than 20 different fullerenes, including fullerenes of mass 60, 70, 80, 84, 120, 130, 140, and 240. For the lowest energy structure of most mass types we have determined the vibrational modes and frequencies, also from first principles. In addition, we have examined the energy and vibrational modes of novel forms of solid carbon which are energetically competitive with solid C_{60}. (This work was supported by ONR-N00014-90-J-130x.)

1. O. F. Sankey and D. J. Niklewski, *Phys. Rev. B,* **40,** 3979 (1989).

614 FUL Synthesis and Characterization of Endohedral Metallofullerenes: *J. M. Alford** and *R. E. Smalley,* Rice Quantum Institute, Dept. of Chemistry, Rice University, Houston, TX 77251-1892

New synthesis techniques developed by this group during the last year now enable the production of macroscopic amounts of endohedral metallofullerenes. These special molecules which completely encapsulate a metal atom or cluster of atoms within their carbon cages can be synthesized using modified versions of either the laser vaporization method or the standard Kratschmer-Huffman (KH) technique. Certain metallofullerenes such as those containing the Group III elements (Sc, Y, La) are easily produced while others such as the alkali metal containing fullerenes prove much more difficult to make. A survey across the periodic table shows which elements can be incorporated inside the fullerene structures. While characterization of a pure metallofullerene remains to be accomplished, some basic studies such as solubility, XPS, and ESR have been performed on samples containing empty and mixed metallofullerenes. These results show that one fullerene, C_{82}, has the unique property of forming both single atom, Y @ C_{82}, and multiple, Y_2 @ C_{82}, metallofullerenes that are soluble in toluene. A more detailed analysis of these results as well as up-to-date results on the characterization of metallofullerenes in general are presented.

615 FUL Structural Studies of Organometallic Derivatives of Fullerenes: *A. L. Balch*, V. J. Catalano, J. W. Lee,* and *M. M. Olmstead,* Dept. of Chemistry, University of California-Davis, Davis, CA 95616

The iridium complex, $In(CO)Cl(PPh_3)_2$, binds reversibly to the exterior surface of fullerenes C_{60} and C_{70}. X-ray crystallographic studies show that binding occurs preferentially at 6:6 ring fusions. Crystal formation is highly sensitive to the solvents used for crystal growth and solvents are incorporated into the solids. The spatial relationship of the occluded solvent and Fullerene is described. New ligands for encircling the fullerenes in these derivatives are described.

616 FUL Adsorption of 1, 1, 2-Trichloro-1, 2, 2-trifluroethane on Fullerenes: *W. L. Bell*, D. T. Wickham,* and *A. L. Schultz,* TDA Research, Inc., Wheat Ridge, CO 80033, *P. Nolan,* U. S. Army CRDEC, Aberdeen Proving Ground, MD 21010-5423

To better understand the surface properties of fullerenes, we have investigated adsorption of the title compound (CFC-113) from the gas phase onto solid fullerenes. Adsorption of organic molecules onto activated carbon is commonly used for separation and purification, and a comparison of fullerenes with activated carbon will be interesting. We measured adsorption by following the change in weight of the fullerene sample as a function of the partial pressure of the adsorbate at a constant temperature. The resulting adsorption isotherms are discussed and compared with results obtained for activated carbon.

617 FUL Quantum Molecular Dynamics Calculations for Fullerenes and Buckytubes: *J. Bernholc*, J.-Y. Yi, Q.-M. Zhang, C. J. Brabec, E. B. Anderson, S. A. Kajihara,* and *B. N. Davidson,* North Carolina State University, Raleigh, NC 27695-8202

We describe the results of extensive *ab initio* molecular dynamics calculations of the properties of fullerenes and buckytubes. Our finite temperature quantum MD simulations for solid C_{60} are in excellent agreement with NMR, photoemission, and neutron scattering data. The C_{60} isomer containing two pairs of adjacent fivefold rings has a binding energy only 1.6 eV smaller than that of perfect C_{60}, but the transformation between these two structures is hindered by a 5.4 eV barrier. It thus requires high temperatures and long annealing times. High temperatures are also needed for the transformation of the lowest energy C_{20} isomer, a dodecahedron, to a corannulene structure, which can be thought of as a fragment of C_{60}. The corannulene structure is a natural precursor for the formation of C_{60}. These results are consistent with the experimental findings that high temperatures are necessary for the formation of substantial quantities of C_{60}. The results of band structure and doping calculations for optimized structures of several buckytubes are also described. (This work was supported by ONR, Grant No. N00014-91-J-1516.)

618 FUL Calculation of Linear and Nonlinear Microscopic Polarizabilities of C_{60} and its Doped Species: *A. Rosen* and *E. Westin,* Dept. of Physics, Chalmers University of Technology and University of Göteborg, S-412 96 Göteborg, Sweden

Molecular cluster calculations (1, 2) within the local density approximation have been performed in a study of the electronic structure of C_{60}, XC_{59} and monosubstituted fullerenes $C_{59}X$, where X = (B, N). Doping with B and N in the center of the cage creates an electronic structure with a partly occupied level in the bandgap, similar to the donor and acceptor levels in traditionally doped semiconductors, while substitution of one of the carbon atoms in the cage with B or N gives a splitting of the HOMO and LUMO levels in the bare C_{60} molecule. Using wavefunctions determined from these molecular calculations the frequency dependent linear and nonlinear optical microscopic polarizabilities, *i.e.*, γ (1), γ(2), and γ(3), tensors, for a process of linear, second and third harmonic generation have been evaluated. The breaking of inversion symmetry for the mono-substituted species results in a large 2nd order response. The relative importance of electric-quadrupole and magnetic interactions are also considered. Our results are found to be in reasonable agreement with experimental data from measurements of susceptibilities of C_{60}, *i.e.*, thin films or solution data (3-5).

1. B. Wastberg and A. Rosén, *Physica Scripta,* **44,** 276 (1991)
2. A. Rosén and B. Wästberg, *Surf. Sci.,* in press.
3. Z. H. Kafafi, Private communication.
4. W. J. Blau *et al., Phys. Rev. Lett.,* **67,** 1423 (1991).
5. X. K. Wang, Private communication.

619 FUL High-Resolution Transmission Electron Microscopy of Fullerenes: *P. R. Buseck** and *S. Wang,* Dept. of Geology and Chemistry, Arizona State University, Tempe, AZ 85287

In spite of the intense research activity that has gone into studying the fullerenes during the last two years, much of the information about their shapes and local structures is inferential. Nonetheless, it is evident that many fullerene samples contain molecules of varied sizes. In some instances these diverse molecules pack into crystals that then contain "defects" consisting of either isolated fullerenes having dimensions different from their hosts, or into domains of one type of fullerene with domain boundaries separating them from fullerenes of other sizes. There are also instances in which large fullerenes occur as isolated molecules or in molecule clusters rather than in crystals. Because of its ability to obtain extremely high spatial resolution images of thin volumes of material, high-resolution transmission electron microscopy is well suited for studying such samples as well as, in ideal cases, isolated molecules. We have observed and imaged domain structures of fullerenes containing up to 130 molecules, and we have indications of far larger units as well as domains smaller than C_{60}. Examples are shown.

620 FUL On the Use of C_{60} or C_{70} Clusters to Nucleate Diamond Crystals: *R. P. H. Chang,* Dept. of Materials Science and Engineering, Northwestern University, Evanston, IL 60208, *R. Meilunas,* Grumman Corp., Corporate Research Center, Bethpage, NY 11714-3580, *S. Liu* and *M. M. Kappes,* Dept. of Chemistry, Northwestern University, Evanston, IL 60208

Chemical vapor deposition is a promising technique for growing diamond films on a variety of substrate materials for protective coatings and the fabrication of active electronic and optical devices. However, a number of requirements in the film growth process are limiting the full technological development and commercialization of this technique. These include the need for high growth temperatures and the necessity of pretreating nondiamond substrates by polishing them with diamond grit. The latter requirement is essential to obtain a high enough initial nucleation density of diamond crystallites on the substrate to form continuous films. Such a pretreatment is not desirable for coating large or nonplanar surface areas. We report a novel method for nucleating diamond crystallites by substituting diamond grit polish with a thin solid film of C_{60} or C_{70} carbon cluster. Our method also allows for the growth of diamond in preselected areas, a potential application in lithography. A simple model of the possible nucleation mechanism is given.

621 FUL Formation of Fullerenes from Molecular Dynamics Simulations: *J. R. Chelikowsky** and *X. Jing,* Dept. of Chemical Engineering and Materials Science, Minnesota Supercomputer Institute, University of Minnesota, Minneapolis, MN 55455

We have examined the nucleation of fullerenes via Langevin molecular dynamics simulations. Two simulations are considered. One simulation (1) focuses on a "hot gas" of sixty carbon atoms. This gas is rapidly quenched. In this simulation, the growth sequence is dominated by the nucleation of long carbon chains in the initial phase. As the nucleation process proceeds, these chains branch and form polycyclic rings. We find an abrupt onset of ring formation at a temperature which corresponds to the melting point of graphite. The resulting structure resembles buckminsterfullerene with a number of defects. A video of this simulation is presented. The second simulation consists of adding monomers at a constant "high" temperature. Initially, open structures are formed. For C_n clusters, with $n \geq 25$, the structures resemble fullerene cages. We find the growth pattern in this simulation is dominated by monomer addition to the edges of the open structures, or to the surface of the fullerene cages. This second simulation illustrates a growth sequence in which atoms are rarely trapped within the fullerene cage. (This work was supported by the U.S. Department of Energy Grant No. DE-FG0289ER45391 and the Petroleum Research Fund.

1. J. R. Chelikowsky, *Phys. Rev. Lett.,* **67,** 2970 (1991).

622 FUL Molecular Dynamics Study of C_{60}, $C_{60}O$ and Alkali-Doped C_{60}: *A. Cheng** and *M. L. Klein,* Dept. of Chemistry and Laboratory for Research on the Structure of Matter, University of Pennsylvania, Philadelphia, PA 19104-6323

Molecular dynamics simulations have been performed for solid C_{60}, $C_{60}O$ and alkali-doped C_{60} using a pair-wise atom-atom potential. At room temperature C_{60} form a face-centered-cubic lattice with C_{60} molecules undergoing hindered rotation. An orientational disorder-order transition occurs upon cooling. $C_{60}O$ has the same lattice symmetry as the C_{60} solid and the presence of oxygen atoms does not change the nature of transition. However, the attached oxygen atom slows down the rotational motion dramatically. $C_{60}O$ molecules prefer pointing along (100) directions so that oxygen atoms stay in the octahedral sites. Alkali-doped C_{60} (M_xC_{60}) is treated as an ionic crystal, assuming that charges are completely transferred from alkali-atom to C_{60} and are equally shared by 60 carbon atoms. A structural transformation from a face-centered-cubic to a body-centered-cubic phase is observed between $x = 3$ and $x = 4$. The results of K_xC_{60} and K_xC_{60} are discussed.

623 FUL Synthesis of Fullerols by Electrophilic Reactions on Fullerene Molecules: *L. Y. Chiang, R. Upasani,* and *J. W. Swirczewski,* Corporate Research Laboratory, Exxon Research and Engineering Co., Annandale, NJ 08801

Fullerene molecules exhibit a high reactivity towards both nucleophilic substitutions and electronic reductions. However, unlike most of highly conjugated aromatics, they are relatively inert to the electronic oxidation showing a remarkable stability even under doping with arsenic pentafluoride at solid state. We demonstrated that the reactivity of electrophilic substitution on fullerenes can be significantly enhanced using the solution chemistry. As an example, we outline three possible methods for the preparation of fullerols as polyhydroxylated fullerene derivatives through the reaction of fullerenes with electrophilic reagents. The synthetic methodology includes an aqueous acid chemistry, the epoxidation reaction, and the interesting nitronium chemistry for the conversion of fullerenes to fullerols. We discovered that the aqueous acid chemistry is an efficient low cost method to introduce multiple hydroxy groups onto the fullerene molecules. The reaction produces fullerols in essentially quantitative yield. We found that the structure of fullerols can be reproduced either through the epoxidation of fullerenes followed by hydrolysis or the electrophilic attack of nitronium ions on fullerene molecules in the presence of organic acid. The strong electrophilicity of nitronium ion develops a carbocationic center on fullerene molecules that is susceptible to the nucleophilic attack of organo carboxylic anion. The resulting nitro-organocarboxylated fullerene derivatives can be transformed into fullerols through the further water treatment and hydrolysis.

624 FUL Preparation and Characterization of C_{60}/C_{70} Crystals and Solutions: *C. W. Chu*, J. G. Lin, Y. K. Tao, Y. Y. Sun, R. L. Meng,* and *P. H. Hor,* Dept. of Physics and Texas Center for Superconductivity at the University of Houston, Houston, TX 77204-5932

We have grown crystals of $(C_{60})_x(C_{70})_{1-x}$ with $x = 0$ to 1, using the sublimation and solution techniques. The effects of the solvent on the structural morphology and symmetry of the crystals grown from the solution technique were examined. For $x = 0$, crystals prepared from solutions of hexane, toluene, benzene, and n-pentane have a fcc structure with a lattice parameter $a = 14.2$ Å, which is identical to that of crystals grown by sublimation. However, the morphology of these crystals depends on the solvent used, *e.g.*, C_{60} crystals grown from benzene are transparent, brown, thin hexagonal platelets; those from hexane and toluene are fibers; those from n-pentane are column-shaped crystals; and those grown by sublimation are dark cubes. Ether appears to be an exception. It bonds to C_{60} and causes the formation of a non-fcc C_{60} crystal which decomposes at ~400°C into fcc crystals. In contrast to C_{60}, C_{70} tends to bind with the solvent molecules and form crystals of a lower symmetry than fcc, such as 10-sided column-shaped crystals, showing a pseudo-ten-fold symmetry due to twinning of a monoclinic cell. Complete solid solutions for $x = 0$ to 1 are formed by the sublimation technique with a continuously increasing lattice constant. However, due to the interaction between C_{60}/C_{70} and solvent molecules, two fcc structures with different lattice constants are synthesized from solvents, corresponding to C_{60} and a specific C_{60}/C_{70} solid solution. (This research is supported in part by NSF, TCSUH, and the T. L. L. Temple Foundation.

625 FUL Application of Real-Time SERS and STM in Studies of C_{60} and C_{70}: *Y. Zhang, X. Gao, G. Edens,* and *M. J. Weaver,** Dept. of Chemistry, Purdue University, West Lafayette, IN 47907

Real-time surface-enhanced Raman spectroscopy (SERS) and scanning tunneling microscopy (STM) have been applied to examine thin films of C_{60} and C_{70} with the aim of understanding the structural effect on structures of adding electrons to the molecules, and to reveal the real-space ring-resolution structures of both fullerenes, and to reveal the centrosymmetric D_{5h} structure of C_{70}. SERS studies (1) were undertaken in acetonitrile with tetrabutylammonium perchlorate as electrolyte on polycrystalline gold under cyclic voltammetric excursions. Besides the ten Raman-active modes, several IR-active modes were also observed for neutral C_{60}, indicating symmetry diminution due to surface binding. Upon electroreduction to the C_{60}^- monoanion, several Raman-active bands downshift significantly in frequency; two of them yield doublets, reflecting anticipated Jahn-Teller distortions in the monoanion. STM (2) images of C_{60} and C_{70} were obtained largely in air on Au(111) except the ring-resolution images, which were obtained on Au(110) in 0.1*M* $HClO_4$ solution with electrode-potential control. Hexagonal close-packed layers were obtained for C_{60} and C_{70} on Au(111), but the C_{70} layers exhibit two different orientations corresponding to the long and short axes being parallel to the surface. While the fullerene layers are less ordered on Au(110), the molecules are less mobile and can yield STM images exhibiting ring-resolution. Electron- (or hole-) driven superexchange mechanism, as discussed in conventional molecular redox chemistry, are proposed to be responsible for the observed molecular- (and ring-) resolution STM images.

1. Y. Zhang, G. Edens, and M. J. Weaver, *J. Am. Chem. Soc.*, **113**, 9395 (1991).
2. Y. Zhang, X. Gao and M. J. Weaver, *J. Phys. Chem.*, In press.

626 FUL Bond Breaking and Bond Making with Fullerenes: *R. Malhotra*, D. S. Tse, R. S. Ruoff, D. F. McMillen,* and *D. C. Lorents,* Molecular Physics Laboratory, SRI International, Menlo Park, CA 94025-3493

In previous work performed in the context of coal liquefaction and pyrolysis we have found that polycyclic aromatic hydrocarbons (PCAH), notably pyrene, catalyze transfer of hydrogen atoms via a bimolecular process and aid in the cleavage of strong aryl-alkyl linkages. We tested the ability of fullerenes, which are also aromatic, in engendering scission of such bonds using 1, 2'-dinaphthylmethane as a model structure. Reactions were conducted at 400°C in a 50:50 mixture of phenanthrene and 9, 10-dihydrophenanthrene solvent system. Addition of the fullerene extract (~85% C_{60} and 14% C_{70}) enhanced the cleavage rate by 50%. The enhanced cleavage rate was also attended by an increase in the selectivity of cleavage at the 1-position of naphthalene leading to the formation of 2-methylnaphthalene. The results are consistent with the view that the fullerenes catalyze the transfer of H atoms to the ipso position of 1, 2'-dinaphthylmethane. The ability of fullerenes in catalyzing H-transfers is also reflected in the products obtained by extracting the raw Kratschmer-Huffman soot with high boiling solvents such as mesitylene and diethylbenzene. While these solvents can be heated under reflux for long periods without any coupling, contact with the fullerenes leads to the formation of dimers, trimers, and other oligomers.

627 FUL The Fullerenes and Fulleroids: Preparation and Properties: *F. Wudl*, Q. Li, T. Suzuki, K. C. Khemani, M. Prato,* and *S. Shi,* Institute for Polymers and Organic Solids and Dept. of Chemistry and Physics, University of California, Santa Barbara, CA 93106

The prepartion of fulleroids (*e.g.*,)

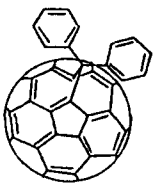

1

Fulleroids are cage molecules which are "inflated" fullerenes. The smallest members have essentially the same electronic structure as fullerene C_{60} and are expected to produce materials with unusual properties, in analogy to their fullerene analogs. Details of their characterization and structure determination such NMR, x-ray crystallography and UV-vis spectroscopy are presented. The electrochemical properties of the fulleroids are also presented. Extension of the fulleroid approach to the preparation of polymers containing the fulleroid unit is also presented. Preliminary results indicate that the polymers have a very high T_g and are insoluble in a large number of solvents.

628 FUL Endohedral Complexes of the C_{60} Cluster: *Ab Initio* Electronic Structure Calculations: *J. Cioslowski,* Dept. of Chemistry and Supercomputer Computations Research Institute, Florida State University, Tallahassee, FL 32306-3006

Although their existence was postulated several years ago, the experimental evidence for endohedral complexes in which atoms, ions, or molecules are trapped inside hollow carbon clusters has become available only very recently. Contrary to popular belief, the guests in these complexes often tend to displace themselves from the cage center. Results of large-scale *ab initio* calculations on several endohedral complexes, including those with the Li^+, Na^+, and Mg^{2+} cations, noble gases, and several diatomic molecules, are presented. Trends in the calculated properties are rationalized in terms of electrostatic interactions between the guests and the cage, and polarization effects. Approximate equations allowing predictions of the complexation energies are derived. Rules guiding the presence or absence of charge transfer between the guest molecule and the C_{60} cage are discussed. The origins of the so-called endohedral effect are explained using concepts of density functional theory.

629 FUL On the Generation, Separation, Physics, and Chemistry of Large Carbon Clusters: *R. N. Compton,* R. L. Hettich, R. H. Ritchie,* and *P. Britt,* Oak Ridge National Laboratory, Oak Ridge, TN 37831, *A. A. Puretzky,* Institute of Spectroscopy U.S.S.R. Academy of Sciences, Moscow, Russia, *W. F. Frey,* Dept. of Physics, Davidson College, Davidson, NC 28036, *A. A. Tuinman, J. L. Adcock,* and *P. Mukherjee,* Dept. of Chemistry, The University of Tennessee, Knoxville, TN 37996, *M. Diack* and *G. Guichon,* Oak Ridge National Laboratory, Oak Ridge, TN 37831

Laser ablation and contact-arc techniques have been used to generate large carbon clusters and many of their derivatives. The effects of various buffer gases (He, Ne, Ar, Kr, Xe) on the growth of fullerenes are described along with spectroscopic analysis of the laser produced plumes. Laser ablation of graphite in the presence of N_2 and H_2 results in C_nN_m and C_nH_m compounds (n, m <20) and is shown to be deleterious to the growth of fullerenes. Separation of the various fullerenes is carried out with liquid chromatography on a C18 chemically bonded silica column as well as with a new sublimation technique. UV/visible, IR, and Raman spectra are recorded for the separated fullerenes and their derivatives. C_{60} was hydrogenated using gas phase catalytic techniques to yield $C_{60}H_{36}$ and $C_{70}H_{40}$. Fluorination results in maximum fluorination corresponding to $C_{60}F_{48}$ and $C_{70}F_{56}$. Sample degradation with time (in C_6F_6 solution) produces $C_{60}F_{36}$ and $C_{70}F_{48}$. Both positive and negative ion high resolution mass spectra are recorded using both surface ionization and gas phase ionization techniques. Laser desorption yields the doubly charged C_{60}^{+2}, C_{70}^{+2}, $C_{60}F_x^{+2}$, and $C_{70}F_y^{+2}$ ions with $x = 37 - 45$ and $y = 45 - 51$ (see also reference 1). Finally, laser desorption negative ion mass spectra of samples produced from laser ablation of boron carbide (B_4C) yields ions of the stoichiometry $C_{60}B_{10}^-$, $C_{82}B_{10}^-$, etc., and weaker peaks at $C_{60}B_8^-$, $C_{82}B_8^-$, etc. Geometrically it is possible for B_8 and B_{10} to fit inside C_{60}. Efforts are underway to prove or disprove this hypothesis.

1. R. L. Hettich, R. N. Compton, and R. H. Ritchie, *Phys. Rev. Lett.*, **67**, 1242 (1991).

630 FUL Synthesis and Characterization of $C_{60}O$: The First Fullerene Epoxide: *D. M. Cox, K. M. Creegan, J. M. Millar, J. L. Robbins, W. K. Robbins, R. D. Sherwood and P. J. Tindall,* Exxon Research and Engineering Company, Annandale, NJ 08801, *J. P. McCauley, Jr., D. R. Jones, R. T. Gallagher* and *A. B. Smith III,* Dept. of Chemistry, University of Pennsylvania, Philadelphia, PA 19104.

Using high pressure liquid chromatography, a new monofunctional fullerene, $C_{60}O$, was separated from the fullerene mixture generated via resistive heating of carbon rods. Characterization by mass spectrometry and ^{13}C NMR solution and solid state, infrared and UV-vis adsorption spectroscopy strongly supports the epoxide

structure 1, and not the isomeric oxo-annulene type structure 2. Solid-state properties of $C_{60}O$ are discussed. $C_{60}O$ can be synthesized at about 7% yield from ultraviolet irradiation of C_{60} in oxygen saturated benzene solutions. Upon addition of benzil to the solution significantly higher yields can be obtained.

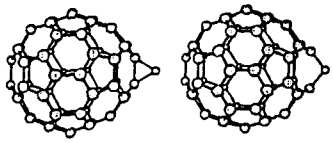

1 2

631 FUL *In situ* Magnetic Circular Dichroism and Fourier Transform Infrared Spectroscopy of C_{60} Species: *D. Scherson*, M. Zhao, S. Kim, I. T. Bae,* and *C. Rosenblatt*, Depts. of Chemistry and Physics, Case Western Reserve University, Cleveland, OH 44106, *D. Dubois* and *K. Kadish*, Dept. of Chemistry, University of Houston, Houston, TX 77204-5641

The solution phase properties of C_{60} and its mono-, di- and trianions in organic electrolytes have been examined *in situ* by magnetic circular dichroism (MCD) in the UV-vis region and Fourier transform infrared spectroscopy. For the MCD measurements, a newly designed instrument was used in which a beam of alternately right- and left-circularly polarized light, aligned essentially parallel to the magnetic field, is allowed to reflect at near normal incidence onto a highly polished gold working electrode surface. Large differences were observed between the *in situ* MCD spectra of the neutral species, characterized by what appears to be a B term at 325 nm, and those of the corresponding electrogenerated anions, for which the signals were much weaker and less well defined. An analysis of these results as well as those obtained with the *in situ* FTIR measurements is discussed. (This work was supported in part by the Gas Research Institute. Valuable discussions with Professor A. Gewirth for University of Illinois are also gratefully acknowledged.)

632 FUL Fullerene Molecular Weight Distributions Determined by Laser Desorption/Fourier Transform Mass Spectrometry: *W. R. Creasy** and *J. A. Zimmerman*, IBM Corp., Endicott, NY 13760

Recent progress has been made in the extraction of high molecular weight fullerenes from graphite soot (1). Fourier transform mass spectrometry (FTMS) using 266 nm laser desorption has proven to be a useful method for obtaining molecular weight distributions of the extracted fullerenes. The advantages and limitations of this technique are discussed. Some examples of the distributions of fullerenes which can be extracted by using different solvents are shown. Since laser desorption can be an energetic method of ion formation, it is necessary to consider the fragmentation of fullerenes into smaller species during the desorption. Alternately, it has also been found that fullerenes can form by growth processes during laser ablation of some materials; in fact, this is the method by which fullerenes were originally observed (2). Both of these processes are discussed in relation to the observed distributions.

1. C. Smart, B. Eldridge, W. Reuter, J. A. Zimmerman, W. R. Creasy, and R. S. Ruoff, *Chem. Phys. Lett.*, In press (1992).

2. E. A. Rolfing, D. M. Cox, and A. Kaldor, *J. Chem. Phys.*, **81**, 3322 (1984).

633 FUL Structure and Electronic Properties of C_{60}-Based Tubules: *M. S. Dresselhaus,* R. Saito, M. Fujita,* and *G. Dresselhaus*, MIT, Cambridge, MA 02139

The concept of a C_{60}-based tubule follows from the relation between the rugby ball shaped C_{70} and the spherical C_{60} molecule. This relation suggests graphene tubules formed from a hemisphere of the C_{60} molecule normal to a five-fold axis. A similar construction can be made normal to a three-fold axis. By viewing the relationship between the honeycomb graphene lattice and a graphene tubule, a general graphene tubule including the chirality of the tubule can be specified and described by a single vector on the honeycomb graphene lattice. A geometric construction provides the key to specifying a nucleating cap for each fiber. This geometrical construction is more generally useful in specifying families of higher order fullerenes. Of particular interest are the 1D dispersion relations for graphene tubules arising from the application of periodic boundary conditions in the circumferential direction. For example, the electronic dispersion relations can be simply determined by zone folding the 2D tight binding energy bands first calculated by Wallace in 1947. The results of this calculation show that approximately 1/3 of the possible graphene tubules are metallic, depending on the fiber diameter and chiral angle. The remaining 2/3 are semiconducting. The implications of these results on mesoscopic structures with cylindrical symmetry are discussed.

634 FUL Symmetry for Lattice Modes in C_{60}, C_{70} and Alkali Metal Doped C_{60}: *G. Dresselhaus* and *M. S. Dresselhaus*, MIT, Cambridge, MA 02139, *P. C. Eklund*, University of Kentucky, Lexington, KY 40506

We present group theoretical analysis relevant to the interpretation of recent experimental observations of Raman and infrared spectroscopy in C_{60}, C_{70} and alkali metal doped C_{60}. The group theoretical analysis for the C_{60}-related materials makes use of two space groups which both reduce the icosahedral point group symmetry of the isolated C_{60} molecule to the cubic point group T_h. The analysis for C_{70} requires going from high to lower symmetry and is closely related to the group theoretical analysis for graphene tubules. The space group for the fcc arrangement of C_{60} molecules is T_h^6 and corresponds to the low temperature solid phase of pristine C_{60}. The bcc arrangement for solid M_6C_{60} is consistent with the space group T_h^1 and is the symmetry identified with the fully doped alkali metal material. The experimental Raman spectra show line splittings which are consistent with a symmetry lowering to T_h symmetry for the C_{60} molecule. However, the polarization selection rules observed experimentally indicate a further lowering of the symmetry, beyond cubic symmetry.

635 FUL Fullerenes and Fullerene Derivatives: *B. I. Dunlap*, Code 6179, U.S. Naval Research Laboratory, Washington, DC 20375-5000

Using both empirical-potential and local-density-functional (LDF) calculations we have computed some properties of a number of available and potentially available fullerene molecules and their derivatives. One of the two most remarkable properties of the fullerenes is that their shell of carbon atoms is not easily penetrated. Large Gaussian-basis-set (corresponding to triple-zeta plus polarization) LDF calculations estimate the barrier for helium penetration at 10 eV. Thus fullerenes have a well-defined inside and outside. We have considered bonding a single carbon atom inside a fullerene and the quantum mechanical motion of single lithium, sodium, and potassium atoms inside various charge states of C_{60}. The question of hydrogenating and fluorinating fullerenes also leads to an endohedral problem. We have found that $C_{60}H_{60}$ is more stable if some of its C-H bonds point inward. The other most remarkable property of fullerenes is their lack of isomerization. We have computed the LDF total energies of some separated-pentagon closed-shell isomers of C_{60}, C_{70}, C_{72}, C_{76}, C_{78}, C_{84}, C_{180}, C_{240} and fullerene tubules to gain insight into the very high selectivity in the process discovered by Krätschmer, Huffman and coworkers. We have also computed the electronic structure and photoemission spectra of these molecules. Remarkably, the icosahedral fullerenes have very similar electronic structure and thus could all form superconducting fullerites.

636 FUL Ellipsometry and Optical Absorption Studies in M_xC_{60} Thin Films (x = 0, 3, 6; M = K, Rb, Cs): *P. C. Eklund*, Dept. of Physics and Astronomy and Center for Applied Energy Research, University of Kentucky, Lexington, KY 40506

Studies have been carried out on M_xC_{60} films (1000-2000 Å) grown on Si (100) and Suprasil substrates and characterized by Raman scattering. Optical absorption (0.5-5.5 eV) has been studied by ellipsometry (x = 0) and reflection/transmission (x = 0, 3, 6). For C_{60}, below the interband threshold at 1.7 eV, the refraction index is n = 1.96. Four strong absorption bands are observed and identified with transitions between narrow (0.5-1 eV) electron energy bands. Sharp absorption structure is also observed for M_xC_{60} which is insensitive to M, indicating the absence of strong charge-transfer excitations and weak hybridization between M and C_{60} orbitals. The structure in the M_xC_{60} is in good agreement with energy band calculations. Films of K_xC_{60} have just been made, and optical studies are in progress, results of these investigations are also presented.

637 FUL Voltammetric Studies of $[(C_6H_5)_3P]_2Pt$ (η^2-C_{60}) and some $([(C_2H_5)_3P]_2M)_n$ (η^2-C_{60})Complexes (M = Ni, Pd and Pt; n = 1, 2, 3 and 6): *P. J. Fagan*, Central Research and Development Dept., E. I. Du Pont de Nemours & Co., Inc., Experimental Station, Wilmington, DE 19880-0328, *S. A. Lerke* and *D. H. Evans*, Dept. of Chemistry and Biochemistry, University of Delaware, Newark, DE 19716

Cyclic voltammetry of the C_{60} complexes bearing one metal fragment reveals a series of reversible reductions displacing 0.2 to 0.3 V in the negative direction from the corresponding C_{60} reductions. Complexes with two, three, and six metal substituents are successively more difficult to reduce. The reductions are thought to be C_{60}-centered with the metal fragments providing electron density to the electron-deficient fullerene, hence causing the observed shift in potential. The mono-complexes undergo cleavage of the metal fragment in the reduced states producing the corresponding reduced C_{60}. Information about the kinetics and equilibria of these cleavage reactions has been extracted from the voltammetric data. The complexes feature irreversible oxidation peaks that appear to be metal-centered. The complexes bearing increasing numbers of metal fragments are more easily oxidized and, for n = 1 and 6, the oxidation potentials become more positive in the order Ni < Pd < Pt.

638 FUL Electron and Oxygen Atom Transfer to C_{60}. Formation of Oxygen Atom and 1,3-Dioxolane Adducts: *C. S. Foote, J. W. Arbogast, M. Kao, Y. Elemes, S. Silverman,* and *C.-M. Sheu*, Dept. of Chemistry and Biochemistry, University of California, Los Angeles, CA 90024-1569

Rates of one-electron reduction of triplet C_{60} by electron donors, especially amines, were measured as a function of oxidation potential in benzonitrile. Although no absorption from C_{60} radical anions was seen, transient spectra from aromatic amine

radical cations were observed. The rate constant for electron-transfer quenching as a function of oxidation potential of the donor follows the Weller relationship, but the rate constant for exothermic reactions is somewhat lower than the diffusion-controlled rate in more common organic solvents because of the high viscosity of benzonitrile. C_{60} reacts with acetone solutions of dimethyldioxirane to give stable oxidation products. Chromatographic separation gave $C_{60}O$, which has the same symmetry as other monoadducts of C_{60} (17 ^{13}C NMR lines). This molecule appears to be an epoxide rather an oxygen-bridged annulene, as shown by a relatively high-field ^{13}C NMR peak. The ^{13}C NMR of the second fraction has many similarities with that of the osmylated C_{60} adduct, and its mass, infrared, and ^1H and ^{13}C spectra show that it is a 1:1 dimethyldioxirane adduct of C_{60} (a 1,3-dioxolane).

639 FUL Analysis of the Raman Spectra of A_3C_{60} and A_6C_{60}: *F. Negri, G. Orlandi* and *F. Zerbetto,** Dipartimento di Chimica "G. Ciamician," Università di Bologna, 40126, Bologna, Italy

The spectroscopy of doped fullerenes is presently attracting considerable interest. Vibrationally resolved Raman spectra of the A_3C_{60} and A_6C_{60} phases are now available. MO-SCF-CI calculations (1) indicate that the ground state of C_{60}^{3-} is a quartet A_u while the ground state of C_{60}^{6-} is of singlet A_g. In previous work (2, 3), we used an upgraded version of the QCFF/PI method (4) to calculate the vibrational frequencies of neutral C_{60}. To investigate the vibrational structure of the Raman spectra of A_3C_{60} and A_6C_{60}, we perform QCFF/PI calculations of the structure, the vibrational frequencies, and the normal modes of vibration of these two anions in the lowest electronic state. The results are compared with similar calculations for neutral C_{60} and with the experiment.

1. F. Negri, G. Orlandi, and F. Zerbetto, *J. Am. Chem. Soc.*, In press.
2. F. Negri, G. Orlandi, and F. Zerbetto, *Chem. Phys. Lett.*, **144**, 31 (1988).
3. F. Negri, G. Orlandi, and F. Zerbetto, *J. Am. Chem. Soc.*, **113**, 6037 (1991).
4. A. Warshel and M. Karplus, *ibid.*, **94**, 5612 (1972).

640 FUL Photoexcitation and Photodissociation Channels of C_{60}: *K. R. Lykke, P. Wurz, D. H. Parker, M. J. Pellin,* and *D. M. Gruen*, Materials Science/Chemistry Div., Argonne National Laboratory, Argonne, IL 60439

The molecule C_{60} is remarkable both in its chemical and physical properties. Understanding the photophysical processes that occur in C_{60} and other fullerenes may even help our insight into the photophysics of other large molecules found in biological and nanomaterials systems. The fullerenes have so many degrees of freedom that they can store large quantities (> 40 eV) of excitation energy for extended periods of time before undergoing fragmentation or ionization. Laser desorption, followed by laser ionization high-resolution mass spectroscopy, has been used to measure direct ionization, fragmentation, detection of neutral fragmentation products, delayed ionization, and velocity distributions. A complex but coherent picture of the processes that occur following photoexcitation and that result in the various decay channels is beginning to emerge. This paper elucidates the measurements that have been done and the fascinating photophysical characteristics of the fullerenes revealed as a result of this work.

641 FUL The Structure and Symmetry of the Orientational Ordering of C_{60}: *A. B. Harris** and *R. Sachidanandam*, Dept. of Physics, University of Pennsylvania, Philadelphia, PA 19104

The symmetry of the orientationally ordered phase of solid C_{60} is discussed. The powder x-ray data of Heiney *et al.* show that this phase has cubic symmetry. The allowed cubic space groups for oriented icosahedra on an fcc lattice are determined to be Pa3, Pn3, and Pm3, each of which has four orientational sublattices. The experimentally determined Pa3 structure is discussed in detail. Orientational order parameters are introduced and using only symmetry considerations we construct a Landau theory to describe the orientational ordering transition. This Landau theory, which is similar to that used by J. R. Cullen *et al.* to describe orientational ordering in solid ortho-H_2, indicates that the transition is discontinuous in agreement with more recent experiments. The spectrum of libron-phonon excitations out of the ground state, as calculated by Yildirim and Harris based on recently proposed orientational potentials is also presented and is shown to be quite similar to that of isostructural ortho-H_2. Experimental implications of these calculations are discussed in some detail. Finally, order parameters to describe a possible orientational glass phase are presented.

642 FUL Nuclear Spin Weights and Gas Phase Spectral Structure of $^{12}C_{60}$ and $^{13}C_{60}$ Buckminsterfullerene: *W. G. Harter** and *T. C. Reimer*, University of Arkansas, Fayetteville, AR 72701

Rotational energy levels and high resolution rovibrational spectra of gas phase Buckminsterfullerene is strongly affected by the Pauli exclusion principle. Very different rovibrational fine structure patterns will be seen for differing arrangements of ^{13}C and ^{12}C isotopes. Only two extreme cases $^{12}C_{60}$ and $^{13}C_{60}$ actually have icosahedral symmetry. Those two cases will have relatively uncluttered spectral patterns and simpler rotational dynamics. Their analysis in turn will be a prerequisite to analyses of rotational dynamics of mixed cases. An understanding of gas phase rotational dynamics may also help to understand dynamics of icosahedral hindered rotors in the fullerite solids.

643 FUL Charge Transfer at Fullerene-Noble Metal Interfaces: J. S. Lannin, Dept. of Physics, Penn State University, University Park, PA 16801

In situ, surface enhanced Raman scattering (SERS) and photoemission of C_{60}/noble metal interfaces have provided information on charge transfer effects. Ultrathin films of C_{60} of less than 1 monolayer thickness were deposited in ultrahigh vacuum on sputtered polycrystalline island and continuous noble metal films. The SERS spectra indicate large shifts of the high frequency Ag(2) symmetry, pentagonal pinch mode of C_{60} increasing in the series Au, Cu, and Ag. In Ag and Cu, UPS difference measurements confirm that the shifts are due to charge transfer as a new LUMO band, derived in part from excited C_{60} states is found. The position of the Fermi energy indicates the formation of a metallic interfacial state for Ag and Cu. Limited changes in the UPS spectra of Au suggest that in addition to charge transfer, substrate polarization effects are present. XPS measurements indicate shifts of the carbon 1s core line that are opposite the SERS trend, also suggest that in addition to charge transfer processes, polarization effects are present. (This work was supported by NSF Grant DMR 8922305.)

644 FUL Recent Results in the Synthesis and Characterization of Discrete Derivatives of C_{60}: *J. M. Hawkins*, Dept. of Chemistry, University of California, Berkeley, CA 94720

Recent results in the synthesis and characterization of discrete derivatives of C_{60} are described, including isometrically pure 2:1 adducts of osmium tetroxide with C_{60}.

645 FUL Molecular Structures of the Gaseous Fullerenes C_{60} and C_{70} from Electron Diffraction: *K. Hedberg** and *L. Hedberg*, Dept. of Chemistry, Oregon State University, Corvallis, OR 97331, *D. S. Bethune, C. A. Brown, R. D. Johnson,* and *M. de Vries*, IBM Research Div., Almaden Research Center, San Jose, CA 95120-6099

In our recent article on C_{60} [*Science*, **254**, 410 (1991)] we reported the r_g bond lengths from refinements in which icosahedral symmetry was assumed and no account was taken of the effects of molecular vibration on the interatomic distances. Although we did not expect this omission to have a significant effect on the bond lengths, we have now introduced a set of vibrational corrections and re-refined the structure. The results are indeed insignificantly different from those previously reported: for the bonds respectively within the five-member ring and connecting five-member rings, the new [old] thermal average bond lengths (r_g/Å) with estimated 2σ uncertainties are 1.460 (6) [1.458 (6)] and 1.403 (10) [1.401 (10)]. We have also undertaken a study of C_{70}. Results are consistent with D_{5h} symmetry. Since C_{70} is a much more complicated molecule than C_{60}, (with assumption of D_{5h} symmetry C_{70} has 12 structural parameters and 143 different interatomic distances), the measured lengths of the individual bonds are much less precise. Preliminary values for the average bond lengths (r_g/Å) within and connecting the five-member rings are respectively 1.452 and 1.398 and the length of the unique bond in the equator of the molecule is 1.510. Details are reported.

646 FUL Orientational Order in Fullerenes: *P. A. Heiney*, Physics Department and Laboratory for Research on the Structure of Matter, University of Pennsylvania, Philadelphia, PA 19104

The discovery (1) of an orientational ordering transition in solid C_{60} has attracted experimental and theoretical interest. The 250 K transition from an orientationally disordered fcc structure to an orientationally ordered simple cubic $Pa\bar{3}$ structure (2) is the first order, and is accompanied by a jump in the lattice parameter of ~0.044 Å. The transition is affected by details of sample preparation, including careful removal of residual solvent. Recent experimental and theoretical results are discussed, and the ordering transition in pure C_{60} is compared with those in C_{70} and $C_{60}O$ as well as effects seen in dilute mixtures of alkali metal atoms in C_{60}. (This work was supported by the National Science Foundation, Grants DMR89-01219 and DMR-88-19885. The assistance of J. E. Fischer, A. R. McGhie, W. J. Romanow, A. M. Denenstein, N. Coustel, G. B. M. Vaughan, D. E. Cox, J. P. McCauley, Jr., and A. B. Smith III, is gratefully acknowledged.)

1. P. A. Heiney, J. E. Fischer, A. R. McGhie, W. J. Romanow, A. M. Denenstein, J. P. McCauley, Jr., and A. B. Smith III, *Phys. Rev. Lett.*, **66**, 2911 (1991).
2. R. Sachidanandam and A. B. Harris, *ibid.*, **67**, 1467 (1991).

647 FUL Structures of Carbon Cluster Ions: *G. von Helden, P. R. Kemper,* and *M. T. Bowers*, Dept. of Chemistry, University of California, Santa Barbara, CA 93106

We have recently developed chromatographic methods based on ion mobilities that allow separation of geometric isomers if they differ sufficiently in shape. These methods have been applied to carbon cluster ions up to n = 84, generated by laser vaporiza-

tion of graphite. Several families of isomers have been detected, starting with linear ($n \leq 10$), then several families of planar ring systems ($n \geq 7$) and finally, fullerenes ($n \geq 30$). A preliminary report has been published (1). We have also developed Monte Carlo methods for calculating mobilities from cluster ion structures in the hard sphere limit. Comparison with experiment allows unambiguous assignment of the structures of the different isomers. Most recently we have begun a series of semi-empirical and *ab initio* calculations on clusters in the C_{20} to C_{30} range for comparison with experiment. Details of both experimental and theoretical results are given.

1. G. von Helden, M-T. Hsu, P. R. Kemper, and M. T. Bowers, *J. Chem., Phys.*, **95**, 3835 (1991).

648 FUL Bandgap, Excitons and Coulomb Interaction in Solid C_{60}: *R. Lof, M. van Veenendaal, B. Koopmans, H. T. Jonkman,* and G. A. Sawatzky,* Laboratory of Applied and Solid State Physics, Materials Science Centre, University of Groningen, 9747 AG Groningen, The Netherlands.

The bandgap of solid C_{60} is determined by a combination of photoelectron and inverse photoelectron spectroscopy and found to be 2.3 eV. The previous reported optical absorption at 1.5-2.0 eV is argued to be of excitonic nature. The on-site molecular C_{60} Coulomb interaction (U) is determined from a comparison of the high resolution KLL Auger spectrum with the structure of the self-convolution of the valence band photoelectron spectrum, and found to be 1.5 eV. This value of U is shown to lead to Frenkel type excitons at 1.5-2.0 eV as observed optically. It is concluded that because of the large value of the Hubbard U as compared with the bandwidth, that C_{60} should be considered as a highly correlated system with U/W comparable to a single band Hubbard model description of the high T_c cuprates.

649 FUL Synthesis, Structure and Superconductivity of Carbon-60 Fullerides: *Z. Iqbal,* Research and Technology, Allied-Signal Inc., Morristown, NJ 07962

Alkali and alkaline earth C_{60} fullerides have been synthesized near ambient temperatures by a novel solution technique. Raman scattering results indicate that single phase materials are obtained in the K, Rb, Ca, and Ba systems. The details of the structures are being investigated by x-ray diffraction as a function of annealing of the as-prepared material. These results are discussed in this paper. Doping in the ternary K-Tl, Rb-Tl, and Cs-Tl systems have been investigated using a temperature gradient under hydrogen during synthesis. Evidence for Tl-intercalation has been obtained from x-ray diffraction and Raman scattering data in the K- and Rb-systems, respectively. Superconductivity (wherever they arise) in both the binary and ternary systems have been investigated using susceptibility and low-field microwave absorption measurements. These data are discussed in some depth. (My collaborators at Allied Signal are: Ray Baughman, Sanjeeva Murthy and Sandeep Khare; at Arizona State University are: B. L. Ramakrishna and Kishay Sinha; at Los Alamos National Laboratory is E. W. Ong; at the Royal Institute of Technology, Stockholm is K. V. Rao and at Morris Research are: Hans Borneman and Don Morris.)

650 FUL Carbon Nanotubes: *S. Iijima,* NEC Corp., Fundamental Research Laboratories, 34 Miyukigaoka Tsukuba, Ibaraki 305, Japan

A novel form of low-dimensional graphitic carbon needles, produced in an arc discharge evaporation method, is examined by means of electron optical methods. Typical needles are only a few nanometers in diameter, and consist of a few layers of graphitic carbon sheets, tubules centered coaxially about needles axes, and hollow inside. The smallest needle was made up of just only two graphitic tubules. On each graphitic tubule the carbon atom hexagons are arranged in a helical fashion about the needle axis. The helix pitch varies from needle to needle and from tubule to tubule in a single needle. The helical structure seems to aid at the growth of the carbon needles. The needles are far from conventional macroscopic crystals in many aspects such as one-dimensional solid, tubular morphology, and helical structure of carbon hexagon. Growth of needles and their electronic properties are also discussed.

651 FUL Solvent, Supporting Electrolyte and Temperature Effects on the Electroreductions of Buckminsterfullerene (C_{60}) in Aprotic Media: *K. M. Kadish,* D. Dubois, G. Moninot, W. Kutner, M. T. Jones,* Dept. of Chemistry, University of Houston, Houston, TX 77204-5641

The electroreductions of Buckminsterfullerene (C_{60}) in aprotic solvents were examined by voltammetry as a function of the solvent, supporting electrolyte and temperature. The reversible half-wave potentials, $E_{1/2}$, for the first three reductions were correlated to the acceptor and donor properties of the solvents as well as to their Dimroth-Reichardt parameter. While the inorganic anions of the supporting electrolyte do not significantly affect the $E_{1/2}$ values, the cations of the supporting electrolyte do to a large extent. The magnitudes of the solvent and supporting electrolyte effects also differ for the various redox processes of C_{60}. The observed shifts in $E_{1/2}$ are rationalized in terms of the following: (*i*) charge density of the fulleride anions, (*ii*) solvophobic effects involving neutral C_{60} (aggregation), (*iii*) solvophobic type interactions involving the C_{60} anions and the larger cations of the supporting electrolyte in polar solvents, (*iv*) ion pairing of the C_{60} anions with smaller cations in non-polar solvents, and (*v*) the acceptor and donor properties of the solvents. Studies of $E_{1/2}$ values as a function of temperature indicate unusually large change of entropy accompanying each reduction step. Diffusion coefficients and apparent solvation number of neutral C_{60} in different systems were also determined and accounted for by the solvophobic effect.

652 FUL Electron Spin Resonance Characterization of Singly, Doubly, and Triply Reduced Buckminsterfullerene, C_{60}, in Aprotic Media: *M. T. Jones,* D. Dubois,* and *K. M. Kadish,* Dept. of Chemistry, University of Houston, Houston, TX 77204-5641

The results of ESR studies on several anion radicals of Buckminsterfullerene, C_{60}^{n-} (n = 1, 2, and 3), in the solvents benzonitrile, dichloromethane, pyridine, and tetrahydrofuran are reported and discussed. The samples are prepared by electrochemical reduction techniques which allow the preparation of samples which contain, quantitatively and selectively, the desired anionic species. The results of ESR spectral studies on the anions in frozen solutions as a function of temperature are presented. The ESR lineshapes and linewidths are dependent upon the solvent and the temperature whereas the g-values are only weakly-dependent upon the temperature. The C_{60}^{-} g-value averages 1.998 over the four solvents and over the temperature range used. The resonances of C_{60}^{2-} are centered at about 2.00 and indicate a triplet ground state with an average separation of 12.6 Å between the two unpaired electrons. The C_{60}^{3-} resonance has a g-value closer to that of the free electron and exhibits features similar to the monoanion, suggesting a spin of 1/2. The results obtained from this study are presented and discussed in terms of the unique physical structure and properties of C_{60}, the lifting of the initial orbital degeneracy of the T_{1u} LUMO of C_{60} and the thermally accessible excited states of the C_{60}^{n-} anions.

653 FUL Intercalation of Amine Functionalized C_{60} in Mica-Type Silicates: *V. Mehrotra* and *E. P. Giannelis,** Dept. of Materials Science and Engineering, Cornell University, Ithaca, NY 14853, *R. F. Ziolo,* Xerox Webster Research Center, Webster, NY 14580

The recent discovery of molecular clusters of carbon has prompted a wide range of theoretical and experimental studies regarding their physical and chemical properties. None of these studies, however, has been concerned with the intercalation of these molecular clusters in a suitable host matrix and the properties of the resulting intercalate. In this paper, we report the synthesis and properties of ethylenediamine-functionalized C_{60}, $[C_{60}(en)_6]$, intercalated fluorohectorite, a synthetic mica-type silicate. X-ray diffraction and spectroscopic measurements show that intercalation leaves the C_{60} cluster intact and that the host galleries are occupied by a monolayer of guest molecules. The intercalated $C_{60}(en)_6$ clusters exhibit a higher thermal stability compared to pristine $C_{60}(en)_6$ and C_{60} with no evidence for reaction with the silicate host. The thermal and electrical properties of the intercalates after elimination of the en ligands at intermediate temperatures are presented and contrasted to those of amorphous and graphitic carbon layers obtained through pyrolysis of intercalated organic molecules or polymers.

654 FUL Theoretical Studies of the Structure, Properties, and Dynamics of Fullerene, Crystals and Superconductors: *W. A. Goddard III,* Y. Guo, G. Chen,* and *N. Karasawa,* Materials Simulation Center—Beckman Institute (139-74), California Institute of Technology, Pasadena, CA 91125

We have developed a force field for Buckyball molecules and for alkali doped fullerenes and have applied this force field to: (*i*) predictions of crystal structures for C_{60} and C_{70} as a function of temperature and pressure; (*ii*) predictions of crystal structures of M_xC_{60} for M = Li, Na, K, Rb, Cs and x = 1, 2, 3, 4, 6, 8 and; (*iii*) predictions of the vibrational frequencies for finite molecules (C_{60}, C_{70}, C_{76} etc.) and of the phonons for the crystal. For K_3C_{60} we used the calculated phonon spectrum and electronic band structure to predict from first principles the superconducting properties of K_3C_{60} (assuming BCS theory). The predicted T_c is within 40% of the observed value, providing strong support for the BCS description of these systems.

655 FUL Studies Related to Extraction and Separation of Fullerenes: *R. S. Ruoff, R. Malhotra,* and *D. Lorents,* SRI-International, Menlo Park, CA 94025

A new technique for large scale separation of C_{60}, C_{70}, and also for subsequent separation of the larger fullerenes, is discussed. Thermodynamic parameters, derived from solubility data and sorption microcalorimetry data of C_{60} in solvents typically employed in extraction and separation, and of C_{60} in solid/solvent mixtures similar to those employed as stationary phase/eluent in chromatographic separations, are presented.

656 FUL ESR Studies of the Reaction of Alkyl Radicals with C_{60}: *P. J. Krusic** and *E. Wasserman,* Central Research and Development, E. I. du Pont de Nemours & Co., Wilmington, DE 19880-0328, *J. R. Morton* and *K. F. Preston,* Steacie Institute for Molecular Sciences, National Research Council of Canada, Ottawa, Ont., Canada K1A OR9

Photochemically and thermally generated organic radials add rapidly to C_{60} to afford radical and nonradical adducts R_nC_{60}. For example, mass spectrometric analyses show the formation of $(CH_3)_nC_{60}$ with n = 1 to at least 36 and of $(C_6H_5CH_2)_nC_{60}$ with n = 1 to at least 15. This paper focuses on the information that can be extracted from electron spin resonance experiments concerning the radical adducts R_nC_{60} with n = 1, 3 and 5. Proton and ^{13}C hyperfine interactions indicate that in the initial radical adducts RC_{60}• (R = *tert*-butyl, 1-adamantyl, isopropyl, ethyl, trichloromethyl, benzyl, etc.) the unpaired electron is mostly confined to two fused six-membered rings on the surface of C_{60} having the substituent R at one of the points of fusion. Each half of the resulting radical structure of C_s symmetry can be compared with a cyclohexadienyl radical. Extensive delocalization of the unpaired electron over the C_{60} sphere is ruled out. The radical adducts with n = 3 and 5 and R = benzyl also have the unpaired electron highly localized on the C_{60} sphere and are exceptionally persistent. ^{13}C labeling of the entering radical in the benzylic position shows that in $(C_6H_5CH_2)_3C_{60}$• the unpaired electron is delocalized in an allylic fashion over three carbons of a five-membered ring of the C_{60} sphere. Similar studies indicate that in $(C_6H_5CH_2)_5C_{60}$• the unpaired electron is shared equally by the carbons of a surface five-membered ring in a cyclopentadienyl fashion. The formation of species with two unpaired electrons is also discussed.

657 FUL Radial Vibrations of an Ion Inside Icosahedral C_{60}: J. L. Ballester and B. I. Dunlap, Dept. of Physics, Emporia State University, Emporia, KS 66801

The very high symmetry of icosahedral C_{60} suggests that as a first approximation an atom trapped inside C_{60} would feel a potential that is radially symmetric about the center. All-electron local-density-functional (LDF) calculations of the total energy of a sodium ion as a function of radial displacement from the center along the fivefold axis of C_{60} serve to refine such a radial potential. In particular, the calculations suggest studying potentials that have minima displaced from the center. A novel analytic functional form for a radial potential having a positive cusp at the origin is proposed and the s-wave radial solutions of the corresponding Schrodinger equation are examined. The extension to nonzero rotational quantum numbers is also considered.

658 FUL Organometallic Chemistry of Fullerenes in the Gas Phase by FTMS: *Y. Huang,* Q. Jiao, S. A. Lee,* and *B. S. Freiser*, Dept. of Chemistry, Purdue University, West Lafayette, IN 47907

The chemistry of fullerene-C_{60} and -C_{70} with transition metal ions in the gas phase was studied by FTMS technique. Fullerene samples heated off a solids probe react with a variety of transition metal ions via condensation to give MC_{60}^+ and MC_{70}^+. Alternatively both C_{60} and C_{70} can react with a ML^+ species (L = an alkene ligand) via displacement to give MC_{60}^+ and MC_{70}^+. Isolation and subsequent fragmentation of these MC_{60}^+ species by collision-induced dissociation give either M^+ or C_{60}^+ or a combination of both depending on the relative IPs of M and C_{60}. Such a fragmentation pattern is distinctly different from those of endohedral $M@C_{60}^+$ ions. The extended reaction of NiC_{60}^+ with C_{60} gives $Ni(C_{60})_2^+$, the first example of perhaps a whole new series of dumbbell complexes. C_{60}^+ undergoes facile reactions with FE(CO)$_5$ to form a variety of $Fe_xC_{60}(CO)_m^+$ species. Electronic consideration suggests that C_{60} acts as a two-electron donor in these species. C_{70}^+ reacts similarly with Fe(CO)$_5$. Interestingly both C_{60} and C_{70} show dramatically higher reactivity with Fe(CO)$_5$ than their neighboring C_n^+ cluster ions.

659 FUL Solubilization of Buckminsterfullerene, C_{60}, in Water and Some Polar Organic Solvents by Cyclodextrin Inclusion Chemistry: *W. Kutner,* P. Boulas,* and *K. M. Kadish*, Dept. of Chemistry, University of Houston, Houston, TX 77204-5641

Highly hydrophobic buckminsterfullerene, C_{60}, is virtually insoluble in most polar solvents, but is shown to solubilize in water as well as in 1:1 (v/v) aqueous methanolic, 1:1 (v/v) aqueous ethanolic, DMF or DMSO solutions by forming inclusion complexes with cyclodextrins (CDs). The internal diameter of the α-, β, and γ-CD cavities is 5.3, 6.5, and 8.3 Å, respectively, while that of the C_{60} molecules is 10-11 Å. This suggests that only a slight penetration of C_{60} into the CD cavities is possible. Surprisingly, however, the α-, β- and γ-isomers of CD all reveal good host properties. UV-vis spectroscopy of C_{60} in each of the above solvent systems indicates that a solubilization of C_{60} in by CD inclusion does not significantly affect its electronic properties. Only slight band shifts and changes in the relative heights of the three intense UV bands of C_{60} are observed as compared to those of C_{60} in aprotic solvents not containing CDs. Measurements of the UV spectra at different CD/C_{60} mole ratios allows one to derive the binding isotherm for each inclusion system and also determine the inclusion complex stoichiometry and stability constant. Cyclic and differential pulse voltammograms of C_{60} in DMF or DMSO solutions containing CDs resemble those reported in pyridine or benzonitrile in the absence of CDs. However, the data in aqueous and mixed aqueous/alcoholic solutions of CDs suggest that electroreduced C_{60} chemically reacts with the solvent.

660 FUL Excited State Behavior of Fullerenes (C_{60} and C_{70}) and Their Reduction in Colloidal Semiconductor Suspensions: *P. V. Kamat* and *N. M. Dimitrijevic*, Radiation Laboratory, University of Notre Dame, Notre Dame, IN 46556

Triplet excited state properties and charge transfer processes of fullerenes in benzene have been investigated by laser flash photolysis and pulse radiolysis techniques. Apart from the previously reported absorption in the visible, the triplet excited states of both C_{60} and C_{70} exhibit interesting spectral features in the UV region. Self quenching processes such as, the ground state quenching (2×10^9 $M^{-1}s^{-1}$ for $^3C_{60}$• and 6×10^8 $M^{-1}s^{-1}$ for $^3C_{70}$•) and triplet-triplet annihilation ($2k = 1.8 \times 10^9$ $M^{-1}s^{-1}$ for $^3C_{60}$• and $2k = 2 \times 10^9$ $M^{-1}s^{-1}$ for $^3C_{70}$•) were responsible for the rapid deactivation of the triplet excited state. Photo-induced charge transfer between ZnO colloids and fullerenes has been achieved with optical excitation of the semiconductor. The reduced fullerenes exhibit absorption characteristics that are quite different from the photogenerated triplet excited state. The efficiency of fullerene reduction increased with increasing concentration of ZnO colloid. At very high ZnO concentrations, the availability of the carbon cluster at the ZnO surface was a limiting factor in controlling the efficiency of reduction. Mechanistic and kinetic details of interfacial charge transfer between the carbon cluster (C_{60} and C_{70}) and colloidal semiconductor are presented. (The research described herein is supported by the Office of the Basic Energy Sciences of the U.S. Department of Energy.)

661 FUL Fluorinated Buckminsterfullerenes: *K. Kniaz, J. E. Fischer, J. P. McCauley,* and *A. B. Smith III*, Dept. of Chemistry, University of Pennsylvania, Philadelphia, PA 19104-6323, *H. Selig*, Dept. of Inorganic Chemistry, Hebrew University, Jerusalem, Israel

Fluorination experiments have been done on samples of pure buckminsterfullerenes C_{60} and C_{70}. Fluorinations have been conducted at different temperatures and under wide range of fluorine pressures. In the analysis of the reaction products we utilized x-ray diffraction, TGA, ^{19}F NMR, UV-vis, IR and mass spectroscopies. Mass spectroscopy revealed many fluorinated fullerenes in the reaction products with the most prominent peaks ranging from $C_{60}F_{40}$ to $C_{60}F_{48}$ for C_{60} and from $C_{70}F_{44}$ to $C_{70}F_{54}$ for C_{70}. The powder x-ray diffraction of the reaction products exhibited a few broad peaks consistent with the fcc lattice with a lattice parameter a = 17.1 A ($C_{60}F_x$) and a = 17.9 A ($C_{70}F_x$). The absence of high-Q peaks suggests a high degree of orientational disorder due to the large number of different molecules in the investigated samples. IR spectroscopy of the reaction products revealed a broad peak at 1165 cm^{-1}. The lubricating properties of thin films of fluorofullerenes cast on silicon wafers have been investigated by means of ellipsometry. The contact angles between water and fluorofullerene films were almost as high as those between water and Teflon. (This work was supported by NSF Grants DMR 88-19885 and DMR 89-01219.)

662 FUL Isomerism and Chirality in Bis-Metal Derivatives of Fullerene C_{60} Ligated in η-6, η-5, η-2 Fashion: *V. I. Sokolov*, Institute of Organo-Element Compounds, Academy of Sciences, 117813 Moscow, Russia

Fullerene O_{80}, a totally unsaturated spheroidal molecule, has to form exohedral complexes with metals wherein it may, in principle, act as η-6, η-5, η-4, η-3, or η-2 ligand. The last structural type is represented by the known platinum or osmylated derivatives whereas hexahapto- and pentahapto-metal complexes (not yet reported) should be analogous to benchrotrene and cymantrene or ferrocene, correspondingly. Symmetry analysis of binary relationships for both 5- and 6-polygonal faces (submitted) has demonstrated that chiral combinations include pairs of nonfused 6-faces only. All pairs involving at least one 5-face are chiral. This suggests that fullerenes, double π-metal complexed on 6-faces, for example, bis(tricarbonychromium) fullerene, will be chiral and resolvable into enantiomers. Their racemization via the η-6 ↔ η-5 haptotropic process is predicted. Metal derivatives of this type can give rise, in a controlled thermal process, to materials $C_{60}M_n$ of superconducting family. Binary relationships between edges reflect isomerism in bis-η -2 derivatives (*e.g.*, osmylated C_{60}). There are 8 different combinations with statistical weights 4:4:4:4:4:4:4:1. The latter applies to the most remote edges separated by the shortest pathway of 8 steps. The pairs of edges separated by odd numbers of steps, except 1, namely, 3, 5, or 7, are chiral. In this analysis only the edges between two 6-faces have been considered because they exhibited a higher reactivity, at least in the camylation.

663 FUL Chemical Oxidation of Buckminsterfullerene (C_{60}): *D. L. Stalling, C. Gao, K. Kuo,* and *K. Kelly*, ABC Laboratories, Inc., Columbia, MO 65205

Two products were obtained and preliminarily characterized when cis-Bis(acetonitrile)chloronitro-palladium (II) (Andrews *et al.*) was used as a C_{60} oxidation catalyst. Reaction products were monitored by UV-liquid chromatography using a newly developed, high performance gel permeation chromatography column-Envirosep-ABC™ (ABC Laboratories, Inc.). This column readily separates C_{60} from C_{70}. The two buckminsterfullerenes elute later than reactions products. Solvent and presence or absence of oxygen influence products of this reaction. When toluene was the solvent, in the presence of dry air, two reaction products

formed which eluted at 3.3 and 6.6 min. The product eluting at 6.6 min first was detected after 20 h, and the component eluting at 3.3 min was detected after 72 h. A decrease in C_{60} concentration correlated with increased amounts of reaction products. Most of the C_{60} and 6.6 min product were depleted after 90 h; after 266 h of reaction, only the 3.3 min product remained. The amount of 6.6 min product was increased by using a solvent system of 15% methylene chloride in toluene (v/v). In the absence of air (argon atmosphere), only product eluting at 3.3 min was observed. Solvent selection is important for this reaction, perhaps due to different solubilities of the catalyst, C_{60} and C_{70}. No reaction occurred in 1,1,1-trichloroethane or t-butyl methyl ether. With methylene chloride as solvent, a black, insoluble solid product was obtained. The UV spectrum of the product eluting at 6.6 min is very similar to that of C_{60}, suggesting that this product has a similar electronic structure, with two absorption bands between 240-350 nM; however, *alpha*-max was shifted to shorter wave lengths. The UV spectrum of the 3.3 min product exhibits one broad absorption band from 220-400 nM (*alpha*-max = 235 nM) suggesting more structural modification occurred. Small amounts of the two compounds isolated from the GPC column were examined by negative ion FAB-MS and ^{13}C-NMR. Formulas of $C_{60}NO_8$ and $C_{60}N_3O_8$ are suggested for the major constituents in the 6.6 and 3.3 min peaks, respectively, and the ^{13}C-NMR support these MS results. Multiple chemical shift signals were observed between 22-69 and 130-148 ppm for the 6.6 min. constituent, indicating opening of double bonds the presence of double bonds other than those of C_{60}. Chemical shifts for the 3.3 min constituent were observed at 13-45 and 128-148 ppm.

664 FUL MNDO Study of Silicon-Substituted Buckminsterfullerene: *X. Xia,** Dept. of Chemistry, State University of New York at Buffalo, Buffalo, NY 14214, *J. R. Bowser* and *D. A. Jelski*, Dept. of Chemistry, State University of New York, College at Fredonia, Fredonia, NY 14063, *T. F. George*, Dept. of Chemistry and Physics, Washington State University, Pullman, WA 99164-1046, *J. Gao*, Dept. of Chemistry, State University of New York at Buffalo, Buffalo, NY 14214

The sequential substitution of silicon atoms into the buckminsterfullerene cage to produce species conforming to the formula ($@C_{60-n}Si_n$) is studied using MNDO. For large n, the fullerene structure becomes unstable, resulting in the collapse of the cage to form three-dimensional networks held together by Si-C σ-bonds (1). For small n, the cage is structurally stable, and it is expected that these systems will have useful properties. For example, ($@C_{58}Si_2$) might provide an avenue for incorporating fullerene cages into polymer backbones. Secondly, the electronic properties of Si-fullerenes may prove useful. Of special interest is ($@C_{48}Si_{12}$), an analog of the ($@C_{12}B_{24}N_{24}$) cluster described in an earlier study (2). A synthetic route to the former from silacyclopentadiene is suggested. (This work was funded by: ACS-PRF, Research Corporation, NSF, and ONR.)

1. Many such species are described in G. Fritz and E. Matern, "Carbosilanes," Springer-Verlag, Berlin (1986).

2. J. R. Bowser, D. A. Jelski, and T. F. George, *Inorg. Chem.*, **31**, 154 (1992).

665 FUL A Systematic Study of Structures and Stabilities for Fullerenes: *B. L. Zhang, C. Z. Wang, K. M. Ho, C. H. Xu,* and *C. T. Chan*, Ames Laboratory-USDOE, Dept. of Physics, Iowa State University, Ames, IA 50011

Combining a very efficient cage network generation scheme with an accurate right-binding potential, we studied every even-numbered fullerene from C_{20} to C_{94}. We found that all the ground-state structures (except C_{22}) consist of five and six-member rings only. Unlike C_{60}, most fullerenes prefer structures with low symmetry. Some of the fullerenes have several isomers very close in energy, and they are expected to coexist in the synthesis. We also calculated the fragmentation energies in the process of C_2 loss and the HOMO-LUMO energy separations. C_{60}, C_{70}, and C_{84} are found to be superstable if both fragmentation and chemical reaction stabilities are considered. (Ames Laboratory is operated for USDOE by Iowa State University under Contract No. W-7405-Eng-82.)

666 FUL Nonlinear Optical Second-Order Harmonic Generation and Suppression in C_{60} Thin Films: *X. K. Wang, T. G. Zhang, W. P. Lin, Z. Y. Xu, S. Liu, M. M. Kappes, G. K. Wong, J. B. Ketterson,* and *R. P. H. Chang*, Materials Research Center, Northwestern University, Evanston, IL 60208

Second harmonic generation and suppression measurements were performed with a Nd:YAG laser and an optical parametric amplifier. It was observed that C_{60} thin film in a corona poling field of 5.5 kV at a nominal temperature of 140°C exhibited a large second-order susceptibility $\chi^{(2)} = 2.2 \times 10^{-8}$ esu, which is about 15 times the $\chi^{(2)}$ value of quartz. When the film is simultaneously illuminated with a second light source, including both pulsed and static illumination, the large second harmonic response of C_{60} films was almost completely suppressed. The response time of the suppression is about 250 ps. These nonlinear optical properties may make fullerene materials very important in a new generation of optical computers.

667 FUL Vapor Pressure and Thermal Oxidation of C_{60} and C_{70}: *M. Balooch** and *W. J. Siekhaus*, Lawrence Livermore National Laboratory, Livermore, CA 94551, *J. Abrefah* and *D. R. Olander*, University of California, Berkeley, CA 94720

The vapor pressure and thermal oxidation of the fullerenes C_{60} and C_{70} have been measured over the temperature range 400-600°C by a thermogravimetric technique. The heats of sublimation of 38 and 45 kcal/mol are obtained for C_{60} and C_{70}, respectively. The vapor pressure of C_{60} ranges from 1.8×10^{-5} and 1.4×10^{-2} Torr and that of C_{70} is between 1.4×10^{-5} and 8.7×10^{-3} Torr over the temperature range investigated. The entropy of vaporization of C_{60} obeys Trouton' rule. The reaction of oxygen with fullerenes proceeds in two different steps. One of them involves adsorption of oxygen by the fullerenes. If uninterrupted by the second step, the oxygen uptake reaches a saturation value. The maximum amount of oxygen uptake increases with decreasing temperature. The second step is the sustained burning of the fullerenes at a constant rate. That rate is almost independent of temperature and the amount of fullerenes.

668 FUL Simultaneous Electrochemical Quartz Crystal Microbalance and Cyclic Voltammetry Study of Electrodeposition, Doping with Countercations and Electrodissolution of Films of Buckminsterfullerene, C_{60}, and Its Anions in Polar Aprotic Solvents: *W. Koh, D. Dubois, W. Kutner, M. T. Jones,* and *K. M. Kadish*, Dept. of Chemistry, University of Houston, Houston, Texas 77204-5641

A simple and efficient method was developed for preparation of insoluble thin films of C_{60}, and salts of C_{60}^- and C_{60}^{2-}. The method consists of first bulk electroreducing a fine suspension of solid C_{60} in acetonitrile solutions under a controlled potential which is sufficiently negative to generate a soluble C_{60}^{3-} anion, followed by electro-oxidative deposition of a film on the surface of a gold/quartz crystal working electrode. The properties of the electrodeposited films were examined by simultaneous cyclic voltammetry and electrochemical quartz crystal microbalance (EQCM) experiments which enabled determination of stoichiometry and film thickness. The C_{60} film is easily doped with different countercations upon electroreduction, leading to the salts of fulleride mono- and dianions. The method of film preparation can also be extended to other solvents in which neutral C_{60} is insoluble. The cyclic voltammetry and EQCM behavior of the film is largely dependent on the nature of the solvent and supporting electrolyte used. These data are discussed with respect to the solution behavior of C_{60}.

669 FUL Nonlinear Optical Properties of Fullerenes in the Visible and Near-Infrared: *Z. H. Kafafi, J. R. Lindle, S. R. Flom, R. G. S. Pong,* and *F. J. Bartoli*, U.S. Naval Research Laboratory, Washington, D.C. 20375

Several nonlinear optical (NLO) experiments have been initiated here at NRL to investigate the NLO properties of the fullerenes (1). Time-resolved degenerate four-wave mixing (DFWM) and Z-scan studies were conducted on solutions and films of the fullerenes, C_{60} and C_{70}. A Q-switched, mode-locked 35 ps Nd:YAG laser was used at 1.064 μm whereas a synchronously pumped, mode-locked 1 ps dye laser, tunable in the visible, was operated near 600 nm. The relationship between the molecular structure/symmetry of the fullerenes and their third-order optical properties is studied. The electronic and dynamic nonlinearities of these molecular clusters, and their time responses are discussed. Mechanisms giving rise to third- and fifth-order optical process in the different time domains are explored.

1. Z. H. Kafafi, J. R. Lindle, R. G. S. Pong, F. J. Bartoli, L. J. Lingg, and J. Milliken, *Chem. Phys. Lett.*, **188**, 492 (1992).

670 FUL Dynamics of Free Fullerenes in Photophysics and Collisions: *W. Kamke,** *E. E. B. Campbell,* and *I. V. Hertel*, Freiburger Materialforschungszentrum and Fakultät für Physik, Albert-Ludwigs-Universität, W 7800 Freiburg, Germany

Buckminsterfullerene (C_{60}) and its associates such as C_{70} and larger fullerenes offer a unique possibility to study the dynamics associated with the absorption of photons in a free large cluster of high symmetry and to compare experimental results to a variety of data available from solids or surfaces. In our experiments, free fullerene molecules or clusters are formed by thermal evaporation from an oven or by laser evaporation. Using multiphoton ionization and a modified time of flight technique delayed ionization of C_{60} has recently been observed. Using single photon ionization with synchrotron radiation the photoionization spectra of fullerenes were measured between threshold (7.54(4) eV for C_{60}) and 35 eV. The ion yield is dominated by a giant plasmon resonance at about 20 eV which was recently predicted theoretically. In our time of flight setups the fullerene ions can easily perform collisions with various target gases. Recent experiments give insight into the collisional fragmentation of fullerenes as well as into the formation of heterogeneous compounds in the collision process. Experiments where C_{60} is used as target vapor are also in progress.

671 FUL Thermophysical Properties of Solid C_{60}, C_{70} and Related Materials: *J. L. Margrave,** *C. Pan, M. S. Chandrasekharaiah, M. P. Sampson,* and *R. H. Hauge*, Dept. of Chemistry and Rice Quantum Institute, Rice University, Houston, TX 77251

The recent availability of gram-quantities of C_{60}/C_{70} mixtures as well as multimilligrams of pure C_{60} and C_{70} and milligrams of

C_{84}, C_{92}, etc. have allowed measurements of (*i*) heats of combustion, (*ii*) vapor pressures, (*iii*) heat capacities, (*iv*) ionization potentials, and (*v*) electron affinities. Also, the reactions of solid C_{60}/C_{70} with O_2, N_2, F_2, Cl_2, H_2, H_2O have been studied.

672 FUL Superconductivity in Metal-Doped C_{60} Solids: *C. M. Lieber, C. C. Chen, Z. Zhang,* and *S. P. Kelty,* Dept. of Chemistry and Division of Applied Sciences, Harvard University, Cambridge, MA 02138

Recently, there has been significant effort directed toward exploring superconductivity in alkali metal doped C_{60} solids and films. The transition temperatures for K-doped C_{60} solids and films. The transition temperatures for K-doped C_{60} (18 K) and Rb-doped C_{60} (28 K) are significantly higher than previously reported for other organic based superconductors, and thus suggests that doped C_{60} represents a new class of high-T_c superconductors. Herein recent results from our laboratory that address the synthesis, characterization and superconducting properties of these materials are discussed. A series of new mixed alkali-metal doped materials have been prepared with the general formulas $K_{3-x}Cs_xC_{60}$ and $Rb_{3-x}Cs_xC_{60}$. Structural and magnetic studies have been used to elucidate the variation of the superconducting transition temperature with lattice size. In addition, extensive low-temperature tunneling measurements of the superconducting energy gap have been carried out. The implications of these and other new data to understanding superconductivity in these materials are discussed.

673 FUL Electrochemical Reactivity of Fullerenes and Their Derivatives: *F. D'Souza, R. Seshadri, R. Nagarajan, G. Raj, V. Krishnan,* C. N. R. Rao,* Solid State and Structural Chemistry Unit, CSIR Centre of Excellence in Chemistry and Dept. of Inorganic and Physical Chemistry, Indian Institute of Science, Bangalore 560012, India

Fullerenes, C_{60} and C_{70}, exhibit favorable one-electron reductions making them valuable acceptor entities. Interaction of fullerenes with typical aromatic amine donors, *viz.*, 2,3,5,6-(dimethylamino) benzene and 1,4-(dimethylamino) benzene has been studied to establish the nature ground-state charge-transfer interaction in these systems. Cyclic vol'ammetric studies of the solutions containing these donors with fullerenes have shown that the oxidation potential of the donors are split while the reduction potentials of the fullerenes are diminished in magnitude indicating possible existence of CT interaction in these systems. In another study involving fullerenes with metalloporphyrins, *viz.* CoTPP, we find that the oxidation potential of Co(II) is shifted to lower potential by about 80 mV accompanied by diminished values of the reduction potentials of fullerenes. This has been interpreted in terms of fulleride anion coordination to Co(III)TPP. Besides partly hydrogenated C_{60} (prepared through diimide reduction), we have prepared alkylamine adducts by nucleophilic addition. We have also prepared bromo and chloro derivatives by reaction with liquid Br_2 and $SbCl_5$, respectively. We have examined these derivatives by cyclic voltammetry.

674 FUL Production and ESR Spectroscopy of Fullerenes Containing Metal Atoms: *R. D. Johnson, C. S. Yannoni, M. S. de Vries, J. R. Salem,* and *D. S. Bethune,** IBM Research Div., Almaden Research Center, San Jose, CA 95120-6099

We report bulk preparation of LaC_{82} and ESR spectra of this species in solution and in the solid state. Samples were prepared by using a graphite/La_2O_3 composite rod as the anode of a carbon arc and extracting the soot with toluene. The extract contained only C_{60}, C_{70} and $La@C_{82}$. The X band (9.112 GHz) ESR spectrum of the degassed dry powder is centered at g =2.001, in the region characteristic of fullerene anion radicals, and has an overall width of ~10 gauss. In solution the spectrum consists of eight extremely narrow (0.125 gauss) equally spaced (1.25 gauss interval) lines of equal intensity also entered at g = 2.0010, unambiguously diagnostic for isotropic hyperfine coupling to a nuclear magnetic moment with spin 7/2 such as ^{139}La. The hyperfine coupling constant (1.25 gauss) is very small, indicating that the unpaired electron resides primarily on the carbon shell and the La is in the +3 oxidation state. Thus the lanthanum 6s electrons pair in the lowest energy C_{82} LUMO while the third electron occupies the next higher energy C_{82} orbital, and the fullerene is a ground state doublet. The captive (La^{+3}) ions are relatively unperturbed and are present in reasonably high concentrations, so that many additional spectroscopic studies may soon be possible.

675 FUL Gas-Phase Characterization of Fullerenes and Endohedral Complexes: *S. W. McElvany,* J. H. Callahan,* and *M. M. Ross,* Code 6113/Chemistry Div., Naval Research Laboratory, Washington, DC 20375-5000

A variety of mass spectrometric (MS) techniques have been used to characterize the gas-phase properties and reactions of fullerenes. Physical properties of fullerenes such as ionization potentials (IPs) and proton affinities (PAs) have been determined by charge-transfer and proton-transfer bracketing measurements. Chemical ionization (CI) has also been shown to be a sensitive method for the analysis of fullerenes and their derivatives in addition to producing gas-phase fullerene derivatives from ion/molecule reactions in the CI plasma. Recent studies have focused on the generation of endohedral fullerene cation complexes using two different production methods. High-energy (keV) collisions of C_n^+ with inert gas atoms results in fragmentation and/or uptake of the neutral target atom. Tandem MS experiments and molecular dynamics simulations of the collision process provide convincing evidence for their endohedral structure, *e.g.*, $He@C_{60}^+$. In other studies, direct laser vaporization of fullerene- and metal-containing samples results in the production of metal-fullerene complexes. Surprisingly, the metal atom(s) in these DLV-generated species (*e.g.*, $Y_xC_n^+$) are shown to reside within the carbon cage by comparison of their CID and ion/molecule reactions with externally bound adducts.

676 FUL Diamond from Fullerenes: *M. Núñez Regueiro* and *P. Monceau,* CRTBT, CNRS, Cedex 9, 38042 Grenoble, France, *J.-L. Hodeau,* L. Crystallographie, CNRS, Cedex 9, 38042 Grenoble, France

High pressures studies have shown that C_{60} molecules are stable under hydrostatic pressures up to at least 20 GPa, with the material conserving the low pressure phase. However, nonhydrostatic loading induces phase transitions to lower symmetry phases that appear to be insulating. It is shown here that extreme nonhydrostatic compressions causes the collapse of the spheroids around 20 GPa at room temperature. Depending on the magnitude and conditions of the applied pressure, the resulting material can be polycrystalline diamond or amorphous material. Our results suggest an alternative route to industrial diamond synthesis.

677 FUL Large Fullerenes: Structures and Growth Mechanism: *Y. Achiba,* Dept. of Chemistry, Tokyo Metropolitan University, Hachioji, Tokyo 192-03, Japan

We here report structural and electronic properties of higher fullerenes up to C158 (C76, C78, C82, C84, C96, C102, C106, C110, etc.) which were isolated from the carbon soot generated by arc heating of graphite, using a preparative HPLC. Mass spectrometric characterization was performed, showing that purity of the isolated fullerenes is better than 95%. UV/visible optical absorption measurements in benzene indicate that absorption threshold shift to the longer wavelength with increasing size of fullerenes. Structural information has been deduced by ^{13}C NMR for well-isolated fullerenes in CS_2 solution. As a result, we found three isomers for C78 ($2 \times C_{2v}$ and D_3), five for C82 (C_2 (major), C_{2v}, $2 \times C_2$, and C_{3v}), and two major isomers (D_2 and D_{2d}) for C84. From the structural evidences obtained for C76, C78, C82, and C84, we see such an interesting tendency that the fullerene cages with the lower symmetry are preferentially formed. The propensities of structures and magic numbers in the formation of the fullerenes would suggest the important role of dynamical aspects in fullerene growth process rather than the thermodynamic stabilities. A new model (ring-stacking model) recently developed by our group for fullerene growth is briefly discussed.

678 FUL Synthesis of a C_{60}-p-Xylylene Copolymer: *D. A. Loy** and *R. A. Assink,* Org. 1812, Sandia National Laboratories, Albuquerque, NM 87185

The preparation and purification of macroscopic quantities of buckminsterfullerenes or buckyballs has ignited an explosion of research into their physical and chemical properties, and a variety of strategies for preparing new fullerene-based materials. Chemical derivatives of C_{60} fullerene can be prepared by a variety of methods. We report a polymeric fullerene material prepared by reacting C_{60} with xylylene. The xylylene, generated by the flash thermolysis of paracyclophane, was reacted with C_{60} in toluene cooled to -78°C to afford an insoluble, brown solid. Analyses of the material by solid state ^{13}C MAS NMR, IR, and thermal gravimetric analysis are consistent with a C_{60}-xylylene copolymer. (This work was supported by the United States Department of Energy under Contract No. DE-AC04-76DP00789.)

679 FUL ESR and Optical Studies of the Radical Ions of Fullerenes: *T. Kato,* T. Kodama, T. Shida, S. Suzuki, and Y. Achiba,* Kyoto University, Kyoto 606, Japan

The electronic absorption spectra of the radical ions of C_{60} and C_{70} are observed in γ-irradiated glassy polyatomic matrices at 77 K. The spectral features of all the radical ions are consistent with the available information in the literature which includes photoelectron and resonance Raman spectra of C_{60} and C_{70}. In addition, the observed spectra compare favorably with the results of CNDO/S calculations. The ESR spectra of the radical anions of C_{60} and C_{70} produced by electrolysis were measured at 77 K. In the case of radical anion of C_{60}, a singlet ESR spectrum with g = 1.9982 appeared. The small value of the g factor was interpreted in terms of a large correction by the second-order perturbation of the residual orbital angular moment. The irregular vibrational structure of the electronic absorption of the radical anion in the frozen matrix was suggested as being due to the Jahn-Teller distortion.

680 FUL Electronic Structures and Superconductivity of Fullerenes and Fullerides: *S. Saito,* A. Oshiyama, Y. Miyamoto, S.-i. Sawada,* and *N. Hamada,* Fundamental Research Laboratories and Microelectronics Research Laboratories, NEC Corp., 34 Miyukigaoka, Tsukuba, Ibaraki 305, Japan

We present the electronic structures of fullerenes and fullerides obtained by using the density-functional theory as well as the realistic tight-binding model. The electronic structures of larger fullerenes, C_{70}, C_{76}, C_{84} etc., as well as C_{60} are reported and are compared to the photoemission spectra. Calculated density of

states of the structural isomers of larger fullerenes are found to be considerably different from one another and did play an important role in determining the actual geometries of larger fullerenes extracted from graphite-arc soot. Cohesive mechanisms and energy bands of solid-state derivatives of C_{60}, *i.e.*, pure solid C_{60}, K_3C_{60}, Rb_3C_{60}, and $C_{60}Br$, are also discussed. The high electronegativity of C_{60} is found to be of significant importance for their properties. The unusual linear relationship between the Fermi-level density of states and the superconducting transition temperature (T_c) in a wide range has been found in K_3C_{60} and Rb_3C_{60}. The validity of the McMillan equation for T_c will be reexamined in these narrow conduction band superconductors with high frequency vibrational modes.

681 FUL Synthesis of Novel Fullerene Derivatives: *G. P. Miller*, Exxon Research & Engineering Co., Annandale, NJ 18042

Immediately after the discovery by Kratchmer and Huffman of a method for the macroscopic synthesis of C_{60}, speculation flourished concerning the potential utility of this novel compound. Organic chemists in particular were compelled by the idea that C_{60} could be a starting point for the construction of a myriad of new materials possessing diverse properties. Several groups, including our own, have developed synthetic strategies for the synthesis of new fullerene materials. It is now possible to add many different functional groups to the C_{60} skeleton. In this presentation, the results of synthetic strategies initiated and investigated in our laboratory are discussed. Particular emphasis is placed upon the preparation of novel derivatives resulting from nucleophilic addition to oxidized C_{60}. The reaction is of broad scope and the derivatives thus formed include alkoxylated and arylated C_{60}.

682 FUL Synthesis, Extraction and Characterization of Fullerenes and Metallofullerenes: *D. H. Parker,* P. Wurz, K. R. Lykke*, and *K. Chatterjee*, Materials Science/Chemistry Divs., Argonne National Laboratory, Argonne, IL 60439, *J. C. Hemminger*, Dept. of Chemistry, University of California, Irvine, CA 92627, *M. J. Pellin, D. M. Gruen*, and *L. M. Stock*, Materials Science/Chemistry Divs., Argonne National Laboratory, Argonne, IL 60439

We report the preparation of fullerenes in very high yield in a plasma discharge. Fullerenes up to C_{190} have been observed in the mass spectrum. By selective solvent extraction, we can isolate different molecular weight ranges of fullerenes for subsequent separation by chromatography. We observe that up to 94% of the soot produced in our plasma discharge is soluble, depending on the choice of solvent. Recently, we have developed a one-step method for the purification of C_{60} in yields of 6% directly from the soot. The one-step method uses much less solvent and is much less labor-intensive than previous methods. Additionally, we have adapted our plasma arc generator to synthesize metallofullerenes. The starting material for the synthesis of the metallofullerenes was either metal wire inserted in graphite rods or a graphite tube filled with a mixture of metal oxide powder and graphite. Both approaches were successful in producing metallofullerenes. We have characterized these species with laser desorption Fourier transform mass spectrometry and time-of-flight mass spectrometry.

683 FUL Larger Fullerenes and Functionalized Fullerenes: Structures and Stabilities: *K. Raghavachari*, AT&T Bell Laboratories, Murray Hill, NJ 07974, *C. M. Rohlfing*, Sandia National Laboratories, Livermore, CA 94551

In this work, we investigate the structures and stabilities of larger fullerenes such as C_{76}, C_{78}, C_{82}, and C_{84} as well as functionalized fullerenes such as $C_{60}O$ and $C_{60}CH_2$. Both semi-empirical and *ab initio* quantum chemical calculations have been used in this study. Larger fullerenes such as C_{76}, C_{78}, C_{82}, and C_{84}, have several structural isomers which have all the pentagons isolated from each other. Total energy minimization techniques have been used to determine the geometries and relative energies of these isomers. The stabilities of the isomers are analyzed in terms of the local environments of the pentagons and hexagons in the structures. Energy parameters have been derived which can characterize such isomers in a predictive manner. Correlations between the structural and electronic properties are discussed. Derivatized fullerenes such as $C_{60}O$ and $C_{60}CH_2$ have a —O or —CH_2 group bridging a naphthalene like structure in the fullerene. The bonding in the derivatized fullerenes is compared to that in C_{60}. In particular, the nature of the bond length across the bridging C—C bond is discussed in detail. Vibrational spectra of derivatized fullerenes are predicted.

684 FUL Coordination Chemistry with Fulleride Ions: *C. A. Reed,* A. Pénicaud, P. Bhyrappa*, and *J. Hsu*, Dept. of Chemistry, University of Southern California, Los Angeles, CA 90089-0744

The perception that the chemistry of C_{60} and C_{70} is a material-limited field is beginning to diminish. We report some procedures which improve the most tedious part of C_{60} and C_{70} isolation—that of chromatography on alumina. In a typical procedure, 1g of soot extract yields 600 mg of high purity C_{60} and 130 mg of good purity C_{70} on a per column, per day basis. Sodium reacts with C_{60} in THF in the presence of a crown ether to give synthetically useful fulleride salts. Strongly reducing metalloporphyrins react readily with C_{60} to give ionic salts of C_{60}^-. The anistropic EPR signal associated with the fulleride ion at low temperatures may be a manifestation of a Jahn-Teller distortion. The extremely weak coordination ability of the C_{60}^- anion gives rise to a notably large shift in redox potential (>650 mV) in the case of the Cr(II/III) porphyrin couple. Characterization of metalloporphyrin products is presented as well as data on nonporphyrinic materials obtained with C_{60}.

685 FUL The Multipole Expansion of Intermolecular Forces Applied to C/60: *G. Lasher*, IBM Research Div., T. J. Watson Research Center, Yorktown Heights, NY 10598

The interaction energy of two molecules determines many properties of their aggregates whether they are crystalline or amorphous and form small clusters or effectively infinite bodies. As relevant experimental data accumulates, the need for a completely empirical description of intermolecular forces becomes more apparent. The obvious choice is a multipole expansion which gives the orientational energy of two interacting molecules as a sum of terms labelled by a total angular momentum quantum number for each molecule. The icosahedral symmetry of C/60 is the highest possible point symmetry, and therefore its multipole expansion eliminates as many terms as possible from the expansion of the orientational energy of two asymmetric molecules. It is a relatively straight forward application of group theory to find an expansion of a function which is invariant to the rotation of either molecule of a pair by an element of its point group. However, the expansion for the energy of the pair must also be unchanged as both molecules are simultaneously rotated by an angle about the line joining their centers. This paper describes a method for computing the multipole functions for any symmetry and for integrating the product of these functions with an arbitrary function to evaluate the coefficients which determine the expansion of that function. The restraints on the coefficients of the icosahedral expansion for C/60 implied by the symmetry of the ground state of fullerite are illustrated.

686 FUL Fullerenes and Fullerides: Photoemission and Scanning Tunneling Microscopy Studies: *J. H. Weaver*, Dept. of Materials Science and Chemical Engineering, University of Minnesota, Minneapolis, MN 55455

This paper focuses on the electronic structures of fullerenes, C_{60} and C_{70}, and the alkali metal fullerides derived from them. Photoemission and inverse photoemission results reveal the distribution of states in the valence bands and conduction bands of these molecular solids. They also show the changes induced by alkali doping, particularly the filling of the first set of conduction band states, and the differences associated with Li, Na, K, Rb, and Cs fullerides. UHV STM results are discussed for thin films of C_{60} and C_{70} and for K_xC_{60} in the metallic and insulating states. The STM results show fullerene trapping at GaAs(110) steps and film growth on the surface by step flow. Novel growth structures are emphasized for these high temperature van der Waals solids. Photoemission results for C_{60} monolayers on metal and semiconductor surfaces show Fermi level alignment, and the implications are examined in terms of surface bonding and dipole formation. Finally, results for fullerenes containing La atoms inside the cage are presented.

687 FUL Electron-Phonon Coupling and Superconductivity in Alkali Intercalated C_{60} Solid: *M. A. Schlüter*, AT&T Bell Laboratories, Murray Hill, NJ 07974

We propose the superconductivity in A_3C_{60} (A = K, Rb) with $T_c \geq 30$ K results from a favorable combination of high phonon frequencies and the existence of two different energy scales optimizing the coupling constant $\lambda = N \cdot V$. Calculations show that electron scattering V is dominated by particular on-ball Jahn-Teller-type modes on the scale of the large on-ball π-hopping energy, while the density of states N is controlled by the weak inter-ball hopping energy. This factorization has several observed experimental consequences. Data on atomic substitution, Raman and neutron scattering, and isotope effect measurements can be explained naturally. Crucial differences to intercalated graphite explain the much smaller T_c values in the graphite compounds. (This work was done in collaboration with M. Lannoo, M. Needels, G. A. Baraff, and D. Tomanek.)

688 FUL The Equilibrium Structure of Big Fullerenes: Spherical or Cylindrical Shape? *G. E. Scuseria*, Dept. of Chemistry and Rice Quantum Institute, Rice University, Houston, TX 77251-1892

The recent experimental discovery [S. Ijima, *Nature*, **354**, 56 (1991)] that a new type of structure consisting of needlelike microtubules of graphitic carbon can be grown using an apparatus very similar to that used to mass produce fullerenes such as C_{60}, challenges the conventional view that big fullerenes such as C_{120} and C_{240} have spherical (or rounded) shapes [H. W. Kroto, *Chem. Rev.*, **91**, 1213 (1991)]. The carbon needles were described as having up to 1 μm in length and ranging from 4 to 30 nm in diameter. These so called "bucky-tubes" —if grown to macroscopic length— might constitute vastly superior carbon fibers. In this work, *ab initio* SCF calculations were carried out in order to predict the equilibrium structures of some of the large fullerenes. Geometries were optimized employing analytic energy gradients within the direct SCF approach. Several electronic states and different

cylindrical and spherical shapes were considered for C_{120}, C_{180} and C_{240}. Results obtained with up to 2400 basis functions are reported.

689 FUL Mass Spectroscopic Characterization of Large Fullerenes and Metallofullerenes: *H. Shinohara,** Dept. of Chemistry for Materials, Mi'e University, Tsu 514 Japan, *Y. Saito*, Dept. of Electrical Engineering, Mi'e University, Tsu 514 Japan

Identification of fullerenes, particularly the fullerenes larger than C70, is a crucial part of the experiment when it comes to the isolation such carbon molecules. Mass spectroscopy is definitely a powerful tool for the identification of fullerenes. However, mass spectrometry usually entails fragmentation of "intact" parent ions which often damages mass spectra. Fullerenes have been known to give even-numbered fragment ions on ionization unless the mildest ionization/desorption conditions are employed. In the first part of the present study, we report the results of the various type of the mass spectrometry of the larger fullerenes, which includes EI, FAB, SIMS, laser desorption (LD), and liquid-MS (LC-Frit-FAB/SIMS and electrospray) technique. Second, the results of LD and FAB mass spectrometry of some metallofullerenes, which were produced by a usual carbon arc method with various metal oxide electrodes, are discussed. Along with the results of absorption and ESR spectroscopy for metallofullerenes, the possible encapsulation of metal(s) in the various size of fullerenes is also discussed.

690 FUL Experimental Heat of Formation, Vapor-Phase UV Spectrum, Vapor Pressure and Heat of Sublimation of C_{60}, Buckminsterfullerene: *D. R. Kirklin*, Chemical Thermodynamics Div., Center for Chemical Physics, National Institute of Standards and Technology, Gaithersburg, MD 20899, *A. L. Smith** and *Y.-W. Hui*, Dept. of Chemistry, Drexel University, Philadelphia, PA 19104, *A. McGhie* and *W. J. Romanow*, Laboratory for Research in the Structure of Matter, University of Pennsylvania, Philadelphia, PA 19104, *G. Zimmerman*, Dept. of Chemistry, Drexel University, Philadelphia, PA 19104

We have measured the energy of combustion of solid C_{60} in the NIST aneroid adiabatic rotating calorimeter. The standard molar enthalpy of combustion is -25,804 ± 6 kJ · mol^{-1}, and the derived enthalpy of formation of solid C_{60} is 2193 ± 10 kJ · mol^{-1}, before the final correction for aliphatic hydrocarbon impurity level. Using the enthalpy of formation of C(gas) and the heat of sublimation of C_{60}, we derive an average carbon-carbon bond energy in C_{60} of 454 kJ · mol^{-1} (109 kcal · mol^{-1}), roughly equal to the weighted average of 1/3 C=C double bond and 2/3 C–C single bond energies. We have also measured the temperature dependence of the vapor pressure of C_{60} from 500 to 680 C by recording the ultraviolet/visible absorption spectrum of C_{60} gas, using methods similar to our previous study of sulfur vapor (1). At these temperatures *in vacuo*, solid C_{60} resists chemical degradation for days, but may exhibit some phase transformation between 620 and 660 C. Clausius-Clapeyron plots of the data give a heat of sublimation of C_{60}. Preliminary values are P_{373} [C_{60}(solid)] = 0.01 Torr at 550 ± 20 C, and heat of sublimation 35 ± 3 Kcal · mol^{-1}.

1. R. I. Billmers and A. L. Smith, *J. Phys. Chem.*, **95**, 4242 (1991).

691 FUL Structure of Superconducting and Ferromagnetic Fullerides: *P. W. Stephens*, Dept. of Physics, SUNY, Stony Brook, NY 11794

We review the crystal structure information determined by the present coworkers (1) and others on superconducting A_3C_{60} (where A is alkali metal Na, K, and Rb) and ferromagnetic TDAE-C_{60} (where TDAE is $C_2N_4(CH_3)_4$). The results provide some explanation for the strongly different behavior of fullerides based on alkali vs. organic donors, and on the detailed mechanisms for the observed properties of these materials.

1. Work performed in collaboration with (so far) P. M. Allemand, D. E. Cox, F. Diederich, A. Hirsch, K. Holczer, S. M. Huang, R. B. Kaner, J. W. Lauher, P. L. Lee, Q. Li, L. Mihaly, J. D. Thompson, R. L. Whetten, J. B. Wiley, and F. Wudl.

692 FUL Isolation, Spectroscopy, and Chemical Reactions of Fullerenes: *R. Taylor, P. R. Birkett, J. H. Holloway, E. C. Hope, J. G. Langley, M. F. Medeine, T. J. Dennis, J. P. Hare, H. W. Kroto*, and *D. R. M. Walton*, School of Chemistry and Molecular Sciences, University of Sussex, Brighton, Sussex, England BN1 9QJ

The chromatographic work that led to the isolation of the first pure samples of C_{60} and C_{70} is described, together with the most recent work on the HPLC separation of the higher fullerenes. Structural features which account for the wide difference in stability of different fullerenes are identified. An account is given of the work of the Sussex group (and their collaborators at Leicester and Southampton Universities) on reduction, photochemical degradation, and halogenation of C_{60}, together with some preliminary work on C_{70}. A number of reactions of the halogenated derivatives are described in detail, especially some nucleophilic substitutions, and reactions as electrophiles in aromatic substitution. The consequences for lubricant potential, of the high reactivity of the halogenated derivatives towards nucleophiles are evaluated. Some general principles guiding the type and magnitude of chemical reactions of C_{60}, and the probable sites involved, are considered. In particular, our results taken along with those of others, indicate the emergence of a reactivity pattern whereby either 2, 3, 4, 6 or 12 of the high-order bonds of C_{60} appear to be commonly involved in chemical reactions. Some reasons for this are suggested.

693 FUL Collective Electronic Excitations in Fullerenes: *D. Tománek*, Dept. of Physics and Astronomy and Center for Fundamental Materials Research, Michigan State University, East Lansing, MI 48824-1116

We have investigated the possible occurrence of collective electronic excitations in carbon fullerene clusters, specifically C_{60}. Our calculations of the electromagnetic response function of isolated fullerenes are based on the random phase approximation (RPA) (1) and the tight-binding formalism for the single-particle levels and wavefunctions. Our results in the low energy region of the spectrum ($\hbar\omega$ < 6 eV) indicate strong to moderately strong screening of the free response to an external dipole field. The spectrum is dominated by a collective excitation at an energy of ≈20 eV, corresponding to a Mie (σ-type) plasmon. The response to general multipolar external fields (L < 9) shows a gradual decay of this 20 eV mode with increasing multipolarity. Beyond the 20 eV plasmon, the response function shows a feature at 6 eV, reminiscent of the π-plasmon in graphite, which persists to fields with a high multipolarity. (Work done in collaboration with G. F. Bertsch, A. Bulgac, N.-J. Ju and Y. Wang; supported by the National Science Foundation under Grant No. PHY-8920927.)

1. G. F. Bertsch, A. Bulgac, D. Tománek, and Y. Wang, *Phys. Rev. Lett.*, **67**, 2690 (1991).

694 FUL NMR Studies of Molecular Dynamics and Electronic Properties of Pure and Doped Buckyballs: *R. Tycko,** *G. Dabbagh, S. E. Barrett, M. J. Rosseinsky, D. W. Murphy, R. M. Fleming*, and *R. C. Haddon*, AT&T Bell Laboratories, Murray HIll, New Jersey 07974

NMR measurements provide important information about molecular reorientational dynamics and phase transitions in pure solid C_{60} and C_{70}, including the rates and activation energies for reorientation and the symmetry of the reorientational motion. NMR also provides information about the phase diagrams of the alkali fullerides A_xC_{60} and about the electronic properties of the metallic and superconducting alkali fullerides, including the densities of electronic states at the Fermi energy in the normal state and the energy gap and magnetic penetration length in the superconducting state. Our most recent NMR results are presented and interpreted.

695 FUL (a) Production and Characterization of Fullerene Encapsulated Metals, and (b) The Search for Fullerenes in Meteorites: *M. S. deVries,** *J. R. Salem, R. D. Johnson, D. S. Bethune, C. S. Yannoni, H. R. Wendt, H. E. Hunziker, K. Reihs*, and *M. Hoinkis*, IBM Corp., Almaden Research Center, San Jose, CA 95120-6099.

We report on studies of metal fullerene complexes, involving various group IIIa elements, *i.e.*, La, Sc, Y, Eu, Tb, and Gd. The complexes are produced by coevaporation of carbon with the various metals in an arc discharge in He. The resulting soot is treated in various ways, such as extraction and sublimation, and studied by laser desorption, laser ionization, mass spectrometry as well as by EPR spectroscopy. Many of the complexes appear to be very stable. The metal C_{60} and metal C_{70} species were found to be unstable upon heating, but could be laser desorbed intact. The species involving heavier fullerenes, such as C_{74} or C_{82} were found to be much more stable. Several complexes were found with two or three metal atoms. Generally there seems to be a greater propensity for finding multiple metals associated with the carbon cage as the ionic radius of the metal decreases. Both the fluence and the wave-length of the ionizing laser were varied to investigate fragmention patterns, ionization efficiency and ionization energies. All tests to date are consistent with metal atoms being inside the carbon cage. We also report the latest results in our search for fullerenes in carbonacious meteorites, relevant to the probability of fullerenes in interstellar space. (Collaborative work with S. Chang and E. Peterson, NASA-Ames Research Center, and R. Fleming, Charles Evans and Associates.)

696 FUL Light and Fullerenes: Photoconductive and Nonlinear Optical Properties: *Y. Wang,** *J. Caspar*, and *L.-T. Cheng*, Du Pont Co., Experimental Station, Wilmington, DE 19880-0356

Fullerenes form charge-transfer complexes with electron donors. There is no appreciable charge separation in the ground state of the complex. However, upon photo-excitation, charge-transfer state is formed which gives rise to novel nonlinear optical and photoconductive properties. In the first part of the paper we report the third order nonlinear optical properties of fullerenes (C_{60} and C_{70}) and the second order nonlinear optical properties of fullerene charge-transfer complexes. Significant optical nonlinearities have been observed in both cases. We then present our recent data demonstrating significant photoconductivity in fullerenes-doped polymers. The performance of this new photoconductor is comparable to some of the best commercial photoconductors such as the thiapyrylium dye aggregates photoconductor. Both field and wavelength dependence data are discussed. The fundamental electron-transfer rate constants of fullerene singlet and triplet states have been determined by time-resolved

laser spectroscopic methods. Several orders-of-magnitude difference in their rate constants have been observed. The explanation and the implication on the photoconductive mechanism are discussed.

697 FUL Synthesis and Characterization of Exo- and Endohedral Metal Fullerides: *J. B. Wiley,* E. G. Gillan, S.-M. Huang, K. Min, M. Alvarez, C. Yeretzian, S. Cho, F. Diederich, R. Whetten, K. Holczer,* and *R. B. Kaner,* Depts. of Chemistry and Physics and Solid State Science Center, University of California, Los Angeles, CA 90024-1569

Fullerene carbon cages continue to produce a wide variety of new and exciting chemistry. Our recent research efforts have concentrated on the synthesis and characterization of metal fullerides. Potassium and rubidium doped C_{60} (FCC M_3C_{60}) exhibit superconducting transition temperatures of 19.3 and 29.6 K, respectively. Experiments with C_{60} and Na, K, and Rb show that although sodium fulleride has an FCC lattice, both it and sodium-containing mixed-metal compounds are not superconducting. X-ray powder diffraction and magnetic susceptibility data are presented on these systems. A series of lanthanide endohedral compounds have been produced from arc-burning of filled graphite rods, and these also are discussed.

*The Fullerenes: Chemistry, Physics and New Directions Symposium was supported in part by the Office of Naval Research.

JOINT RECENT NEWS PAPER SESSION

Electronics/Dielectric Science and Technology

Promenade Ballroom A, 2nd Level

Thursday, May 21, 1992

JOINT RECENT NEWS PAPER SESSION
Electronics/Dielectrics Science and Technology

D. E. Bailey, Chairman; L. K. White, Vice-Chairman
Promenade Ballroom A, 2nd Level

Processing

8:50	Electrochemical *In-Situ* Diagnostics for Light-Induced Wet Etching of Multilayer Structures - Th. Fink and R. M. Osgood, Jr.	698 RNP
9:00	The Effect of Energetic Ion Bombardment on the Activation Energy of the Etching Reaction Between Silicon and Fluorine - P. M. Kopalidis and J. Jorne	699 RNP
9:10	Microtrench Formation During Plasma Etching - T. J. Dalton, J. C. Arnold, H. H. Sawin, S. Swan, and D. Corliss	700 RNP
9:30	Adaption of Clean Technology to Semiconductor Manufacturing Equipment: 8-Inch Vertical Furnaces as an Example - T. Matsuo	701 RNP
9:50	Rapid Thermal Anneal Repeatability using Wafer Expansion Thermometry - W. DeHart, B. Peuse, C. Rau, A. Rosekrans and K. Snow	702 RNP
10:00	Ten-minute intermission	

Materials

10:10	Phosphorus Concentration Dependence of the Sodium Passivation by TEOS-PECVD Phosphosilicate Glasses - J. K. Cramer, S. P. Murarka, K. V. Srikrishnan, and W. Patrick	703 RNP
10:30	Oxygen Precipitation in CZ Si During Various Simulated 4MB DRAM Processing Steps - J.-G. Park, S.-P. Choi, C.-K. Shin, L. Shive, W. Angelberger, J. Partanen, T. Tuomi, and S. Hahn	704 RNP
10:50	Electrical Conduction in Buried Oxide (BOX) in SIMOX Structures - G. A. Brown and A. G. Revesz	705 RNP
11:10	Minority Carrier Recombination Lifetime of Lightly-Doped Cz Silicon Measured by Microwave PCD, ELYMAT, and SPV - L. Coates, L. Caubin, and S. Hahn	706 RNP
11:30	Study on Surface Photovoltage Measurement of Long Diffusion Length Silicon: Analytical Approach - O. J. Anttila and S. K. Hahn	707 RNP
11:50	Thermal Decomposition Mechanism of MOCVD Precursor, Cu(acetylacetonate)^2 Studied by Differential Scanning Calorimetry (DSC) - Y.-N. Chang	708 RNP

Solution Chemistry

12:00	Hydration Models for Trivalent Transcurium Element ^{254}Es(III) in Aqueous Solutions at 298^{0}K - H. Latrous, N. Ouerfelli, and J. Olivier	709 RNP

RNP

Abstracts

698 RNP Electrochemical *In Situ* Diagnostics for Light-Induced Wet Etching of Multilayer Structures: *Th. Fink* and *R. M. Osgood, Jr.*, Microelectronics Sciences Laboratories, Columbia University, New York, NY 10027

This work presents an electrochemical method for *in situ* monitoring of heterostructure etching. Experiments with AlGaAs/GaAs multilayer samples showed that measurement of the current in the electrochemical cell or of the potential of the sample clearly indicate the passing of an interface between two epilayers during light-induced etching. Therefore, the technique can be used for the controlled localized layer-by-layer etching of multilayers which makes it important for the processing of multi-quantum well materials.

699 RNP The Effect of Energetic Ion Bombardment on the Activation Energy of the Etching Reaction Between Silicon and Fluorine: *P. M. Kopalidis* and *J. Jorne*, Dept. of Chemical Engineering, University of Rochester, Rochester, NY 14627

Energetic ion bombardment has a profound effect on the etch rate of silicon in dry etching processes. In this work, a combined theoretical and experimental approach is followed to investigate this phenomenon. A mathematical model of a showerhead-type reactive ion etching reactor is developed. Experimental measurements of the plasma density, electron energy, and exit gas composition in this system are used to provide information on the gas phase reactions taking place and the values of kinetic coefficients. The concentration distribution of molecules and radicals are obtained by solving the mass balances with finite differences. Surface recombination and competition between fluorine and oxygen atoms to adsorb on the silicon surface are considered, and the chemical etch rate of silicon is calculated. A correlation between the activation energy of the etching reaction and the energy and density of bombarding ions is obtained, by comparing the calculated chemical etch rate distribution with the one measured experimentally.

700 RNP Microtrench Formation during Plasma Etching: *T. J. Dalton, J. C. Arnold,* and *H. H. Sawin*, MIT, Dept. of Chemical Engineering, Cambridge, MA 02139, *S. Swan* and *D. Corliss*, Digital Equipment Corp, Hudson, MA 01749-2809

Microtrenches have been observed in submicron features etched with an existing plasma process. In contrast to previous reports, these microtrenches occurred a small distance away from the sidewall. We examined possible causes of microtrench formation, including surface diffusion of reactants, reflection of ions from the sidewalls, and localized charging of the feature. A simple numerical model indicated that ion reflection was the dominant cause.

701 RNP Adaptation of Clean Technology to Semiconductor Manufacturing Equipment: 8 Inch Vertical Furnaces as an Example: *T. Matsuo*, Tokyo Electron Ltd., 650 Nitsueane Hosaka-cho, Nirasaki City, Yamanashi-pre. 407-01, Japan

The construction of a total clean system requires the technological trends such as that to microminiaturize LSI, expand the diameter and highly concentrate the density, and the breakthrough with mass production technology emphasizing clean technology. As the first equipment adapted with the total clean technology, we have developed Series "α - 8" φ 8 Vertical Furnace.

702 RNP Rapid Thermal Anneal Repeatability Using Wafer Expansion Thermometry: *W. DeHart, B. Peuse, C. Rau, A. Rosekrans,* and *K. Snow*, Peak Systems Inc., Fremont, CA 94538

Rapid thermal processing (RTP) is considered an essential technology for submicron processing. However, it has been restricted in its use because of the inherent limitations of pyrometer temperature control. A new method of temperature control has recently been introduced that measures the thermal expansion of a wafer to determine its temperature. This thermal micrometer works by using a laser autofocus mechanism to determine the change in wafer diameter due to temperature.

703 RNP Phosphorus Concentration Dependence of the Sodium Passivation by TEOS-PECVD Phosphosilicate Glasses: *J. K. Cramer* and *S. P. Murarka*, Center for Integrated Electronics, Rensselaer Polytechnic Institute, Troy, NY 12180, *K. V. Srikrishnan* and *W. Patrick*, IBM General Technology Div., Hopewell Junction, NY 10953

Mobile ions like sodium are known to cause device (MOS) instabilities. Phosphosilicate glasses have been used as passivating layers to isolate the active devices from such contamination. In this study we have examined the effectiveness of TEOS-PECVD P-glasses, as the barrier to sodium diffusion, as a function of the phosphorus concentration. The results of C-V and I-V studies on

contaminated and annealed P-glasses are presented and discussed.

704 RNP Oxygen Precipitation in Cz Si during Various Simulated 4 Mb DRAM Processing Steps: *J.-G. Park, S. P. Choi,* and *C. K. Shen,* Samsung Electronics, Kihung-Eup, Kyungki-do, Korea, *L. Shive,* MEMC Electronic Materials, Inc., St. Peters, MO 63376, *W. Angelberger,* Wacker-Chemitronic, D-8263 Burghausen, Germany, *J. Partanen* and *T. Tuomi,* Helsinki University of Technology, 02150 Espoo, Finland, *S. Hahn,* Dept. of Materials Science and Engineering, Stanford University, Stanford, CA 94305

Interstitial oxygen is perhaps the most important consideration in silicon crystals for VLSI/ULSI fabrication. The relevance of oxygen to integrated circuit fabrication is primarily due to oxygen's ability to form oxide precipitates and to generate lattice defects in a controlled manner for impurity gettering during device processing. In this investigation, we studied oxygen precipitation in Cz Si during various simulated 4 Mb DRAM processing thermal cycles using infrared absorption, chemical etch/cross-section optical microscopy and synchrotron section topography. In this paper we discuss effects of initial oxygen concentration and various thermal cycles (pre- and post-intrinsic gettering heat-treatments) upon oxygen precipitation, bulk microdefect, and denuded zone formation.

705 RNP Electrical Conduction in Buried Oxide (BOX) in SIMOX Structures: *G. A. Brown,* Texas Instruments, Inc., Dallas, TX 75243, *A. G. Revesz,* Revesz Associates, Bethesda, MD 20817

BOX layers in SIMOX structures exhibit strongly localized defect conduction and nonlocalized background ("bulk") conduction. In the latter case, the current increases linearly with the electrode area. For both annealed (at 1325°C) and unannealed samples the I-V characteristics are quasi-linear at low fields (<0.8 MV/cm for unannealed samples and <2 MV/cm for the annealed ones) but super-linear at higher fields. The current densities in the quasi-linear regime are several orders of magnitude higher for the unannealed samples than for the annealed ones and their time-dependence indicates pronounced trapping phenomena. Annealed pseudo-SIMOX samples (top Si layer removed) which were heat-treated in oxygen at 1100°C behave similarly to thermally grown SiO_2 films in the sense that the current is practically at the noise level (10^{-11} A/cm^2). This observation indicates that conduction in BOX is related to defects associated with oxygen deficiency (*e.g.*, Si – Si bonds) that are present even in annealed samples without additional treatment. (This work was funded by Naval Research Laboratory under the Contract No. N00014-88-C-2492.)

706 RNP Minority Carrier Recombination Lifetime of Lightly Doped Cz Silicon Measured by μ-PCD, ELYMAT, and SPV: *L. Coates,* Kokusai Electric Co., Ltd., San Jose, CA 95131-1729, *L. Caubin,* Kawasaki Wafer Technology, Inc., Santa Clara, CA 95051, *S. Hahn,* Dept. of Materials Science and Engineering, Stanford University, Stanford, CA 94305

The minority carrier recombination lifetime which determines the diffusion length is a very sensitive parameter for crystallographic defects for recombination centers. The three most commonly used recombination lifetime methods are microwave photoconductive decay (μ-PCD), surface photovoltage (SPV), and electrolytic metal tracer (ELYMAT). Even though all three of these techniques are well established in semiconductor industry, to the best of our knowledge, few experiments have been carried out so far to correlate the data by one method with those from others. In this study we measured the lifetime of lightly doped oxidized Cz Si wafers with three commercially available μ-PCD lifetime testers, ELMAT, and SPV. In this paper, we compare our lifetime data with each other, and discuss some potential correlations among them.

707 RNP Study on Surface Photovoltage Measurement of Long Diffusion Length Silicon: Analytical Approach: *O. J. Anttila,* Dept. of Electrical Engineering, Stanford University, Stanford, CA 94305, *S. K. Hahn,* Dept. of Materials Science and Engineering, Stanford University, Stanford, CA 94305

The limitations of SPV, using the analytical solution for the minority carrier distribution, are studied in detail. The principal source of error in long diffusion length material is the back surface recombination. The possibility of measuring large diffusion lengths in a reliable manner is discussed. Measurement of minor amounts of iron contamination in p-type material is possible, but a correction factor is required for the traditionally used relationship to convert the observed diffusion length change to iron concentration. The value of the correction factor varies between 1 and 1.5 for high back surface recombination velocity; the magnitude depends on the ratio between wafer thickness and the diffusion length of the minority carriers. The sensitivity of the measured diffusion length to different sources of errors and requirements for sample preparation are discussed. Finally, the use of SPV to measure the denuded zone width in precipitated material is briefly analyzed.

708 RNP Thermal Decomposition Mechanism of MOCVD Precursor, Cu(acetylacetonate)^2 Studied by Differential Scanning Calorimetry (DSC): *Y.-N. Chang,* Dept. of Chemical Engineering, Iowa State University, Ames, IA 50010

The pyrolysis kinetics of the MOCVD precursor, Cu(acetylacetonate)^2 (Cu(acac)^2), was studied by differential scanning calorimetry (DSC) at atmospheric pressure. Solid Cu(acac)^2 sample was programmed heated with a constant heating rate from 25 to 400°C. For each thermogram, energy exchange rates between sale and ambient were recorded with respect to temperature. Pure He, N_2, dry air, or mixture of He + O_2 were used as the inert or reactive gas ambient. From DSC results, the thermal decomposition of Cu(acac)^2 started at 250°C, and ended by 350°C. The peak temperature-heating rate relationship, as analyzed by the Kissinger equation, was used to estimate the activation energy for the respective kinetic step. Solid residuals after Cu(acac)^2 pyrolysis were analyzed by FTIR, which revealed a mixed content of Cu_2O, CuO, and carbonates.

709 RNP Hydration Models for Trivalent Transcurium Element ^{254}Es(III) in Aqueous Solutions at 298 K: *H. Latrous* and *N. Ouerfelli,* Faculté des Sciences de Tunis, Tunis, Tunisia, *J. Olivier,* Oak Ridge National Laboratory, Oak Ridge, TN 37831

Self-diffusion coefficient data for ^{254}Es(III) and ^{170}Tm(III) in neodymium perchlorate solutions are reported for concentrations up to 1.14 mol dm^{-3} at 25°C. The open end capillary method (OECM) has been used for the determination of the self-diffusion coefficient in perchlorate solutions at pH 2.5 labeled with tracer ^{254}Es(III) or ^{170}Tm(III). The experimental diffusion coefficients for ^{254}Es(III) and ^{170}Tm(III) were fitted to polynomials of the following form $D/D_o = \Sigma_i b_i (I)^{i/2}$ where D_o is the limiting diffusion coefficient value against the square root of the ionic strength (I). The data have been analyzed by using the simple hydration models to obtain realistic estimates of the effective cation hydration. In solution at pH 2.5, the data show that there is a similarly in the ionic transport process of ^{254}Es(III) and ^{170}Tm(III) ions. As a further consequence, it may be argued that ^{254}Es(III) and ^{170}Tm(III) ions have the same hydration as a tripositive ion in the absence of hydrolysis ion-pairing or complexing. The limiting diffusion coefficients, D_o [10^{-6} cm^2 s^{-1}], for actinide trivalent ion ^{254}Es(III) is 5.80 ± 0.05 and for lanthanide trivalent ion ^{170}Tm(III) is 5.85 ± 0.05.

INDEX TO AUTHORS FOR SYMPOSIA WITH EXTENDED DEADLINES
Authors of Recent News Papers are not included in this Index.

APPLICATION FOR ADMISSION

TO

The Electrochemical Society, Inc.

Return completed application to:

Secretary
The Electrochemical Society, Inc.
10 South Main Street, Pennington, New Jersey 08534-2896
609-737-1902

For office use only

Date Rec'd. $

Notice of Ackn.

Checked:

Approved:

To the Board of Directors of The Electrochemical Society, Inc:

Please print complete name and address as it should appear on mailings.

Name:

Address:

Business Telephone: (include area code)

I hereby make application for admission to The Electrochemical Society, Inc., as an _____ member, and enclose the amount of $____ covering the first year's dues. (Please see reverse side for proper class of membership and dues applying thereto, noting the options with regard to the date of election and active life membership and the credit available for nonmember meeting registration.)

1. Date of Birth: _____ (month) _____ (day) _____ (year)

2. Please check LOCAL SECTION with which you wish to affiliate:

—— Boston (05)	—— Columbus (20)	—— Midland (Mich.) (40)	—— Philadelphia (70)	—— Southern Wisconsin (92)
—— Canadian (60)	—— Detroit (25)	—— Natl. Capital Area (45)	—— Pittsburgh (75)	—— Twin Cities (96)
—— Chicago (10)	—— European (27)	—— North Texas (55)	—— San Francisco (85 & 86)	—— None (99)
—— Cincinnati (12)	—— Japan (33)	—— Oregon (62)	—— South Texas (88)	
—— Cleveland (15)	—— Metropolitan N.Y. (35)	—— Pacific Northwest (65)	—— So. Calif.-Nevada (90)	

3. Please indicate your DIVISIONAL and GROUP interests, noting your primary interest(s) with the number 1 and secondary interest(s) with the number 2.

—— Battery (AO)	—— Electronics (EO)	—— Luminescence and Display Materials (KO)
—— Corrosion (BO)	—— Energy Technology (GO)	—— Organic & Biological Electrochemistry (FO)
—— Dielectric Science and Technology (CO)	—— High Temperature Materials (HO)	—— Physical Electrochemistry (JO)
—— Electrodeposition (DO)	—— Industrial Electrolysis and Electrochemical Engineering (IO)	—— Sensor (LO)

4. Education:

Institution	Dates Attended	Major Subject	Degree Earned

5. Work Experience:

Name of Employer (current, followed by previous)	Dates	Position

6. The Society's Constitution provides that two Active Members of the Society (who can substantiate the above record) must recommend you for admission to membership. It will facilitate the handling of your application if you are able to have your references sign this application form; if this is not convenient, please list their names and addresses. On a student application, only a single faculty member recommendation with signature (including title and institution) is required.

Name (please print)	Signature	Address
Name (please print)	Signature	Address

The undersigned certifies that the above statements are correct and agrees, if elected to the Society, to be governed by its Constitution and Bylaws and to promote the objects of the Society as stated in its Constitution.

Date _____ 19__

_____
(Signature)

Rev. 11/91

EXTRACTS FROM THE CONSTITUTION AND BYLAWS

CONSTITUTION—Article II

Membership

Section 1. The individual membership shall consist of Active, Honorary and Emeritus Members. The Board of Directors may from time to time authorize other classifications of membership as defined in the Bylaws of the Society.

(Active Member—Annual Dues $85.00)

Active Member

Section 2. An Active Member shall be interested in electrochemistry or allied subjects and possess a Bachelor's degree, or its equivalent, in engineering or natural science. In lieu of a Bachelor's degree, or its equivalent, any combination of years of undergraduate study and years of relevant work experience in electrochemistry or allied subjects adding to at least seven years shall be required. Election to Active Membership shall require the recommendation of two Active Members in good standing.

BYLAWS—Article II

Non-Voting Membership
(Student Member—Annual Dues $10.00)

Student Member

Section 1. Student Member. A Student Member shall be a full-time undergraduate or graduate student registered for a degree in natural science or engineering or a full-time postdoctoral student in natural science or engineering in a degree-granting institution. The applicant for Student Membership shall be recommended by a member of the faculty of the school. Upon graduation with a Bachelor's degree or equivalent in natural science or engineering, or upon departure from postdoctoral status, the Student Member may apply for Active Membership. The application shall be approved by two Active Members of the Society in good standing. If the Student Member enters graduate school as a full-time student, or enters a qualifying postdoctoral appointment after completing a doctoral degree, the person may choose to apply for Active Membership or may remain a Student Member. A person may hold Student Membership as a postdoctoral student for no more than two years.

BYLAWS—Article XXI

Dues and Fees

Dues

Section 1. The annual dues for Active Members shall be eighty-five dollars. The annual dues for Student Members shall be ten dollars. Each member shall receive the JOURNAL OF THE ELECTROCHEMICAL SOCIETY.

Date of Election

Section 2. When individuals are elected to membership, they must elect to initiate their membership as of January 1 or July 1 of the year of election; or, if elected during the last quarter, January 1 of the year following election. In the case of a July 1 election for starting membership, dues will be prorated.

Active Life Membership

Section 3. Any Active Member who shall pay in one lump sum the amount equivalent to two-thirds of the remaining dues to age sixty-five at the time of payment, but not less than an amount of 5 years of full dues, shall be exempt from payment of any further dues and shall be considered an Active Member during the remainder of his or her life.

BOARD OF DIRECTORS ACTION OF OCTOBER 9, 1960

Nonmember Meeting Registration Credit

If application for new membership is received within four months of the payment of nonmember registration at a Society Meeting by the applicant, the difference between the nonmember and member registration fees shall be credited toward the first year's dues.

CONSTITUTION—Article III

Admission and Dismissal of Members

Section 1. Application for individual membership shall be in writing on a form adopted by the Board of Directors.

Section 2. The Admissions Committee shall be a rotating committee consisting of three members. One member shall be appointed each year by the President with the approval of the Board of Directors for a term of three years to replace the outgoing member. This Committee shall receive from the Secretary all properly executed and properly recommended applications for admission which he has received from persons desirous of becoming members of the Society. It shall be the duty of this Committee, after examining the credentials of applicants, to make appropriate recommendation to the Board as to approval or rejection of the applications. Unanimous approval of an applicant by this Committee shall be required before the candidate's name may be submitted to the Board of Directors for election. The election to membership shall be by a mail vote of the Board of Directors. The candidate shall be considered elected two weeks after the date the proposed membership list is mailed to the Board if no negative votes have been received by the Secretary. If a candidate receives one negative vote, his application shall then be considered and voted upon at the next meeting of the Board of Directors. Two negative votes cast at this meeting shall exclude a candidate. The Board of Directors may refuse to elect a candidate who, in its opinion, is not qualified for membership. The names of those elected shall be announced to the Society. Duly elected candidates shall have all the rights and privileges of membership as soon as their entrance fee, if any, and dues for the current year have been paid.

Section 3. A member desiring to resign shall send a written resignation to the Office of the Society.

Section 4. Upon the written request of ten or more Active Members that, for cause stated therein, a member be dismissed, the Board of Directors shall consider the matter and, if there appears to be sufficient reason, shall advise the accused of the charges against him. He shall then have the right to present a written defense, and to appear in person before a meeting of the Board of Directors, of which meeting he shall receive notice at least twenty days in advance. Not less than two months after such meeting the Board of Directors shall finally consider the case and, if in the opinion of the majority of the Board of Directors a satisfactory defense has not been made and the accused member has not in the meantime tendered his resignation he shall be dismissed from the Society.

Section 7. The entrance fee, if any, annual dues and any other payments to be made by the members of the Society shall be paid in accordance with regulations set forth in the Bylaws.

Section 8. Any member delinquent in dues after April 1 shall not receive the Society's publications and will not be allowed to vote in any Society election until such dues are paid. All members in arrears for one year after April 1 shall lose their membership status and can be reinstated only by action of the Board of Directors.

All members receive a subscription to the Journal of The Electrochemical Society.

PROCEEDINGS VOLUME ORDER FORM

Qty.	PV #	Proceedings Volume Title	Price Ea.	Total

PREPAYMENT REQUIRED TOTAL $ _____

Send completed order form with payment to: The Electrochemical Society, Inc., 10 South Main St., Pennington, NJ 08534-2896.
Phone (609-737-1902) or FAX (609-737-2743) orders are accepted with bank card payment.

This is your shipping label ***Important: Please provide complete mailing address, including postal code and country.***

CONTENTS
BOOKS
Return Postage
Guaranteed

from-
The Electrochemical Society, Inc.
10 South Main Street
Pennington, NJ 08534-2896

Name_____
Address_____
_____
_____
_____

Your Order No._____

_____

Name_____
Address_____
_____
_____
_____

Payment in U.S. funds, drawn on U.S. Bank, must accompany order.
- or -
☐ Mastercard ☐ Visa, Card#_____
Exp. date _____Signature_____

For ECS use only:
C/A#_____

PO#_____Recap_____

SL-P

The Electrochemical Society, Inc.

PROCEEDINGS VOLUME ORDERING INFORMATION

HOW TO ORDER

1. Please be sure to complete this special order form carefully. Photocopies of the form are acceptable. Type or print your complete name and address to which publications are to be shipped and send to The Electrochemical Society, Inc., 10 South Main Street, Pennington, New Jersey 08534-2896. Telephone 609-737-1902 or FAX 609-737-2743 orders are accepted with bank card payment.

2. Indicate the quantity and price (member or nonmember) for each volume to be ordered. The total should be indicated in the space provided.

3. Shipping is by fourth class mail. First class and airmail services are available for an additional charge. Please contact us in advance for rates if you desire this service (609) 737-1902 and indicate on your order if you desire special postage.

4. A copy of the order must accompany your check. The Electrochemical Society, Inc. requires prepayment for all orders.

INQUIRING ABOUT YOUR ORDER

1. Have on hand verification that the order was paid. We require prepayment and no orders will be shipped until payment has been received.

2. Contact The Electrochemical Society, Inc., Book Order Department, 10 South Main St., Pennington, NJ 08534-2896. Telephone (609) 737-1902

CREDIT CARDS

The Electrochemical Society, Inc. accepts Visa and MasterCard. Please include your credit card account number, expiration date and signature as indicated on the order form.

DISCOUNTS

1. All publications are discounted for members of The Electrochemical Society, Inc. only. All others must pay the nonmember price.

2. To become a member of The Electrochemical Society, Inc. and qualify for the special member prices, on future orders, contact The Electrochemical Society, Inc., 10 South Main Street, Pennington, NJ 08534-2896 for a Membership Application and Information. The 1992 Membership Dues are $85.00.

RETURNS

All sales are final except for damaged or incorrect shipments.

SHIPPING INFORMATION

1. Domestic
   4th Class 1 to 4 weeks
   First Class 7 to 14 days
2. Foreign
   4th Class (surface mail) 6-10 weeks
   Air Mail 2 to 4 weeks

CLAIMS

Claims for missing publications will be honored if received within 30 days of normal delivery date.

THE ELECTROCHEMICAL SOCIETY CONTRIBUTING MEMBERS

BENEFACTOR MEMBERS

ELTECH Systems Corporation
Chardon, OH
Fairport Harbor, OH

International Business Machines Corp.
Armonk, NY

Olin Corporation
Stamford, CT

PATRON MEMBERS

AT&T Bell Laboratories
Murray Hill, NJ

Dow Chemical Company
Central Research
Midland, MI

Eveready Battery Co., Inc.
Danbury, CT

Fujitsu Limited
Tokyo, Japan

Hitachi, Ltd.
Central Research Laboratory
Tokyo, Japan

Lam Research Corporation
Fremont, CA

Texas Instruments Inc.
Dallas, TX

SUSTAINING MEMBERS

The Aerospace Corp.
Los Angeles, CA

Aluminum Co. of America
Pittsburgh, PA

Alupower, Inc.
Warren, NJ

AMP Inc.
Harrisburg, PA

Analog Devices, Inc.
Norwood, MA

ASEA Brown Boveri, Ltd.
Corporate Research
Baden, Switzerland

Ballard Power Systems, Inc.
North Vancouver, B.C., Canada

Battelle Memorial Institute
Columbus, OH

The BOC Group
Murray Hill, NJ

Boeing Co.
Seattle, WA

BP Research Centre
Middlesex, England

Comalco Aluminum Ltd.
Melbourne, Victoria, Australia

COMSAT Laboratories
Clarksburg, MD

Corning Incorporated
Corning, NY

CSIRO Division of Mineral Products
Port Melbourne, Victoria, Australia

Duracell Research Center
Needham, MA

ECO Energy Conversion
Somerville, MA

EG&G Princeton Applied Research Corp.
Princeton, NJ

Electrochemical Technology Corp.
Seattle, WA

Electronics and Telecommunications Research Institute
Chung Nam, Korea

Ever Ready Co. (Holdings) Ltd.
Whetstone, London, England

Exxon Research & Engineering Co.
Engineering Technology Division
Florham Park, NJ

General Electric Co.
Corporate Research & Development
Schenectady, NY

SUSTAINING MEMBERS (CONTINUED)

General Motors Corp.
Delco-Remy Division
Anderson, IN

General Motors Research Laboratories
Warren, MI

Giner, Inc.
Waltham, MA

GTE Laboratories
Waltham, MA

GTE Sylvania Inc.
Chemical & Metallurgical Div.
Towanda, PA

Hewlett Packard Co.
Circuit Technology Group
Santa Clara, CA

High Energy Batteries (India) Ltd.
Madras, India

Hoechst-Uhde Corp.
Philadelphia, PA

Honeywell, Inc.
Micro Switch-Optoelectronics
Richardson, TX

ICI Canada Inc.
Mississauga, Ont., Canada

ICI Chemicals & Polymers, Ltd.
Cheshire, England

International Lead Zinc Research Organization, Inc.
Research Triangle Park, NC

Japan Storage Battery Co., Ltd.
Kyoto, Japan

Johnson Controls, Inc.
Milwaukee, WI

Kerr-McGee Chemical Corp.
Kerr-McGee Center
Oklahoma City, OK

Kerr-McGee Corp.
Technology Division
Oklahoma City, OK

Lawrence Berkeley Laboratory
Berkeley, CA

Leclanche S. A.
Yverdon, Switzerland

Lockheed Missiles & Space Co., Inc.
Research Laboratory
Palo Alto, CA

LONZA Ltd.
Sins, Switzerland

LSI Logic Corp.
Santa Clara, CA

M&T Harshaw
Somerset, NJ

Max-Planck-Institut f. Festkorperforschung
Stuttgart, Germany

Medtronic Energy Technology
Minneapolis, MN

Metkem Silicon Limited
Madras, India

Mobil Solar Energy Corp.
Billerica, MA

Molycorp, Inc.
a Unocal company
White Plains, NY

Motorola Inc.
Phoenix, AZ

National Semiconductor
Fairchild Research Center
Santa Clara, CA

NEC Corporation Central Research Laboratories
Kawasaki, Japan

NIFE AB
Oskarshamn, Sweden

Noranda Research Centre
Pointe Claire, Que., Canada

Northern Telecom
Ottawa, Ont., Canada

NTT Electrical Communication Laboratories
Atsugi, Japan

Occidental Chemical Corporation
Research & Development
Grand Island, NY

Orbit Semiconductor, Inc.
Sunnyvale, CA

Philips Laboratories, Inc.
Briarcliff Manor, NY

RAYOVAC Corp.
Madison, WI

Sandia National Laboratories
Albuquerque, NM

Schlumberger Instruments
Canyon Lake, CA

J. C. Schumacher Co.
Carlsbad, CA

SHARP Corporation
Nara, Japan

Shipley Company, Inc.
Newton, MA

Siemens Aktiengesellschaft
Munich, Germany

Siltec Corp.
Menlo Park, CA

Sumitomo Metal Industries Ltd.
Amagasaki, Japan

Tektronix, Inc.
Beaverton, OR

Texas A&M University
Department of Chemical Engineering
College Station, TX

Texas Instruments Inc.
Attleboro, MA

3M Company
St. Paul, MN

Toshiba Corp.
Toshiba Research and
Development Center
Kawasaki, Japan

Toyota Central Research and Development Labs, Inc.
Nagoya, Japan

VARTA Batterie AG
Kelkheim, Germany

Wacker Chemitronic
Burghausen, Germany

Wilson Greatbatch Ltd.
Clarence, NY

Xerox Corp.
Webster Research Center
Rochester, NY

Yuasa Battery Co., Ltd.
Osaka, Japan

LOCAL SECTIONS OF THE SOCIETY

Boston
Purush Chalilpoyil, Chm.
Thomas J. Blakley, V-Chm.
John F. Reardon, Sec.
Daniel J. Eustace, Treas.
James M. Fenton*

Canadian
Andrzej Lasia, Chm.
David F. Tessier, V-Chm.
Christopher P. Wilde, Sec.
Dennis Dong, Treas.
Thomas Z. Fahidy*
Pierre Roberge*

Chicago
Shu-Hwa Lu, Chm.
Scott Barnett, V-Chm.
Daniel J. Kuchynka, Sec.
William Buttner, Treas.
Alanah Fitch*
Kevin Krist*

Cincinnati
Farhad Radpour, Chm.
Arthur T. Hubbard, V-Chm.
Neil M. Poley, Treas.

Cleveland
John C. Bailey, Chm.
Donald A. Tryk, V-Chm.
Daniel W. Gibbons, Sec.
Doris Britton, Treas.
Margaret A. Reid*
Brooke Schumm, Jr.*

Columbus
Irvine I. Tingley, Chm.
David G. Vutetakis, V-Chm.
Han Wu, Sec-Treas.
Steve Bibyk*
M. Ken Han*

Detroit
Frederick T. Wagner, Chm.
M. Ahsan Habib, V-Chm.
Khalil Najafi, V-Chm.
Jerry C.-J. Huang, Sec-Treas.
Tadeusz Malinski*
Gholamabbas Nazri*

European
Georges G. Perrault, Chm.
Jack J. Van Humbeeck, V-Chm.
Wahlfried Plieth, V-Chm.
Alain Olivier, Sec.
Jan Augustynski, Treas.
Helmut Tannenberger*
K. J. Whitlaw*

Japan
Yasuhiro Horiike, Chm.
Katsuro Sugawara, V-Chm.
Koichi Tokuda, V-Chm.
Kenji Murata, Sec.
Ikuo Shiota, Treas.
Hiroshi Ishiwara*
Katsumi Niki*
Isamu Uchida*

Metropolitan New York
Madhav Datta, Chm.
Panayotis C. Andricacos, V-Chm.
Hariklia Deligianni, Sec-Treas.
John Dukovic*
Joseph M. Rosamilia*

Midland
D. Phillip Murray, Chm.
Robert D. Mussell, V-Chm.
Richard D. Varjian*

National Capital
Paul Natishan, Chm.
Graham T. Cheek, V-Chm.
Regis K. Conrad, V-Chm.
Lori Lipkin, Sec.
Frederic D. Bogar, Treas.
Kenneth W. Pratt*
Patricia P. Trzaskoma*

North Texas
Dane E. Bailey, Chm.
Gabriel G. Barna, V-Chm.
Warren O. Kinstley, Sec.
Jimmy W. Hosch, Treas.
Thomas W. Orent*
Richard L. Yeakley*

Oregon
Not available at press time

Pacific Northwest
Not available at press time

Philadelphia
Michael F. Carolan, Chm.
Terrence M. Noveske, V-Chm.
Michael F. Carolan, Sec.
Sudhan S. Misra, Treas.
Walter O. Freitag*

Pittsburgh
John W. Burgman, Chm.
T. David Burleigh, V-Chm.
Chia-Tsun Liu, Sec-Treas.
Alfred F. Lacamera*

San Francisco
Solid State Science & Technology Subsection
Emily I. Bromley, Chm.
Kenneth N. Ritz, V-Chm.
John M. De Larios, Sec.
Izak Bencuya, Treas.
Patrice Geraghty*
Electrochemical Science & Technology Subsection
C. Mark Seymour, Chm.
Francis L. Tanzella, V-Chm.
S. Bhakta, Sec.
Neil Robertson, Treas.
Gina M. Whitney*

South Texas
H. S. Burney, Jr., Chm.
Supramaniam Srinivasan, V-Chm.
Ralph E. White, Sec.
Stephen L. Kelly, Treas.
Demetre Economou*
Richard Pollard*

Southern California-Nevada
Fotios Deligiannis, Chm.
Burton Otzinger, V-Chm.
Thomas P. Barrera, Sec.
Walter A. Tracinski, Treas.
David F. Pickett, Jr.*

Southern Wisconsin
James J. Bolstad, Chm.
Ronald C. Miles, V-Chm.
Benjamin A. Feinberg, Sec-Treas.
Robert B. Dopp*
Kathryn A. Bunding Lee*

Twin Cities
Jing-Yih Cherng, Chm.
Erik R. Scott, V-Chm.
Donald B. Deal, Sec.
H. W. Kalweit, Treas.
William G. Howard*
Henry White*

*Representatives on the Council of Local Sections

Council of Local Sections of the Society

Robert B. Dopp, Chairman
Wayne E. Bailey, Vice-Chairman
Jennifer A. Rathwell, Secretary
William G. Howard, Representative on the Board
Robert B. Dopp, Representative on the Board

OFFICERS OF THE SOCIETY

PRESIDENT
Larry R. Faulkner

VICE-PRESIDENTS
Robert P. Frankenthal — Wayne L. Worrell — James A. Amick

SECRETARY
Eric W. Brooman

TREASURER
Ralph E. White

EXECUTIVE SECRETARY
Roque J. Calvo

DIVISIONS AND GROUPS OF THE SOCIETY

Battery

James McBreen, Chairman
Kathryn R. Bullock, Vice-Chairman
Frank R. McLarnon, Secretary
Samuel C. Levy, Treasurer
Kathryn R. Bullock, Division Advisor

Corrosion

William H. Smyrl, Chairman
Hugh S. Isaacs, Vice-Chairman
Barry R. MacDougall, Secretary-Treasurer
Kathryn R. Bullock, Division Advisor

Dielectric Science and Technology

Geraldine C. Schwartz, Chairman
Robin A. Susko, Vice-Chairman
Y. H. Wong, Secretary
John R. Susko, Treasurer
Vik J. Kapoor, Division Advisor

Electrodeposition

Keith G. Sheppard, Chairman
Milan Paunovic, Vice-Chairman
Dexter D. Snyder, Secretary-Treasurer
Mordechay Schlesinger, Division Advisor

Electronics

Carlton M. Osburn, Chairman
Ralph Jaccodine, First Vice-Chairman
George K. Celler, Second Vice-Chairman
Hisham Z. Massoud, Secretary
Richard L. Yeakley, Treasurer
Paul A. Kohl, Division Advisor

Energy Technology

Micha Tomkiewicz, Chairman
Albert R. Landgrebe, Vice-Chairman
Bruce A. Parkinson, Secretary
Krishnan Rajeshwar, Treasurer
Paul A. Kohl, Division Advisor

High Temperature Materials

Subhash C. Singhal, Chairman
William B. Johnson, Senior Vice-Chairman
Karl E. Spear, Junior Vice-Chairman
Ashok Khandkar, Secretary-Treasurer
John P. Dismukes, Division Advisor

Industrial Electrolysis and Electrochemical Engineering

Dale E. Hall, Chairman
Richard D. Varjian, Vice-Chairman
Eric J. Rudd, Secretary-Treasurer
Mordechay Schlesinger, Division Advisor

Luminescence and Display Materials

Thomas F. Soules, Chairman
William M. Yen, Vice-Chairman
Alok M. Srivastava, Secretary
Thomas E. Sisneros, Treasurer
Vik J. Kapoor, Group Advisor

Organic and Biological Electrochemistry

Essie Kariv-Miller, Chairman
Fred M. Hawkridge, Vice-Chairman
Norman L. Weinberg, Secretary-Treasurer
Therese Cotton, Division Advisor

Physical Electrochemistry

Gregory C. Farrington, Chairman
Brian E. Conway, Vice-Chairman
Daniel A. Scherson, Secretary-Treasurer
Therese Cotton, Division Advisor

Sensor

Richard P. Buck, Chairman
Rupert G. Cuzzon, Vice-Chairman
Michael A. Butler, Secretary-Treasurer
John P. Dismukes, Group Advisor